A Novel Mechanism For The Anti-Cancer Activity Of Aspirin And Its Analogues

BASHIR ASMA'U ISMAIL JUNAIDU B.Pharm, MSc.

A thesis submitted in partial fulfilment of the requirements of the University of Wolverhampton for the degree of Doctor of Philosophy

University of Wolverhampton

September 2017

Declaration

This work or any part hereafter has not previously been presented in any form to the University or to any other body whether for the purpose of assessment, publication or for any other purpose (unless otherwise stated). Save for any express acknowledgments, reference and/or bibliographies cited in the work, I can confirm that the intellectual content of the work is the result of my own efforts and no other person.

The right of Bashir Asma'u Ismail Junaidu to be identified as an author of this work is asserted in accordance with ss.77 and 78 of the Copyright, Designs and Patents Act 1988. At this date copyright is owned by the author.

Signature……

Date…….....

Abstract

Colorectal cancer (CRC), which includes cancer of the large bowel and rectum is the third most common cancer in men and the second in women and there is a poorer survival rate in less developed regions of the world such as West Africa mainly due to the 'out of reach' costs of chemotherapy.

Evidence suggests that aspirin, a non-steroidal anti-inflammatory drug (NSAID) has the potential to decrease incidence of, or mortality from a number of cancers including CRC through several mechanisms of action. However, this evidence is dampened by aspirin's gastrointestinal (GI) toxicity, which have been found to be mostly age-dependent. The search for potential aspirin-related compounds with the same or better cytotoxic effects against cancer cells accompanied by a safer toxicity profile has been ongoing over the years and led to us to synthesise a number of novel aspirin analogues. One of the mechanisms of action suggested for the anticancer property of aspirin is the COX-dependent pathway. In this thesis SW480 cell line, a CRC cell line that is COX-2 negative and mismatch repair (MMR) proficient was used to study the possible COX-independent mechanism of action for aspirin, its analogues and diflunisal at 0.5 mM. Diflunisal was included in this study because it is also a salicylate with reports of having cytotoxic effects. OE33 and FLO1 oesophageal cancer cells were also employed in the epidermal growth factor receptor (EGFR) and synergy experiments to show effects were not just specific to SW480 cells alone. These aspirin analogues were synthesised, identified using nuclear magnetic resonance (NMR) and infra-red (IR) spectroscopy, and tested for purity using thin layer chromatography (TLC) and melting point. The findings of this study suggest that these compounds breakdown into salicylates and perturb epidermal growth factor (EGF) internalization with PN517 (fumaryldiaspirin) and PN590 (*ortho*-thioaspirin) also driving EGF co-localization with early-endosome antigen-1 (EEA1). The perturbation of the internalization of EGF by aspirin and PN517 was also observed by a time-lapse assay using live confocal imaging. These compounds also had specific effects on different tyrosine phosphorylation sites of the EGFR, with none but PN590 inhibiting

phosphorylation at Y1068, and all but PN502 (*ortho*-aspirin), PN548 (*meta*-aspirin) and PN549 (*para*-aspirin) inhibiting phosphorylation at Y1045 and Y1173. Given that the EGF internalization assay involved the cells being treated with compounds for 2 h, cells were also treated for this same time period and probed with pEGFR 1045, which resulted in the compounds having no significant effect on phosphorylation at that site which is responsible for the ubiquitination of the EGFR. Most of these compounds were apoptotic with some showing a combination of apoptosis and necrosis. Aspirin and its isomers drove apoptotic cell death in SW480 cells via the BCL2-BAX pathway while the thioaspirins appear to follow the p21 pathway by decreasing the expression of the protein. In addition, it was shown that PN502 (aspirin), PN517 and PN590 had synergistic effects when used in combination with oxaliplatin at ED_{50}, ED_{75} and ED_{90} in SW480 CRC cells. The cytotoxicity of these compounds individually or in combination was determined using MTT assay followed by the use of the CompuSyn and CalcuSyn software to calculate combination index (CI), which indicated whether a drug combination was synergistic, antagonistic or additive. PN517 and PN524 were synergistic when used in combination with cisplatin in OE33 oesophageal cancer cells. Effect of these compounds on the EGFR indicates a delay or disruption of the signalling pathway involved in the proliferation of cancer cells, thus, translating into protection against tumour formation or progression while the synergistic effects of these compounds when used in combination with platinum compounds can provide patients with less toxic chemotherapeutic regimen especially in patients with CRC tumours that harbour mutant *TP53* gene and normally resistant to oxaliplatin.

It is therefore proposed that the perturbation of EGF internalization is a novel mechanism of action for aspirin and its analogues in cancer therapy.

These positive findings shed light on the understanding of the possible mechanism of action for aspirins and gives hope for a more affordable, less toxic therapy for the prevention, treatment and management of cancer.

Acknowledgement

All praises due to the Lord of the worlds, the Most Beneficent, the Most Merciful for keeping me alive and healthy and for giving me the strength to complete this phase of my life.

I will like to sincerely show my gratitude to my supervisors, Dr. Iain Nicholl, Dr. Steve Safrany and Dr. Chris Perry. Thank you for your constructive criticisms, support, encouragement and guidance. I have learnt a great deal.

Special thanks to the academic staff; Dr. A. Armesilla, Prof. W. Wang, Dr. S. Jones, Dr. V. Kannapan, Dr. S. Kilari, the technical staff; David Townrow, Henrik Townsend, Clare Murcott and Karen Hollyhead; and my colleagues; Haider, Satish, Patricia, Maggie, Lawrence, Shaima, Aisha, Fakhra, Karim and Kate.

To my dear husband, Bashir Abdullahi, words cannot express my gratitude. Thank you for your emotional and financial support throughout this journey and beyond.

To my children Nadima, Abdullah, Khadija, Rahama, Aisha and brother, Siraj. Thank you for your unconditional support and putting up with ‘Grumpy Mum’.
I will also like to thank my Parents, Professor Ismail Junaidu and Aisha Indo Junaidu for their continuous support and prayers. Thank you to my siblings and entire family for your encouragement and prayers.

And last but not least, my sincere appreciation to my Wolverhampton family, Hauwa, Hussaina, Fatima and so many well wishers. God bless you all.

Dedication

This work is dedicated to all those that lost the battle to cancer because they could not afford the treatment.

Table of Contents

Abstract **3**

Acknowledgement **5**

Table of Contents **7**

Table of figures **11**

List of tables **19**

Abbreviations **21**

Chapter 1. Introduction **26**

1.1 Cancer **26**

1.2 The Hallmarks of Cancer **26**

1.2.1 'Sustaining Growth Signalling' 27

1.2.2 'Evading Growth Suppressors' 28

1.2.3 'Resisting Cell Death' 29

1.2.4 'Enabling Replicative Immortality' 30

1.2.5 'Inducing Angiogenesis' 31

1.2.6 'Activating Invasion and Metastasis' 31

1.2.7 'Cancer-related Inflammation' 32

1.2.8 'Genome Instability and Mutation' 33

1.2.9 'Deregulating Cellular Energies' 34

1.2.10 'Avoiding Immune Destruction' 34

1.3 Colorectal cancer **35**

1.3.1 Types of Colorectal cancer (CRC) 37

1.3.2 Pathways involved in the development of CRC 38

1.4 Treatment of CRC **43**

1.4.1 Cetuximab 46

1.4.2 Panitumumab 46

1.4.3 Bevacizumab 46

1.4.4 5-Fluorouracil (5-FU) 46

1.4.5 Oxaliplatin 47

1.4.6 Immunotherapy....48
1.4.7 Aspirin....51
1.5 Aims and Objectives....57
Chapter 2. Materials & Methods....59
2.1 Materials....59
2.1.1 Lab instruments....59
2.1.2 Media and Reagents/Chemicals....61
2.1.3 Buffers and solutions....65
2.1.4 Primary antibodies....66
2.1.5 Secondary antibodies....68
2.1.6 Cell lines....69
2.2 Methods....71
2.2.1 Tissue Culture....71
2.2.2 Preparation of compounds as stock solutions....73
2.2.3 Synthesis of aspirin analogues....73
2.2.4 Chemistry of aspirin analogues....75
2.2.5 Cytotoxicity, Toxicity and Breakdown of aspirin analogues....77
2.2.6 Salicylic acid Analysis....80
2.2.7 DEREK Analysis....82
2.2.8 SDS-PAGE for separation of proteins and Western blot for detection 82
2.2.9 Flow cytometry....88
2.2.10 YO-PRO®-1 and PI....90
2.2.11 Epidermal Growth Factor Binding....91
2.2.12 Epidermal Growth Factor Internalization....91
2.2.13 EGF internalization using Live Confocal Imaging....92
2.2.14 Quantification of EGF internalization....93
2.2.15 EGF co-localisation with EEA1....94
2.2.16 Synergy experiments....95
2.2.17 Statistical Analysis....97
Chapter 3. Chemistry of Aspirin analogues....98
3.1 Introduction....98

3.2 Aims and Objectives 99
3.3 Methodology 99
3.4 Results 99
3.4.1 Synthesis of aspirin analogues 99
3.4.2 Identification/Confirmation of aspirin analogues structures 100
3.4.3 Purity of aspirin analogues synthesised 120
3.4.4 Stability/Breakdown of aspirin analogues 126
3.5 Discussion 134

Chapter 4. Cytotoxicity and Synergy of Aspirin analogues with platinum compounds 137

4.1 Introduction 137
4.1.1 Cytotoxicity of Aspirin analogues 137
4.1.2 Synergy 139
4.2 Aims and Objectives 146
4.3 Methodology 146
4.4 Results 147
4.4.1 Cytotoxicity results 147
4.4.2 DEREK analysis 159
4.4.3 Drug combinations 161
4.5 Discussion 216

Chapter 5. Apoptosis or Necrosis? 223

5.1 Introduction 223
5.1.1 Apoptosis 223
5.1.2 Beta catenin 227
5.2 Aims and Objectives 228
5.3 Methodology 228
5.4 Results 229
5.4.1 Effects of aspirin analogues on p21 expression 229
5.4.2 Effects of aspirin analogues on BAX and BCL2 expression 231
5.4.3 Effects of aspirin analogues on apoptosis 231
5.4.4 Effect of ortho-thioaspirin on the localization of β-catenin 244
5.5 Discussion 245

Chapter 6. Effect of Aspirin analogues on the EGFR.....251
6.1 Introduction 251
6.1.1 The EGF Receptor.....251
6.1.2 Early Endosome Antigen1 (EEA1).....260
6.2 Aims and Objectives 262
6.3 Methodology 263
6.4 Results 263
6.4.1 Perturbation of EGF internalization and effect on its co-localization with EEA1 by aspirin and its analogues 263
6.4.2 Effect of aspirin and its analogues on the Tyrosine phosphorylation sites of the EGF receptor 303
6.5 Discussion 325
Chapter 7. General Discussion and Future Studies.....332
7.1 General Discussion.....332
7.2 Future Studies 340
Chapter 8. Appendix 343
8.1 ^{13}C NMR Spectra for aspirin and its analogues 343
8.2 IR Spectra for aspirin and its analogues.....352
8.3 Supplementary: Screen shots and Legend for Live Imaging Movies (on DVD) of EGF in cells incubated with aspirin and aspirin analogue. 365
Reference List 367

Table of figures

Figure 1.1 The seven hallmarks of Cancer. 27
Figure 1.2 Therapeutic Targeting of the Hallmarks of Cancer. 33
Figure 1.3 CRC tumourigenesis. 36
Figure 1.4 Different steps in the pathways to genetic instability and relationship between ploidy and CIN in terms of tumour initiation and growth. 42
Figure 1.5 Intensive and less intensive treatment lines for metastatic CRC. 45
Figure 1.6 COX-dependent and COX-independent mechanisms of antitumoural effects of aspirin. 55
Figure 2.1 Chemical reaction for the synthesis of isomers of thioaspirin. 74
Figure 2.2 Illustrated explanation of the principle behind MTS activity. 78
Figure 2.3 Gating of cells undergoing apoptosis and necrosis using flow cytometry. 89
Figure 3.1 NMR Spectrum for o-acetoxybenzoic acid (o-aspirin). 101
Figure 3.2 ^{13}C NMR PN502. 102
Figure 3.3 ^{13}C NMR PN508. 104
Figure 3.4 ^{13}C NMR PN517. 106
Figure 3.5 ^{13}C NMR PN548. 108
Figure 3.6 ^{13}C NMR PN549. 110
Figure 3.7 ^{13}C NMR PN590. 112
Figure 3.8 ^{13}C NMR PN591. 114
Figure 3.9 ^{13}C NMR PN592. 116
Figure 3.10 TLC of aspirin analogues assessing purity. 121
Figure 3.11 Standard curve for salicylic acid detection using the As(III)-SA system. 127
Figure 3.12 Fluorescence reading of salicylic acid (SA) at different time points. 128
Figure 3.13 Percentage of salicylic acid (SA) produced by aspirin analogues. 129
Figure 3.14 Percentage of salicylic acid (SA) produced by aspirin analogues. 130

Figure 3.15 TLC of aspirin analogues against their salicylates and extracts (S). 132
Figure 3.16 Salicylate formation from PN502 in solution at different storage conditions.....134
Figure 4.1 Morphology of the cell lines used in this study.....139
Figure 4.2 Drug combination plots and their interpretations based on the Chou and Tatalay combination index (CI) theorem. 144
Figure 4.3 Standard curve for MTS solution. 147
Figure 4.4 Standard curve for MTT solution.....148
Figure 4.5 Percentage cell viability of SW480 CRC cells in different organic solvents.....149
Figure 4.8 Dose response curves of aspirin analogues and platinum compounds in OE33 (A) and FLO1 (B) oesophageal cell lines.....156
Figure 4.9 Drug combination plots for cisplatin and ortho-aspirin (CP+PN502[1:200]) in SW480 CRC cells. 163
Figure 4.10 Drug combination plots for cisplatin and meta-aspirin (CP+PN548[1:400]) in SW480 CRC cells. 164
Figure 4.11 Drug combination plots for cisplatin and para-aspirin (CP+PN549[1:250]) in SW480 CRC cells. 165
Figure 4.12 Drug combination plots for cisplatin and fumaryldiaspirin (CP+PN517[1:10]) in SW480 CRC cells. 167
Figure 4.13 Drug combination plots for cisplatin and diaspirin (CP+PN508[1:17.5]) in SW480 CRC cells. 168
Figure 4.14 Drug combination plots for cisplatin and m-bromobenzoylsalicylate (CP+PN524[1:40]) in SW480 CRC cells. 169
Figure 4.15 Drug combination plots for cisplatin and ortho-thioaspirin (CP+PN590[1:20]) in SW480 CRC cells. 171
Figure 4.16 Drug combination plots for cisplatin and meta-thioaspirin (CP+PN591[1:20]) in SW480 CRC cells 172
Figure 4.17 Drug combination plots for cisplatin and para-thioaspirin (CP+PN592[1:70]) in SW480 CRC cells. 173

Figure 4.18 Drug combination plots for oxaliplatin and ortho-aspirin (OX+PN502[1:80]) in SW480 CRC cells. 175
Figure 4.19 Drug combination plots for oxaliplatin and meta-aspirin (OX+PN548[1:80]) in SW480 CRC cells. 176
Figure 4.20 Drug combination plots for oxaliplatin and para-aspirin (OX+PN549[1:100]) in SW480 CRC cells. 177
Figure 4.21 Drug combination plots for oxaliplatin and fumaryldiaspirin (OX+PN517[1:8]) in SW480 CRC cells. 179
Figure 4.22 Drug combination plots for oxaliplatin and diaspirin (OX+PN508[1:14]) in SW480 CRC cells. 180
Figure 4.23 Drug combination plots for oxaliplatin and m-bromobenzoylsalicylate (OX+PN524[1:8]) in SW480 CRC cells. 181
Figure 4.24 Drug combination plots for oxaliplatin and ortho-thioaspirin (OX+PN590[1:8]) in SW480 CRC cells. 183
Figure 4.25 Drug combination plots for oxaliplatin and meta-thioaspirin (OX+PN591[1:10]) in SW480 CRC cells. 184
Figure 4.26 Drug combination plots for oxaliplatin and para-thioaspirin (OX+PN592[1:14]) in SW480 CRC cells. 185
Figure 4.27 Drug combination plots for carboplatin and ortho-aspirin (CB+PN502[1:20]) in SW480 CRC cells. 187
Figure 4.28 Drug combination plots for carboplatin and meta-aspirin (CB+PN548[1:20]) in SW480 CRC cells. 188
Figure 4.29 Drug combination plots for carboplatin and para-aspirin (CB+PN549[1:50]) in SW480 CRC cells. 189
Figure 4.30 Drug combination plots for carboplatin and fumaryldiaspirin (CB+PN517[1:2]) in SW480 CRC cells. 191
Figure 4.31 Drug combination plots for carboplatin and diaspirin (CB+PN508[1:1.75]) in SW480 CRC cells. 192
Figure 4.32 Drug combination plots for carboplatin and m-bromobenzoylsalicylate (CB+PN524[1:1]) in SW480 CRC cells 193
Figure 4.33 Drug combination plots for carboplatin and ortho-thioaspirin (CB+PN590[1:2]) in SW480 CRC cells. 195

Figure 4.34 Drug combination plots for carboplatin and meta-thioaspirin (CB+PN591[1:5]) in SW480 CRC cells. 196
Figure 4.35 Drug combination plots for carboplatin and para-thioaspirin (CB+PN592[1:1.75]) in SW480 CRC cells. 197
Figure 4.36 Drug combination plots for cisplatin and ortho-aspirin (CP+PN502[1:100]) in OE33 oesophageal cancer cells. 199
Figure 4.37 Drug combination plots for cisplatin and fumaryldiaspirin (CP+PN517[1:50]) in OE33 oesophageal cancer cells. 200
Figure 4.38 Drug combination plots for cisplatin and m-bromobenzoylsalicylate (CP+PN524[1:50]) in OE33 oesophageal cancer cells. 201
Figure 4.39 Drug combination plots for cisplatin and methyl-benzoylsalicylate (CP+PN528[1:160]) in OE33 oesophageal cancer cells. 202
Figure 4.40 Drug combination plots for oxaliplatin and ortho-aspirin (OX+PN502[1:20]) in OE33 oesophageal cancer cells. 204
Figure 4.41 Drug combination plots for oxaliplatin and fumaryldiaspirin (OX+PN517[1:20]) in OE33 oesophageal cancer cells. 205
Figure 4.42 Drug combination plots for oxaliplatin and m-bromobenzoylsalicylate (OX+PN524[1:10]) in OE33 oesophageal cancer cells. 206
Figure 4.43 Drug combination plots for oxaliplatin and methyl-benzoylsalicylate (OX+PN528[1:32]) in OE33 oesophageal cancer cells. 207
Figure 4.44 Drug combination plots for carboplatin and ortho-aspirin (CB+PN502[1:40]) in OE33 oesophageal cancer cells. 209
Figure 4.45 Drug combination plots for carboplatin and fumaryldiaspirin (CB+PN517[1:40]) in OE33 oesophageal cancer cells. 210
Figure 4.46 Drug combination plots for carboplatin and m-bromobenzoylsalicylate (CB+PN524[1:20]) in OE33 oesophageal cancer cells. 211
Figure 4.47 Drug combination plots for carboplatin and methyl-benzoylsalicylate (CB+PN528[1:32]) in OE33 oesophageal cancer cells. 212
Figure 5.1 Morphological features of the different types of PCD. 224

Figure 5.2 Effect of 5-FU on the expression of p21 using different antibodies. 229
Figure 5.3 Effect of aspirin analogues on p21, BAX and BCL2 expression in SW480 CRC cells. 230
Figure 5.4 Representation of flow cytometric analysis and ICC for negative control (untreated) and control for apoptosis. 232
Figure 5.5 Representation of flow cytometric analysis and ICC for negative control (untreated) and control for necrosis. 233
Figure 5.6 Representation of flow cytometric analysis and ICC for PN502 (aspirin). 234
Figure 5.7 Representation of flow cytometric analysis and ICC for PN548 (meta-aspirin). 235
Figure 5.8 Representation of flow cytometric analysis and ICC for PN549 (para-aspirin). 236
Figure 5.9 Representation of flow cytometric analysis and ICC for PN590 (ortho-thioaspirin). 237
Figure 5.10 Representation of flow cytometric analysis and ICC for PN591 (meta-thioaspirin). 238
Figure 5.11 Representation of flow cytometric analysis and ICC for PN592 (para-thioaspirin). 239
Figure 5.12 Flow cytometric analysis of aspirin analogues showing induced apoptosis in SW480 CRC cell line. 241
Figure 5.13 Flow cytometric analysis of aspirin analogues showing induced necrosis in SW480 CRC cell line. 242
Figure 5.14 Effect of PN590 (ortho-thioaspirin) on β-catenin localization. 244
Figure 6.1 Structure of the EGFR, sites of phosphorylation and effector signalling pathways triggered. 253
Figure 6.2 EGFR signalling pathway. 257
Figure 6.3 Structure of diflunisal and salicylic acid. 265
Figure 6.4 Quantification of the effect on aspirin analogues on EGF binding. 266
Figure 6.5 Effect of aspirin analogues on EGF binding. 267

Figure 6.6 Effect of aspirins with PBS on EGF-100 ng/ml internalization and EGF co-localization with EEA1. 270
Figure 6.7 Effect of thioaspirins with PBS on EGF-100 ng/ml internalization and EGF co-localization with EEA1. 273
Figure 6.8 Effect of diaspirins with PBS on EGF-100 ng/ml internalization and EGF co-localization with EEA1. 276
Figure 6.9 Aspirin analogues dissolved in acetone to 50 mM and further diluted with buffer to adjust pH. 278
Figure 6.10 Effect of aspirins and thioaspirins with HEPES on EGF-100 ng/ml internalization and EGF co-localization with EEA1. 282
Figure 6.11 Effect of diaspirins with HEPES on EGF-100 ng/ml internalization and EGF co-localization with EEA1. 285
Figure 6.12 Effect of salicylates with HEPES on EGF-100 ng/ml internalization and EGF co-localization with EEA1. 288
Figure 6.13 Effect of aspirin analogues with HEPES on EGF-20 ng/ml internalization and EGF co-localization with EEA1. 293
Figure 6.14 Effect of aspirin analogues with HEPES on EGF-20 ng/ml internalization in oesophageal cells. 296
Figure 6.15 Effect of aspirin analogues on EGF-20 ng/ml internalization in oesophageal cells. 299
Figure 6.16 Effect of aspirin analogues on EGF-20 ng/ml internalization in MG cells.....301
Figure 6.17 EGFR expression levels with aspirin analogues buffered with PBS in SW480 cells. 305
Figure 6.18 EGFR expression levels with aspirin analogues buffered with HEPES (pH8) in SW480 cells. 307
Figure 6.19 Time response to EGFR expression levels with aspirin analogues in SW480 cells. 309
Figure 6.20 EGF dose and exposure time optimization for pY1068 and pY1173 antibodies. 311
Figure 6.21 EGF dose and exposure time optimization for EGFR stimulation against pY1045 antibody. 312

Figure 6.22 EGF dose and exposure time optimization for EGFR stimulation against pY992 and p1101 antibodies. 313
Figure 6.23 Effect of aspirin and its analogues on pEGFR tyrosine kinase phosphorylation sites. 315
Figure 6.24 Dose response effect of the thioaspirins on the pEGFR Y1045 and Y1173 tyrosine kinase phosphorylation sites. 317
Figure 6.25 Dose response effect of 'diaspirins' on the pEGFR Y1045 and Y1173 tyrosine kinase phosphorylation sites. 319
Figure 6.26 Effect of aspirin and its analogues on pEGFR Y1045 site. 321
Figure 6.27 Effect of aspirin analogues on stat-3. 322
Figure 6.28 Effect of aspirin analogues on stat-3 and Tyr705 phosphorylation. 324
Figure 8.1 ^{13}C NMR spectrum for aspirin (PN502). 344
Figure 8.2 ^{13}C NMR spectrum for PN508. 345
Figure 8.3 ^{13}C NMR spectrum for PN517. 346
Figure 8.4 ^{13}C NMR spectrum for PN548 347
Figure 8.5 ^{13}C NMR spectrum for PN549. 348
Figure 8.6 ^{13}C NMR spectrum for PN590. 349
Figure 8.7 ^{13}C NMR spectrum for PN591. 350
Figure 8.8 ^{13}C NMR spectrum for PN592. 351
Figure 8.9 IR Spectrum of PN502. 352
Figure 8.10 IR Spectrum of PN517. 353
Figure 8.11 IR Spectrum of PN548. 354
Figure 8.12 IR Spectrum of PN549. 355
Figure 8.13 IR Spectrum of PN590. 356
Figure 8.14 IR Spectrum of PN591. 357
Figure 8.15 IR Spectrum of PN592. 358
Figure 8.16 IR Spectrum of Salicylic acid. 359
Figure 8.17 IR Spectrum of Thiosalicylic acid. 360
Figure 8.18 IR Spectrum of 3-hydroxybenzoic acid. 361
Figure 8.19 IR Spectrum of 4-hydroxybenzoic acid. 362
Figure 8.20 IR Spectrum of 3-mercaptobenzoic acid. 363

Figure 8.21 IR Spectrum of 4-mercaptobenzoic acid. 364
Figure 8.22 Screen shots of Movies showing SW480 CRC cells untreated (control), treated with aspirin and PN517 at 0 min and 30 min after stimulation. 365

List of tables

Table 1.1 Structure and Properties of Platinum-based antineoplastics. 48
Table 2.1 List of instruments and equipment used in this study. 60
Table 2.2 List of Reagents, Drugs, Culture media and other chemicals used in this study. 64
Table 2.3 List of buffers used in this study. 65
Table 2.4 List of Primary antibodies used in this study. 67
Table 2.5 List of Secondary antibodies used in this study. 68
Table 2.6 Characteristics of cancer cell lines used in this study. 70
Table 2.7 Recipe for preparation of stacking gel. 83
Table 2.8 Recipe for preparation of separating gel. 83
Table 3.1 IR interpretation of aspirin analogues and their precursor compounds. All spectra recorded on neat powdered samples using a Genesis II ATR FTIR Spectrometer. 118
Table 3.2 R_f value of aspirin analogues and their respective precursors. 120
Table 3.3 Structure and Properties of aspirin analogues. Lit. (Literature). 125
Table 4.1 Example of a DRI Data for Drug Combination involving drugs A and B. 142
Table 4.2 Description and Interpretation of CI values. 145
Table 4.3 IC_{50} values of aspirin analogues, NSAIDs and platinum compounds on SW480 CRC cell line, OE33 and FLO1 oesophageal cell lines. 158
Table 4.4 IC_{50} values of some aspirin analogues, NSAIDs and platinum compounds on SW480 CRC cell line after 12- day cytotoxicity assay. 158
Table 4.5 List of compounds, endpoints and results produced by *in silico* analysis using the DEREK software. 160
Table 4.6 Summary of drug combination CI values in SW480 CRC cell line. .214
Table 4.7 Summary of drug combination CI values in OE33 oesophageal cancer cell line. 215
Table 5.1 List of various apoptosis detection kits from different companies with the type of cell used in the documentation/protocol sheet. 248

Table 6.1 EGFR phosphorylation sites used in this study and their functions.....
.....255
Table 7.1 Summary of the effect of aspirin analogues on SW480 CRC cells .....
.....334

Abbreviations

5-FU	5-fluorouracil
Ab	Antibody
AIF	Apoptosis inducing factors
APC	Allophycocyanin
APC	Adenomatous polyposis coli
APS	Ammonium persulphate
APPL1	Adaptor protein, phosphotyrosine interaction, PH domain and Leucine zipper containing 1
ATCC	American Type Culture Collection
BAX	Bcl2 associated X-protein
BAK	BCL-2 homologous antagonist killer
BCL-2	B-cell lymphoma 2
BID	BH3 interacting-domain death agonist
BIM	BCL-2-like protein 11
BCL-W	BCL-2-like protein 2
BCL-XL	B-cell lymphoma-extra large
BSA	Bovine Serum Albumin
CEA	Carcinoembryonic antigen
CI	Combination Index
CIN	Chromosome instability
CO_2	Carbon dioxide
CRUK	Cancer Research UK
CRC	Colorectal cancer

CTLA-4	Cytotoxic T-lymphocyte-associated protein
DMEM	Dulbecco's Modified Eagle's Medium
DMSO	Dimethyl sulphoxide
DNA	Deoxyribonucleic acid
ECACC	European Collection of Authenticated Cell Collection
ECL	Enhanced chemiluminescence
ECM	Extracellular matrix
EDTA	Ethylenediaminetetraacetic acid
EEA1	Early endosome antigen-1
EGF	Epidermal Growth Factor
EGFR	Epidermal Growth Factor Receptor
EMT	Epithelial-mesenchymal transition
ESCRT	Endosome Sorting Complexes Required for Transport
FBS	Foetal Bovine Serum
Fig.	Figure
FITC	Fluorescein isothiocyanate
g	grams
GI	Gastrointestinal
h	hour
HCl	Hydrochloric acid
HNPCC	Hereditory non-polyposis colorectal cancer
HRP	Horseradish peroxidase
kDa	KiloDalton
L	Litre

L-15	Leibovitz's medium
LBM	Lean body mass
mAb	monoclonal Antibody
MAPK	Mitogen-activated protein-kinase
mCRC	metastatic colorectal cancer
MHC	major histocompatibility complexes
min	minutes
ml	millilitres
mM	millimolar
MMR	Mismatch Repair
MIN	Microsatellite instability
mpt	melting point
MTS	[3-(4,5-dimethylthiazol-2-yl)-2,5-diphenyltetrazolium bromide]
MTT	3-(4,5-dimethylthiazol-2-yl)-5-(3-carboxyphenyl)-2-(4-sulfophenyl)-2H-tetrazolium]
MW	Molecular weight
NF-κB	Nuclear factor kappa-light-chain-enhancer of activated B-cells
NFM	Non-Fat Milk
NSAID	Non-Steroidal Anti-Inflammatory Drugs
p21	protein-21
pAb	polyclonal Antibody
PAGE	Polyacrylamide Gel Electrophoresis
PBS	Phosphate Buffered Saline
PD-1	Programmed death-1

pH	potential of Hydrogen
PI	Propidium Iodide
PI3K	Phosphatidylinositol-4,5-biphosphate 3-kinase
PLC	Phospholipase C
PKC	Protein Kinase C
PI 3-K	Phosphoinositide-3-kinase
PE	Phycoerythrin
PN502	ortho-aspirin
PN548	meta-aspirin
PN549	para-aspirin
PN590	ortho-thioaspirin
PN591	meta-thioaspirin
PN592	para-thioaspirin
PN517	Fumaryldiaspirin
PN508	Diaspirin
PN524	m-bromobenzoylsalicylate
PN528	methyl-benzoylsalicylate
PVDF	Polyvinylidene difluoride
RER	Replication errors
RONS	Reactive oxygen and nitrogen species
rpm	revolutions per minute
RT	room temperature
SA	Salicylic acid
SD	Standard deviation

SDS	Sodium dodecyl sulphate
SDS-PAGE	Sodium dodecyl sulphate- Polyacrylamide Gel Electrophoresis
SEM	Standard error of the mean
TCR	T-cell receptors
TEMED	N,N,N',N'-tetramethylethylenediamine
TGF	Tumour Growth Factor
THF	Tetrahydrofuran
TIL	Tumour infiltrating lymphocytes
TLR	Toll-like receptors
V	volts
VEGF	Vascular endothelial growth factor
UCA	Ulcerative colitis-associated
UPAR	Urokinase plasminogen activator receptor gene
v/v	volume/volume
w/v	weight/volume
w/w	weight/weight
yrs	years
µg	microgram
µM	micromolar
µm	micrometre
°C	degree Celsius
%	percentage

Chapter 1. Introduction

1.1 Cancer

Cancer arises as a consequence of the accumulation of genomic changes, which include genetic mutations, disruption in the functionality of these genes and deregulation of signalling pathways. These genetic mutations result in an increase in functionality of oncogenes and a decrease or loss in the functionality of tumour suppressor genes (Hanahan and Weinberg, 2000). These genetic changes result in alterations in cell physiology termed as the hallmarks of cancer (Colotta *et al.*, 2009, Hanahan and Weinberg, 2000, Hanahan and Weinberg, 2011).

1.2 The Hallmarks of Cancer

The genomic changes were initially thought to be as a result of six alterations in cell physiology termed as the six hallmarks of cancer. They include sustaining proliferative signalling, evading growth suppressors, activating invasion and metastasis, enabling replicative immortality, inducing angiogenesis and resisting apoptosis (Hanahan and Weinberg, 2000). Later on, cancer-related inflammation has been included as the seventh hallmark of cancer (Colotta *et al.*, 2009) (Figure 1.1).

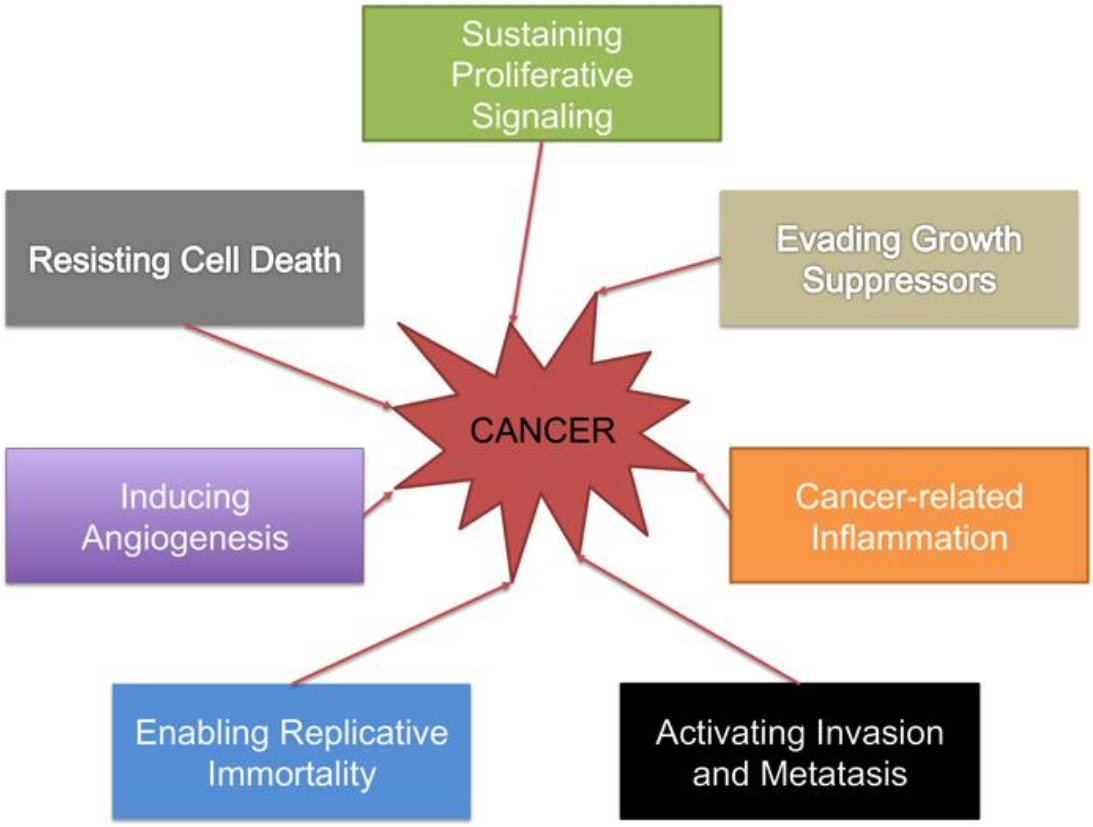

Figure 1.1 The seven hallmarks of Cancer.
Cancers acquire these capabilities during development in order to progress and invade other neighbouring tissues. These capabilities also contribute to poor prognosis [Adapted from (Colotta *et al.*, 2009, Hanahan and Weinberg, 2000, Hanahan and Weinberg, 2011)].

1.2.1 'Sustaining Growth Signalling'

Mitogenic growth signals are required for cell to change from a rest phase to a proliferative phase by transmembrane receptors (Bhowmick and Moses, 2005). Normal growth signals are mimicked by oncogenes (Liotta and Kohn, 2001). This enables tumour cells to generate their own signalling programme. For example, cancer cells do not rely on normal cells for the production of growth factors such as platelet-derived growth factor (PDGF) and tumour growth factor α (TGFα), but rather produce these growth factors independently. In addition, cancer cells may also send signals to normal cells, which in turn supply the

cancer cells with various growth factors (Cheng *et al.*, 2008). Cell surface receptors responsible for this signalling also undergo deregulation resulting in overexpression. For example, the epidermal growth factor receptor (EGFR) when overexpressed becomes hyper-responsive to background levels of growth factor (Sebastian *et al.*, 2006, Yarden and Ullrich, 1988) or ligand-independent signalling (Di Fiore *et al.*, 1987). Similarly, somatic mutations in the DNA of cancer cells result in an increase in signalling through the Raf to mitogen-activated protein-kinase (MAPK) pathway (Davies and Samuels, 2010) and the phosphoinositide 3-kinase (PI 3-K) signalling pathway (Jiang and Liu, 2009).

Cancer cells can also choose to express extracellular receptors that produce proliferative signals, which could lead to resistance to apoptosis and entry into the active cell cycle. An example is the effects of integrin on growth factors (Giancotti and Ruoslahti, 1999).

In some contexts however, oncoproteins such as Ras and Raf, producing high levels of signalling can stimulate apoptosis or entry into the rest phase of the cell cycle (Collado and Serrano, 2010, Lowe *et al.*, 2004)

1.2.2 'Evading Growth Suppressors'

Antiproliferative signals are responsible for maintaining tissue homeostasis. Antigrowth signals from tumour suppressor genes block cell proliferation either by forcing the cell cycle into rest (G_0) phase or by causing apoptosis (Hanahan and Weinberg, 2000, Hanahan and Weinberg, 2011). Examples of tumour suppressors include *RB* (retinoblastoma-associated) and *TP53*. The *RB* gene, as part of a wider network acts as a 'gatekeeper' to cells for entry or

progression into the cell cycle (Burkhart and Sage, 2008) and its inactivation can lead to cellular proliferation. *TP53* regulates cell growth or division by halting cell cycle progression or activating apoptosis when stress signals, as a result of damage to the genome, are received (Hanahan and Weinberg, 2011). Another mechanism in which cancer cells operate to evade growth suppressors is by corrupting the TGF-β pathway (Ikushima and Miyazono, 2010), where TGF-β regulates the G_1 phase of the cell cycle by suppressing *c-myc* gene and also causes synthesis of p21 and p15 proteins, which inhibits G_1 cyclin CDK leading to cell apoptosis (Datto *et al.*, 1997).

1.2.3 'Resisting Cell Death'

Resisting apoptosis, also known as programmed cell death, is a contributing factor in cancer development (Adams and Cory, 1998, Adams and Cory, 2007, Lowe *et al.*, 2004) and thus, a hallmark of cancer. Apoptosis is a step-by-step process that takes place within 2 h. It involves disruption of the cellular membrane; break down of the cytoplasmic and nuclear organelles, degradation of the chromosomes, and fragmentation of the nucleus. Finally, the shrivelled cell is engulfed by nearby cells by a process known as phagocytosis (Wyllie *et al.*, 1980). The mitochondria release cytochrome C, a catalyst for apoptosis when proapoptotic signals are received (Green and Reed, 1998). Apoptosis can either be caspase-dependent or caspase-independent, where the former involves the triggering of caspase by the release of apoptosis inducing factors (AIF) (van Gurp *et al.*, 2003) and the latter entails translocation of AIF into the nucleus, which induces chromatin condensation (Cregan *et al.*, 2004).

Proapoptotic proteins include BCL-2 associated X protein (BAX), BCL-2 homologous antagonist killer (BAK), BH3 interacting-domain death agonist (BID) and BCL-2-like protein 11 (BIM) while the antiapoptotic proteins include B-cell lymphoma 2 (BCL-2), B-cell lymphoma-extra large (BCL-XL) and BCL-2-like protein 2 (BCL-W), all of which are of the BCL-2 family (Gross *et al.*, 1999). Upon DNA damage, p53 tumour suppressor upregulates BAX, which results in the release cytochrome C by the mitochondria (Hanahan and Weinberg, 2000). Autophagy, another form of cell death, is a degradation system that enables the delivery of cytoplasmic materials of aged cells during starvation conditions to lysosomes and is important in maintaining cell homeostasis (Jiang *et al.*, 2015, Seglen *et al.*, 1996). Insufficiency of survival signals leads to the downregulation of the PI 3-K signalling pathway, which results in the stimulation of autophagy and/or apoptosis (Levine and Kroemer, 2008).

1.2.4 'Enabling Replicative Immortality'

Telomeres, which are composed of several thousand repeats of a short 6-base-pair sequence element, protect the ends of chromosomes and are mainly responsible for proliferation in cells (Blasco, 2005). The loss of a number of telomeric DNA base-pair from the ends of every chromosome occurs after every cell cycle. Progressive reduction in number of the telomeres results in their inability to protect the ends of chromosomal DNA, triggering cell senescence and eventually death. In other words, end-to-end chromosomal fusion occurs due to the chromosome being unprotected, which eventually leads to cell death (Counter *et al.*, 1992). Telomerase, an enzyme that adds telomeres to the ends

of chromosomes permits indefinite replication and is almost absent in nonimmortalized cells but expressed in high levels in immortalized/cancer cells (Hanahan and Weinberg, 2011). This means that cells are resistant to apoptosis and replicate continuously.

1.2.5 'Inducing Angiogenesis'

Angiogenesis, the growth of new blood vessels is carefully regulated. It begins with the birth of new endothelial cells and their assembly into tubes (vasculogenesis) (Risau and Flamme, 1995) and then the sprouting of new vessels from existing ones (angiogenesis) (Hanahan and Weinberg, 2000, Ramjiawan *et al.*, 2017). This happens to be switched on and off in processes such as wound healing and female reproductive cycling. However, in tumour progression, the switch remains turned on causing continuous sprouting of blood vessels that feed cancer cells (Hanahan and Folkman, 1996). An inducer of angiogenesis is the vascular endothelial growth factor-A (VEGF-A), which can be upregulated by hypoxia and signalling by oncogenes (Ferrara, 2009). Thrombospondin-1, fragments of plasmin and type 18 collagen function as inhibitors to angiogenesis (Ribatti, 2009) and has been shown to suppress tumour growth (Kazerounian *et al*., 2008).

1.2.6 'Activating Invasion and Metastasis'

Metastasis, the distant travel or spread of tumour cells, is the cause of about 90% of mortality from cancer (Sporn, 1996). The shape and ability of cells to attach to other cells is altered in cancer cells due the loss of E-cadherin, a cell-to-cell adhesion molecule. The loss of E-cadherin enables cancer cells to move

away from assembled epithelial cell sheets and move freely thereby losing its state of quiescence (Berx and van Roy, 2009, Canel *et al.*, 2013). N-cadherin, an adhesion molecule expressed in migrating neurons is upregulated in invasive cancer cells (Cavallaro and Christofori, 2004, Qian *et al.*, 2014).

1.2.7 'Cancer-related Inflammation'

As far back as the 17th century, the relationship between cancer and inflammation was hypothesised by Rudolf Virchow (Balkwill and Mantovani, 2001). This hypothesis has since then been reiterated by other scientists (Colotta *et al.*, 2009, Hanahan and Weinberg, 2011) and can easily be proven due to the development of better markers for histochemical staining that can accurately identify distinct cell types of the immune system (Pages *et al.*, 2010). Inflammation, a simple but powerful defence mechanism programmed to halt tissue damage and stimulate repair (Munn, 2017), leads to the progression of the other six hallmarks of cancer by activating growth factors, which sustain proliferative signalling, survival factors that resist cell death, factors that induce angiogenesis, stimulating genetic mutation (Grivennikov *et al.*, 2010, Hanahan and Weinberg, 2011) due to increased levels of nuclear factor-κB (NF-κB), reactive oxygen and nitrogen species (RONS), cytokines, prostaglandins and microRNAs (Schetter *et al.*, 2010).

Ten hallmarks of cancer with corresponding therapeutic targets were subsequently described in 2011 (Hanahan and Weinberg, 2011) (Figure 1.2).

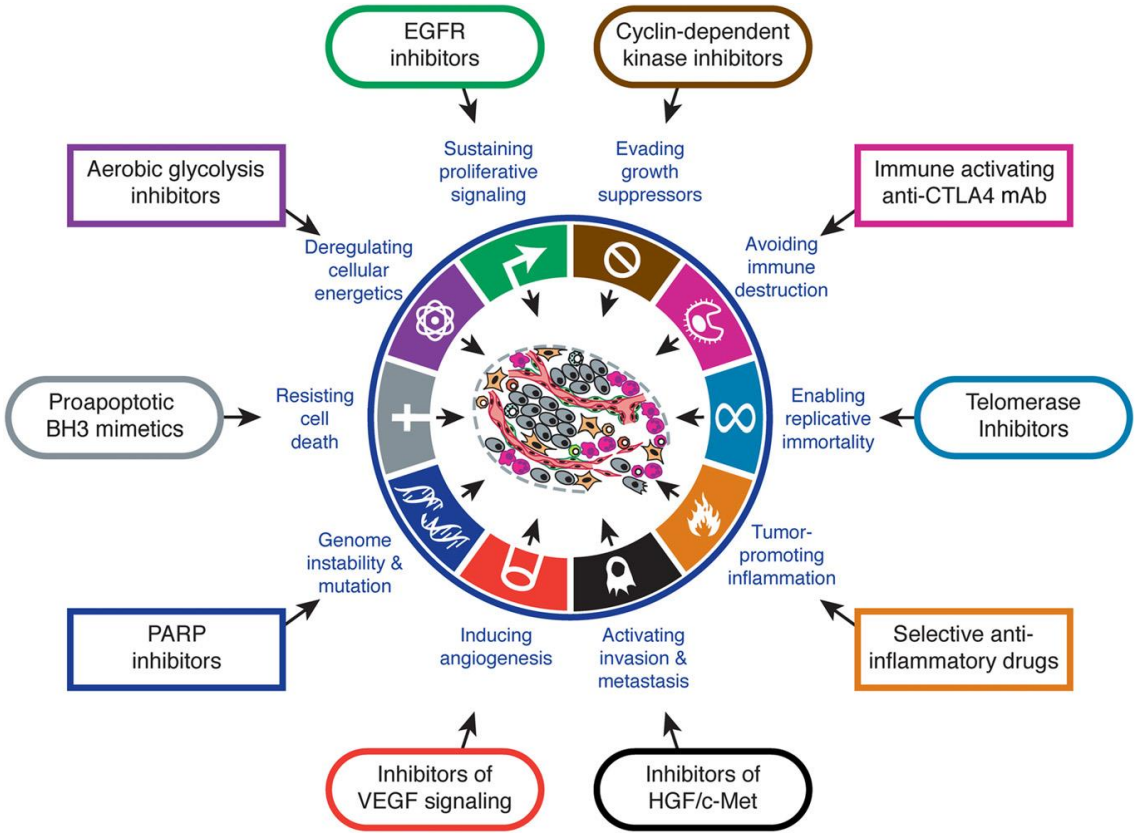

Figure 1.2 Therapeutic Targeting of the Hallmarks of Cancer.
These drugs are used in combination therapies for the treatment of cancers (Hanahan and Weinberg, 2011). EGFR inhibitors such as cetuximab act by inhibiting the cell growth regulatory pathway (Kohne and Lenz, 2009).

The additional hallmarks are:

1.2.8 'Genome Instability and Mutation'

Mutations found in certain genes of cancer cells lead to their dominance in population (Hanahan and Weinberg, 2011). For example, inactivation of tumour suppressor genes due to *TP53* mutations (Goh *et al.*, 2015, Lane, 1992), inactivation of MMR genes due to mutations (Negrini *et al.*, 2010), chromosome instability (CIN) and microsatellite instability (MIN) (Artandi and DePinho, 2010).

1.2.9 ‘Deregulating Cellular Energies’

In normal cells, under anaerobic conditions, glycolysis is the main process for energy metabolism with a small amount of pyruvate delivered to the mitochondria (Hanahan and Weinberg, 2011). However, cancer cells are able to redirect their energy metabolism even under aerobic conditions to glycolysis. This process known as ‘aerobic condition’ is accompanied by low adenosine triphosphate (ATP) production and often compensated for by an increase in uptake and utilization of glucose (DeBerardinis *et al.*, 2008), even though the preference for glycolysis is quite puzzling (Hanahan and Weinberg, 2011). Two different cell populations can be found in some cancer cells with different pathways for energy metabolism. One of the populations are glucose-dependent cells that produce lactate (Warburg-effect) while the other uses the lactate produced by neighbouring cells as their source of energy (Kennedy and Dewhirst, 2010). This indicates that normoxia or hypoxia is not a permanent condition for survival in cancer cells but this fluctuates depending on the condition the cells find themselves (Hardee *et al.*, 2009).

1.2.10 ‘Avoiding Immune Destruction’

Hanahan and Weinberg (2011) suggested this hallmark with some considerations that it was not a firmly established contributing factor. However, the emergence of immunotherapy in the treatment of cancer reiterates failure of the immune system to detect and destroy cancer cells as one of the hallmarks of cancer (Lynch and Murphy, 2016, Morse *et al.*, 2013, Xiang *et al.*, 2013). For example, there is better prognosis in colon and ovarian tumour patients with

high levels of killer lymphocytes as compared to those that lack such cells as part of their immune system (Pages *et al.*, 2010). It has also been found that cancer cells are able to secrete immunosuppressive factors that disable T lymphocytes/killer cells (Lynch and Murphy, 2016) and thus the emergence of checkpoint inhibitors such as ipilimumab, tremelimumab and pembrolizumab (Section 1.4.6.5) used in the treatment of some cancers (Gangadhar and Salama, 2015, Gong *et al.*, 2017, Wherry, 2011).

1.3 Colorectal cancer

Colorectal cancer (CRC), which includes cancer of the large bowel and rectum, is the third most common cancer in men with over 750,000 cases and the second in women (GLOBOCAN 2012) with about 600,000 cases worldwide (Garcia-Albeniz and Chan, 2011). While this is becoming a global phenomenon, over 50% of these cases are found in more developed regions of the world, the estimated incidence rates being higher in Australia/New Zealand and the lowest in West Africa. However, there is a poorer survival rate in the less developed regions of the world such as West Africa. In the UK, over 40,000 people were diagnosed with this disease in 2014 alone with almost 16,000 deaths that same year, which translates to roughly over forty deaths per day (CRUK). Unfortunately, incidence rates of CRC in the UK have increased by 6% over the last ten years. The median survival duration of patients with metastatic CRC is about six months if untreated (Van Cutsem and Geboes, 2007).

Over 90% of colorectal cancers are adenocarcinomas and about 1% of these are lymphomas (CRUK).

CRC arises as a consequence of the accumulation of variable and specific changes to the genome, which includes mutations to genes such as *KRAS* oncogene resulting in deregulation of the EGFR signalling pathway or the up-regulation of β-catenin resulting in deregulation of the Wnt signalling pathway. These genomic changes alter normal cell function (Figure 1.3).

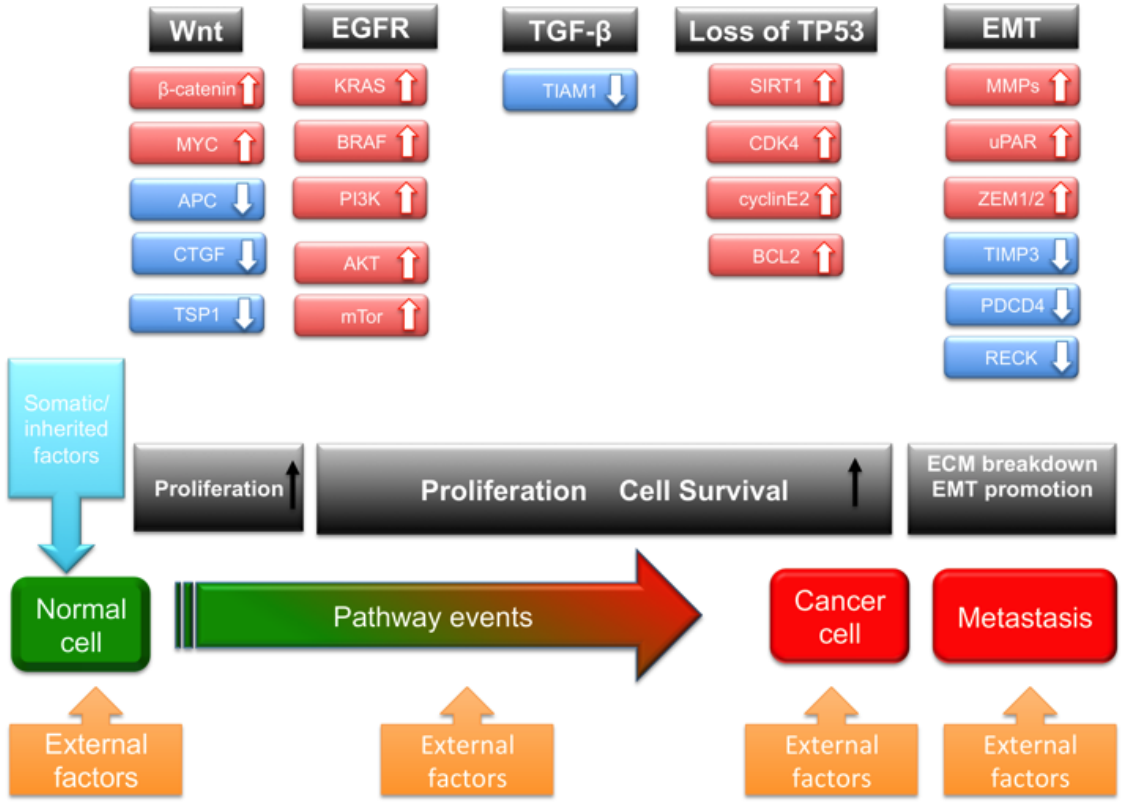

Figure 1.3 CRC tumourigenesis.
Progression of CRC to metastasis from normal cells is as a result of the accumulation of abnormalities in the signalling pathways. Most CRC harbour *APC* mutations (Rowan *et al.*, 2000), which usually occur in the early stages of carcinogenesis leading to the deregulation of the Wnt signalling pathway. Some tumours harbour *TP53* mutations that lead to loss of activity while others bear mutations of the *KRAS* oncogene, which leads to deregulation of the EGFR signalling pathway. ECM (extracellular matrix), EMT (epithelial-mesenchymal transition). [Adapted from (Bustin and Murphy, 2013)].

1.3.1 Types of Colorectal cancer (CRC)

Based on clinical and pathological data, CRC can be divided into three main types (Tomlinson *et al.*, 1998); namely:

1.3.1.1 Adenocarcinomas

An adenocarcinoma can be described as a lesion in the colon or rectum containing clear abnormality in tissue growth (epithelial neoplasia) (Quirke *et al*., 2011). Adenocarcinomas develop from the adenoma and are the most common type of CRC. They are found mostly in the left hand side of the large intestine.

1.3.1.2 Replication errors (RER) Colorectal cancer

Replication errors (RER) CRC has tumours with widespread RERs. They make up about 90% of CRC in patients with hereditary non-polyposis colorectal cancer (HNPCC) syndrome (Papadopoulos *et al.*, 1994, Peltomaki, 1995). They are mostly found on the right hand side of the bowel (Aaltonen *et al.*, 1993).

1.3.1.3 Ulcerative colitis-associated Colorectal cancer (UCACRC)

Ulcerative colitis-associated (UCA) CRC are found mostly on the left hand side of the bowel and usually develop from a distant dysplasia, which can be found in the rectum or sigmoid colon (Connell *et al.*, 1994). Mutations at APC and KRAS loci occur less frequently in UCACRC when compared with the other types of CRC (Tomlinson *et al.*, 1998).

1.3.2 Pathways involved in the development of CRC

Cancer is as a result of the accumulation of gene mutations that eventually lead to uncontrolled cell proliferation (Garraway and Lander, 2013). Sources of which include hereditary [(H) germline mutations], environmental factors [(E) such as exposure to UV, cigarette smoke] or due to Replicative mutations (R) (Tomasetti *et al.*, 2017). Approximately three mutations occur whenever a normal human stem cell divides (Tomasetti *et al.*, 2013) and the number of these normal cell divisions determines cancer risk in most mouse model organs (Zhu *et al.*, 2016).

Genetic instability drives cell mutations, which result in the development of different cancers (Loeb, 1991). Genetic alterations in tumours can be divided into four main categories; namely; (i) Subtle sequence changes comprising of a few base pair substitutions, deletions or insertion of nucleotides, (ii) Alterations in chromosome number, which involves losses or gains of whole chromosomes, (iii) Chromosome translocations that results in fusions between two different genes, and (iv) Gene amplifications that results in the formation of ‘amplicons’, which contain 0.5-10 mega bases of DNA (Lengauer *et al.*, 1998). Hereditary CRC syndromes are as a result of germline mutations while sporadic CRC is by alteration of DNA structure [mutation] or DNA function [epigenetics] (Obuch and Ahnen, 2016).

1.3.2.1 Chromosome Instability (CIN)

Chromosomal instability (CIN) is more common than microsatellite instability (MIN) and occurs in about 70% of human cancers (Obuch and Ahnen, 2016).

This involves gains and losses of whole chromosomes known as chromosome missegregation and has an important role in tumourigenesis (Lengauer *et al.*, 1998). CIN is driven by activation of mutations in oncogenes such as *KRAS* and tumour suppressor genes such as *APC* or *P53* (Obuch and Ahnen, 2016), which results in aneuploidy, the presence of an abnormal number of chromosomes in a cell and a cause for tumorigenesis (Boveri, 2008, Thompson and Compton, 2008) (Figure 1.3). Individuals with medical conditions characterised by aneuploidy such as Down syndrome and Turner syndrome have been found to show high incidence of cancer (Sullivan *et al.*, 2007). However, in CIN, aneuploidy found in the tumour cell population is heterogeneous and has the capability of selective evolution resulting in metastasis (Bakhoum and Compton, 2012).

Studies have shown that CIN is responsible for tumorigenesis (Schvartzman *et al.*, 2010). For instance, chromosome misseggregation was induced in mice by perturbing microtubule attachments to chromosomes. This led to the formation of lymphomas and lung tumours (Weaver *et al.*, 2007). However, disruption or inactivation of the *P53/P21* pathway was required for aneuploidy karyotypes to survive because chromosome misseggregation in cells with a functional *P53/P21* system will lead to cell cycle arrest. CRC cell lines SW480, HRT-18, HT-29, DLD-1 have been found to possess mutation status at *P53* gene (Din *et al.*, 2004), which suggests that chromosomal misseggregation in CRC is mainly via the CIN pathway.

1.3.2.2 Microsatellite Instability (MIN)

Microsatellite instability (MIN) pathway results in about 5% of CRCs with the chromosome number not affected (diploid). It is caused by germline mutations in one of the DNA MMR genes, which are responsible for recognising and repairing errors that occur during DNA replication and also repair of DNA damage (Iyer *et al.*, 2006). Mutations in MMR genes eventually leads to Lynch syndrome CRCs (Obuch and Ahnen, 2016). Mutations found in regulatory regions of the MMR genes *MSH2, MSH6, MLH1* and *PMS2*, which leads to MIN are one of the hallmarks (1.2.8) for the development of CRC in humans (Fishel and Kolodner, 1995, Herman *et al.*, 1998, Kane *et al.*, 1997, Modrich and Lahue, 1996). About 90% of mutations in Lynch Syndrome are caused by *MLH1* and *MSH2* mutations, with 7-10% by *MSH6* mutations, less than 5% by *PMS2* (Tutlewska *et al.*, 2013) and about 3% by *EPCAM* gene mutation (Kuiper *et al.*, 2011). The *EPCAM* gene is responsible for intercellular adhesion and intracellular signalling, migration and proliferation with its deletion leading to *MSH2* silencing (Tutlewska *et al.*, 2013). MIN occurs in most patients with HNPCC (Aaltonen *et al.*, 1993) and is as a result of defects in the MMR genes, *mutS* homologue (hMSH2) and *mutL* homologue (hMLH1) (Strand *et al.*, 1993) (Figure 1.4). There are six *mutL* and *mutS* homologues all of which when deactivated as a result of mutation will lead to the development of cancer through the MIN pathway (Peltomaki and de la Chapelle, 1997).

1.3.2.3 CpG island Methylator Phenotype (CIMP)

CpG island methylator phenotype (CIMP) is also known as the serrated pathway, which results in CRCs that are DNA MMR deficient (MSI) or DNA MMR proficient (MSS), and make up about 25% of CRCs. The CIMP phenotype can be grouped into CIMP-high and CIMP-low with the BRAF oncogene mutation often found in CIMP-high CRC characterised by increased cell proliferation, progression of carcinogenesis (Ogino *et al.*, 2009). Unlike CIN and MIN pathways, CIMP does not involve the activation of *KRAS* mutations (Janne and Mayer, 2000). However, in some contexts, *KRAS* mutations are found in CIMP CRCs and referred to as CIMP-low (Colussi *et al.*, 2013).

CRCs that are formed via MIN and CIMP pathways may be more difficult to diagnose than those that are formed via CIN pathway because they are commonly found in the proximal region of the colon are not detected easily by endoscopy and may develop quickly into cancer (Patel and Ahnen, 2014).

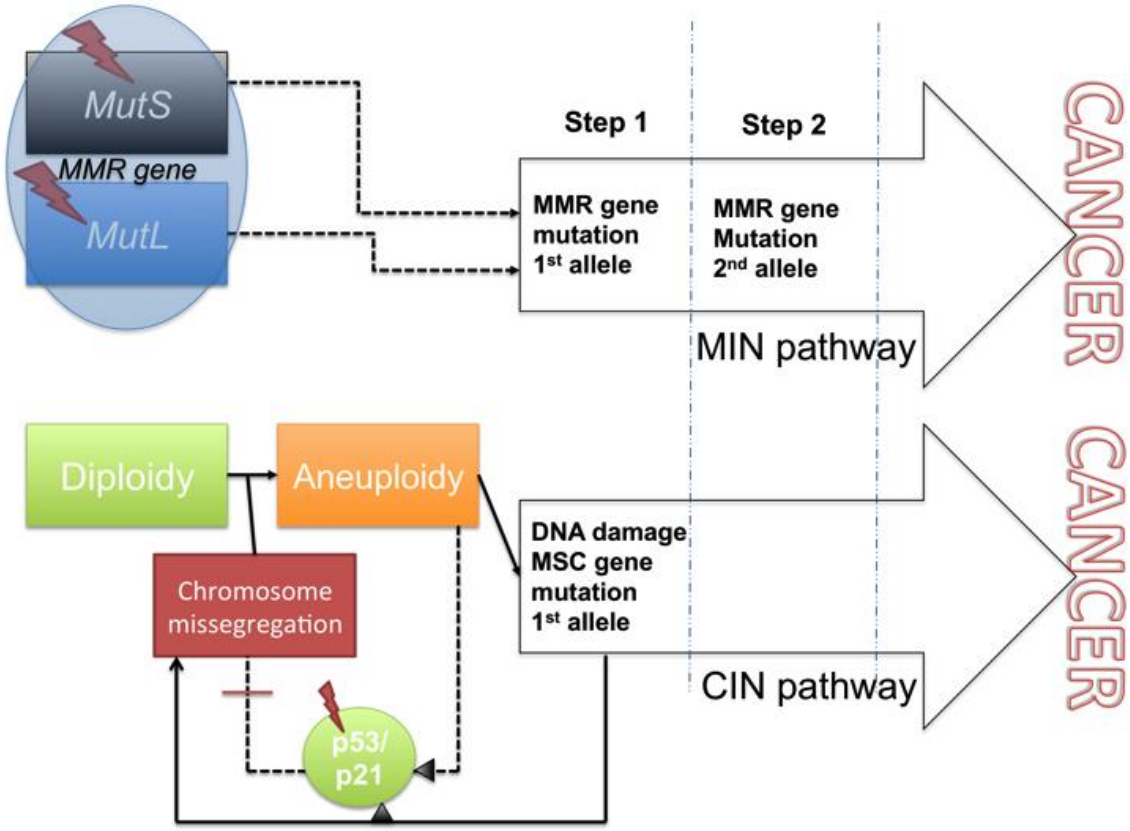

Figure 1.4 Different steps in the pathways to genetic instability and relationship between ploidy and CIN in terms of tumour initiation and growth.
Different number of mutational 'hits' are required by each pathway to result in instability of either the microenvironment or the chromosome. In a heterozygote with one defective MMR allele, the MIN pathway commences only when there is inactivation of the normal allele inherited from the unaffected parent (step 2). For the CIN pathway, however, only one mutational 'hit' is required to produce the CIN phenotype. An example of a gene that follows the CIN pathway is *hBUB1*, a component of the mitotic spindle checkpoint (MSC), which is responsible for controlling mitotic checkpoints and chromosome segregation. Loss-of-function mutations of the *BUB1* gene results in aneuploidy (Cahill *et al.*, 1998). Aneuploidy leads to additional chromosome missegregation and DNA damage. p53/p21 tumour suppressor pathway is triggered as a result of aneuploidy to limit further proliferation of aneuploidy cells. However, if the *p53/p21* gene is mutated, this function becomes null and void [Adapted from (Bakhoum and Compton, 2012, Lengauer *et al.*, 1998)].

1.4 Treatment of CRC

Prognosis for patients with metastatic CRC (mCRC) is still poor (Lynch and Murphy, 2016). In CRC, when detected early (while still localized), surgical removal may be curative. However, the early detection happens in only 39% of cases (Kohne and Lenz, 2009) and chemotherapy is often the only option.

Up until 1996, 5-fluorouracil (5-FU)-based therapy was the only one used in mCRC. Irinotecan, a topoisomerase inhibitor, was then approved that year and the platinum compound, oxaliplatin in 2004. A combination of 5-FU with irinotecan is termed FOLFIRI while the combinations of 5-FU and leucovorin plus oxaliplatin is termed FOLFOX (Kohne and Lenz, 2009). To further improve chemotherapy regimens, monoclonal antibodies; bevacizumab, cetuximab and panitumumab were then introduced as combinations with FOLFIRI and FOLFOX (Goldberg *et al.*, 2007, Kohne and Lenz, 2009) (Figure 1.5).

The new trend in CRC therapy however is the emergence of immunotherapy, which is as a result of decades of research and the understanding of the relationship between the immune system and cancer. This has led to the development of therapies approved by the FDA such as a cancer vaccine in 2010 known as sipuleucel-T and immunomodulatory antibodies, iplimumab in 2011, nivolumab and pembrolizumab (Callahan *et al.*, 2013, DeFrancesco, 2010, Lynch and Murphy, 2016). Whole-cancer-cell immunotherapies also have a promising future in the treatment of CRC with OncoVAX® in its confirmatory Phase IIIb clinical trials (Melero *et al.*, 2014). Various success stories about the

use of immunotherapy in the treatment of cancer have been published. Such treatments include T-cell transfer therapy involving tumour-infiltrating lymphocytes (TIL) consisting of CD8+ T-cells obtained from a patient with mCRC which was able to recognise cancer cells harbouring mutant *KRAS* G12D gene (Tran *et al.*, 2016). Many human cancers harbour mutations in the *KRAS* oncogene with reports of *KRAS* G12D expressed in about 13% of CRCs (Vaughn *et al.*, 2011). A patient receiving TILs consisting of about 75% CD8+ T-cells reactive to KRAS G12D, showed regression of all seven metastatic lung lesions in the patient after 40 days of therapy with only one of the lesions progressing after 9 months (Tran *et al.*, 2016).

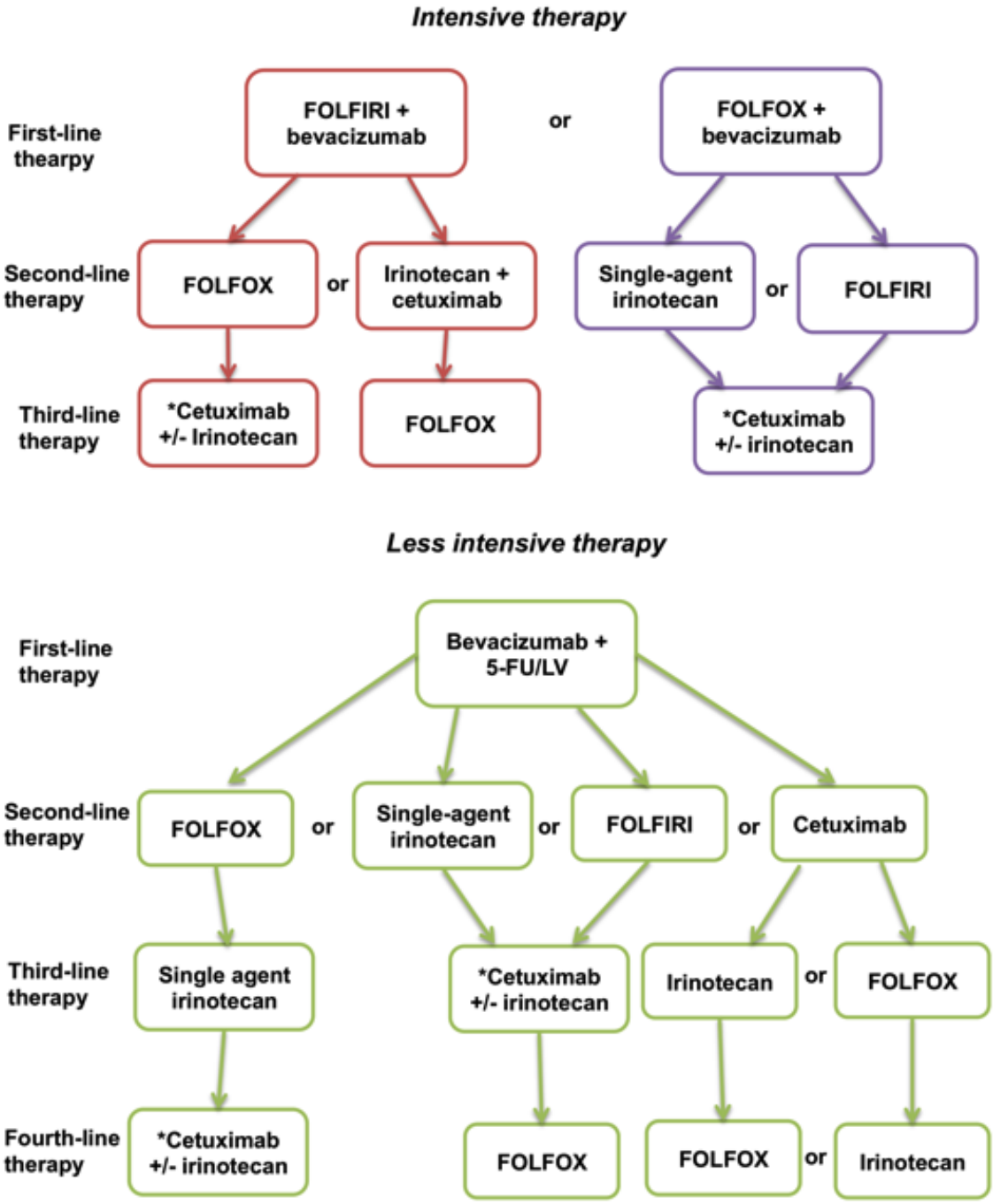

Figure 1.5 Intensive and less intensive treatment lines for metastatic CRC. *Cetuximab maybe be administered alone for patients intolerant to irinotecan (Goldberg *et al.*, 2007).

1.4.1 Cetuximab

Cetuximab is marketed as Erbitux® and is an inhibitor of the EGFR. It targets the EGF-mediated cell growth regulatory pathway (Kohne and Lenz, 2009). Cetuximab is administered in combination with irinotecan or alone for patients intolerant to irinotecan (Goldberg *et al.*, 2007) (Figure 1.5).

1.4.2 Panitumumab

Panitumumab is marketed as Vectibix® and also an EGFR inhibitor that targets the EGF pathway (Kohne and Lenz, 2009).

1.4.3 Bevacizumab

Bevacizumab, marketed as Avastin® targets the VEGF-mediated angiogenesis pathway by interfering with VEGF-A binding to the receptor, thus blocking VEGF-mediated intracellular signalling for angiogenesis and tumour growth (Hicklin and Ellis, 2005). This is used in combination with FOLFIRI or FOLFOX (Figure 1.5).

1.4.4 5-Fluorouracil (5-FU)

5-Fluorouracil (5-FU) is converted to fluorodeoxyuridine monophosphate by thymidine phophorylase enzyme. In the presence of reduced folate, fluorodeoxyuridine reacts with thymidylate synthase to form a complex that interferes with DNA synthesis and subsequently causing apoptosis in the tumour cells. Leucovorin (folinic acid) is often added to 5-FU because of its

ability to enhance binding between fluorodeoxyuridine monophosphate and thymidylate synthase (1992, Kohne and Lenz, 2009).

1.4.5 Oxaliplatin

Oxaliplatin is a third-generation diaminocyclohexane platinum compound, which is effective in cisplatin-resistant tumours (Ramanathan *et al.*, 2003). Similar to other platinum derivatives (Table 1.1), oxaliplatin mediates its action via formation of platinum-DNA adducts with N(7) guanines of DNA to form monoadducts (Levi *et al.*, 2000) and subsequently diadducts, which are capable of blocking DNA replication (Knox *et al.*, 1986). This results in oxaliplatin inducing primary and secondary DNA lesions leading to cell-cycle arrest, autophagy and apoptosis in human cancer cells (Liu *et al.*, 2015, Raymond *et al.*, 1998). Oxaliplatin in combination with 5-FU and Leucovorin (Figure 1.5) resulted in an improvement in disease-free survival of patients from CRC and a 23% relative reduction in the risk of recurrence (Andre *et al.*, 2004).

Peripheral neuropathy is the main safety concern associated with oxaliplatin. Frequent, transient, distal paresthesias are induced by oxaliplatin shortly after administration (Andre *et al.*, 2004). Lean body mass (LBM) have been found to be a significant predictor in toxicity and neuropathy in patients undergoing FOLFOX therapy such that patients with low LBM are susceptible to oxaliplatin toxicity, which has led to a cut off dose point of 3.09 mg oxaliplatin/kg LBM. It is therefore essential to use conventional body surface area dosing in order to reduce such serious side effects (Ali *et al.*, 2016).

Drug and Structure	Mechanism of action	Major Side Effects	Mechanisms of Resistance
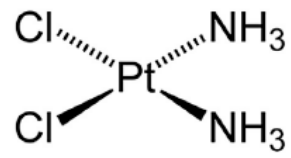 cisplatin	DNA crosslinker	nephrotoxicity; neurotoxicity; ototoxicity	decreased uptake; increased efflux; increased DNA repair capacity; enhanced replication bypass; failure of death pathways
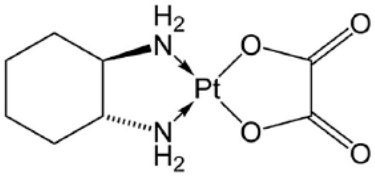 oxaliplatin	DNA crosslinker	hepatotoxicity; neurotoxicity; pulmonary toxicity	
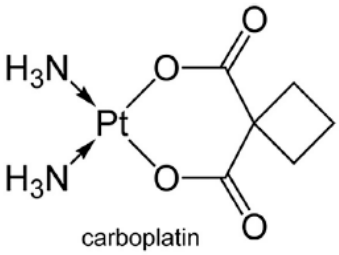 carboplatin	DNA crosslinker	myelosuppression	

Table 1.1 Structure and Properties of Platinum-based antineoplastics.
[Adapted from (Cheung-Ong *et al.*, 2013, Weiss and Christian, 1993)].

1.4.6 Immunotherapy

Immunotherapy has the ability to cause the immune system to attack and destroy cancer cells by recognising specific antigens that are found on tumour cells.

Carcinoembryonic antigen (CEA) is the most widely studied tumour associated antigen (TAA) in CRC and has been on-going since the 1960s (Gold and Freedman, 1965). CEA is a plasma membrane-associated glycoprotein expressed by adult tissues and overexpressed by adenocarcinomas of the colon, breast lungs, which can be found in the serum (Hammarstrom, 1999).

Another TAA targeted in immunotherapy is MUC1 (mucin), a transmembrane glycoprotein, found on the surface of secretory epithelial cells which protects the body from bacterial invasion by binding to pathogens (Hollingsworth and Swanson, 2004). The overexpression of MUC1 in CRC regulates β-catenin and Ras tumour promoting signalling pathways leading to poor prognosis (Singh and Hollingsworth, 2006). An adenoviral gene delivery platform encoding CEA antigen, *Ad5* has been shown to cause cell mediated immunity in over 60% of patients with advanced stage CRC (Morse *et al.*, 2013).

1.4.6.1 Cancer vaccines

Cancer vaccines stimulate the immune system in to recognising tumour-specific antigens harboured by cancer cells as foreign bodies. This facilitates the attack of cancer cells by the immune system (Lynch and Murphy, 2016). Cancer vaccines can be categorised into autologous tumour cell vaccines, dendritic cell vaccines, DNA vaccines and viral vector-based vaccines (Xiang *et al.*, 2013).

1.4.6.2 Cytokine therapy

Studies on the use of cytokine therapy in CRC is quite limited (Lynch and Murphy, 2016). PEGylated recombinant IL-10 (AM0010) in a phase I study resulted in a sustained systemic Th 1 immune stimulation with a CRC patient having the cancer under control for over 40 weeks (Lynch and Murphy, 2016).

1.4.6.3 Toll-like receptors (TLR) agonists

Toll-like receptors (TLR) agonists act by targeting the innate immune system (Wittig *et al.*, 2015) with TLR-9 out of the ten human TLRs (TLR-1 to TLR-10)

exhibiting protective role against malignant transformation in colorectal mucosa (Eiro *et al.*, 2012). Examples of TLR agonists in early clinical trials include CpG-oligodeoxynucleotides (CpG-ODN) and MGN1703, a synthetic DNA-based immunomodulator with a dumbbell-like structure, which are being designed as maintenance therapy in mCRC patients after standard first-line therapy (Lynch and Murphy, 2016).

1.4.6.4 Adoptive cell transfer (ACT)

Adoptive cell transfer (ACT) involves the harvesting of autologous T-cells from TILs, activating and expanding them in number *ex vivo* after which they are then re-introduced into the patient host. This method of introducing large numbers of T-cells has been beneficial in tumour regression (Rosenberg *et al.*, 2011). This method of therapy is particularly attractive because it targets driver mutations, which are tumour-specific and may likely be harboured by all the tumour cells (McGranahan *et al.*, 2015). However, limitations in this therapy include lack of immune memory, protracted time and cost of T-cells production and risk of severe side effects (Xiang *et al.*, 2013).

1.4.6.5 Checkpoint inhibition

Checkpoint inhibitors are monoclonal antibodies that deregulate the Major Histocompatibility Complexes T-cell Receptor signalling pathways by targeting co-inhibitory molecules that are responsible for the suppression of the immune system via stimulating T-cell dysfunction or apoptosis (Schreiber *et al.*, 2011). These co-inhibitory molecules include CTLA-4, PD-1, PD-L1/2, lymphocyte-

activation gene-3, T-cell immunoglobulin, T-cell immunoglobulin mucin-3 (Lynch and Murphy, 2016).

1.4.6.5.1 CTLA-4 (Cytotoxic T-lymphocyte associated protein-4) inhibitors:

CTLA-4 is a receptor found on the surface of CD4 and CD8 T cell membranes responsible for inhibiting the activation of the immune system. Examples of CTLA-4 inhibitors include ipilimumab and tremelimumab used for melanoma (Lynch and Murphy, 2016). These inhibitors however have not been successful in CRC therapy (Chung *et al.*, 2010).

1.4.6.5.2 PD-1 (Programmed death-1) inhibitors:

PD-1 receptor induces exhaustion in effector T-cells (Wherry, 2011). PD-1 inhibitors such as pembrolizumab block the interaction between PD-1 receptor and its ligands, PD-L1 and PD-L2 in order to enable T-cell activation and subsequent antitumor immune response (Gangadhar and Salama, 2015). About 50% of CRCs express PD-L1 (Dong *et al.*, 2002). Pembrolizumab has been shown to be effective in patients with MSI (DNA MMR deficient) and also in a patient with MSS (DNA MMR proficient) CRC (Gong *et al.*, 2017, Kieler *et al.*, 2016).

1.4.7 Aspirin

Aspirin, a non-steroidal anti-inflammatory drug (NSAID) is an old drug commonly used for pain, inflammatory conditions and fever therapy (Langley *et al.*, 2011). Its active metabolite is known to be salicylic acid, which was used over two centuries ago by a Greek physician as extracts of the willow bark to

treat fever (Gensini and Conti, 2009). The elimination of salicylates depends on two major pathways: formation of salicyluric acid and salicyl phenolic glucoronide. As these pathways are readily saturated, salicylates behave differently from most other drugs in that they show pseudo-zero order kinetics, meaning their half-life in the serum is directly proportional to its concentration (Paulus *et al.*, 1971).

1.4.7.1 Pharmacology of Aspirin

Several modes of action for aspirin as an antiproliferative and chemopreventative agent have been suggested. They include:

i. The accepted pathway by which aspirin acts as an anti-inflammatory agent: irreversible cyclooxygenase inactivation through non-enzymatic acetylation of a single serine residue, which ultimately leads to the inhibition of prostaglandin biosynthesis (Patrignani *et al.*, 2017, Patrono *et al.*, 2008, Schror, 2011, Warner *et al.*, 1999).
ii. The inhibition of NF-κB activity (Gurpinar *et al.*, 2013, Kopp and Ghosh, 1994).
iii. Inhibition of the JNK pathway (Schwenger *et al.*, 1997).
iv. Activation of AMP kinase (AMPK) (Hawley *et al.*, 2012).
v. Aspirin has been found to cause apoptosis through the Wnt-β-catenin pathway (Deng *et al.*, 2009), which provides a link between the Wnt-β-catenin pathway and apoptosis.
vi. Normalising EGFR expression (Li *et al.*, 2015).

vii. Increase in the expression of hMLH1, hPMS2, hMSH2 and hMLH1, which are DNA MMR proteins (Goel *et al.*, 2003).

viii. Inhibition of VEGF, which leads to the suppression of angiogenesis (Borthwick *et al.*, 2006, Ouyang *et al.*, 2008).

The general pharmacology of aspirin and other NSAIDs is known to be the inhibition of COX-1 and COX-2 (cyclooxygenase) (Figure 1.6) to prevent the generation of prostanoids from arachidonic acid. These prostanoids, which are biologically active lipid mediators, play significant roles in many physiologic pathways and include prostaglandin PGD_2, PGE_2, $PGF_{2\alpha}$, prostacyclin and thromboxane $(TX)A_2$ (Bruno *et al.*, 2012). Prostanoids have an effect in various health conditions such as inflammation, pain, asthma, platelet function, renal function, cardiovascular homeostasis and cancer (Smyth *et al.*, 2009).

It has been shown that repeated doses of aspirin at a low dose (75-100 mg/day) causes maximal inhibition of platelet COX-1 activity after several days without greatly affecting cells elsewhere in the body. This effect lasts to about 24 hours (Bruno *et al.*, 2012). Aspirin is primarily absorbed in the stomach when taken orally and goes through the GI tract and hepatic first-pass metabolism (Hatori *et al.*, 1984). Aspirin undergoes hydrolysis by non-specific esterases and inhibits COX by acetylation before it is absorbed into the system and thus the reason for reduced systemic levels of aspirin and high levels of salicylic acid which is not as potent (Bruno *et al.*, 2012).

1.4.7.2 Chemoprevention with Aspirin

Chemopreventitive and chemotherapeutic effects of aspirin in cancer have been widely studied (Elwood et al., 2009) and it has been found to reduce the risk of CRC.

Despite a population-based cohort study that concluded non-aspirin NSAIDs to have a greater effect than aspirin in reducing the risk of CRC (Garcia Rodriguez *et al.*, 2001), over the years a number of randomised controlled studies have been carried out which have suggested a protected effect or reduced risk against colorectal adenoma/cancer with the regular use of aspirin (Benamouzig *et al.*, 2012, Bosetti *et al.*, 2012, Burn *et al.*, 2011a, Burn *et al.*, 2011b, Chan *et al.*, 2012, Johnson *et al.*, 2010, Sandler *et al.*, 2003), which also led to the recommendation of low dose aspirin for the prevention of CRC by the United States preventative services task force (Chan and Ladabaum, 2016).

An analysis of individual patient data from three large UK trials based on daily aspirin versus non-aspirin with approximately four years duration of treatment was the first proof in man that indeed aspirin reduced mortality from several cancers (Rothwell *et al.*, 2011). Aspirin has a dose-dependent effect on CRC risk with probably the highest risk reduction in patients taking a lower dose with a reduction of CRC after five years of continuous use (Din *et al.*, 2010).

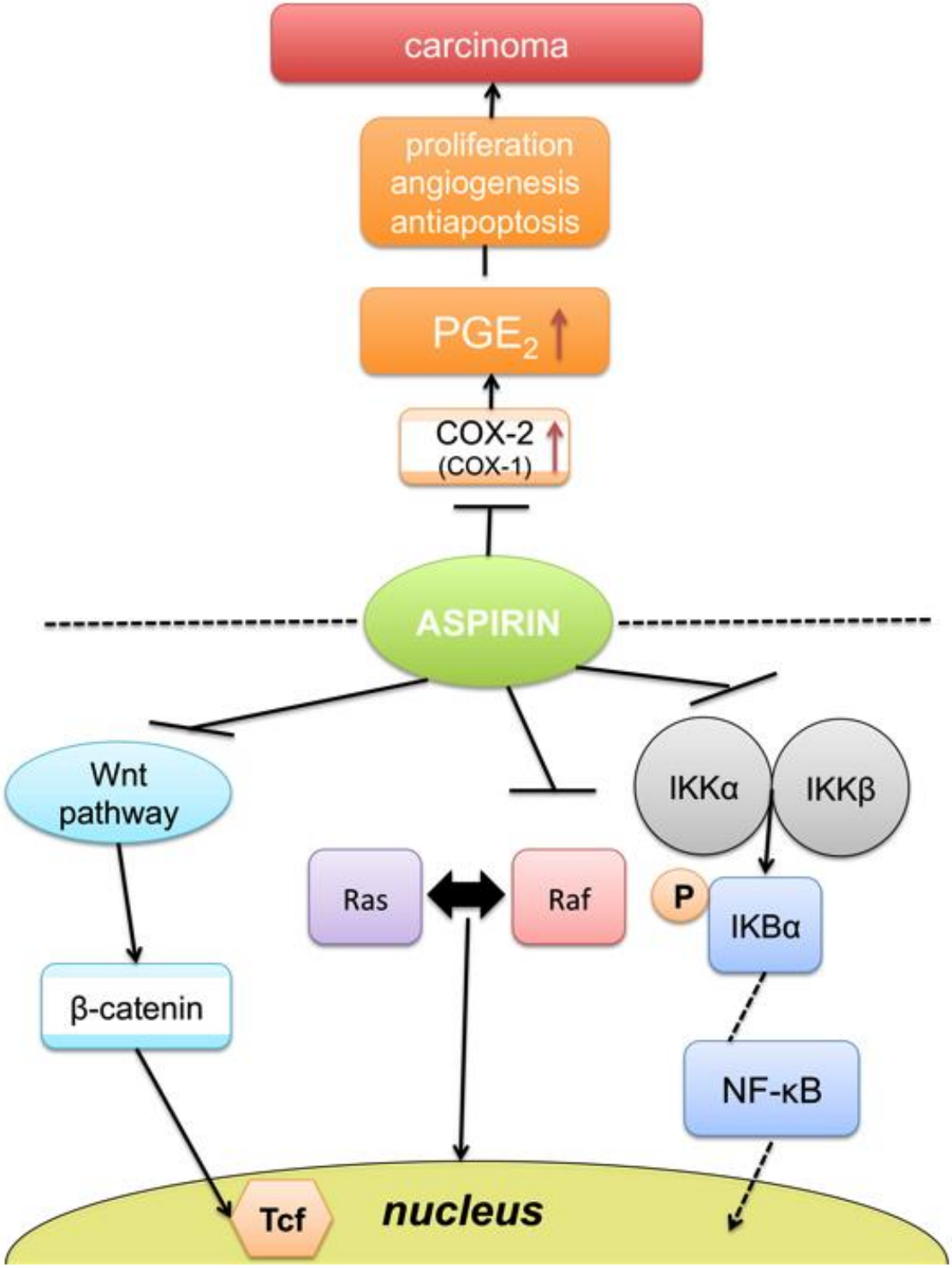

Figure 1.6 COX-dependent and COX-independent mechanisms of antitumoural effects of aspirin. Mechanisms of action include: (i) inhibition of the Wnt/β-catenin pathway, which targets gene expression involved in tumorigenesis when β-catenin interacts with T-cell factor (Tcf) in the nucleus; (ii) inhibition of the binding of c-Raf to Ras resulting in the inhibition of extracellular signal-regulated protein kinase (ERK) pathway, which is involved in various downstream signals that cause proliferation, cell differentiation and cell survival; (iii) inhibition of I-kappa kinase (IκK), thereby preventing the activation by NF-κB and its ability to regulate gene expressions that cause antiapoptosis in cancer cells; (iv) inhibition of COX-2 derived PGE_2 formation and recovery of apoptosis [Adapted from (Bruno *et al.*, 2012, Schror, 2011)].

1.4.7.3 Risks associated with aspirin therapy

There is increasing evidence of the benefits of aspirin in the prevention of CRC and it is a standard treatment used in the prevention of cardiovascular events. However, it still presents with some health risks such as gastrointestinal (GI) toxicity, in particular GI bleeding and peptic ulcer, which have been found to be mostly age-dependent (Li *et al.*, 2017, Patrono *et al.*, 2005) and rarely fatal (Roderick *et al.*, 1993).

Data from randomised, controlled, trials have shown there to be about a two-fold increase in the risk of GI complications (Roderick *et al.*, 1993) regardless of the aspirin being in enteric-coated or buffered formulation (Garcia Rodriguez *et al.*, 2001). However, administration of proton-pump inhibitors in combination with aspirin greatly reduced GI effects (Garcia Rodriguez *et al.*, 2016).

There are contradicting facts in regards to the effect of dose and duration of aspirin usage on risk of GI bleeding (Huang *et al.*, 2010). Some data suggest that the GI mucosa adapts to the side effect of aspirin when used for a long duration of time and an increased risk of GI bleeding when used for a shorter duration (Griffin *et al.*, 1991, Langman *et al.*, 1994). But other studies show that this increased risk in GI bleeding is cumulative overtime (Nelson *et al.*, 1994). However, these contradictions may be due to heterogeneous conditions of the individual studies (Huang *et al.*, 2010).

The symptoms of GI complications are made worse in the presence of *H. pylori* infection even though it does not initiate or predispose to NSAID gastropathy (Goggin *et al.*, 1993). It is thus recommended for patients to undergo *H. pylori*

screening before commencing on aspirin therapy to reduce the possibility of GI side effects.

1.5 Aims and Objectives

In this study it is intended to synthesize novel aspirin analogues, identify and study their chemical and pharmacological properties/effects as anti-cancer agent in SW480 CRC cell line. The research questions include:

i. Are these aspirin analogues stable at room temperature when in solution?
ii. Do these compounds breakdown into salicylates?
iii. What is the best organic solvent to dissolve these compounds with the least effect on cell viability?
iv. How cytotoxic are these compounds against SW480 CRC cells, OE33 and FLO1 oesophageal cell lines *in vitro*?
v. Do these compounds cause cell death through apoptosis, necrosis or a mixture of both?
vi. Do these aspirin analogues affect the pharmacology of the EGFR and its signalling pathway? If so, what is the possible mechanism of action?
vii. Do these compounds synergise with platinum compounds in SW480 CRC and OE33 oesophageal cell lines *in vitro*?
viii. Are these aspirin analogues toxic *in silico*?

These investigations will be carried out using different laboratory tools and techniques, which include; Cell tissue culture, MTT assays, TLC (thin layer chromatography), IR (infra-red) and NMR (nuclear magnetic resonance)

spectroscopy, salicylate assay developed using fluorescent quantification of salicylic acid, flow cytometry, western blots using SDS-PAGE gels and immunocytochemistry using confocal microscopy. The CompuSyn®/CalcuSyn® software will also be adopted for the synergy experiments and DEREK software for possible toxicities of these compounds based on pre-existing stored data.

The main aim of this chapter is to find out whether these aspirins can be used as a more affordable adjunct or in combination with other anti-cancer agents in the prevention, maintenance and possible cure for colorectal and oesophageal cancer.

Chapter 2. Materials & Methods

2.1 Materials

2.1.1 Lab instruments

Equipment used is listed in Table 2.1

Instrument	Company
Amersham Biosciences Storm 860 3-Scan Mode Phospho Lab imager	Amersham Biosciences Ltd. Amersham place, Little Chalfont Buckinghamshire HP7 9NA, UK
AmScope Pre-cleaned Microscope slides	AmScope
BD Accuri™ C6 flow cytometer	Becton Dickinson (BD) The Danby Building Edmund Halley Road Oxford Science Park, Oxford OX4 4DQ, UK
Beckman Z1 Coulter® Single threshold particle counter	Beckman Coulter (UK) Ltd. Oakley Court Kingsmead Business Park London Road, High Wycombe HP11 1JU, UK
Bio-Rad Power Pac 200/2.0 Electrophoresis Power Supply	164-5050, Bio-Rad laboratories Ltd. Bio-Rad House, Maxted Road Hemel Hempsted, Hertfordshire HP2 7DX, UK
CLARIOstar® monochromator microplate reader	BMG LABTECH 5 Alton House Office Park Gatehouse Way Aylesbury HP19 8XU, UK
Glass base dish (Glass)	IWAKI brand Asahi Glass Co., Ltd. Japan
Microplate Reader Thermo Multiskan Ascent 96 & 384	MTX Lab Systems, LLC 1114 Palma Sola Blvd. Bradenton FL 34209, USA
Mono-Mixer	Desaga, Sarstedt-Gruppe Sarstedt AG & Co. Sarstedtstraße 1 51588 Nümbrecht Germany

Instrument	Company
Non-vented tissue culture flasks	Sarstedt Ltd. 68 Boston Road Leicester LE4 1AW, UK
Olympus Microscope CK2-TR	Olympus KeyMed House Stock Road, Southend-on-Sea SS2 5QH, UK
Panasonic Direct Heat CO_2 incubator	Panasonic Healthcare Co. Ltd. 1-1-1 Sakata, Oizumi-Machi Ora-Gun, Gunma 370-0596 Japan
Square cover glass (22X22mm)	AmScope
Storm System Optical Scanner	Amersham Biosciences UK Limited Amersham Place Little Chalfont Buckinghamshire HP7 9NA, UK
Stuart® SMP 10 Melting Point Apparatus	Bibby Scientific Ltd. Beacon Road Stone, Staffordshire ST15 0SA, UK
Vented tissue culture flasks	Sarstedt Ltd. 68 Boston Road Leicester LE4 1AW, UK
VWR Digital Heat Block	VWR Hunter Boulevard, Magna Park Lutterworth, Leicestershire LE17 4XN, UK
Zeiss LSM 880 Confocal Microscope	Carl Zeiss Ltd. 509 Coldhams Lane, Cambridge Cambridgeshire CB1 3JS, UK

Table 2.1 List of instruments and equipment used in this study.

2.1.2 Media and Reagents/Chemicals

All media and reagents/chemicals used were standard grade or higher and purchased from Sigma-Aldrich unless otherwise stated. Details are provided in Table 2.2.

Name	Product code	Company
40% Acrylamide Solution (Acrylamide: Bis-Acrylamide, 29:1), Electrophoresis Grade	BP1408-1	Fisher Scientific Bishop Meadow Road Loughborough LE11 5RG, UK
Acetaminophen	1706	TOCRIS Bioscience The Watkins Building Atlantic Road Avonmouth, Bristol BS11 9QD, UK
Acetic acid, 99.5% pure	124040025	ACROS ORGANICS Fisher Scientific Ltd. Bishop Meadow Road Loughborough LE11 5RG, UK
Acetone	40308	Sigma® Sigma-Aldrich Company Ltd., The Old Brickyard, New Road Gillingham Dorset SP8 4XT, UK
Acetylsalicylic acid (Aspirin)	A5376	Sigma® Sigma-Aldrich Company Ltd.
Annexin-V-FLUOS Staining kit	11 858 777 001 1 988 549	Roche Diagnostics Ltd. Applied Science Charles Avenue Burgess Hill West Sussex RH15 9RY, UK
Ammonium Persulphate (APS)	A-3678	Sigma® Sigma-Aldrich Company Ltd.
Bovine Serum Albumin (BSA)	BP9702-100	Fisher Scientific
Bromophenol blue	B-5525	Sigma® Sigma-Aldrich Co.

Name	Product code	Company
Carboplatin	S1215	Stratech Scientific Ltd. Unit 7, Business Centre, Oaks Drive Newmarket CB8 7SY, UK
CellTiter 96® Aqueous One Solution Cell Proliferation Assay kit	G3580	Promega Corporation Delta House Southhampton Sience Park, Southhampton SO16 7NS, UK
Cisplatin	S1166	Stratech Scientific Ltd.
Diclofenac sodium salt	4454	TOCRIS Bioscience The Watkins Building Atlantic Road Avonmouth, Bristol BS11 9QD, UK
Diflunisal	D3281	Sigma-Aldrich® Sigma-Aldrich Inc.
Dimethyl sulfoxide (DMSO)	D5879	Honeywell Sigma-Aldrich Company Ltd
Dulbecco's Modified Eagle Medium (DMEM)	11965-092	gibco® life technologies™ ThermoFisher Scientific
Epidermal Growth Factor, Biotinylated, complexed to Alexa Fluor® 555 Streptavidin (Alexa Fluor® 555 EGF complex)	E35350	Molecular Probes Eugene, Oregon, USA
Ethyl acetate, 99.8% pure	270989	Sigma-Aldrich® Sigma-Aldrich Inc.
Foetal Bovine Serum (FBS)	FB-1001/500	Labtech International Ltd. 2 Birch House Brambleside Bellbrook Ind. Est. Uckfield, East Sussex TN22 1QQ, UK
Glycerol	G5516	Sigma-Aldrich® Sigma-Aldrich Inc.
Glycine powder	J64365	Alfa Aesar, Shore Road, Port of Heysham Industrial Park, Lancashire LA3 2XY, UK

Name	Product code	Company
Hexane, ≥95% pure	439177	Sigma-Aldrich® Sigma-Aldrich Inc.
Hydrogen peroxide	H-1009	Sigma® Sigma-Aldrich Co.
Indomethacin	1708	TOCRIS Bioscience
Leibovitz's L-15 Medium	11415-049	gibco® life technologies™ ThermoFisher Scientific
Methanol	34860-1L-R	Sigma® Sigma-Aldrich Company Ltd
N,N,N',N'-Tetramethylethylenediamine (TEMED)	T9281	Sigma-Aldrich® Sigma-Aldrich Inc.
Naproxen	2655	TOCRIS Bioscience
Oxaliplatin	S1224	Stratech Scientific Ltd.
Penicillin streptomycin (10,000U/ml)	15140122	ThermoFisher Scientific, Scientific
Phosphate Buffered Saline (PBS) pH 7.4 (1X)	10010-015	gibco® life technologies™ ThermoFisher Scientific 3 Fountain Drive Inchinnan business Park, Paisley PA4 9RF
Protease Inhibitor Cocktail (100X)	5871S	Cell Signalling Technology, Inc. New England Biolabs 75-77 Knowl Piece
Protein Plus Protein™ Dual Color Standards	161-0374	Bio-Rad Laboratories Ltd., Bio-Rad House, Maxted Road, Hemel Hempstead, Hertfordshire HP2 7DX, UK
RPMI Medium	11875-093	gibco® life technologies™ ThermoFisher Scientific
Salicylic acid	105910	Sigma-Aldrich®, Sigma-Aldrich Co.
Sodium chloride	301237S	BDH GPR™, VWR International Ltd. Poole BH15 1TD, UK

Name	Product code	Company
Sodium dodecyl sulphate (SDS)		Sigma® Sigma-Aldrich Co.
Staurosporine	S1421	Selleckchem.com Stratech Scientific Ltd. Unit 7 Acorn Business Centre Oaks Drive Newmarket, Suffolk CB8 7SY, UK
Thermo Scientific™ Pierce™ ECL 2 western Blotting Substrate	80196	Thermo Scientific Hunter Boulevard Magna Park Lutterworth Leichestershire LE17 4XN, UK
Thiazolyl Blue Tetrazolium Bromide	M2128	Sigma® Sigma-Aldrich Company Ltd
Tris-(hydroxymethyl) aminomethane	443866G	VWR BDH PROLABO® Unit 15, The Birches Willard Way Imberhorne Industrial Estate East Grinstead West Sussex RH19 1XZ, UK
Trypsin solution	T4674	Sigma-Aldrich® Sigma-Aldrich Inc.
Trypsin-EDTA 1X [0.25%(w/v)-0.53mM EDTA] solution	T3924	Sigma-Aldrich® Sigma-Aldrich Inc.
Tween®-20	P1379	Sigma-Aldrich® Sigma-Aldrich Inc.
Vectashield® Mounting Medium with DAPI		Vector Laboratories Inc. 3 Accent Park Bakewell Road Orton Southgate Peterborough PE2 6XS, UK
Vybrant® Apoptosis Assay Kit #4, YO-PRO®-1/Propidium Iodide	V13243	Life Technologies Corporation

Table 2.2 List of Reagents, Drugs, Culture media and other chemicals used in this study.

2.1.3 Buffers and solutions

According to each experimental protocol, different buffers and solutions were required to be made up. A list of buffers used in this study is provided in Table 2.3.

Buffers	Ingredients
Antibody dilution buffer #1	5%(w/v) non-fat dry milk (NFM), 0.1%(v/v) Tween-20 in Tris Buffered Saline (TBS)
Antibody dilution buffer #2	5%(w/v) BSA, 0.1%(v/v) Tween-20 in TBS
Blocking buffer #1	5%(w/v) NFM, 0.1%(v/v) Tween-20 in TBS
Blocking buffer #2	5%(w/v) BSA, 0.1%(v/v) Tween-20 in TBS
Blocking buffer #3	3%(w/v) BSA, 0.2%(v/v) Tween-20 in Phosphate Buffered Saline (PBS)
Freezing solution	FBS+10%(v/v) DMSO
Running buffer	Tris base 3g, Glycine 14.4g, 10%SDS 10ml, Water to 1L
Transfer buffer	Tris base 3g, Glycine 14.4g, Methanol 200ml, Water to 1L
Laemmli Sample buffer (2X)	Tris 0.125M pH 6.8, 4% SDS, 20% Glycerol, 10% β-mercaptoethanol, 0.004% bromophenol blue
Phosphate Buffered Saline (PBS)	1 tablet of PBS dissolved in 200ml of deionised water
Tris Buffered Saline (TBS) 10X	24g Tris base, 88g NaCl, dissolved in 900ml Water; Solution was pH adjusted to 7.6 with 12M HCl and Water to 1L
Tris Buffered Saline with Tween-20 (TBST) 1X	100ml TBS (10X), 900ml dWater, 1ml Tween-20
Fixing Solution	50%(v/v)Acetone, 50%(v/v)Methanol
Acid stripping buffer	0.2% BSA in L-15 medium (0.1g BSA in 50ml of L-15 medium); Solution was pH adjusted to 3.5 with HCl

Table 2.3 List of buffers used in this study.

2.1.4 Primary antibodies

Primary antibodies were used to detect the levels of antigen or protein of interest. Find below the primary antibodies used in this study.

Antibody	Isotype	Working dilution
EGF Receptor (D38B1) XP® Rabbit mAb #4267 Cell Signalling Technology Inc. Schuttersveld 2 2316 ZA Leiden The Netherlands	Rabbit IgG	1:1000
EGFR (phospho Y1068) Ab #ab5644 Abcam, 330 Cambridge Science Park Cambridge CB4 0FL, UK	Rabbit IgG	1:1000
EGFR (phospho Y1172) Ab #ab135560 Abcam	Rabbit IgG	1:1000
EGFR (phospho Y1045) Ab #2237S Cell Signalling Technology Inc.	Rabbit IgG	1:1000
EGFR (phospho Y992) Ab #9922 Cell Signalling Technology Inc.	Rabbit IgG	1:1000
EGFR (phospho Y1101) Ab #ab76195 Abcam	Mouse IgG	1:1000
Anti-β-Tubulin antibody #ab15568 Abcam	Rabbit IgG	1:2000
GAPDH (FL-335) antibody #sc-25778 Santa Cruz Biotechnology Inc. Bergheimer Str. 89-2 69115 Heidelberg Germany	Rabbit IgG	1:1000
Anti-p21 antibody [EPR3993] #ab109199 Abcam	Rabbit IgG	1:1000
Anti-Bcl-2 antibody [E17] #ab32124 Abcam	Rabbit IgG	1:1000

Antibody	Isotype	Working dilution
BAX (N-20) antibody #sc-493 Santa Cruz Biotechnology Inc.	Mouse IgG	1:200
Stat3 (79D7) Rabbit mAb #4904 Cell Signalling Technology Inc.	Rabbit IgG	1:2000
Phospho-Stat3 (Tyr705) Antibody #9131 Cell Signalling Technology Inc.	Rabbit IgG	1:1000
Anti-EEA1 antibody [1G11]- Early Endosome Marker #ab70521 Abcam	Mouse IgG	1:1000
Anti-β-Catenin antibody #ab6302 Abcam	Rabbit IgG	1:2000

Table 2.4 List of Primary antibodies used in this study.

2.1.5 Secondary antibodies

Secondary antibodies bind to primary antibodies and are normally linked to a fluorophore or horseradish peroxidase (HRP) to enable detection when excited by laser or enhanced chemiluminescence (ECL) substrate.

The secondary antibodies used in this study are shown in the table below.

Isotype	Species	Working dilution
Anti-Rabbit IgG-Phycoerythrin (PE) #ab72465 Abcam 330 Cambridge Science Park, Cambridge CB4 0FL, UK	Goat	1:1000
Anti-Rabbit IgG-Horseradish Peroxidase (HRP) #ab16284 Abcam	Donkey	1:2000
Anti-Mouse IgG+IgM+IgA-Allophycocyanin (APC) #ab130775 Abcam	Goat	1:1000
Anti-Mouse IgG-Fluorescein isothiocyanate (FITC) #ab6728 Abcam	Rabbit	1:1000
Anti-Rabbit IgG (FITC) #ab6717	Goat	1:200
Anti-Rabbit IgG (HRP) #7074S Cell Signalling Technology Inc. Schuttersveld 2 2316 ZA Leiden The Netherlands	Goat	1:2000

Table 2.5 List of Secondary antibodies used in this study.

2.1.6 Cell lines

SW480 CRC cells were originally purchased from European Collection of Authenticated Cell Cultures (ECACC).

Characteristics and morphology of these cell lines are presented in Table 2.6.

The CRC cell line, SW480 is from a colorectal adenocarcinoma and is adherent to the floor of the tissue culture flask (Leibovitz *et al.*, 1976). This cell line was cultured in L-15 medium supplemented with 10% (v/v) of FBS and 1% (v/v) penicillin-streptomycin. The cells were cultured in non-vented flasks and incubated at 37°C in the presence of 5% CO_2.

The oesophageal cell line, OE33 and FLO-1 were generously provided by Mr Tim Underwood, Cancer Sciences Division, University of Southhampton and was cultured in RPMI-1640 medium supplemented with 10% (v/v) FBS and 1% (v/v) penicillin-streptomycin. This cell line originates from an oesophageal adenocarcinoma and also grows adherent to floor of the tissue culture flask. These cells were grown in vented tissue culture flasks and incubated at 37°C with an atmosphere of 5% CO_2. U251 MG cells were kindly provided by Prof. W. Wang. FLO1 and U251 MG cell lines were originally derived from an oesophageal adenocarcinoma and a malignant glioblastoma tumour respectively. All these cell lines were cultured in DMEM medium supplemented with 10% (v/v) FBS and 1% (v/v) 10,000 U/ml penicillin-10 mg/ml streptomycin (Table 2.6). Vented tissue culture flasks were used and incubated at 37°C in the presence of 5% CO_2.

Cell line	**SW480 (ATCC®CCL-228™)**	**OE33**	**FLO1**	**U251 MG**
Organism	*Homo sapiens*	*Homo sapiens*	*Homo sapiens*	*Homo sapiens*
Tissue	Colon	Oesophagus	Oesophagus	Brain
Cell line origin	Metastatic site of colorectal adenocarcinoma of a 50 year old male Caucasian	Adenocarcinoma of the lower oesophagus of a 73 year old female patient	Primary distal oesophageal adenocarcinoma in a 68 year old male Caucasian	Derived from a malignant glioblastoma tumour
Disease	Duke's type B	Barrett's metaplasia	Adenocarcinoma	Human glioblastoma astrocytoma
Culture properties	Adherent	Adherent	Adherent	Adherent
Morphology	Epithelial	Epithelial	Epithelial	Pleumorphic/ astrocytoid
Culture media	L-15, 10%(v/v) FBS, 1%(v/v) 10,000 U/ml penicillin-10 mg/ml streptomycin	RPMI-1640, 10%(v/v) FBS, 1%(v/v) 10,000 U/ml penicillin-10 mg/ml streptomycin	DMEM, 10%(v/v) FBS, 1%(v/v) 10,000 U/ml penicillin-10 mg/ml streptomycin	DMEM, 10%(v/v) FBS, 1%(v/v) 10,000 U/ml penicillin-10 mg/ml streptomycin

Table 2.6 Characteristics of cancer cell lines used in this study.
(Adapted from ATCC (American Type Culture Collection); ECACC (European Collection of Authenticated Cell Cultures) General Cell Collection, Public Health England, (Leibovitz *et al.*, 1976).

2.2 Methods

2.2.1 Tissue Culture

The procedures and experiments requiring mammalian cells were all carried out aseptically in a laminar tissue culture hood using sterile materials and reagents. Cell morphology and confluency were observed using an inverted phase contrast microscope (OLYMPUS CK2-TR, Japan).

The cancer cell lines were regularly split in the appropriate medium supplemented with 10% FBS and 1% antibiotic solution (10,000 U/ml penicillin-10 mg/ml streptomycin) warmed to room temperature to maintain growth and confluency of cells for experiments.

Prior to splitting the cells, they were always washed gently with PBS before being detached from the floor of the culture flask using 0.25% (w/v) Trypsin-0.53 mM EDTA. After the cells had completely detached, medium was added to inactivate trypsin. The cells were then seeded in a splitting ratio of 1:6 into either T75 (75 cm^2) or T175 (175 cm^2) tissue culture flasks with fresh medium and incubated at 37°C. OE33, FLO1 and U251 cell lines were seeded in vented flasks while SW480 CRC cell line was seeded in non-vented flask. This was done twice a week.

2.2.1.1 Cell Counting

Cells were counted using the Coulter counter (Beckman Z1 Coulter® Single threshold particle counter). Twenty µl of the detached cell solution was pipetted out into 10ml of isotonic solution (ISOTON® II Diluent, 20 L, Item No: 8546719,

Beckman Coulter) and then inserted into the Coulter counter for cell counting. Five hundred µl of the diluted cell suspension were counted, representing the number of cells per µl of the original material.

2.2.1.2 Cryopreservation of cells

Cells were grown to about 80-90% confluency, harvested using 0.25% (w/v) trypsin-EDTA before cryopreservation and then centrifuged at 250 x g for 10 min. The supernatant was aspirated and the cells then washed in PBS and centrifuged again. The supernatant PBS was aspirated and cells suspended gently in 2 ml of freeze medium [90% (v/v) FBS and 10% (v/v) DMSO]. One ml aliquots of cell suspension were pipetted out into cryovials, labelled appropriately and cooled slowly to -80°C over 48 h. The frozen cells were then transferred to liquid nitrogen (-180°C) for long-term storage.

2.2.1.3 Resuscitation of frozen cell lines and Sub culturing

Frozen cells were removed from liquid nitrogen and thawed quickly by dipping in a 37°C water bath. The cells were then quickly transferred drop-wise into a T25 flask containing 10 ml of warm medium, which had been left in the incubator to warm up and to equilibrate the flask with CO_2 where appropriate. This was then incubated at 37°C overnight to allow cells to recover and get attached to the flask. The media was then aspirated and replaced with fresh media. Cells were washed with PBS in order to remove any traces of DMSO. Cells were then allowed to grow to confluency and sub-cultured accordingly.

2.2.2 Preparation of compounds as stock solutions

Aspirin and analogues were always freshly prepared in acetone (Section 2.2.5.1.1) at a concentration of 50 mM and then either diluted with PBS (pH7.4) or HEPES (pH8) to adjust the pH. These solutions were then further diluted in appropriate media supplemented with 10% (v/v) FBS and 1% (v/v) 10,000 U/ml penicillin-10 mg/ml streptomycin to either 1 mM or 0.5 mM final concentrations for studies. This resulted in 20 mM or 10 mM respectively as the final concentration of HEPES, which is known as a suitable buffer for biological studies (Good *et al.*, 1966) and within the recommended 10 mM to 25 mM concentration for tissue culture (Eagle, 1971).

2.2.3 Synthesis of aspirin analogues

2.2.3.1 PN591 (meta-thioaspirin)

The procedure was started by dissolving 0.616 g of 3-mercaptobenzoic acid in 5.6 ml (0.10 mole) of ice cold sodium hydroxide solution. To this solution was added 5 g of ice and 0.5 g acetic anhydride whilst stirring for 15 min. The resulting mixture was then acidified with HCl drop wise. The precipitate was then filtered and washed with water. The powder was left to dry. Mpt is ideally 152°C - 153°C (Bordwell and Boutan, 1956). This powder is known as PN591.

2.2.3.2 PN592 (para-thioaspirin)

Synthesis of this compound was carried out in accordance to the method described by Bordwell and Boutan, 1956. 5 g of ice accompanied by 0.5 g acetic anhydride were added to an ice-cold solution of 4-mercaptobenzoic acid in sodium hydroxide. This mixture was stirred for 15 min and then acidified with hydrochloric acid. The precipitate was filtered off and washed with water. The powder was then left to dry. Mpt was found to be 189°C - 190°C. The product is known as PN592.

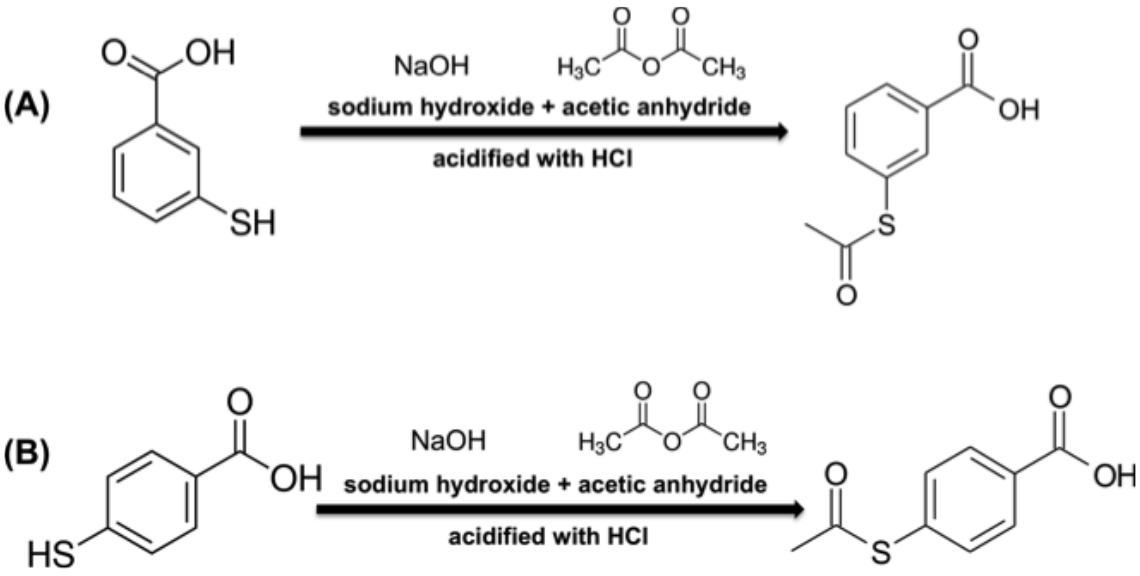

Figure 2.1 Chemical reaction for the synthesis of isomers of thioaspirin.
Synthesis of *meta*-thioaspirin (PN591) from 3-mercaptobenzoic acid (A) Synthesis of *para*-thioaspirin (PN592) from 4-mercaptobenzoic acid (B).

2.2.4 Chemistry of aspirin analogues

2.2.4.1 Melting point analysis

The mpts of the compounds were determined using the Stuart® SMP 10 melting point apparatus. Methodology was in line with the Stuart® SMP 10 instructions manual. Samples were placed in a glass capillary tube by tapping gently and then placed in the aluminium block inside the sample chamber. The block is then heated and the sample observed through the magnifying lens until it melted. The melting point temperature was then read on the LED display and recorded. Values represent mean of n=3.

2.2.4.2 Thin Layer Chromatography (TLC)

TLC is one of the most widely used separation techniques. This is because it is quite easy and fast to use, can be applied to a wide range of samples, highly sensitive, and relatively cheap (Touchstone, 1992). The main aim is to demonstrate purity (or very high concentration of the compound of interest) by elution as a single spot in more than one solvent if possible. This is a good, practical indicator of relatively high purity.

It works by allowing an analyte to move up a layer of stationary phase under the influence of a mobile phase, which also moves through the stationary phase by capillary action (Watson, 2005).

The test samples made up of aspirin and its analogues dissolved in diethylether (or other suitable volatile solvent) and placed as spots about 2cm from the bottom of the silica-60 plate (12804281, ALUGRAM UV254). The suitable

eluent used in this case was 65:30:5 (v/v) mixtures of hexane (≥95%, 439177, Sigma Aldrich), ethylacetate (99.8%, 270989, Sigma Aldrich) and acetic acid (99.5%, pure, 124040025, ACROS ORGANICS). The plates were then spotted with the compounds in solution (diethylether) and allowed to dry. These plates were then placed in the chamber. After elution, ultraviolet light was used to detect the travelled compounds (seen as spots). The R_f value was calculated by dividing the distance travelled by the compound from the origin (point of compound application) by the distance travelled by the solvent from the origin.

$$R_f = \frac{\text{Distance moved by spot}}{\text{Distance migrated by solvent}}$$

TLC was used to test the purity of aspirin analogues synthesized and also to observe any possible breakdown of compounds.

2.2.4.3 Infrared (IR) Spectroscopy

IR spectroscopy is a technique used to check the fingerprint that is unique to the compound being examined (Williams and Fleming, 2008). This is then compared with a standard stored in a database to determine the purity of that compound. The bonds between the molecules in the sample of interest absorb electromagnetic radiation ranging between 400 cm^{-1} and 4000 cm^{-1}, causing them to stretch or bend. These bonds are then determined by the radiation wavelength absorbed (Watson, 2005).

The powdered compound was transferred to the diamond stage of a Genesis II ATR FTIR (Attenuated Total Reflection Fourier Transform IR) instrument, which

enables analysis without the need for further sample preparations (Perkin Elmer Life and Analytical Sciences, 2005) and the spectrum obtained using the WinFIRST software, which controls the FTIR spectrometer.

The spectrum was then analysed for each sample and the key functional group wavenumbers were catalogued.

(See appendix for the individual spectra of compounds).

2.2.4.4 Nuclear Magnetic Resonance (NMR) Spectroscopy

^{13}C NMR was used to confirm the structures of the aspirin analogues before use by interpretation using aspirin as a standard and point of reference (http://sdbs.db.aist.go.jp/sdbs/cgi-bin/cre_index.cgi). David Townrow using a JEOL ECZ-YH 400 MHz NMR spectroscopy machine carried this out.

(See appendix for the individual spectra of aspirin analogues).

2.2.5 Cytotoxicity, Toxicity and Breakdown of aspirin analogues

2.2.5.1 MTS assay for Cell Viability

Viability of cells after being treated with different aspirin analogues was measured using the CellTiter 96 AQ_{ueous} One solution Cell Proliferation Assay kit in accordance to Spruce *et al*., 2004. Prior to this, the cell viability of SW480 cells was determined using different solvents as a dissolution medium. The principle behind this is the formation of formazan, which is yellow in colour (Marker) due to the reduction of tetrazolium compounds by NADPH or NADH produced in metabolically active cells (Figure 2.2).

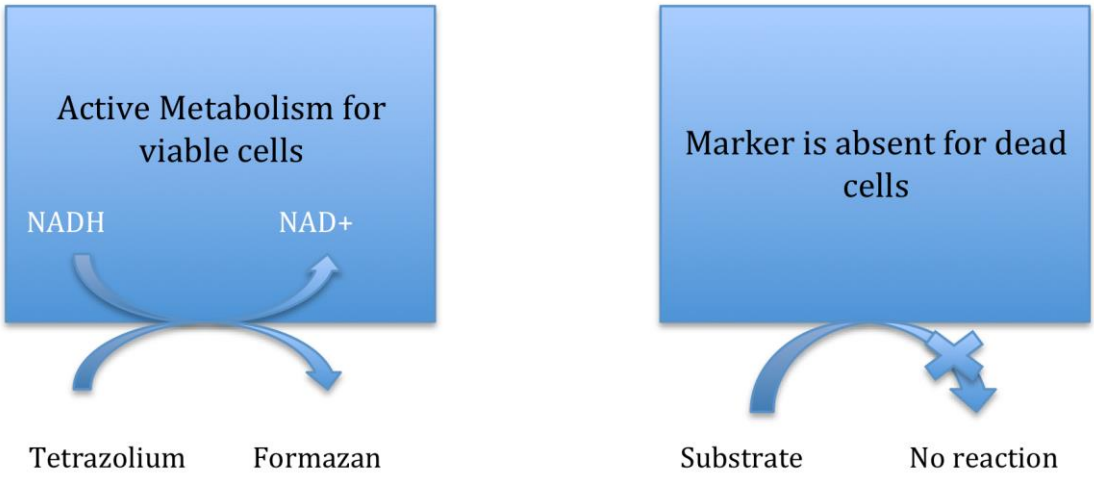

Figure 2.2 Illustrated explanation of the principle behind MTS activity.

A standard curve was plotted to show the relationship between concentration and absorbance at 490 nm (Figure 4.3).

The experiments were performed in duplicates and the viable cells were calculated as a percentage relative to the negative control cells. The equation used.

$$\%\text{Cell viability} = \frac{\text{Absorbance 490 nm(treated cells-blank)}}{\text{Absorbance 490 nm(control cells-blank)}} \times 100$$

2.2.5.1.1 MTS Assay to determine most suitable dissolution Solvent

To determine the most appropriate solvent, SW480 cells were seeded in growth media at a density of 10,000 cells/well in 96 well plates and incubated overnight. The cells were treated with acetone, DMSO or tetrahydrofuran (THF) in serial dilutions and incubated for 48 h. A negative control containing only cell culture media was also included. 10 µl of CellTiter 96 AQ_{ueous} (1 ml MTS solution:50 µl

coupling agent) was added to each well and readings were taken using a Multiskan microplate reader at 490 nm absorbance for 0-4 h (Spruce *et al.*, 2004).

SW480 cells were seeded in growth media at a density of 1 X 10^4 cells/well in 96 well plates and incubated overnight. Aspirin and aspirin analogues (3 mM - 0.1 mM) were prepared in stock solutions of 100 mM with either acetone or DMSO and diluted with PBS and Penicillin-Streptomycin solution. The cells were further incubated for 48 h. Ten µl of CellTiter 96 AQ_{ueous} one solution reagent was then pipetted into each well to determine the cell viability in control and cell treated populations. Using a plate reader, absorbance of the colorimetric solution was read at 490 nm at 0 h and after 6 h. A negative and vehicle control was also included containing cells treated with medium only and medium treated with acetone respectively.

2.2.5.2 MTT assay

Cell viability was also measured by 3-(4,5-Dimethyl-2-thiazolyl)-2,5-diphenyl-2H-tetrazolium bromide (MTT) reduction assay (Mosmann, 1983) with modifications (Carmichael *et al.*, 1987). SW480 cells were seeded at a density of 1 X 10^4 or 5 X 10^3 cells per well in a 96-well plate and incubated overnight at 37°C. After 24 h of seeding, the culture medium was then replaced with medium containing the drugs at required concentrations and further incubated for 48 h. A control that had cells with no treatment was also included in these experiments. The medium was then aspirated from each well and cells washed once with fresh medium to completely remove drugs and replaced with 300 µl of

MTT reagent (0.5 mg/ml). Cells were incubated at 37°C for 3 h at which time the medium was aspirated and replaced with 200 µl dimethyl sulfoxide (DMSO). The plates were incubated at 37°C for a further 30 min at which time the conversion of MTT into formazan crystals by living cells was measured by recording changes in the absorbance at 540 nm in a microplate reader (Microplate Reader Thermo Multiskan Ascent 96 & 384). Plates were protected from light throughout the procedure. Dosage of drugs ranged from 0 to 3 mM. A standard curve for formazan was constructed to examine the relation between formazan concentration and absorbance. GraphPad Prism was used to plot dose-response curves and to determine IC_{50} values. All assays were performed in duplicate (n=3) and the viable cells were expressed as a percentage relative to the negative control. The equation used can be found below.

$$\%\text{Cell viability} = \frac{\text{Absorbance 540nm(treated cells-blank)}}{\text{Absorbance 540nm(control cells-blank)}} \times 100$$

2.2.6 Salicylic acid Analysis

This analysis was used to measure the amount of salicylic acid as the breakdown product of the aspirin analogues of interest (Section 3.4.4.1). It is based on the fluorescence enhancement of the As(III)-salicylic acid system (Karim *et al*., 2006). In other words, fluorescence excitation and emission spectra of salicylic acid (λ_{ex} =315 nm, λ_{em} =408 nm) were measured due to the formation of a As(III)-salicylic acid complex in the presence of sodium dodecyl sulphate (SDS).

2.2.6.1 Dilution curve for Salicylic acid

A dilution curve for salicylic acid and aspirin boiled with sodium hydroxide (NaOH) for 1 h in order to hydrolyse aspirin into salicylic acid was made to make sure the assay was specific to salicylates (Figure 3.11). Different concentrations of salicylic acid were prepared in serial dilutions starting from 10 mM.

10 µl of 1 mM SDS, 1 µl of 0.1 mM As_2O_3, 10 µl of 100 mM HEPES buffer (pH7) were pipetted into wells of a white flat bottom 96-well assay plate. To this was added 50 µl of the prepared salicylic acid compounds. The volume of each well was made up to 100 µl with distilled water, which made the final concentration of salicylic acid to be 5 mM. The plate was incubated for 10 min and placed into the CLARIOStar® fluorescence monochrome microplate reader. The fluorescence intensity of the solution in each well was then measured at 408 nm with excitation at 315 nm against a reagent blank without salicylic acid.

The dilution curves of salicylic acid, aspirin boiled with NaOH for 1 h and aspirin alone were compared and can be seen in section 3.4.4.1.

2.2.6.2 Rate of metabolism of Aspirin analogues on SW480 cells using salicylic acid analysis

24-Well tissue culture plates (Sarstedt Ltd.) were prepared with each well containing $5X10^4$ SW480 cells and left to incubate for 24 h at 37°C, 5% CO_2. The cells were then treated with different aspirin analogues at 1mM concentration for 48 h.

The amount of salicylic acid was measured in duplicates for each well containing cells treated with the compounds.

2.2.7 DEREK Analysis

The recommended system for the prediction of toxicity in compounds of known chemical structure is the Derek Nexus software (Dobo *et al.*, 2012, Sutter *et al.*, 2013) as it generates clear and scientifically robust predictions. Toxicity of compounds can be predicted without the need of animal studies. Thus, the Nexus Suite 2.1 Derek Nexus (Version 5.0.1) was used to predict the toxicity profile of each compound using its basic chemical structure.

One of the shortcomings of this software however is that it can only work with chemical compounds already stored in its data bank. This led to it not recognising the chemical structure of some aspirin analogues and thus not providing an accurate prediction.

2.2.8 SDS-PAGE for separation of proteins and Western blot for detection

2.2.8.1 Preparation of SDS gels

Gels were prepared in accordance to the recipe given in Tables 2.7 and 2.8 below. The various volumes of ingredients needed for separation gel were made up and 3.5ml of that poured into already set up glass plates (150 X 100 X 0.75 mm, Bio Rad mini gel). To the gel was then added 200 µl of isopropanol so as to ensure a horizontal upper surface and to get rid of bubbles. The gel was then allowed to set.

The gel was then rinsed with water and the excess water dabbed off using strips of filter paper, after which the stacking gel was prepared and pipetted into the glass set up, on top of the separating gel. The gel comb was then immediately inserted in order to form the gel wells. This was then allowed to set, gel comb removed and the wells were ready of loading of protein samples. Table 2.7 and 2.8 shows the recipes for stacking and separating gels.

Ingredients	**Volume (ml)**
40% acrylamide (29:1)	1.0
0.5 M Tris base buffer (pH 6.8)	2.5
10% SDS	0.1
Water	6.0
TEMED	0.05
APS*	0.05

Table 2.7 Recipe for preparation of stacking gel.
*Always made fresh by dissolving 0.02 g APS per 0.2 ml of water.

Ingredients	**Volumes for different % of acrylamide**		
	6%	**8%**	**10%**
40% acrylamide (29:1)	1.5	2.0	2.5
1.5 M Tris base buffer (pH 8.8)	2.5	2.5	2.5
10% SDS	0.1	0.1	0.1
Water	6.0	5.5	5.0
TEMED	0.05	0.05	0.05
APS*	0.05	0.05	0.05

Table 2.8 Recipe for preparation of separating gel.
*Always made fresh by dissolving 0.02 g APS per 0.2 ml of water.

2.2.8.2 Western blot for detection of proteins

Treated samples were prepared in accordance with the western blotting protocol on the Cell Signalling Technology® website.

The SDS-PAGE loaded with the sample protein of interest was then run using electrophoresis for 1.5 h at 150 V in 'running buffer'. After this, the protein was then transferred on to Polyvinylidene difluoride (PVDF) transfer membrane at 100V for 2 h in the presence of 'transfer buffer'. The blots were blocked in blocking buffer for 1h at room temperature (RT) with gentle rocking. The membrane was then probed with the appropriate primary antibodies overnight on a rocker at 4°C. The probed membrane was then washed in TBST three times for 5 min each and re-probed with a corresponding HRP-linked secondary antibody diluted in blocking buffer for 1 h on a rocker at room temperature. The HRP bound protein-labelled antibody was visualised using ECL (GE Healthcare Amersham™ ECL™ Prime Western Blotting Detection Reagent, RPN2232) for 5 min and exposed to CL-XPosure™ Film.

2.2.8.2.1 Effect of aspirin and its analogues on EGFR expression

The effect of aspirin and its analogues on the EGF receptor expression over time was observed using western blotting.

About $5X10^4$ SW480 CRC cells per well were plated in a 6-well tissue culture plate and treated with aspirin, thioaspirin and their isomers at 0.5 mM for 24 h, and subsequently for 0 h, 1 h, 3 h, 6 h and overnight.

200 µl of Laemmli protein buffer containing 0.01% of protease inhibitor cocktail (100X) was added to the cells before being scraped off and transferred into 1.5 ml microcentrifuge tubes. The cells were then treated at 100°C for 20 min and centrifuged (20,000 rpm) for 5 min. The samples were analysed by electrophoresis in 10% polyacrylamide gels in the presence of 0.1% SDS at 150 V for 1.2 h. After protein transfer on to PVDF transfer membrane at 100V for 2 h, the blots were blocked in blocking buffer #1 (Table 2.3) for 1 h at room temperature (RT). The blots were then probed with primary antibodies EGFR (D38B1, Cell Signalling Technology) rabbit mAb at 1:1000 and GAPDH (sc-25778, Santa Cruz Biotechnology) rabbit polyclonal IgG at 1:1000 overnight on a rocker at 4°C. The blots were then washed in TBST three times for 5 min each and probed with anti-rabbit IgG (7074S, Cell Signalling Technology) HRP-linked secondary antibody diluted in blocking buffer #1 for 1 h on a rocker at room temperature. The HRP bound protein-labelled antibody was visualised using ECL (GE Healthcare Amersham™ ECL™ Prime Western Blotting Detection Reagent, RPN2232) for 5 min and exposed to CL-XPosure™ Film.

2.2.8.2.2 Effect of aspirin and its analogues on EGFR tyrosine phosphorylation sites

The effects on the EGFR phosphorylation sites by aspirin analogues were examined using western blot analysis.

About 5 X10^4 SW480 cells per well were plated on a 6-well tissue culture plate, serum-starved for 2 h. The cells were then treated with aspirin and its analogues for 24 h at 0.5 mM. The cells were subsequently also treated at various doses to determine a dose response on the phosphorylation sites.

To abolish effects on the phosphorylation sites due to pH change, another set of SW480 cells were treated with compounds that have been pH adjusted with HEPES.

Briefly, cells were washed with cold (4°C) PBS and suspended in 2X Laemmli sample buffer containing 10% β-mercaptoethanol (Laemmli, 1970) and 0.01% of protease inhibitor cocktail (100X) (5871S, Cell Signalling Technology). The cells were then scraped off and transferred into 1.5 ml microcentrifuge tubes and treated at 100°C for 20 min and centrifuged (14,000 rpm) for 5 min. The samples were analysed by electrophoresis in 6% and 10% polyacrylamide gels in the presence of 0.1% SDS at 150 V for 1.2 h. After protein transfer on to PVDF transfer membrane at 100 V for 2 h, the blots were blocked in blocking buffer #2 (Table 2.3) on a rocker for 1 h at RT. The blots were then subjected to immunoblot analysis by probing with either rabbit pEGFR Y1068 (ab5644, Abcam) Ab at 1:1000 dilution, rabbit pEGFR Y1045 (2237S, Cell signalling technology) Ab at 1:0000, rabbit pEGFR Y1172 (ab135560, Abcam) Ab at 1:2000, rabbit pEGFR Y992 (9922, Cell Signalling Technology) Ab or mouse pEGFR Y1101 (ab7195, Abcam) Ab as primary antibodies overnight on a rocker at 4°C. Either GAPDH (sc-25778, Santa Cruz Biotechnology) Ab or beta-tubulin (ab15568, Abcam) Ab were used as loading controls. The blots were then washed in TBST three times for 5 min each and probed with the

corresponding secondary antibody (anti-rabbit or anti-mouse) conjugated with HRP all diluted in blocking buffer #2 (Table 2.3) for 3 h on a rocker at room temperature. The HRP bound protein-labelled antibody was visualised using ECL 2 Western blotting substrate kit (80196, Thermo Scientific) and film.

2.2.8.2.3 Effects of aspirin analogues on pro-apoptotic and anti-apoptotic proteins

About 5 $X10^4$ SW480 CRC cells per well were plated in a 6-well tissue culture plate and treated with aspirin and some of its analogues at 0.5 mM for 24 h.
150 µl of Laemmli protein buffer was added to the cells before being scraped off and transferred into 1.5 ml microcentrifuge tubes. The cells were then treated at 100°C for 20 min and centrifuged (14,000 rpm) for 5 min. The samples were analysed by electrophoresis in 10% polyacrylamide gels in the presence of 0.1% SDS at 120V for 1 h. After protein transfer on to PVDF transfer membrane at 100V for 2 h, the membrane was blocked in blocking buffer #1 (Table 2.3) for 1 h at RT. The blots were then probed with primary antibodies p21 (ab109199, Abcam) rabbit mAb at 1:1000, BCL-2 (ab32124, Abcam) rabbit mAb at 1:1000 and BAX (sc-493, Santa Cruz Biotechnology) mouse mAb at 1:200. Anti-beta Tubulin Ab (ab15568, Abcam) at 1:2000 was used as loading control overnight on a rocker at 4°C. The blots were then washed in TBST three times for 5 min each and probed with the corresponding HRP-linked secondary antibody diluted in blocking buffer #1 (Table 2.3) for 1 h on a rocker at RT. The HRP bound protein-labelled antibody was visualised using ECL (GE Healthcare

Amersham™ ECL™ Prime Western Blotting Detection Reagent, RPN2232) for 5 min and exposed to CL-XPosure™ Film.

2.2.9 Flow cytometry

Flow cytometry was used to sort out a population of cells (Figure 2.3) into apoptotic cells that are stained with Annexin V due to interaction with phosphatidylserine protein exposed by the flipped cell membrane (Vermes *et al.*, 1995) and necrotic cells that are stained by propidium iodide (PI) due to its ability to interact with DNA of cells under stress or dead (Chou *et al.*, 1987). 2 X 10^5 of SW480 cells per well were plated out in a 6-well tissue culture plate and left in the incubator for 24 h after which they were treated with either aspirin analogues, staurosporine as a control for apoptosis (Jacobson *et al.*, 1993) or hydrogen peroxide (H_2O_2) as a control for necrosis (Teramoto *et al.*, 1999). The cells were dissociated from the wells using trypsin, 0.25% (w/v) after 16h and 40 h and centrifuged at 200 X g for 5 min to separate cell pellets from the supernatant media. 0.25% (w/v) trypsin lacking EDTA was used in order to minimize damage to the cell membrane. The cell pellets were then washed in PBS and centrifuged again. The cells were then resuspended in binding buffer containing the dyes FITC-Annexin V and PI. After 15 min of incubation at room temperature, each sample was then analysed using the BD Accuri™ C6 flow cytometer installed with the BD Accuri™ C6 software (Version 1.0.264.21). Cells were treated with 0.5 mM, 0.3 mM and 0.1 mM concentrations of aspirin and its analogues with staurosprine (Maciel *et al.*, 2014) at 500 nM and H_2O_2 at 5 mM. 10,000 cells were acquired for each experimental condition.

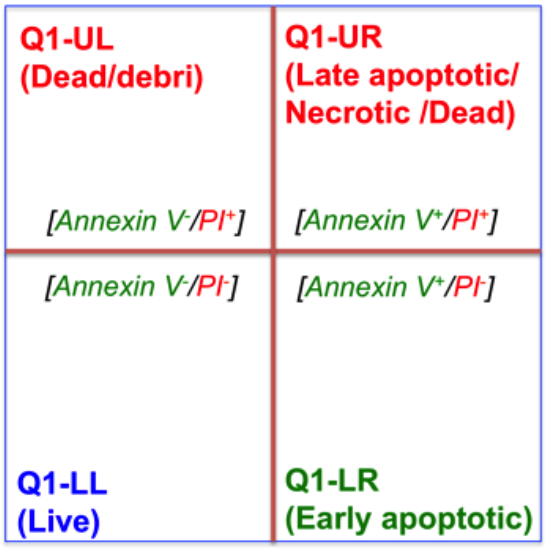

Figure 2.3 Gating of cells undergoing apoptosis and necrosis using flow cytometry.
The cytogram is divided into four different quadrants in which cell populations are grouped according to the fluorescence dye it is stained with. Cell populations that do not take up any of the dyes are the live healthy cells and are grouped in the lower-left quadrant (Q1-LL) as shown by the BD Accuri™ C6 software. Cells that take up the Annexin V dye are those undergoing early apoptosis and are grouped in the lower-right quadrant (Q1-LR). Cell populations that take up both dyes are undergoing late apoptosis, necrosis or considered dead and fall in the upper-right quadrant (Q1-UR). Populations that only take up the PI dye are considered either dead cells or debri and fall in the upper-left quadrant (Q1-UL) (Wlodkowic *et al.*, 2011).

2.2.10 YO-PRO®-1 and PI

YO-PRO®-1 is a green florescent dye that selectively passes through the membrane of apoptotic cells whereas dyes like the red florescent PI cannot (Idziorek *et al.*, 1995). Thus, a combination of these two dyes provides a sensitive assay for apoptosis.

SW480 CRC cells were plated on glass cover slips in 6-well-pates to obtain 70% confluency after 24 h. These cells were then treated with staurosporine and H_2O_2 as controls for apoptosis and necrosis respectively for 16 and 40 h after which were washed with cold PBS once and then treated with 1 µl each of YO-PRO®-1 and PI stock solution in 1 ml of PBS per well on ice for 30 min. This step was then followed by two washes with cold PBS, left on ice in PBS for a further 30 min and then coverslips placed onto a drop of VectaShield® mounting medium. Microscopy was done using a Zeiss LSM 880 confocal microscope, equipped with 405 and 561 nm excitation lasers using 40X/1.30 oil immersion DIC M27 objective. The Zeiss: ZEN2 (blue edition) software was used to process images. Cells were treated with 0.5 mM concentrations of aspirin and its analogues with the exception of PN590 at 0.3mM. Cells were treated with staurosprine at 500 nM and H_2O_2 at 5 mM as control for apoptosis and necrosis respectively.

2.2.11 Epidermal Growth Factor Binding

The effect of aspirin analogues on EGF binding was assayed using immunocytochemistry/confocal microscopy and quantified using ImageJ.

SW480 cells were cultured on glass coverslips to approximately 70% confluency in 6-well tissue culture plates and serum-starved for 48 h. Monolayers were cooled to 4°C, and incubated for 1 h in the presence of 100 ng/ml AlexaFluor 555 EGF on ice. For experiments testing compounds, serum-starved cells were pre-incubated at 37°C for 30 min in the absence or presence of compounds at 0.5 mM, then 15 min at 4°C, prior to addition of equivalent volume of cold serum-free culture medium containing 200ng/ml AlexaFluor 555 EGF for 1 h to allow EGF binding, which resulted in a final concentration of 100ng/ml EGF. Cells were then washed with cold PBS 3 times and fixed for 5 min with acetone/methanol (1:1) on ice, and the coverslips then placed onto a drop of VectaShield® mounting medium. Microscopy was done using a Zeiss LSM 880 confocal microscope, equipped with 405 and 561 nm excitation lasers using 40X/1.30 oil immersion DIC M27 objective. ImageJ (1.48v) was used to quantify bound EGF by analysing fifty cells per compound in the red channel.

2.2.12 Epidermal Growth Factor Internalization

The effect of aspirin and its analogues on EGF internalisation was studied using immunocytochemistry/confocal microscopy.

SW480 cells were cultured on glass coverslips to approximately 70% confluency in 6-well tissue culture plates and serum-starved for 48 h. Monolayers were cooled to 4°C, and incubated for 1 h in the presence of 100

ng/ml AlexaFluor 555 EGF on ice (In subsequent experiments this concentration was reduced to 20 ng/ml in order to target the EGFR recycling pathway). For experiments testing compounds, serum-starved cells were pre-incubated at 37°C for 30 min in the absence or presence of compounds, then 15 min at 4°C, prior to addition of equivalent volume of cold serum-free culture medium containing 200 ng/ml AlexaFluor 555 EGF for 1 h to allow EGF binding. Cells were warmed to 37°C for 30 min to stimulate EGF internalization, washed with cold PBS 3 times and fixed for 5 min with acetone/methanol (1:1) on ice, and the coverslips then placed onto a drop of VectaShield® mounting medium. Microscopy was done using a Zeiss LSM 880 confocal microscope, equipped with 405 and 561 nm excitation lasers using 40X/1.30 oil immersion DIC M27 objective. The Zeiss: ZEN2 (blue edition) software was used to process images. For preliminary experiments, cells were incubated with 0.5 mM aspirin and its analogues.

2.2.13 EGF internalization using Live Confocal Imaging

SW480 CRC cells were plated in 3 ml DMEM medium (Thermofisher, 11965-092) supplemented with 10% FBS and 1% antibiotic solution (10,000 U/ml penicillin-10 mg/ml streptomycin) on a confocal dish (IWAKI® glass base dish) to achieve approximately 70% confluency the next day. DMEM medium was used in this assay because phenol-red free medium was needed for clear viewing under the microscope and DMEM was the only medium we had that had a phenol-red free version. The cells were then serum starved for 24 h because starving for 48 h in the confocal dish reduced cell viability. Monolayers

were cooled to 4°C, and incubated for 1 h in the presence of 200 ng/ml AlexaFluor 555 EGF on ice. For experiments testing compounds, serum-starved cells were pre-incubated at 37°C for 30 min in the presence of compounds, then for 15 min on ice, prior to addition of equivalent volume of cold serum-free culture medium containing 400 ng/ml AlexaFluor 555 EGF to give a final volume of 200 ng/ml for 1 h to allow EGF binding. Cells were then washed with cold PBS once and medium replaced with 3 ml Phenol-red-free DMEM (D1145, Sigma®) to enable clear viewing of cells under the confocal microscope. Microscopy was done using a Zeiss LSM 880 confocal microscope, equipped with 405 and 561 nm excitation lasers using EC Plan-Neofluar 20X/0.50 DIC M27 objective using the incubation chamber at 37°C, 5% CO_2. Time series was 120 cycles at 0.5 min intervals. For preliminary experiments, cells were either incubated with 0.5 mM PN502 or PN517.

2.2.14 Quantification of EGF internalization

Quantification of EGF internalization was attempted using flow cytometry as described by Li *et al*., 2008. 6 X 10^5 SW480 cells per well were plated in a 6-well plate and incubated overnight. The cells were then serum-starved in pre-warmed L-15 medium for 48 h. Receptor internalization was set in motion by treating the cells with L-15 medium containing 100 ng/ml EGF or without at 37°C for 0 and 30 min. This was halted by shifting the cells to ice for 10 min and then washed twice in cold PBS for 10 min each at 4°C with gentle shaking. The cells were then washed with freshly prepared ice-cold acid stripping buffer thrice for 5 min each to remove non-internalized ligand after which they were

washed with ice-cold PBS with gentle shaking for 5 min. The next step was to incubate the cells in pre-chilled FACS buffer containing 3 µg/ml of Anti-EGFR antibody at 4°C for 1 h and washed again three times with cold PBS for 5 min each. Cells were then incubated in pre-chilled FACS buffer containing secondary antibody conjugated to FITC for 1 h on ice. After washing with PBS, the cells were then trypsinised with 300 µl trypsin per well, centrifuged at 1,100 g for 3 min and washed again with ice-cold FACS buffer. 1% PI in FACS buffer was added per tube for 15 min at room temperature prior to flow cytometry to distinguish live cells from the dead ones. 20,000 cells were acquired for each experiment.

Another method was attempted by plating 6 X 10^5 CRC cells and starving for 48 h after which the cells were incubated with and without an aspirin analogue at 37°C for 30 min and then at 4°C for 15 min. The cells were then treated with an equivalent volume of 200 ng/ml AlexaFluor® 555 EGF resulting in a final concentration of 100 ng/ml AlexaFluor® 555 EGF on ice for 1 h. Cells were trypsinized with trypsin, neutralized with cell medium and centrifuged at 200 X g for 10 min. FACS buffer was added to wash cells and centrifuged once more. Cells were then analysed in FACS buffer using flow cytometry. 20,000 cells were acquired for each experiment.

2.2.15 EGF co-localisation with EEA1

SW480 cells were cultured on glass coverslips (AmScope) to approximately 70% confluency in 6-well tissue culture plates and serum-starved for 48 h. For experiment testing compounds, serum-starved cells were pre-incubated at 37°C

for 30 min in the absence or presence of compounds, then for 15 min at 4°C, prior to addition of equivalent volume of cold serum-free culture medium containing 200 ng/ml AlexaFluor® 555 EGF, resulting in a final concentration of 100 ng/ml AlexaFluor® 555 EGF on ice for 1 h to allow EGF binding (In later experiments, this concentration was reduced to 20 ng/ml). Cells were then warmed to 37°C for 30 min to stimulate EGF internalization, washed with cold PBS 3 times and fixed for 5 min with acetone/methanol on ice. The cells were washed in cold PBS again followed by being blocked in blocking buffer #3 (Table 2.3) for 2 h in the dark at room temperature. Anti-EEA1 antibody [1G11] Early Endosome Marker (ab70521, Abcam) as primary antibody was added to cells at 1:1000 and kept at 4°C overnight with gentle rocking. The cells were then washed with cold blocking buffer thrice after which Goat Anti-Mouse IgG H&L-FITC (ab6785, Abcam) as secondary antibody was added for 2 h at room temperature, washed with cold blocking buffer 3 times and finally with cold PBS before cover-slips were placed onto a drop of VectaShield® mounting medium. Microscopy was performed using a Zeiss LSM 880 confocal microscope, equipped with 405 and 561 nm excitation lasers using 40X/1.30 oil immersion DIC M27 objective. For preliminary experiments, cells were incubated with 0.5 mM of aspirin and its analogues.

2.2.16 Synergy experiments

SW480 cells were plated in a 96-well plate at a density of 500 cells/well/100µl of medium and allowed to set overnight at 37°C. The cells were the treated the next day with serial dilutions of cisplatin, oxaliplatin, carboplatin and aspirin with

its analogues either for 12 days with drug being replenished at day 6 (McPherson *et al.*, 2014) or for 72 h (Chan *et al.*, 2014, Luo *et al.*, 2010, Toscano *et al.*, 2007, Yan *et al.*, 2010, Zhou *et al.*, 2010). Cell viability was measured by MTT assay to determine the IC_{50} for each drug.

Combination drug treatments were then performed as above by pairing cisplatin, oxaliplatin or carboplatin with each of the other drugs in a constant ratio design based on the IC_{50}. Once these ratios were set, a mixture of the two drugs was made at 2-fold and then serially diluted to 1-fold, 0.5-fold, 0.125-fold and 0.0625-fold. All assays were performed in duplicates (n=3). CompuSyn Inc. software (Paramus, NJ., 2005) was used to calculate the Combination Index (CI) and Dose Reduction Index (DRI). This produces multiple drug dose-effect calculations using the Median Effect methods described by Chou and Tatalay (Chou and Talalay, 1984). The CI is the quantitative measure of the degree of drug interaction in terms of additive effect (CI = 1), synergism (CI < 1), or antagonism (CI > 1) while the DRI is the measure of favourable dose reduction when two drugs are used in combination.

Graphpad Prism 7 software (Version 7.0a, April 2016) was used to calculate the IC_{50} of individual compounds and their respective combinations. This software was also used for statistical analysis.

2.2.17 Statistical Analysis

Statistical analyses were carried out using GraphPad Prism 7 software (GraphPad software Inc., San Diego, CA, USA). The test used to determine statistical significance was ordinary one-way ANOVA. Differences between control were considered as statistically not significant at $p>0.05$, and significant at $p<0.05$, $p<0.01$, $p<0.001$ or $p<0.0001$.

Chapter 3. Chemistry of Aspirin analogues

3.1 Introduction

Evidence suggests that the NSAID, aspirin, has the potential to decrease incidence of, or mortality from, a number of cancers through several mechanisms of action (Benamouzig *et al.*, 2012, Goel *et al.*, 2003, Hawley *et al.*, 2012, Li *et al.*, 2015, Patrono *et al.*, 2008, Schror, 2011). However, despite these evidences, long-term use of aspirin has a potential to cause GI toxicity, in particular GI bleeding and peptic ulcer, which have been found to be mostly age-dependent (Laine, 2002, Patrono *et al.*, 2005). The search for potential aspirin-related compounds with the same or better cytotoxic effects against cancer cells accompanied by a safer toxicity profile has been on going over the years, which include, mesalazine (5-aminosalicylic acid) in HCT-116 CRC cells (Gasche *et al.*, 2005), MDC-43 (4-[(diethoxyphosphoryloxy)methyl]phenyl 2-acetoxybenzoate) in colon, liver, pancreas and breast cancer cells (Zhao *et al.*, 2009), NX-4016 (2-(acetoxy)benzoic acid 3-[(nitrooxy)methyl]phenyl ester) in ovarian cancer (Selvendiran *et al.*, 2008), PN517 (fumaroyldiapirin) and PN514 (benzosalin) in SW480 CRC cell line (Claudius *et al.*, 2014, Deb *et al.*, 2011).

The *meta*- and *para*- isomers of aspirin were found to exhibit the same biological profiles from the *ortho*- isomers accompanied with safer profiles in regards to GI toxicity (Kodela *et al.*, 2013). Thus, this chapter includes study in the synthesis, identification and stability profile of *meta*- and *para*- isomers of aspirin and thioaspirin in order to find out if they chemically behave similarly to the *ortho*- form.

3.2 Aims and Objectives

The reason for the work done in this chapter is to confirm that the compounds synthesised match with the structures of aspirin analogues of interest and that the compounds are of acceptable purity and fit for purpose. The stability of these aspirin analogues and rate of breakdown into salicylates was also assessed.

3.3 Methodology

The methodology has been discussed extensively in chapter two (2.2.5 and 2.2.7) of this thesis.

3.4 Results

The results in this chapter comprise of the synthesis of aspirin analogues, the identification and confirmation of their chemical structures, determination of their purity and percentage breakdown into salicylate.

3.4.1 Synthesis of aspirin analogues

PN591 (meta-thioaspirin) and PN592 (para-thioaspirin) were synthesised from 3-mercaptobenzoic acid and 4-mercaptobenzoic acid respectively. The rest of the aspirin analogues were synthesised by Dr. Chris Perry (School of Pharmacy, University of Wolverhampton).

3.4.2 Identification/Confirmation of aspirin analogues structures

NMR and IR spectroscopy were used in combination to confirm the structures and approximate purity of the aspirin analogues synthesised. TLC was used as an additional technique in order to demonstrate that the compounds used in the cell studies were eluting as a single spot, before use.

3.4.2.1 NMR

Nuclear Magnetic Resonance (NMR) was first invented in 1946 and its spectra have been in use within the field of organic chemistry since 1960 (Williams and Fleming, 2008). This method can easily be used to determine chemical structures of compounds without the need of an expert.

^{13}C NMR was carried out on each of the following compounds (Full sized Spectra of compounds can be found in appendix 8.1).

3.4.2.1.1 PN502 (*ortho*-acetoxybenzoic acid/o-acetylsalicylic acid/aspirin)

Aspirin is a very common substance and a standard spectrum is available on the Spectral Database for Organic Compounds Spectral Data Base System (SDBS) from the Japanese National Institute of Advanced Industrial Science and Technology (AIST) (http://sdbs.db.aist.go.jp/sdbs/cgi-bin/cre_index.cgi) for comparison (Figure 3.1). NMR data from in-house PN502 (Figure 3.2) can be favourably compared with data from Figure 3.1.

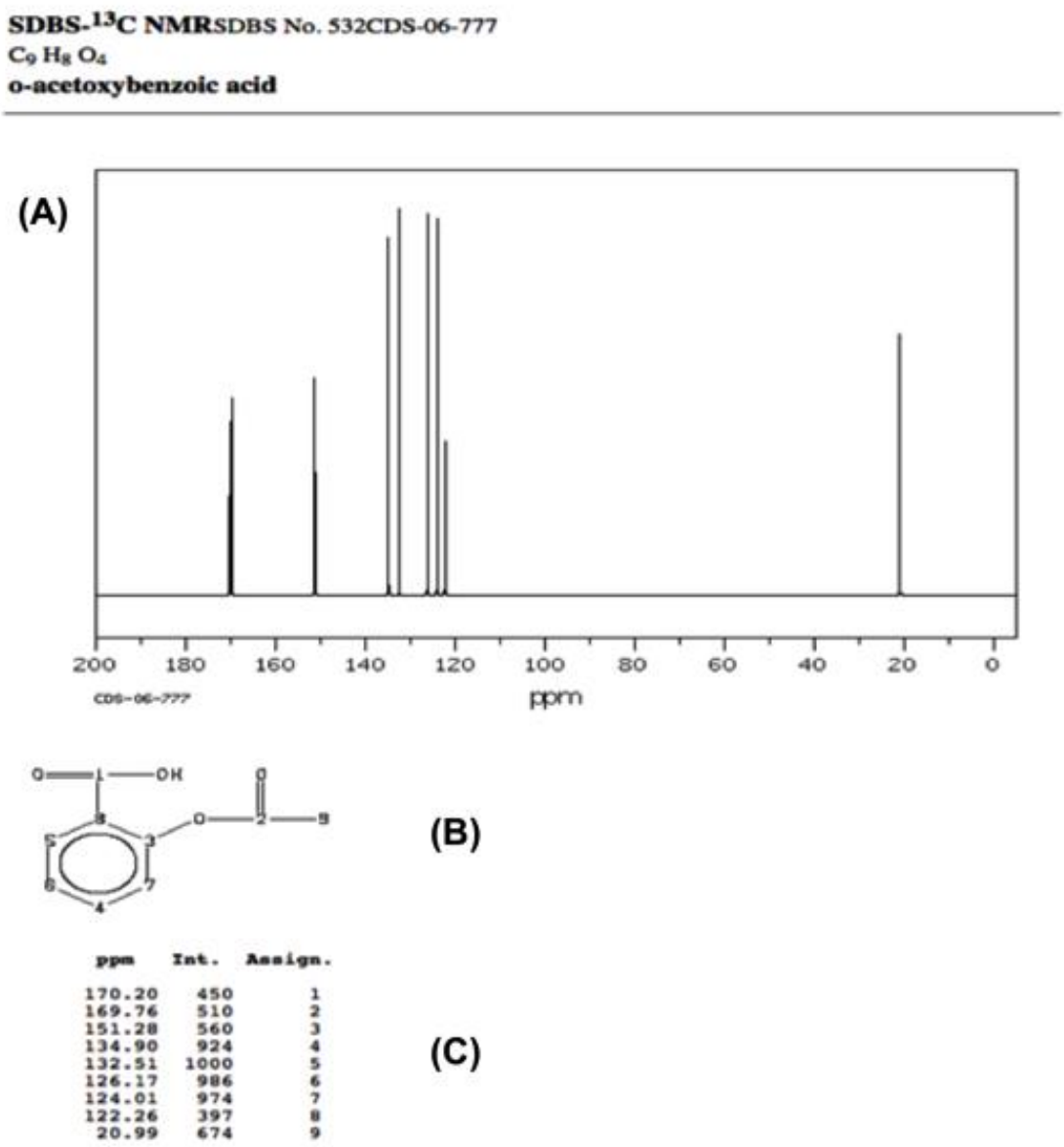

Figure 3.1 NMR Spectrum for o-acetoxybenzoic acid (o-aspirin).
^{13}C NMR spectrum for aspirin (A). Chemical structure and assigned C atom numbering in relation to C peaks on spectrum for interpretation (B) Table for C number assignment and corresponding ppm (C). Molecular Formula: $C_9H_8O_4$, Molecular Weight: 180.2 g/mol. (http://sdbs.db.aist.go.jp/sdbs/cgi-bin/cre_index.cgi).

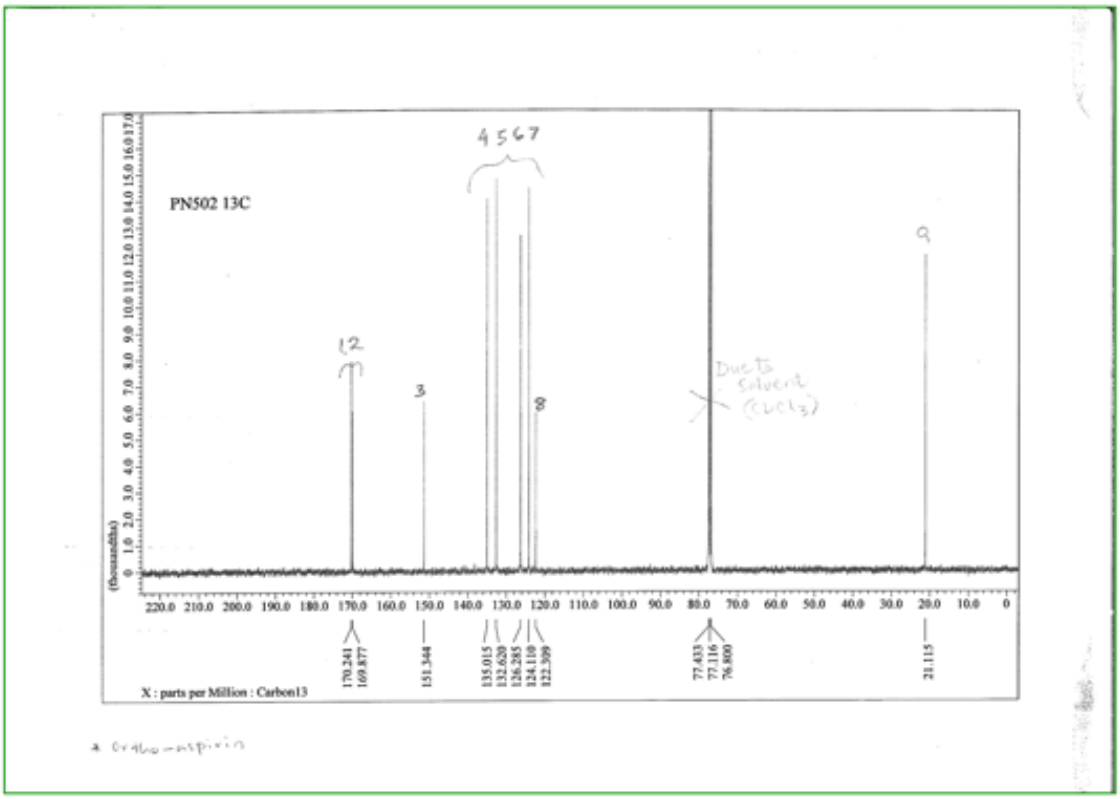

(A)

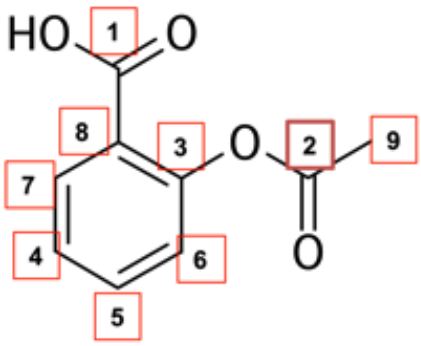

(B)

Assigned number	ppm
1	170.24
2	169.88
3	151.34
4	135.02
5	132.62
6	126.29
7	124.11
8	122.31
9	21.16

(C)

Figure 3.2 ^{13}C NMR PN502.
^{13}C NMR spectrum for PN502 [Appendix figure 8.1] (A). Chemical structure and assigned C atom numbering in relation to C peaks on spectrum for interpretation (B) Table for C number assignment and corresponding ppm (C). Molecular Formula: $C_9H_8O_4$, Molecular Weight: 180.2 g/mol.

This compound has nine carbon (C) nuclei and in comparison with the aspirin spectrum found in the database, shows peak assignments and chemical shifts that are remarkably similar between the two spectra.

On the PN502 ^{13}C NMR spectra, a triplet of peaks are seen at 77 ppm, which is classically due to the carbon nucleus in $CDCl_3$ coupling with deuterium, arising from the deuterochloroform used as the solvent for compound dissolution. This will be excluded from peaks considered in the analysis.

From the spectrum, nine separate C peaks (excluding solvent bands) are seen which confirms the fact that this compound is correct and pure. No impurity carbons are visible in the spectrum shown (appendix 8.1) because each C nucleus should have a different environment and thus a single peak.

3.4.2.1.2 PN508 (Diaspirin)

PN508 is a diaspirin, made up of two aspirin structures joined together at the methyl groups of the acetyl (CH_3CO-) parts of the molecule. It also has nine C environments all similar to that in aspirin with the exception of C9 due to it having a longer carbon chain of $–CH_2CH_2$- instead of CH_3. The NMR data confirm the structure of PN508 (Figure 3.3B).

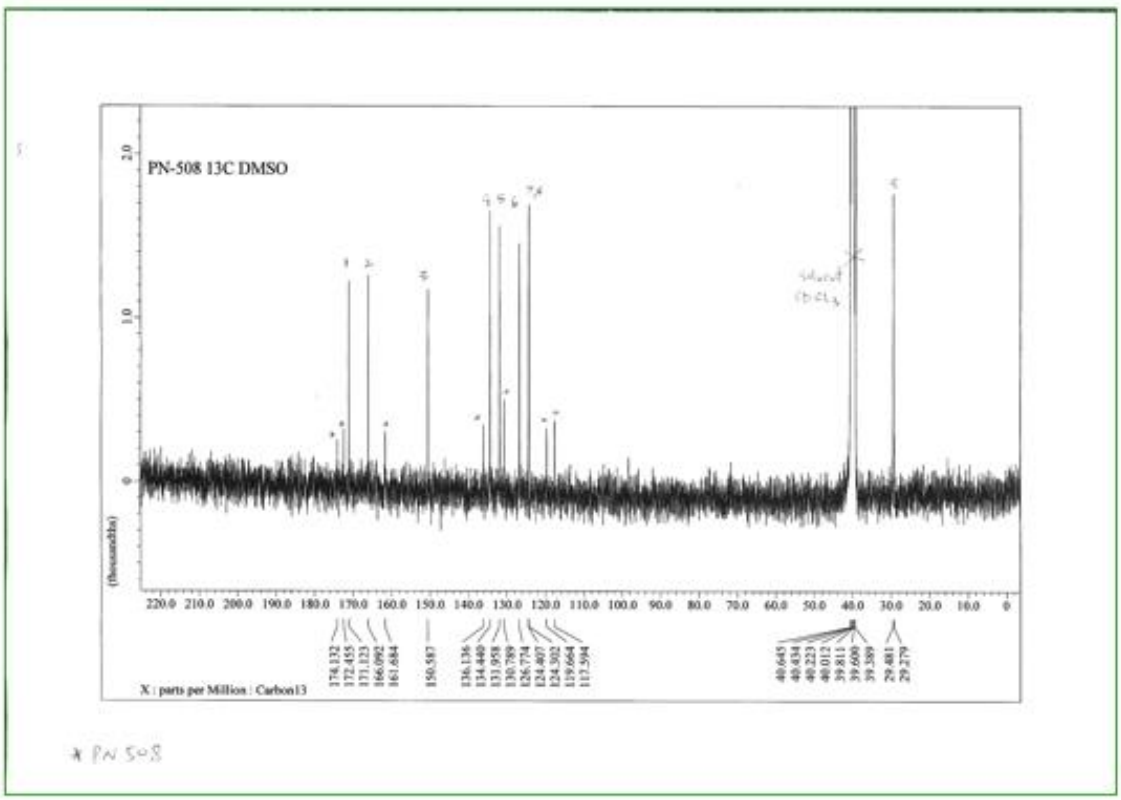

(A)

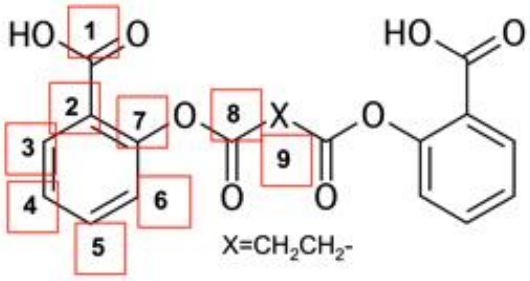

(B)

Assigned number	ppm
1	171.12
2	124.30
3	150.59
4	134.44
5	131.96
6	126.77
7	124.41
8	166.09
9	29.48

(C)

Figure 3.3 ^{13}C NMR PN508.
^{13}C NMR spectrum for PN508 [Appendix Figure 8.2] (A). Chemical structure and assigned C atom numbering in relation to C peaks on spectrum for interpretation (B) Table for C number assignment and corresponding ppm (C). Molecular Formula: $C_{16}H_{14}O_8$, Molecular Weight: 358 g/mol.

3.4.2.1.3 PN517 (Fumaryldiaspirin)

PN517 is also made up two aspirin molecules connected by an alkene grouping (Figure 3.4A).

To analyse this NMR (Figure 3.4A), it is helpful to bisect the molecule at the centre of symmetry and look for the nine C environments. In comparison to the aspirin molecule/chemical structure, two separate C peaks are seen at 165.92 ppm and 163.54 ppm representing the C nucleus at position 1 and 2 respectively of the chemical structure. These are lower than aspirin, which could be due to the electron donating effect of the double bond found in PN517 (X=-CH=CH-).

The peak representing position 3 of the chemical structure can be found at 150.04 ppm as compared to 151.28 ppm in aspirin. C 5 and 6 are found at position 132.03 ppm and 127.24 ppm respectively on the spectrum. This leaves us with C 4 and 7, which appear as two single peaks at 134.43 ppm and 134.58 ppm at peak 4 and 124.34 ppm and 124.64 ppm at peak 7. The C 9 in aspirin is now an alkene C, which shifts completely away from the 21 ppm methyl position to a position between 110 ppm and 140 ppm. This is thus at the 134 ppm region close to C 4. At the 124 ppm region, C 7 and 8 can be seen. C 8 has shifted from 122.26 ppm in aspirin to either 124.34 ppm or 124.64 ppm. Thus, 9 C peaks have been accounted for (Figure 3.4A).

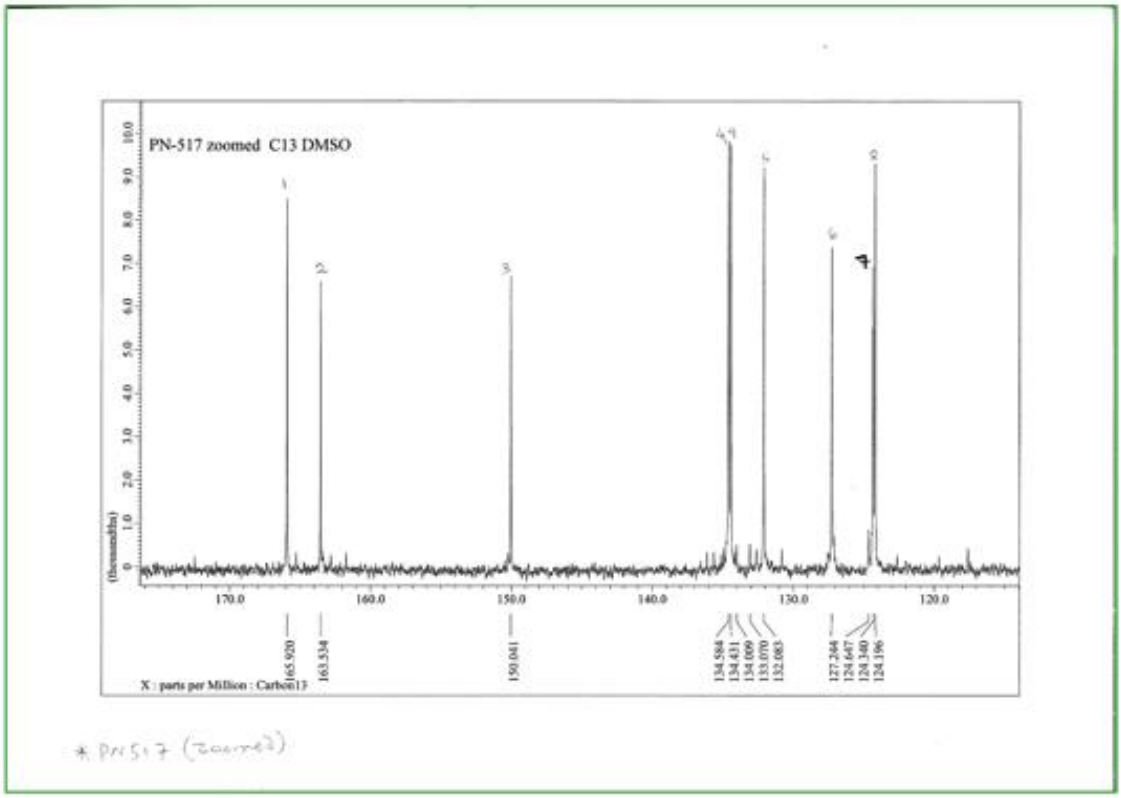

(A)

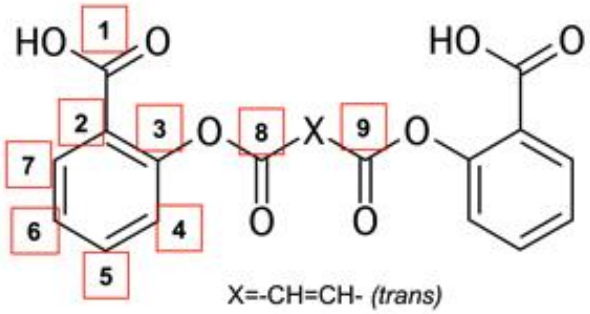

Assigned number	ppm
1	165.92
2	124.34/124.64
3	150.04
4	134.43/134.58
5	132.08
6	127.24
7	124.34/124.64
8	163.54
9	134.43/134.58

(B) **(C)**

Figure 3.4 ^{13}C NMR PN517.
^{13}C NMR spectrum for PN517 [Appendix Figure 8.3] (A). Chemical structure and assigned C atom numbering in relation to C peaks on spectrum for interpretation (B) Table for C number assignment and corresponding ppm (C). Molecular Formula: $C_{16}H_{12}O_8$, Molecular Weight: 356 g/mol.

3.4.2.1.4 PN548 (*meta*-aspirin)

The difference between PN548 and aspirin is that PN548 has got the carboxylic group attached -*meta* position of the benzene ring (Figure 3.5B).

The large signals seen at 77 ppm are due to the solvent $CDCl_3$ (deuterochloroform) (Figure 3.5A). Comparing this spectrum to that of aspirin, signals 1 and 2 can be seen at 171.19 and 169.32 represent the two C contained in the carboxylic groups (C=O). They are probably more apart than in aspirin because of the lack of H-bonding between the two groups seen in aspirin. This is because in PN548, the groups are too far apart to interact with each other. The ring C with the ester (acetoxy) group falls at 150.75 ppm and two of C atoms appear as having a weaker signal compared to the others (signal 3 and 4). This is because they both do not have a hydrogen (H) atom attached to them and this phenomenon is a consequence of the Nuclear Overhauser effect (NOE) (Williams and Fleming, 2008). The other four C atoms attached to the ring appear between 129.68 and 123.53 ppm.

The C atom carrying the acetyl group ($-CH_3$) appears at 21.14 ppm, which is almost the same frequency as 20.99 ppm in aspirin.

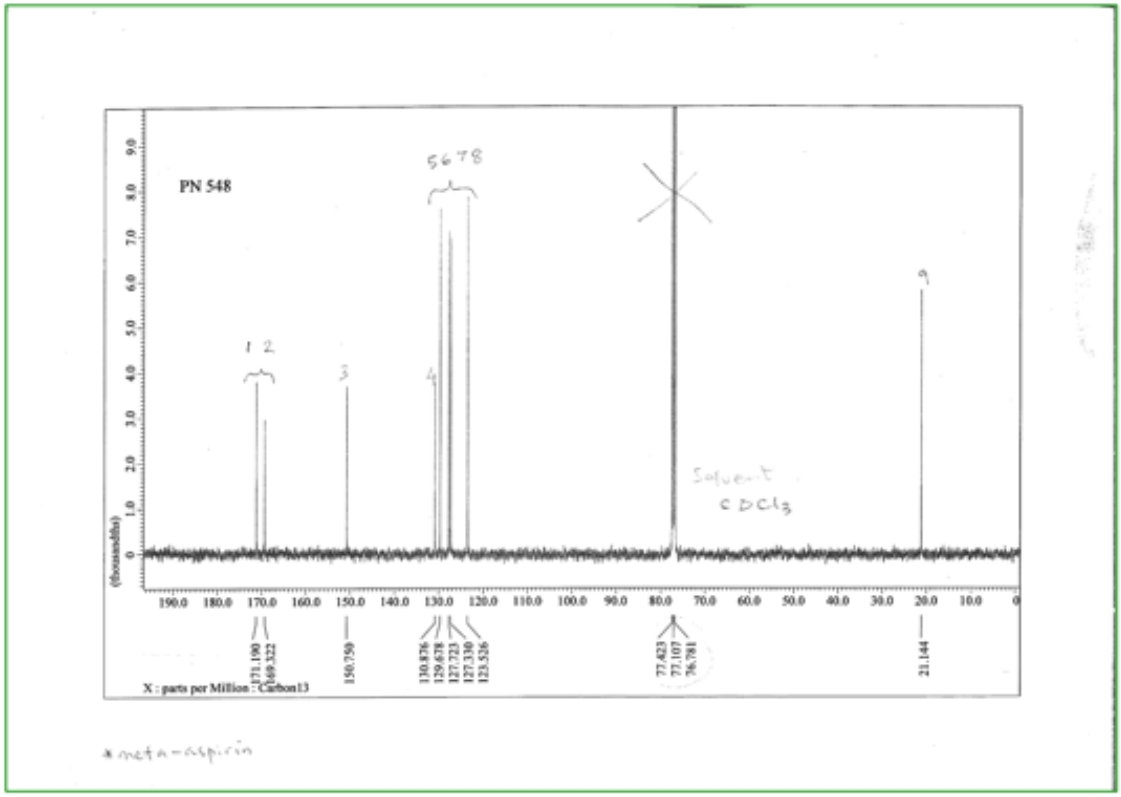

(A)

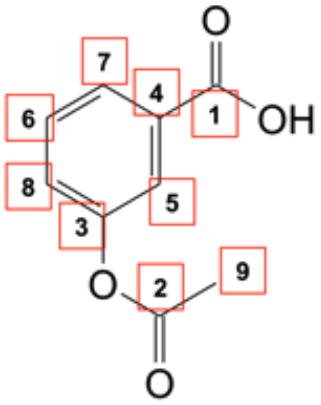

(B)

Assigned number	ppm
1	171.19
2	169.32
3	150.75
4	130.88
5	129.68
6	127.72
7	127.33
8	123.53
9	21.14

(C)

Figure 3.5 ^{13}C NMR PN548.
^{13}C NMR spectrum for PN548 [Appendix Figure 8.4] (A). Chemical structure and assigned C atom numbering in relation to C peaks on spectrum for interpretation (B) Table for C number assignment and corresponding ppm (C). Molecular Formula: $C_9H_8O_4$, Molecular Weight: 180.2 g/mol.

3.4.2.1.5 PN549 (*para*-aspirin)

Here, the carboxylic group is attached to the benzene ring at the *para*- position (Figure 3.6B).

In PN549 chemical structure, the two C atoms ortho- to the carboxyl group and the two C atoms meta- to the carboxyl group are equivalent. This results in an extra symmetry and due to this we expect to see only seven and not nine signals on the spectrum (Figure 3.6A). At C 7 with the methyl group, which corresponds to C 9 in aspirin, the signal appears at 21.25 ppm. The two C=O signals are clearly visible at 171.31 ppm and 168.96 ppm. The ring C bearing the $–CH_3COO$ group at position 3 appears at 155.06 and because it has no H atoms (quarternary C) attached to it, the signal is seen to be small. C 5 is also a quartenary C at 126.88 ppm. Due to equivalence peaks at 131.96 ppm and 121.85 ppm each represent 2 Cs at positions 4, 4‘ and 6, 6‘ respectively.

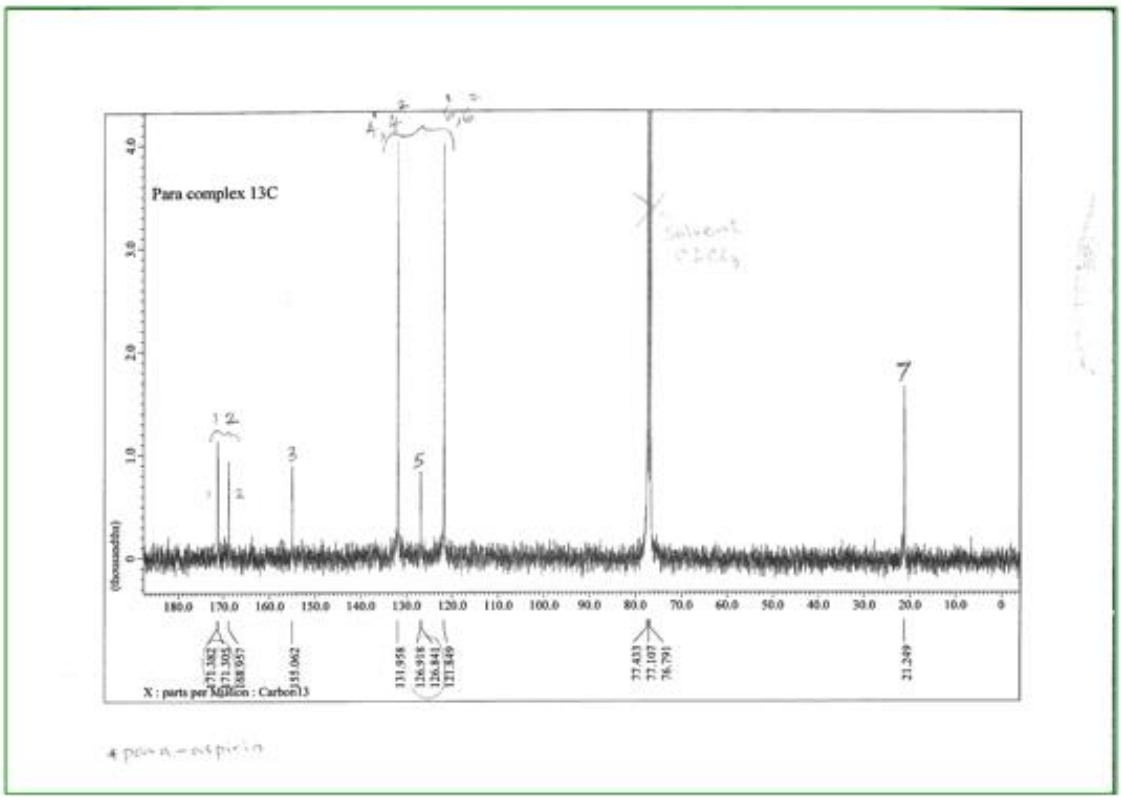

(A)

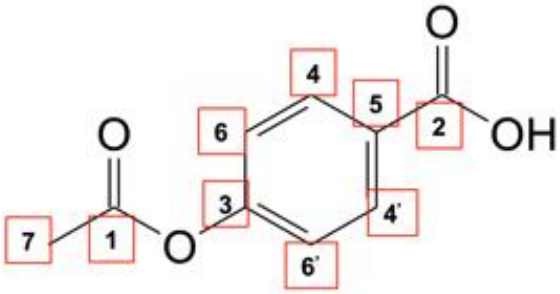

Assigned number	ppm
1	171.31
2	168.96
3	155.06
4	131.96
4'	131.96
5	126.88
6	121.85
6'	121.85
7	21.25

(B) (C)

Figure 3.6 ^{13}C NMR PN549.
^{13}C NMR spectrum for PN549 [Appendix Figure 8.5] (A). Chemical structure and assigned C atom numbering in relation to C peaks on spectrum for interpretation (B) Table for C number assignment and corresponding ppm (C). Molecular Formula: $C_9H_8O_4$, Molecular Weight: 180.2 g/mol.

3.4.2.1.6 PN590 (*ortho*-thioaspirin)

The chemical structure for o-thioaspirin has a sulfur (S) atom attached to the C=O instead of an oxygen (O). Nine peaks should be expected with nine different C environments (Figure3.7B).

The peak at 171.48 ppm represents C 1 and is pretty much the same as in aspirin (170.24 ppm) while the peak at C 2 has shifted significantly to a lower field (bigger ppm) at 193.27 ppm. The significant change is because the C atom has become much more deshielded because of the S atom not feeding electrons to the C=O group as well as the O ester in aspirin. Sulfur has got a higher nuclear charge and so shifts the C down the spectrum. C 3 is attached to S instead of O found in aspirin. This accounts for the shift away from 151.28 ppm to 132.66 ppm. C 3 to C 8 fall between 129 ppm and 137 ppm. The attachment to S atom also accounts for the shift of C 9 (methyl group) from 21 ppm to 30.45 ppm. The peak at 77 ppm indicates the $CDCl_3$ solvent used. No impurity peaks are evident in the spectrum (Figure 3.7A).

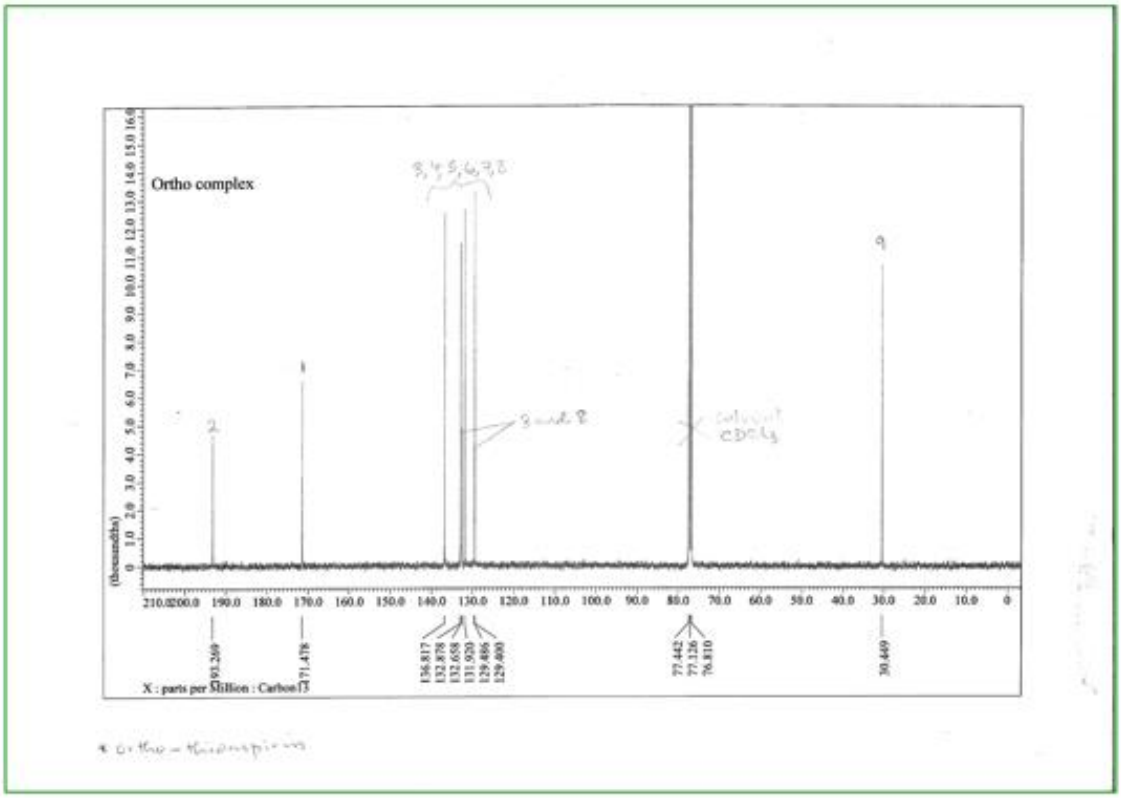

(A)

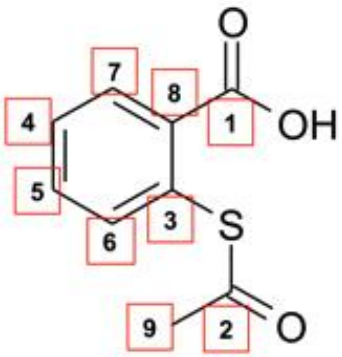

(B)

Assigned number	ppm
1	171.48
2	193.27
3	132.66
4	136.82
5	132.88
6	131.92
7	129.49
8	129.40
9	30.45

(C)

Figure 3.7 ^{13}C NMR PN590.
^{13}C NMR spectrum for PN590 [Appendix Figure 8.6] (A). Chemical structure and assigned C atom numbering in relation to C peaks on spectrum for interpretation (B) Table for C number assignment and corresponding ppm (C). Molecular Formula: $C_9H_8O_3S$, Molecular Weight: 196 g/mol.

3.4.2.1.7 PN591 (*meta*-thioaspirin)

The S group is attached at the *meta*- position of the benzene ring (Figure 3.8B). Here also nine peaks representing nine separate C environments are expected to be seen in the spectrum.

Similar to o-thioaspirin, the C at position 1, 2 and 9 fall at the same position in the spectra. However, there are distinct differences at C positions 3 to 8 with C 3 and 8 showing a smaller signal due to its attachment to the $–SCOCH_3$ and –COOH groups respectively and thus, are quartenary Cs. Their peaks appear at 130.43 and 128.88 ppm. C 4, 5, 6 and 7 come at 139.85, 136.16, 131.19 and 129.46 although hard to ascertain each C environment to its individual peak. The peak indicating the solvent $CDCl_3$ used is seen at 77 ppm (Figure 3.8A).

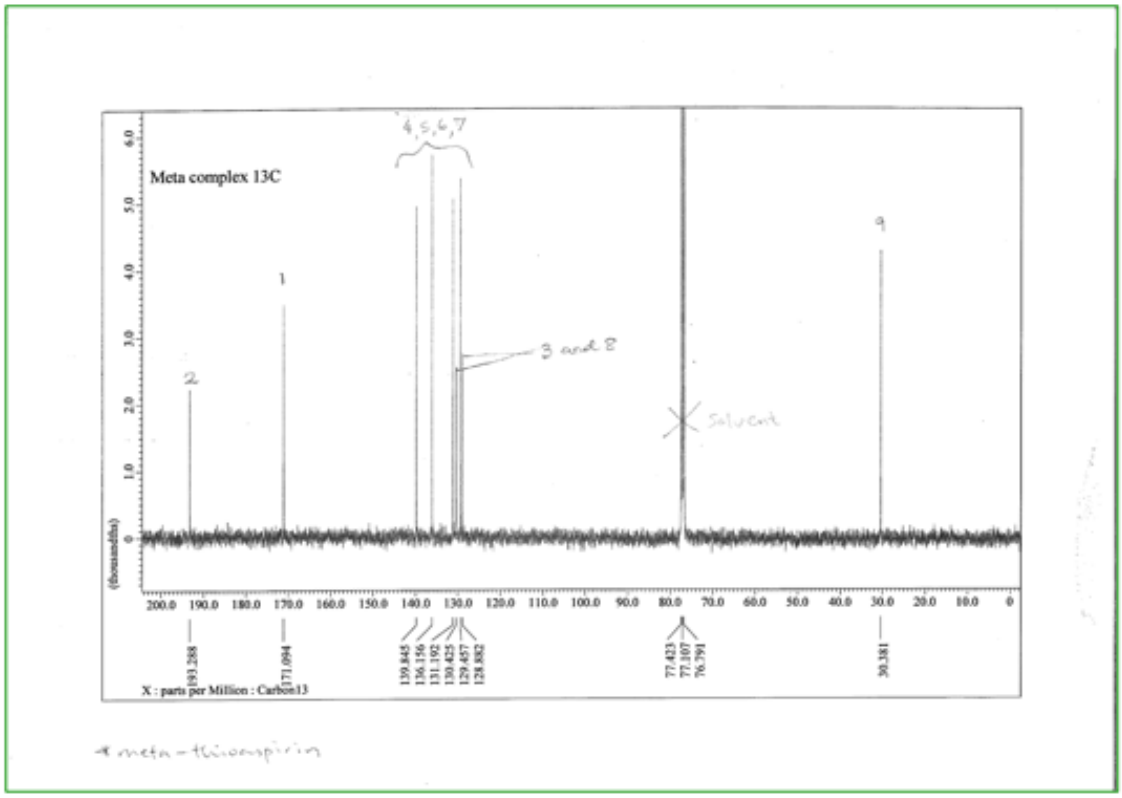

(A)

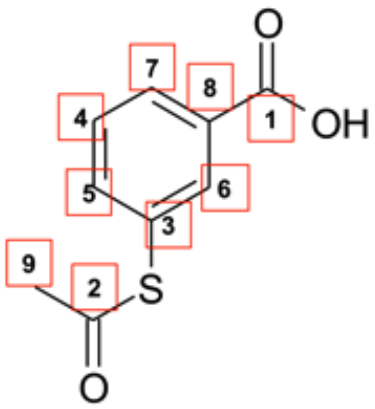

(B)

Assigned number	ppm
1	171.09
2	193.29
3	130.43
4	139.85
5	136.16
6	131.19
7	129.46
8	128.88
9	30.38

(C)

Figure 3.8 ^{13}C NMR PN591.
^{13}C NMR spectrum for PN591 [Appendix Figure 8.7] (A). Chemical structure and assigned C atom numbering in relation to C peaks on spectrum for interpretation (B) Table for C number assignment and corresponding ppm (C). Molecular Formula: $C_9H_8O_3S$, Molecular Weight: 196 g/mol.

3.4.2.1.8 PN592 (*para*-thioaspirin)

The S group is attached to the *para*- position of the benzene ring (Figure 3.9B). Similar to PN549 (Figure 3.6A), only seven peaks are expected because of the extra symmetry of the *para* isomer.

Two peaks representing the C=O group; C 2 at 192.62 ppm for the thioester and C 1 at 166.74 ppm for the COOH nucleus. The relative positions of these are for the same reason as PN590 and PN591.

In comparison to the aspirins, here the thioester group is significantly deshielded at the C=O carbon due to S being a poorer electron donor than O. The four ring C environments show peaks at 134.20 ppm (C 4 and 4'), 132.97 ppm (C 3), 131.54 ppm (C 6) and 129.94 ppm (C 5 and 5'). The two substituted ring C nuclei (C 3 and C 6) show as small peaks because they are quatenary C atoms while the unsubstituted ring C nuclei appear as larger peaks (C 4, 4', 5, 5') because there are two C nuclei in each band and they have a H attached. The only remaining peak is C 7 representing the methyl C nucleus of the acetyl group. This was observed to shift upfield to about 30 ppm in PN590 and PN591. The same is observed for PN592 at 30.45 ppm (Figure 3.9A).

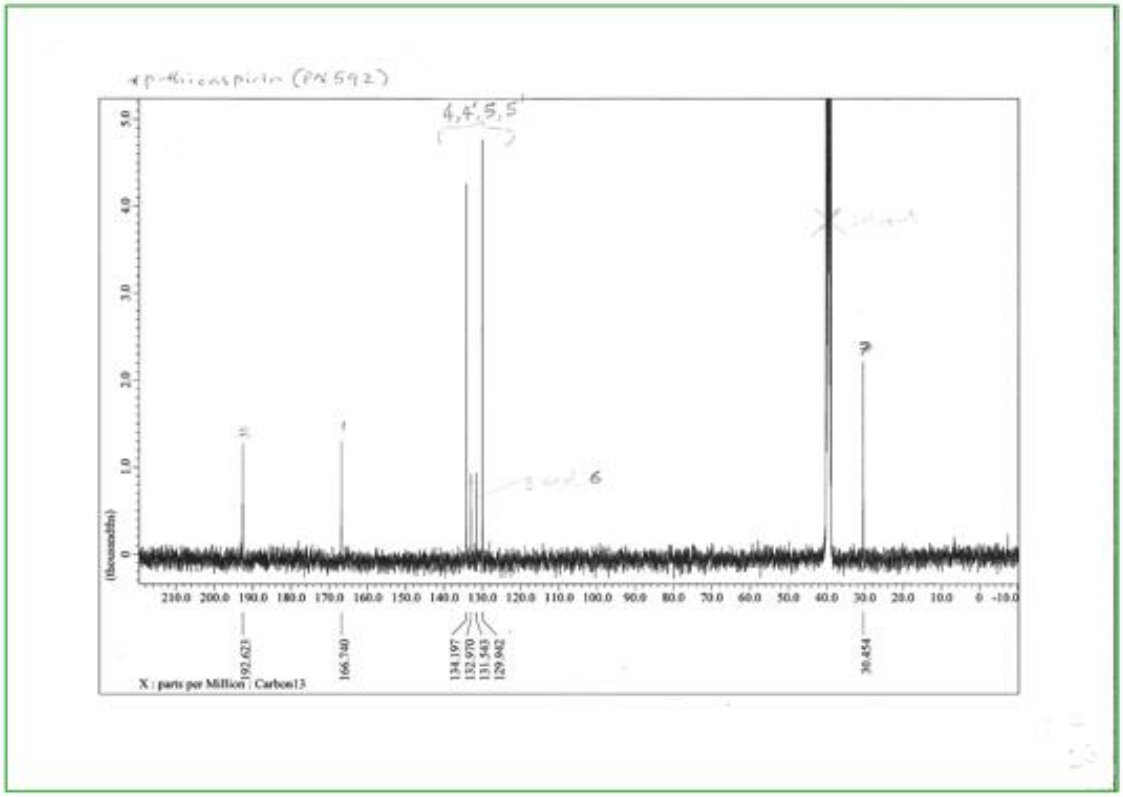

(A)

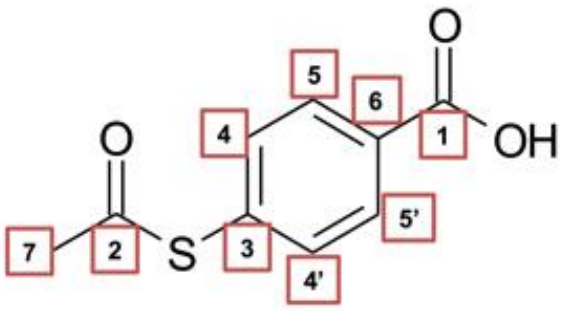

Assigned number	ppm
1	166.74
2	192.62
3	132.97
4	134.20
4'	134.20
5	129.94
5'	129.94
6	131.54
7	30.45

(B)

(C)

Figure 3.9 ^{13}C NMR PN592.
^{13}C NMR spectrum for PN592 [Appendix Figure 8.8] (A). Chemical structure and assigned C atom numbering in relation to C peaks on spectrum for interpretation (B) Table for C number assignment and corresponding ppm (C). Molecular Formula: $C_9H_8O_3S$, Molecular Weight: 196 g/mol.

3.4.2.2 IR

IR spectra involve the movement of nuclei between vibrational energy levels. To enable identification, many functional groups have characteristic vibration frequencies. This method is a simple, quick and reliable method for identifying functional groups in chemical compounds (Williams and Fleming, 2008).
An IR correlation chart (https://chem.libretexts.org/Reference/Reference_Tables/Spectroscopic_Parameters/Infrared_Spectroscopy_Absorption_Table) was used to interpret the bands and stretches on the spectra. Spectra of compounds can be found in appendix 8.2 [Appendix Figures 8.9 to 8.21].

Key to band intensities: w = weak band, m = medium band, s = strong band. BA = Benzoic acid. str = stretch.

Product ID	OH/SH stretch (Phenol/thiol) / cm^{-1}	OH stretch (Carboxylic acid) / cm^{-1}	C=O stretch Ester / cm^{-1}	C=O stretch Carboxylic acid / cm^{-1}	C=C stretch (Alkene) Aromatic / cm^{-1}	Notes
PN502	-	≈3390-2180	1752 (s)	1680 (s)	1604 (m)	
PN508	-	≈3300-2200	1762 (s)	1681 (s)	1607 (m)	
PN517	-	≈3470-2170	1738 (s)	1685 (s)	[≈1575 (w)] 1607 (m)	
PN548	-	≈3400-2200	1758 (s)	1675 (s)	1584 (m)	
PN549	-	≈3500-2200	1754 (s)	1677 (s)	1602 (m)	
PN590	-	≈3380-1960	1694 (s)	1676 (s)	1582 (m)/1565 (m)	Overlapping C=O str
PN591	-	≈3380-1990	1685 (s)	1685 (s)	1593 (m)/1573 (m)	Overlapping C=O str
PN592	-	≈3380-1950	1683 (s)	1683 (s)	1592 (m)/1566 (m)	Overlapping C=O str
Salicylic acid	3230 (OH) (m)	≈3500-1760	-	1656 (s)	1608 (m)	
Thiosalicylic acid	2520 (SH) (m)	≈3300-1750	-	1672 (s)	1586 (m)/1562 (m)	
3-Hydroxy-BA	3330 (OH) (m)	≈3500-1800	-	1680 (s)	1596 (m)	
4-Hydroxy-BA	3510 (OH) (m)	≈3600-1950	-	1670 (s)	1606 (m)/1594 (m)	
3-Mercapto-BA	2548 (SH) (m)	≈3300-2000	-	1678 (s)	1598 (w)/1572 (m)	
4-Mercapto-BA	2555 (SH) (m)	≈3280-1950	-	1670 (s)	1592 (m)/1564 (m)	

Table 3.1 IR interpretation of aspirin analogues and their precursor compounds. All spectra recorded on neat powdered samples using a Genesis II ATR FTIR Spectrometer.

From the IR table (Table 3.1), it can be seen that the appropriate functional groups have been identified in the samples synthesised thus, confirming that they are indeed the compounds of interest.

A hydroxyl (–OH) group (4000-3000 cm^{-1}) belonging to carboxylic acid, C=O group also part of carboxylic acid (1870-1540 cm^{-1}) and the C=C (alkene) bonds found in aromatic rings (1670-1600 cm^{-1}) have been identified for all of the compounds which is very much expected.

The C=O group as part of the ester group (1870-1540 cm^{-1}) has been identified in all but the precursor compounds. This also concurs with the chemical structure of the compounds (Table 3.3).

A distinct feature of the precursor chemical compounds is the presence of a thiol (-SH) or –OH group which gets acetylated to a –S and –O producing final products of the compounds of interest.

Last but not least are the thioaspirins with a distinctive feature of having their two C=O group stretches (1870-1540 cm^{-1}) overlapping each other (Appendix 8.13, 8.14 and 8.15). As seen on the table (Table 3.1), only the thioaspirins exhibited this feature.

The differences in the IR specrtra of the precursor compounds from their final products confirms that the precursor have been successfully converted into the aspirin analogues of interest. And when coupled to NMR evidence there is little doubt that this is the case.

3.4.3 Purity of aspirin analogues synthesised

3.4.3.1 TLC

Thin Layer Chromatography (TLC) and melting point (Table 3.3) was used in this chapter to assess the presence of impurities in the compounds synthesised and to also find out if the product compound is different from the precursor compound.

Precursor compound	R_f	Product compound	R_f
SA	1.0	PN502	0.8
3HBA	0.8	PN548	0.9
4HBA	0.6	PN549	0.7
TSA	0.9	PN590	0.8
3MBA	0.9	PN591	0.8
4MBA	0.7	PN592	0.6
SA	0.9	PN517	0.4

Table 3.2 R_f value of aspirin analogues and their respective precursors with solvent system hexane:ethylacetate:acetic acid [65:30:5 (v/v)].
The precursors with their corresponding product compounds. Aspirin, Salicylic acid (SA), *meta*-aspirin (PN548), 3-hydoxybenzoic acid (3HBA), *para*-aspirin (PN549), 4-hydroxybenzoic acid (4HBA), *ortho*-thioaspirin (PN590), thiosalicylic acid (TSA), *meta*-thioaspirin (PN591), 3-mercaptobenzoic acid (3MBA), *para*-thioaspirin (PN592), 4-mercaptobenzoic acid (4MBA), fumaryldiaspirin (PN517).

Using qualitative appearance of the spots on the TLC plates, the precursors are clearly different from the product compound. The PN502 is light grey in appearance (Figure 3.10A) and has R_f value of 0.8 (Table 3.2). This is clearly different from the blue spot of SA (Figure 3.10A) with 1.0 as its R_f value (Table 3.2).

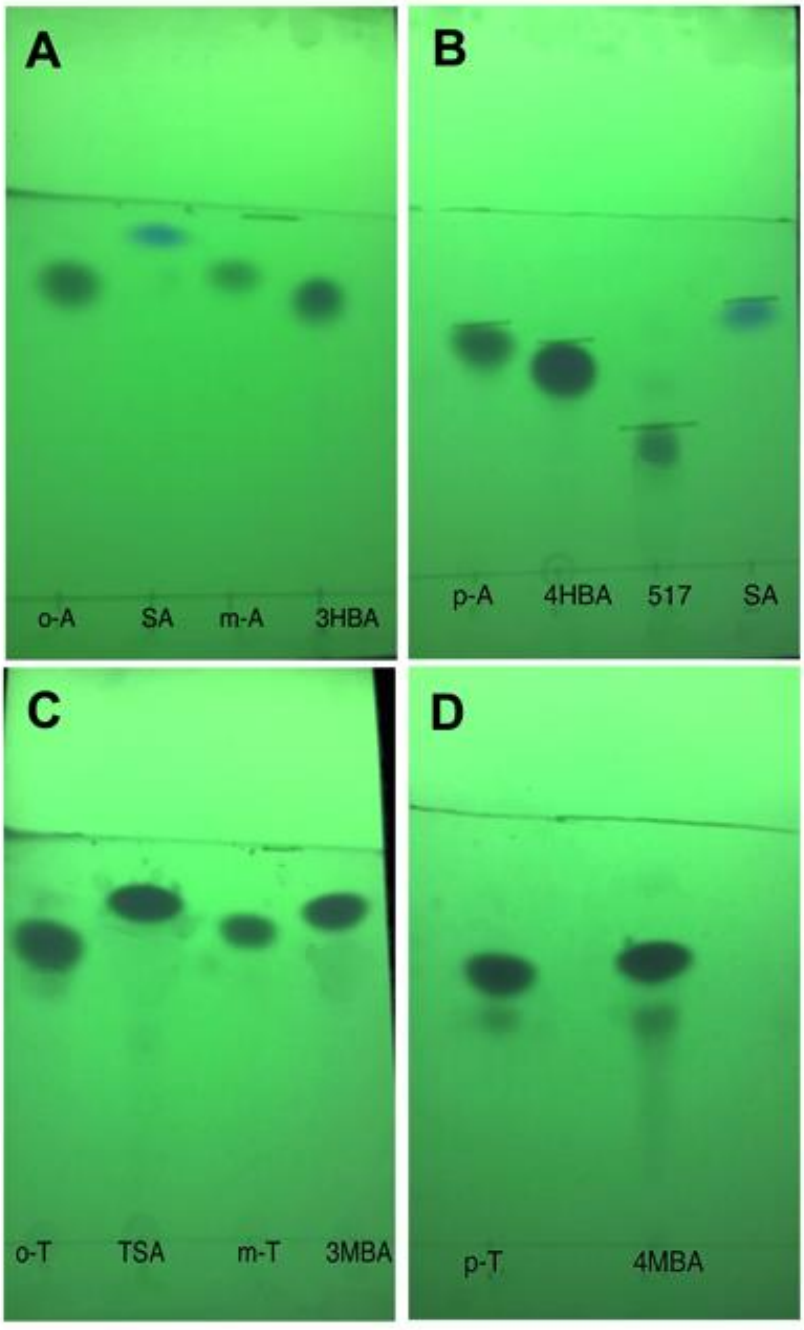

Figure 3.10 TLC of aspirin analogues assessing purity.
Samples were chromatographed on silica-coated plates developed with hexane/ethylacetate/acetic acid (65:30:5, v/v), and the spots were visualised under UV254 light. Separation and detection of aspirin (o-A), Salicylic acid (SA), PN548 (m-A) and 3-hydroxybenzoic acid (3HBA) (A). Separation and detection of PN549 (p-A), 4-hydroxybenzoic acid (4HBA), PN517 (517) and SA (B). Separation and detection of PN590 (o-T), Thiosalicylic acid (TSA), PN591 (m-T) and 3-mercaptobenzoic acid (3MBA) (C). Separation and detection of PN592 (p-T) and 4-mercaptobenzoic acid (4MBA) (D).

PN548 appears as a light grey spot (Figure 3.10A) with R_f value of 0.9 (Table 3.2) while its precursor, 3HBA appears as a darker shade of grey with R_f value of 0.8 (Table 3.2). PN549 spot colour appeared as grey and its precursor compound as a charcoal grey (Figure 3.10B). R_f values for PN549 and 4HBA are 0.7 and 0.6 respectively (Table 3.2). PN517 appeared as a light grey spot against a blue spot for its precursor, SA (Figure 3.10B) with 0.4 and 0.9 as their respective R_f values. TSA and 3MBA appear as darker spots than their respective product compounds, PN590 and PN591 (Figure 3.10C). The R_f value was 0.9 for TSA and 3MBA; and 0.8 for PN590 and PN591 (Table 3.2). PN592 spot appeared as the same colour shade as that of its precursor 4MBA (Figure 3.10D) with the distinguishing difference between the two being the R_f value of 0.6 and 0.7 respectively (Table 3.2). Both PN592 and 4MBA appear as multiple spots (Figure 3.10D). The multiple spots could be due to impurities in the precursor compound, which was commercially purchased, that have also been transferred to the product compound PN592.

In summary, salicylic acid shows up as blue (Figure 3.10A and 3.10B), but the aspirin analogues (Figure 3.10A, 3.10B, 3.10C and 3.10D) are all shades of grey varying from quite pale for PN517 to deep grey-almost charcoal for 4-MBA. This is probably due, partly, to loading on the plate as well as natural colour variation.

Note also that one of the commercial samples (4MBA in Figure 3.10D) show significant amounts of impurity and is not a single spot. The ‘in-house’ synthesised compounds are pretty good by comparison.

3.4.3.2 Melting point analysis

The melting point of compounds was determined using the Stuart® SMP 10 melting point apparatus. The individual melting points taken all correlate with the melting points in the literature with the exception of PN592, whose melting point was lower (Table 3.3) than that found in the literature indicating presence of impurities stemming from the precursor compound, 4MBA (Figure 3.10D).

ID number	Chemical name	Structure	Molecular weight (g/mol)	Melting point (°C)	TLC	IR	NMR
PN502	ortho-aspirin [2-acetoxybenzoic acid]	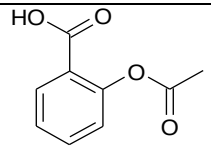	180	134-136		✓	
PN548	meta-aspirin [3-acetoxybenzoic acid]	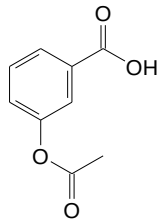	180	132-134 Lit. 129-131 (Edwin *et al*., 1942)		✓	
PN549	para-aspirin [4-acetoxybenzoic acid]	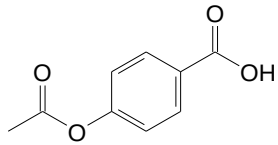	180	183-185 Lit. 188.7-189.4 (Nelander, 1964)		✓	
PN590	ortho-thioaspirin [2-acetylthiobenzoic acid]	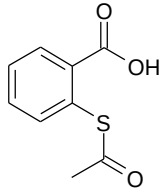	196	122-125 Lit. 125.5-126 (Nelander, 1964)		✓	
PN591	meta-thioaspirin [3-acetylthiobenzoic acid]	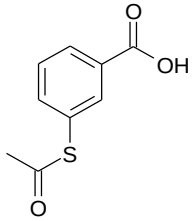	196	153-156 Lit. 152-153 (Bordwell, 1956)		✓	

PN592	para-thioaspirin [4-acetylthiobenzoic acid]	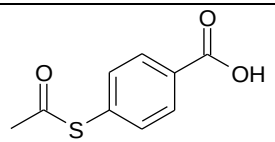	196	189-190 Lit. 202.8-203.6 (Nelander, 1964)		✓	
PN517	fumaryldiaspirin, F-DiA [bis-(2-carboxyphenyl) fumarate]	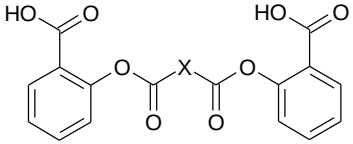 X= -CH=CH- (*trans*)	356	190-192 Lit. 178-180 (Zaugg *et al.*, 1980)		✓	
PN508	diaspirin, DiA [bis-(2-carboxyphenyl) succinate]	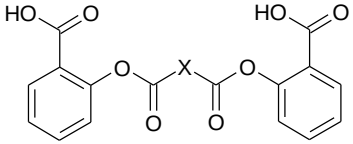 X= -CH_2-CH_2-	358	169-171 Lit. 160-165 (Aldrich)			✓
PN524	m-bromobenzoylsalicylate [(3-bromobenzoyl)salicylic acid]	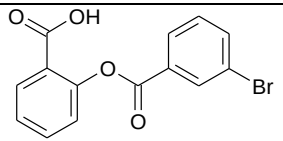	321	Lit. 140-142 (Claudius *et al.*, 2014)		✓	
PN528	benzosalin, [methyl-bromobenzoylsalicylate]	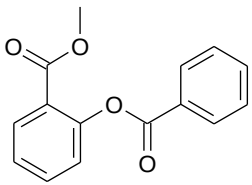	256	84-86 Lit. 83.8-84 (Claudius *et al.*, 2014)		✓	
PN529	Isopropyl (3-bromobenzoyl)salicylate	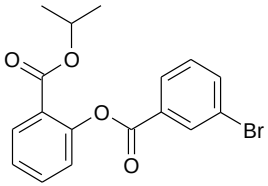	363	Lit. 49-51 (Claudius *et al.*, 2014)		✓	

Table 3.3 Structure and Properties of aspirin analogues. Lit. (Literature), ✓ = Analysis carried out on compounds.

3.4.4 Stability/Breakdown of aspirin analogues

3.4.4.1 Salicylic Acid Analysis

The salicylic acid analysis assay was based on fluorescence enhancement of the As (III)-salicylic acid system (Karim *et al.*, 2006).

3.4.4.1.1 Dilution Curve for Salicylic Acid

A dilution curve was plotted for SA and aspirin boiled in the presence of sodium hydroxide (NaOH) for 1 h in order to hydrolyse aspirin into salicylic acid. SA caused fluorescence in a concentration dependant manner within the concentrations used. Aspirin was without effect. Alkaline hydrolysis of aspirin, caused by boiling for 1 h in the presence of NaOH caused quantitative cleavage of aspirin, as determined by the curve overlaying the SA standard curve (Figure 3.11). The purpose of this dilution curve is to make sure that the assay is robust enough.

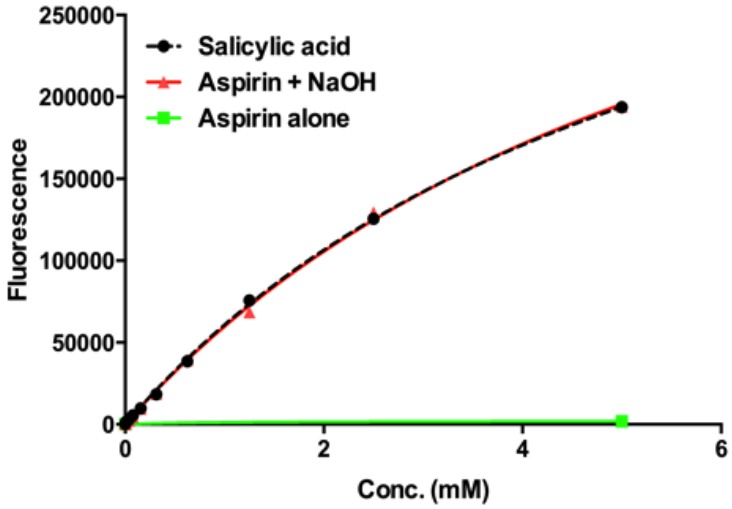

Figure 3.11 Standard curve for salicylic acid detection using the As(III)-SA system.
SA, aspirin broken down into salicylic acid when boiled with NaOH for 1 h and aspirin alone were serially diluted (from 5mM) in wells and fluorescence taken at 315 nm excitation and 408 nm emission wavelenghths.

The standard curve shows that the assay is specific for salicylic acid and does not react with aspirin (Figure 3.11).

To further test the robustness of the assay, the fluorescence reading of different concentrations of salicylic acid (SA) was taken at different time points.

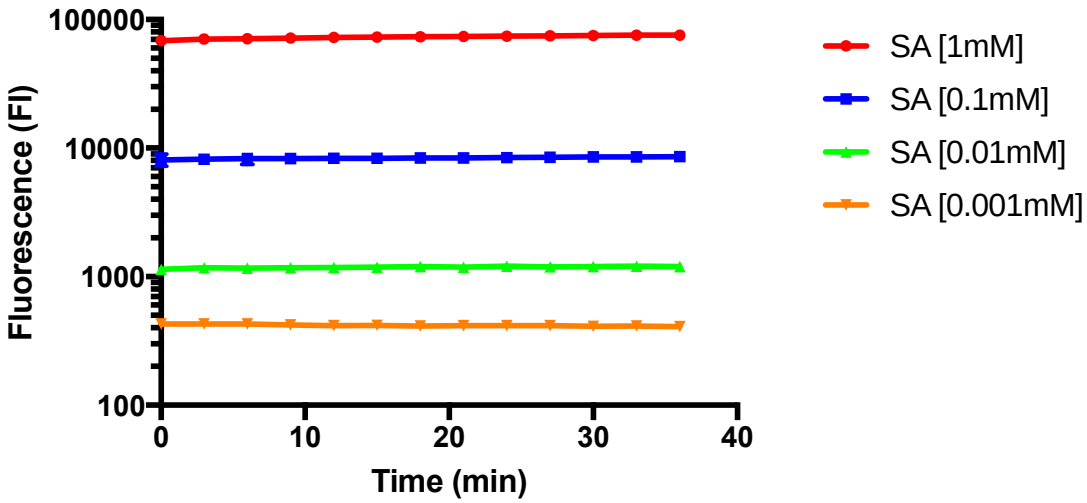

Figure 3.12 Fluorescence reading of salicylic acid (SA) at different time points. Twelve time points were taken every 3 min. Fluorescence scale is at Log_{10}.

The fluorescence reading for SA remained constant for over 30 min when assessed at four different concentrations (Figure 3.12). Thus, indicating a robust assay for measuring salicylic acid.

A major setback that was encountered with this assay is its reducing property. The reducing property of the assay rendered it insensitive to most of the compounds in this study, which also possess reducing characteristics. This assay was only sensitive to PN502, PN517 and PN548. The reason for its insensitivity to PN549 is unclear.

3.4.4.1.2 Assessment of breakdown of compounds into salicylic acid using salicylic acid assay

Aspirin is hydrolysed into SA, also known as 2-hydroxybenzoic acid as soon as it enters the circulatory system (Elliot Cham *et al.*, 1982, Karim *et al.*, 2006). The serum concentration of SA is found to be 20-30 times higher than aspirin after 5 min of administration with aspirin being 20 times more potent (Higgs *et*

al., 1987). The aspirin analogues used in this chapter have been observed to exert their antiproliferative effect when cells were treated for 48 h. It was therefore, rational to study and observe the rate at which they metabolise to salicylic acid during this duration of treatment. In this case the supernatant cell media was used to assess the percentage of SA present after 48 h because levels of intracellular SA was difficult to measure using the As (III)-SA system.

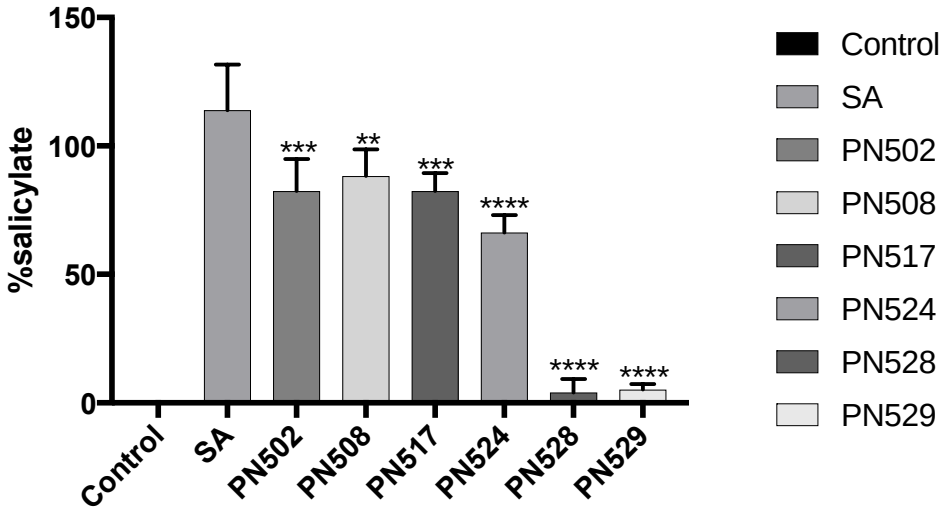

Figure 3.13 Percentage of salicylic acid (SA) produced by aspirin analogues. SW480 cells were treated at 1 mM of aspirin analogues for 48 h at 37°C. Control contains no compound, SA [salicylic acid], PN502 [ortho-aspirin], PN508 [diaspirin], PN517 [fumaryldiaspirin], P524 [m-bromobenzoylsalicylate], PN528 [methyl(benzoylsalicylate](benzosalin) and PN529 [isopropyl(m-bromobenzoylsalicylate)]. The other compounds not included in this figure did not show any sensitivity to the SA analysis. Data plotted as mean ± SEM (*n=5*), $^{**}p<0.01$, $^{***}p<0.001$,$^{****}p<0.0001$.

PN528 and PN529 showed the least amount of SA (Figure 3.13), which indicates that they are not easily metabolised into SA. Although PN502 and PN517 showed some level of SA after 48 h, the levels were still significantly different from the positive control (SA). If PN502 and PN517 metabolised into same levels of SA after 48 h (Figure 3.13), was it also at the same rate? This prompted a comparison between PN502 and PN517 of the rate of breakdown into salicylate with time.

The reading for salicylate was therefore measured for PN502 and PN517 at nine time points for duration of 90 min.

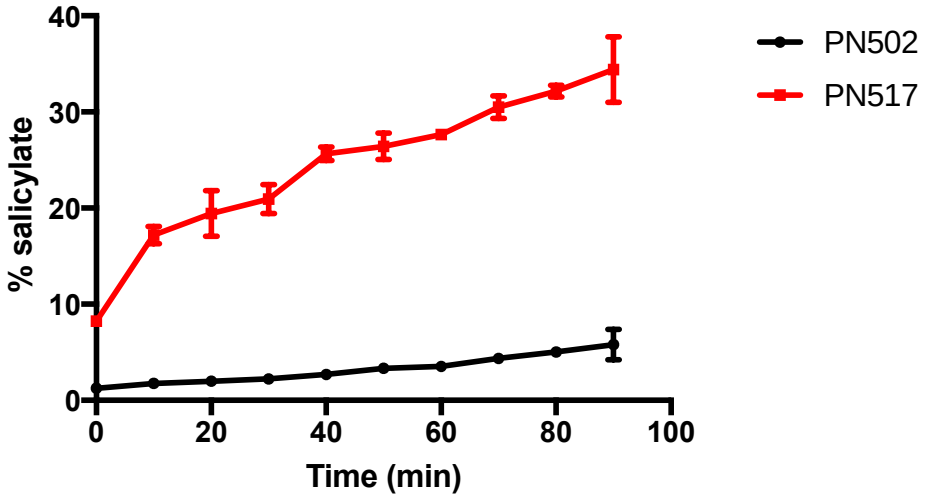

Figure 3.14 Percentage of salicylic acid (SA) produced by aspirin analogues.
SW480 cells were treated with 1mM of PN502 [aspirin] and PN517 [fumaryldiaspirin] for 90 min at 37°C. Readings were taken every 10 min using the As (III)-SA system.

Results show for PN517, metabolism slows down with time. The rate of breakdown of PN517 into SA is seen to be much higher than PN502 (Figure 3.14) because it appears to be metabolised to the same level of SA after 48 h (Figure 3.13) but then PN517 appearing to be metabolised into higher levels of

SA than PN502 for the first 90 min. However, metabolism into SA is still significantly different from SA alone after 48 h (Figure 3.13).

Due to this salicylic acid analysis being insensitive to thioaspirins and para-aspirin, it was decided to use a different approach in investigating the breakdown of the mentioned aspirin analogues. The approach taken was TLC.

3.4.4.1.3 Assessment of breakdown of compounds using TLC

TLC of supernatant containing compounds of treated cells was run against salicylates (precursors) of the aspirin analogues. Prior to spotting, the supernatant was acidified using conc. HCl after which ether was added in order to extract the compounds of interest (ether layer). Ether layers containing aspirin (o-A), PN548 (m-A), PN549 (p-A), PN590 (o-T), PN591 (m-T) and PN592 (p-T) were named S1, S2, S3, S4, S5 and S6 respectively.

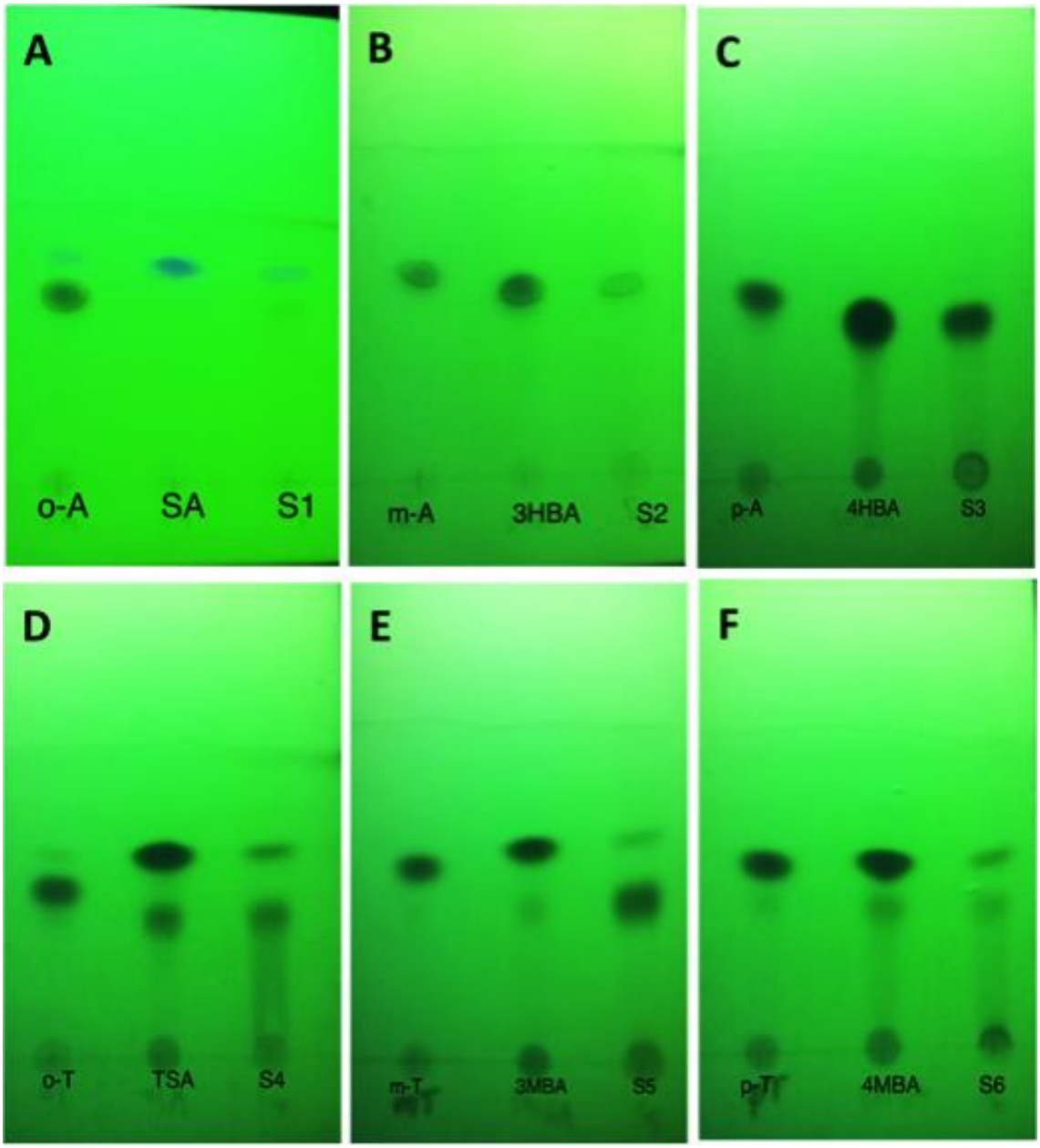

Figure 3.15 TLC of aspirin analogues against their salicylates and extracts (S). Samples were chromatographed on silica-coated plates developed with hexane/ethylacetate/acetic acid (65:30:5, v/v), and the spots were visualised under UV254 light. Separation and detection of PN502 (o-A), Salicylic acid (SA) and extract of supernatant media of cells after treatment with PN502 (S1) (A). Separation and detection of PN548 (m-A), 3-hydroxybenzoic acid (3HBA) and extract after treatment with PN548 (S2) (B). Separation and detection of PN549 (p-A), 4-hydroxybenzoic acid (4HBA) and extract after treatment with PN549 (S3) (C). Separation and detection of PN590 (o-T), Thiosalicylic acid (TSA) and extract after treatment with PN590 (S4) (D). PN591 (m-T), 3-mercaptobenzoic acid (3MBA) and extract after treatment with PN591 (S5) (E). Separation and detection of PN592 (p-T), 4-mercaptobenzoic acid (4MBA) and extract after treatment with PN592 (S6) (F).

The spot for PN502 appears to be black in colour with its precursor, SA as blue and closer to the solvent front. Extract S1 appears to be made up of SA due to the colour and distance from the solvent front being the same as in SA (Figure 3.15A). Extract S2 appears to have the same R_f value as 3HBA, which suggests that PN548 has broken down into its salicylate (Figure 3.15B). Extract S3 also share the same R_f value as the salicylate of PN549, 4HBA (Figure 3.15C). Extract S4 show two spots suggesting that PN590 has been broken down into two compounds, which corresponds to the separation into two spots by TSA (Figure 3.15D). For PN591, the extract, S5 appears to be about 10% of the salicylate, 3MBA and 90% of something else which could be a dimer (Figure 3.15E). The same effect is seen with PN592 with the extract and salicylate both separating into two spots suggesting two different compounds (Figure 3.15F).

3.4.4.1.4 Stability of PN502

In order to carry out experiments/assays using these aspirin analogues, knowledge of their stability in solution is of utmost importance. PN502 was used as a ‘benchmark’ to find out the relative stability of these compounds at room temperature (RT), at +4°C and at -20°C.

PN502 dissolved in acetone at 50mM was stored at RT, +4°C and -20°C for 24 h and the level of salicylic acid measured from each sample.

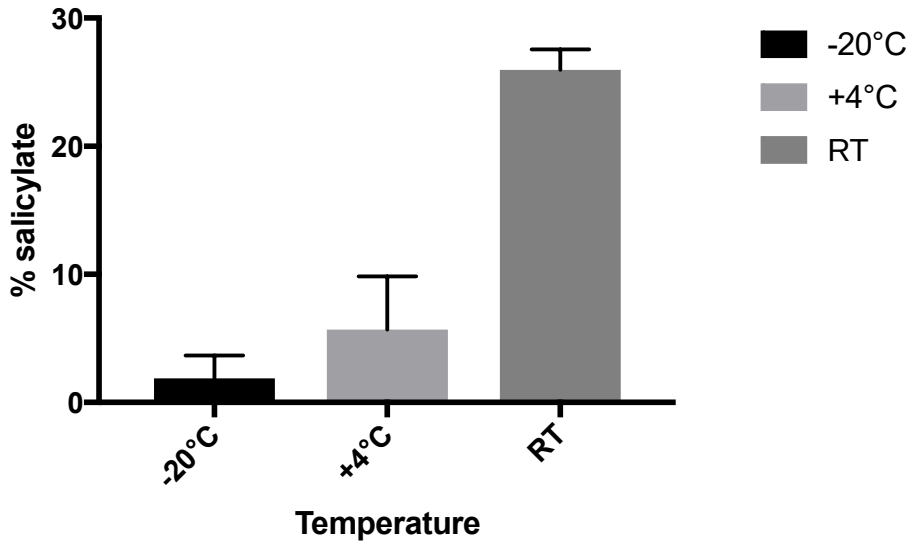

Figure 3.16 Salicylate formation from PN502 in solution at different storage conditions.
PN502 was dissolved in acetone and stored at the temperature stated for 24 h before testing for the presence of SA using the As (III)-SA system. Data are from n=3 performed in duplicate. Error bars represent SEM.

Using the SA assay, over 20% of PN502 had been hydrolysed to SA when in solution in acetone and kept at RT for 24 h. At +4°C, hydrolysis was slowed down and only about 5% was hydrolysed to salicylic acid and about 2% was hydrolysed when stored at -20°C (Figure 3.16).

3.5 Discussion

The aspirin analogues synthesised were identified and chemical structure verified using NMR spectroscopy (Figure 3.1 to 3.9) in combination with IR spectroscopy (Table 3.1). In order to make sure that the compounds were free of impurities, an assessment was made using TLC (Table 3.2 and Figure 3.10) where it was observed that the compounds of interest separated as a single spot distinct from the precursor salicylate compound with the exception of PN592 of which even its commercially bought precursor, 3MBA (Figure 3.10D)

showed significant amounts of impurity. Melting point was also used to assess the state of purity for these compounds and found to be close to the readings given in literature (Table 3.3). Signs of impurities present in the PN592 sample can also be confirmed by the melting point which was low at 189-190°C (Table 3.3) as compared to the melting point found in the literature as a reference point (202.8-203.6°C). However, the other 'in-house' synthesised compounds show high purity. The rate and extent of hydrolysis or breakdown of these compounds were studied using a newly developed salicylic acid assay based on a published paper (Karim *et al.*, 2006). The assay was also tested for its sensitivity to SA and robustness (Figure 3.11 and 3.12) before commencing with the aspirin analogues of interest (Figure 3.13). It was observed that PN528 and PN529 were the least affected by hydrolysis with only about 5% metabolised to SA. PN502 and PN517 were metabolised quantitatively at the same level to SA, which raised the question to whether this hydrolysis was also at the same rate. Assessment of the rate of hydrolysis at nine time points suggested that PN517 is hydrolysed at a faster rate than PN502 (Figure 3.14). A major set back was encountered in that the assay developed is enhanced by the reducing property of As(III) to the salicylic system (Karim *et al.*, 2006) and so thioaspirins due to their reducing property could not be used in this assay. Thioaspirins have a sulfhydryl group attached to their benzene rings which reacts with As(III) and reduces it (Scott *et al.*, 1993) thereby rendering the assay null and void.

Thus, TLC was adopted to assess the breakdown of the thioaspirins into their respective thiosalicylate forms (Figure 3.15). In PN502, the hydroxyl bond (-OH)

is more strongly bonded to the carboxy group as compared to its affinity to the TLC plate (Watson, 2005). This is why its distance from the solvent front is more than that of Salicylic acid, thus, moves at a slower rate as compared to its meta- and para- isomer. It was observed that the extracts for the cells treated with thioaspirins separated into two spots, as the salicylates. Thiols are known to lose a proton above a given pH, this being relevant to the biological system, which leads to the formation of disulphide bonds (Rowland *et al.*, 2011). An increase in pH leads to a 50% oxidation to 2-2'-disulfanediyldibenzoic acid (2,2'-DSBA), which contains a disulphide bond/bridge (Rowland *et al.*, 2011). However, the experimental conditions differ. There might be a formation of disulphide bonds by 3MBA and 4MBA (Rowland *et al.*, 2010), which explains the multiple spots for the extracts observed on the TLC plate. The oxidation of thioaspirins is likely to make the products more polar.

Using PN502 as a 'benchmark' (Figure 3.16), it can be said that these aspirin analogues are not very stable when in solution especially at RT (Kim *et al*., 2013) and as such are always freshly prepared before each experiment.

The aspirin analogues synthesised were thus declared fit for use in experimental studies.

Chapter 4. Cytotoxicity and Synergy of Aspirin analogues with platinum compounds

4.1 Introduction

The discovery of a positive effect of aspirin on CRC (Kune *et al.*, 1988) was a stepping stone for the study of aspirin on various cancers. Evidence later emerged that indeed the daily intake of aspirin reduced mortality (Rothwell *et al.*, 2011), incidence and metastasis of CRC (Algra and Rothwell, 2012). These discoveries geared studies carried out on the effects caused by aspirins in different cancers (Drew *et al.*, 2016, Nan *et al.*, 2015, Thorat and Cuzick, 2015).

4.1.1 Cytotoxicity of Aspirin analogues

The cell line primarily used in this study was the SW480 CRC cell line, which has been well characterized by Leibovitz *et al.,* (1976) and more recently genetically characterized (Ahmed *et al.*, 2013) . The cell line was isolated from the primary adenocarcinoma in the colon of a 50-year-old Caucasian male (Ahmed *et al.*, 2013, Leibovitz *et al.*, 1976). The cells are polygonal in shape with microvilli on their cell surfaces when viewed under an electron microscope (Leibovitz *et al.*, 1976) with an intermediate growth rate (Ahmed *et al.*, 2013). They are also known to be hyperdiploid and a low producer of CEA and are considered a good candidate for experimental studies in CRC research (Leibovitz *et al.*, 1976).

The SW480 cell line is DNA MMR proficient (Din *et al.*, 2004) and thus a good model for the study of changes involved in the progression of late CRC (Hewitt *et al.*, 2000). Semi quantitative analysis reveals the SW480 cell line to express low levels of COX1 and undetectable levels of COX2 (Li *et al.*, 2001, Richter *et al.*, 2001), thus making it a good model for the study of mechanism of action of compounds following COX-independent pathways.

The cytotoxicity of aspirin and its analogues have been reported in various cancers (Claudius *et al.*, 2014, Din *et al.*, 2004, Gurpinar *et al.*, 2013). In this study, it has been found out that aspirin and several synthesised novel analogues have cytotoxic effects on the SW480 cell line and oesophageal cancer cell lines OE33 and FLO1.

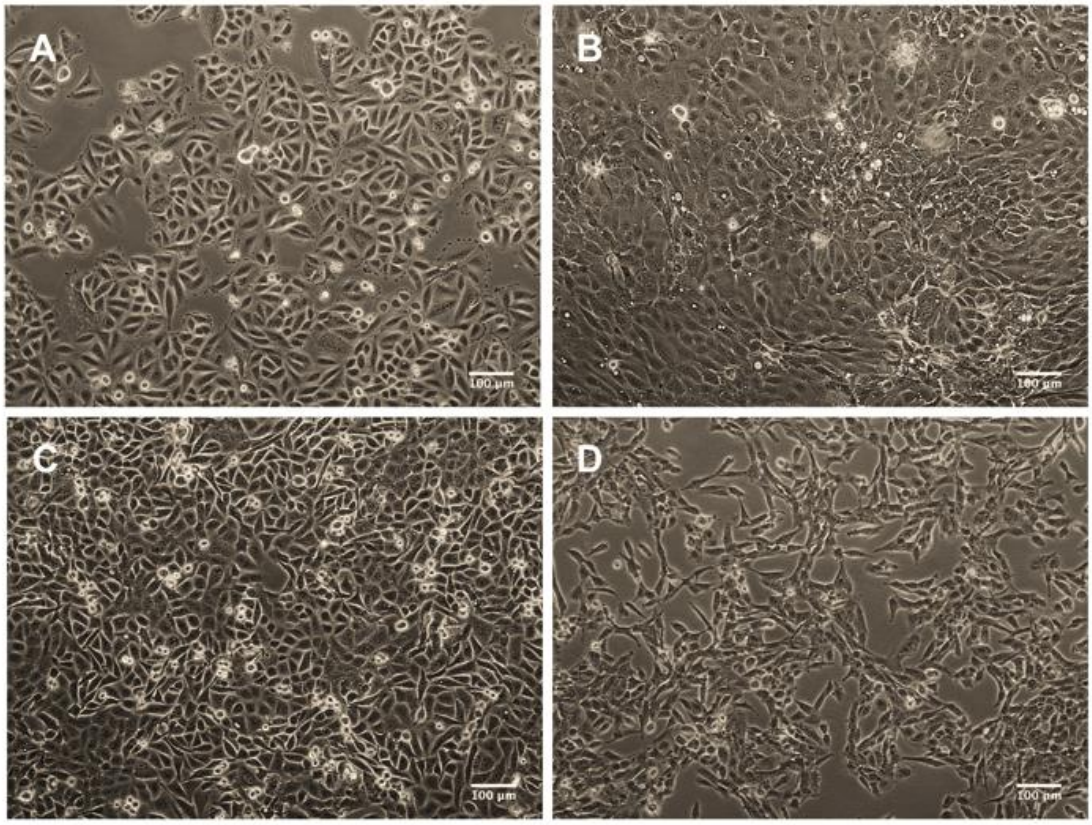

Figure 4.1 Morphology of the cell lines used in this study.
SW480 CRC cell line (A), OE33 Oesophageal cell line (B), FLO1 Oesophageal cell line (C) and U251 MG tumour cell line. Phase Contrast images of cell lines taken at 100X Magnification. Bar scale is at 100 µm.

4.1.2 Synergy

The adaption of combined therapy using several active ingredients to produce a desired effect in the treatment of different diseases by both traditional and modern medical practitioners (Foucquier and Guedj, 2015) dates back thousands of years when the Chinese and African herbalists used a combination of naturally occurring herbs to treat ailments (Odugbemi *et al.*, 2007, Yuan and Lin, 2000). One of the reasons behind the increased interest in the development of combination therapies can be attributed to the enhanced understanding that cancer as a disease involves the disruption of different

molecular pathways, which are all connected and better tackled with the combined action of two or more drugs (Podolsky and Greene, 2011, Zimmermann *et al.*, 2007). Another reason for the increased interest in combination therapy is the desire to achieve therapeutic effects at reduced doses, which will result in toxicity reduction and also delay or minimize the induction of drug resistance (Chou, 2010). Drug combination therapy has increased in popularity for the treatment of complicated diseases such as cancer and AIDS (Chou, 2006).

Synergy can be defined as the greater effect for drugs in combination than in the simple additive effect produced by each drug individually (Foucquier and Guedj, 2015). For example, 1+1 should be >2 for a synergistic effect while an antagonistic effect is less than an additive effect (Foucquier and Guedj, 2015). The term 'combination index' (CI) is used to quantitatively depict synergism (CI<1), additive effect (CI=1) or antagonism (CI>1) (Chou and Talalay, 1984).

With emphasis on the treatment of CRC involving platinum compounds, oxaliplatin has been used in several combinations with other drugs. As far back as 1992, a study was published on the effects that resulted from the combination of oxaliplatin, folinic acid and 5-FU with an objective response from 58% of the patients (Levi *et al.*, 1992). FOLFOX was later introduced which comprises of 5-FU, folinic acid (leucovorin) and oxaliplatin, which resulted in a high response rate in CRC patients (Andre *et al.*, 2009, de Gramont *et al.*, 1997). Bevacizumab, a VEGF antagonist is also used in combination with FOLFOX, the oxaliplatin-containing regimen in the treatment of metastatic CRC

and has produced promising results (Saltz *et al.*, 2008). EGFR antagonists, cetuximab or panitumumab have also produced improved response rates when used in combination with FOLFOX in patients harbouring the *KRAS* gene mutation (Alcindor and Beauger, 2011). Unfortunately, these combinations do not improve overall survival (Bendell *et al.*, 2017, Saltz *et al.*, 2008).

Oxaliplatin, as part of a neoadjuvant chemotherapy regimen is administered to CRC patients in order to shrink tumours before surgery/main treatment (Andre *et al.*, 2004, Yang *et al.*, 2016). However resistance to oxaliplatin is an encroaching menace especially in cancers that harbour a mutation of the *TP53* gene of the tumour suppressor protein p53 (Lowe *et al.*, 1993). p53 as a transcription factor acts as guard to the cell in response to stress signals and is responsible for the regulation of the cell cycle (Brown *et al.*, 2009) and several metabolic enzymes, which are in turn responsible for drug metabolism (Lowe *et al.*, 1993, Yang *et al.*, 2016). For example, mutations found in the *TP53* gene affect cytochrome P450, an enzyme involved in the metabolism of drugs such as oxaliplatin (Lee *et al.*, 2008, Yang *et al.*, 2016), thereby leading to resistance. It was therefore aimed to establish whether these aspirin analogues used in combination with platinum compounds could have an effect in either a synergistic, additive or antagonistic manner.

4.1.2.1 Terminologies and plots used in the interpretation of drug combination results

There are certain terminologies and graph plots used to interpret whether a certain combination of drugs result in synergy, additive effect or antagonism. They include CI, which has been earlier mentioned, an isobologram, which is "a graph with equipotency sum of doses" (Chou, 2006), Fa-CI and Fa-DRI plots. The Fa-CI plot (Figure 4.2A) is a graph showing the CI of each combination in relation to the fraction affected (Fa), which means the growth inhibitory effect of each drug [Fa = 1 − (%growth／100)] (Bijnsdorp *et al.*, 2011). Isobologram is a plot that indicates synergism, antagonism or additive effect depending on whether the data points fall on the left, right or on the curve (Chou, 2006). Chou (2006) further explains that if the data points fall on the left side, right side or on the curve, the combination is synergistic, antagonistic or additive respectively (Figure 4.2B). Another plot found in both the CalcuSyn and CompuSyn software is the Fa-dose-reduction index (Fa-DRI) plot (Figure 4.2C). As alluded before, one of the main reason for synergistic studies is to develop drug combinations with desired effects at reduced doses in order to decrease toxicity effects (Chou, 2006). The dose-reduction-index, DRI>1 indicate favourable dose-reduction while DRI<1 indicate unfavourable dose-reduction. For example (Table 4.1), Fa=0.5 means at 50% inhibition of cell proliferation;

Fa	**Dose A**	**Dose B**	**DRI A**	**DRI B**
0.5	3.7260	4.1938	3.2163	3.5924

Table 4.1 Example of a DRI Data for Drug Combination involving drugs A and B.

For a 50% inhibition of cell growth, 3.7 μM of drug **A** and 4.2 μM of **B** is required. However, 3.2163-fold less **A** plus 3.5924-fold less **B** is required to achieve the same 50% inhibition at the chosen combination ratio (i.e., 3.7260 μM/3.2163 = 1.1585 μM of drug **A** plus 4.1938 μM/3.5924 = 1.1674 μM of drug **B**).

CI values can also be interpreted as descriptive words or by symbols (Table 4.2).

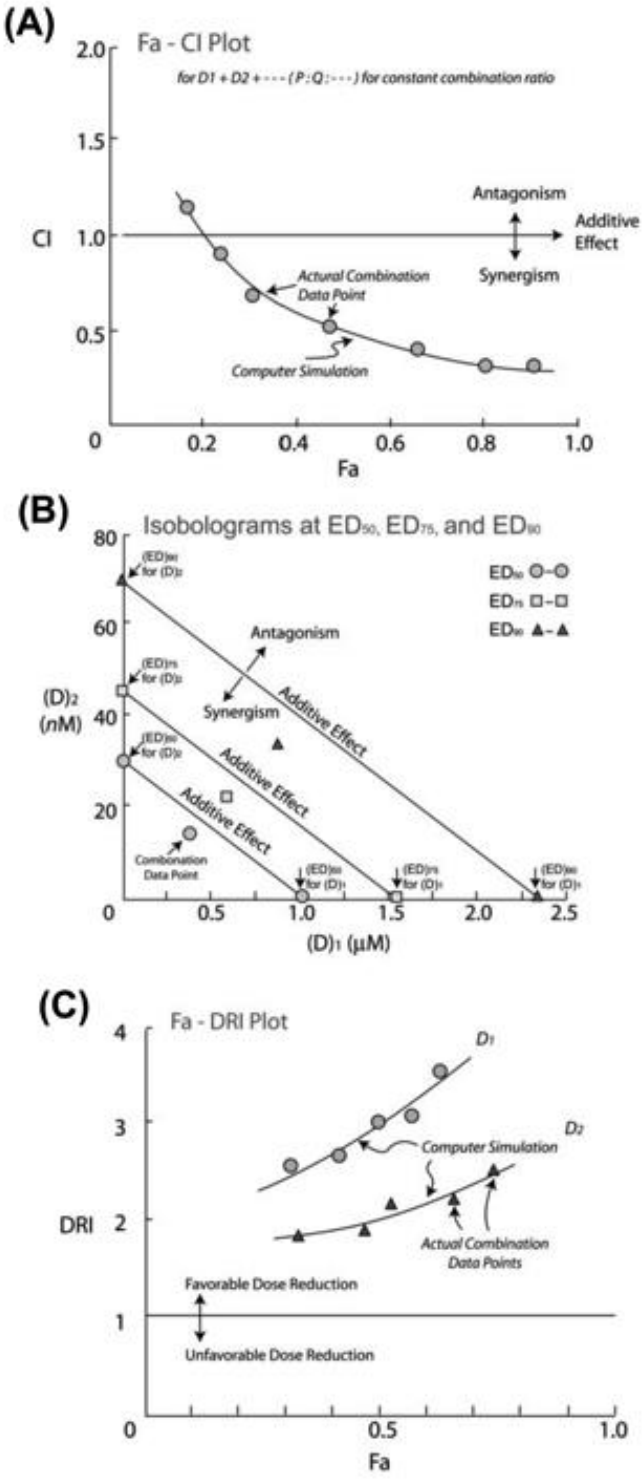

Figure 4.2 Drug combination plots and their interpretations based on the Chou and Tatalay combination index (CI) theorem.
Fa-CI plot (A), Isobologram at ED_{50}, ED_{75} and ED_{90} (B), Fa-DRI plot (C) (Chou, 2006). These plots are generated automatically by using the CompuSyn (Chou and Martin, 2005) or CompuSyn (Chou, 2005) software. Fa = fraction affected.

Combination Index (CI)	Graded Symbols	Interpretation
<0.1	+++++	Very strong synergism
0.1-0.3	++++	Strong synergism
0.3-0.7	+++	Synergism
0.7-0.85	++	Moderate synergism
0.85-0.9	+	Slight synergism
0.9-1.1	•	Nearly additive
1.1-1.2	−	Slight antagonism
1.2-1.45	−−	Moderate antagonism
1.45-3.3	−−−	Antagonism
3.3-10	−−−−	Strong antagonism
>10	−−−−−	Very strong antagonism
Simplified CI values and their interpretation		
<0.8	Synergism	
0.8-1.2	Additive	
>1.2	Antagonism	

Table 4.2 Description and Interpretation of CI values.
A table showing the description and interpretation of synergism or antagonism in combination studies using CI method of analysis [Adapted from (Bijnsdorp *et al.*, 2011, Chou, 2006)].

The synergy experiments carried out in this chapter involved the combination of aspirin analogues and DNA-damaging platinum compounds in SW480 CRC and OE33 oesophageal cell lines.

Based on their respective IC_{50}, compounds were combined at different ratios. Doses and FA of individual compounds and combinations were fed into the CompuSyn software, which calculated CI and DRI at ED_{50}, ED_{75} and ED_{90}.

4.2 Aims and Objectives

Kankipati (2014) and Kilari (2014) have reported cytotoxic effects of some of these aspirin analogues on colorectal and oesophageal cell lines respectively. In this chapter, it was aimed to investigate the cytotoxic effects of a wider range of these analogues, which include the meta- and para- isomers of aspirin and thioaspirin. It was also aimed to study if their cytotoxic effect against SW480 CRC and OE33 oesophageal cell lines will result in a synergistic effect when in combination with DNA-damaging platinum compounds known to be used as chemotherapeutic agents using the CalcuSyn® and CompuSyn® softwares.

4.3 Methodology

The methodology used in this chapter is given in detail in chapter two for materials and methods (2.2.6 and 2.2.17). The MTT assay was later adopted to investigate cytotoxic effects of compounds after it was discovered that the MTS reagent became insensitive to the thioaspirins because of their reducing effect (Mert *et al*., 2006), which rendered the MTS reagent inactive. There is evidence for the dimerization of thiosalicylic acid which varies with pH (Rowland *et al*., 2011) and thus has the capacity to interfere with any assay that utilises reagents capable of undergoing a redox reaction (For example, MTS assays and SA assays using As(III) or Fe(III) salts). MTT assay was preferred in this case because there was a step in the procedure that enabled the washing out of compounds before addition of MTT reagent thus avoiding/minimizing interaction, whereas the MTS reagent is used as a single solution added

directly to assay wells. The combination ratios for the synergy experiments were based on the individual IC_{50} values for each compound.

4.4 Results

4.4.1 Cytotoxicity results

A standard curve for the MTS solution was plotted, which resulted in a very good R-square value indicating that absorbance readings were directly proportional to the concentration or percentage of MTS solution.

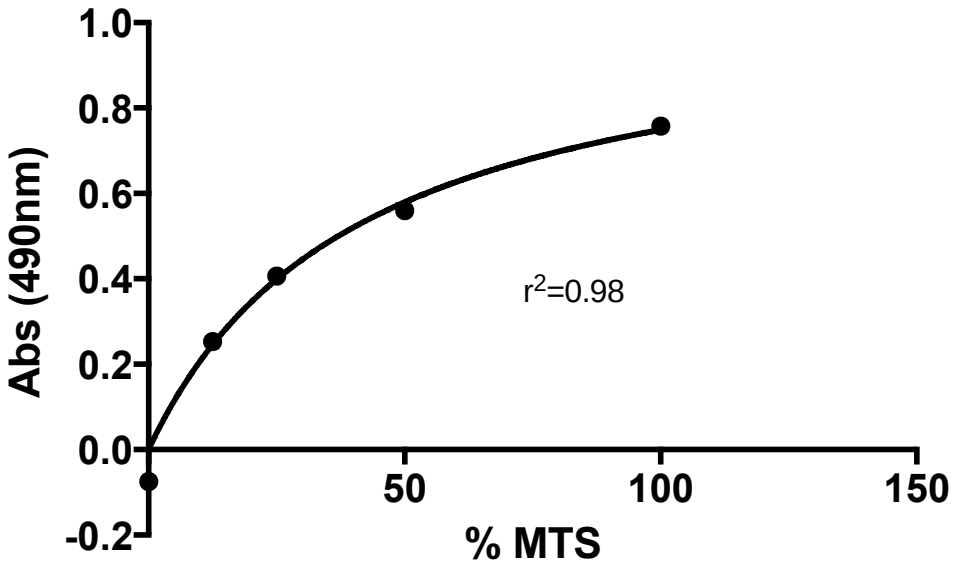

Figure 4.3 Standard curve for MTS solution.
MTS solution was serially diluted with acetone. Linear regression analysis shows "R-square" value as 0.98, which indicates it is a good fit. Absorbance was used in relation to cell activity/viability.

The MTS solution was thus fit for determining cell viability in accordance with the absorbance readings at 490 nm (Figure 4.3).

The standard curve for the MTT assay was also determine to make sure that the concentration of formazan was directly proportional to the absorbance at 540 nm (Figure 4.4).

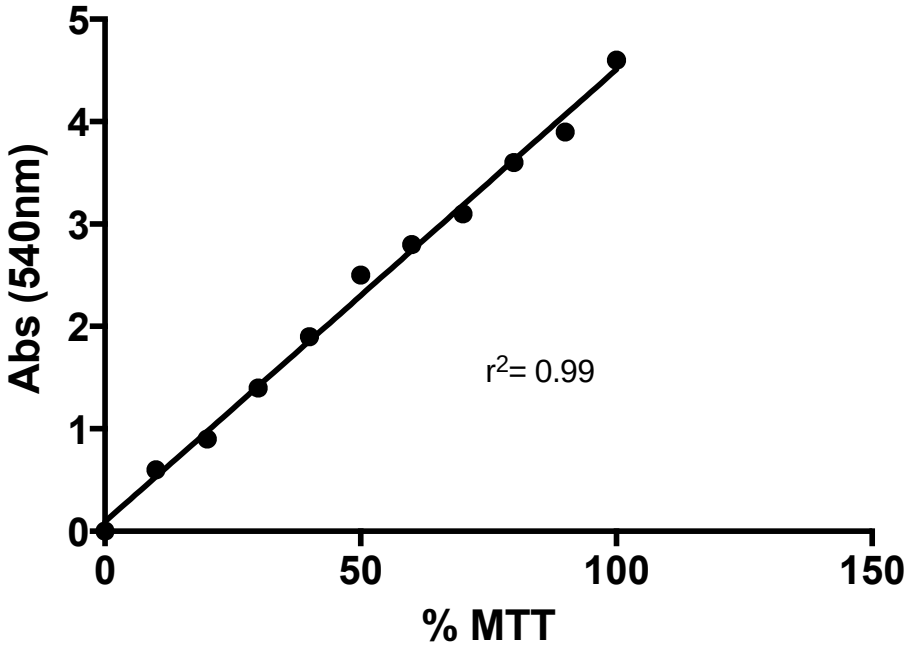

Figure 4.4 Standard curve for MTT solution.
Formazan crystals were diluted with DMSO to make a solution. Linear regression analysis shows "R-square" value as 0.99, which indicates it is a very good fit. Absorbance was used in relation to cell activity/viability.

The absorbance recorded at 540nm appears to be directly proportional to the percentage of MTT solution thus rendering the assay fit for purpose (Figure 4.4). The percentage viability of cells was assessed using this MTT assay and IC_{50} values calculated using GraphPad Prism.

Prior to analysing the cell viability of cells after treatment with aspirin analogues, the most appropriate dissolution solvent for these compounds had to be determined. Assays had initially been carried on these compounds using DMSO

as a dissolution solvent. It was thus decided to compare other organic solvents with DMSO based on their ability to dissolve the aspirin analogues and their effect on cell viability. Acetone, THF, DMSO and water were chosen to test solubility of compounds and effect on cell viability.

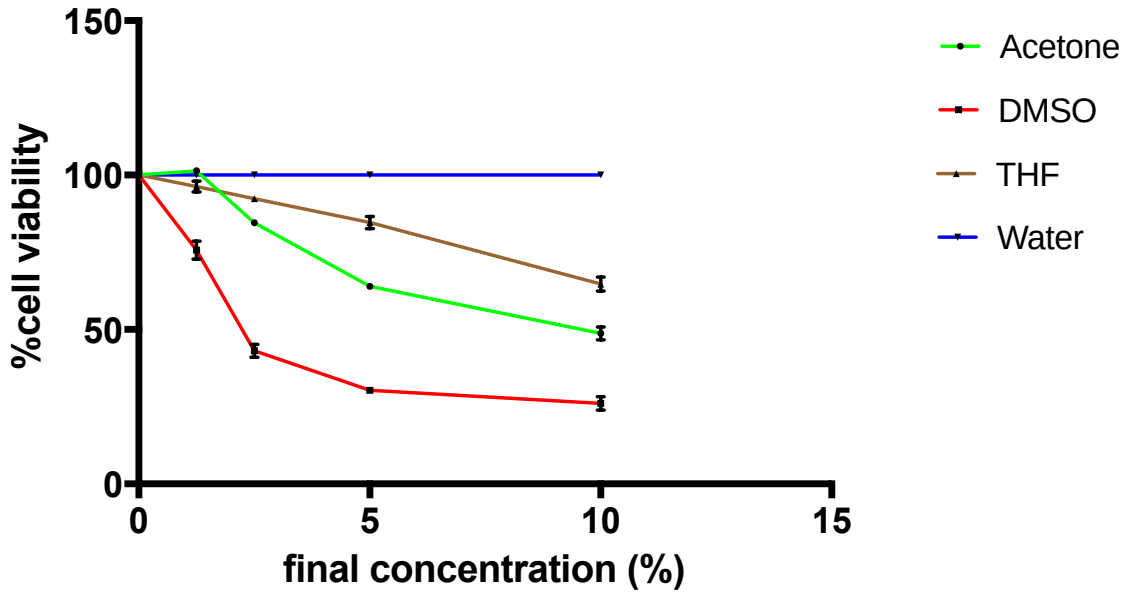

Figure 4.5 Percentage cell viability of SW480 CRC cells in different organic solvents.
SW480 cells were incubated with organic solvents in media to different final concentrations at 37°C for 48 h. Mean ± SEM (*n=3)*.

Although ultrapure water had no cytotoxic effect on the cells at the concentrations tested, water was a poor dissolution solvent for the compounds used in this study. Likewise, THF also failed to dissolve some of the aspirin analogues. The aspirin analogues completely dissolved in acetone and DMSO, with less toxicity to cell viability noted with acetone in particular (Figure 4.5). Although DMSO is generally known as the 'universal solvent' for biological

experiments due to its ability to dissolve most molecules at high concentrations of up to 100 mM (Pereira and Williams, 2007), acetone was found to have a lesser effect on cell viability. Acetone was thus chosen as the dissolution solvent for the experiments carried out with aspirin analogues in this thesis. Compounds were always dissolved in acetone to a concentration of 50 mM, which was further diluted with a buffer and finally diluted to the desired final concentration with cell culture media (e.g. L-15, DMEM, etc).

SW480 CRC cells were treated with aspirin analogues dissolved in acetone and NSAIDs for 48 h at doses between 1 μM and 3 mM. Platinum compounds were treated at doses between 0.1 μM and 0.3 mM. The IC_{50} values were then determined from the dose response curves plotted.

Acetone was used to dissolve aspirin analogues and NSAIDs with the exception of diflunisal, which was only soluble in DMSO. Dissolution with DMSO was also avoided in platinum compounds; cisplatin, oxaliplatin and carboplatin as DMSO react with platinum complexes thereby decreasing their cytotoxic effect (Hall *et al.*, 2014). The nucleophilic sulphur in DMSO reacts with platinum complexes thereby displacing their ligands, which result in a structure change, and thus making the compounds unstable in DMSO (Farrell *et al.*, 1990, Kerrison and Sadler, 1985). Due to these facts, cisplatin was dissolved using PBS while both oxaliplatin and carboplatin were dissolved using water as suggested by Hall *et al*., (2014). SW480 cells were also treated with aspirin analogues and platinum compounds for 12 days in order to determine if cytotoxicity of compounds will follow the same pattern, slow down or come to a halt. Furthermore, increased

cytotoxic effect of any of these compounds over long period of time means such compounds have a longer duration of action than expected.

The oesophageal cancer cell lines, OE33 and FLO1 are both from human and originate from the oesophagus. OE33 is originally from the adenocarcinoma of the lower oesophagus (Barrett's metaplasia) in a 73-year-old female patient (ECACC). FLO1 is originally from the primary distal oesophageal adenocarcinoma in a 68-year-old Caucasian male (ECACC).

OE33 and FLO1 oesophageal cell lines were also treated with a few of the aspirin analogues and platinum compounds in order to determine the IC_{50} as a base needed for synergy experiments later carried out. The same dissolution conditions for compounds used to treat SW480 cells were also applied for oesophageal cancer cell lines.

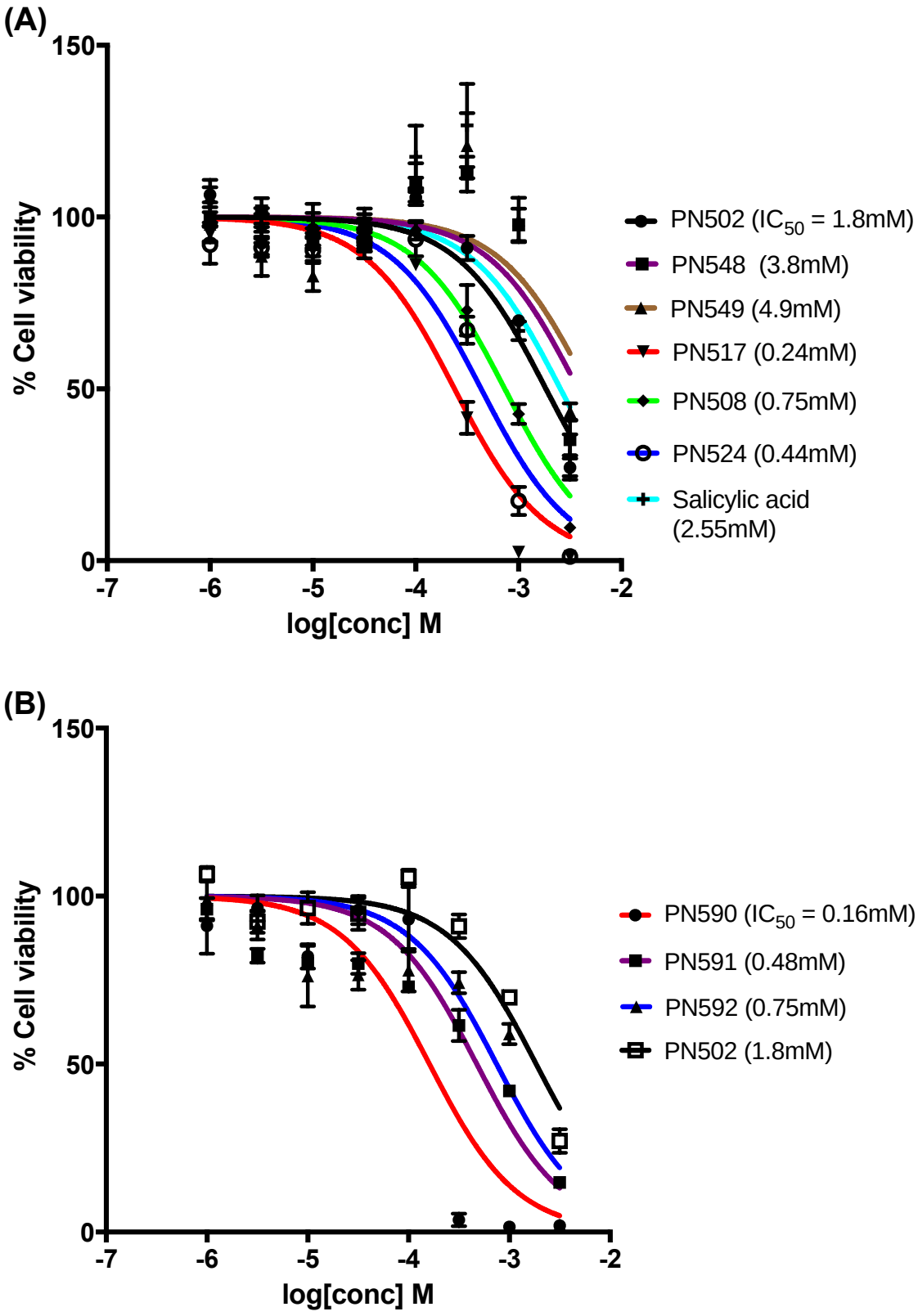

Figure 4.6 Dose response curves of aspirin analogues in SW480 CRC cell line.
SW480 CRC cell lines were treated with compounds (1 μM-3 mM) and incubated at 37°C for 48 h. The anti-proliferative effects were measured using MTT assay. Data plotted as mean ± SEM (*n=3*). Where error are absent, SEM is smaller than size of data point. IC_{50} was calculated using GraphPad Prism.

SW480 CRC cells treated with aspirin and its analogues for 48 h resulted in an inhibitory concentration of 50% of the cell population for aspirin as 1.8 mM (Figure 4.6A). PN548 (meta-aspirin) and PN549 (para-aspirin) had IC_{50} at 3.8 mM and 4.9 mM respectively when cells were treated for 48 h (Figure 4.6A), which appears to not have much cytotoxicity. This could be due to the short duration of treatment. In comparison to PN502, PN517 (fumaryldiaspirin) and PN524 (m-bromo benzoylsalicylate), both 'diaspirins' were very cytotoxic against SW480 cells with an IC_{50} of 0.24 mM and 0.44 mM respectively (Figure 4.6A). PN508, also one of the 'diaspirins' was quite cytotoxic with 0.75 mM as its IC_{50} which suggests that even though 'diaspirins' are dimers of aspirin, they are more than twice more potent. Cytotoxicity against SW480 cells was higher when cells were treated with the thioaspirins as compared to aspirin with IC_{50} for PN590 (ortho-thioaspirin), PN591 (meta-thioaspirin) and PN592 (para-thioaspirin) as 0.16 mM, 0.48 mM and 0.75 mM respectively (Figure 4.6B).

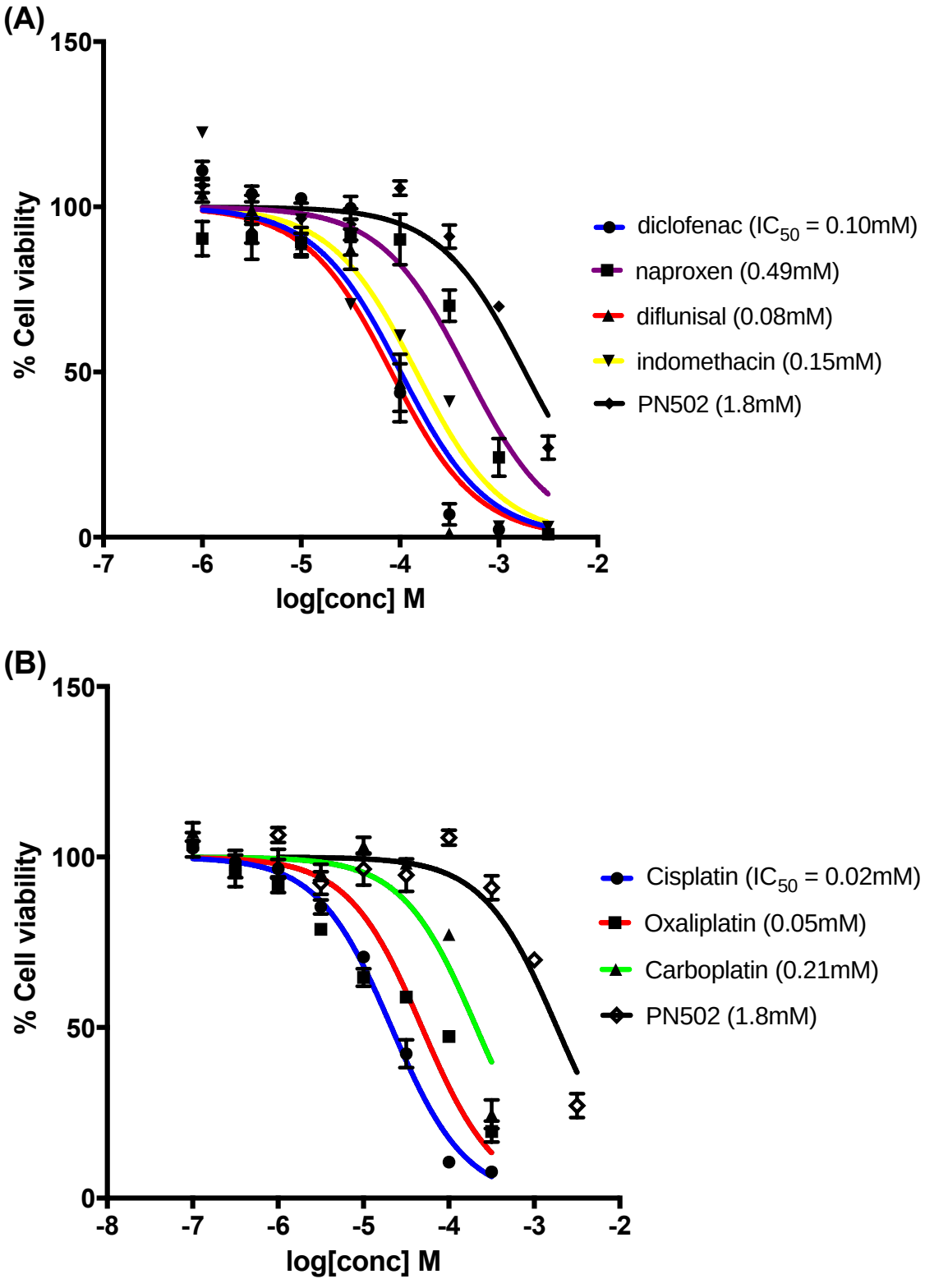

Figure 4.7 Dose response curves of NSAIDs and platinum compounds in SW480 CRC cell line. SW480CRC cell lines were treated with compounds (0.1 µM-0.3 mM) and incubated at 37°C for 48 h. The anti-proliferative effects were measured using MTT assay. Data plotted as geometric mean ± SEM (*n=3*). Where error are absent, SEM is smaller than size of data point. IC_{50} was calculated using GraphPad Prism.

SW480 cells were also treated with NSAIDs for 48 h, which resulted in diflunisal as the most cytotoxic NSAID against this cell line with an IC_{50} of 0.08 mM (Figure 4.7A). Treatment with diclofenac, indomethacin and naproxen resulted in IC_{50} of 0.1 mM, 0.15 mM and 0.49 mM respectively (Figure 4.7A). Cytotoxicity of NSAIDs against SW480 cells is much higher than aspirin and 'diaspirins' with the exception of PN517 (Figure 4.6A). The DNA-damaging platinum compounds had IC_{50} of 0.02 mM for cisplatin, 0.05 mM for oxaliplatin and 0.21 mM for carboplatin, all of which were more cytotoxic than aspirin (Figure 4.7B).

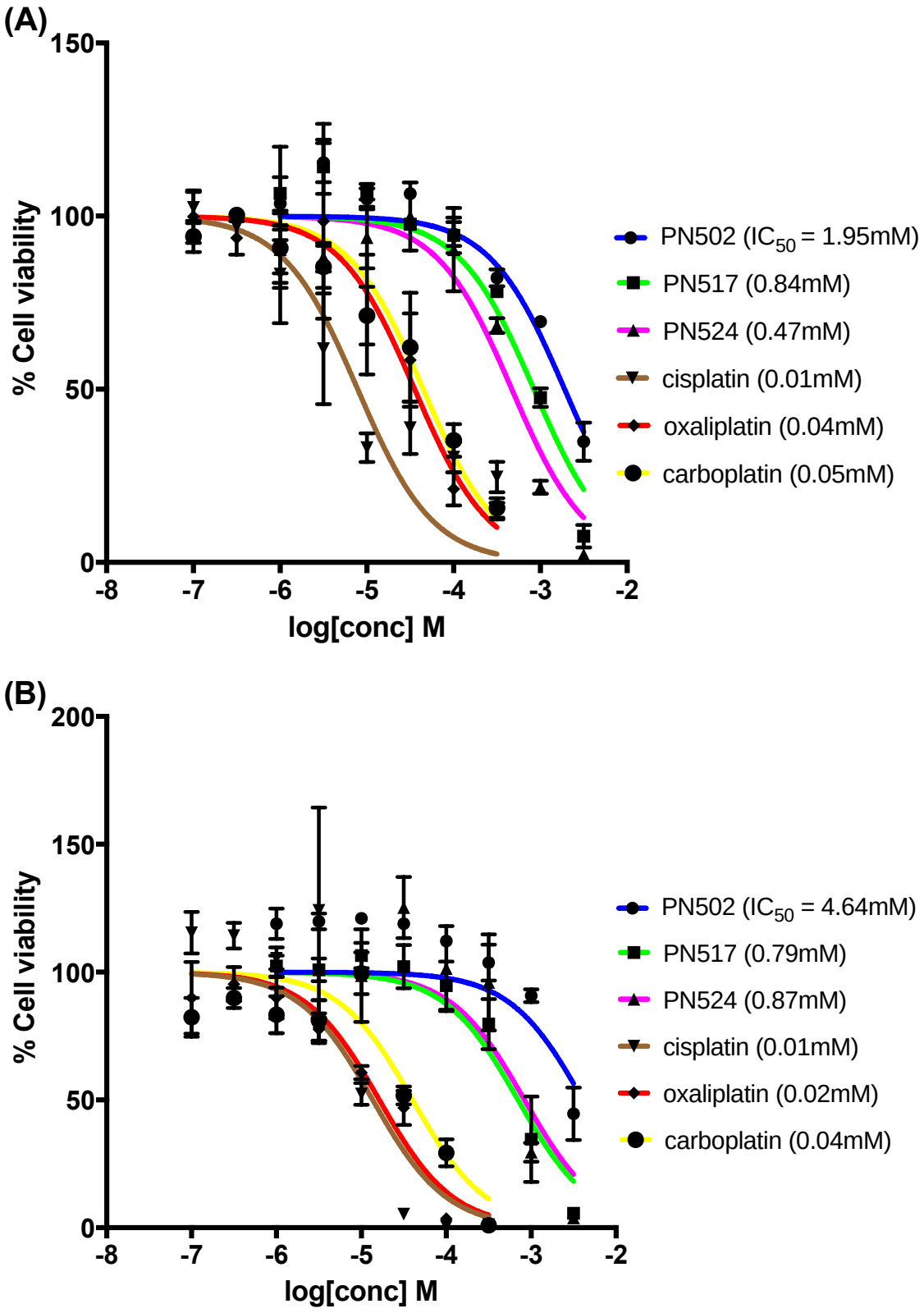

Figure 4.6 Dose response curves of aspirin analogues and platinum compounds in OE33 (A) and FLO1 (B) oesophageal cell lines.

Figure 4.8 Dose response curves of aspirin analogues and platinum compounds in OE33 (A) and FLO1 (B) oesophageal cell lines.
Oesophageal cells were treated with aspirin analogues (1 µM-3 mM) and platinum compounds (0.1 µM-0.3 mM) and then incubated at 37°C for 48 h. The anti-proliferative effects were measured using MTT assay. Data plotted as geometric mean ± SEM (*n=3*). Where error are absent, SEM is smaller than size of data point. IC_{50} was calculated using GraphPad Prism.

The oesophageal cell lines, OE33 and FLO1 were also treated with some of the aspirin analogues and DNA-damaging platinum compounds for 48 h. PN502 (aspirin) appeared not to be very cytotoxic against FLO1 cells with 4.64 mM as IC_{50} (Figure 4.8B) as compared to OE33 cells (Figure 4.8A) and SW480 cells (Figure 4.6) with 1.95 mM and 1.8 mM as IC_{50} respectively. PN524 was also found to be more cytotoxic in OE33 cells, IC_{50} as 0.47 mM (Figure 4.8A) than in FLO1 cells, IC_{50} as 0.87 mM (Figure 4.8B). However, PN517 and the platinum compounds had similar cytotoxic effects in both oesophageal cell lines. In OE33 cells, PN517, cisplatin, oxaliplatin and carboplatin had IC_{50} at 0.84 mM, 0.01 mM, 0.04 mM and 0.05 mM respectively (Figure 4.8A). While in FLO1 cells, PN517, cisplatin, oxaliplatin and carboplatin resulted in IC_{50} values of 0.79 mM, 0.01 mM, 0.02 mM and 0.04 mM respectively (Figure 4.8B).

Compounds	Geometric mean of IC_{50} values (mM)		
	SW480	OE33	FLO1
PN502	1.8	1.95	4.64
PN548	3.8	-	-
PN549	4.9	-	-
PN517	0.24	0.84	0.79
PN508	0.75	-	-
PN524	0.44	0.47	0.87
Salicylic acid	2.55	-	-
PN590	0.16	-	-
PN591	0.48	-	-
PN592	0.75	-	-
Diclofenac	0.10	-	-
Naproxen	0.49	-	-
Diflunisal	0.08	-	-
Indomethacin	0.15	-	-
Cisplatin	0.02	0.01	0.01
Oxaliplatin	0.05	0.04	0.02
Carboplatin	0.21	0.05	0.04

Table 4.3 IC_{50} values of aspirin analogues, NSAIDs and platinum compounds on SW480 CRC cell line, OE33 and FLO1 oesophageal cell lines.
Cells were treated for 48 h. IC_{50} values were obtained by non-linear regression analysis from dose-response curves using Graphpad Prism. Data are presented as geometric mean (*n=4*),

Compounds	Geometric mean of IC_{50} values (mM)
PN502	0.10
PN508	0.16
PN517	0.06
PN590	0.08
PN591	0.04
PN592	0.03
Diclofenac	0.05
Naproxen	0.09
Indomethacin	0.05
Cisplatin	0.003
Oxaliplatin	0.0004
Carboplatin	0.009

Table 4.4 IC_{50} values of some aspirin analogues, NSAIDs and platinum compounds on SW480 CRC cell line after 12- day cytotoxicity assay.
Cells were treated for 12 days with cells replenished on the sixth day. IC_{50} values were obtained by non-linear regression analysis from dose-response curves using Graphpad Prism. Data are presented as geometric mean (*n=3*).

4.4.2 DEREK analysis

Aspirin and its analogues were analysed *in silico* for their toxicity profile. The toxicological endpoints assessed include hepatoxicity, nephrotoxicity, mitochondrial dysfunction and skin sensitisation in humans. The knowledge database used is the DEREK KB 2015 2.0, version 1.0, certified by Lhasa Limited, Leeds, Yorshire, UK.

A major setback in this analysis is that the software did not recognise the chemical structures of some of the compounds and so did not produce any predictions for its toxicological profile.

The aspirin analogues that the programme did recognise were identified as salicylates and thus produced predictions for their toxicological profile as that of salicylic acid. Salicylates have anti-inflammatory, analgesic and antipyretic effects and are known to cause liver injury that could lead to fatality in humans at doses that exceed 4g orally (Cao et al., 2015, Hamdan et al., 1985, Seaman et al., 1974). Mitochondrial dysfunction is also included in the toxicological profile of the salicylates (Zhang et al., 2009).

Nephrotoxicity have also been reported to be caused by salicylates in the form of renal failure, nephrotic syndrome and interstitial nephritis (Perazella and Markowitz, 2010).

Compound	Endpoint	Result
PN502 (ortho-aspirin)	Hepatotoxicity	Positive
	Mitochondrial dysfunction	Positive
	Nephrotoxicity	Positive
	Skin sensitisation	Plausible
PN548 (meta-aspirin)	Hepatotoxicity	'The query structure does not match any structural alerts or examples in Derek'
	Mitochondrial dysfunction	
	Nephrotoxicity	
	Skin sensitisation	
PN549 (para-aspirin)	Hepatotoxicity	'The query structure does not match any structural alerts or examples in Derek'
	Mitochondrial dysfunction	
	Nephrotoxicity	
	Skin sensitisation	
PN590 (ortho-thioaspirin)	Hepatotoxicity	'The query structure does not match any structural alerts or examples in Derek'
	Mitochondrial dysfunction	
	Nephrotoxicity	
	Skin sensitisation	
PN591 (meta-thioaspirin)	Hepatotoxicity	'The query structure does not match any structural alerts or examples in Derek'
	Mitochondrial dysfunction	
	Nephrotoxicity	
	Skin sensitisation	
PN592 (para-thioaspirin)	Hepatotoxicity	'The query structure does not match any structural alerts or examples in Derek'
	Mitochondrial dysfunction	
	Nephrotoxicity	
	Skin sensitisation	
PN508 (diaspirin)	Hepatotoxicity	Positive
	Mitochondrial dysfunction	Positive
	Nephrotoxicity	Positive
	Skin sensitisation	Plausible
PN517 (fumaryldiaspirin)	Hepatotoxicity	Positive
	Mitochondrial dysfunction	Positive
	Nephrotoxicity	Positive
	Skin sensitisation	Plausible

Table 4.5 List of compounds, endpoints and results produced by *in silico* analysis using the DEREK software.

4.4.3 Drug combinations

Platinum compounds in combination with aspirin and its analogues were used to treat SW480 CRC cells and OE33 oesophageal cancer cells for 72 h. The cytotoxic effect and fraction of cells affected (Fa) was then calculated and fed into the CompuSyn software where The CI was determined at ED_{50}, ED_{75} and ED_{90}. The dose-effect graph to compare the fraction of cells affected by single compounds with the fractions of cells affected by drug combinations; Fa-log (DRI) graphs to show the effective ED_{50} of compounds decreased or increased when in combination were also plotted by the software. Against the colorectal cell line, SW480, cisplatin had synergistic effects when combined with all the aspirin analogues with the exception of the meta- (PN591) and para- (PN592) thioaspirin (Figure 4.16 and 4.17 respectively). Oxaliplatin in combination with PN548, PN524 and PN592 had synergistic effects at lower doses i.e. ED_{50} and lower. Although there appears to be a synergistic effect, antagonism sets in at ED_{75} and ED_{90}. PN517 also has a synergistic effect with carboplatin at ED_{50}, which decreased and effect became antagonistic at ED_{90} (Table 4.5). Carboplatin and PN549 [1:50] was the only combination that had a favourable synergistic effect. These combination effects between aspirin and its analogues with platinum compounds have been summarised on Table 4.5.

Against the oesophageal cell line, OE33, cisplatin had synergistic effects when used in combination with PN517, PN524 and PN528. PN528 (methyl-bromobenzoylsalicylate) was included in this study against the OE33 cell line because of its high cytotoxic effects and specificity against three different oesophageal cell lines namely; FLO1, OE33 and OE21 (Kilari, 2014). The other

platinum compounds however, did not show any synergistic effects when used in combination with PN502 (aspirin), PN517, PN524 and PN528.

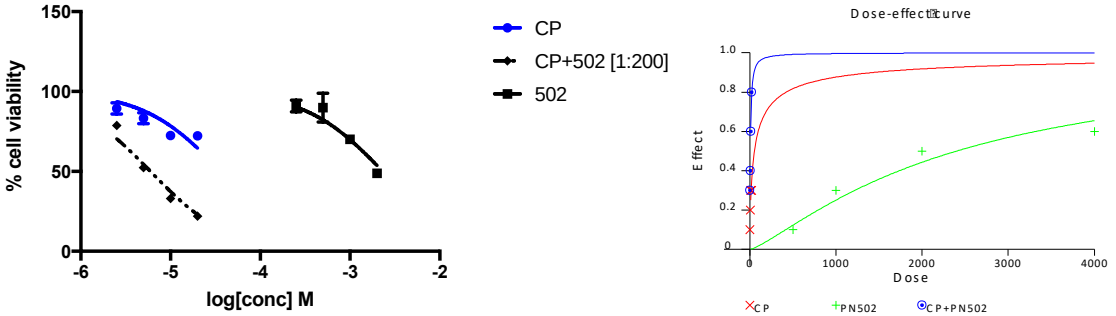

(A)

(B)

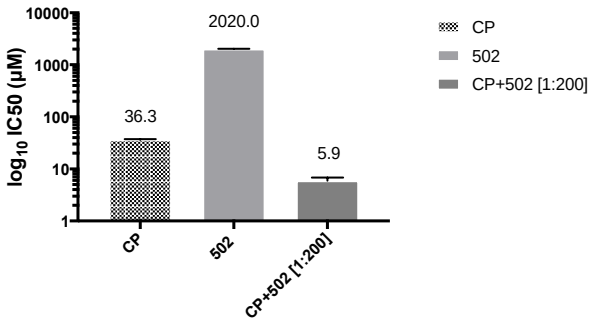

(C)

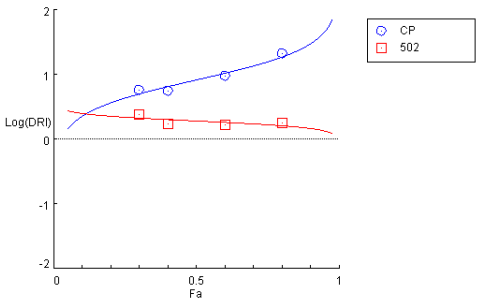

(D)

CI values at:

Drug Combo	ED50	ED75	ED90
CP+PN502 [1:200]	0.64	0.66	0.71

(E)

Figure 4.7 Drug combination plots for cisplatin and ortho-aspirin (CP+PN502[1:200]) in SW480 CRC cells.
Dose response curve (A). Dose-effect curve as plotted by CalcuSyn (B). Bar chart representation of IC_{50} by single compounds and their combination (C). Fa-log(DRI) plot as plotted by CompuSyn (D). CI values as calculated by CompuSyn at ED_{50}, ED_{75} and ED_{90}. CP=Cisplatin.

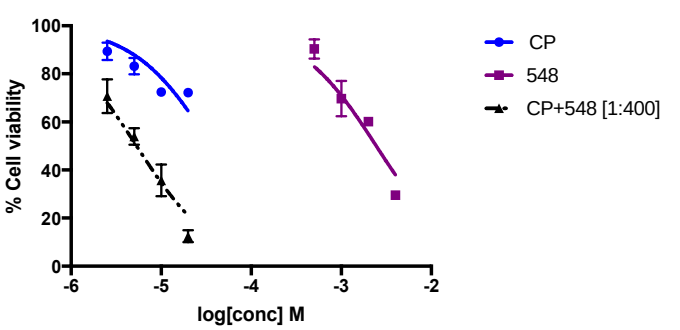

(A)

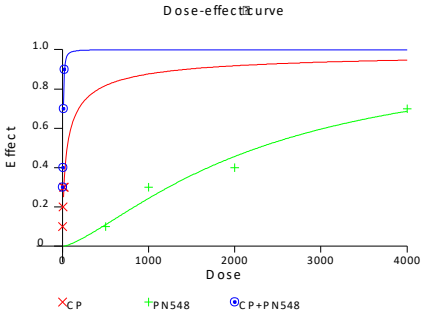

(B)

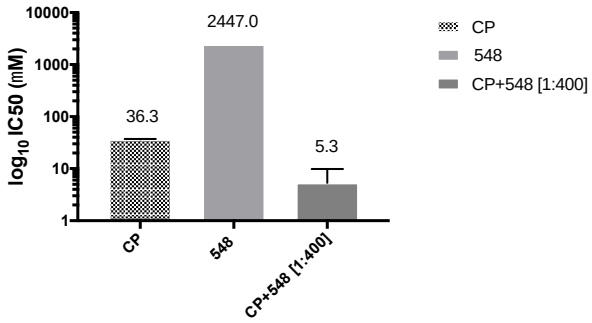

(C)

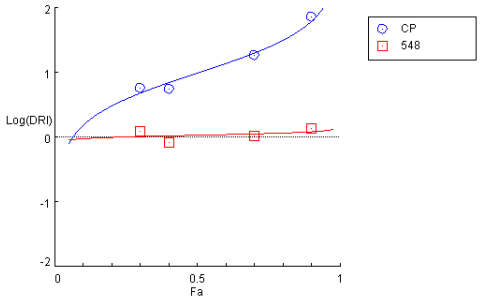

(D)

CI values at:

Drug Combo	ED50	ED75	ED90
CP+PN548 [1:400]	1.03	0.91	0.83

(E)

Figure 4.8 Drug combination plots for cisplatin and meta-aspirin (CP+PN548[1:400]) in SW480 CRC cells.

Dose response curve (A). Dose-effect curve as plotted by CalcuSyn (B). Bar chart representation of IC_{50} by single compounds and their combination (C). Fa-log(DRI) plot as plotted by CompuSyn (D). CI values as calculated by CompuSyn at ED_{50}, ED_{75} and ED_{90}. CP=Cisplatin.

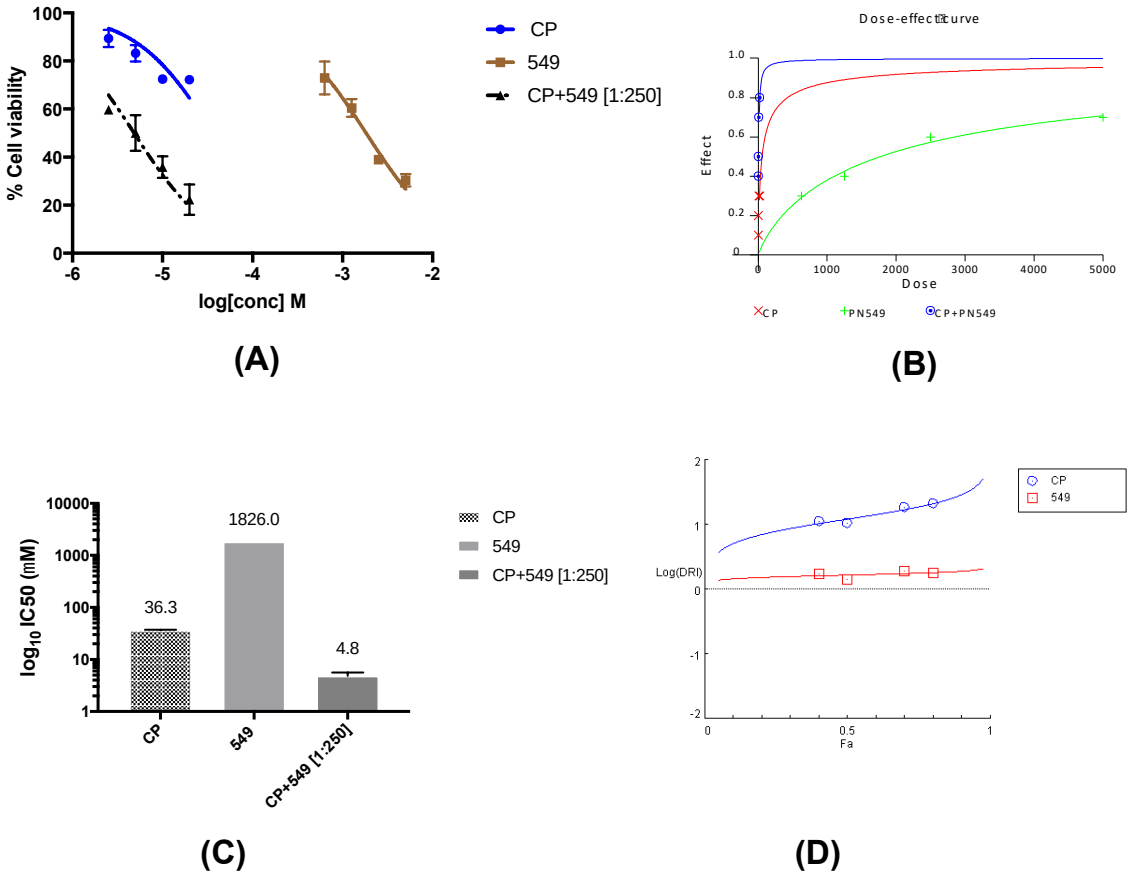

CI values at:

Drug Combo	ED50	ED75	ED90
CP+PN549 [1:250]	0.69	0.61	0.56

(E)

Figure 4.9 Drug combination plots for cisplatin and para-aspirin (CP+PN549[1:250]) in SW480 CRC cells.
Dose response curve (A). Dose-effect curve as plotted by CalcuSyn (B). Bar chart representation of IC_{50} by single compounds and their combination (C). Fa-log(DRI) plot as plotted by CompuSyn (D). CI values as calculated by CompuSyn at ED_{50}, ED_{75} and ED_{90}. CP=Cisplatin.

Cisplatin was used in combination with aspirin and its isomers, PN502 (aspirin), PN548 (meta-aspirin) and PN549 (para-aspirin) at 1:200 (Figure 4.9A, B, C, D and E), 1:400 (Figure 4.10A, B, C, D and E) and 1:250 (Figure 4.11A, B, C, D and E) respectively.

Combination index (CI) values for cisplatin and PN502 [1:200] indicated a synergistic effect (Figure 4.9E) with ED_{50} for cisplatin when used in combination with PN502 reduced from 51.9μM to 6.2μM (Figure 4.9D). The DRI calculated by CompoSyn software for SW480 CRC cells showed that cisplatin and PN548 [1:400] resulted in a decrease in concentration to kill 50% of the cell population (ED_{50}) for cisplatin and PN548 from 51.9μM and 2265.0μM to 5.2μM and 2097.6μM respectively in combination (Figure 4.10D). The ED_{50} for cisplatin when used in combination with PN549 [1:250] reduced from 51.9μM to 4.2μM (Figure 4.11D).

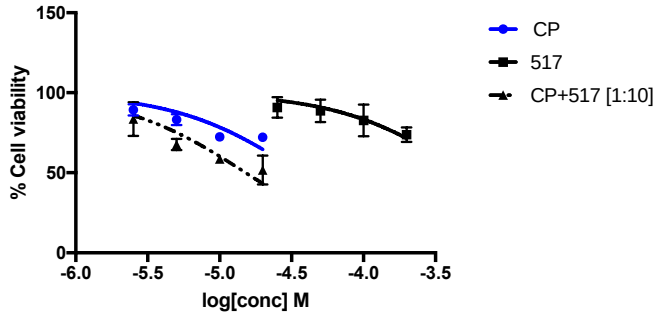

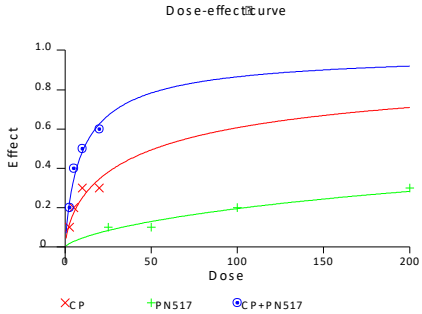

(A) **(B)**

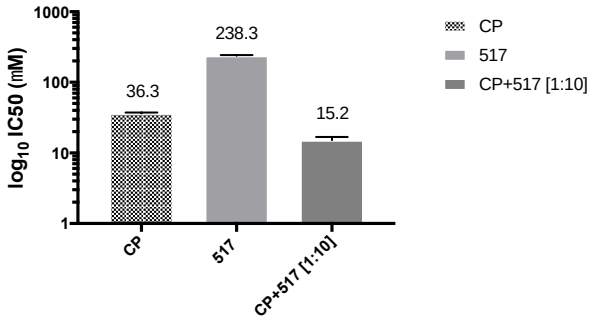

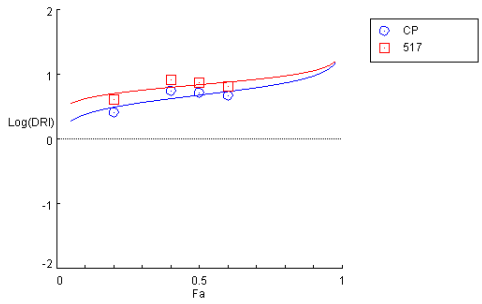

(C) **(D)**

CI values at:

Drug Combo	ED50	ED75	ED90
CP+PN517 [1:10]	0.35	0.26	0.20

(E)

Figure 4.10 Drug combination plots for cisplatin and fumaryldiaspirin (CP+PN517[1:10]) in SW480 CRC cells.
Dose response curve (A). Dose-effect curve as plotted by CalcuSyn (B). Bar chart representation of IC_{50} by single compounds and their combination (C). Fa-log(DRI) plot as plotted by CompuSyn (D). CI values as calculated by CompuSyn at ED_{50}, ED_{75} and ED_{90}. CP=Cisplatin.

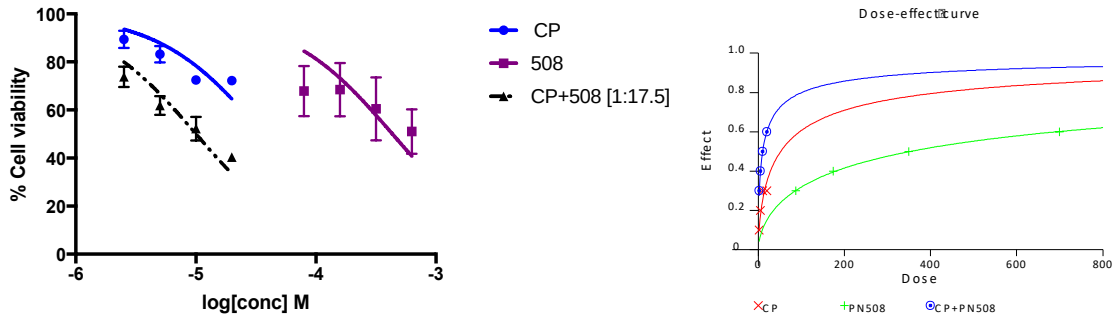

(A) (B)

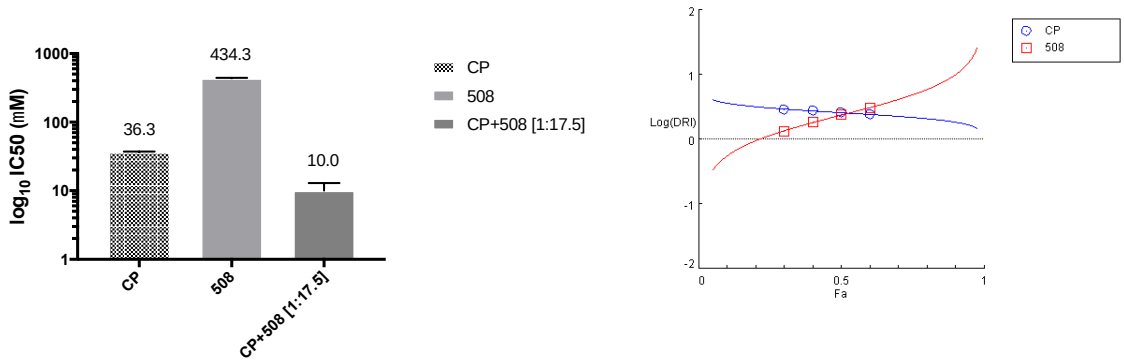

(C) (D)

CI values at:

Drug Combo	ED50	ED75	ED90
CP+PN508 [1:17.5]	0.81	0.66	0.64

(E)

Figure 4.11 Drug combination plots for cisplatin and diaspirin (CP+PN508[1:17.5]) in SW480 CRC cells.
Dose response curve (A). Dose-effect curve as plotted by CalcuSyn (B). Bar chart representation of IC_{50} by single compounds and their combination (C). Fa-log(DRI) plot as plotted by CompuSyn (D). CI values as calculated by CompuSyn at ED_{50}, ED_{75} and ED_{90}. CP=Cisplatin.

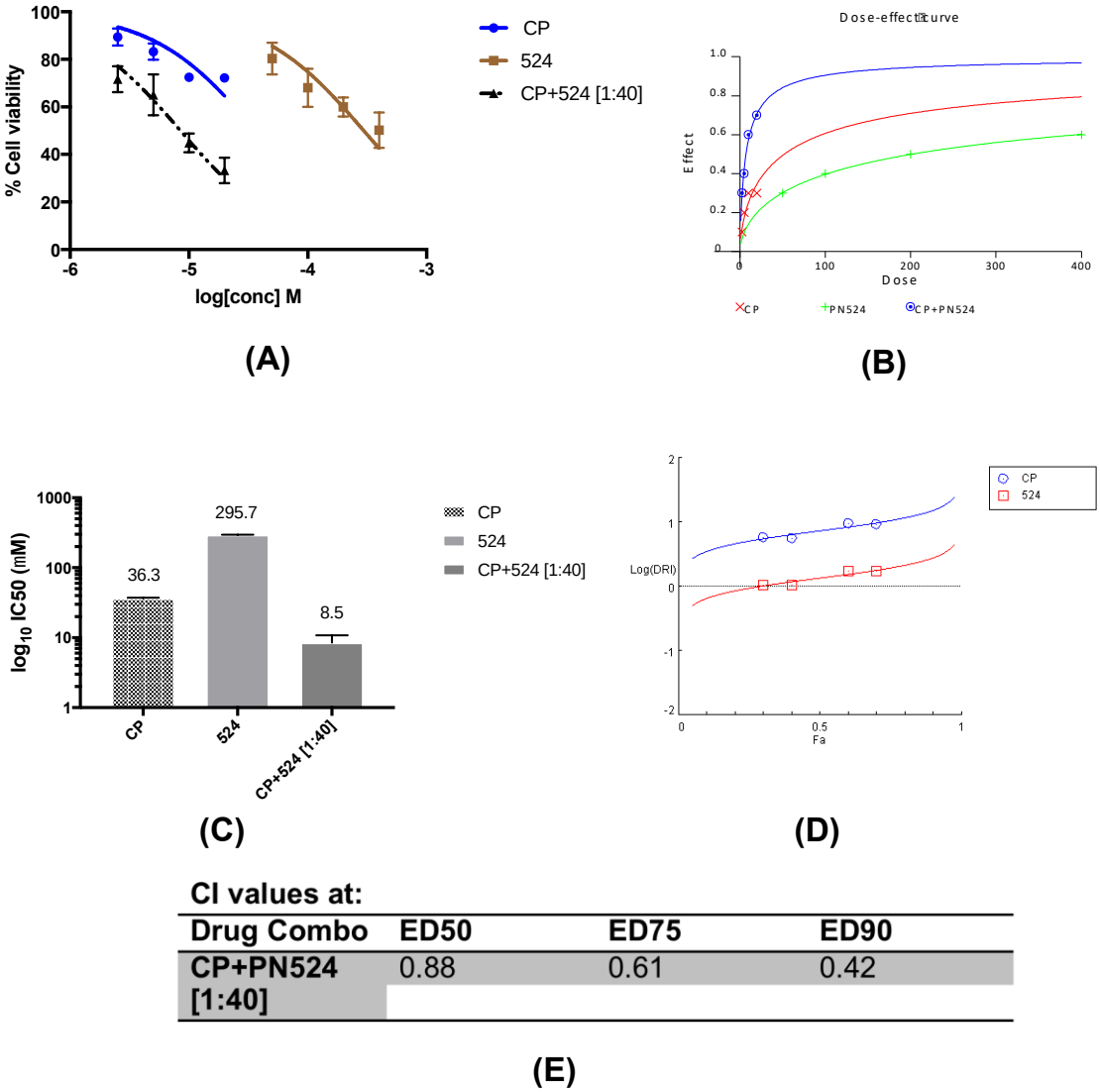

CI values at:

Drug Combo	ED50	ED75	ED90
CP+PN524 [1:40]	0.88	0.61	0.42

(E)

Figure 4.12 Drug combination plots for cisplatin and m-bromobenzoylsalicylate (CP+PN524[1:40]) in SW480 CRC cells.
Dose response curve (A). Dose-effect curve as plotted by CalcuSyn (B). Bar chart representation of IC_{50} by single compounds and their combination (C). Fa-log(DRI) plot as plotted by CompuSyn (D). CI values as calculated by CompuSyn at ED_{50}, ED_{75} and ED_{90}. CP=Cisplatin.

Cisplatin used in combination with the ‘diaspirins’, PN517, PN508 and PN524 against SW480 cells at 1:10 (Figure 4.12A, B, C, D and E), 1:17.5 (Figure 4.13A, B, C, D and E) and 1:40 (Figure 4.14A, B, C, D and E) concentrations respectively resulted in synergistic effects at ED_{50}, ED_{75} and ED_{90}.

When cisplatin was used in combination with PN517 [1:10], PN508 [1:17.5] and PN524 [1:40], the ED_{50} of the platinum compound reduced from 51.9 μM to 10.7μM (Figure 4.12D), 20.1μM (Figure 4.13D) and 7.1μM (Figure 4.14D) respectively. PN517 in combination with cisplatin had its ED_{50} reduced from 751.1μM to 107.1μM (Figure 4.12). The ED_{50} of PN508 in combination with cisplatin was decreased from 838μM as calculated by CompuSyn to 352.1μM (Figure 4.13). PN524 also had ED_{50} reduced from 382.1μM to 282.8μM (Figure 4.14).

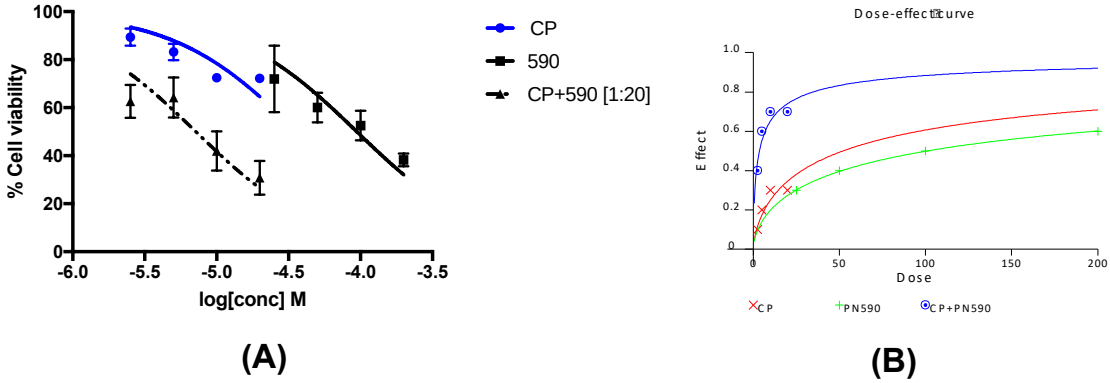

(A) (B)

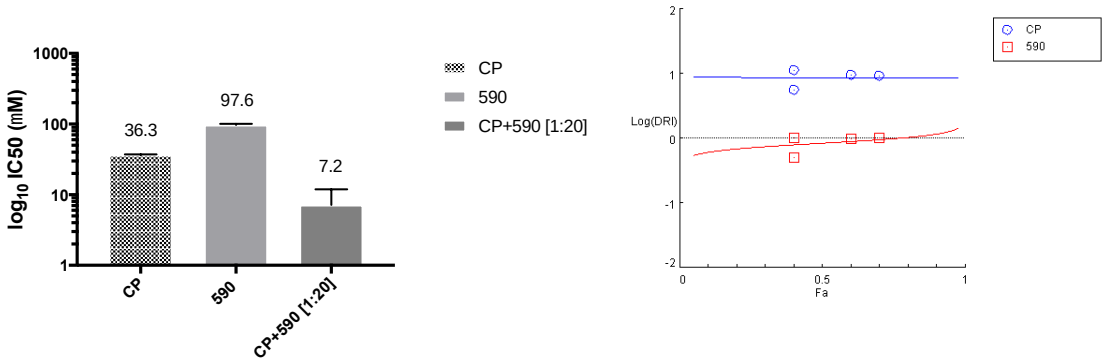

(C) (D)

CI values at:

Drug Combo	ED50	ED75	ED90
CP+PN590 [1:20]	1.30	1.13	0.98

(E)

Figure 4.13 Drug combination plots for cisplatin and ortho-thioaspirin (CP+PN590[1:20]) in SW480 CRC cells.
Dose response curve (A). Dose-effect curve as plotted by CalcuSyn (B). Bar chart representation of IC_{50} by single compounds and their combination (C). Fa-log(DRI) plot as plotted by CompuSyn (D). CI values as calculated by CompuSyn at ED_{50}, ED_{75} and ED_{90}. CP=Cisplatin.

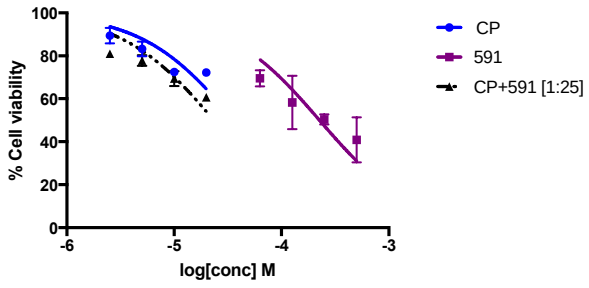

(A)

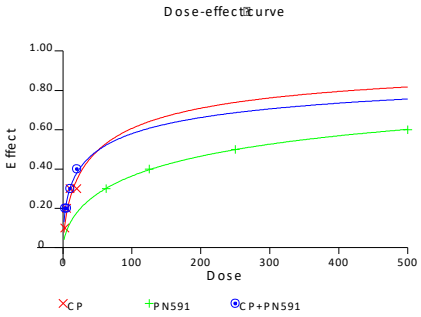

(B)

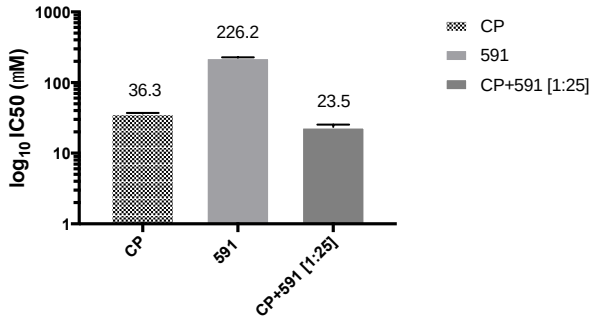

(C)

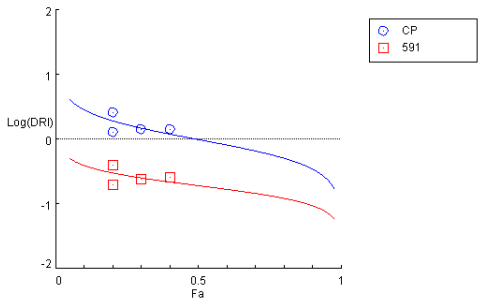

(D)

CI values at:

Drug Combo	ED50	ED75	ED90
CP+PN591 [1:25]	6.22	9.17	>10

(E)

Figure 4.14 Drug combination plots for cisplatin and meta-thioaspirin (CP+PN591[1:20]) in SW480 CRC cells .
Dose response curve (A). Dose-effect curve as plotted by CalcuSyn (B). Bar chart representation of IC_{50} by single compounds and their combination (C). Fa-log(DRI) plot as plotted by CompuSyn (D). CI values as calculated by CompuSyn at ED_{50}, ED_{75} and ED_{90}. CP=Cisplatin.

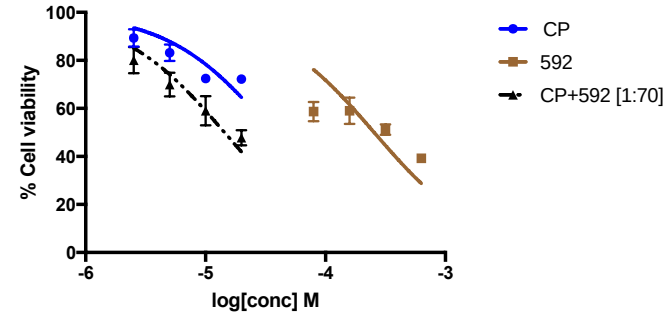

(A)

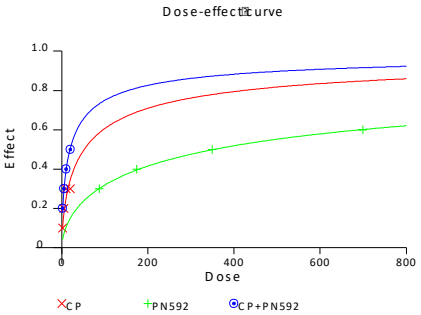

(B)

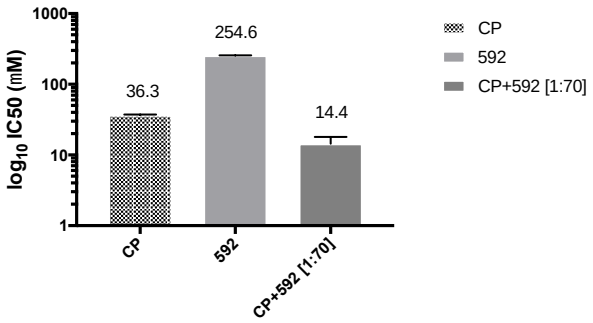

(C)

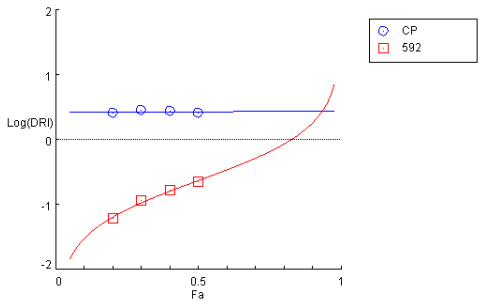

(D)

CI values at:

Drug Combo	ED50	ED75	ED90
CP+PN592 [1:70]	4.59	1.88	0.91

(E)

Figure 4.15 Drug combination plots for cisplatin and para-thioaspirin (CP+PN592[1:70]) in SW480 CRC cells.

Dose response curve (A). Dose-effect curve as plotted by CalcuSyn (B). Bar chart representation of IC_{50} by single compounds and their combination (C). Fa-log(DRI) plot as plotted by CompuSyn (D). CI values as calculated by CompuSyn at ED_{50}, ED_{75} and ED_{90}. CP=Cisplatin.

Cisplatin when used in combination with thioaspirin, PN590 and its isomers, PN591 (meta-thioaspirin), PN592 (para-thioaspirin) resulted in different effects, which ranged from antagonistic, additive and synergistic effects.

The DNA-damaging platinum compound, cisplatin in combination with PN590 [1:20] (Figure 4.15A, B, C, D and E), resulted in its ED_{50} reduced from 51.9μM to 5.9μM (Figure 4.15D). The combination effect of cisplatin and PN590 was slightly antagonistic at ED_{50} and progressed to additive effect at ED_{75} and ED_{90} (Figure 4.15, Table 4.5). Strong antagonistic effects (Figure 4.16D) resulted when cisplatin was used in combination with PN591 [1:20] (Figure 4.16A, B, C, D and E) and also when used in combination with PN592 [1:70] (Figure 4.17A, B, C, D and E). The ED_{50} of cisplatin was not reduced in combination with either of the thioaspirin isomers, which defeats the purpose of drug combinations.

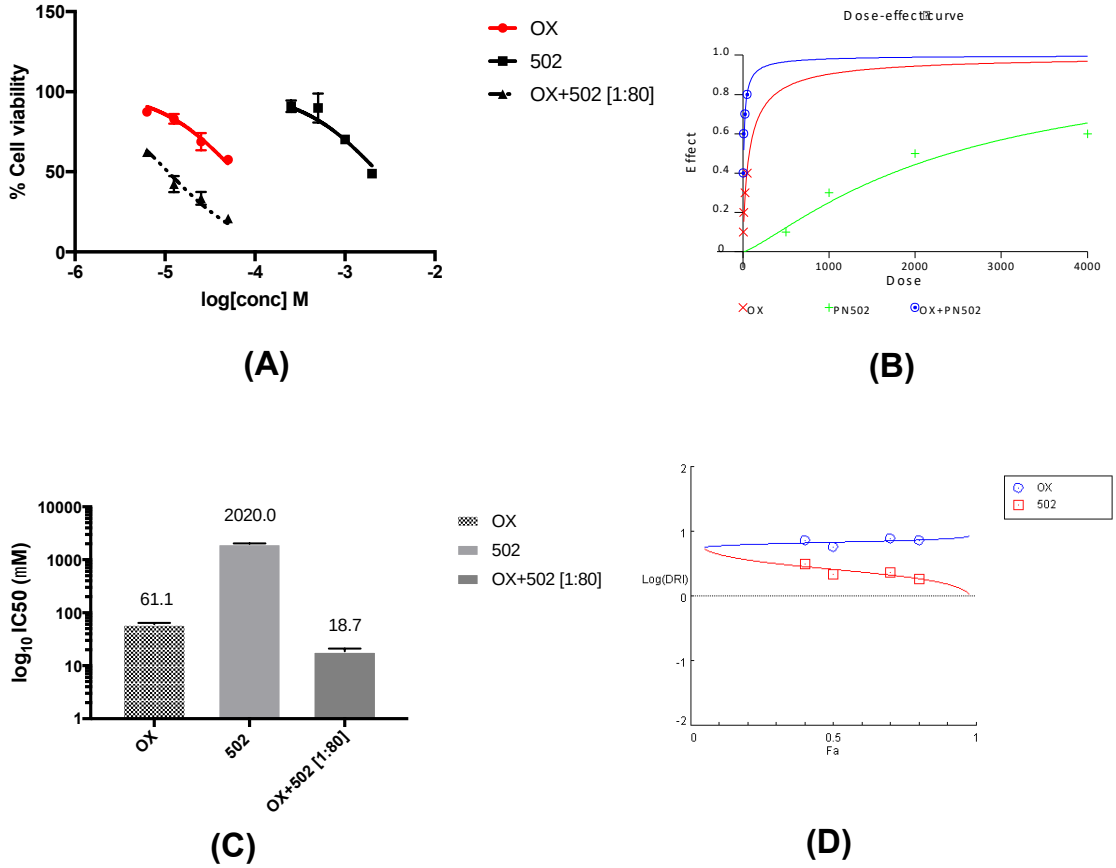

CI values at:

Drug Combo	ED50	ED75	ED90
OX+PN502 [1:80]	0.53	0.64	0.78

(E)

Figure 4.16 Drug combination plots for oxaliplatin and ortho-aspirin (OX+PN502[1:80]) in SW480 CRC cells.
Dose response curve (A). Dose-effect curve as plotted by CalcuSyn (B). Bar chart representation of IC_{50} by single compounds and their combination (C). Fa-log(DRI) plot as plotted by CompuSyn (D). CI values as calculated by CompuSyn at ED_{50}, ED_{75} and ED_{90}. OX=Oxaliplatin.

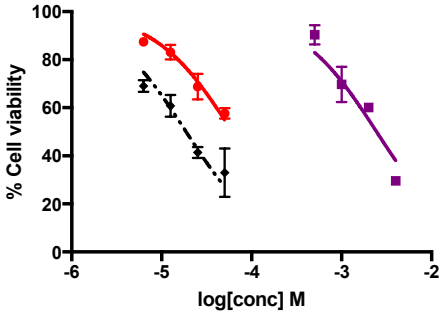

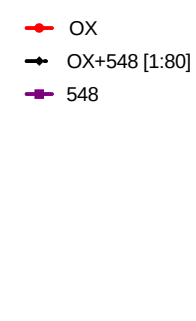

(A)

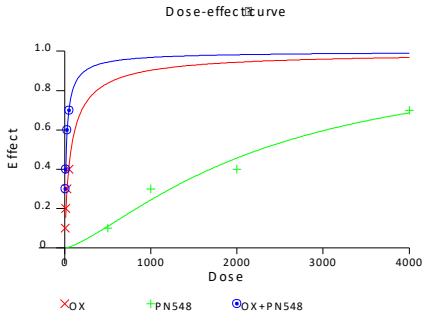

(B)

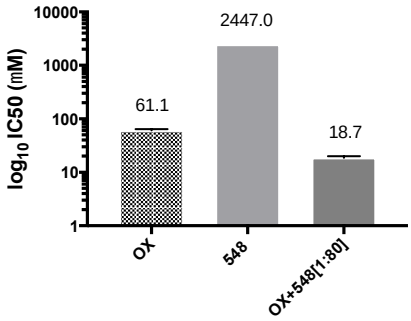

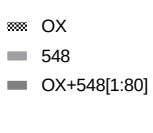

(C)

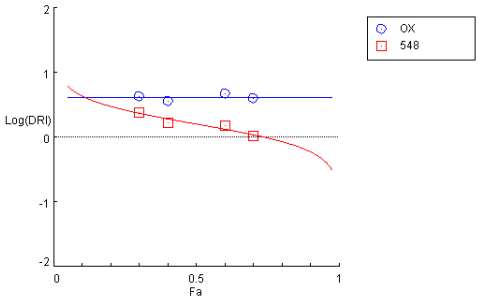

(D)

CI values at:

Drug Combo	ED50	ED75	ED90
OX+PN548 [1:80]	0.87	1.27	1.93

(E)

Figure 4.17 Drug combination plots for oxaliplatin and meta-aspirin (OX+PN548[1:80]) in SW480 CRC cells.
Dose response curve (A). Dose-effect curve as plotted by CalcuSyn (B). Bar chart representation of IC_{50} by single compounds and their combination (C). Fa-log(DRI) plot as plotted by CompuSyn (D). CI values as calculated by CompuSyn at ED_{50}, ED_{75} and ED_{90}. OX=Oxaliplatin.

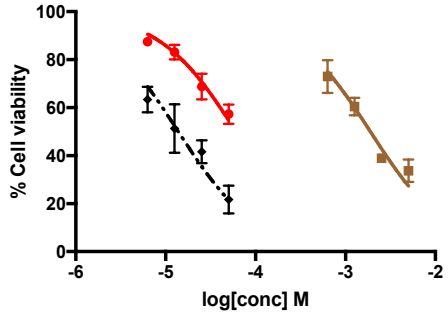

(A)

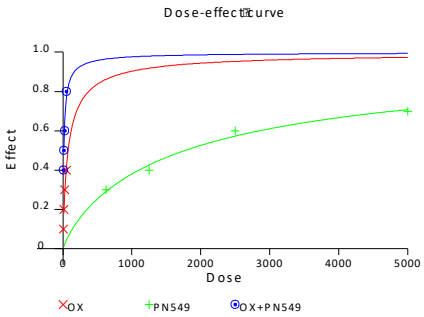

(B)

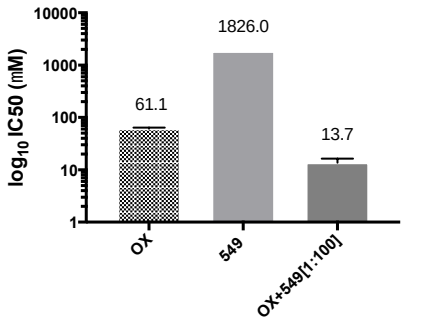

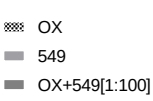

(C)

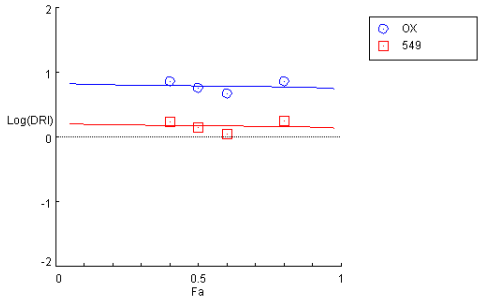

(D)

CI values at:

Drug Combo	ED50	ED75	ED90
OX+PN549 [1:100]	0.82	0.84	0.86

(E)

Figure 4.18 Drug combination plots for oxaliplatin and para-aspirin (OX+PN549[1:100]) in SW480 CRC cells.
Dose response curve (A). Dose-effect curve as plotted by CalcuSyn (B). Bar chart representation of IC_{50} by single compounds and their combination (C). Fa-log(DRI) plot as plotted by CompuSyn (D). CI values as calculated by CompuSyn at ED_{50}, ED_{75} and ED_{90}. OX=Oxaliplatin.

Oxaliplatin was used in combination with aspirin and its isomers, PN502 (aspirin), PN548 (meta-aspirin) and PN549 (para-aspirin) at 1:80 (Figure 4.18A, B, C, D and E), 1:80 (Figure 4.19A, B, C, D and E) and 1:100 (Figure 4.20A, B, C, D and E) respectively.

Oxaliplatin in combination with PN548 had synergistic effects at lower doses i.e. ED_{50} and lower, but the combinations became antagonistic with increase in concentration at ED_{75} and ED_{90} (Table 4.5). This is unfavourable in anticancer therapy because high cytotoxicity to the cancer cells is needed for the combination to be effective (Chou, 2010). However, there was a synergistic effect when oxaliplatin was combined with PN502 [1:80] against SW480 CRC cells (Figure 4.18) and the ED_{50} of oxaliplatin was decreased from 72.9μM to 10.6μM. The ED_{50} for oxaliplatin when in combination with PN549 [1:100] also decreased from 72.9μM to 11.7μM (Figure 4.20).

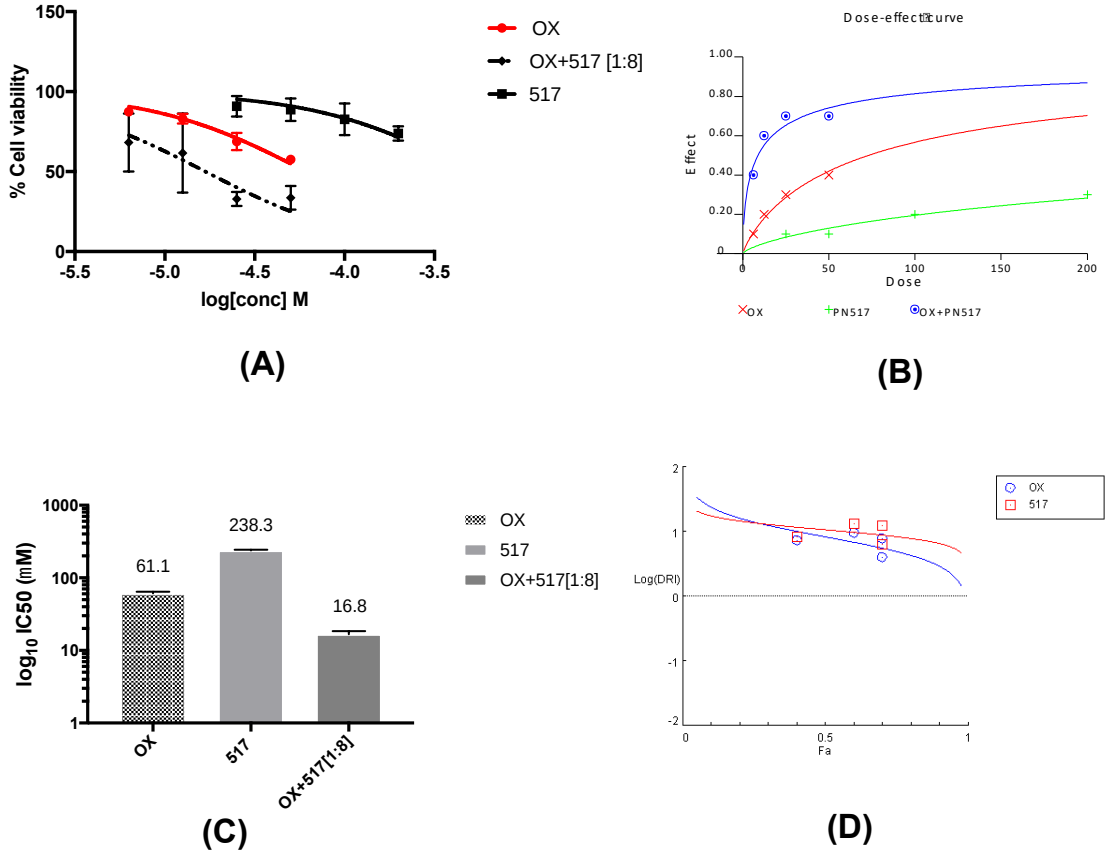

CI values at:

Drug Combo	ED50	ED75	ED90
OX+PN517 [1:8]	0.21	0.32	0.50

(E)

Figure 4.19 Drug combination plots for oxaliplatin and fumaryldiaspirin (OX+PN517[1:8]) in SW480 CRC cells.
Dose response curve (A). Dose-effect curve as plotted by CalcuSyn (B). Bar chart representation of IC_{50} by single compounds and their combination (C). Fa-log(DRI) plot as plotted by CompuSyn (D). CI values as calculated by CompuSyn at ED_{50}, ED_{75} and ED_{90}. OX=Oxaliplatin.

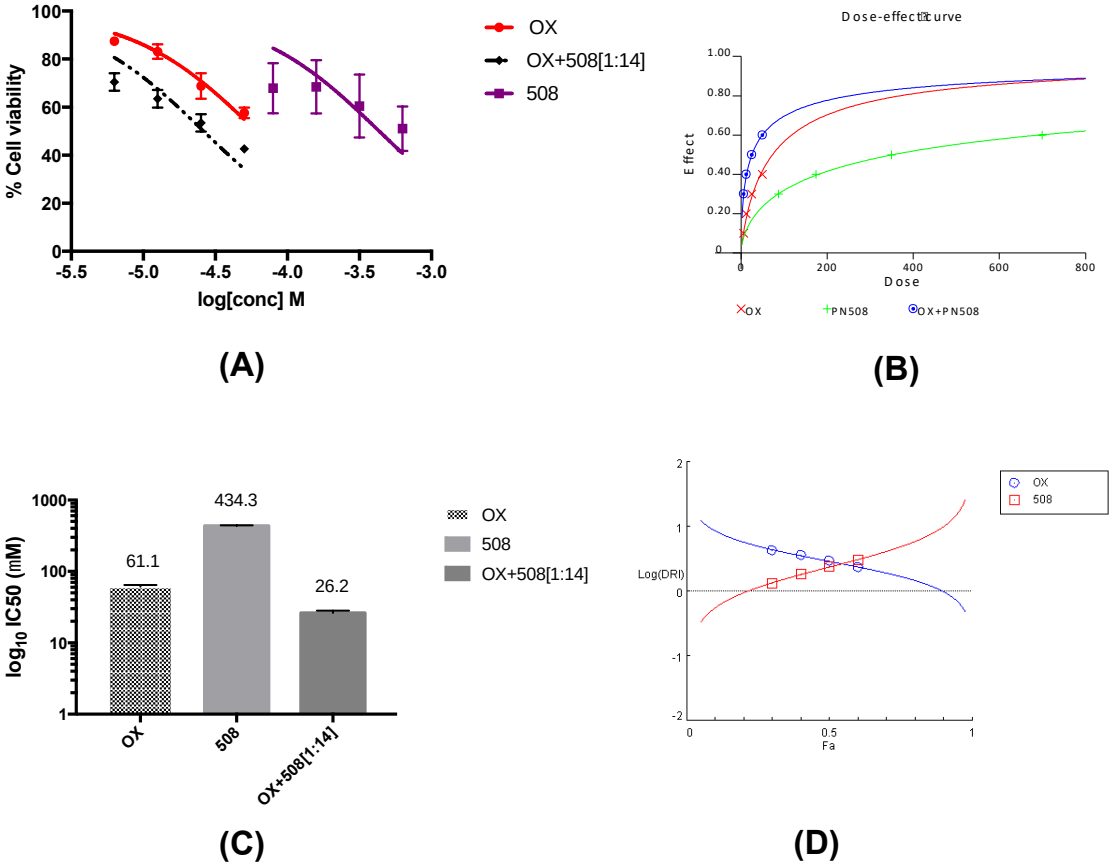

CI values at:

Drug Combo	ED50	ED75	ED90
OX+PN508 [1:14]	0.77	0.80	1.12

(E)

Figure 4.20 Drug combination plots for oxaliplatin and diaspirin (OX+PN508[1:14]) in SW480 CRC cells.
Dose response curve (A). Dose-effect curve as plotted by CalcuSyn (B). Bar chart representation of IC_{50} by single compounds and their combination (C). Fa-log(DRI) plot as plotted by CompuSyn (D). CI values as calculated by CompuSyn at ED_{50}, ED_{75} and ED_{90}. OX=Oxaliplatin.

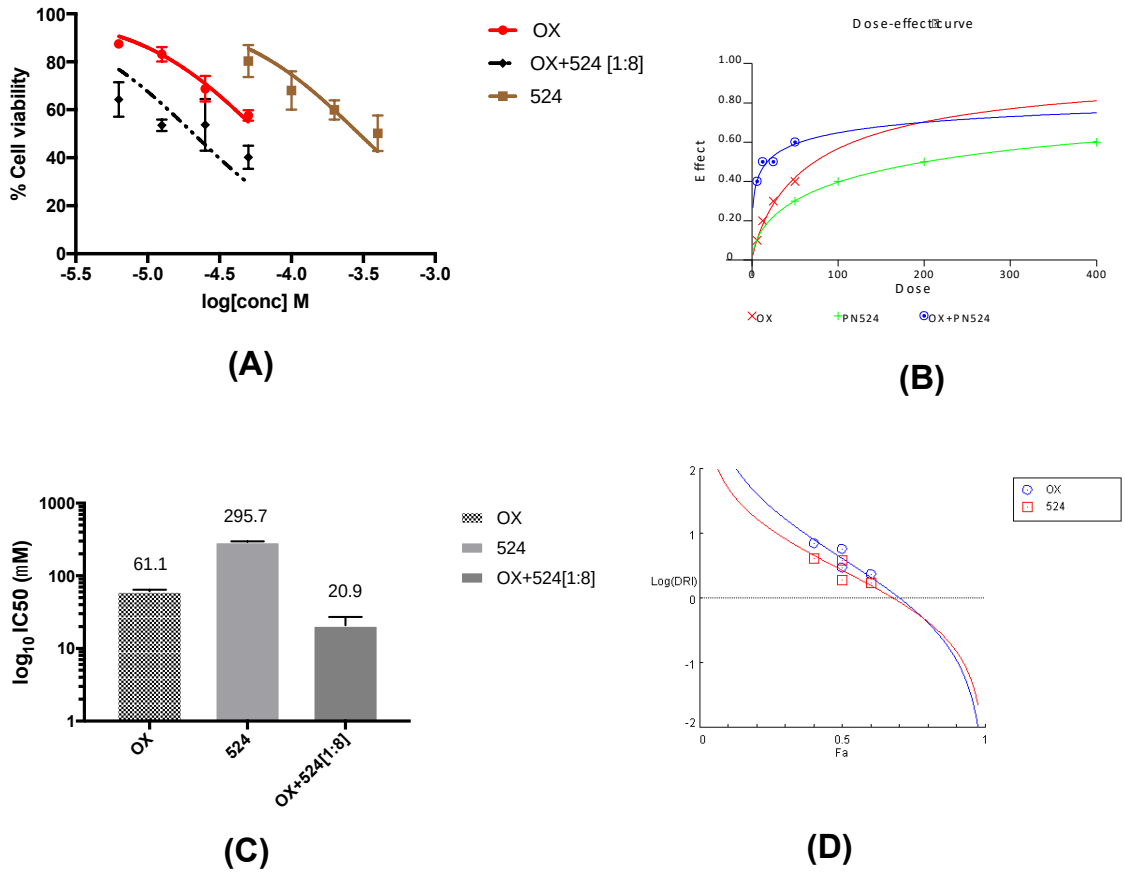

CI values at:

Drug Combo	ED50	ED75	ED90
OX+PN524 [1:8]	0.61	3.10	>10

(E)

Figure 4.21 Drug combination plots for oxaliplatin and m-bromobenzoylsalicylate (OX+PN524[1:8]) in SW480 CRC cells.
Dose response curve (A). Dose-effect curve as plotted by CalcuSyn (B). Bar chart representation of IC_{50} by single compounds and their combination (C). Fa-log(DRI) plot as plotted by CompuSyn (D). CI values as calculated by CompuSyn at ED_{50}, ED_{75} and ED_{90}. OX=Oxaliplatin**.**

Oxaliplatin used in combination with the ‘diaspirins’, PN517, PN508 and PN524 against SW480 cells at 1:8 (Figure 4.21A, B, C, D and E), 1:14 (Figure 4.22A, B, C, D and E) and 1:8 (Figure 4.23A, B, C, D and E) concentrations respectively resulted in a combination of synergistic and antagonistic effects at ED_{50}, ED_{75} and ED_{90}.

Oxaliplatin in combination with PN517 [1:8] had a synergistic effect on SW480 CRC cells (Figure 4.21) with a decrease in oxaliplatin ED_{50} from 72.9 μM to 8.8 μM (Figure 4.21D). ED_{50} for oxaliplatin in combination with PN580 [1:14] and in combination with PN524 [1:8] decreased from 72.9 μM to 25.2 μM (Figure 4.22D) and 17.7 μM (Figure 4.23D) respectively.

PN517 (Figure 4.21) had synergistic effects at ED_{50}, ED_{75} and ED_{90} with PN508 (Figure 4.22) and PN524 (Figure 4.23) having synergistic effects at ED_{50} but antagonistic when the dose was increased to ED_{90}.

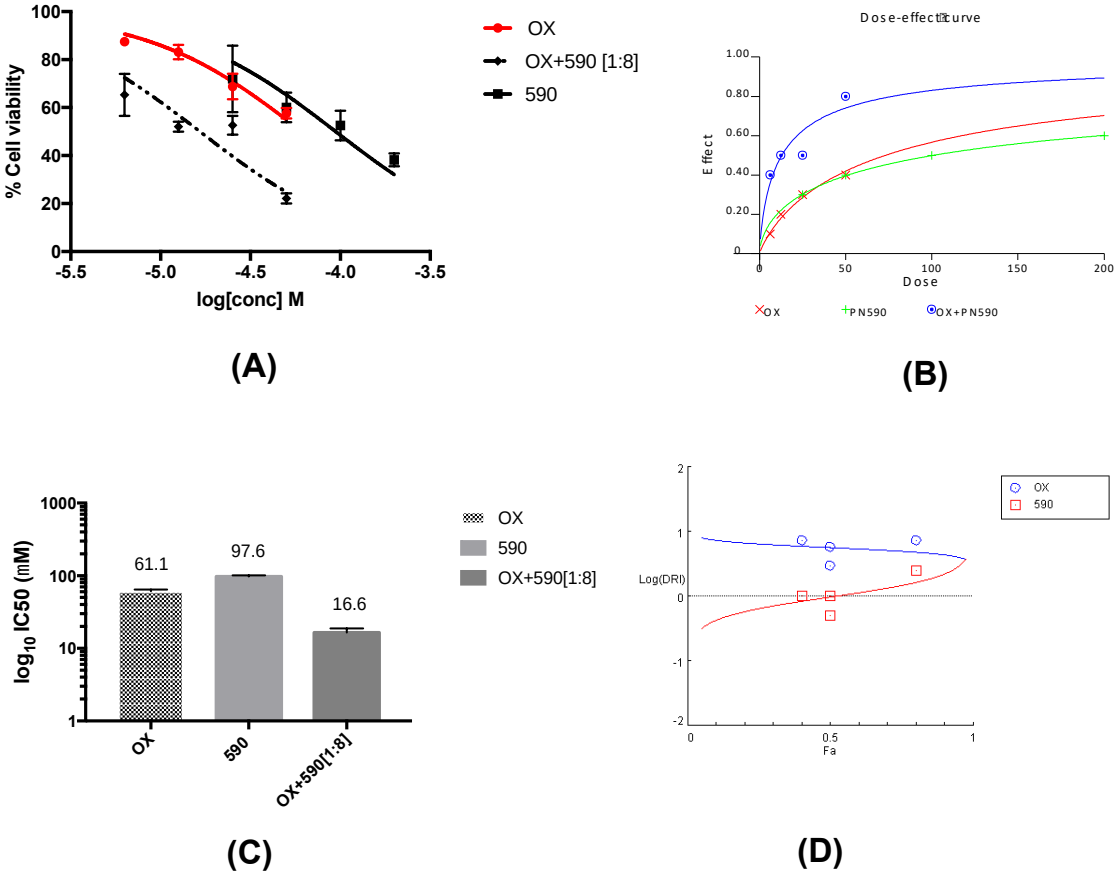

CI values at:

Drug Combo	ED50	ED75	ED90
OX+PN590 [1:8]	1.20	0.88	0.68

(E)

Figure 4.22 Drug combination plots for oxaliplatin and ortho-thioaspirin (OX+PN590[1:8]) in SW480 CRC cells.
Dose response curve (A). Dose-effect curve as plotted by CalcuSyn (B). Bar chart representation of IC_{50} by single compounds and their combination (C). Fa-log(DRI) plot as plotted by CompuSyn (D). CI values as calculated by CompuSyn at ED_{50}, ED_{75} and ED_{90}. OX=Oxaliplatin.

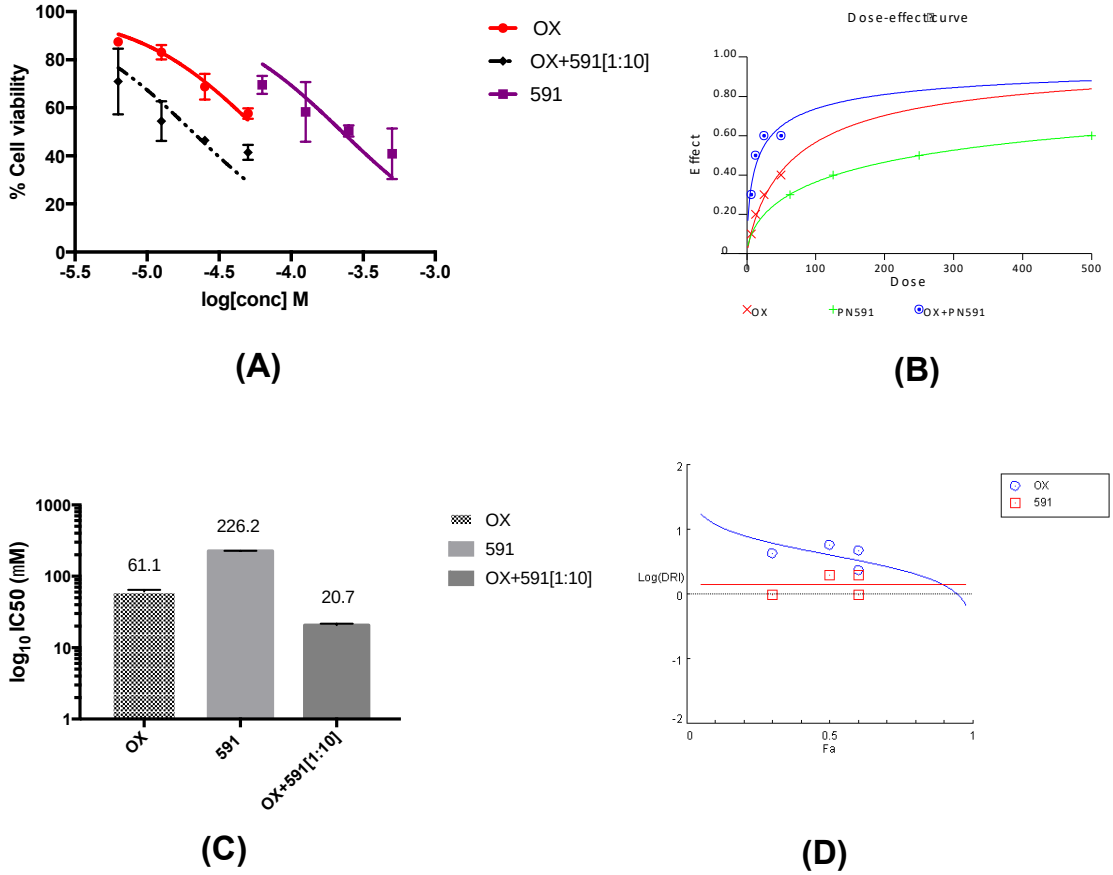

CI values at:

Drug Combo	ED50	ED75	ED90
OX+PN591 [1:10]	0.96	1.14	1.44

(E)

Figure 4.23 Drug combination plots for oxaliplatin and meta-thioaspirin (OX+PN591[1:10]) in SW480 CRC cells.
Dose response curve (A). Dose-effect curve as plotted by CalcuSyn (B). Bar chart representation of IC_{50} by single compounds and their combination (C). Fa-log(DRI) plot as plotted by CompuSyn (D). CI values as calculated by CompuSyn at ED_{50}, ED_{75} and ED_{90}. OX=Oxaliplatin.

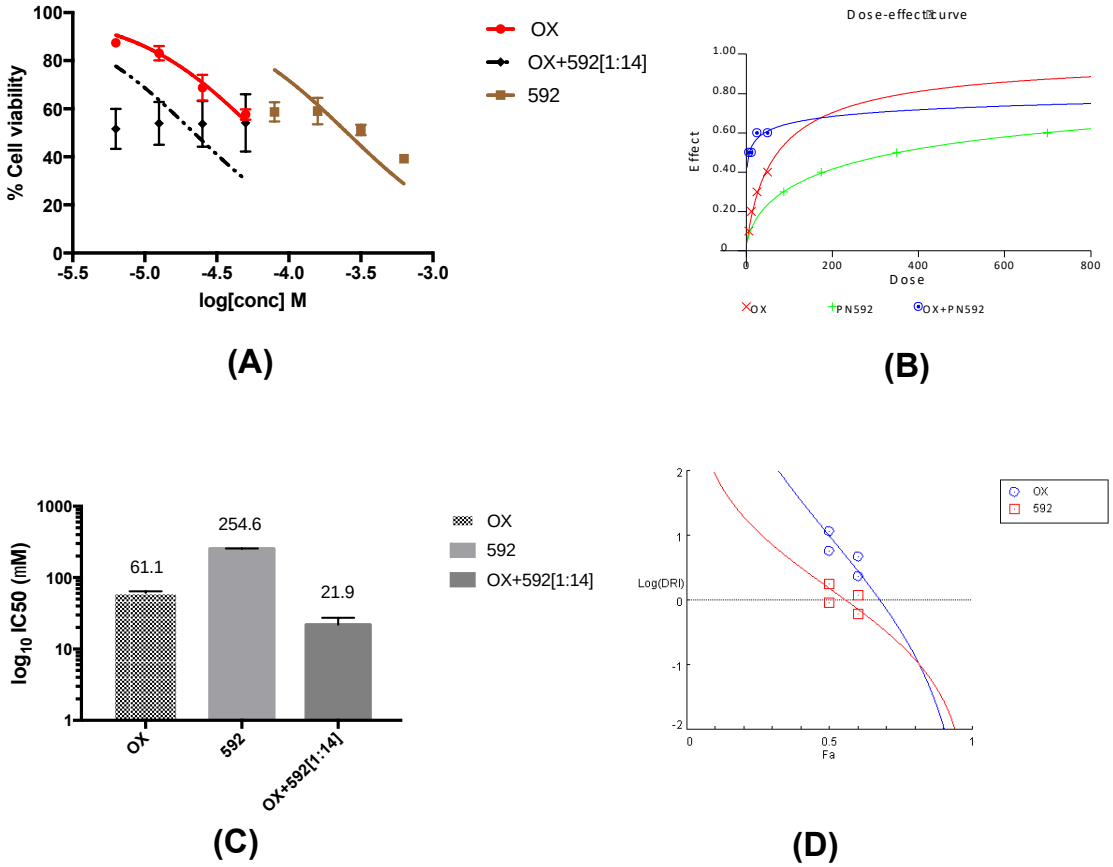

CI values at:

Drug Combo	ED50	ED75	ED90
OX+PN592 [1:14]	0.76	7.99	>10

(E)

Figure 4.24 Drug combination plots for oxaliplatin and para-thioaspirin (OX+PN592[1:14]) in SW480 CRC cells.
Dose response curve (A). Dose-effect curve as plotted by CalcuSyn (B). Bar chart representation of IC_{50} by single compounds and their combination (C). Fa-log(DRI) plot as plotted by CompuSyn (D). CI values as calculated by CompuSyn at ED_{50}, ED_{75} and ED_{90}. OX=Oxaliplatin.

Oxaliplatin when used in combination with thioaspirin, PN590 (Figure 4.24A, B, C, D and E) and its isomers [PN591 (Figure 4.25A, B, C, D and E) and PN592 (Figure 4.26A, B, C, D and E)] resulted in synergistic and antagonistic effects respectively.

Oxaliplatin in combination with PN592 had synergistic effects at lower doses i.e. ED_{50} and lower, but the combinations became antagonistic with increase in concentration at ED_{75} and ED_{90} (Table 4.5). This is unfavourable in anticancer therapy because high cytotoxicity to the cancer cells is needed for the combination to be effective. Synergistic effects between two compounds when used in combination at ED_{50} and above is favourable in the treatment of cancer as a maximum kill of the cancer cells accompanied by a decrease in dose required to make that kill is required for an ideal combination for cancer therapy (Chou, 2010).

The ED_{50} for oxaliplatin when used in combination with PN590 was reduced from 72.9 μM to 12.9 μM (Figure 4.24D). However, combinations with PN591 (Figure 4.25) and PN592 (Figure 4.26) had antagonistic effects.

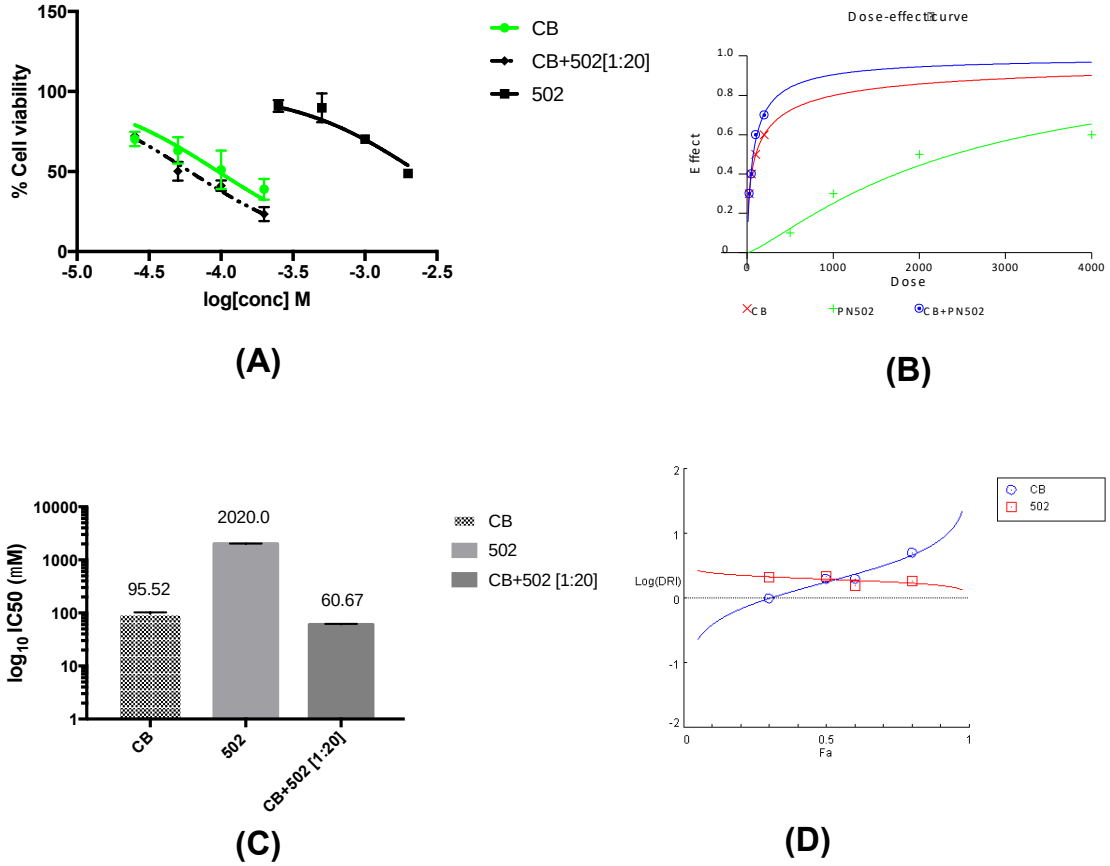

CI values at:

Drug Combo	ED50	ED75	ED90
CB+PN502 [1:20]	1.29	1.30	1.58

(E)

Figure 4.25 Drug combination plots for carboplatin and ortho-aspirin (CB+PN502[1:20]) in SW480 CRC cells.
Dose response curve (A). Dose-effect curve as plotted by CalcuSyn (B). Bar chart representation of IC_{50} by single compounds and their combination (C). Fa-log(DRI) plot as plotted by CompuSyn (D). CI values as calculated by CompuSyn at ED_{50}, ED_{75} and ED_{90}. CB=Carboplatin.

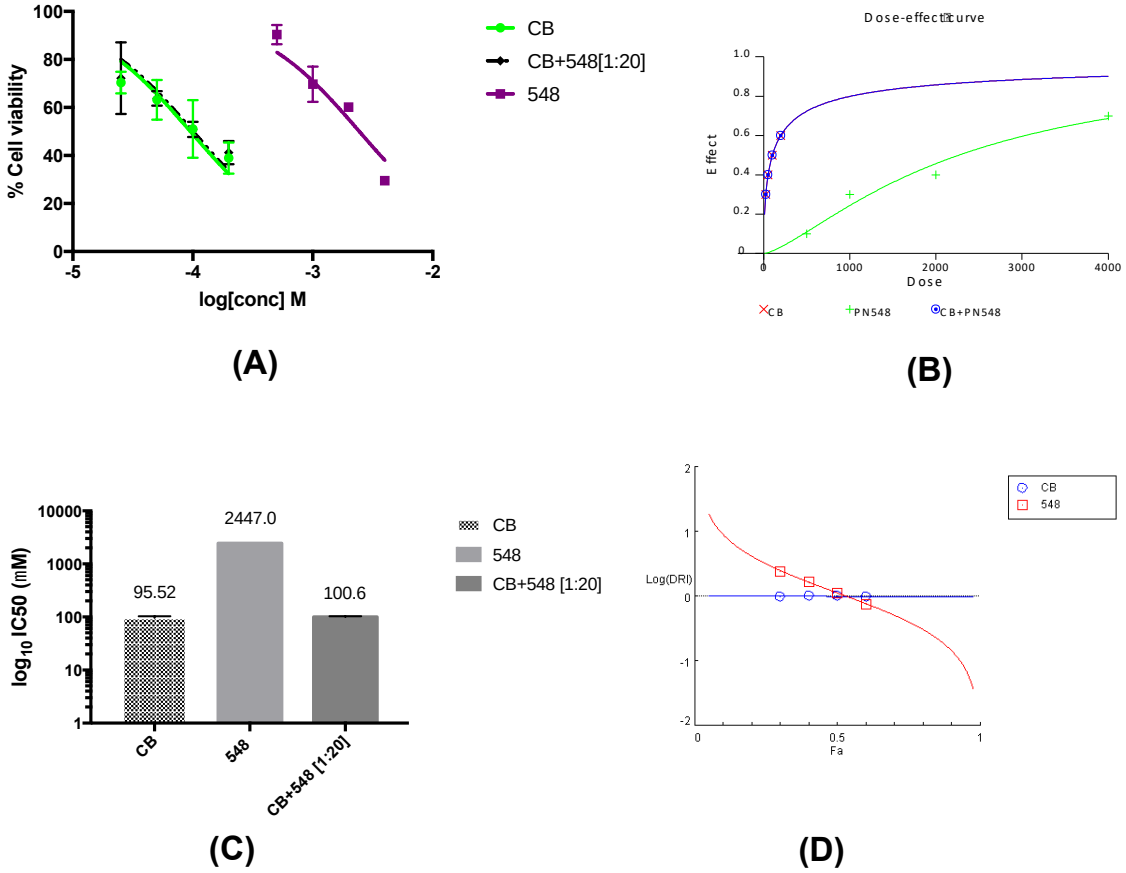

CI values at:

Drug Combo	ED50	ED75	ED90
CB+PN548 [1:20]	1.89	3.50	8.02

(E)

Figure 4.26 Drug combination plots for carboplatin and meta-aspirin (CB+PN548[1:20]) in SW480 CRC cells.
Dose response curve (A). Dose-effect curve as plotted by CalcuSyn (B). Bar chart representation of IC_{50} by single compounds and their combination (C). Fa-log(DRI) plot as plotted by CompuSyn (D). CI values as calculated by CompuSyn at ED_{50}, ED_{75} and ED_{90}. CB=Carboplatin.

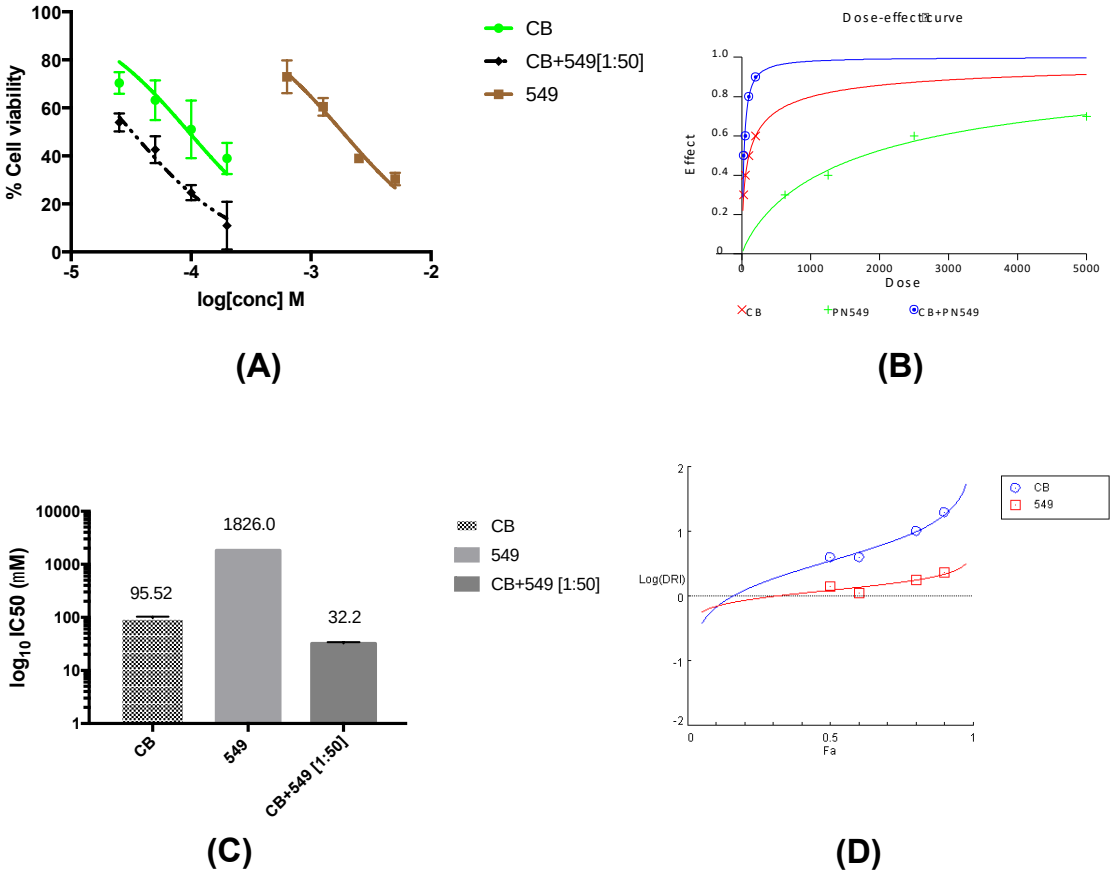

CI values at:

Drug Combo	ED50	ED75	ED90
CB+PN549 [1:50]	1.08	0.73	0.51

(E)

Figure 4.27 Drug combination plots for carboplatin and para-aspirin (CB+PN549[1:50]) in SW480 CRC cells.
Dose response curve (A). Dose-effect curve as plotted by CalcuSyn (B). Bar chart representation of IC_{50} by single compounds and their combination (C). Fa-log(DRI) plot as plotted by CompuSyn (D). CI values as calculated by CompuSyn at ED_{50}, ED_{75} and ED_{90}. CB=Carboplatin.

Carboplatin was used in combination with aspirin and its isomers, PN502 (aspirin), PN548 (meta-aspirin) and PN549 (para-aspirin) at 1:20 (Figure 4.27A, B, C, D and E), 1:20 (Figure 4.28A, B, C, D and E) and 1:50 (Figure 4.29A, B, C, D and E) respectively.

Amongst the aspirin isomers, PN549 stood out as the only one that had a synergistic effect when used in combination with carboplatin against SW480 CRC cells (Figure 4.29). The ED_{50} for carboplatin in combination with PN549 [1:50] reduced from 100.6μM to 28μM. Carboplatin in combination with aspirin and PN548 had antagonistic effects (Figure 4.27 and 4.28 respectively).

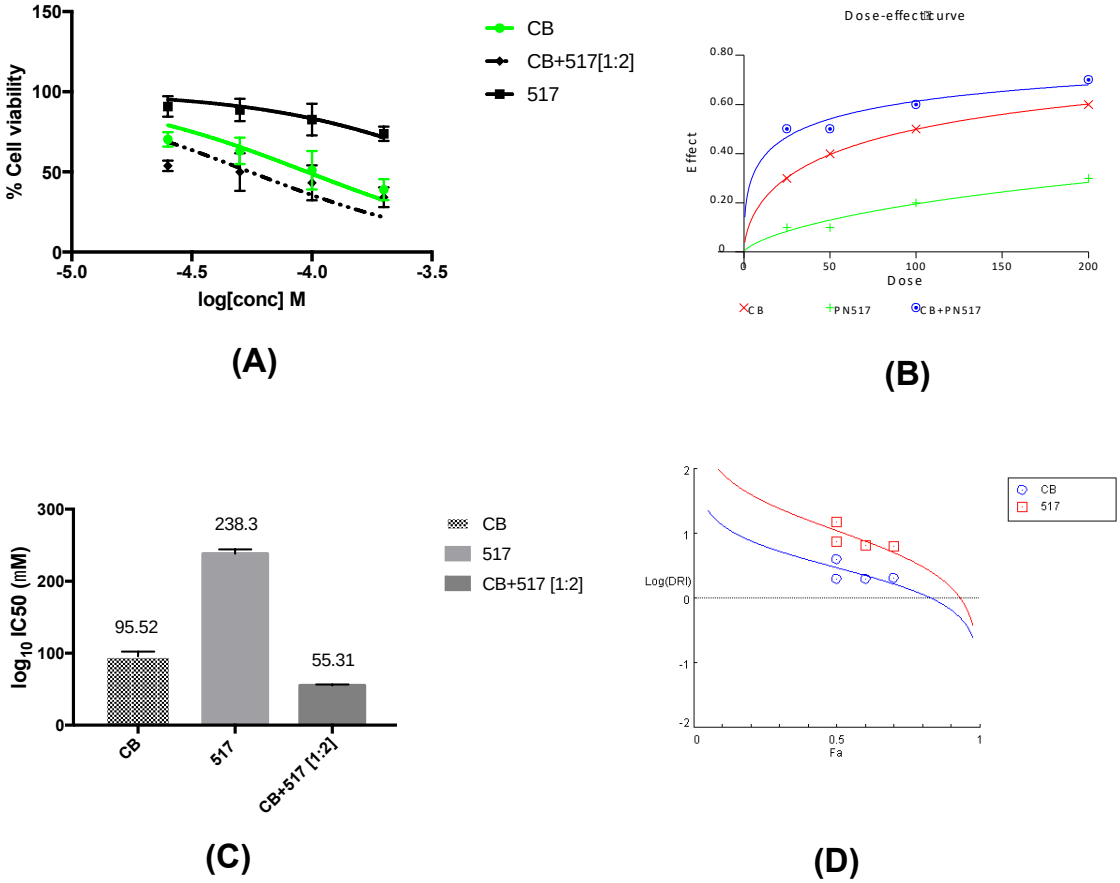

CI values at:

Drug Combo	ED50	ED75	ED90
CB+PN517 [1:2]	0.43	0.97	2.21

(E)

Figure 4.28 Drug combination plots for carboplatin and fumaryldiaspirin (CB+PN517[1:2]) in SW480 CRC cells.
Dose response curve (A). Dose-effect curve as plotted by CalcuSyn (B). Bar chart representation of IC_{50} by single compounds and their combination (C). Fa-log(DRI) plot as plotted by CompuSyn (D). CI values as calculated by CompuSyn at ED_{50}, ED_{75} and ED_{90}. CB=Carboplatin.

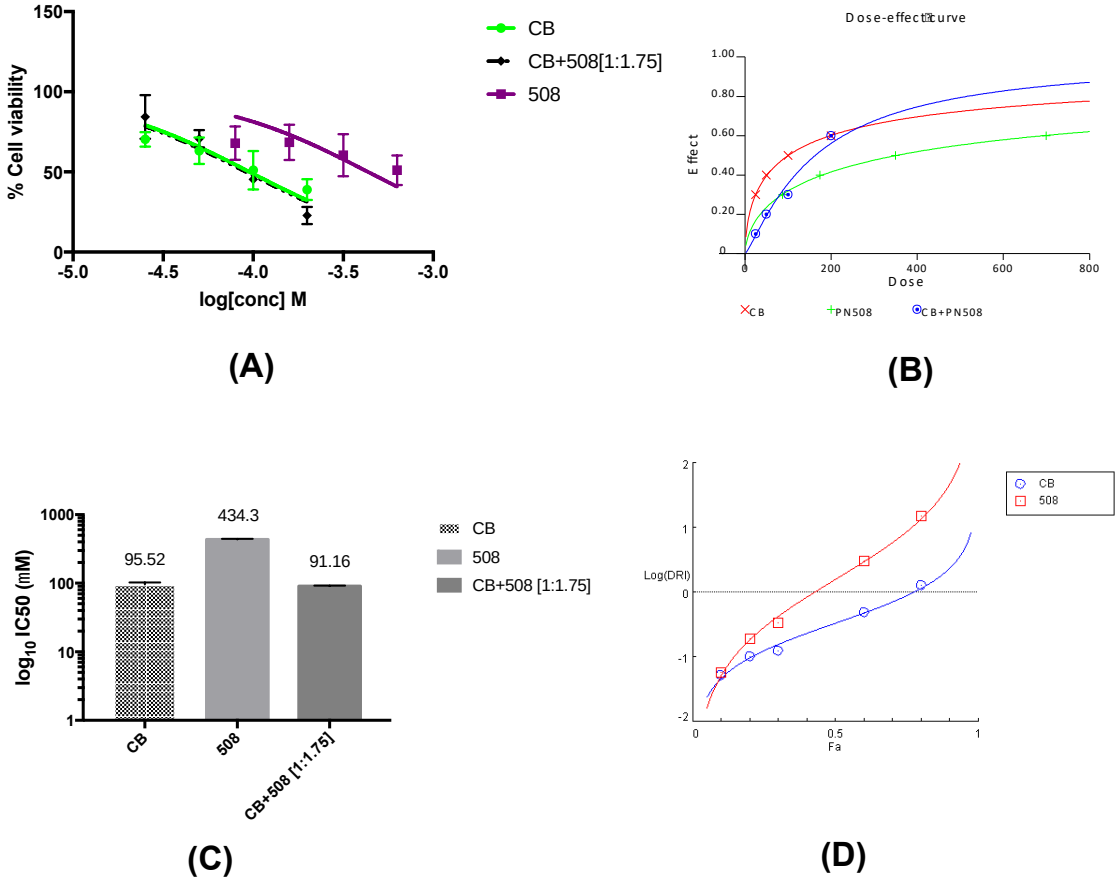

CI values at:

Drug Combo	ED50	ED75	ED90
CB+PN508 [1:1.75]	3.62	1.24	0.44

(E)

Figure 4.29 Drug combination plots for carboplatin and diaspirin (CB+PN508[1:1.75]) in SW480 CRC cells.
Dose response curve (A). Dose-effect curve as plotted by CalcuSyn (B). Bar chart representation of IC_{50} by single compounds and their combination (C). Fa-log(DRI) plot as plotted by CompuSyn (D). CI values as calculated by CompuSyn at ED_{50}, ED_{75} and ED_{90}. CB=Carboplatin.

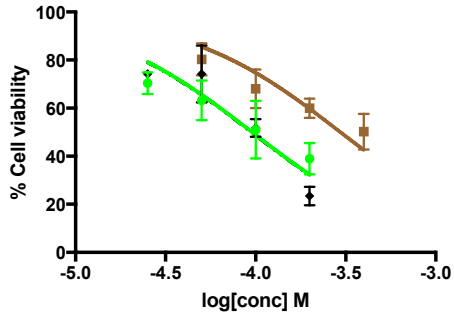

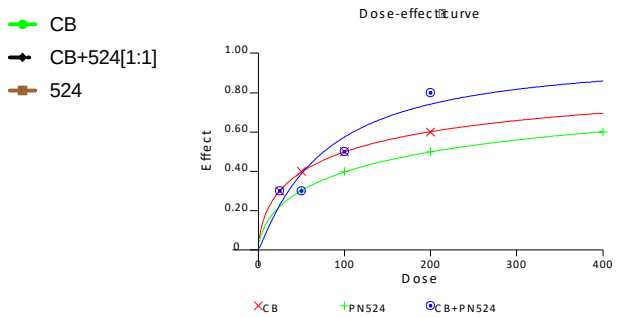

(A)

(B)

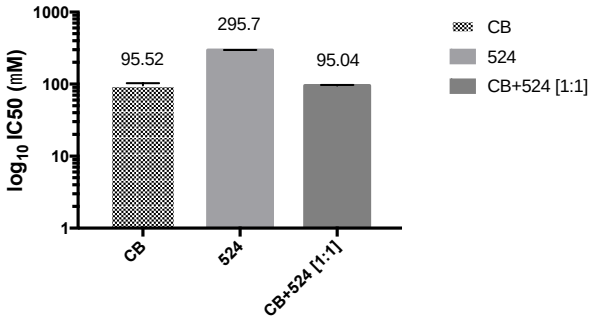

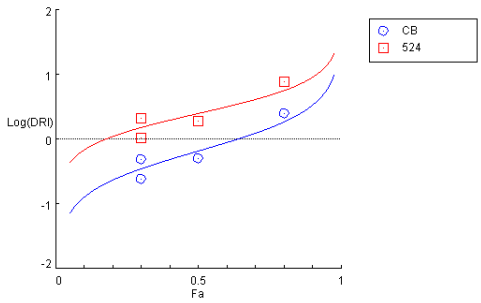

(C)

(D)

CI values at:

Drug Combo	ED50	ED75	ED90
CB+PN524 [1:1]	1.91	0.87	0.40

(E)

Figure 4.30 Drug combination plots for carboplatin and m-bromobenzoylsalicylate (CB+PN524[1:1]) in SW480 CRC cells .
Dose response curve (A). Dose-effect curve as plotted by CalcuSyn (B). Bar chart representation of IC_{50} by single compounds and their combination (C). Fa-log(DRI) plot as plotted by CompuSyn (D). CI values as calculated by CompuSyn at ED_{50}, ED_{75} and ED_{90}. CB=Carboplatin.

Carboplatin used in combination with the ‘diaspirins’, PN517 (Figure 4.30A, B, C, D and E), PN508 (Figure 4.31A, B, C, D and E) and PN524 (Figure 4.32A, B, C, D and E) against SW480 cells resulted in a combination of synergistic and antagonistic effects at ED_{50}, ED_{75} and ED_{90}.

PN517, PN508 and PN524 did not have favourable anticancer effects against SW480 CRC cells when used in combination with carboplatin (Figure 4.30, 4.31 and 4.32 respectively). Although, there was what seemed to be a synergistic effect between carboplatin with PN508 and PN524 at ED_{50}, the doses of carboplatin at ED_{50} increased rather than decrease when used in combination with the diaspirins. This increase in ED_{50} of carboplatin when in combination defeats one of the main reasons of combination therapy, which is to achieve a decrease in effective dose in order to reduce or alleviate side effects (Chou, 2010).

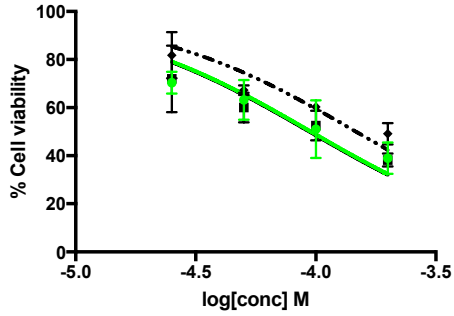

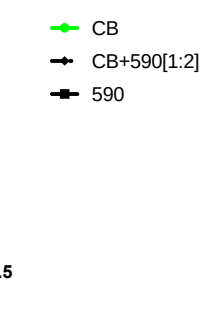

(A)

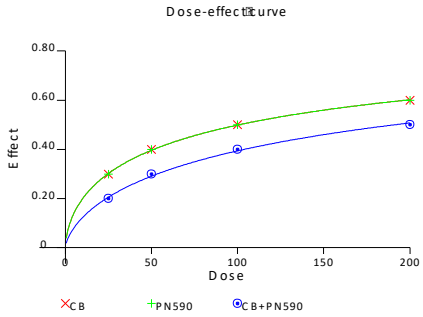

(B)

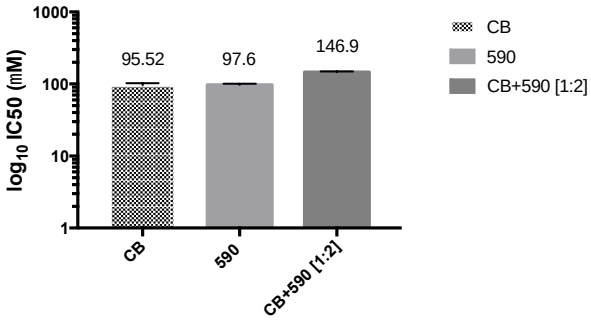

(C)

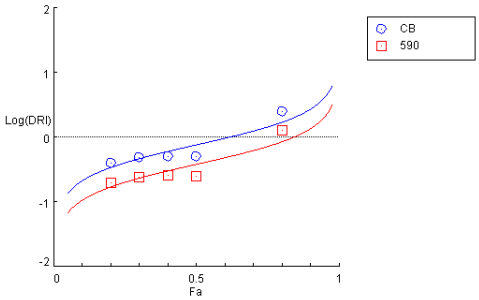

(D)

CI values at:

Drug Combo	ED50	ED75	ED90
CB+PN590 [1:2]	3.91	2.07	1.09

(E)

Figure 4.31 Drug combination plots for carboplatin and ortho-thioaspirin (CB+PN590[1:2]) in SW480 CRC cells.
Dose response curve (A). Dose-effect curve as plotted by CalcuSyn (B). Bar chart representation of IC_{50} by single compounds and their combination (C). Fa-log(DRI) plot as plotted by CompuSyn (D). CI values as calculated by CompuSyn at ED_{50}, ED_{75} and ED_{90}. CB=Carboplatin.

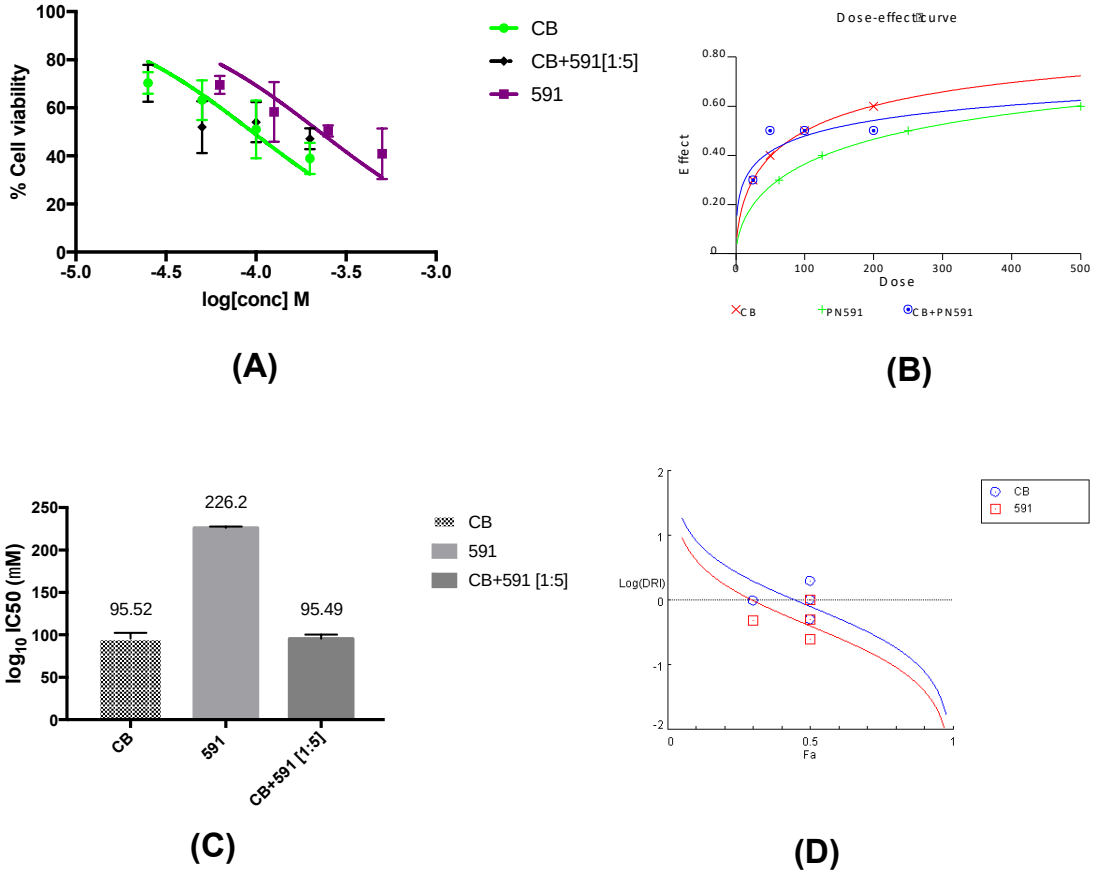

CI values at:

Drug Combo	ED50	ED75	ED90
CB+PN591 [1:5]	3.76	>10	>10

(E)

Figure 4.32 Drug combination plots for carboplatin and meta-thioaspirin (CB+PN591[1:5]) in SW480 CRC cells.
Dose response curve (A). Dose-effect curve as plotted by CalcuSyn (B). Bar chart representation of IC_{50} by single compounds and their combination (C). Fa-log(DRI) plot as plotted by CompuSyn (D). CI values as calculated by CompuSyn at ED_{50}, ED_{75} and ED_{90}. CB=Carboplatin.

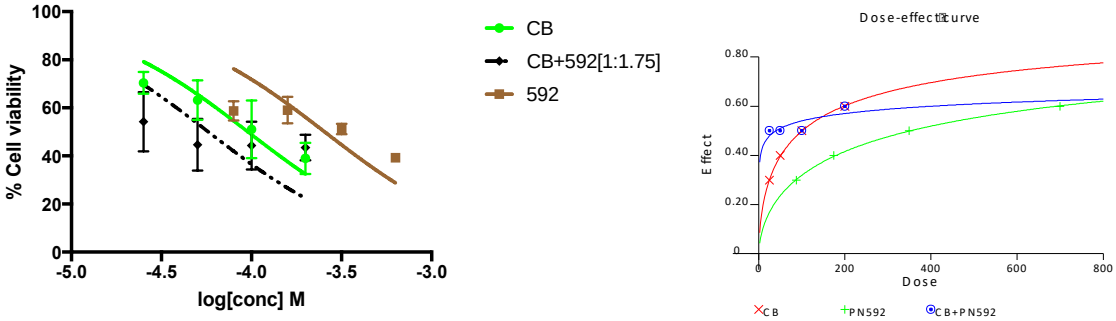

(A)

(B)

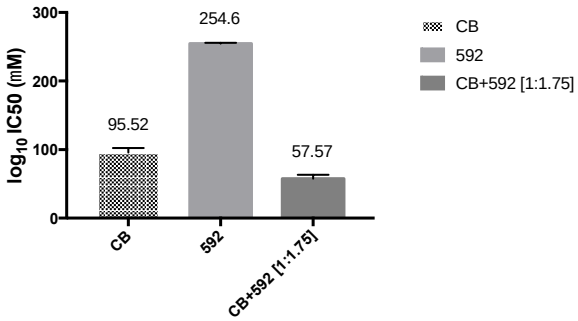

(C)

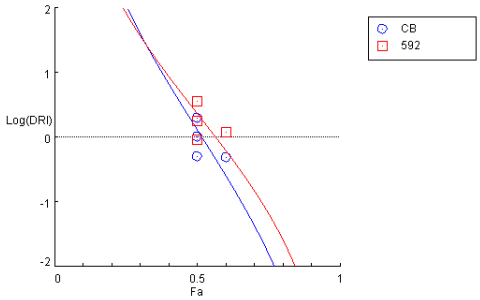

(D)

CI values at:

Drug Combo	ED50	ED75	ED90
CB+PN592 [1:1.75]	1.23	>10	>10

(E)

Figure 4.33 Drug combination plots for carboplatin and para-thioaspirin (CB+PN592[1:1.75]) in SW480 CRC cells.
Dose response curve (A). Dose-effect curve as plotted by CalcuSyn (B). Bar chart representation of IC_{50} by single compounds and their combination (C). Fa-log(DRI) plot as plotted by CompuSyn (D). CI values as calculated by CompuSyn at ED_{50}, ED_{75} and ED_{90}. CB=Carboplatin.

Carboplatin when used in combination with thioaspirins, PN590, PN591 (meta-thioaspirin) and PN592 (para-thioaspirin) resulted in antagonistic effects.

Carboplatin, in combination with PN590 (Figure 4.33A, B, C, D and E), PN591 (Figure 4.34A, B, C, D and E) and PN592 (Figure 4.35A, B, C, D and E) all had strong synergistic effects against the colorectal cell line. Some of the combinations showed strong antagonism due to very high CI values. This is possible in some combinations as the synergy scale is from 1 to 0 and the antagonism scale is from 1 to infinity (Chou, 2010).

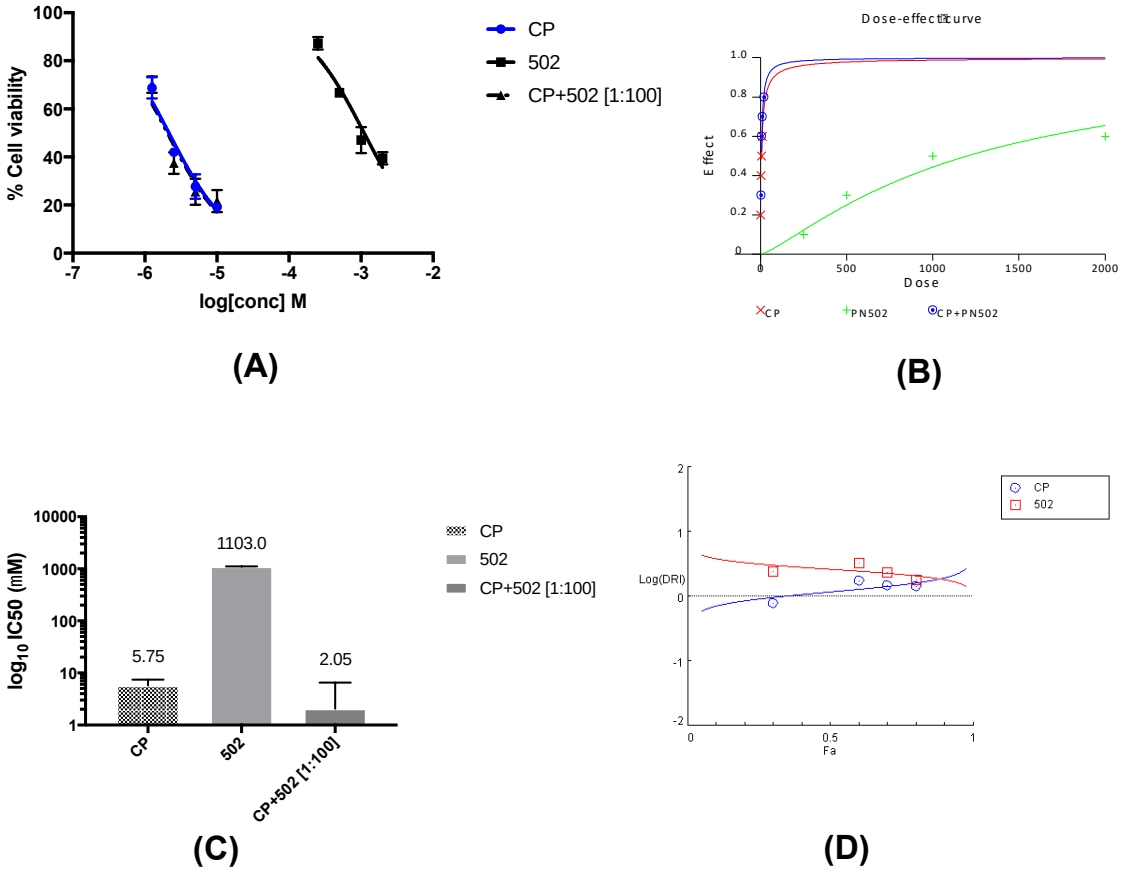

CI values at:

Drug Combo	ED50	ED75	ED90
CP+PN502 [1:100]	1.24	1.12	1.07

(E)

Figure 4.34 Drug combination plots for cisplatin and ortho-aspirin (CP+PN502[1:100]) in OE33 oesophageal cancer cells.
Dose response curve (A). Dose-effect curve as plotted by CalcuSyn (B). Bar chart representation of IC_{50} by single compounds and their combination (C). Fa-log(DRI) plot as plotted by CompuSyn (D). CI values as calculated by CompuSyn at ED_{50}, ED_{75} and ED_{90}. CP=Cisplatin.

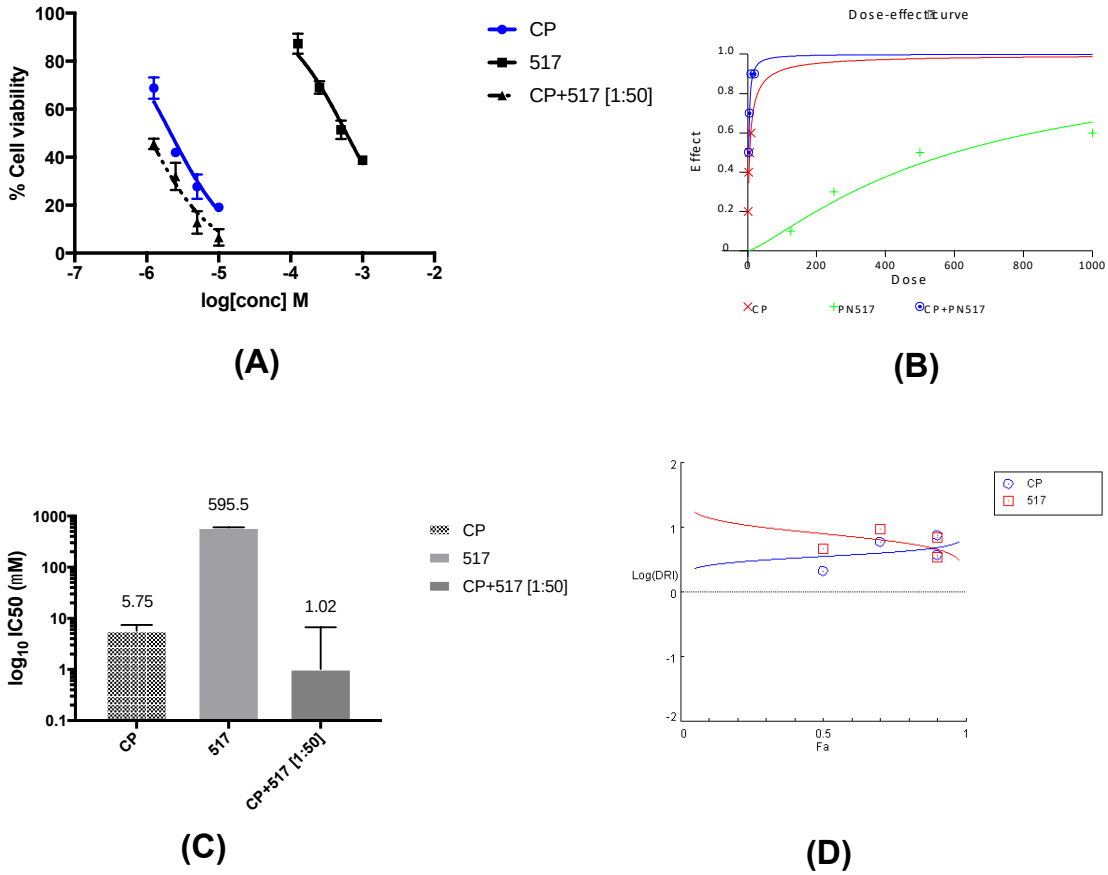

CI values at:

Drug Combo	ED50	ED75	ED90
CP+PN517 [1:50]	0.40	0.40	0.45

(E)

Figure 4.35 Drug combination plots for cisplatin and fumaryldiaspirin (CP+PN517[1:50]) in OE33 oesophageal cancer cells.
Dose response curve (A). Dose-effect curve as plotted by CalcuSyn (B). Bar chart representation of IC_{50} by single compounds and their combination (C). Fa-log(DRI) plot as plotted by CompuSyn (D). CI values as calculated by CompuSyn at ED_{50}, ED_{75} and ED_{90}. CP=Cisplatin.

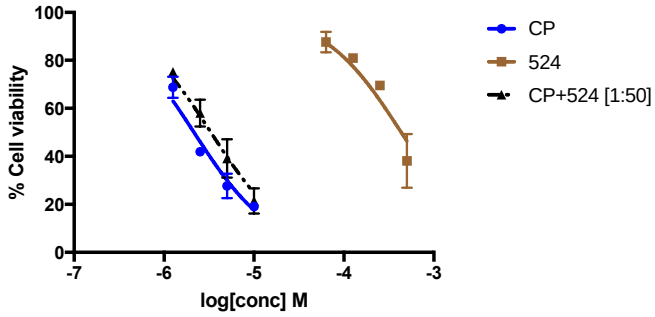

(A)

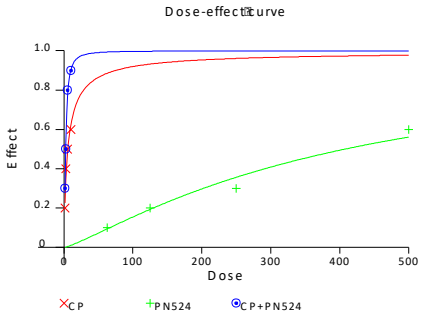

(B)

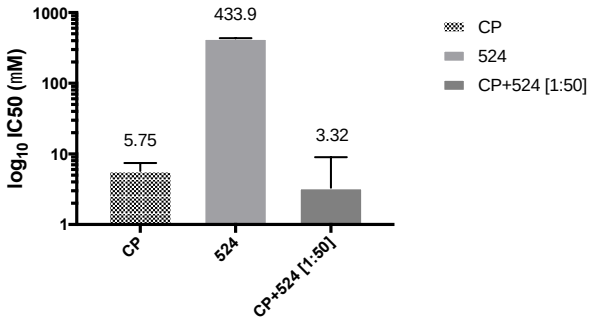

(C)

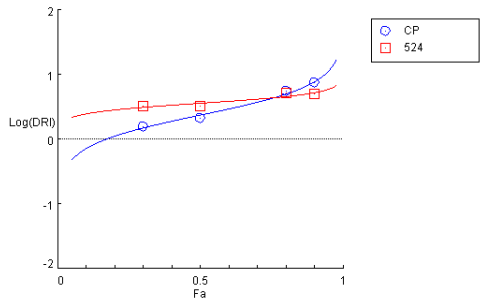

(D)

CI values at:

Drug Combo	ED50	ED75	ED90
CP+PN524 [1:50]	0.70	0.46	0.32

(E)

Figure 4.36 Drug combination plots for cisplatin and m-bromobenzoylsalicylate (CP+PN524[1:50]) in OE33 oesophageal cancer cells.
Dose response curve (A). Dose-effect curve as plotted by CalcuSyn (B). Bar chart representation of IC_{50} by single compounds and their combination (C). Fa-log(DRI) plot as plotted by CompuSyn (D). CI values as calculated by CompuSyn at ED_{50}, ED_{75} and ED_{90}. CP=Cisplatin.

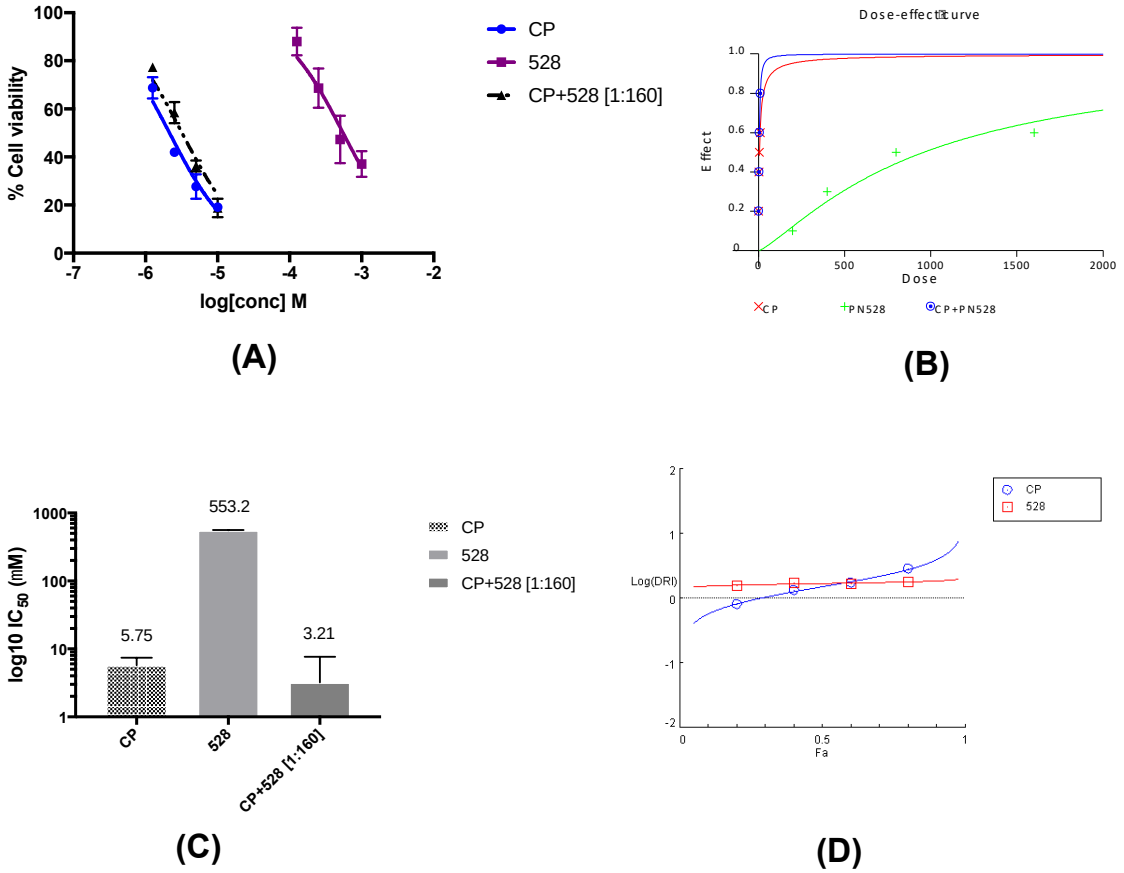

CI values at:

Drug Combo	ED50	ED75	ED90
CP+PN528 [1:160]	1.25	0.97	0.79

(E)

Figure 4.37 Drug combination plots for cisplatin and methyl-benzoylsalicylate (CP+PN528[1:160]) in OE33 oesophageal cancer cells.
Dose response curve (A). Dose-effect curve as plotted by CalcuSyn (B). Bar chart representation of IC_{50} by single compounds and their combination (C). Fa-log(DRI) plot as plotted by CompuSyn (D). CI values as calculated by CompuSyn at ED_{50}, ED_{75} and ED_{90}. CP=Cisplatin.

Cisplatin in combination with PN502 [1:100] against OE33 oesophageal cancer cells had an additive effect (Figure 4.36A, B, C, D and E). Synergistic effects were achieved when cisplatin was combined with PN517 [1:50] with the ED_{50} for cisplatin reduced from 5.36μM to 1.49μM (Figure 4.37A, B, C, D and E). Synergistic effects at ED_{50}, ED_{75} and ED_{90} were also observed when cisplatin was combined with PN524 [1:50] against the oesophageal cell line and accompanied by a reduction in the ED_{50} of cisplatin from 5.36μM to 2.25μM (Figure 4.38A, B, C, D and E). PN528 in combination with cisplatin had an additive effect at ED_{50}, however, at higher doses, synergistic effects were achieved (Figure 4.39A, B, C, d and E) with a drop in ED_{50} for cisplatin from 5.36μM to 3.54μM.

In OE33 oesophageal cancer cell line, the ED_{50} for cisplatin when used in combination with PN517 [1:50] reduced from 5.4μM to 1.5μM while that of PN517 reduced from 599.7μM to 74.6μM. ED_{50} reduced from 5.4μM and 407.7μM to 2.3μM and 112.6μM respectively for cisplatin and PN524 [1:50] when in combination.

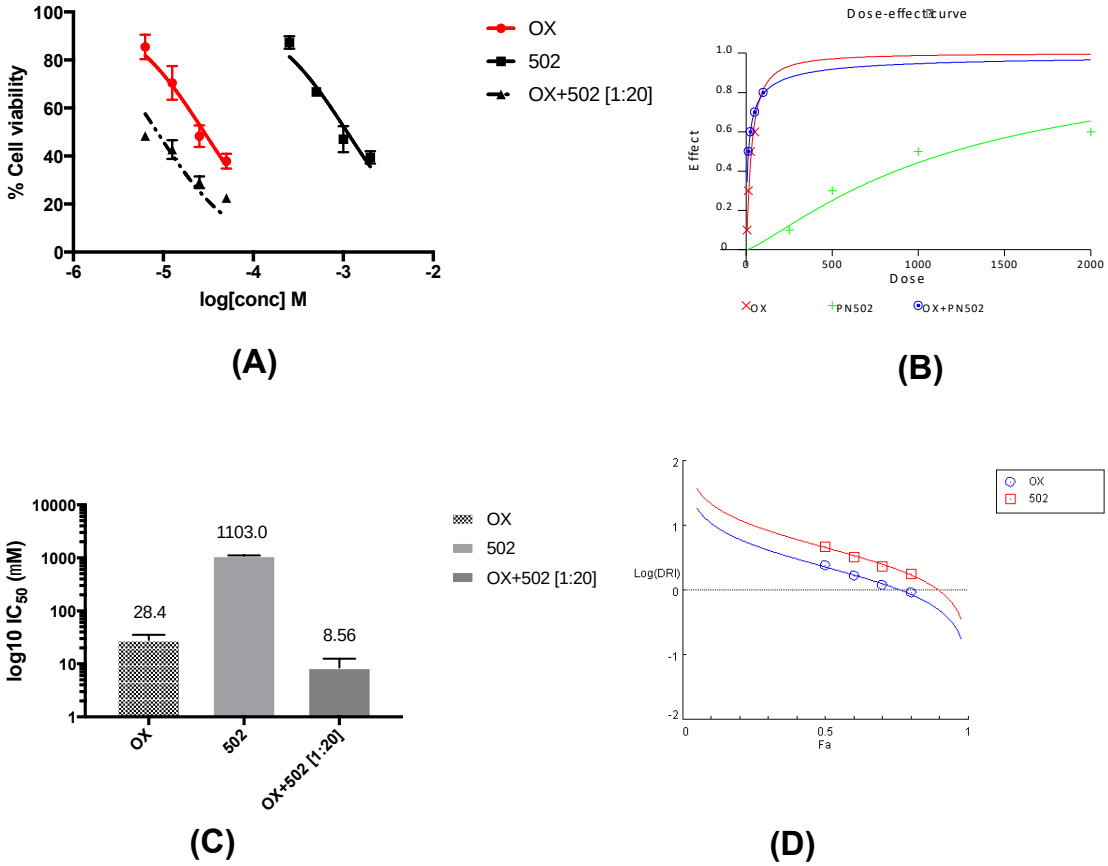

CI values at:

Drug Combo	ED50	ED75	ED90
OX+PN502 [1:20]	0.65	1.42	3.09

(E)

Figure 4.38 Drug combination plots for oxaliplatin and ortho-aspirin (OX+PN502[1:20]) in OE33 oesophageal cancer cells.
Dose response curve (A). Dose-effect curve as plotted by CalcuSyn (B). Bar chart representation of IC_{50} by single compounds and their combination (C). Fa-log(DRI) plot as plotted by CompuSyn (D). CI values as calculated by CompuSyn at ED_{50}, ED_{75} and ED_{90}. OX=Oxaliplatin.

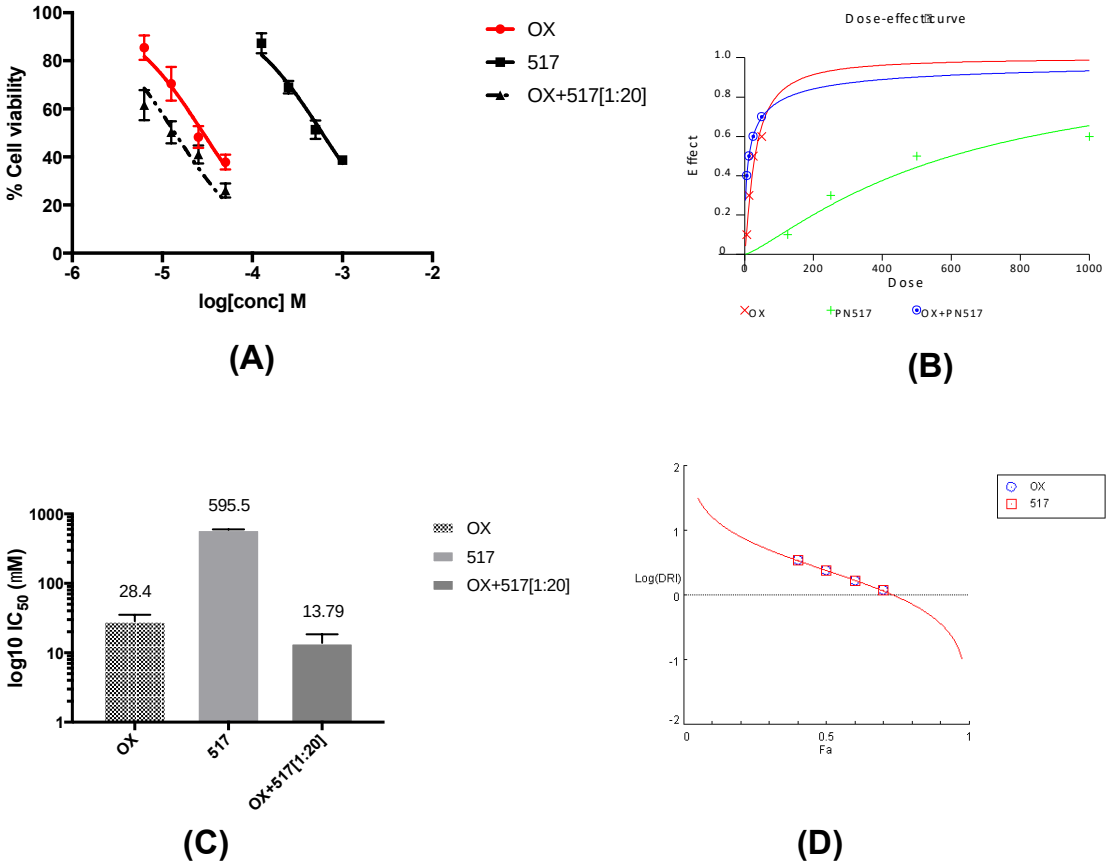

CI values at:

Drug Combo	ED50	ED75	ED90
OX+PN517 [1:20]	0.83	2.14	5.53

(E)

Figure 4.39 Drug combination plots for oxaliplatin and fumaryldiaspirin (OX+PN517[1:20]) in OE33 oesophageal cancer cells.
Dose response curve (A). Dose-effect curve as plotted by CalcuSyn (B). Bar chart representation of IC_{50} by single compounds and their combination (C). Fa-log(DRI) plot as plotted by CompuSyn (D). CI values as calculated by CompuSyn at ED_{50}, ED_{75} and ED_{90}. OX=Oxaliplatin.

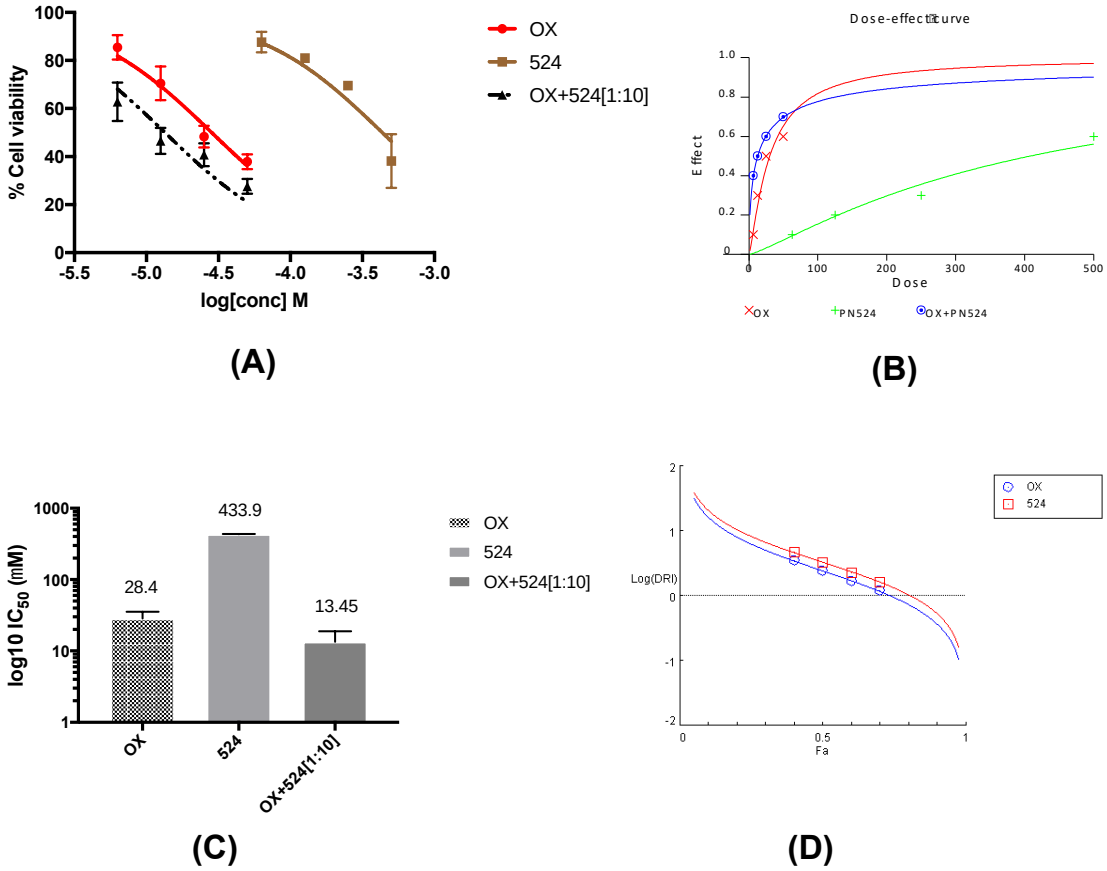

CI values at:

Drug Combo	ED50	ED75	ED90
OX+PN524 [1:10]	0.72	1.83	4.67

(E)

Figure 4.40 Drug combination plots for oxaliplatin and m-bromobenzoylsalicylate (OX+PN524[1:10]) in OE33 oesophageal cancer cells.
Dose response curve (A). Dose-effect curve as plotted by CalcuSyn (B). Bar chart representation of IC_{50} by single compounds and their combination (C). Fa-log(DRI) plot as plotted by CompuSyn (D). CI values as calculated by CompuSyn at ED_{50}, ED_{75} and ED_{90}. OX=Oxaliplatin.

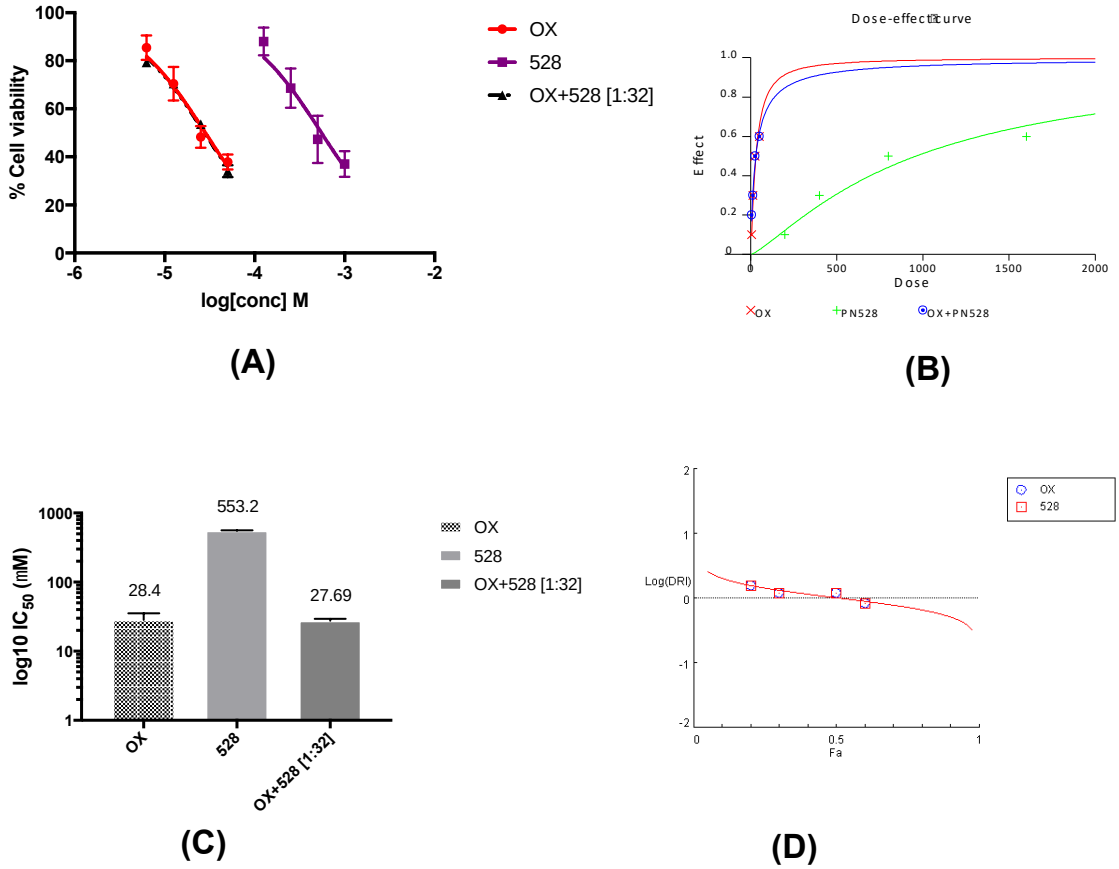

CI values at:

Drug Combo	ED50	ED75	ED90
OX+PN528 [1:32]	1.96	2.77	3.90

(E)

Figure 4.41 Drug combination plots for oxaliplatin and methyl-benzoylsalicylate (OX+PN528[1:32]) in OE33 oesophageal cancer cells.
Dose response curve (A). Dose-effect curve as plotted by CalcuSyn (B). Bar chart representation of IC_{50} by single compounds and their combination (C). Fa-log(DRI) plot as plotted by CompuSyn (D). CI values as calculated by CompuSyn at ED_{50}, ED_{75} and ED_{90}. OX=Oxaliplatin.

Oxaliplatin in combination with PN502 [1:20] against OE33 oesophageal cancer cells had synergistic effects at ED_{50} and below, which indicates synergy at low doses with little cytotoxic effects. This is not relevant in cancer therapy (Figure 4.40A, B, C, D and E). The platinum compound, oxaliplatin in combination with PN517 (Figure 4.41A, B, C, D and E) and PN524 (Figure 4.42A, B, C, D and E) against OE33 oesophageal cancer cell line had antagonistic effects ED_{75} and ED_{90} with synergy at ED_{50} and below. The platinum compound in combination with PN528 (Figure 4.43A, B, C, D and E) had antagonistic effects with CI values above 0.9 at ED_{50}, ED_{75} and ED_{90}.

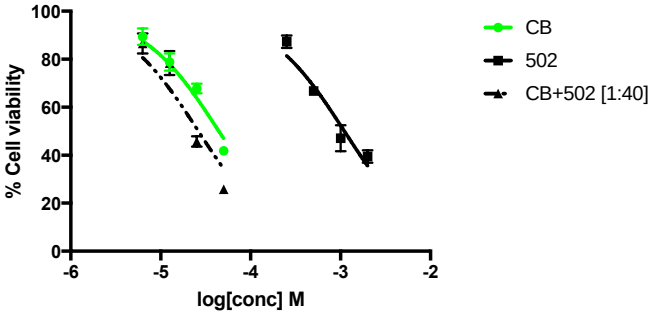

(A)

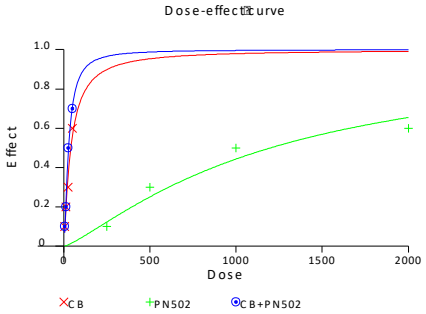

(B)

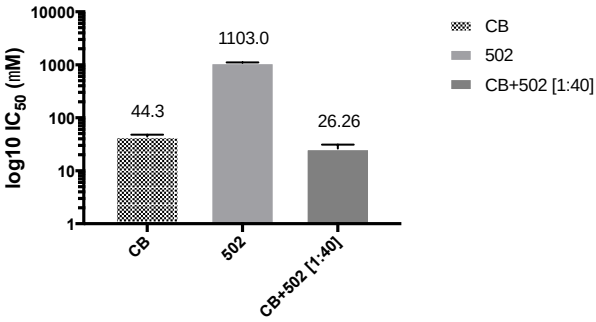

(C)

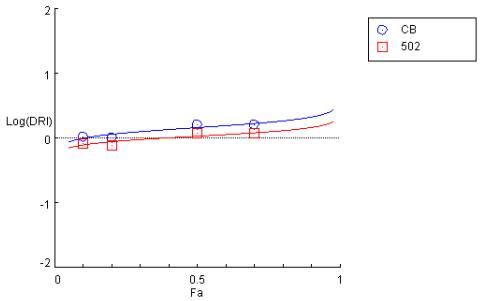

(D)

CI values at:

Drug Combo	ED50	ED75	ED90
CB+PN502 [1:40]	1.61	1.36	1.14

(E)

Figure 4.42 Drug combination plots for carboplatin and ortho-aspirin (CB+PN502[1:40]) in OE33 oesophageal cancer cells.
Dose response curve (A). Dose-effect curve as plotted by CalcuSyn (B). Bar chart representation of IC_{50} by single compounds and their combination (C). Fa-log(DRI) plot as plotted by CompuSyn (D). CI values as calculated by CompuSyn at ED_{50}, ED_{75} and ED_{90}. CB=Carboplatin.

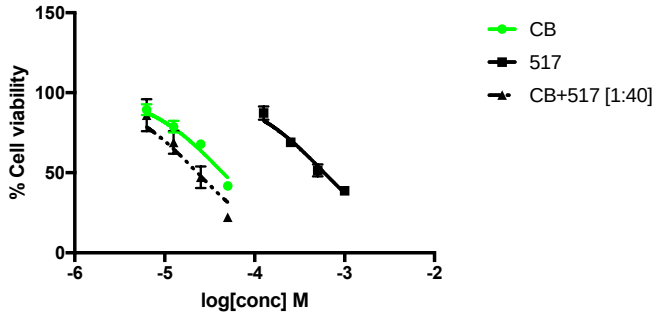

(A)

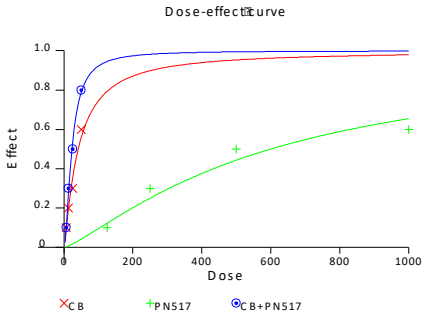

(B)

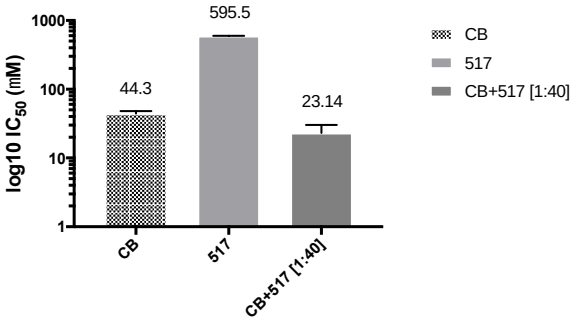

(C)

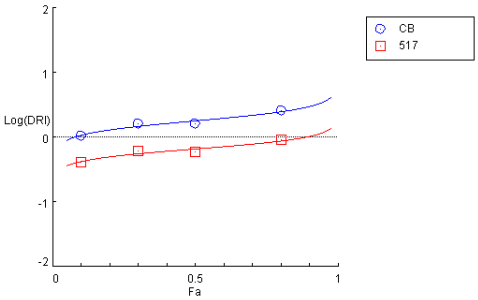

(D)

CI values at:

Drug Combo	ED50	ED75	ED90
CB+PN517 [1:40]	2.07	1.64	1.30

(E)

Figure 4.43 Drug combination plots for carboplatin and fumaryldiaspirin (CB+PN517[1:40]) in OE33 oesophageal cancer cells.
Dose response curve (A). Dose-effect curve as plotted by CalcuSyn (B). Bar chart representation of IC_{50} by single compounds and their combination (C). Fa-log(DRI) plot as plotted by CompuSyn (D). CI values as calculated by CompuSyn at ED_{50}, ED_{75} and ED_{90}. CB=Carboplatin.

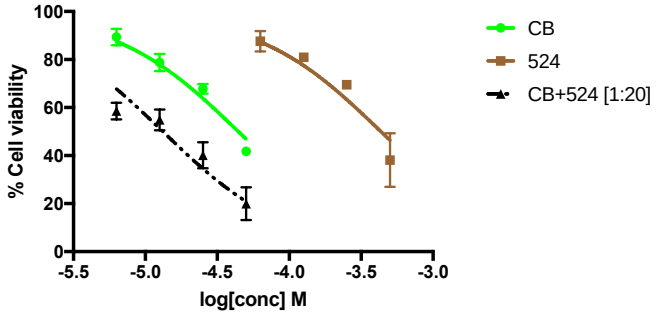

(A)

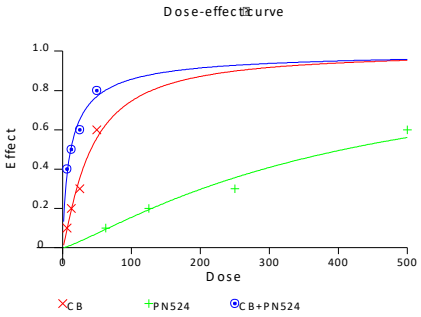

(B)

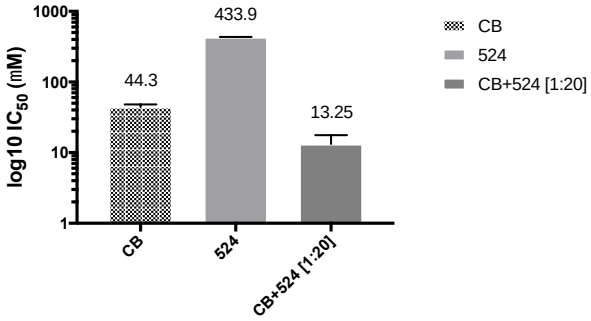

(C)

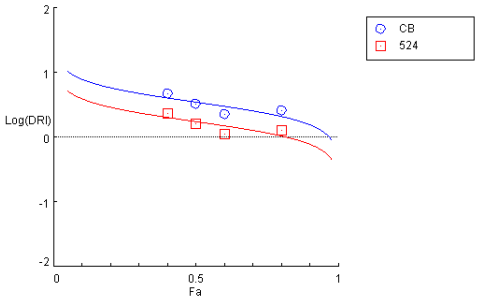

(D)

CI values at:

Drug Combo	ED50	ED75	ED90
CB+PN524 [1:20]	0.86	1.29	1.93

(E)

Figure 4.44 Drug combination plots for carboplatin and m-bromobenzoylsalicylate (CB+PN524[1:20]) in OE33 oesophageal cancer cells.
Dose response curve (A). Dose-effect curve as plotted by CalcuSyn (B). Bar chart representation of IC_{50} by single compounds and their combination (C). Fa-log(DRI) plot as plotted by CompuSyn (D). CI values as calculated by CompuSyn at ED_{50}, ED_{75} and ED_{90}. CB=Carboplatin.

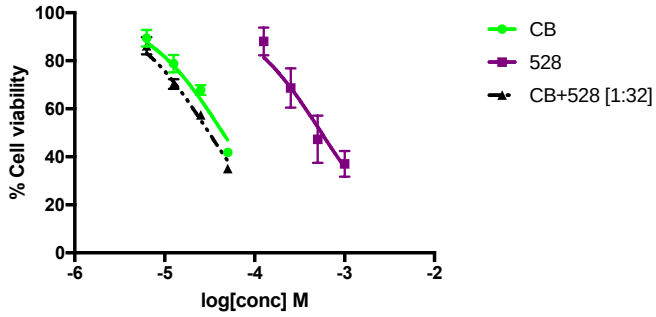

(A)

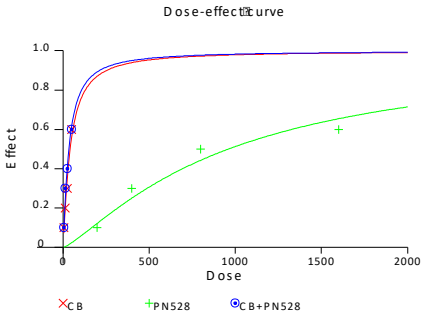

(B)

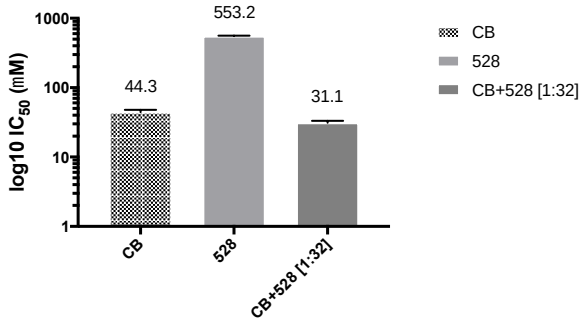

(C)

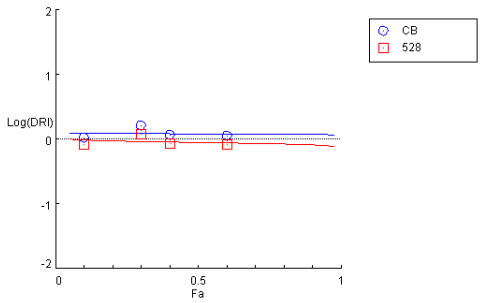

(D)

CI values at:

Drug Combo	ED50	ED75	ED90
CB+PN528 [1:32]	1.94	1.99	2.06

(E)

Figure 4.45 Drug combination plots for carboplatin and methyl-benzoylsalicylate (CB+PN528[1:32]) in OE33 oesophageal cancer cells.
Dose response curve (A). Dose-effect curve as plotted by CalcuSyn (B). Bar chart representation of IC_{50} by single compounds and their combination (C). Fa-log(DRI) plot as plotted by CompuSyn (D). CI values as calculated by CompuSyn at ED_{50}, ED_{75} and ED_{90}. CB=Carboplatin.

Antagonistic effects were observed when carboplatin was used in combination with PN502 (Figure 4.44A, B, C, D and E), PN517 (Figure 4.45A, B, C, D and E) and PN528 (Figure 4.47A, B, C, D and E) against the oesophageal cancer cell line. The platinum compound in combination with PN524 [1:20], however, had a synergistic effect at ED_{50} and below but combinations had antagonistic effects at ED_{75}, ED_{90} and above (Figure 4.46A, B, C, D and E). The ED_{50} of carboplatin was combined with PN524 reduced from 40.77μM to 11.67μM, which is about a 4-fold reduction in dose to kill 50% of the oesophageal cancer cells.

PN524 in combination with oxaliplatin and carboplatin have synergistic effects at ED_{50} and lower. This is not favourable in cancer chemotherapy because drugs are needed to be highly cytotoxic to the cancer cells in order to ensure maximal kill. The DRI for cisplatin and PN528 combination resulted in a decrease in ED_{50} for cisplatin from 5.4μM to 3.5μM.

A summary of the effects of all the combinations in this thesis as determined by their CI values against SW480 CRC cell line and OE33 oesophageal cancer cell line calculated by CompuSyn and CalcuSyn can be found on Table 4.6 and 4.7.

Compounds	Cisplatin (CP)			Oxaliplatin (OX)			Carboplatin (CB)		
	CI values at								
	ED_{50}	ED_{75}	ED_{90}	ED_{50}	ED_{75}	ED_{90}	ED_{50}	ED_{75}	ED_{90}
PN502	**+++**	**+++**	**++**	**+++**	**+++**	**++**	**−−**	**−−**	**−−−**
PN548	+	+	++	+	−	−−	•	−−−	−−−−
PN549	+++	+++	+++	++	++	+	•	+++	+++
PN517	+++	++++	++++	++++	++++	+++	+++	+	−−−
PN508	++	+++	+++	++	++	•	−−−−	−−	+++
PN524	+	+++	+++	+++	−−−	−−−−−	•	+	+++
PN590	−	−	•	−	+	+++	−−−	−−−	•
PN591	−−−−	−−−−	−−−−−	•	•	−−	−−−	−−−−−	−−−−−
PN592	−−−−	−−−	•	+	−−−−	−−−−−	−	−−−−−	−−−−−

Table 4.6 Summary of drug combination CI values in SW480 CRC cell line.
Drug combinations with CI values at effective dose for 50% kill of the cell population (ED_{50}), 75% of the population (ED_{75}) and 90% of the population (ED_{90}). Effect for each combination is synergistic [+], additive [•] or antagonistic [−] (Table 4.2).

Compounds	Cisplatin (CP)			Oxaliplatin (OX)			Carboplatin (CB)		
	CI values at								
	ED_{50}	ED_{75}	ED_{90}	ED_{50}	ED_{75}	ED_{90}	ED_{50}	ED_{75}	ED_{90}
PN502	−	−	•	+++	−−	−−−	−−−	−−−	−
PN517	+++	+++	+++	++	−−−	−−−−	−−−	−−−	−−
PN524	+++	+++	+++	++	−−−	−−−−	++	−−	−−−
PN528	−	+	++	−−−	−−−	−−−	−−−	−−−	−−−

Table 4.7 Summary of drug combination CI values in OE33 oesophageal cancer cell line.
Drug combinations with CI values at effective dose for 50% kill of the cell population (ED_{50}), 75% of the population (ED_{75}) and 90% of the population (ED_{90}). Effect for each combination is synergistic [+], additive [•] or antagonistic [−] (Table 4.2).

4.5 Discussion

In comparison to PN502 (aspirin), the other aspirin analogues and NSAIDs with the exception of meta- (PN548) and para- (PN549) isomers of aspirin appear to be more cytotoxic to SW480 CRC cells (Figure 4.5 and 4.6). The IC_{50} for PN502 after buffering with HEPES and treating for 48 h is found to be at 1.8 mM with the meta- and para-isomers, PN548 and PN549 at 3.8 mM and 4.9 mM respectively (Figure 4.5A). However, higher cytotoxic effects of aspirin (PN502) have been reported; for example, the IC_{50} for aspirin has been found to be 1.48 mM (Din *et al.*, 2004). This difference in cytotoxicity could be as a result of the difference in dissolution solvent used for stock solutions, buffers used to adjust pH or duration of treatment. Din *et al*., (2004) used distilled water to make up stock solutions of aspirin at a concentration of 500 mM and further diluted to desired concentrations using media. However, stocks were made up at concentrations of 50 mM with acetone, diluted down to 25 mM (1:1) using HEPES buffer (pH8) and then further diluted to the desired concentration using media, after which cells were treated for 48 h. The 'diaspirins' PN517 and PN508, caused a 50% growth inhibition at 0.24 mM and 0.75 mM respectively (Figure 4.5A), which is substantially more cytotoxic than 0.87 mM and 2.43 mM respectively (Claudius *et al.*, 2014). These differences in cytotoxicity may be due to different reasons such as dissolution solvents used; for example acetone or DMSO, buffering solutions used such as HEPES or PBS to adjust pH of compounds and duration of treatment. The IC_{50} of salicylic acid is higher than that of aspirin at 2.55 mM (Figure 4.5A), which suggests that the cytotoxic effect of aspirin does not solely depend on its salicylate moiety but on the parent

compound. Thioaspirin (PN590) and its meta- (PN591) and para- (PN592) appear to be very cytotoxic with their IC_{50} as 0.16 mM, 0.48 mM and 0.75 mM respectively. The mutational status of *TP53* gene in SW480 CRC, OE33 and FLO1 oesophageal cancer cells (Din *et al.*, 2004, Liu *et al.*, 2017), indicate that cancers made up such cell lines will have reduced sensitivity to platinum compounds and thus cytotoxicity is reduced (Perego *et al.*, 1996, Toscano *et al.*, 2007, Yang *et al.*, 2016, Zhang *et al.*, 2014) in cancers. This could explain why the cytotoxic effect of the platinum compounds was not very high (Table 4.3) and possibly due to the p53 dependence for sensitivity to oxaliplatin (Toscano *et al.*, 2007, Yang *et al.*, 2016) and other platinum compounds (Perego *et al.*, 1996, Zhang *et al.*, 2014) in other cancers. Likewise, in CRC cell lines, p53 is essential for chemotherapy-induced cytotoxicity exhibited by oxaliplatin (Yang *et al.*, 2016). In addition, MMR proficient CRC cells are known to survive high doses of cisplatin or oxaliplatin (Sergent *et al.*, 2002). Aspirin was found to have higher cytotoxicity in SW480 cells with IC_{50} of 1.8 mM as compared to in FLO1 with IC_{50} of 4.1 mM (Table 4.3). Sensitivity to these aspirin analogues clearly differ from cell type to cell type due to differences in specific targets by different compounds (Din *et al.*, 2004). Din *et al*. (2004) compared sensitivity to aspirin in CRC cell lines to non-CRC cell lines and found out that the dose of aspirin used was inversely proportional to cell viability in CRC cells while non-CRC cells did not show this relationship.

In regards to the 12-day cytotoxicity assay (Table 4.4), it was observed that the degree of cytotoxicity for some of these compounds was not the same as when cells were treated for 48 h (Table 4.3**)**. The 12-day IC_{50} values for cisplatin and

oxaliplatin (Table 4.4) are similar to 2.22 μM and 0.34 μM respectively (McPherson *et al.*, 2014). Based on their respective IC_{50} values determined at 48 h compared to that determined after 12 days of treatment, cisplatin and carboplatin both had about 10-fold increase in cytotoxicity after 12 days while oxaliplatin had about 100-fold increase in cytotoxicity, thus increase in cytotoxicity varies from compound to compound. PN502 and naproxen had a 8-fold and 5-fold increase in cytotoxicity after 12 days of treatment. The 12-day cytotoxicity assay revealed PN517, PN590, diclofenac and indomethacin to have a 3-fold increase in cytotoxicity against SW480 CRC cells. The thioaspirin isomers, PN591 and PN592 had a big increase in cytotoxicity after 12 days of treatment against SW480 CRC cells. The increase in cytotoxicity is about 12-fold and 25-fold for PN591 and PN592 respectively with the cytotoxic effects overtaking that of their ortho- isomer, which is usually more cytotoxic. This unusual finding suggests that meta- and para- isomers of thioaspirin are more cytotoxic against SW480 CRC cells after treatment for lengthy periods, thus exhibiting a longer duration of action for reasons that are not known. Furthermore, increase in cytotoxicity of these compounds could be due to replenishment of cells on day six of treatment, which will lead to an increase in drug concentration.

The combination of cisplatin and PN548 [1:400] in SW480 CRC cells (Figure 4.10) had a slight synergistic effect at ED_{50} and ED_{75} with the synergistic effect increasing to moderate at a higher dose of ED_{90}. In addition, the ED_{50} for cisplatin in this combination reduced by about 10-fold, which is favourable in cancer therapy (Chou, 2010). The ED_{50} of cisplatin reduced by almost 10-fold

when in combination with PN549 (para-aspirin) [1:250] accompanied by a synergistic effect at ED_{50}, ED_{75} and ED_{90} (Figure 4.11). Strong synergy was observed when cisplatin was combined with PN517 [1:10] with a 5-fold decrease in ED_{50} for cisplatin (Figure 4.12). Cisplatin in combination with PN508 [1:18] (Figure 4.13) and PN524 [1:40] (Figure 4.14) had synergistic effects in SW480 CRC cells with about a 2-fold and 7-fold decrease in ED_{50} for cisplatin respectively. In addition, the synergistic effects of these combinations increased at higher dose, which is advantageous in chemotherapy (Chou, 2010). Cisplatin in combination with PN590 [1:20] (Figure 4.15) had an additive effect in SW480 CRC cells with both of its isomers, PN591 (Figure 4.16) and PN592 (Figure 4.17) having an antagonistic effect when used in combination with all three platinum compounds. This antagonism between the isomers of thioaspirin and the platinum compounds could be because they had low cytotoxic effects against these CRC cells after 72 h (Table 4.1), which later on greatly improved overtaking PN590 after cells were treated for a period of 12 days (Table 4.2).

In this study, combinations of oxaliplatin with PN548 [1:80] (Figure 4.19) and PN524 [1:8] (Figure 4.23) had antagonistic effects at ED_{75} and ED_{90}. Even though there was synergistic effects at ED_{50} and below, this is unfavourable in cancer therapy because maximum cytotoxicity against the cancer cells is key to effective therapy (Chou, 2010). Oxaliplatin combination with PN548 [1:80] (Figure 4.19) resulted in slight synergistic effects at ED_{50} and ED_{75} increasing to moderate synergism at ED_{90} with a 4-fold decrease in oxaliplatin ED_{50}. The ED_{50} for the platinum compound, oxaliplatin had a 7-fold decrease when

combined with PN549 (Figure 4.20), PN590 (Figure 4.24) and PN517 (Figure 4.21) with strong synergistic effects with PN517 and synergistic effects with PN549 and PN590 (Table 4.5). Although there was a synergistic effect when oxaliplatin was combined with PN508 [1:14] (Figure 4.22) and PN524 [1:8] (Figure 4.23) at ED_{50}, the effect regressed to antagonism with dose increase (ED_{75} and ED_{90}). This effect will not produce the maximum cytotoxicity needed in cancer therapy (Chou, 2010). With the prominent side effect of oxaliplatin being peripheral neuropathy (Alcindor and Beauger, 2011), a reduction in its ED_{50} as a result of the combinations with aspirin (Figure 4.18), PN549 (Figure 4.20), PN517 (Figure 4.21) and PN590 (Figure 4.24) may reduce or totally alleviate this side effect because a reduction in drug concentration will result in toxicity reduction and also delay or minimize the induction of drug resistance (Chou, 2010). Although, there was what seemed to be a synergistic effect between carboplatin with PN508 (Figure 4.31) and PN524 (Figure 4.32) at ED_{50}, the doses of carboplatin at ED_{50} increased rather than decreased when used in combination with the 'diaspirins'. This increase in ED_{50} of carboplatin when in combination defeats one of the main reasons of combination therapy, which is to achieve a decrease in effective dose in order to reduce or alleviate side effects. Carboplatin, in combination with the thioaspirins, PN590 (Figure 4.33), PN591 (Figure 4.34) and PN592 (Figure 4.35) also had strong synergistic effects against the colorectal cell line. Some of the combinations showed strong antagonism due to very high CI values. This is possible in some combinations as the synergy scale is from 1 to 0 and the antagonism scale is from 1 to infinity (Chou, 2010). PN549 [1:50] (Figure 4.29) was the only aspirin analogue that

showed synergistic effects against the colorectal cell line when in combination with carboplatin. There was a 3-fold decrease in carboplatin ED_{50}.

In the OE33 oesophageal cancer cell line, none of the platinum compounds synergised with aspirin (Figure 4.36, 4.40 and 4.44). Although there was synergy when oxaliplatin and aspirin [1:20] were combined at ED_{50}, this effect regressed at ED_{75} and ED_{90} and thus is not favourable in the treatment of cancer. In gastric cancer cells however, cell growth was significantly inhibited when cisplatin was used in combination with aspirin (Dong *et al.*, 2014). Combinations of cisplatin and aspirin were also seen to have synergistic effects in human cervical carcinoma HeLa cells (Wang *et al*., 2010). The combination of cisplatin and PN517 [1:50] (Figure 4.37) maintained its synergistic effects through ED_{50}, ED_{75} and ED_{90}, which make this a promising combination for the treatment of cancer. Oxaliplatin and carboplatin in combination with PN517 (Figure 4.41 and 4.45 respectively) had an antagonistic effect. Although there was moderate synergy between oxaliplatin and PN517 at ED_{50}, the positive effect decreased as doses increased, which is thus not favourable. Cisplatin and PN524 [1:50] (Figure 4.38) had synergistic effect at ED_{50}, ED_{75} and ED_{90}. Even though oxaliplatin and carboplatin also had synergistic effects with PN524 at ED_{50}, this was not maintained at ED_{75} and ED_{90} (Figure 4.42 and 4.46 respectively). Slight synergy was observed when cispaltin was in combination with PN528 [1:160] (Figure 4.39). Oxaliplatin and carboplatin in combination with PN528 had antagonistic effects (Figure 4.43 and 4.47 respectively). The decrease in doses needed for these platinum compounds are of utmost importance because of their narrow therapeutic index (Alcindor and Beauger,

2011). The differences in outcomes for each drug combination in different cell lines may be due to differences in specific targets by different compounds (Din *et al.*, 2004).

In the treatment of CRC, oxaliplatin has been used in combination with a variety of cytotoxic agents producing different levels of desired effects (Alcindor and Beauger, 2011). Due to oxaliplatin not having any effect on the drug biotransformation enzyme, P450, its combination with commonly used drugs such as aspirins does not raise any concerns (Masek *et al.*, 2009). Some of these aspirin analogues thus show promising results when combined with platinum compounds for the treatment of cancer and should be investigated further *in vivo*.

Chapter 5. Apoptosis or Necrosis?

5.1 Introduction

Regulation of various cellular processes such as proliferation, differentiation and apoptosis have been linked to activation of mitogen-activated protein kinase (MAPK), Akt, PI 3-K and STAT proteins, all found in the EGFR signalling pathway (Grant *et al.*, 2002).

There are a series of published studies linking activation of pro-apoptotic mechanisms with inhibition of the EGFR signalling pathway as a mechanism of action found in established anti cancer compounds (Mendelsohn and Baselga, 2000), which resulted in the extension of these studies to the possible effects of aspirin analogues on the EGFR found in the next chapter of this thesis. It has already been established that the diaspirins (PN508, PN517 and PN524) induce apoptotic death in cancer cells (Claudius *et al.*, 2014). Here, in this chapter, it was investigated whether the isomers of aspirin namely PN502 (aspirin), PN548 (meta-aspirin), PN549 (para-aspirin) and isomers of thioaspirin namely PN590 (ortho-thioaspirin), PN591 (meta-thioaspirin) and PN592 (para-thioaspirin) induce apoptotic, necrotic cell death or a mixture of both in SW480 CRC cell line was investigated.

5.1.1 Apoptosis

Cell death was classified as occurring via two separate morphological patterns, one of which is known as ‘coagulative necrosis’ where there is swelling and rupture of organelle membranes and disintegration of their structure and the

other pattern is known as apoptosis. In apoptosis, the cell organelles maintain their integrity with the membrane forming different bulges that eventually separate and form membrane-bound globules ready to be phagocytized (Wyllie *et al.*, 1980). However, it is now believed that programmed cell death (PCD) occurs via different pathways with more than one of these pathways triggered simultaneously (Leist and Jaattela, 2001, Nikoletopoulou *et al.*, 2013).

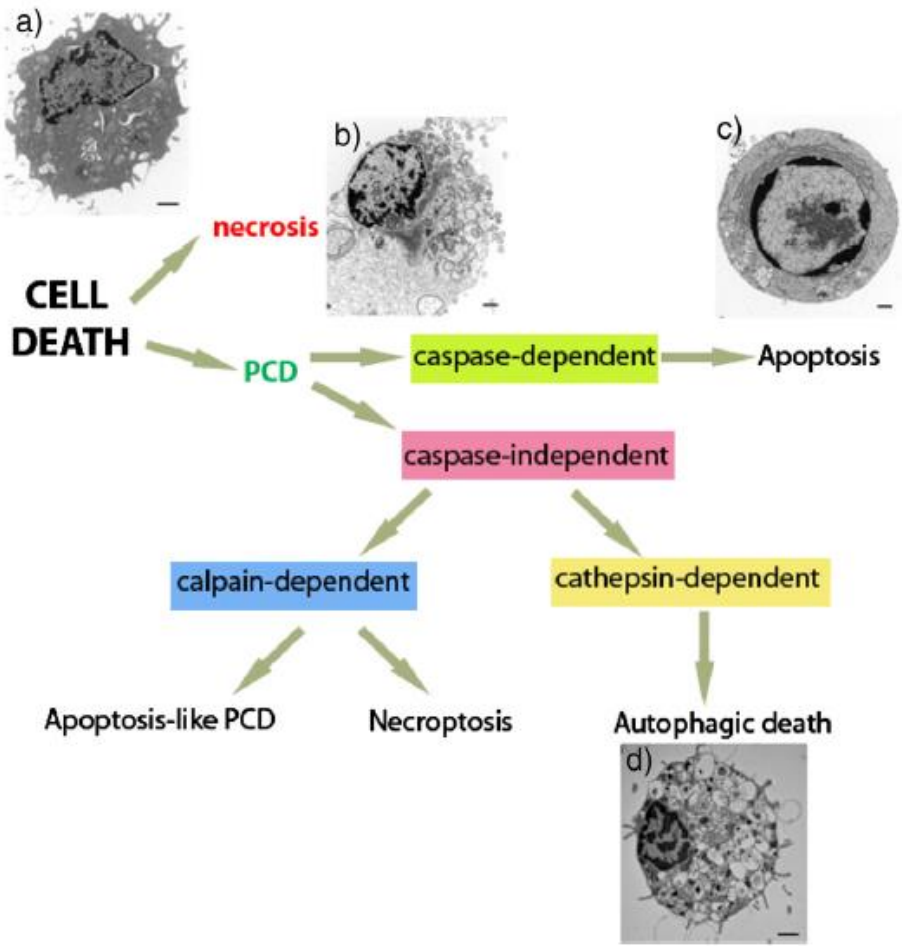

Figure 5.1 Morphological features of the different types of PCD.
Healthy cell (a). Necrotic cell (b). Apoptotic cell (c). Autophagic cell (d) (Edinger and Thompson, 2004, Nikoletopoulou *et al.*, 2013).

Cell death could be as a result of apoptosis, necrosis or autophagy (Leist and Jaattela, 2001, Nikoletopoulou *et al.*, 2013). PCD is particularly important in the

life cycle of a cell as a balance between cell proliferation and cell death is essential for the maintenance of homeostasis (Schwartzman and Cidlowski, 1993). During apoptosis, the phosphatidylserine (PS) normally found in the inner leaflet of the phospholipid cell membrane flips and is exposed (Leist and Jaattela, 2001, van Engeland *et al.*, 1996).

5.1.1.1 Cell cycle and apoptosis

The cell cycle was initially divided into two stages; mitosis and interphase with the mitosis stage made up of prophase, metaphase, anaphase and telophase. This division was later on reviewed, which included G_1, S, G_2 and M phases as part of interphase (Norbury and Nurse, 1992). Cells undergo DNA replication in the G_1 phase before which some enter the G_0 phase also known as the resting phase where cells are dormant and thus do not proliferate (Vermeulen *et al.*, 2003).

In cancer, mutations normally occur in two classes of genes known as the proto-oncogenes and the tumour suppressor genes. The proto-oncogenes are responsible for the stimulation of cell proliferation. However, when mutated this process is uncontrolled and promotes tumour growth. As the name implies, tumour suppressor genes are responsible for inhibiting the cell cycle progression where and when necessary. When mutated, these get inactivated (McDonald and El-Deiry, 2000).

The cyclin-dependent kinase inhibitor p21, also known as WAF1 controls many biological activities by functioning as an anti-apoptotic protein, promoting cell cycle arrest by inhibiting proliferating cell nuclear antigen (PCNA) via binding to it and thus, inhibiting DNA synthesis at G_1 phase of the cell cycle, which then allows for DNA repair and this correlates with an increase in expression (Abbas and Dutta, 2009, Karimian *et al.*, 2016, Pan *et al.*, 1995). However, in certain conditions, p21 can also act as an oncogene (Gartel, 2006, Roninson, 2002), thus not having classical tumour suppressor activities (Abbas and Dutta, 2009). The expression of p21 is dependent on p53, a tumour suppressor gene (el-Deiry *et al.*, 1993). Nevertheless, there is evidence of it being activated independently of p53 (Abbas and Dutta, 2009, Gartel, 2005, Halevy *et al.*, 1995). p21 expression is found to be inversely related to the expression of the p53 protein (Zirbes *et al.*, 2000). The p53 protein regulates DNA repair, cell arrest and apoptosis after treatment with cytotoxic drugs (Goldstein *et al.*, 2011, Vousden and Prives, 2009). Activation of *TP21* gene leads to cell cycle arrest halting replication of damaged DNA (Abbas and Dutta, 2009, Ko and Prives, 1996). This is necessary particularly in human CRCs (Polyak *et al.*, 1997).

BAX (BCL2 associated X protein) is an important member of the BCL2 family located in the cytosol and translocates to the mitochondria after an apoptotic stimulus (Wolter *et al.*, 1997). However, in cases where BAX is overexpressed, apoptosis is triggered even in the absence of stimuli (Jurgensmeier *et al.*, 1998).

The BCL2 family is important for regulating apoptosis because too little or too much apoptosis leads to the progression of cancer or ischaemic conditions respectively (Czabotar *et al.*, 2014). BCL2 regulates apoptosis by exhibiting anti-apoptotic functions and it is regulated either by other proteins in the BCL2 family or phosphorylation which could also inactivate it (Haldar *et al.*, 1995). Interestingly, very high levels of BCL2 reverse its role, thus making it cause cell death (Shinoura *et al.*, 1999). BCL2 also causes cells to exit the cell cycle and enter into the resting phase and prevents re-entry (Adams and Cory, 1998, Mazel *et al.*, 1996) as well as inhibiting BAX, which is a promoter of cell apoptosis (Mazel *et al.*, 1996). This suggests it has multiple functions. However, its main function is prolonging G_1 to S phase transition in the cell cycle to enable supplementary time for the cell to either synthesise or repair damaged DNA (Mazel *et al.*, 1996).

PCNA is a protein responsible for DNA replication and damage repair (Wang *et al.*, 2006).

5.1.2 Beta catenin

The adenomatous polyposis coli suppressor (*APC*) gene is responsible for the regulation and destruction of β-catenin (Munemitsu *et al.*, 1995). Mutation in the *APC* gene occurs in CRC and colorectal adenomas, which leads to the accumulation of β-catenin in the cell cytoplasm, thus, activation of the Wnt/β-catenin pathway (Schror, 2011). β-catenin is normally degraded by phosphorylation in its amino terminus which leads to a reduction in its signalling (Yost *et al.*, 1996) and absence of phosphorylatable residues due to mutation leads to an increase in its signalling (Morin *et al.*, 2016).

The translocation of β-catenin to the nucleus leads to its interaction with DNA-bound transcription factor proteins (TCF1, TCF2 or TCF3) which in turn causes the activation of several target genes such as Cyclin D1 (Thorstensen *et al.*, 2005).

5.2 Aims and Objectives

As opposed to necrosis, apoptosis is the preferred method for drug-induced cell death, otherwise the leaked cell contents cause damage to neighbouring cells in an uncontrolled manner. However, more often these patterns of cell death go hand in hand (Leist and Jaattela, 2001).

These aspirin analogues have been found to have cytotoxic effects on SW480 CRC cells. Thus, it was planned to find out if the mode of cell death was caused via apoptosis, necrosis or a mixture of both and whether a change in the isomeric positions of the acetyl group to the benzene ring might be responsible for this change in behaviour.

5.3 Methodology

The effect of aspirin analogues on pro-apoptotic and anti-apoptotic proteins was tested using SDS-PAGE resolution and western blot analysis (2.2.9.2.3). Annexin-V dye to detect apoptotic cells and PI to detect necrotic cells using flow cytometry (2.2.9) was also used. To further confirm these findings, YO-PRO®-1 and PI dyes to detect apoptosis and necrosis respectively were later employed using confocal microscopy (2.2.10).

5.4 Results

5.4.1 Effects of aspirin analogues on p21 expression

The effect on the expression of p21 was first of all observed using a drug in chemotherapy as control. The fluoropyrimidine, 5-fluorouracil (5-FU), is the most common drug used in the treatment of colorectal cancer and has been in use for almost 60 years (Chu *et al.*, 2009), thus, it was a the drug of choice to use in order to compare with the compounds in this study.

Interestingly, p21 protein was repeatedly downregulated by high doses of 5-FU (Figure 5.2).

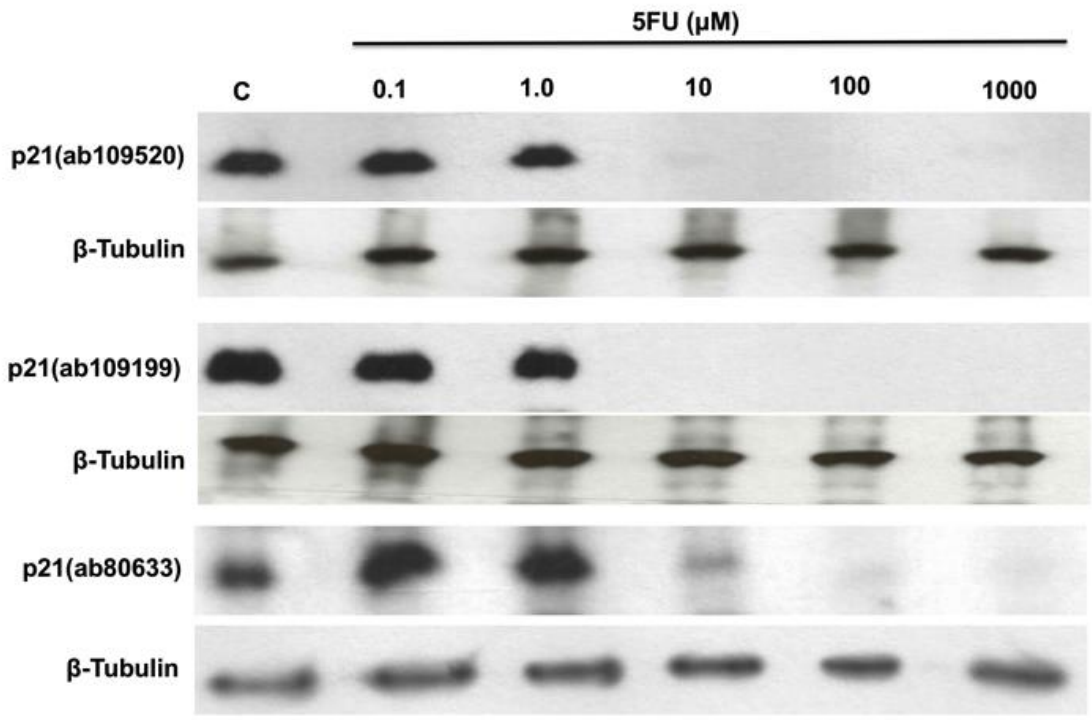

Figure 5.2 Effect of 5-FU on the expression of p21 using different antibodies. SW480 CRC cells were treated with increasing doses of 5-FU for 24 h, lysed with Laemelli buffer, resolved using SDS-PAGE and probed with different antibodies to p21 (21 kDa) from Abcam. β-Tubulin (55 kDa) was used as loading control.

In comparison to the untreated cells (C), 5-FU at 0.1 μM and 1.0 μM upregulated the expression of p21 protein. However, at higher concentrations the expression was reduced and ultimately abolished (Figure 5.2).

With this consistent result across different p21 antibodies, it was decided to compare this with the effects to p21 expression caused by some of the aspirin analogues.

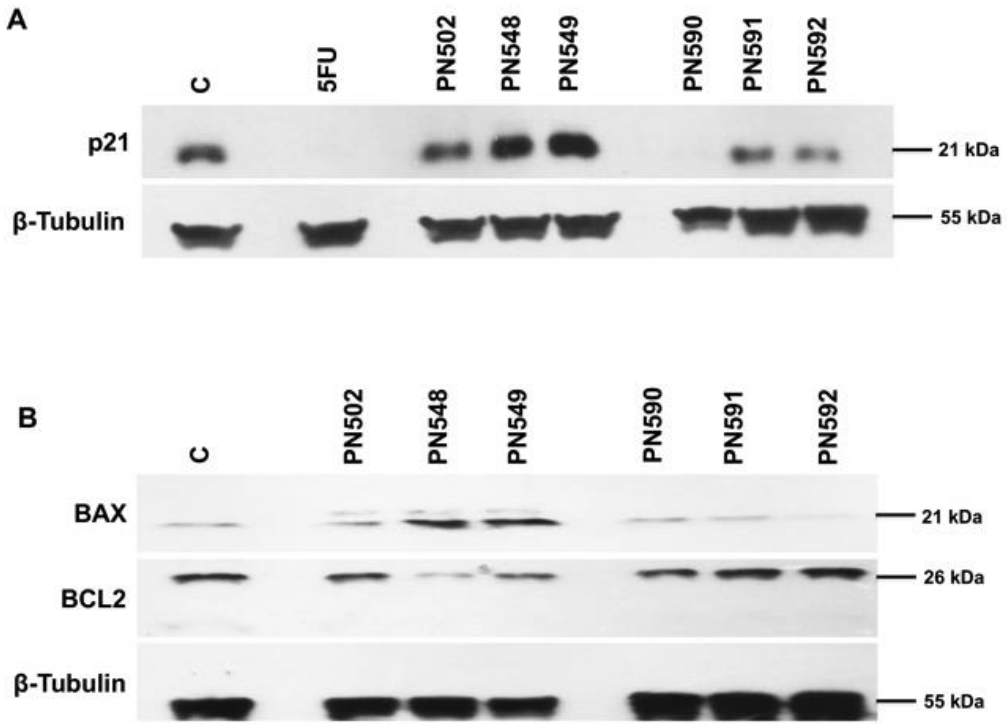

Figure 5.3 Effect of aspirin analogues on p21, BAX and BCL2 expression in SW480 CRC cells.

Effect of aspirin analogues on p21 expression in SW480 CRC cells (A). Effect of aspirin analogues on BAX and BCL2 expression in SW480 CRC cells (B). Cells were treated with compounds at 0.5 mM for 24 h. The concentration of 5-FU used was 100 μM. Lysed cells were resolved and probed with p21 (ab109520), BAX (sc-493) or BCL2 (ab32124) antibodies. β-Tubulin was used as loading control.

There was complete suppression of p21 expression by 5-FU and PN590. However, PN548 and PN549 caused an increase in p21 expression with a decrease in expression by PN502, PN591 and PN592 (Figure 5.3A).

Similarities in effects to p21, BAX and BCL2 have been consistent between the *meta*- and *para*- isomers of these aspirin analogues [PN548 and PN549] and [PN591 and PN592] (Figure 5.3A and 5.3B).

5.4.2 Effects of aspirin analogues on BAX and BCL2 expression

The effect of these compounds on the expression of the BAX and BCL2 proteins, which are pro-apoptotic and anti-apoptotic proteins respectively, were also studied.

It was observed that the expression of BAX was increased when cells were treated with PN548 and PN549. All the other compounds did not have any effect on BAX expression (Figure 5.3B). Similarly, only PN548 and PN549 decreased the expression of BCL2 with the others having no effect (Figure 5.3B).

To further study the effects of these compounds on apoptosis, it was decided to use flow cytometry and immunocytochemistry (ICC).

5.4.3 Effects of aspirin analogues on apoptosis

SW480 CRC cells were treated with the isomers of these aspirin analogues at 0.5 mM with the exception of PN590, which was treated at 0.3 mM because of its high cytotoxic effect (Table 4.3) for 16 h and 40 h, using staurosporine as a control for apoptosis and hydrogen peroxide (H_2O_2) as control for necrosis.

Staurosporine is a potent kinase protein inhibitor (Kiyoto *et al.*, 1987), which has been shown to induce apoptosis in a number of cell lines (Bertrand *et al.*, 1994, del Solar *et al.*, 2015, McKeague *et al.*, 2003) while H_2O_2, a reactive oxygen species is produced naturally during metabolism and high levels causes necrosis (McKeague *et al.*, 2003, Miyoshi *et al.*, 2006).

A large number of late apoptotic/dead cells were detected using flow cytometry after treatment with compounds and even in samples of untreated cells.

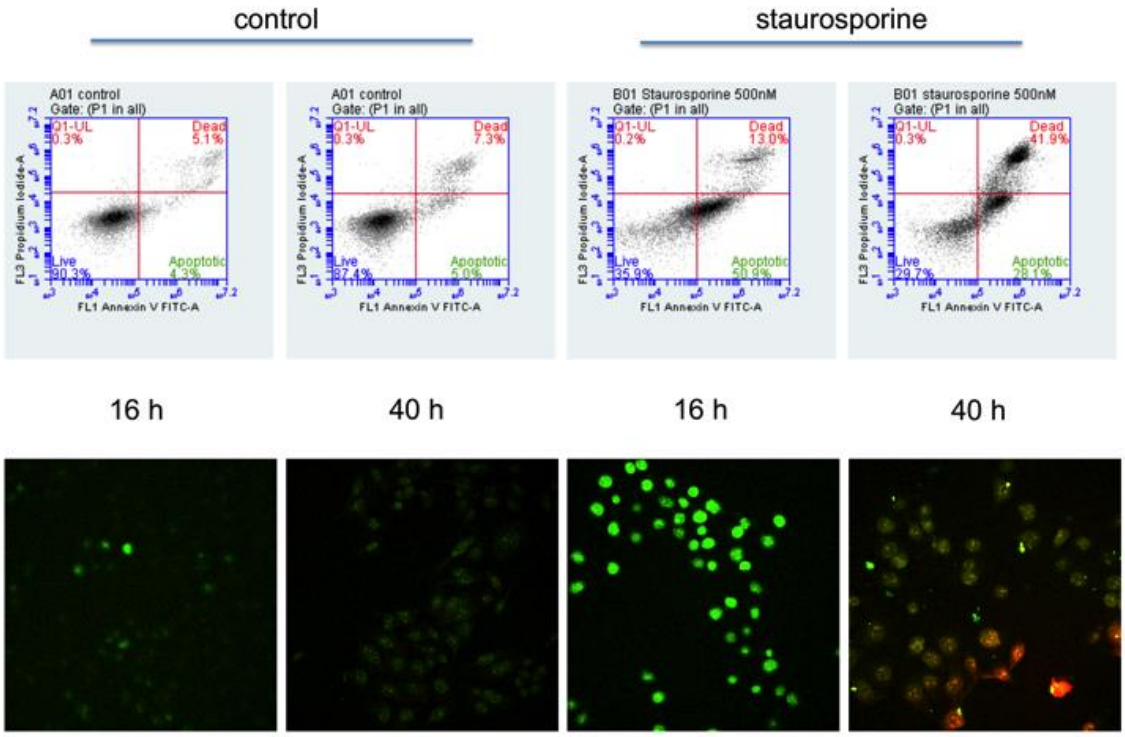

Figure 5.4 Representation of flow cytometric analysis and ICC for negative control (untreated) and control for apoptosis.
SW480 cells were treated with 500 nM of staurosporine for 16 h and 40 h. This is compared with a control (untreated cells). The fluorescent dyes used for flow cytometry are Annexin-V-FITC (green) for apoptotic cells and PI (red) for necrotic cells. The fluorescent dyes used for ICC were YO-PRO®-1 (green) for apoptotic cells and PI (red) for late apoptotic/necrotic cells. Representative confocal images were taken at 40X oil/1.30 oil immersion objective. *n=3.*

Flow cytometric analysis of untreated cells detects the presence of dead cells after 16 h and the percentage increases after 40 h of incubation. However, using ICC, dead cells are not detected in the untreated cells after 16 h and 40 h (Figure 5.4). This could be because only adherent cells were analysed as the dead cells get washed off during washes. The treatment with staurosporine in both flow cytometry and ICC detected a significant amount of apoptotic cells after 16 h. Both methods also detected a combination of apoptotic and late apoptotic/necrotic cells after 40 h of treatment (Figure 5.4).

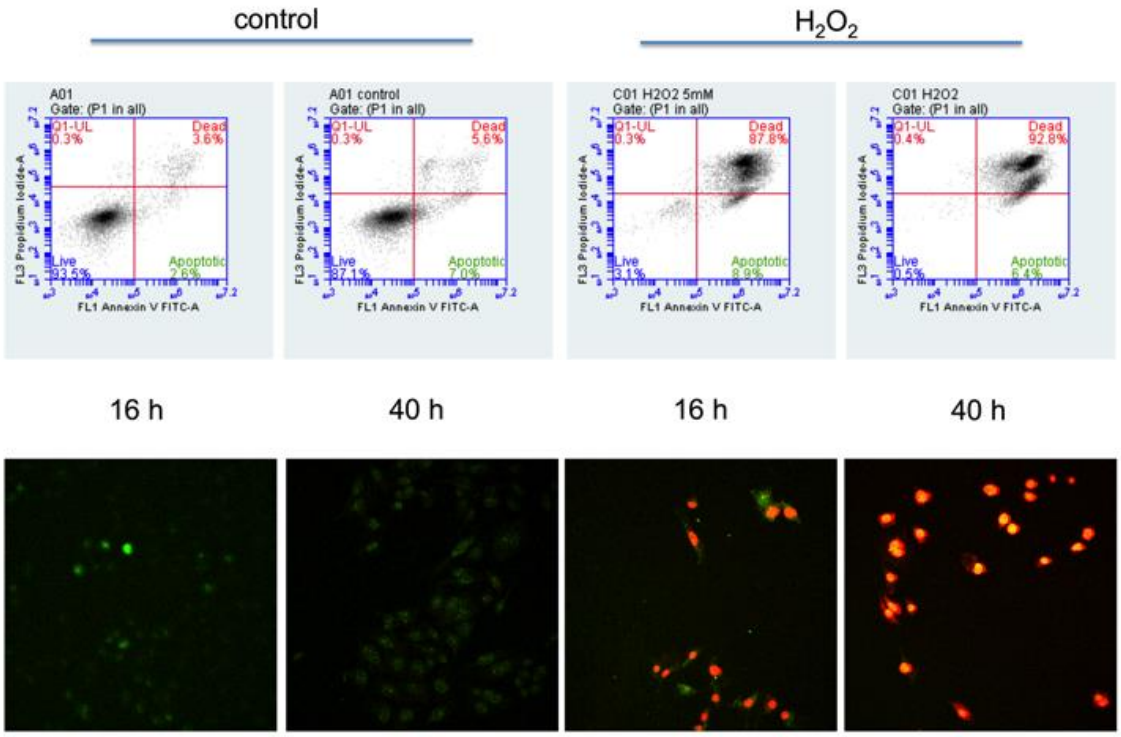

Figure 5.5 Representation of flow cytometric analysis and ICC for negative control (untreated) and control for necrosis.
SW480 cells were treated with 5 mM of H_2O_2 for 16 h and 40 h. This is compared with a control (untreated cells). The fluorescent dyes used for flow cytometry are Annexin-V-FITC (green) for apoptotic cells and PI (red) for necrotic cells. The fluorescent dyes used for ICC were YO-PRO®-1 (green) for apoptotic cells and PI (red) for late apoptotic/necrotic cells. Representative confocal images were taken at 40X oil/1.30 oil immersion objective. *n=3.*

Both the flow cytometric analysis and ICC experiments indicate a few apoptotic cells with most being late apoptotic/necrotic in samples treated with H_2O_2 for 16 h. The SW480 cells all turn necrotic after 40 h of treatment with 5 mM H_2O_2 (Figure 5.5).

Using staurosporine and H_2O_2 in both analysis produced very similar outcomes and thus good controls for detecting apoptotic and late apoptotic/necrotic cells respectively in SW480 CRC cell line.

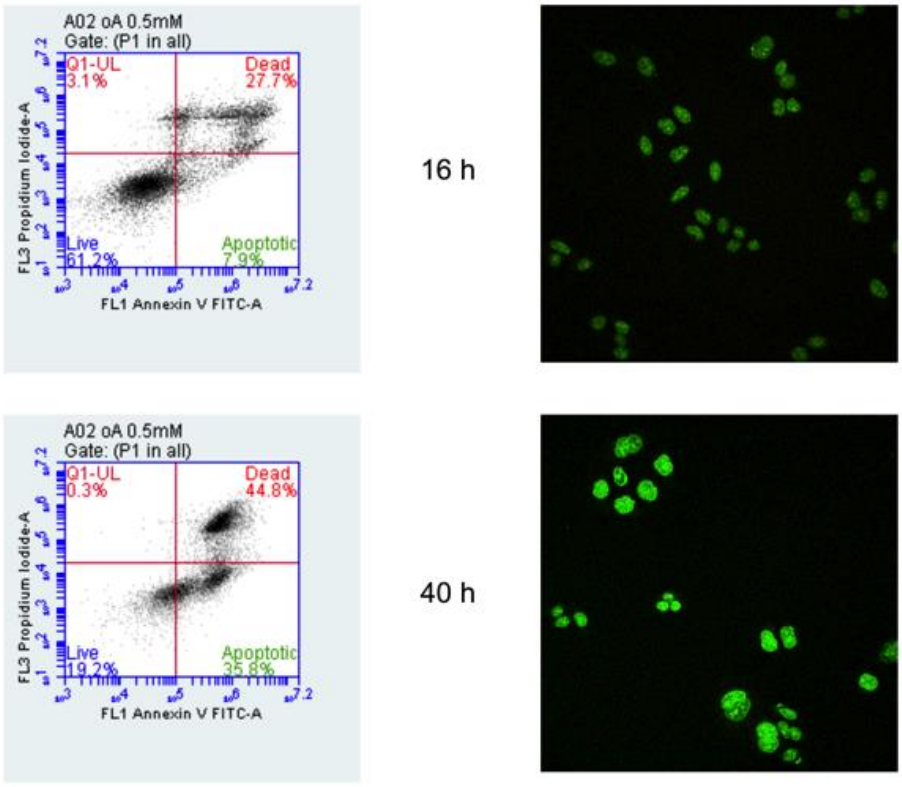

Figure 5.6 Representation of flow cytometric analysis and ICC for PN502 (aspirin). SW480 cells were treated with 0.5 mM of PN502 for 16 h and 40 h. The fluorescent dyes used for flow cytometry are Annexin-V-FITC (green) for apoptotic cells and PI (red) for late apoptotic/necrotic cells. The fluorescent dyes used for ICC were YO-PRO®-1 (green) for apoptotic cells and PI (red) for late apoptotic/necrotic cells. Representative confocal images were taken at 40X oil/1.30 oil immersion objective. *n=3.*

The flow cytometric analysis detected a large number of necrotic cells after treatment with 0.5 mM of PN502 after 16 h and a larger percentage of necrotic cells after 40 h of treatment. About 8% of cells were apoptotic after the 16 h treatment, which increased to about 35% after 40 h of treatment with PN502. The levels of apoptotic cells detected correlates with the ICC method however, in the ICC method, late apoptotic/necrotic cells were not detected (Figure 5.6). This could be because a dominant number of the cells analysed have undergone early apoptosis and a negligible number of necrotic cells are present.

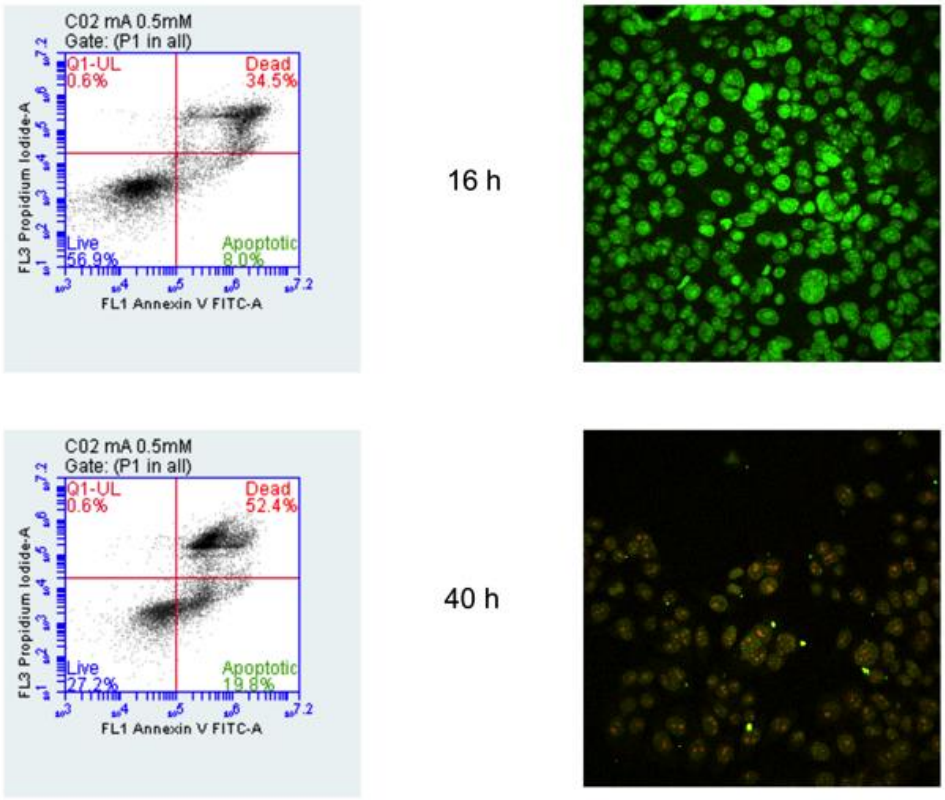

Figure 5.7 Representation of flow cytometric analysis and ICC for PN548 (meta-aspirin).
SW480 cells were treated with 0.5 mM of PN548 for 16 h and 40 h. The fluorescent dyes used for flow cytometry are Annexin-V-FITC (green) for apoptotic cells and PI (red) for late apoptotic/necrotic cells. The fluorescent dyes used for ICC were YO-PRO®-1 (green) for apoptotic cells and PI (red) for late apoptotic/necrotic cells. Representative confocal images were taken at 40X oil/1.30 oil immersion objective. *n=3.*

About 8% of the SW480 cells became apoptotic after treatment with 0.5 mM of PN548 after 16 h, which increased to about 20% after 40 h of treatment and accompanied with over 50% of necrotic cells. A lot of the cells can be seen to be apoptotic after 16 h of treatment and analysed using the ICC method with some of the cells showing some necrosis after 40 h of treatment (Figure 5.7).

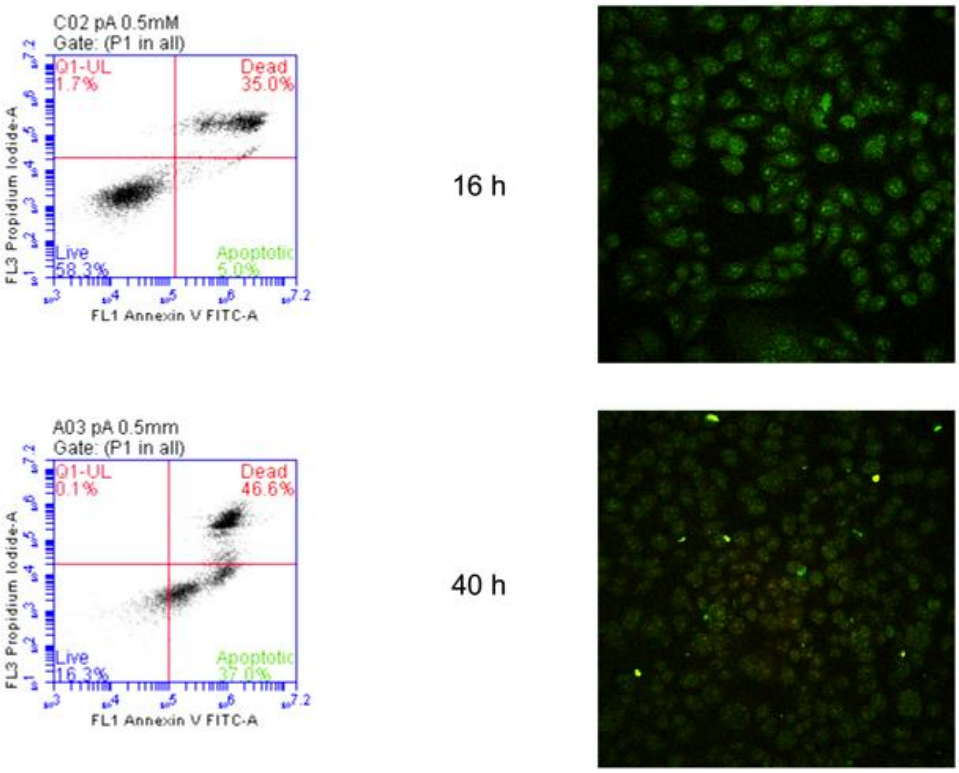

Figure 5.8 Representation of flow cytometric analysis and ICC for PN549 (para-aspirin).
SW480 cells were treated with 0.5 mM of PN549 for 16 h and 40 h. The fluorescent dyes used for flow cytometry are Annexin-V-FITC (green) for apoptotic cells and PI (red) for late apoptotic/necrotic cells. The fluorescent dyes used for ICC were YO-PRO®-1 (green) for apoptotic cells and PI (red) for late apoptotic/necrotic cells. Representative confocal images were taken at 40X oil/1.30 oil immersion objective. *n=3.*

Apoptotic cell cells increased from about 5% after being treated with 0.5 mM of PN549 for 16 h to about 37% after 40 h of treatment. Although a large number of late apoptotic/necrotic cells are detected by the flow cytometric analysis, this is also reflected by the qualitative results shown from the ICC method after 40 h of treatment with this isomer (Figure 5.8), which is more similar to the staurosporine image (Figure 5.4) than the H_2O_2 image (Figure 5.5). Cells treated with H_2O_2 went straight to dead (red fluorescence) unlike staurosporine and PN549 where there was accumulation of cells in the early apoptotic region.

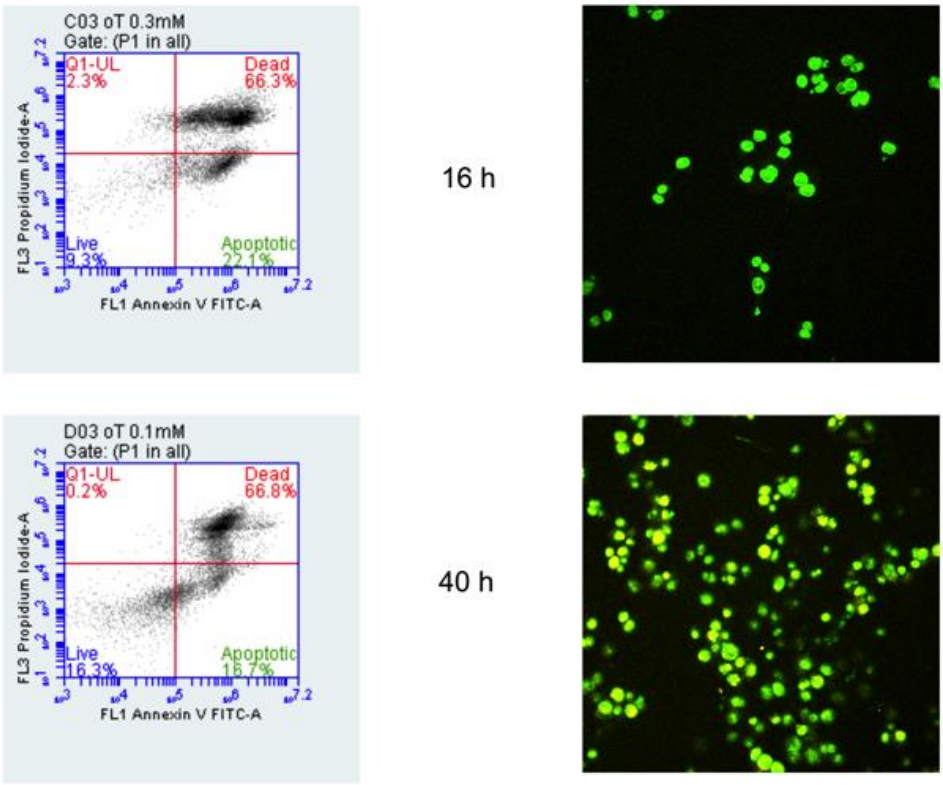

Figure 5.9 Representation of flow cytometric analysis and ICC for PN590 (ortho-thioaspirin).

SW480 cells were treated with 0.3 mM of PN590 for 16 h and 40 h. The fluorescent dyes used for flow cytometry are Annexin-V-FITC (green) for apoptotic cells and PI (red) for late apoptotic/necrotic cells. The fluorescent dyes used for ICC were YO-PRO®-1 (green) for apoptotic cells and PI (red) for necrotic cells. Representative confocal images were taken at 40X oil/1.30 oil immersion objective. *n=3.*

The flow cytometric analysis here again detects a large percentage of necrotic cells after treatment with 0.3 mM PN590 for 16 h and 40 h. The apoptotic cells seem to decrease in percentage with increase duration of treatment. This can also be seen in the ICC slides where the cells after 40 h treatment start to turn necrotic [yellow fluorescence] (Figure 5.9) unlike the brownish/red fluorescence when cells were treated with H_2O_2 (Figure 5.5).

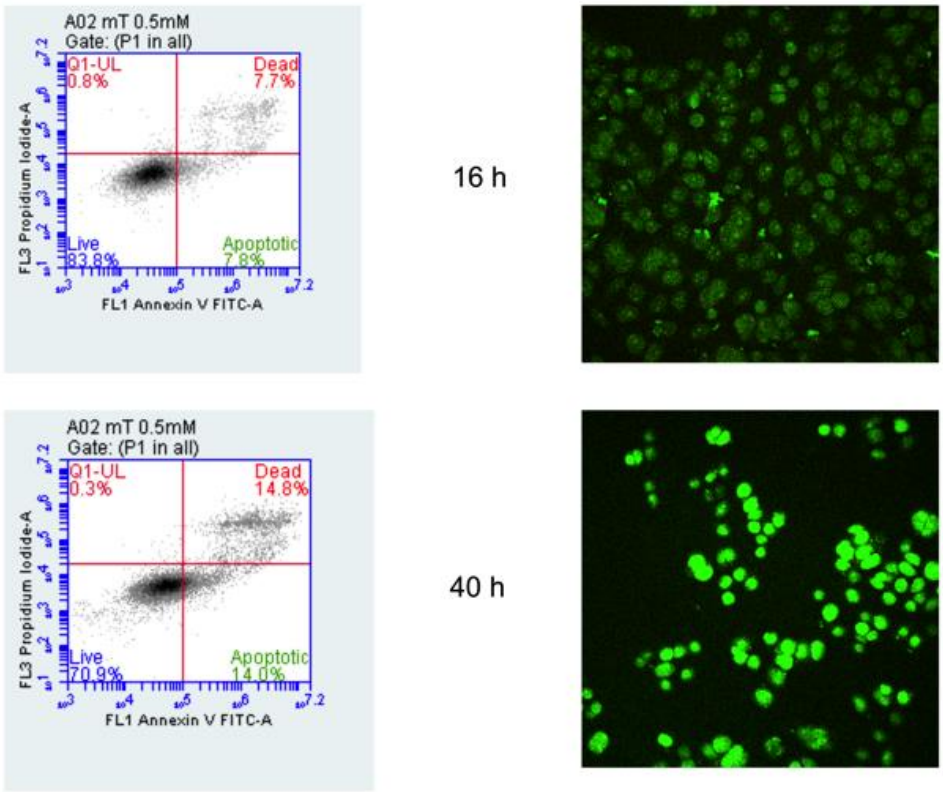

Figure 5.10 Representation of flow cytometric analysis and ICC for PN591 (meta-thioaspirin).
SW480 cells were treated with 0.5 mM of PN591 for 16 h and 40 h. The fluorescent dyes used for flow cytometry are Annexin-V-FITC (green) for apoptotic cells and PI

(red) for late apoptotic/necrotic cells. The fluorescent dyes used for ICC were YO-PRO®-1 (green) for apoptotic cells and PI (red) for necrotic cells. Representative confocal images were taken at 40X oil/1.30 oil immersion objective. *n=3.*

Treatment with 0.5 mM PN591 after a duration of 16 h resulted in about 8% of apoptotic cells, which increased to about 14% after 40 h as shown by flow cytometry. The increase in apoptotic cells with time is reflected by the ICC confocal images by fluorescing bright green apoptotic cells (Figure 5.10).

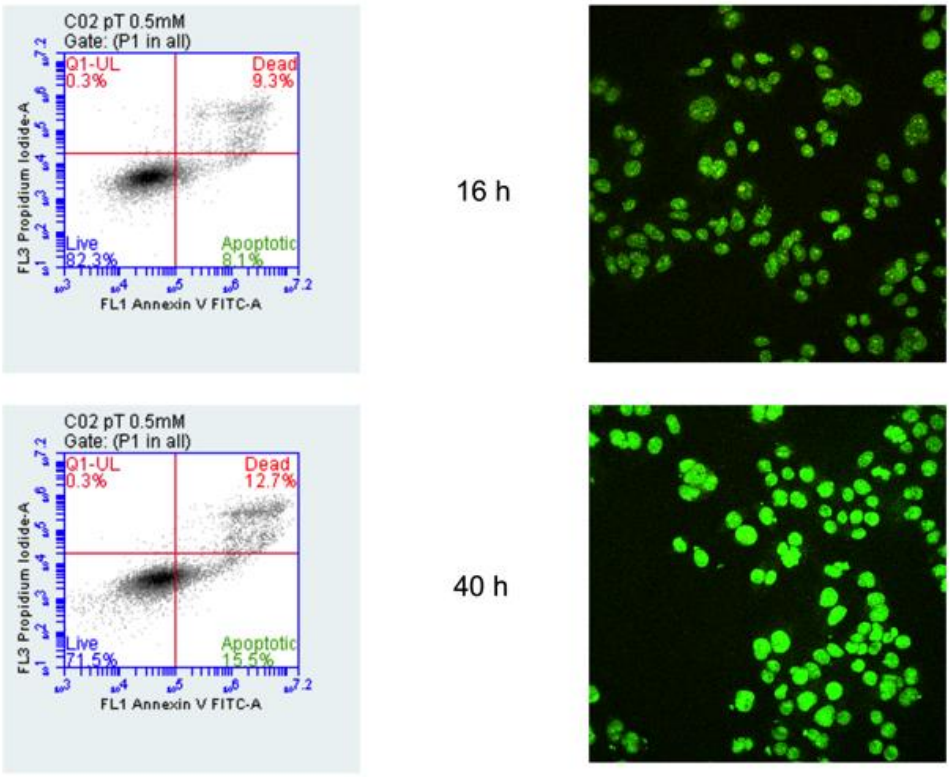

Figure 5.11 Representation of flow cytometric analysis and ICC for PN592 (para-thioaspirin).
SW480 cells were treated with 0.5 mM of PN592 for 16 h and 40 h. The fluorescent dyes used for flow cytometry are Annexin-V-FITC (green) for apoptotic cells and PI (red) for late apoptotic/necrotic cells. The fluorescent dyes used for ICC were YO-PRO®-1 (green) for apoptotic cells and PI (red) for necrotic cells. Representative confocal images were taken at 40X oil/1.30 oil immersion objective. *n=3.*

Apoptotic cells increased after treatment with 0.5 mM PN592 from about 8% after 16 h to about 15% after treatment for 40 h as shown by flow cytometric

analysis. About 10% of necrotic cells were detected using flow cytometry. However, necrotic cells were not detected using the ICC method with apoptotic cells also increasing with duration of treatment with PN592 [from 16 h to 40 h] (Figure 5.11).

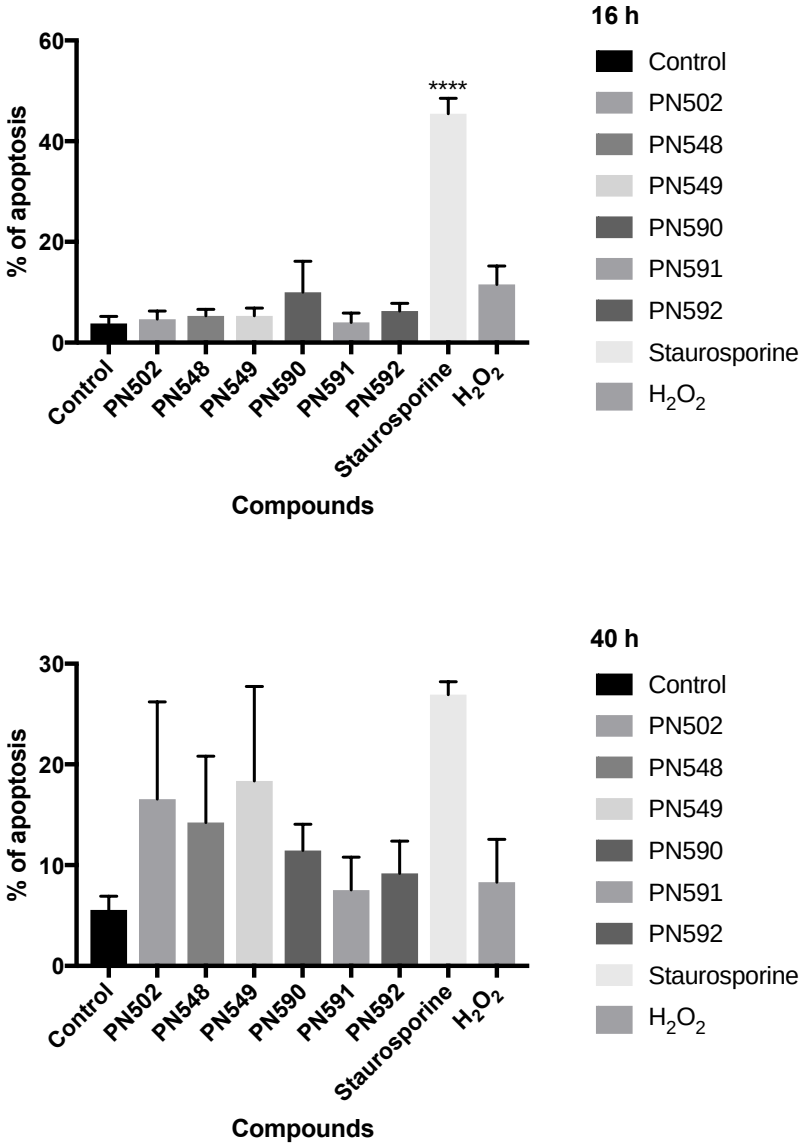

Figure 5.12 Flow cytometric analysis of aspirin analogues showing induced apoptosis in SW480 CRC cell line.
SW480 CRC cells were treated with compounds for 16 h and 40 h, stained with Annexin-V-Fluos and counterstained with PI fluorescence dye and analysed using flow cytometry. Data plotted as mean ± SEM (*n=3*), *****p<0.0001.*

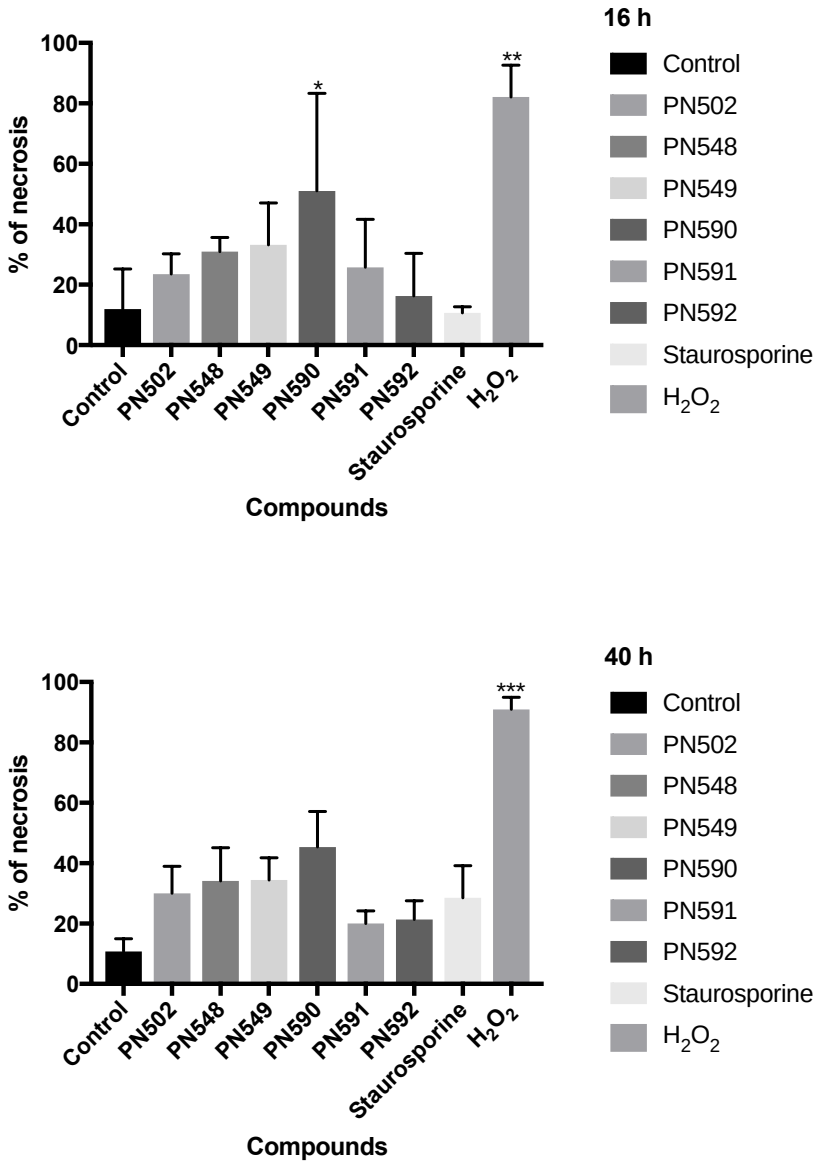

Figure 5.13 Flow cytometric analysis of aspirin analogues showing induced necrosis in SW480 CRC cell line.
SW480 CRC cells were treated with compounds for 16 h and 40 h, stained with Annexin-V-Fluos and counterstained with PI fluorescence dye and analysed using flow cytometry. Data plotted as mean ± SEM (*n=3*) **p<0.05,**p<0.01,***p<0.001.*

Using flow cytometric analysis, the percentage of induced apoptosis in SW480 cells was quite low after treatment with all aspirin analogues. However, the percentage apoptosis did increase after 40 h of treatment with the exception of staurosporine, the compound used as a positive control to apoptosis (Figure 5.12). Necrotic/dead cells also increased in percentage with duration of treatment. The longer the cells were under treatment, the more necrotic cells appeared (Figure 5.13). This also applies to control cells, which could be attributed to the nature of the cells or the methodology/protocol followed.

5.4.4 Effect of ortho-thioaspirin on the localization of β-catenin

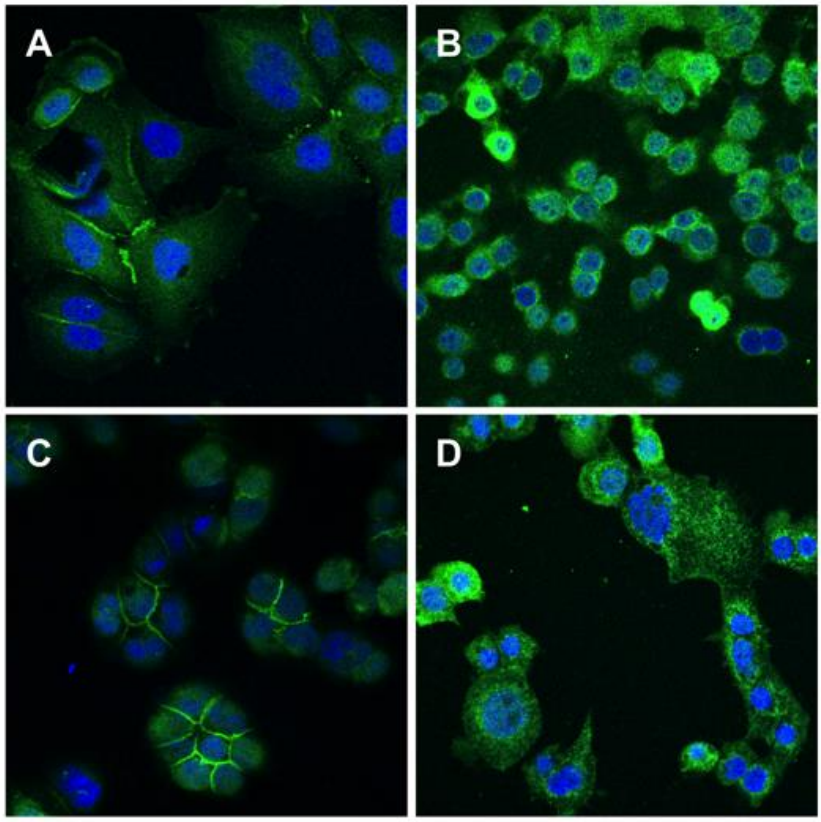

Figure 5.14 Effect of PN590 (ortho-thioaspirin) on β-catenin localization.
DMSO as vehicle control [untreated cells] (A) Cells treated with PN590 dissolved in DMSO (B) Acetone as vehicle control [untreated cells] (C) Cells treated with PN590 dissolved in acetone (D). SW480 CRC cells were treated with PN590 dissolved in either acetone or DMSO for 24 h.

Translocation of β-catenin towards the nucleus from the cytoplasmic membrane can be seen when the cells were treated with PN590 dissolved in DMSO (Figure 5.14B). The translocation of β-catenin from the cytoplasmic membrane when cells were treated with PN590 dissolved in acetone was more to the cytoplasm and not towards the nucleus (Figure 5.14D). Acknowledging that PN590 has a very reactive sulfhydryl group (Scott *et al.*, 1993), reaction with

DMSO may be possible which eventually leads to translocation of β-catenin towards the nucleus.

5.5 Discussion

Programmed cell death (PCD), also known as apoptosis, occurs via different pathways with more than one of these pathways triggered simultaneously (Leist and Jaattela, 2001, Nikoletopoulou *et al.*, 2013). As mentioned in section 1.3.2.1, the SW480 cell line contains a mutation at *TP53* gene of the p53 protein (Din *et al.*, 2004), which p21 is dependent on in its expression and status (el-Deiry *et al.*, 1993). Although p21 is not a reliable protein to conclude induction of apoptotic or anti-apoptotic cell death caused by compounds due to its multiple functions, it does control cell proliferation by causing cell cycle arrest at G1/S transition of the cell cycle. (Abbas and Dutta, 2009, Karimian *et al.*, 2016). Thus, its application to cancer therapy must be approached with caution with emphasis on inhibiting only the oncogenic activities of p21 (Karimian *et al.*, 2016). There was a decrease in p21 expression when SW480 CRC cell line was treated with aspirin (PN502), PN591, PN592 and completely abolished when treated with 100 μM 5-FU, a known anti-cancer drug used in the treatment of CRC (Chu *et al.*, 2009) and PN590 (Figure 5.2 and 5.3A). Contrary to the results obtained in regards to p21 expression after treatment of cells with 5-FU, Li *et al*. found p21 to be up-regulated in oral cancer cell lines, NA and HSC-4 treated with 10 mg/ml and 1 mg/ml 5-FU respectively for a period of 12 h (Li *et al.*, 2004). This could be due to different cell lines having different responses to 5-FU or a difference in dose or duration of treatment. In this study, SW480 CRC cells were treated with 100 μM of 5-FU for a period of 24 h while

Li *et al*. (2004) treated NA and HSC-4 cells with 10 mg/ml and 1 mg/ml, which is equivalent to 76.9 mM and 7.69 mM of 5-FU respectively. Lee *et al*. (2005) also found an increase in p21 expression after treatment of hypopharyngeal cancer cell line, PNUH-12 with 5-FU. However, lung cancer cells, Calu-6 and colon cancer cells, HCT 116 treated with 100 μM of 5-FU for a period of 24 h also down-regulated p21 expression (Esposito *et al.*, 2014), which concurs with the findings in this study. Clinically, investigations by immunohistochemistry in pre- and post-therapeutic tumour samples in patients with rectal carcinoma revealed a decrease in p21 expression to be related to better disease-free survival, indicating the induction of p21 to be linked with lower proliferative activity but poor prognosis after treatment (Noske *et al.*, 2009, Rau *et al.*, 2003). Furthermore, it was observed that the untreated cells (control) expressed p21, which is consistent with p21 being overexpressed in a variety of cancers (Abbas and Dutta, 2009) and could be due to DNA damage and subsequent induction of cell cycle arrest (Karimian *et al.*, 2016) . Expression of p21 is also found to be inversely related to the expression of the p53 protein (Zirbes *et al.*, 2000) and in this study could be due to *TP53* gene mutations harboured by SW480 cells. A number of studies have linked the overexpression of p21 to inhibition of apoptosis. An example includes a study in breast cancer cell lines that revealed a decrease in sensitivity to IR-induced apoptosis when p21 was overexpressed (Soria and Gottifredi, 2010). An increase in the expression of p21 therefore suggests inhibition of apoptosis thus promoting cell survival and cell cycle arrest due to potential DNA damage, while a decrease in the expression of p21 suggests either induction of apoptosis or non-interference in the cell cycle. The

isomers of aspirin, PN548 and PN549 did not seem to have an effect in the expression of p21 (Figure 5.3A). This suggests that PN548 and PN549 may maintain stable biological activity through cell cycle arrest. These isomers of aspirin again stand out when SW480 cells were treated (Figure 5.3B) with them and appeared to be the only compounds that had an effect on the proteins that suggests induction of apoptosis via the BAX-BCL2 pathways. The expression of BAX was increased and the expression of BCL2 decreased simultaneously by both the meta- and para-isomers of aspirin. It can thus be concluded that PN548 and PN549 induce apoptosis via BAX-BCL2 pathways but not through the p21 pathways. However, decrease in the expression of p21 caused by treatment with 5-FU, PN502, PN590, PN591 and PN592 is favourable in cancer therapy because researchers have found out that the knockdown of p21 by radiation leads to a decrease in tumourigenesis suggesting that p21 functions as an oncogene by inhibiting apoptosis (Prives and Gottifredi, 2008). It was therefore concluded that p21 can have dual outcomes in regards to cell proliferation. It can have inhibitory or stimulatory effect on cell division either through apoptosis or cell cycle arrest (Karimian *et al.*, 2016).

The comparison between the quantitative apoptotic status of cell populations using flow cytometry and ICC led to the rise of two main concerns about flow cytometry in the quantitative determination of adherent cells.

The first concern is false PI staining as a result of damaged cells due to trypsinization in order to make a suspension out of the monolayers ready for analysis using the flow cytometer. It was found out that some of the cells got

damaged due to the addition of trypsin thereby taking up PI and thus giving a false result for necrotic/dead cells. Further investigation revealed that all manufacturers of apoptosis kits use cells that are in suspension as sample cells for quantitative analysis of their products found on the protocol sheets (Table 5.1).

Product	Company	Type of cells	Culture properties
⋆Annexin V-FLUOS kit	Roche® Life Sciences	U937 lymphocyte cells	Suspension
FITC Annexin V/PI	invitrogen® Molecular probes®	Jurkat cells (T-cell Leukaemia,human)	Suspension
Annexin V Reagents for apoptosis	IncuCyte®	Jurkat cells	Suspension
FITC Annexin V apoptosis detection kit with 7-AAD	Biolegend®	Jurkat cells	Suspension
PE Annexin V apoptosis kit I	BDPharminogen™	Jurkat cells	Suspension
Annexin V-CF Blue 7-AAD apoptosis staining/detection kit	Abcam	Jurkat cells	Suspension
Annexin V apoptosis detection kit PE	e Bioscience™	Mouse thymocytes	Suspension
Annexin V/7-AAD apoptosis kit	Abnova	Jurkat cells	Suspension

Table 5.1 List of various apoptosis detection kits from different companies with the type of cell used in the documentation/protocol sheet.

(⋆Product used for this study).

The inclusion of adherent cells in samples used for quantitative analysis of apoptosis detection kits will make the product more versatile for use and false PI staining will surely be taken care of by the manufacturers due to damage inflicted on the cell membranes during harvesting in order to produce more robust and reliable data. Some protocols suggest harvesting the cells by incubation in standard trypsin with EDTA, trypsin without EDTA, EDTA without trypsin or mechanical scraping with a rubber policeman. However, all these methods result in damage of the cell membrane (van Engeland *et al.*, 1996). Such damage is likely to happen when attempts are made to harvest adherent cells from the surface of tissue culture plates and was thus suggested to allow for Annexin V binding to cells before harvesting (van Engeland *et al.*, 1996). The second concern is that late apoptotic cells also appear in the UR quadrant positive for PI staining. This means that the analysis is unable to differentiate between late apoptotic, necrotic and dead cells. Part of this issue is raised by Rieger *et al*., (2011) in that about 40% of PI stain results could be due to staining of RNA within the cytoplasm and thereby producing false positive events (Rieger *et al.*, 2010). They suggest a protocol, which includes the addition of 16 µl of 1:100 diluted RNase A (Sigma, R4642) to give a final concentration of 50 µg/ml and incubated before analysis (Rieger *et al.*, 2011). This enables the removal of cytoplasmic RNA and thus eliminates any false necrotic values due to PI staining.

Results from ICC confocal images after treatment with isomers of aspirin and thioaspirins revealed that SW480 CRC cells treated with 0.5 mM of PN502

(aspirin), PN591 and PN592 for 16 h caused few cells to undergo early apoptosis, which increased substantially after 40 h of treatment (Figures 5.6, 5.10 and 5.11 respectively). Aspirin has previously been reported to cause cell death in SW480 cells via apoptosis (Stark *et al.*, 2001). Treatment of this cell line with 0.5 mM of PN548, 0.5 mM of PN549 and 0.3 mM of PN590 caused the cells to undergo early apoptosis after treatment for 16 h and then progressed to late apoptosis and necrosis after 40 h of treatment (Figures 5.7, 5.8 and 5.9 respectively). Here again the same trend is followed by the isomers of aspirin, PN548 and PN549 and the isomers of thioaspirin, PN591 and PN592.

Inactivation of the pathways that involves *APC* tumour suppressor gene and β-catenin is usually the beginning of a chain of genetic changes involved in colorectal cancer development (Morin *et al.*, 2016, Morin *et al.*, 1997). These changes include translocation of β-catenin to the nucleus which leads to its interaction with DNA-bound transcription factor proteins (TCF1, TCF2 or TCF3), which in turn causes the activation of several target genes such as Cyclin D1 (Thorstensen *et al.*, 2005). Thus, the ability of PN590 to drive β-catenin towards the nucleus is a disadvantage to its properties as a compound with cytotoxic effects. However, this translocation towards the nucleus is seen more clearly when PN590 is dissolved in DMSO, which suggests that PN590 dissolution in DMSO should be avoided (Figure 5.15B).

Chapter 6. Effect of Aspirin analogues on the EGFR

6.1 Introduction

6.1.1 The EGF Receptor

EGF was discovered while in the process of isolating and characterizing a salivary gland protein that caused growth developments in new-born mice back in 1960 (Cohen, 1962). In 1975, Graham Carpenter published his findings of a receptor, as a membrane protein with a molecular weight of 170-kDa (Carpenter *et al.*, 1975).

The EGF receptor (EGFR) is one of the 20 subfamilies of the receptor tyrosine kinases (RTKs), which are the main mediators of many cell signals in living organisms. The EGFR family, also known as ErbB tyrosine kinase receptors or type I receptor tyrosine kinases (Mendelsohn and Baselga, 2000) is made up of four receptors; namely, EGFR (ErbB1), HER2 (ErbB2/neu), HER3 (Erb3) and HER4 (ErbB4) (Hackel *et al.*, 1999, Klapper *et al.*, 2000, Olayioye *et al.*, 2000).

Levels of EGFR in the neoplastic tissue of the colorectal mucosa in comparison to the surrounding unaffected mucosa, assessed by enzyme immunoassay and Western blotting procedure are raised in up to 80% of CRC cases (Messa *et al.*, 1998, Porebska *et al.*, 2000). EGFR overexpression in cancer cells is primarily due to mRNA instability caused by a mutation that lead to mononucleotide or dinucleotide deletions within the A13/A14 repeat sequence in the 3'-untranslated region of the EGFR gene (Yuan *et al.*, 2009). This condition can be reversed by treatment with anti-EGFR agents that bind competitively with EGF to the receptor such as cetuximab (Cunningham *et al.*, 2004) and more

recently by aspirin treatment, leading to improved clinical outcomes (Algra and Rothwell, 2012, Chan and Lippman, 2011, Li *et al.*, 2015). In about 10% of lung tumours however, mutation occurs as a result of threonine being substituted with methionine at amino acid 790 (T790M). This mutation enables activation of EGFR even after drug-receptor interaction, thus, causing resistance to EGFR inhibitor drug, gefitinib and leads to poor prognosis (Kobayashi *et al.*, 2005, Pao *et al.*, 2005).

The percentage of EGFR expression and its significance in clinical outcomes differ quite widely in the literature as a result of the absence of a standardized methodology for assessment (Krasinskas, 2011). For example, while EGFR is reported to be overexpressed in about 80% of CRC cases with no correlation to increased patient mortality (Spano *et al.*, 2005), it is also reported to be overexpressed in 35% of CRC cases which has been related to increased patient mortality (Resnick *et al.*, 2004). In comparison to lung cancer, the defect found in CRC is mainly due to overexpression of the EGFR and rarely protein/gene mutation (Barber *et al.*, 2004, Lee *et al.*, 2005). However, the prevalence in Korean CRC patients is 22.4% in a small clinical study of 58 patients (Oh *et al.*, 2011).

Thus, overexpression of the EGFR is often found in a number of cancers and related to the development and enhancement of tumourigenesis.

6.1.1.1 Structure of the EGFR

The EGF receptor is made up of three domains. The extracellular ligand binding domain, the transmembrane lipophilic domain and the intracellular protein kinase domain that consists of a regulatory carboxyl terminal segment (Mendelsohn and Baselga, 2000), which harbours the different phosphorylation sites (Wheeler *et al.*, 2010) (Figure 6.1).

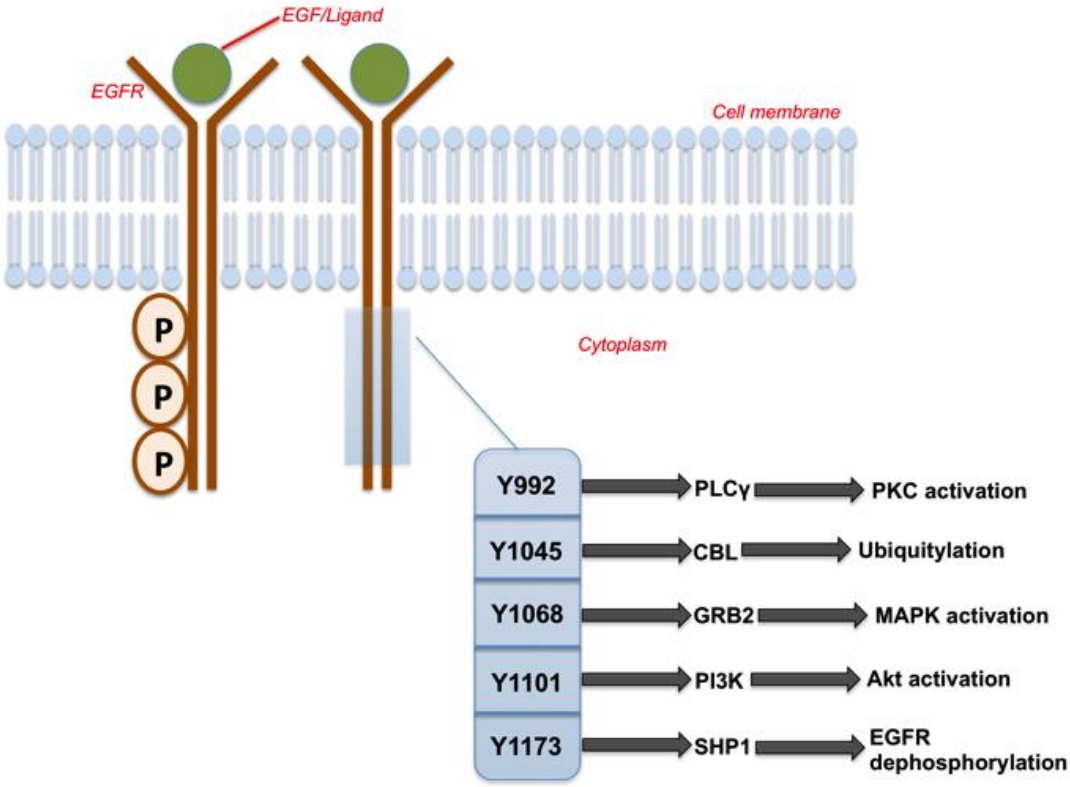

Figure 6.1 Structure of the EGFR, sites of phosphorylation and effector signalling pathways triggered.
Homodimerization or heterodimerization occurs after ligand binding to the EGFR. This leads to autophosphorylation of the tyrosine kinase residues located on the cytoplasmic tail of the receptor. The tyrosine kinase sites include Y992, Y1045, Y1068, Y1101 and Y1173 and their biological activities indicated after the arrows [(Adapted from (Nyati *et al.*, 2006) and (Wheeler *et al*., 2010)].

Proteins that connect the RTKs to downstream signalling pathways include Shc, Grb2, Grb7 and Nck while the enzymes include phospholipase Cγ (PLCγ), PI 3-K and Src, which is phosphorylated and thus activated (Hackel *et al*., 1999).

6.1.1.2 Epidermal Growth Factor (EGF)

Epidermal growth factor (EGF) was first discovered while in the process of isolating and characterizing a salivary gland protein that caused growth developments in new-born mice back in 1960 and was found out to make up about 0.5% of the protein content of the submaxillary gland (Carpenter and Cohen, 1979, Cohen, 1962).

Endogenous EGF in normal cells has a positive function that is wound healing (Schultz *et al.*, 1991, Werner and Grose, 2003). The EGF family members are considered as one of the most important growth factors responsible for the growth and differentiation of keratinocytes, which is a process involved in wound healing of the skin (Shirakata *et al.*, 2005).

EGF only has a negative effect in cancer due to the overexpression and deregulation of its signalling pathway.

6.1.1.3 The phosphorylation sites

Upon stimulation of the EGF receptor, phosphorylation is activated on its various tyrosine residues (Margolis, 1992, Wheeler *et al.*, 2010).

EGFR phosphorylation sites/Tyrosine residues	**Function**
Tyr 1068	The activation of EGFR leads to a series of protein-protein interactions involving Grb2, a protein found in the site's downstream signalling pathway. This serves as an adaptor protein, which binds to the phosphorylated Tyr 1068. This is particularly important in the protein kinase-signalling pathway. Phosphorylation at this site is responsible for the activation of Ras and Mitogen-activated protein kinase (MAPK) pathway (Nyati *et al.*, 2006, Rojas *et al.*, 1996, Wheeler *et al.*, 2010).
Tyr 992	PLCγ has two SH2 domains which both bind to this phosphorylation site to activate PLCγ mediated downstream signalling (Emlet *et al.*, 1997, Wheeler *et al.*, 2010).
Tyr 1045	The EGFR is downregulated by c-Cbl adaptor proteins via mobilizing ubiquitin-activating and ubiquitin-cojugating enzymes. This leads to endocytosis (internalisation) and degradation of ligand-receptor complexes (Levkowitz *et al.*, 1998, Nyati *et al.*, 2006)
Tyr 1173	This provides the docking site for Shc and Grb2 adaptor proteins in which its phosphorylation causes the activation of the Ras oncogene after Erk phosphorylation (Jorissen *et al*., 2003)
Tyr 1101	The function of this phosphorylation site is uncertain (Biscardi *et al.*, 1999). However, Wheeler *et al*. described it as having an effect on the activation of PI3K and subsequently Akt (Wheeler *et al.*, 2010).

Table 6.1 EGFR phosphorylation sites used in this study and their functions.

6.1.1.4 Biological function of the EGFR

In healthy cells, dimerization occurs when the EGFR becomes activated as a result of ligand binding to the receptor or overexpression of the receptor (Cochet *et al.*, 1988, Lemmon and Schlessinger, 1994, Yarden and Schlessinger, 1987). This leads to the formation of homo or heterodimeric complexes for Src homology (SH2) and phosphotyrosine binding (PTB) domain-containing proteins by phosphorylation of specific tyrosine residues (Lemmon and Schlessinger, 2010). An asymmetric dimer with only one bound ligand is created when the first ligand binds to the receptor and the idle site of the dimer becomes structurally unable to interact with any ligand. Thus, reducing the possibility of a second ligand to bind onto the same receptor. This process is known as negative co-operativity (Alvarado *et al.*, 2010).

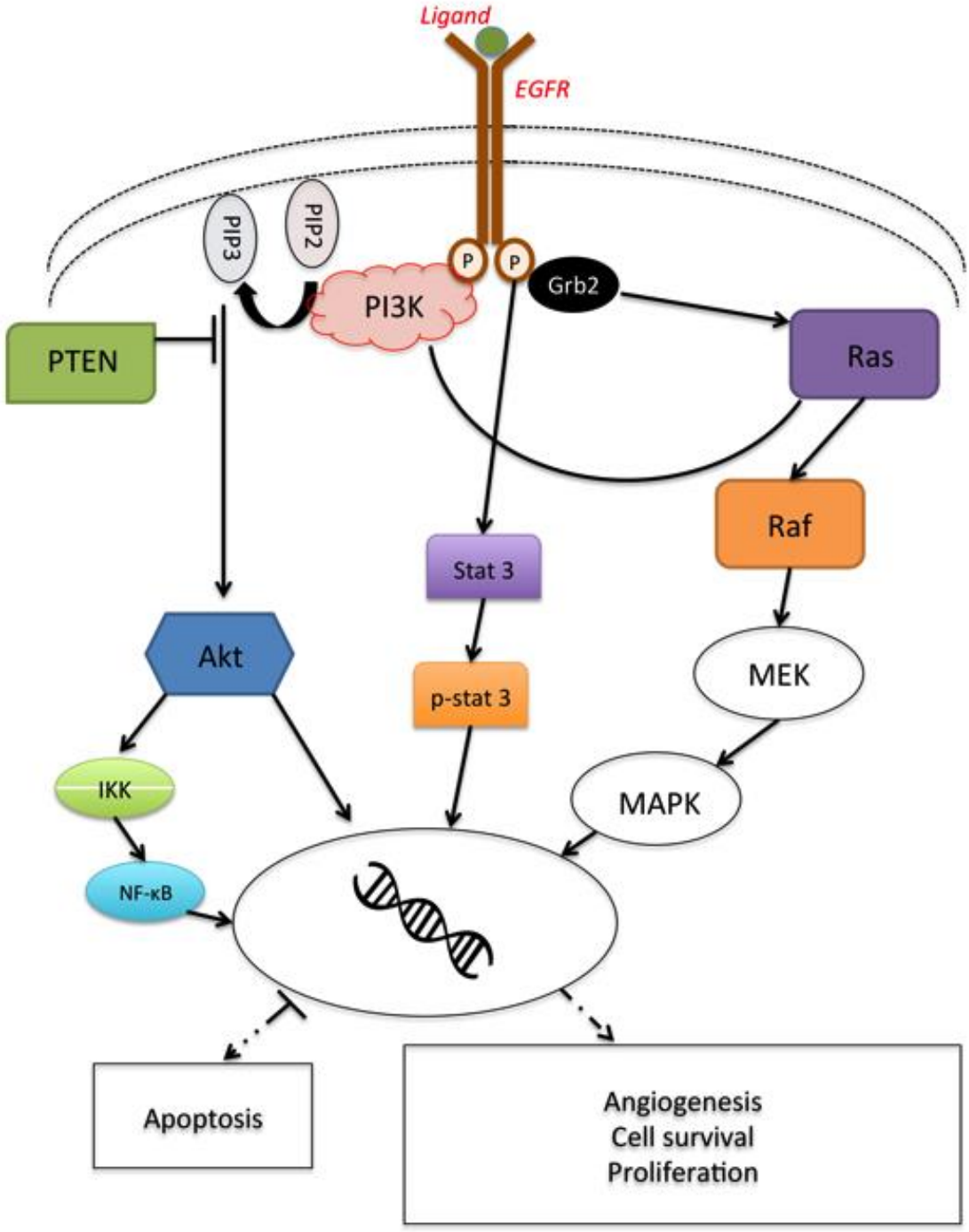

Figure 6.2 EGFR signalling pathway.
Dimerization occurs after ligand binding to the receptor. Autophosphorylation of tyrosine kinase residues leads to a cascade of downstream signalling. [Adapted from (Krasinskas, 2011, Schlessinger, 2000)].

Activation of the protein tyrosine kinases is then set-off with subsequent autophosphorylation of the sites resulting in the activation of different signalling pathways and cellular activities (Alroy and Yarden, 1997), which include apoptosis, gene expression, cellular differentiation and proliferation (Chan *et al.*, 1999). These phosphorylated tyrosines cause a change in charge and shape of the receptors, permitting the recruitment of particular signalling protein. Adaptor proteins that contain Src homology 2 domains (SH2) or phosphotyrosine-binding domains such as c-Cbl (Y1045) or Grb2 (Y1068) are later recruited (Levkowitz *et al.*, 1998, Ushiro and Cohen, 1980). One of the branches of the EGFR signalling pathway is the Ras-Raf-MEK-MAPK pathway (Figure 6.2).

It should be mentioned that there are different conflicting theories and explanations on endocytosis of the EGFR, which could be due to differences in experimental designs or possibly different clones of the same cell type (Benmerah and Lamaze, 2007).

PTEN, a tyrosine phosphatase enzyme, is known to inhibit PI 3-K by dephosphorylating phosphatidylinositol 3,4,5-trisphosphate (PIP_3) in the 3-position, which ultimately results in Akt inactivation and cell death (Krasinskas, 2011).

The EGFR pathway is complicated, and signalling needs to be strictly controlled due to different negative and positive feedback mechanisms linked to the pathway and activation of different transcription factors all with different outcomes depending on which type of cell it is (Citri and Yarden, 2006). Otherwise, this results in anti-apoptosis, cell proliferation, angiogenesis and metastasis (Mitsudomi and Yatabe, 2010). Tumour formation or progression is

especially due to the activation of EGFR downstream regulators such as the Akt, *KRAS* and MAPK (Krasinskas, 2011). The inhibition of these effectors/regulators will be beneficial in therapy. However, study of these individual regulators commonly results in different outcomes (Krasinskas, 2011). For example, *KRAS* proto-oncogene encodes a GTPase at the beginning of the MAPK pathway. Mutation of *KRAS* leads to the prolonged activation of the MAPK pathway. Samowitz et al., (2000), Belly et al., (2001) and Andreyev et al., (2010) reported *KRAS* mutation status to be linked with shorter patient survival whereas Roth et al., (2010) and Tejpar et al., (2010) reported otherwise.

EGFR stimulation also leads to the continuous activation of certain STAT (Signal transducers and activators of transcription) proteins, which include Stat-3 having anti-apoptotic effects (Grandis *et al.*, 2000). Thus, its inhibition will lead to the activation of the apoptotic process.

Currently, seven STATs are recognised, namely STAT 1, -2, -3, -4, -5A, -5B and -6 (Garcia and Jove, 1998). In comparison to normal human cells, Stat-3 activation is greatly increased in a range of human cancer cells and have been linked to poor prognosis in breast and colon cancers (Khazaie *et al.*, 1993). Activation of Stat-3 subsequently leads to activation of Bcl-2 (Catlett-Falcone *et al.*, 1999), which is also anti-apoptotic. EGFR degradation is one of two results of its stimulation by EGF (Decker, 1990).

A number of studies have found out that the internalization of the EGFR induced by ligand binding is a crucial step in the EGFR signalling pathway (Schlessinger, 2000, Weiner and Zagzag, 2000).

6.1.1.5 Medical relevance

The epidermal growth factor receptor (EGFR) is one of the numerous molecular targets suggested as candidate targets for cancer therapy (Mendelsohn and Baselga, 2000) and is one of four receptor tyrosine kinases with its overexpression resulting in poor prognosis (Madshus and Stang, 2009). A number of human cancers have been identified to show overexpression, mutations and gene amplification of the receptor (Zwang and Yarden, 2006) with colorectal cancer amongst those known to exhibit such characteristics (Ciardiello *et al.*, 2001).

Apart from observed mutations in receptor tyrosine kinase (RTK) pathways in different subtypes of human CRC, which are one of the main oncogenic mechanisms, there is also overexpression in some oncogenic RTKs (Yao *et al.*, 2013). Thus, a complete understanding on the EGFR signalling pathway will be of great use to researchers (Hynes and Lane, 2005). In patients undergoing cancer therapy using gefitinib, mutations at the tyrosine kinase domain were found in those that responded to the therapy and none of these mutations were seen in those that did not (Jorissen *et al.*, 2003). Stimulation of these downstream pathways can lead to different pathways responsible for cell migration, proliferation and cell survival and their alterations can lead to positive prognostic effects (Krasinskas, 2011).

6.1.2 Early Endosome Antigen1 (EEA1)

The early endosome antigen1 (EEA1) is an effector protein required at the early endosome, which is a compartment responsible for the sorting of ligand-

receptor complexes into late endosomes and lysosomes for degradation or back to the cell surface for recycling (Mu *et al.*, 1995, Shepherd, 1989). This compartmentalization takes place after endocytosis of a receptor, which is part of the signalling pathway of the EGFR (Schlessinger, 2000). Two models have been proposed for transition from early endosomes to late endosomes, one of which proposes that early endosomes progressively mature into late endosomes and lysosomes (Murphy, 1991). However, Griffiths and Gruenberg (1991) disagrees and proposes that early and late endosomes are 'two distinct pre-existing cellular organelles' and linked by a microtubule communicating system. Proteins specific to these compartments include Rab5, a GTP-binding rab protein (Chavrier *et al.*, 1990) and EEA1 both localizing to the early endosome, Rab4 or Rab11 localizing the recycling compartments and Rab7, localizing to the late endosome and are all GTP-binding rab proteins (Flores-Rodriguez *et al.*, 2015, Mu *et al.*, 1995). Ligand stimulation of the EGFR leads to it being rapidly internalised and transported to the early endosomes with some of the receptor recycled back to the cell membrane but most of it delivered into intraluminal vesicles (ILVs) within the endosome, which matures into the multivesicular body (MVB) (Flores-Rodriguez *et al.*, 2015, Sorkin and Goh, 2009). The endosomes then undergoes biochemical changes via fusion and fission leading to development into late endosomes that eventually delivers the EGFR to the lysosomes where it undergoes degradation (Foret *et al.*, 2012). Within the early endosome network, the EGFR is delivered to the Rab5 situated at the periphery of the early endosomes enriched with APPL1 (adaptor protein, phosphotyrosine interaction, PH domain and leucine zipper containing 1), an

adaptor protein that regulates AKT signalling before being delivered to EEA1-positive endosomes (Schenck *et al.*, 2008). However, it is also reported that the receptor employs endosomal-sorting complex required for transport (ESCRT), protein complexes that deliver the receptor into ILVs (Hanson and Cashikar, 2012) before being sorted to EEA1-positive endosomes (Flores-Rodriguez *et al.*, 2015).

CHMP4C and *CAV1*, genes essential in the endosomal-sorting network are regulated by the transcription factor, P53 (Yu *et al.*, 2009). *CHMP4C* is harboured by one of the ESCRT protein complex situated on the MVB (Woodman, 2009) while CAV1 is harboured by caveolin-1 protein involved in the caveolae-mediated pathway for EGFR endocytosis (Le Roy and Wrana, 2005, Yu *et al.*, 2009).

6.2 Aims and Objectives

In the previous chapters of this thesis and previous publications, it has been seen that the cytotoxic effects of aspirin and its analogues on SW480 CRC cell lines in varying degrees. Their capacity to induce apoptosis (Deb *et al.*, 2011), inhibit NF-κB *in vitro* and cyclin D1 expression and also suppress tumour growth *in vivo* in a murine model of colorectal cancer with no evidence of toxicity observed (Claudius *et al.*, 2014). Cytotoxic effects on oesophageal cancer cell lines have also been reported by Kilari, R.S. (2014) *Roles of Inositol Diphosphate in DNA Repair And Effects of Aspirin Analogues on Oesophageal Cancer.* Ph.D. Thesis, University of Wolverhampton.

In this chapter, it was intended to find out if these compounds have an effect on the molecular pharmacology of the EGFR; namely its internalization, its co-localization with EEA1 and the effect of these analogues on the different tyrosine kinase phosphorylation sites responsible for its ubiquitination and recycling. The pursuit to study whether the EGFR phosphorylation state was altered, leading to regulation of downstream effects, was determined using selective antibodies prepared against particular targets. Fluorescent dyes and selective antibodies have been used to study this signalling pathway. SW480 CRC cell line is a good candidate for this study because it is known to over-express EGFR (Goetz *et al.*, 2010).

The ability of aspirins and analogues to alter tyrosine phosphorylation may be a general effect, or it may target specific tyrosines. Selective sites were looked at in order to determine (i) whether the EGFR is a target for these drugs and (ii) whether all phosphorylation sites are affected.

6.3 Methodology

The experimental methods used in this chapter are as stated in chapter two (2.2.12 to 2.2.16).

6.4 Results

6.4.1 Perturbation of EGF internalization and effect on its co-localization with EEA1 by aspirin and its analogues

A long standing proposal has been that the internalization of the EGFR is a way of attenuating the signalling pathway as the receptor is removed from the cell surface (Wells, 1999). However, evidences from von Zastrow and Sorkin,

(2007) generated by observations made in 1996 by Vieira et al., show that internalization is an essential part of the signalling pathway in which inhibition could lead to disruption of a number of mechanisms in the signalling pathway (Sigismund *et al.*, 2008). Internalization removes the EGFR from the cell surface and routes it to either be recycled or degraded in endosomes and lysosomes (Sorkin and von Zastrow, 2009). Nuclear EGFR has been found to act as a transcription factor, activating genes such as cyclin D1 responsible for cell proliferation (Lin *et al.*, 2001). A recent study from Ortega *et al*., discovered that the phosphorylation of PCNA by EGFR in the nucleus led to the inhibition of DNA MMR thereby promoting proliferation of cells with damaged DNA (Ortega *et al.*, 2015) and thus tumour growth.

Effects of these compounds could be due to the salicylate moiety of the chemical structure. Diflunisal, containing salicylate as part of its substructure is an NSAID, and also included in this study. Diflunisal works similarly to salicylic acid as an anti-inflammatory and has been found to inhibit the growth of cancer cells *in vitro* and *in vivo* (Shirakawa *et al.*, 2016).

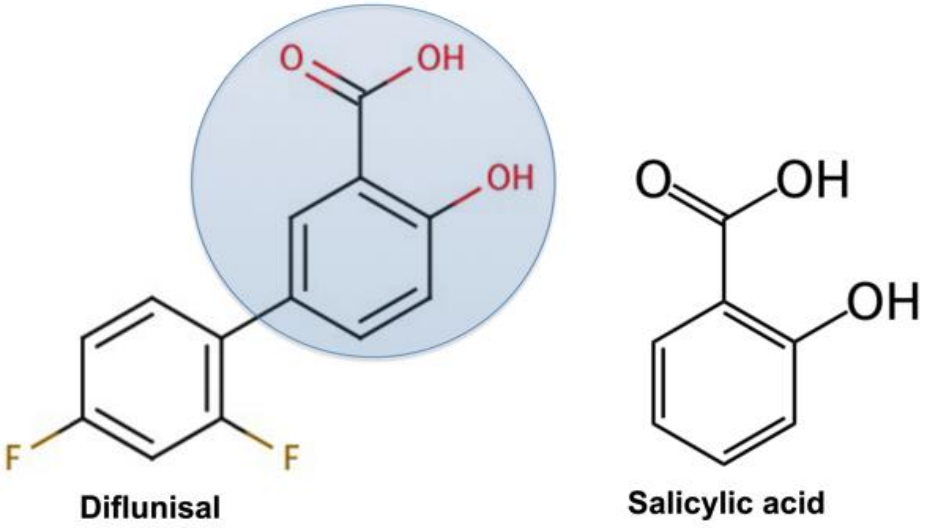

Figure 6.3 Structure of diflunisal and salicylic acid.
Diflunisal has a salicylic acid moiety as part of its chemical structure.

The compounds used were dissolved in acetone and either buffered in HEPES (pH8) or PBS (pH7.4) and then made up to the required 0.5 mM final concentration as in all the experiments prior to this chapter. The cells were initially treated with the compounds and EGF without ‘chasing’ (Activating internalization) at 37°C to ensure that there was no competitive binding between the compounds and EGF to the receptor.

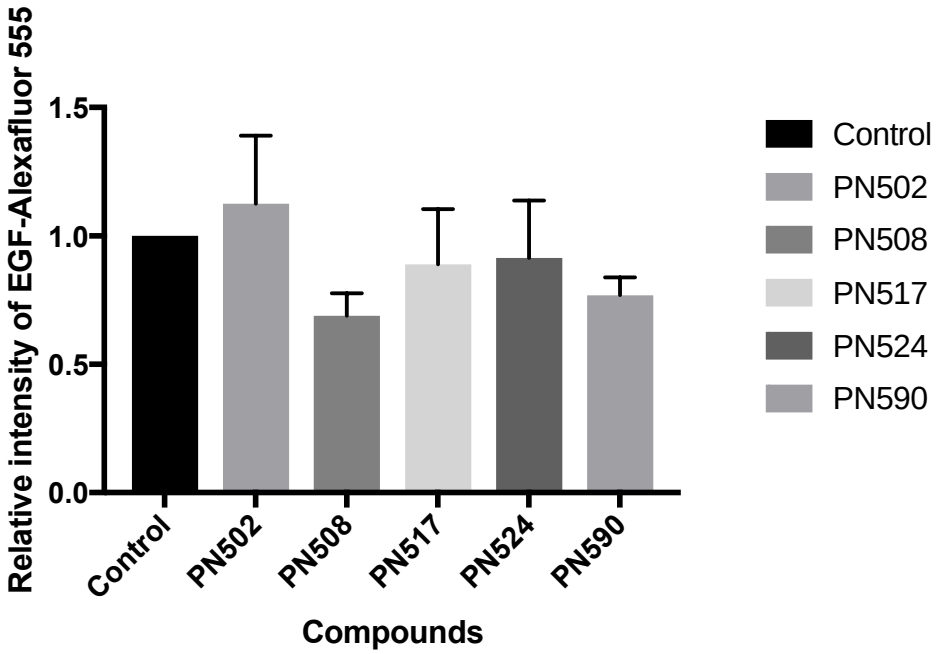

Figure 6.4 Quantification of the effect on aspirin analogues on EGF binding.
The effect of aspirin analogues on EGF binding was quantified using Image J software. 50 cells were analysed per compound and data plotted as mean ± SEM (*n=3*).

The difference in EGF bound along the membrane of the cytoplasm in untreated SW480 CRC cells was not significantly different from the cells treated with the aspirin analogues (Figure 6.4). Intensity of EGF-Alexafluor 555 measured for treated cells is relative to the intensity of EGF in the control (untreated cells).

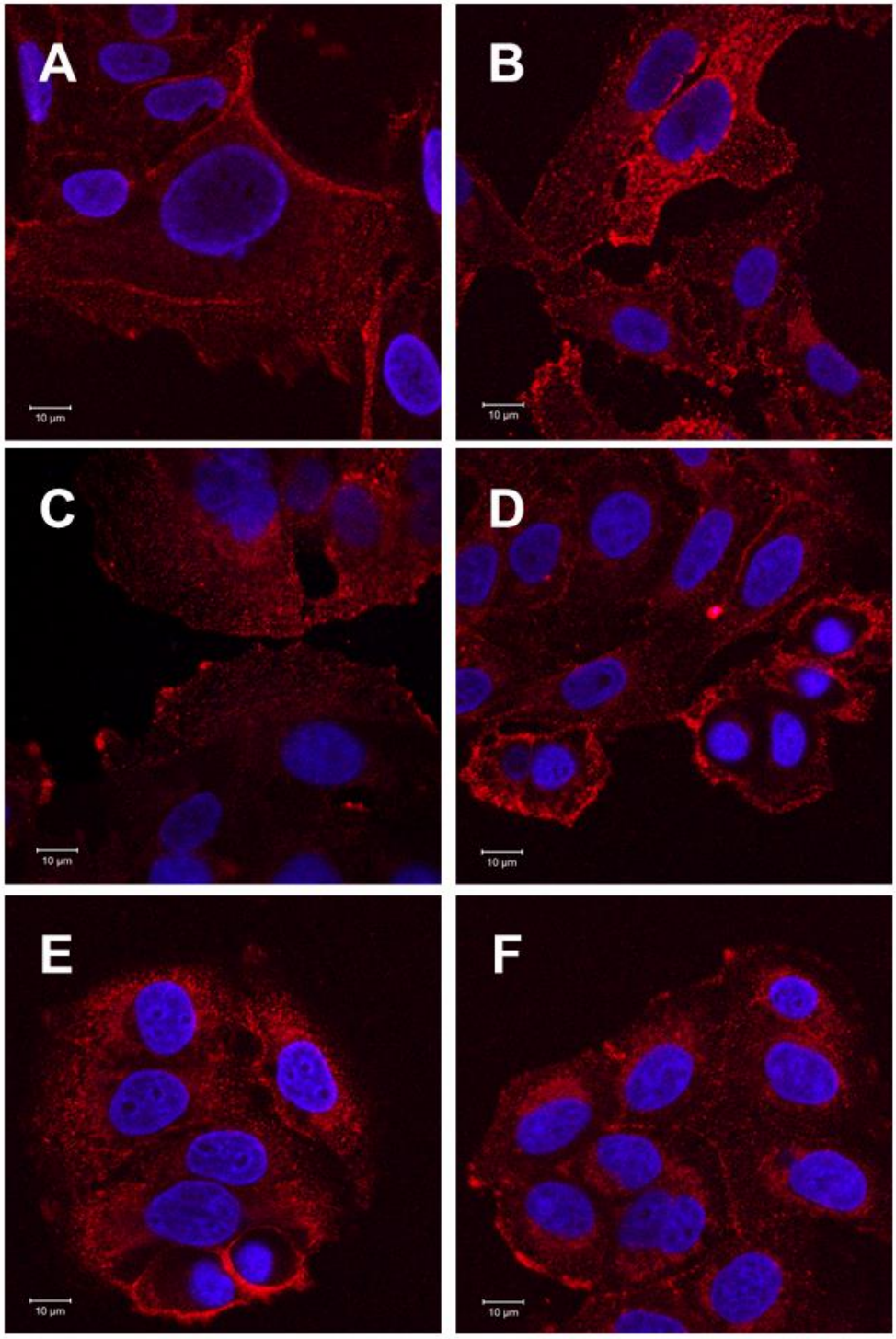

Figure 6.5 Effect of aspirin analogues on EGF binding.
Confocal images of SW480 CRC cells treated with or without compounds; Control [untreated] (A), PN502 [ortho-aspirin] (B), PN508 [diaspirin] (C), PN517 [fumaryldiaspirin] (D), PN524 [m-bromobenzoylsalicylate] (E), PN590 [ortho-thioaspirin] (F). Cells (with the exception of control) were treated with 0.5 mM (pH adjusted with PBS) for 30 min. The EGF used is complexed to Alexa Fluor® 555 (100 ng/ml) for 1 h on ice and fixed. Images were acquired at 405 nm-DAPI (blue) and 561 nm-Alexa Fluor (red) for EGF. Representative images are shown taken at 40X oil/1.30 oil immersion objective. Scale bar represents 10 µm.

Semi-quantitative (Figure 6.4) and qualitative (Figure 6.5) analysis revealed that there was no significant difference between the intensity of EGF bound to the control cells that were untreated (Figure 6.5A) with the cells that were treated with PN502 (Figure 6.5B), PN517 (Figure 6.5D), PN524 (Figure 6.5E), PN590 (Figure 6.5F) and PN508 (Figure 6.5C). This enabled further experiments to be carried out with the knowledge that these compounds do not alter EGF binding. The images below have been grouped into aspirins, diaspirins, thioaspirins and salicylate-like compounds for easy visualisation using the same positive and negative controls to all aspirin analogues for same experimental conditions.

In the controls where there was only ligand stimulation and no treatment with compounds for the EGF-EEA1 co-localization experiments, the EGF was observed not to have co-localized with EEA1 even though internalization had taken place. This suggests that degradation did not take place but perhaps the receptors were recycled back to the cell surface and so signalling pathways remained activated.

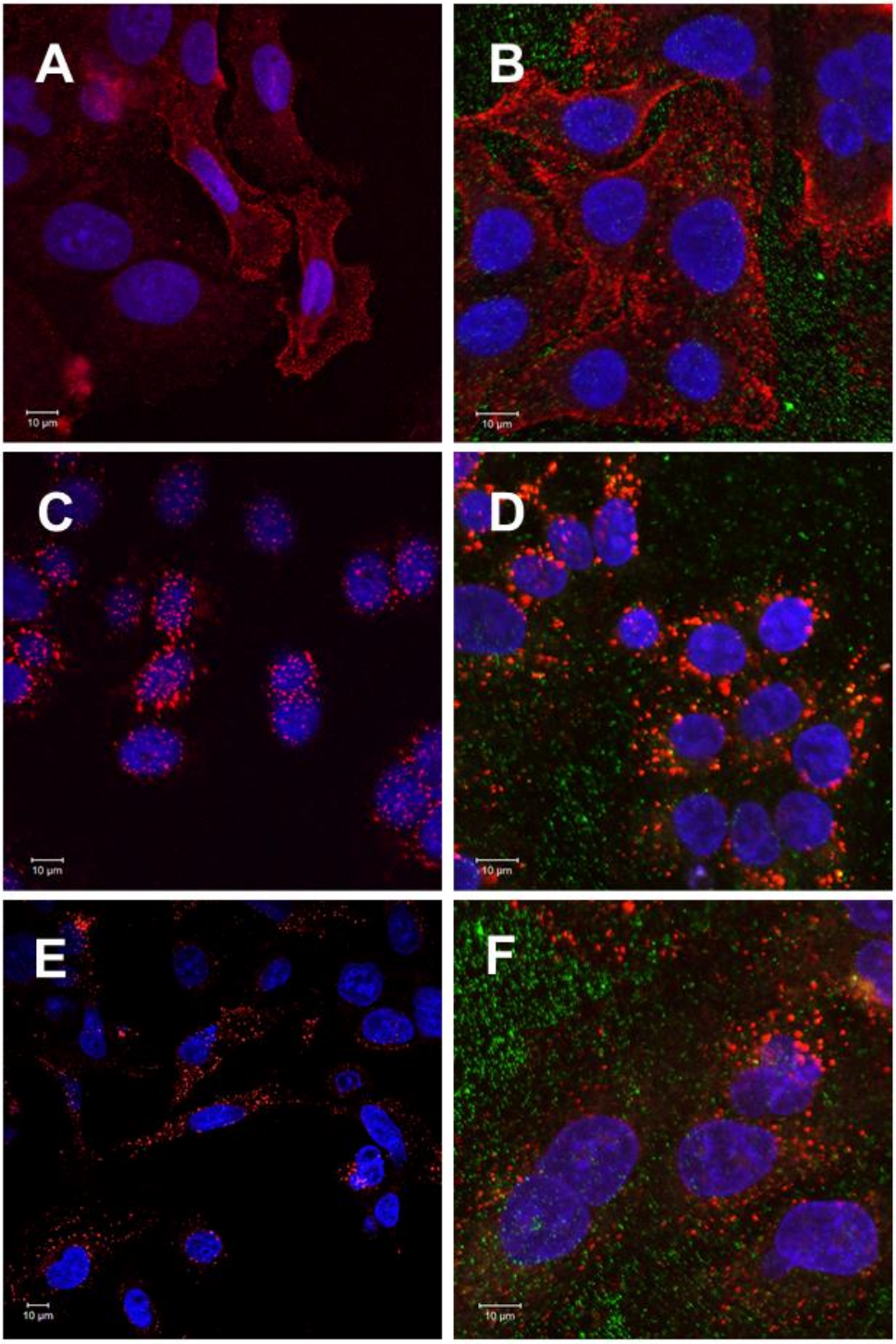

Figure 6.6 (A – F) Effect of aspirins with PBS on EGF-100 ng/ml internalization and EGF co-localization with EEA1.

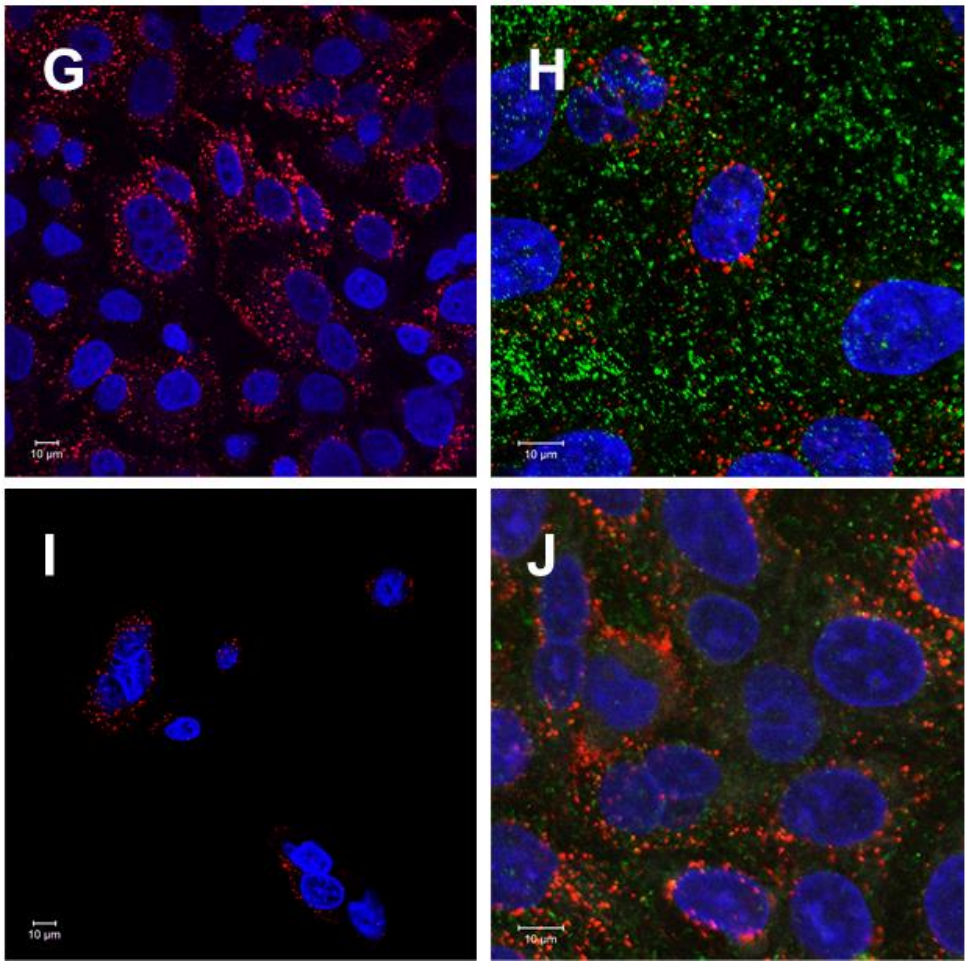

Figure 6.6 Effect of aspirins with PBS on EGF-100 ng/ml internalization and EGF co-localization with EEA1.

Confocal images of SW480 CRC cells treated with or without compounds, negative control [EGF receptor unstimulated] (A), negative control with EEA1 (B), positive control [EGF receptor stimulated] (C), positive control with EEA1 (D), PN502 [ortho-aspirin] (E), PN502 showing EEA1 (F), PN548 [meta-aspirin] (G), PN548 showing EEA1 (H), PN549 [para-aspirin] (I), PN549 showing EEA1 (J). Cells were treated with 0.5 mM aspirin analogue (pH adjusted with PBS) for 30 min. The EGF used is complexed to Alexa Fluor® 555 (100 ng/ml) for 1 h on ice after which it was 'chased' at 37°C for 30 min. The cells were then fixed for 5 min. For EEA1 co-localization, the slides were then treated with EEA1 primary antibody and a corresponding secondary antibody. Images were acquired at 405 nm-DAPI (blue) for nucleus, 561 nm-Alexa Fluor (red) for EGF and 488 nm-FITC for EEA1 (green). Representative images are shown taken at 40X oil/1.30 oil immersion objective *(n=3*). Scale bar represents 10 µm.

EGF can be seen along the cell membrane for the negative control cells (Figure 6.6A) because the receptor has not been stimulated by incubation at 37°C. As EGF binds to EGFR, this represents the EGFR along the cell membrane before internalization when stimulated. The positive control represents the state of the EGF after it has been 'chased', which means stimulating the receptor by incubating the cells for 30 min at 37°C stimulating the receptor leads to its internalization towards the nucleus as seen in Figure 6.4C.

The presence of yellow fluorescence signifies co-localization. Upon observation, the EGF, with the receptor not stimulated showed no signs of co-localization with EEA1 (Figure 6.6B). This was expected. However, what was not expected was the stimulated receptor to also show no signs of co-localization with EEA1 (Figure 6.6D).

Internalization of EGF (100ng/ml) was clearly perturbed by PN502 (Figure 6.6E), PN548 (Figure 6.6G) and PN549 (Figure 6.6I) in varying degrees with the perturbation strongest in cells treated with PN502. Downregulation of EGFR internalization is a significant process in regulating its signalling (Roepstorff *et al.*, 2009). However, effect on the co-localisation of EGF and EEA1 in the cells treated with PN548 (Figure 6.6H) and PN549 (Figure 6.6J) was no different from the unstimulated (Figure 6.6B) and stimulated (Figure 6.6G) receptors with slight co-localization seen in the cells treated with PN502 (Figure 6.6F).

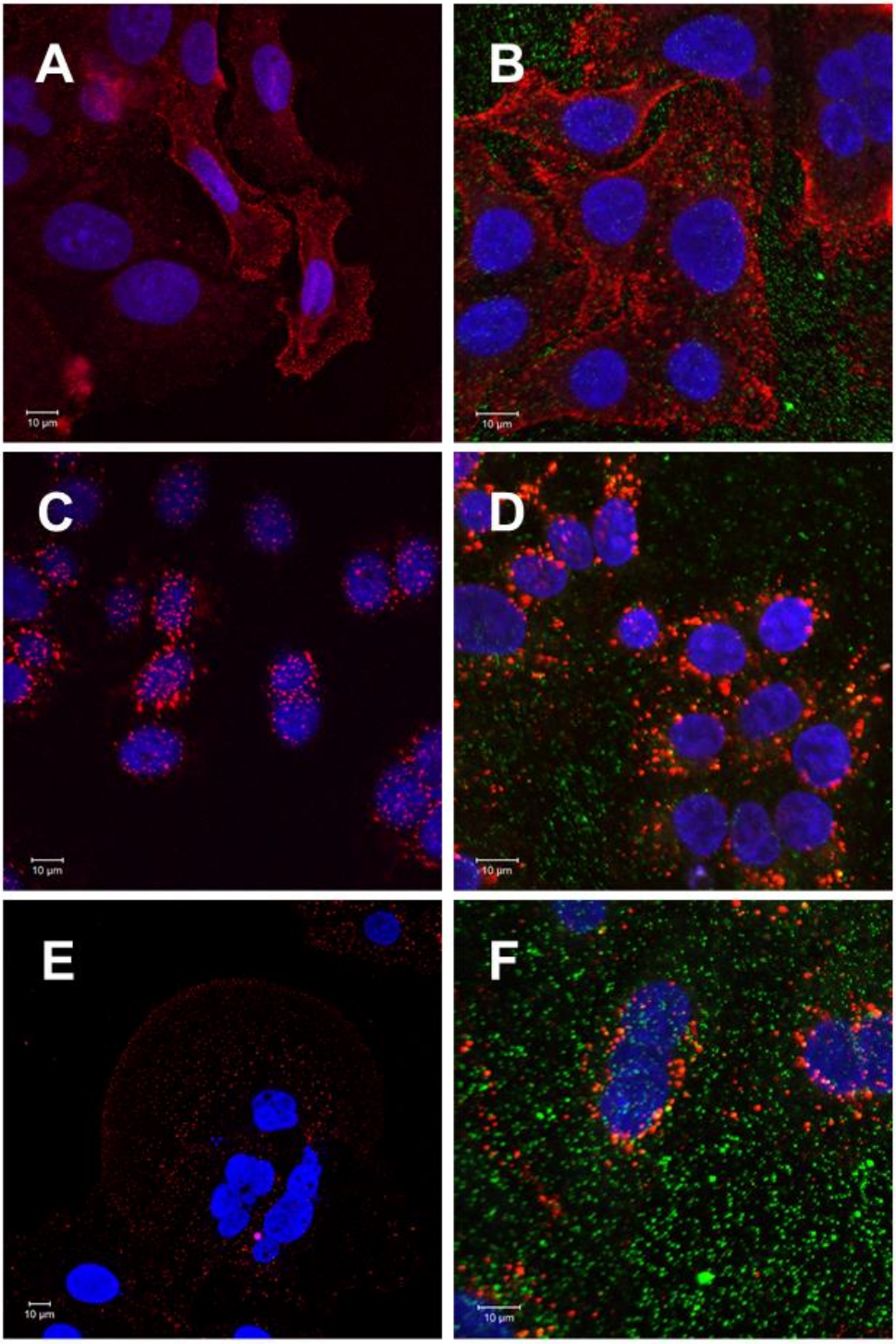

Figure 6.7 (A – F) Effect of thioaspirins with PBS on EGF-100 ng/ml internalization and EGF co-localization with EEA1.

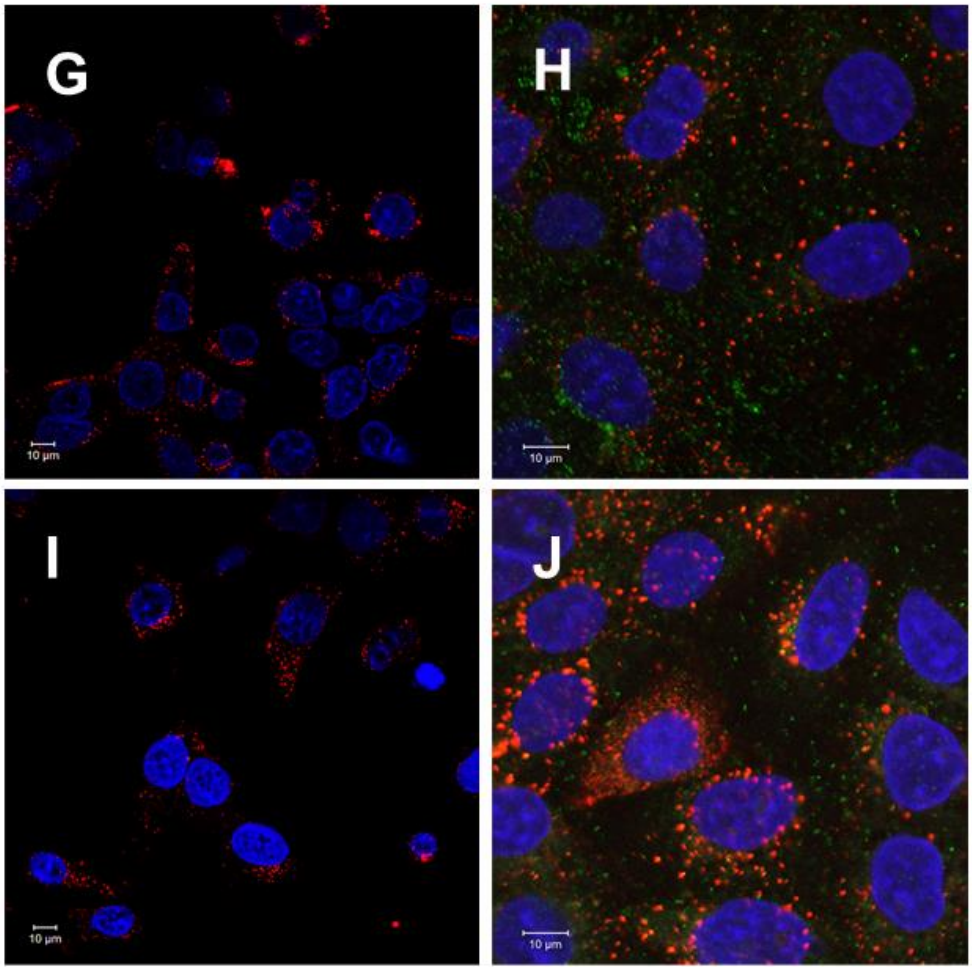

Figure 6.7 Effect of thioaspirins with PBS on EGF-100 ng/ml internalization and EGF co-localization with EEA1.
Confocal images of SW480 CRC cells treated with or without compounds, negative control [EGF receptor unstimulated] (A), negative control with EEA1 (B), positive control [EGF receptor stimulated] (C), positive control with EEA1 (D), PN590 [ortho-thioaspirin] (E), PN590 showing EEA1 (F), PN591 [meta-thioaspirin] (G), PN591 showing EEA1 (H), PN592 [para-thioaspirin] (I), PN592 showing EEA1 (J). Cells were treated with 0.5 mM aspirin analogue (pH adjusted with PBS) for 30 min. The EGF used is complexed to Alexa Fluor® 555 (100 ng/ml) for 1 h on ice after which it was 'chased' at 37°C for 30 min. The cells were then fixed for 5 min. For EEA1 co-localization, the slides were then treated with EEA1 primary antibody and a corresponding secondary antibody. Images were acquired at 405 nm-DAPI (blue) for nucleus, 561 nm-Alexa Fluor (red) for EGF and 488 nm-FITC for EEA1 (green). Representative images are shown taken at 40X oil/1.30 oil immersion objective *(n=3)*. Scale bar represents 10 µm.

PN590 clearly perturbs EGF internalization with the formation of small rounded vesicle-like structures (Figure 6.7E) and in comparison to the positive and negative controls; this compound causes slight co-localization between EGF and EEA1.

Disruption of EGF internalization was not as significant when the cells were treated with PN591 (Figure 6.7G) and PN592 (Figure 6.7E). Co-localization of EGF and EEA1 was also not observed in cells treated with PN591 (Figure 6.7H) and PN592 (Figure 6.7J). This indicated that the thioaspirins also perturbed the EGF signalling pathway by inhibiting or delaying the internalization of the stimulated receptor.

The cells were then treated with the diaspirins, namely, PN517, PN508 and PN524.

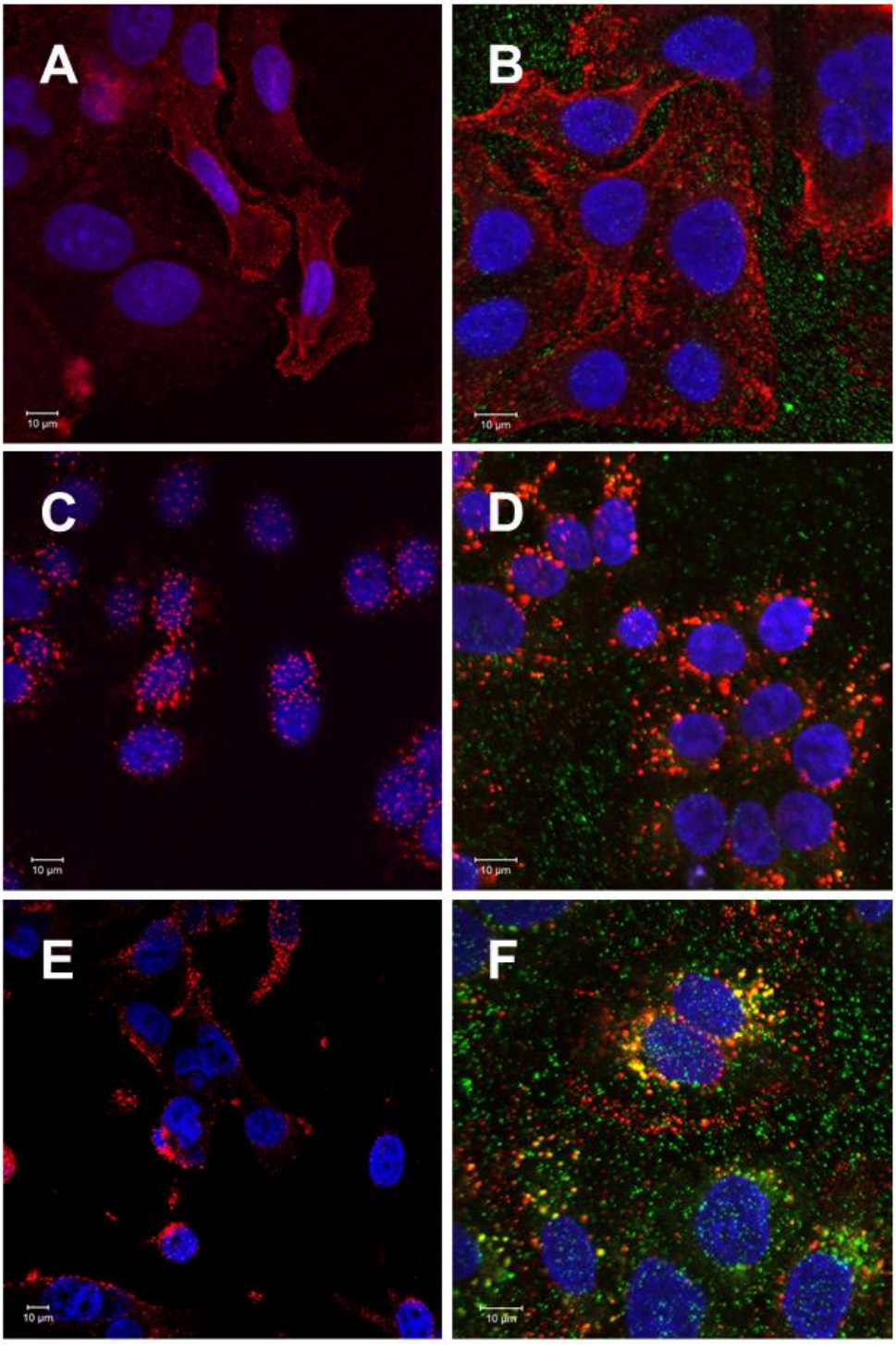

Figure 6.8 (A – F) Effect of diaspirins with PBS on EGF-100 ng/ml internalization and EGF co-localization with EEA1.

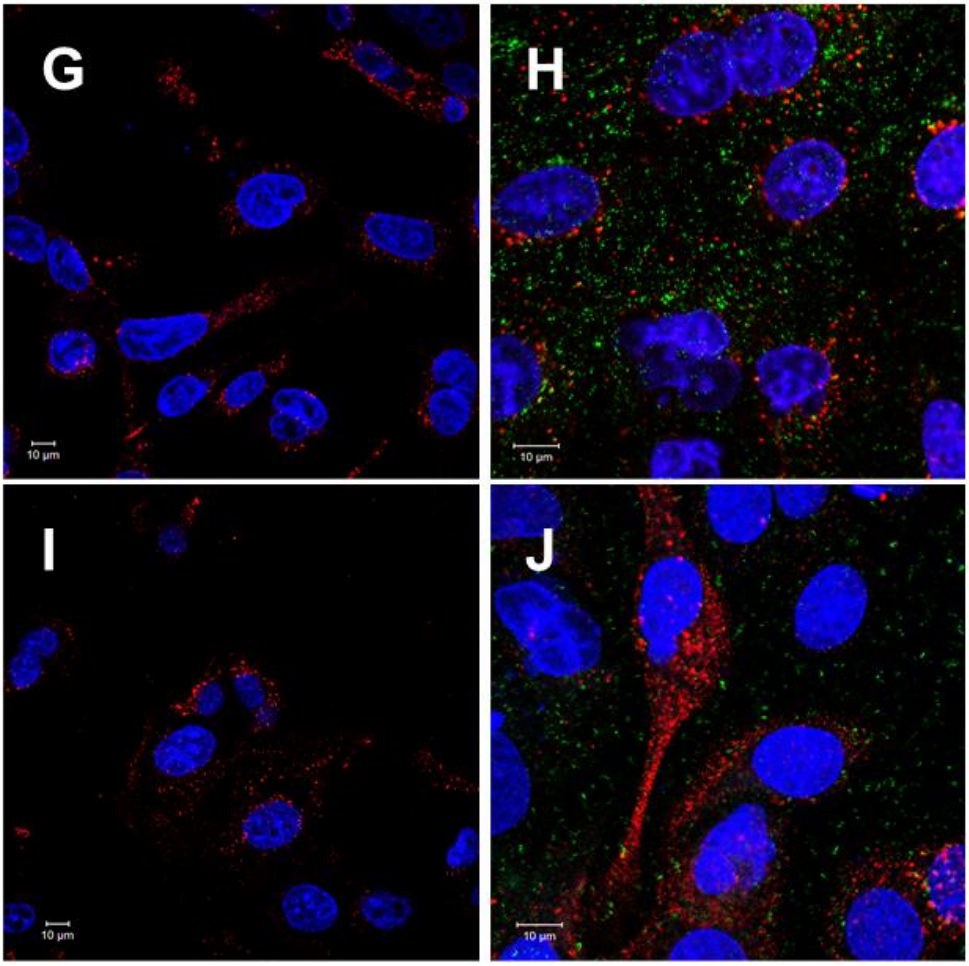

Figure 6.8 Effect of diaspirins with PBS on EGF-100 ng/ml internalization and EGF co-localization with EEA1.

Confocal images of SW480 CRC cells treated with or without compounds, negative control [EGF receptor unstimulated] (A), negative control with EEA1 (B), positive control [EGF receptor stimulated] (C), positive control with EEA1 (D), PN517 [fumaryldiaspirin] (E), PN517 showing EEA1 (F), PN508 [diaspirin] (G), PN508 showing EEA1 (H), PN524 [m-bromobenzoylsalicylate] (I), PN524 showing EEA1 (J). Cells were treated with 0.5mM aspirin analogue (pH adjusted with PBS) for 30 min. The EGF used is complexed to Alexa Fluor® 555 (100 ng/ml) for 1 h on ice after which it was 'chased' at 37°C for 30 min. The cells were then fixed for 5 min. For EEA1 co-localization, the slides were then treated with EEA1 primary antibody and a corresponding secondary antibody. Images were acquired at 405 nm-DAPI (blue) for nucleus, 561 nm-Alexa Fluor (red) for EGF and 488 nm-FITC for EEA1 (green). Representative images are shown taken at 40X oil/1.30 oil immersion objective *(n=3)*. Scale bar represents 10 µm.

PN517 clearly perturbed EGF internalization along with the formation of small round vesicle-like structures (Figure 6.8E). EGF and EEA1 highly co-localized when the SW480 CRC cells were treated with PN517 (Figure 6.8F). The yellow colouring is clearly seen due to the overlapping of red for EGF and green for EEA1. Cells treated with PN508 also showed EGF internalization being perturbed (Figure 6.8G). However, EGF co-localization with EEA1 was ever so slight (Figure 6.8H). PN524 perturbed EGF internalization as well with the formation of small rounded vesicle-like structures (Figure 6.8I) but did not cause any co-localization between EGF and EEA1 (Figure 6.8J).

Overall, all the aspirin analogues pH adjusted with PBS perturbed EGF internalization with PN517 and PN590 causing significant co-localization between EGF and EEA1. These results raised a few questions. Why did PN517 and PN590 cause co-localization of EGF and EEA1? Could these aspirin analogues be forcing the EGF back into the appropriate signalling pathway? In other words, is it a pharmacological effect?

Could this just be a pH effect? This question was raised because aspirins are known to be acidic in nature. Even though the pH had been adjusted with PBS, it was decided to use another buffer just to make sure that the effect was not due to pH. This is important because an appropriate pH of between 6 and 8 is required for tissue culture preparations (Good *et al.*, 1966) and it has been asserted that ligand binding can be affected by low pH due to the EGF dissociating itself from the receptor (Roepstorff *et al.*, 2009).

Good *et al*. (1966) described *N*-2-hydroxyethylpiperazine-*N*'-2-ethanesulfonic acid (HEPES) as an effective buffering agent for biological research. Thus,

HEPES was also used as a buffering agent and the above experiments repeated accordingly to confirm if the effects seen are consistent.

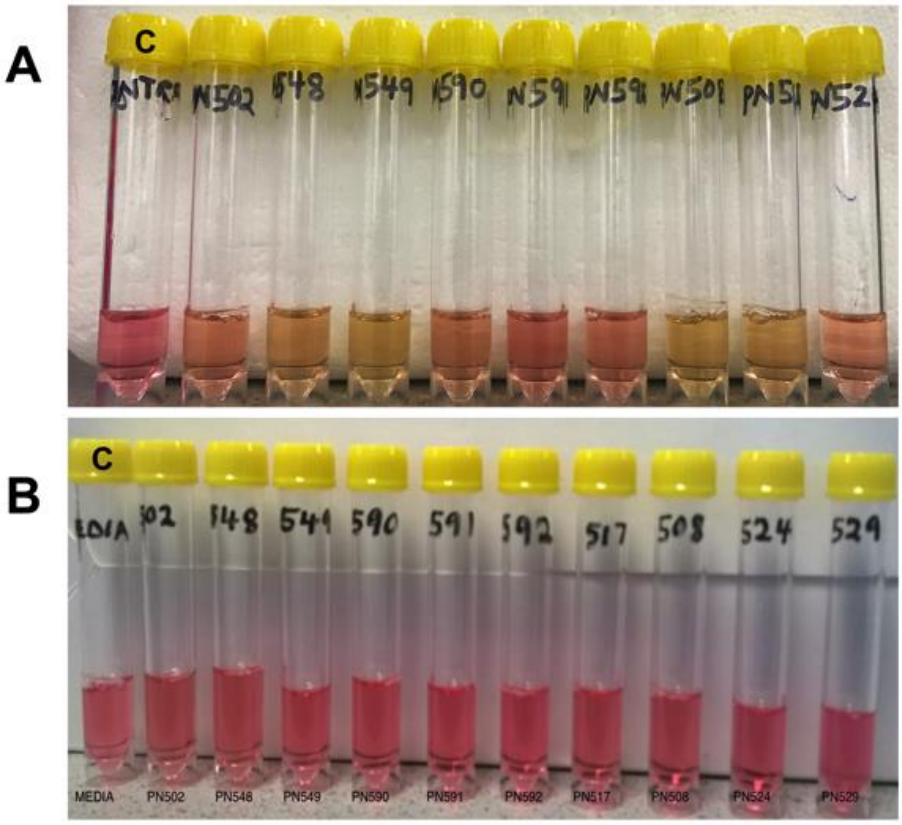

Figure 6.9 Aspirin analogues dissolved in acetone to 50 mM and further diluted with buffer to adjust pH.
C represents L-15 media without any aspirin analogue. Compounds dissolved in acetone to 50 mM concentration and further diluted to 0.5 mM with media (A) Compounds dissolved in acetone to an initial 50 mM concentration, diluted to adjust pH to 25 mM with HEPES (pH8) and further diluted to a concentration of 0.5 mM with media (B).

Compounds dissolved in acetone without a buffering agent clearly changed the colour of the media indicating a change in pH (Figure 6.9A). The pH of these compounds were therefore adjusted, only this time with HEPES (pH8) (Figure 6.9B) instead of PBS to see if the same effects on EGF internalization and EEA1 co-localization will be seen. All the compounds of interest were studied

for effect on EGF internalization; however, only the compounds that had some effect on EGF co-localization with EEA1 in previous experiments were included for this experimental condition to confirm the effects seen. Thus, PN524, PN517, PN508, PN590 and PN502 for comparison were included for the EGF-EEA1 co-localization experiments with pH being adjusted with HEPES.

To find out if the effects these aspirin analogues have on the EGF are due to its metabolite, salicylate, salicylic acid and diflunisal were also included in the experiments. Diflunisal, having salicylate as part of its chemical structure works similarly to salicylic acid as an anti-inflammatory and has been found to have anticancer properties (Shirakawa *et al.*, 2016)

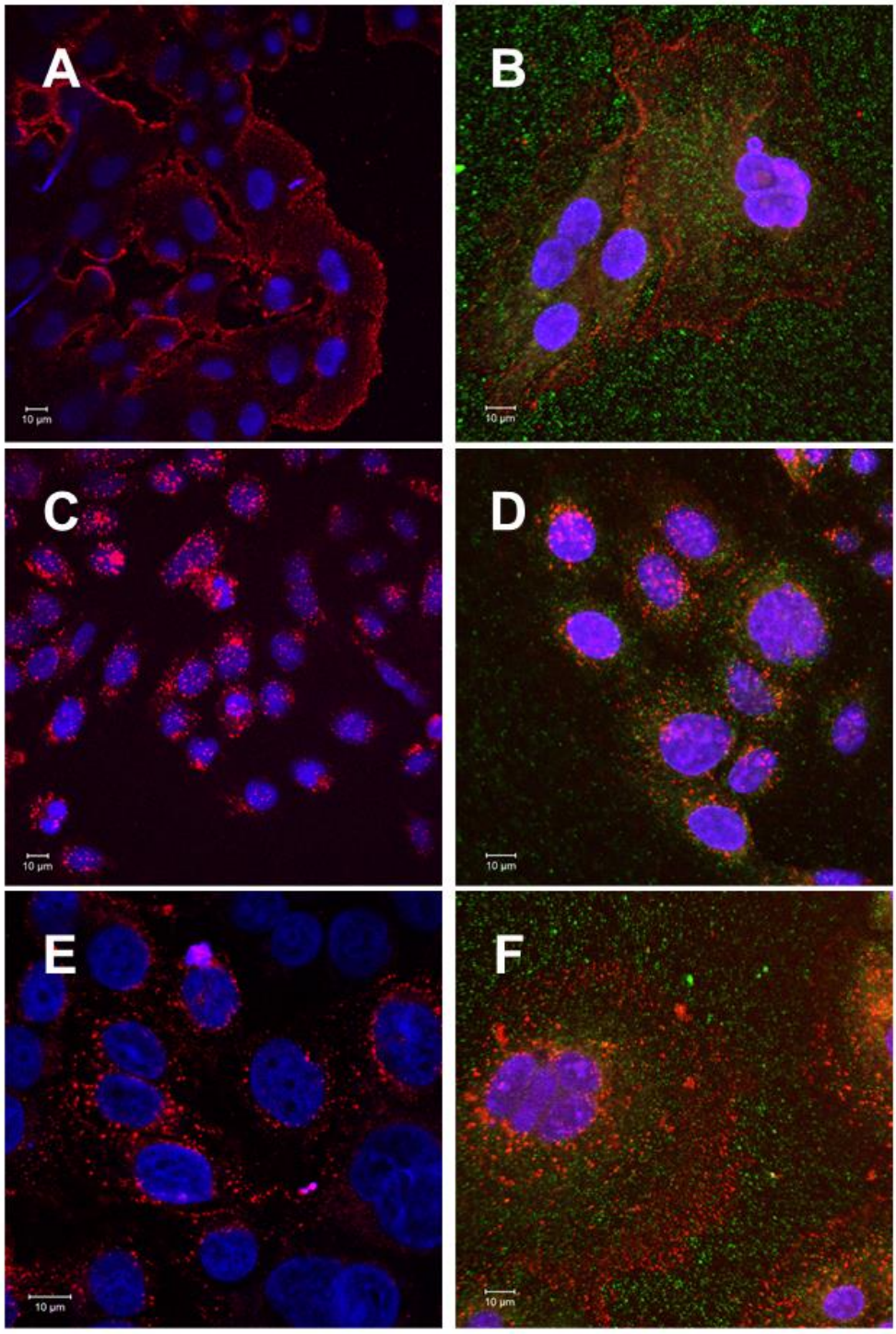

Figure 6.10 (A – F) Effect of aspirins and thioaspirins with HEPES on EGF-100 ng/ml internalization and EGF co-localization with EEA1.

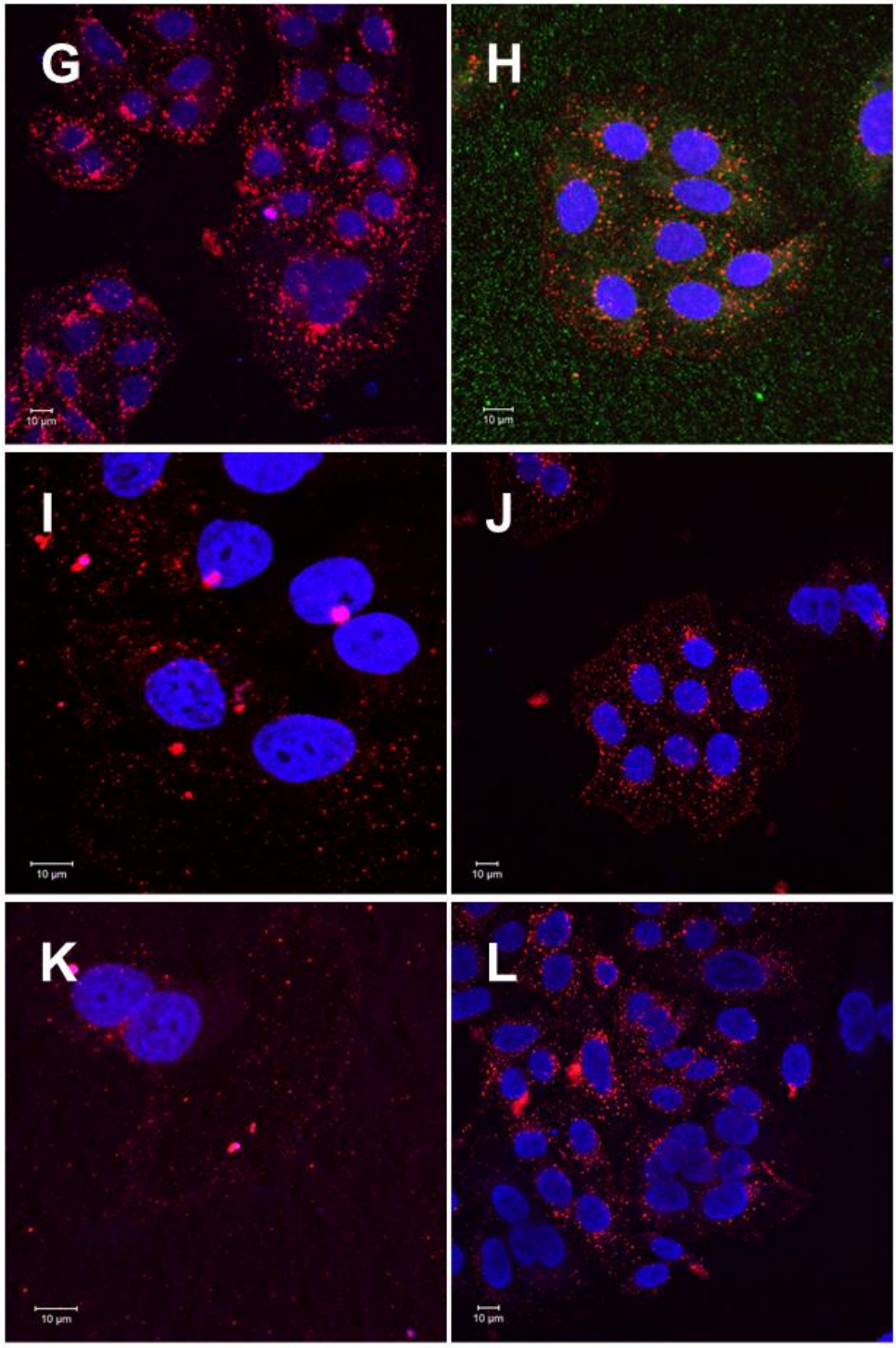

Figure 6.10 (G – L) Effect of aspirins and thioaspirins with HEPES on EGF-100 ng/ml internalization and EGF co-localization with EEA1.

Figure 6.10 Effect of aspirins and thioaspirins with HEPES on EGF-100 ng/ml internalization and EGF co-localization with EEA1.
Confocal images of SW480 CRC cells treated with or without compounds, negative control [EGF receptor unstimulated] (A), negative control with EEA1 (B), positive control [EGF receptor stimulated] (C), positive control with EEA1 (D), PN502 [ortho-aspirin] (E), PN502 showing EEA1 (F), PN590 [ortho-thioaspirin] (G), PN590 showing EEA1 (H), PN548 [meta-aspirin] (I), PN549 [para-aspirin] (J), PN591 [meta-thioaspirin] (K), PN592 [para-thioaspirin] (L). Cells were treated with 0.5 mM aspirin analogue (pH adjusted with HEPES, pH8) for 30 min. The EGF used is complexed to Alexa Fluor® 555 (100 ng/ml) for 1 h on ice after which it was 'chased' at 37°C for 30 min. The cells were then fixed for 5 min. For EEA1 co-localization, the slides were then treated with EEA1 primary antibody and a corresponding secondary antibody. Images were acquired at 405 nm-DAPI (blue) for nucleus, 561 nm-Alexa Fluor (red) for EGF and 488 nm-FITC (green) for EEA1. Representative images are shown taken at 40X oil/1.30 oil immersion objective *(n=3)*. Scale bar represents 10 µm.

Cells labelled as negative control were not subjected to incubation at 37°C following EGF binding so as not to stimulate the receptor into internalization. Images representing this had the EGF (red dye) seen along the surface of the cell membrane (Figure 6.10A). Likewise, negative control that included EEA1 antibody (green dye) was also subjected to the same condition and had the EGF along the cell membrane that did not co-localise with EEA1 (Figure 6.10B). The cells that had their slides subjected to incubation at 37°C (EGF 'chased') for 30 min after EGF binding were observed as having the EGF as large rough-edged cluster of vesicle-like structures at close proximity to the nucleus (Figure 6.10C). These images are a representation of the positive control where internalization has taken place after ligand stimulation. Figure 6.10D also represents the positive control with EEA1 antibody included. Co-localization between EGF and EEA1 was not observed even after ligand stimulation.

PN502 perturbed EGF internalization (Figure 6.10E) but did not cause EGF and EEA1 co-localization (Figure 6.10F). Likewise, PN590 also perturbed EGF internalization with EGF forming tiny rounded vesicle-like structures that spread far away from the nucleus (Figure 6.10G). PN590 did lead to EGF and EEA1

co-localizing (Figure 6.10H). PN548 had an effect on the internalization of EGF but in this case the vesicle-like structures were not very visible (Figure 6.10I). With PN549, the EGF was clearly spread across the cytoplasm as tiny vesicles (Figure 6.10J). PN591 and PN592 also had the EGF spread across the cytoplasm as tiny vesicle-like structures that were not clustered in close proximity to the nucleus (Figures 6.10K and 6.10L respectively).

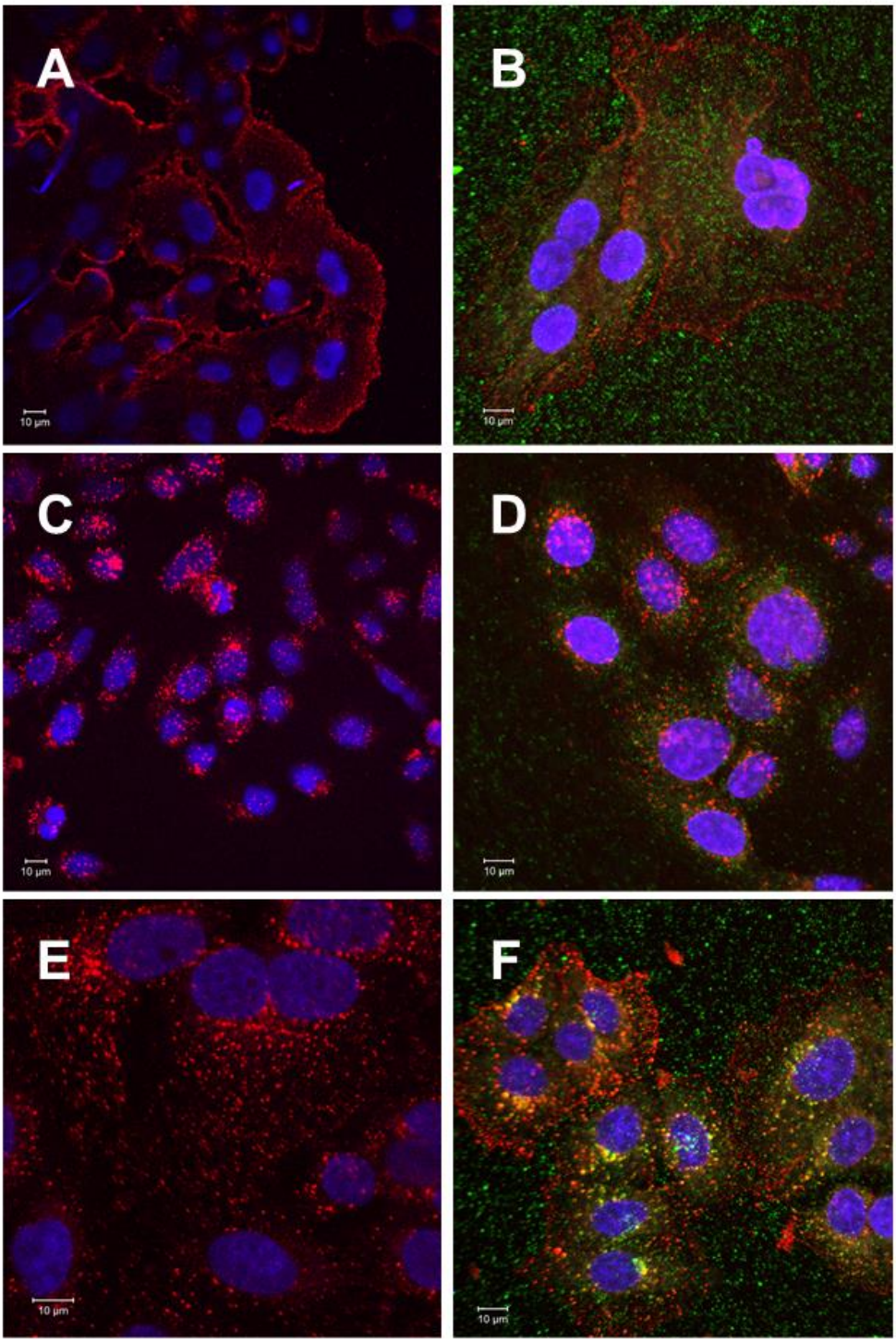

Figure 6.11 (A – F) Effect of diaspirins with HEPES on EGF-100 ng/ml internalization and EGF co-localization with EEA1.

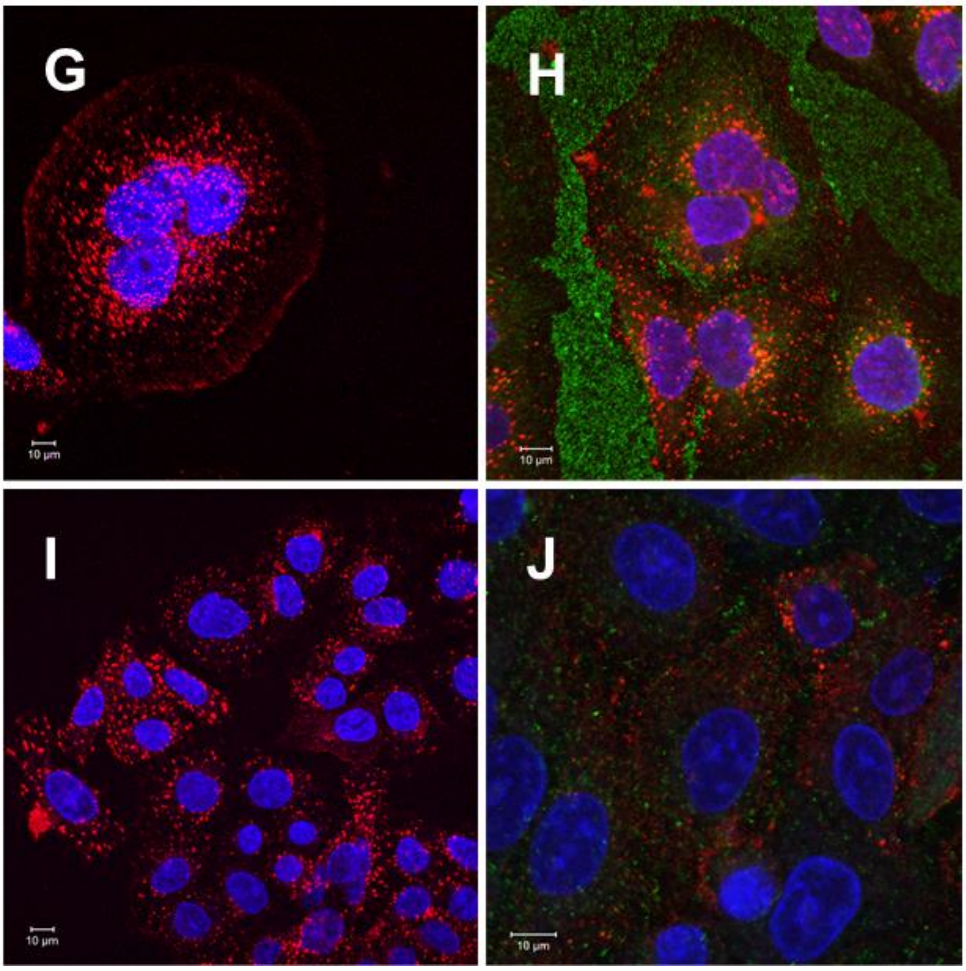

Figure 6.11 Effect of diaspirins with HEPES on EGF-100 ng/ml internalization and EGF co-localization with EEA1.
Confocal images of SW480 CRC cells treated with or without compounds, negative control [EGF receptor unstimulated] (A), negative control with EEA1 (B), positive control [EGF receptor stimulated] (C), positive control with EEA1 (D), PN517 [fumaryldiaspirin] (E), PN517 showing EEA1 (F), PN508 [diaspirin] (G), PN508 showing EEA1 (H), PN524 [m-bromobenzoylsalicylate] (I), PN524 showing EEA1 (J). Cells were treated with 0.5 mM aspirin analogue (pH adjusted with HEPES, pH8) for 30 min. The EGF used is complexed to Alexa Fluor® 555 (100 ng/ml) for 1 h on ice after which it was 'chased' at 37°C for 30 min. The cells were then fixed for 5 min. For EEA1 co-localization, the slides were then treated with EEA1 primary antibody and a corresponding secondary antibody. Images were acquired at 405 nm-DAPI (blue) for nucleus, 561 nm-Alexa Fluor (red) for EGF and 488 nm-FITC (green) for EEA1. Representative images are shown taken at 40X oil/1.30 oil immersion objective *(n=3)*. Scale bar represents 10 µm.

The negative and positive controls in Figure 6.11 are the same as in Figure 6.10 because they all belong to the same experimental conditions but separated into different figures for easy visualisation and comparison. PN517 is seen to disturb the internalization of EGF by causing it to spread across the cytoplasm as small rounded vesicle-like structures (Figure 6.11E) instead of clustering close to the cytoplasm as in the positive control (Figure 6.11C). Many EGF foci co-localized with EEA1 when the cells were treated with PN517. This can be observed qualitatively due to the yellow fluorescence seen in close proximity to almost all the nuclei (Figure 6.11F). PN508 and PN524 also caused the EGF to appear as tiny vesicles spread across the cytoplasm of each cell (Figure 6.11G and 6.11I respectively) but with only PN508 causing slight co-localization between EGF and EEA1 seen as yellow fluorescence in about 10% of the sample area (Figure 6.11H).

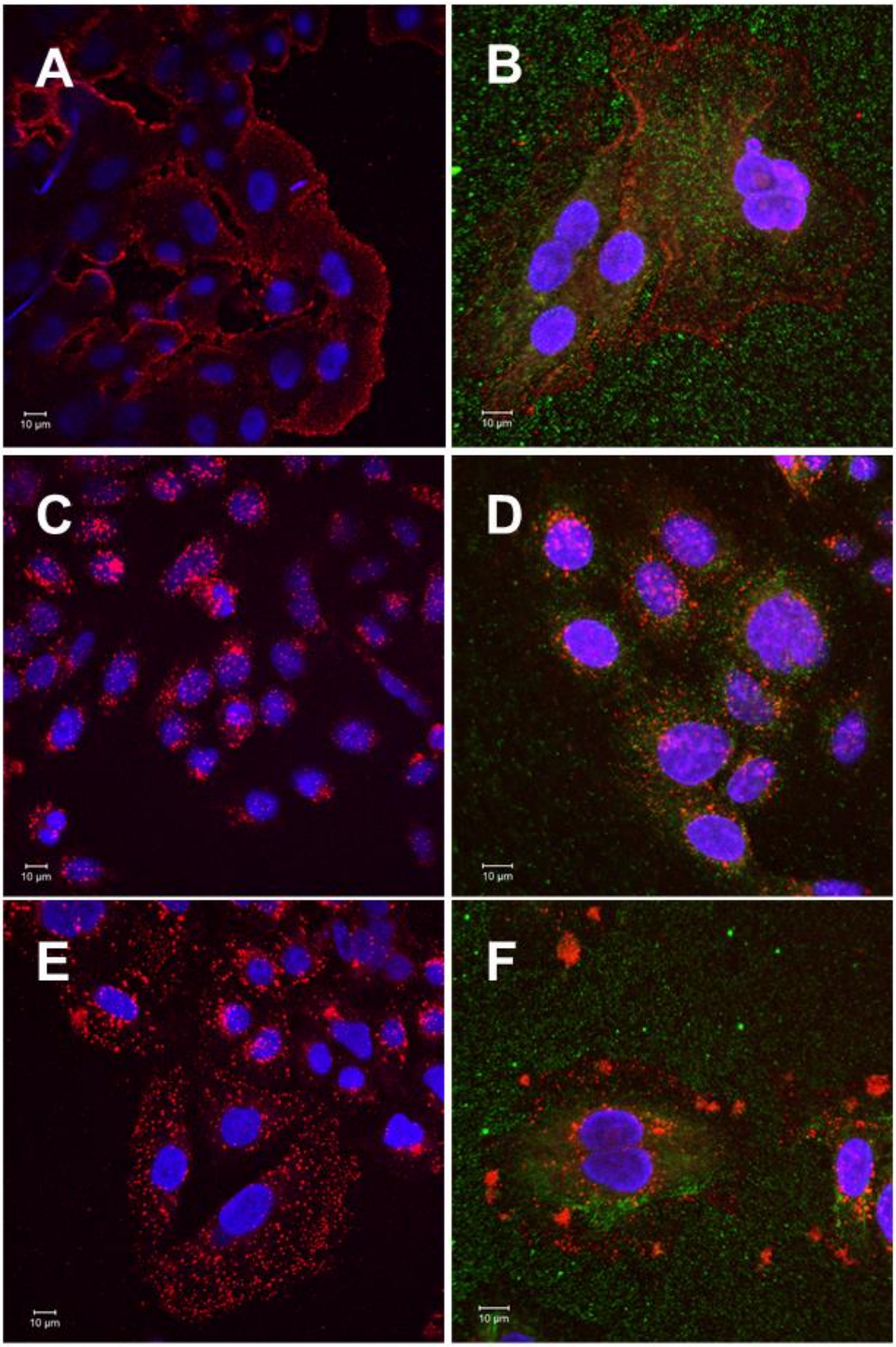

Figure 6.12 (A – F) Effect of salicylates with HEPES on EGF-100 ng/ml internalization and EGF co-localization with EEA1.

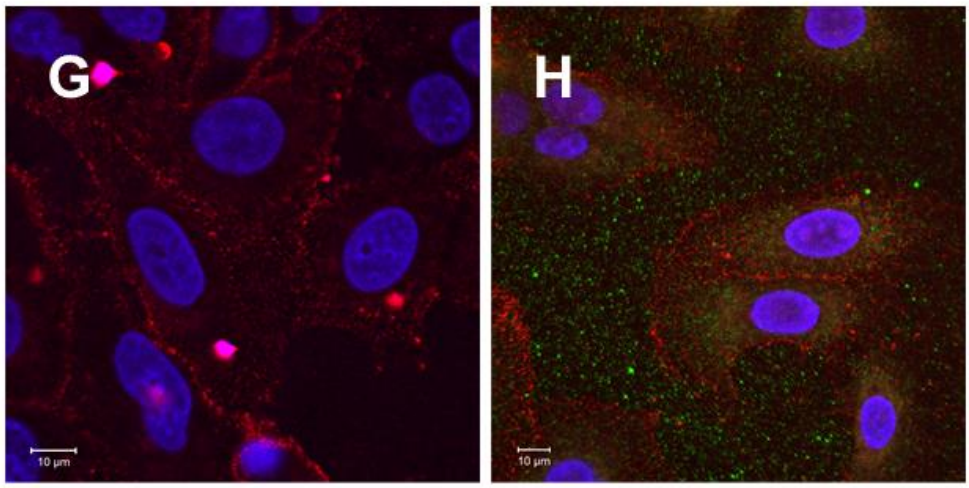

Figure 6.12 Effect of salicylates with HEPES on EGF-100 ng/ml internalization and EGF co-localization with EEA1.
Confocal images of SW480 CRC cells treated with or without compounds, negative control [EGF receptor unstimulated] (A), negative control with EEA1 (B), positive control [EGF receptor stimulated] (C), positive control with EEA1 (D) Salicylic acid (E), Salicylic acid showing EEA1 (F), Diflunisal (G), Diflunisal showing EEA1 (H). Cells were treated with 0.5 mM aspirin analogue (pH adjusted with HEPES, pH8) for 30 min. The EGF used is complexed to Alexa Fluor® 555 (100 ng/ml) for 1 h on ice after which it was 'chased' at 37°C for 30 min. The cells were then fixed for 5 min. For EEA1 co-localization, the slides were then treated with EEA1 primary antibody and a corresponding secondary antibody. Images were acquired at 405 nm-DAPI (blue) for nucleus, 561 nm-Alexa Fluor (red) for EGF and 488 nm-FITC (green) for EEA1. Representative images are shown taken at 40X oil/1.30 oil immersion objective *(n=3)*. Scale bar represents 10 µm.

Negative and positive controls for EGF internalization and EGF co-localization with EEA1 in Figure 6.12 is the same as in Figures 6.10 and 6.11 because all experiments were carried out at the same time and under the same conditions. Salicylic acid, a precursor and metabolite of these aspirin analogues also disrupted EGF internalization (Figure 6.12E) with EGF as rounded structures spread across the cytoplasm. These tiny structures were accompanied by larger clusters of EGF, which are also seen in Figure 6.12 F. However, it did not cause EGF co-localization with EEA1. Interestingly, diflunisal did not only perturb but inhibited EGF internalization altogether (Figure 6.12D) as the EGF

can still be seen along the cell membrane similar to the negative control, thus, appearing to be unstimulated. Same as the negative control, there was no co-localization between EGF and EEA1 when cells were treated with diflunisal (Figure 6.12H).

Henriksen et al. (2013) had previously suggested that EGF used in a concentration greater than 20 ng/ml as a stimulant could lead to the receptor following different pathways. This apparently means that low doses of EGF as stimulant lead to the internalization of the receptor through the clathrin pathway, which ultimately results in the receptor being recycled back to the cell surface (Sigismund *et al.*, 2008) but stimulating with high doses of EGF will lead to internalization through clathrin-independent pathways (Sigismund *et al.*, 2005). Little is known of the clathrin-independent pathway and it could be made up of a single or multiple pathways all with similar features (Mayor and Pagano, 2007). To address these points it was decided to carry the same experiment only this time using a concentration of 20 ng/ml EGF instead of 100 ng/ml as used previously.

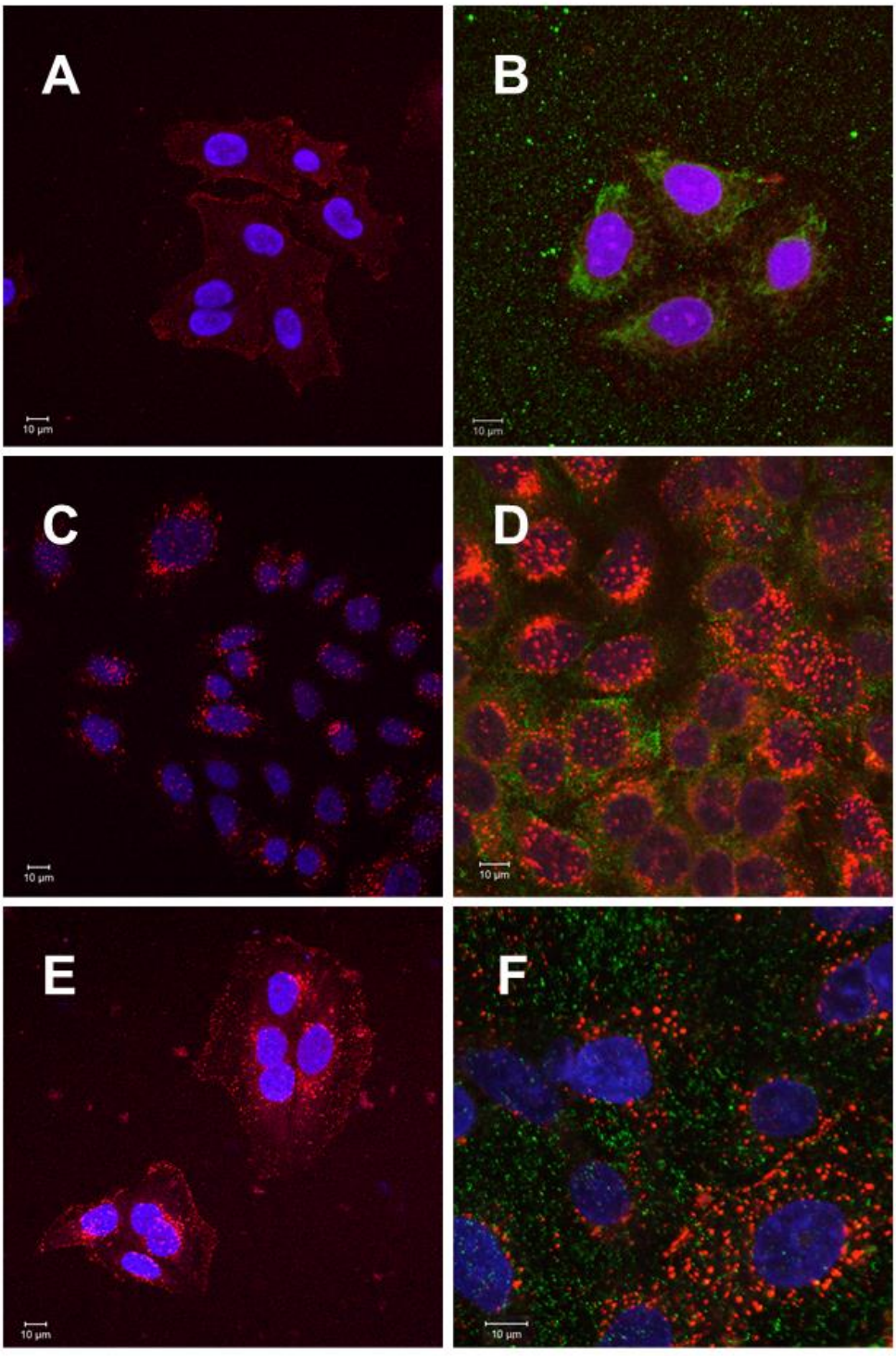

Figure 6.13 (A – F) Effect of aspirin analogues with HEPES on EGF-20 ng/ml internalization and EGF co-localization with EEA1.

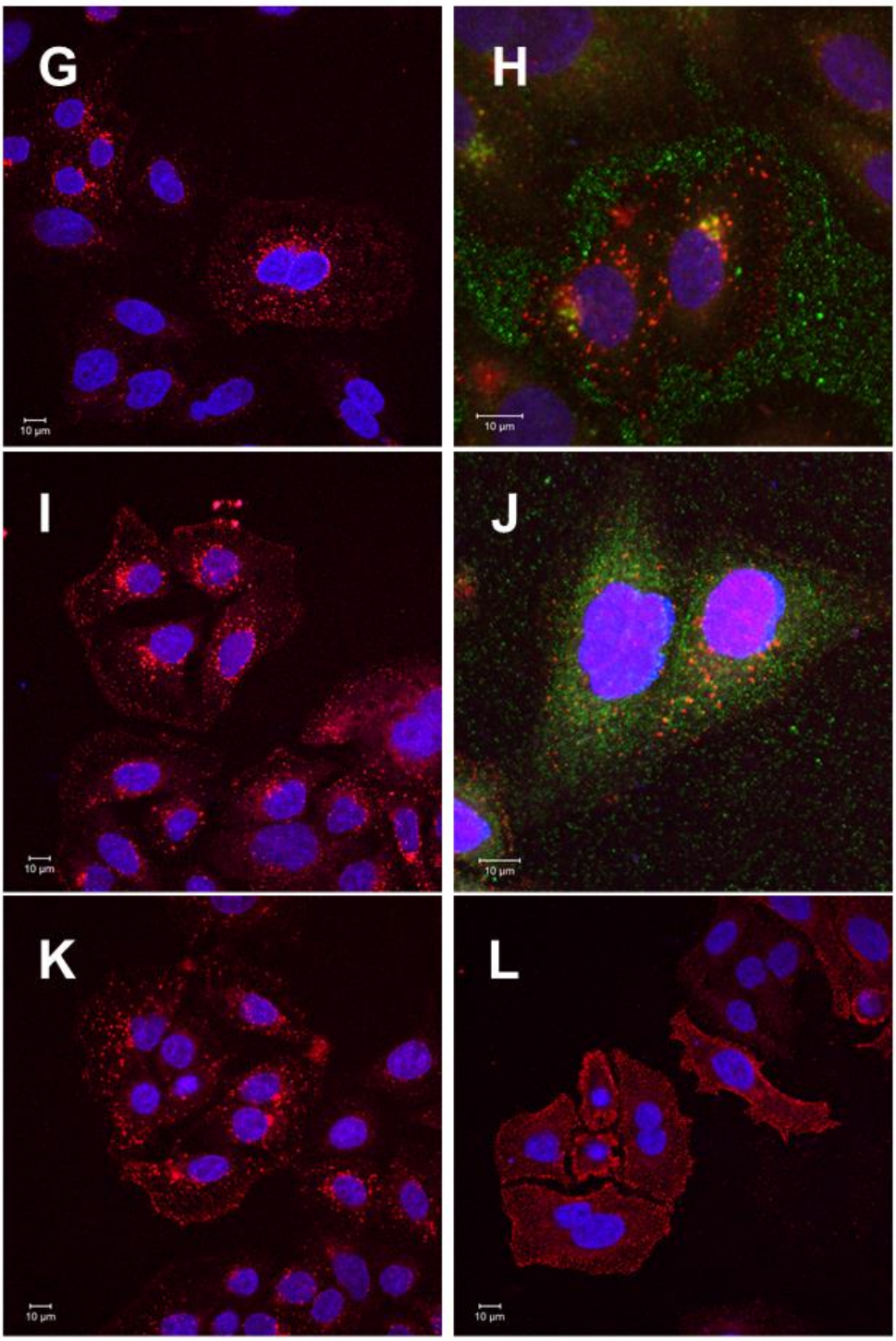

Figure 6.13 (G – L) Effect of aspirin analogues with HEPES on EGF-20 ng/ml internalization and EGF co-localization with EEA1.

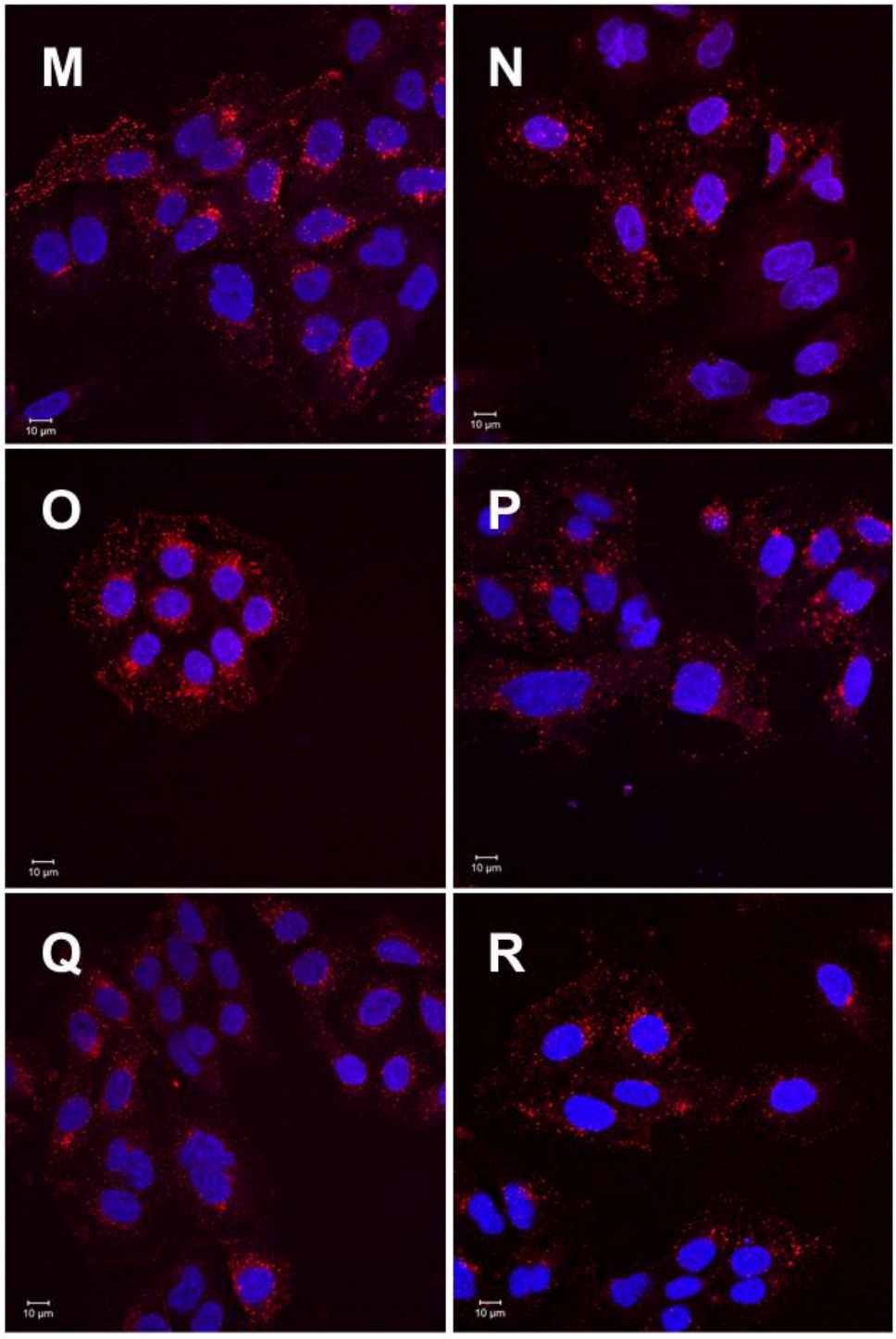

Figure 6.13 (M – R) Effect of aspirin analogues with HEPES on EGF-20 ng/ml internalization and EGF co-localization with EEA1.

Figure 6.13 Effect of aspirin analogues with HEPES on EGF-20 ng/ml internalization and EGF co-localization with EEA1.
Confocal images of SW480 CRC cells treated with or without compounds, negative control [EGF receptor unstimulated] (A), negative control with EEA1 (B), positive control [EGF receptor stimulated] (C), positive control with EEA1 (D) PN502 [ortho-aspirin] (E), PN502 showing EEA1 (F), PN517 [fumaryldiaspirin] (G), PN517 showing EEA1 (H), Salicylic acid (I), Salicylic acid showing EEA1 (J), PN590 [ortho-thioaspirin] (K), Diflunisal (L), PN548 [meta-aspirin] (M), PN549 [para-aspirin] (N), PN591 [meta-thioaspirin] (O), PN592 [para-thioaspirin] (P), PN508 [diaspirin] (Q), PN524 [m-bromobenzoylsalicylate] (R). Cells were treated with 0.5 mM aspirin analogue (pH adjusted with HEPES, pH8) for 30 min. The EGF used is complexed to Alexa Fluor® 555 (20 ng/ml) for 1 h on ice after which it was 'chased' at 37°C for 30 min. The cells were then fixed for 5 min. For EEA1 co-localization, the slides were then treated with EEA1 primary antibody and a corresponding secondary antibody. Images were acquired at 405 nm-DAPI (blue) for nucleus, 561 nm-Alexa Fluor (red) for EGF and 488 nm-FITC (green) for EEA1. Representative images are shown taken at 40X oil/1.30 oil immersion objective *(n=3)*. Scale bar represents 10 µm.

Ligand stimulation with 20 ng/ml EGF at 37°C showed the EGF endocysed as large round vesicles at close proximity to the nuclei (Figure 6.13C) that did not show co-localization with EEA1 (Figure 6.13D). With the negative controls however, the EGF can be seen along the surface of the cell membrane (Figure 6.13A) that also showed no co-localization with EEA1 (Figure 6.13B). Even at 20ng/ml, the internalized EGF presented as tiny vesicles spread along the cytoplasm (Figure 6.13E) consistent with the results observed when the cells were stimulated with 100ng/ml EGF. The EGF however, did not co-localize with EEA1 (Figure 6.13F). PN517 also caused the EGF to appear as small vesicles spread across the cytoplasm (Figure 6.13G). EGF and EEA1 co-localization was also seen, which has been consistent across all the different experimental conditions (Figure 6.13H). Salicylic acid also resulted in the EGF to co-localize with EEA1 (Figure 6.13J) that was accompanied with disruption of the internalization of the EGF (Figure 6.13I). As with the previous experimental conditions all the other analogues disturbed the normal appearance of

internalized EGF with diflunisal showing the most prominent effect, as the EGF still appeared to be along the surface of the cell membrane (Figure 6.13L).

EGFR internalization pathways could differ between cell lines due to the expression of proteins involved in the mechanisms (Henriksen *et al.*, 2013). This led to the application of the same experimental conditions on different cell lines that also have high EGFR expression. Cell lines found to exhibit this characteristic include OE33 and FLO1 oesophageal cancer cell lines (Song *et al.*, 2015), which were chosen.

The EGFR has been found to be overexpressed and responsible for the growth progression in a number of cancers including brain tumours, particularly in primary glioblastomas (Mendelsohn and Baselga, 2000) and a number of earlier studies have shown the EGFR to be an effective target for anti cancer therapy in gliomas found in humans (Kang *et al.*, 2006). For this reason it was decided to include U251 MG cell line as a candidate for this assay.

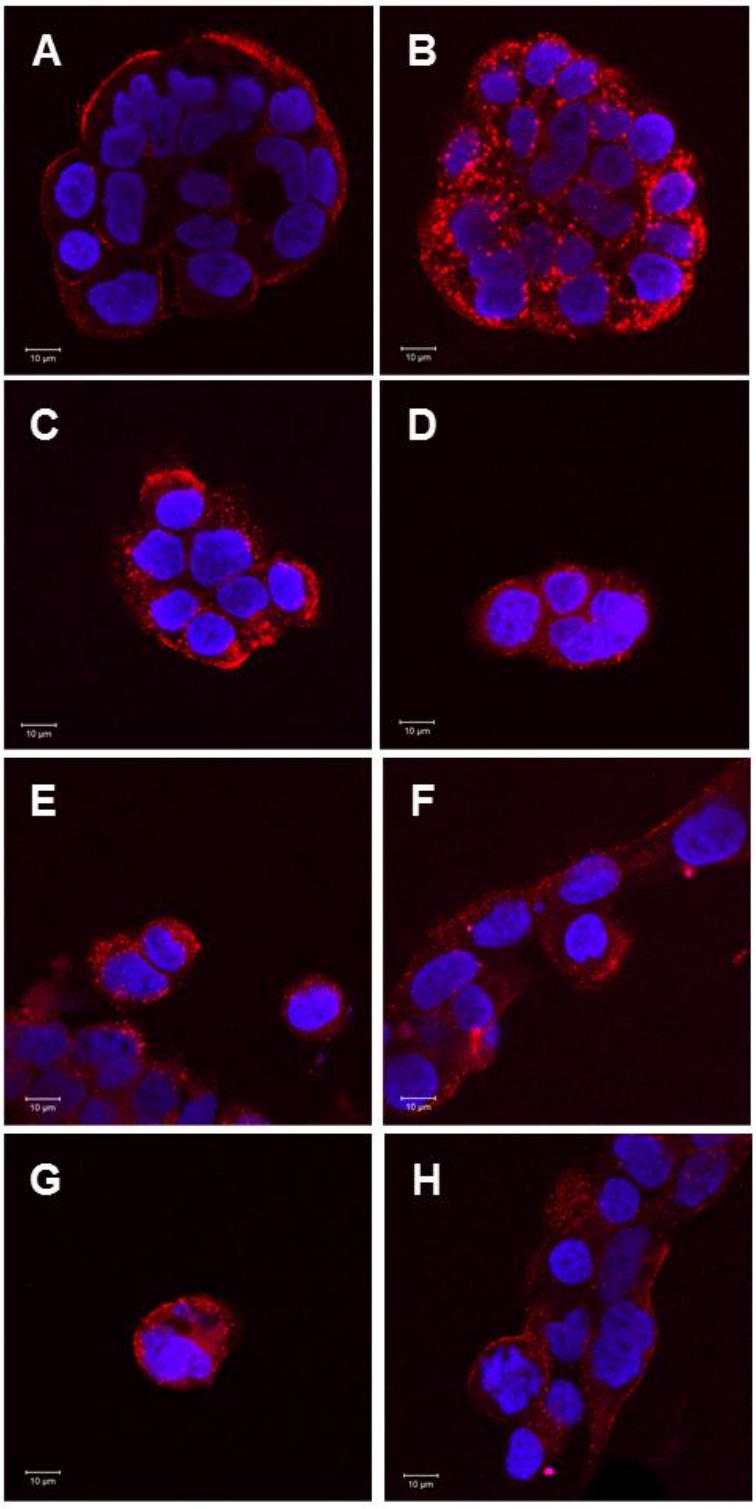

Figure 6.14 (A – H) Effect of aspirin analogues with HEPES on EGF-20 ng/ml internalization in oesophageal cells.

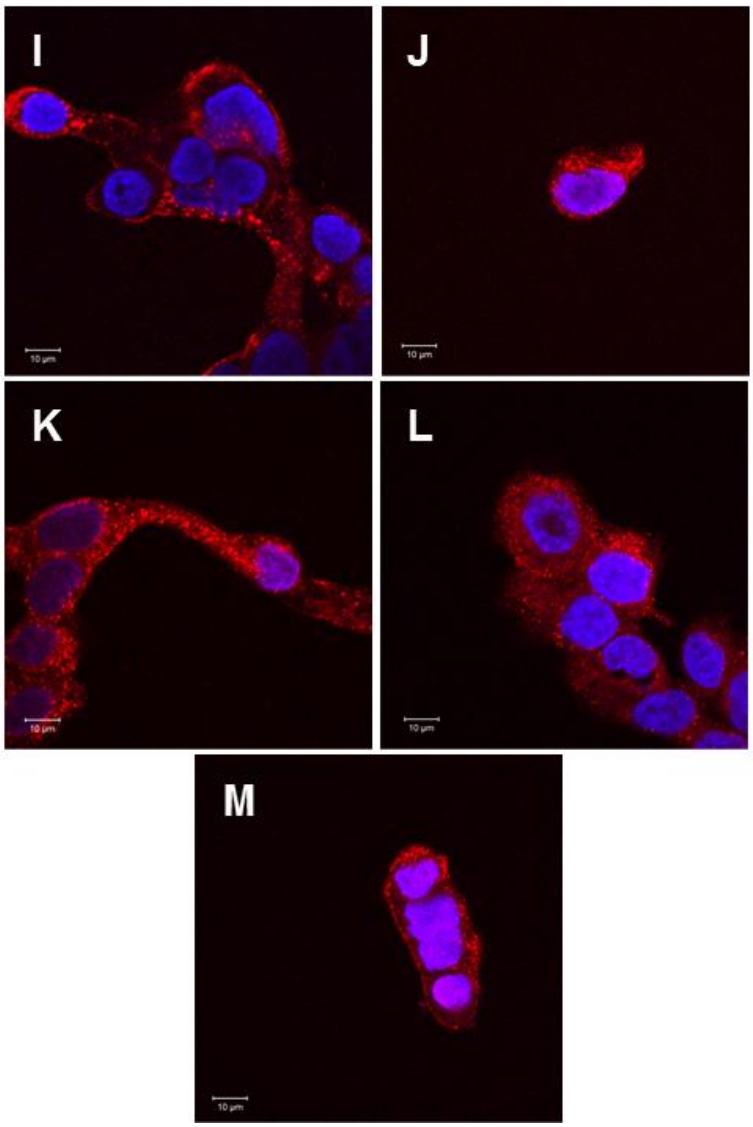

Figure 6.14 Effect of aspirin analogues with HEPES on EGF-20 ng/ml internalization in oesophageal cells.
Confocal images of OE33 oesophageal cancer cells treated with or without compounds, negative control [EGF receptor unstimulated] (A), positive control [EGF receptor stimulated] (B), PN502 [ortho-aspirin] (C), PN548 [meta-aspirin] (D), PN549 [para-aspirin] (E), PN590 [ortho-thioaspirin] (F), PN591 [meta-thioaspirin] (G), PN592 [para-thioaspirin] (H), PN517 [fumaryldiaspirin] (I), PN508 [diaspirin] (J), PN524 [m-bromobenzoylsalicylate] (K), Salicylic acid (L), Diflunisal (M). Cells were treated with 0.5 mM aspirin analogue (pH adjusted with HEPES, pH8) for 30 min. The EGF used is complexed to Alexa Fluor® 555 (20 ng/ml) for 1 h on ice after which it was 'chased' at 37°C for 30 min. The cells were then fixed for 5 min. Images were acquired at 405 nm-DAPI (blue) for nucleus and 561 nm-Alexa Fluor (red) for EGF. Representative images are shown taken at 40X oil/1.30 oil immersion objective *(n=3)*. Scale bar represents 10µm.

The distance between the cell membrane and the nucleus in OE33 oesophageal cancer cells appeared to be much closer than in SW480 CRC cells and so distinguishing between complete internalization and perturbed internalization was more of the position of the EGF rather than the distance away from the nucleus.

The negative control, which has the EGF not stimulated, is seen to have the EGF along the surface of the cell membrane (Figure 6.14A). However, when stimulated by subjecting the cells to 30 min of incubation time at 37°C, the EGF forms large vesicle-like structures that are in much closer proximity to the nucleus (Figure 6.14B). This is labelled as the positive control. After cell treatment with PN502, about 50% of the EGF had been internalized with the other half still along the surface of the cell membrane (Figure 6.14C), thus, internalization disturbed. PN548 treated cells showed the EGF as round vesicle at close proximity to the nuclei (Figure 6.14D). Very little EGF was along the surface of the cytoplasmic membrane after cells were treated with PN549 (Figure 6.14E) with about 70% along the cell membrane in cells treated with PN590 (Figure 6.14F). PN591 and PN508-treated cells presented the EGF away from the cytoplasm and closer to the nucleus as small vesicle-like structures (Figure 6.14G and 6.14J) respectively. About 60% of the EGF remained along the cell membrane in cells treated with PN592 (Figure 6.14H) and a large amount also found along the cell surface in cells treated with PN517 (Figure 6.14I). PN524 disrupted the internalization of some of the EGF (Figure 6.14K) and for the cells treated with salicylic acid, none of the EGF could be seen along the cell membrane (Figure 6.14L) indicating that EGF internalization

was not perturbed. For cells treated with diflunisal, most of the EGF could still be seen along the surface of the cell membrane (Figure 6.14M).

The images show that these aspirin analogues also perturb EGF internalization in OE33 cells, which means this could be applied to oesophageal cancer.

A few of the compounds, namely PN502 and PN517 were chosen to see if they had the same effect in FLO1 oesophageal cancer and U251 malignant glioblastoma (MG) cell lines. These compounds were chosen because PN517 had the most significant effect on the EGF internalization and PN502 was like a standard ‘yard stick’ for comparison.

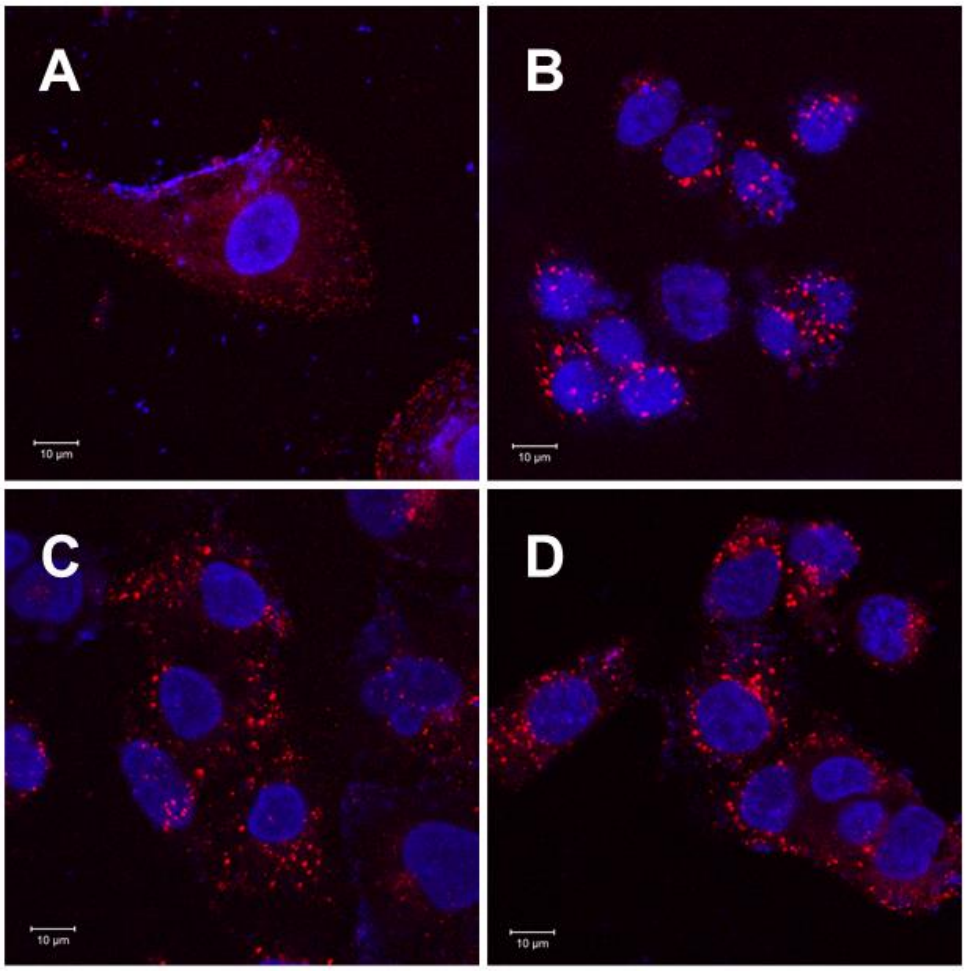

Figure 6.15 Effect of aspirin analogues on EGF-20 ng/ml internalization in oesophageal cells.
Confocal images of FLO1 oesophageal cancer cells treated with or without compounds, negative control [EGF receptor unstimulated] (A), positive control [EGF receptor stimulated] (B), PN502 [ortho-aspirin] (C), PN517 [fumaryldiaspirin] (D). Cells were treated at 0.5 mM (pH adjusted with HEPES, pH8) for 30 min. The EGF used is complexed to Alexa Fluor® 555 (20 ng/ml) for 1 h on ice after which it was 'chased' at 37°C for 30 min. The cells were then fixed for 5 min. Images were acquired at 405 nm-DAPI (blue) for nucleus and 561 nm-Alexa Fluor (red) for EGF. Representative images are shown taken at 40X oil/1.30 oil immersion objective *(n=2)*. Scale bar represents 10 µm.

The negative control, which are the FLO1 cells with unstimulated EGF appear to have the EGF along the surface of the cell membrane (Figure 6.15A). However, when stimulated by subjecting to 37°C for 30 min, the EGF gets internalized toward the nucleus of each cell (Figure 6.15B). The cells treated with PN502 and PN517 in this cell line also appeared to have the EGF farther away from the nucleus when compared to the control (Figure 6.15C and 6.15D) respectively. But for this cell line the vesicle-like structures of the EGF in the treated cells appear to be the same size as the ones in the positive control (the EGF that have undergone internalization).

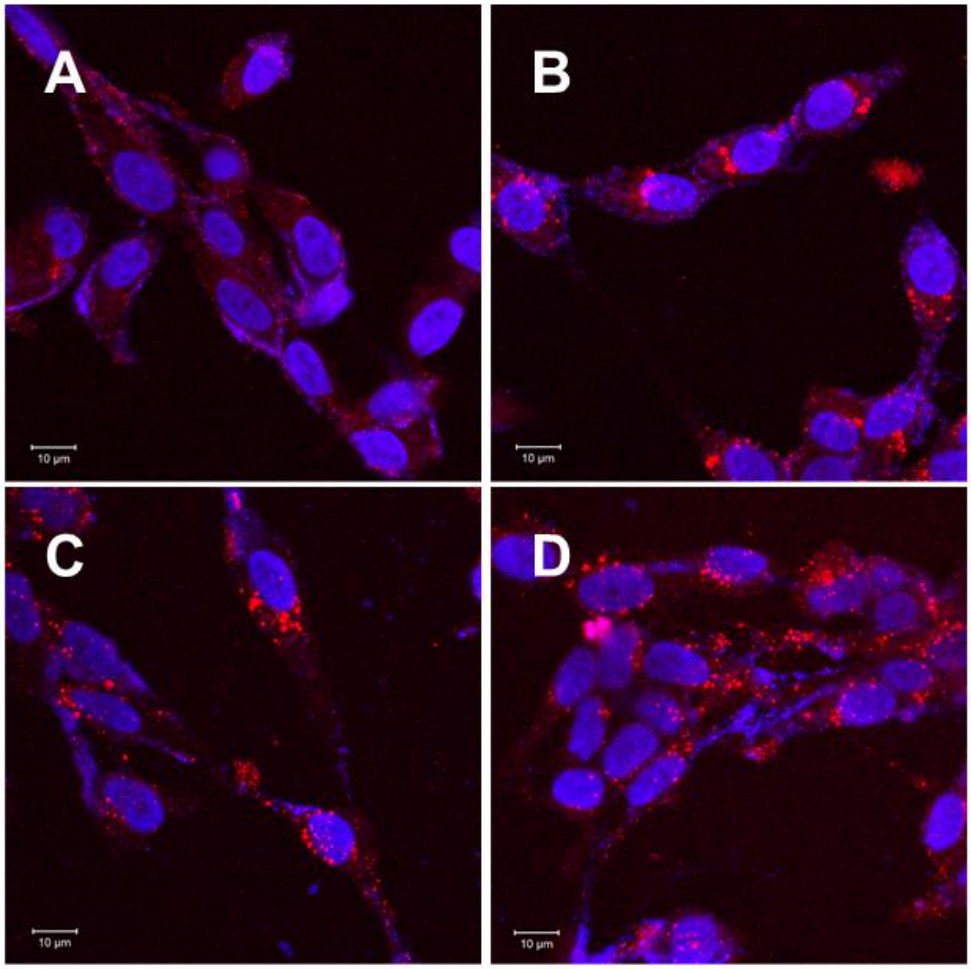

Figure 6.16 Effect of aspirin analogues on EGF-20 ng/ml internalization in MG cells.
Confocal images of U251 MG cells treated with or without compounds, negative control [EGF receptor unstimulated] (A), positive control [EGF receptor stimulated] (B), PN502 [ortho-aspirin] (C), PN517 [fumaryldiaspirin] (D). Cells were treated at 0.5 mM (pH adjusted with HEPES, pH8) for 30 min. The EGF used is complexed to Alexa Fluor® 555 (20 ng/ml) for 1 h on ice after which it was 'chased' at 37°C for 30 min. The cells were then fixed for 5 min. Images were acquired at 405 nm-DAPI (blue) for nucleus and 561 nm-Alexa Fluor (red) for EGF. Representative images are shown taken at 40X oil/1.30 oil immersion objective *(n=2)*. Scale bar represents 10 µm.

The EGF is seen along the cell membrane in the cells that have not been stimulated (Figure 6.16A) and then internalized towards the nucleus in the cells that have been ligand stimulated (Figure 6.16B).

In this particular cell line, however, the compounds appeared not to disturb the internalization of EGF. Cells treated with PN502 appeared as vesicle-like structure in close proximity to the nucleus (Figure 6.16C). PN517 also failed to disturb the EGF internalization as the EGF is seen in a close distance to the nucleus (Figure 6.16D).

PN502 and PN517 both affected EGF internalization in FLO1 oesophageal cell line. However, it did not or the effect was not clear in U251 MG. Perhaps, this can be clarified in the future by assessing if the aspirin analogues of interest affect any of the tyrosine kinase phosphorylation sites responsible for EGFR downstream signalling.

6.4.2 Effect of aspirin and its analogues on the Tyrosine phosphorylation sites of the EGF receptor

The binding of EGF activates EGF receptor and this leads to a series of signalling pathways involved in multiple mechanisms. This signalling pathway is ultimately attenuated by the degradation of the receptor through binding to the Cbl site, internalization of Y1045 and sorting into lysosomes for degradation. Mutation of this binding site found in cancer cells leads to impaired ubiquitination of the receptor (Grovdal *et al.*, 2004).

A series of phosphorylation sites were examined; namely pEGFR: Y992, Y1045, Y1068, Y1101 and Y1173 to detect the ones sensitive to EGF stimulation in SW480 cell line and to also find out if the compounds in this study stimulated degradation of the EGF receptor. The characteristics and functions of these phosphorylation sites have been mentioned in the beginning of this chapter.

Image J software was used to measure the level of EGFR expression and level of phosphorylation. EGFR expression was in relation to the EGFR expressed by untreated cells (Control). The level of phosphorylated tyrosine relative to EGF stimulation was normalized using the controls. The result gives a comparative measure of the phosphorylation level of tyrosine residues to that obtained after stimulation with 200 ng/ml of EGF. This particular dose for EGF was chosen because it gave the highest signal to the tyrosine kinase antibodies.

A series of time and dose response/sensitivity tests to EGF was carried out to determine the optimal dose and stimulation time of EGF to the different tyrosine kinase phosphorylation sites used in this study.

The first question that needed to be answered was if these compounds affected the expression of EGFR.

Cells were treated with some of the aspirin analogues buffered with PBS (pH7.4) for 24 h and it was discovered that there was a slight change in the level of EGFR expression.

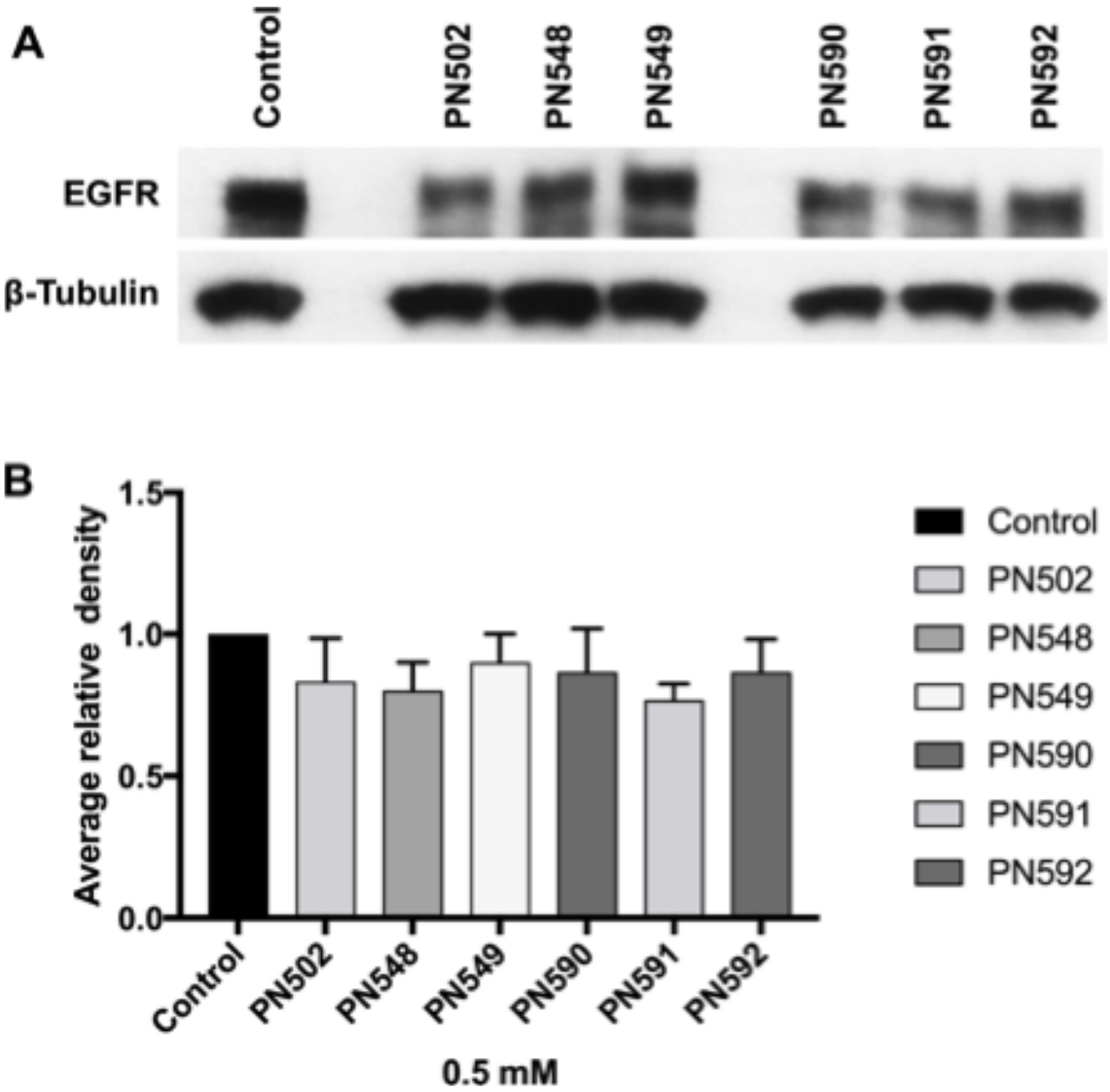

Figure 6.17 EGFR expression levels with aspirin analogues buffered with PBS in SW480 cells.
Cells were treated with 0.5 mM of compounds for 24 h and resolved by SDS-PAGE and western blotting. β-Tubulin was used as a loading control (A). Quantitative analysis of the blots using Image J software. The average relative density of EGFR expression in relation to the control (*n*=*3*) (B).

In comparison to EGFR expression level of control, the aspirin analogues PN502, PN548, PN549, PN590, PN591 and PN592 did not significantly affect the EGFR levels under the conditions tested (Figure 6.17A and 6.17B).

It was noted that compound addition alters the pH of the tissue culture media used (See Figure 6.9A). HEPES is one of the buffers recommended for biological studies (Good *et al.*, 1966) and was thus also employed as a buffering agent. To this end, HEPES (pH8) was added to make a final concentration of 10 mM prior to addition of compounds to cells.

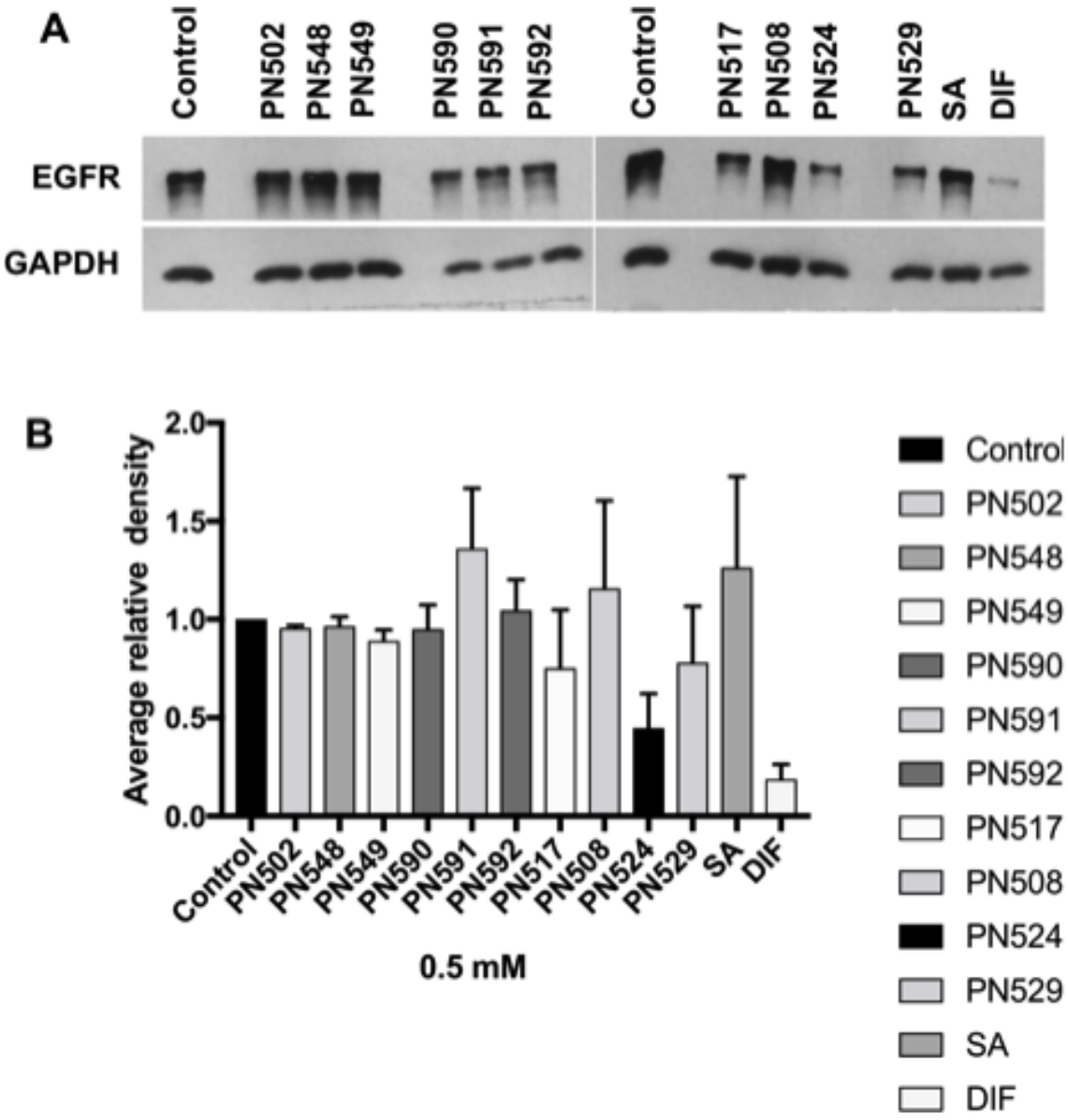

Figure 6.18 EGFR expression levels with aspirin analogues buffered with HEPES (pH8) in SW480 cells.
Cells were treated with 0.5 mM of compounds for 24 h and resolved by SDS-PAGE and western blotting. GAPDH was used as a loading control (A). Quantitative analysis of the blots using Image J software. The average relative density of EGFR expression is in relation to the control *(n=3)* (B).

The expression levels of EGFR was found to be reduced when SW480 CRC cells were treated with 0.5 mM diflunisal with slight changes observed when cells were treated with PN517, PN524 and PN529 for a period of 24 h (Figure

6.18A and B). This prompted the need to carry out a time-lapse observation of receptor expression levels after treatment. If perturbation of EGF internalization was visualized after approximately 2 h of treatment and effects of compounds on tyrosine kinase phosphorylation sites overnight, could this all be due to receptor binding and thus, less signalling travelling through the cell?

The cells were therefore treated for a period between 1 h and overnight to see the effect of these aspirin analogues on EGFR expression levels.

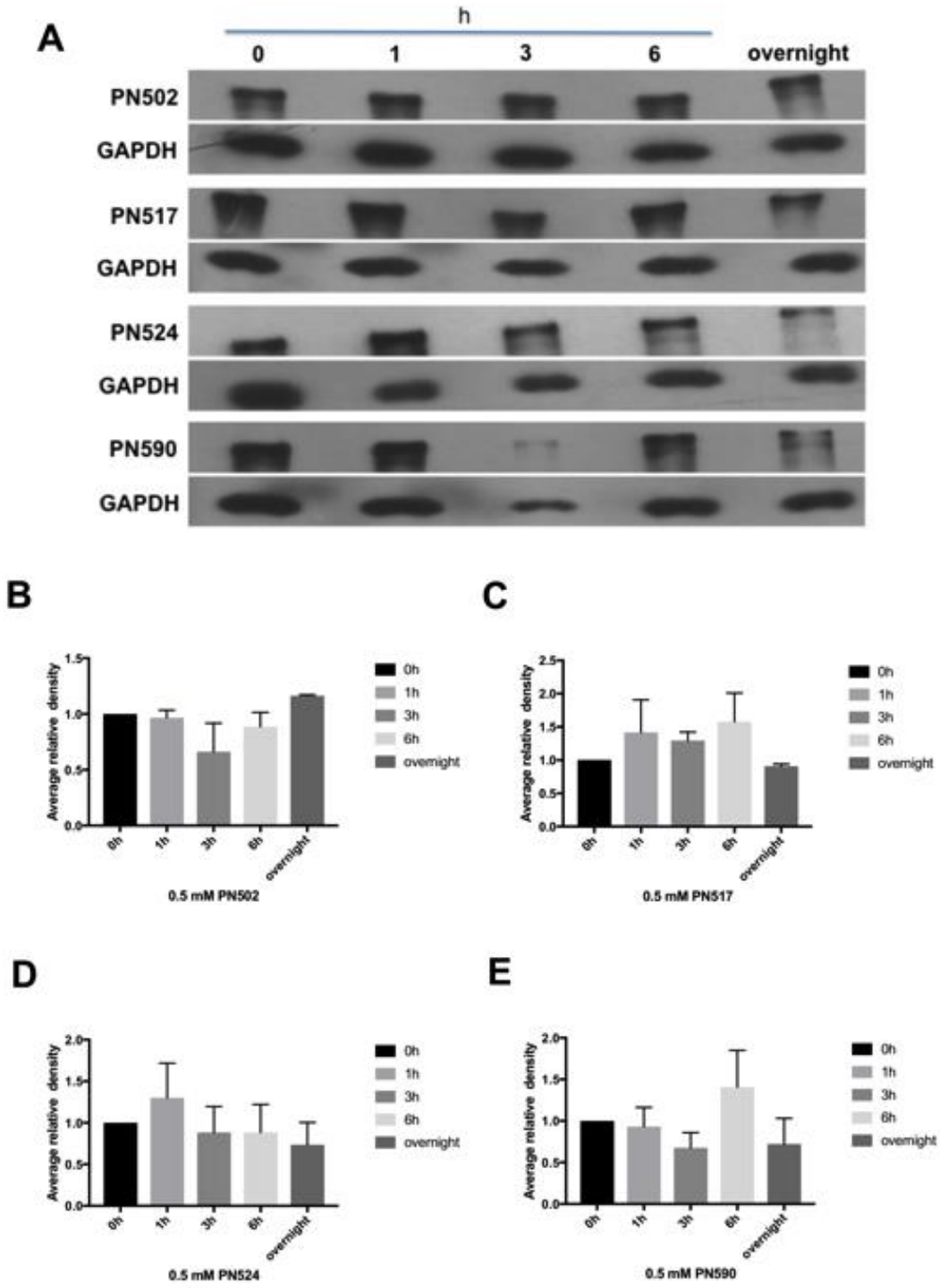

Figure 6.19 Time response to EGFR expression levels with aspirin analogues in SW480 cells.

Cells were treated with 0.5 mM of compounds (PN502, PN517, PN524 and PN590) for 0, 1, 3, 6 h and overnight. The protein extracts were resolved by SDS-PAGE and western blotting. GAPDH is used as a loading control (A). Densitometry of the blots using Image J software (*n=3*) for PN502 (B) PN517 (C) PN524 (D) and PN590 (E). The average relative density of EGFR expression is in relation to the control (0 h).

Levels of EGFR expression levels decreased significantly after cells were treated for 3 h with PN502 but then levels rose to similar levels to the control after 6 h (Figure 6.19B). However, when cells were treated with PN517, EGFR levels increased after an hour and then started to decrease when cells were treated overnight (Figure 6.19C). A slight increase of EGFR levels was observed after 1 h when treated with PN524, which normalised after 3 h (Figure 6.19D). Expression levels with PN590 dipped after 3 h, shot up after 6 hours of treatment and normalised overnight.

Over a time period of up to about 18 h (overnight), these compounds at 0.5mM did not significantly decrease EGFR expression levels which suggests that they do not competitively bind to the receptor thereby not causing a reduced signal altogether.

If these compounds are perturbing the internalization of the EGFR, what happens to the tyrosine kinase phosphorylation process? Does selective phosphorylation of particular sites affect trafficking, or do aspirin analogues prevent phosphorylation of multiple sites. The tyrosine kinase phosphorylation site responsible for the EGF receptor ubiquitination and degradation is pEGFR Y1045. While pY1173, pY1068, pY992 and pY1101 are responsible for GRB2/MAPK activation, PLC/PKC activation and PI3K/AKT activation respectively.

In order to find out the optimal dose and exposure time to enable receptor stimulation by EGF, the protein extract from SW480 cells exposed to different doses of EGF at different times was probed with pEGFR Y1068 antibody.

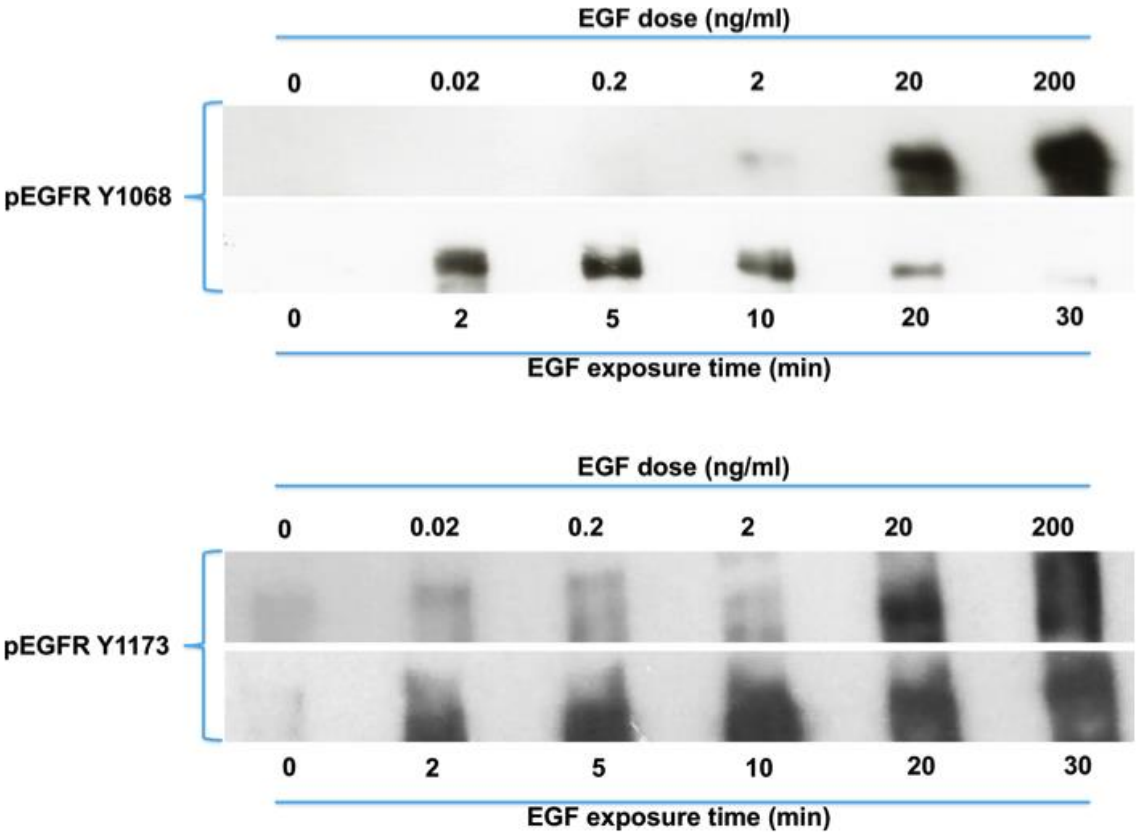

Figure 6.20 EGF dose and exposure time optimization for pY1068 and pY1173 antibodies.
SW480 CRC cells were exposed to EGF for 5 min at 0.02 ng/ml, 0.2 ng/ml, 2 ng/ml and 200 ng/ml. Cells were also exposed to EGF at 200 ng/ml for 2 min, 5 min, 10 min, 20 min and 30 min. The cells were then lysed in Laemmli buffer, resolved by SDS-PAGE and western blotting. Bands were seen at about 180 kDa.

The highest signal to pEGFR Y1068 was seen to be when exposed to EGF at 200 ng/ml for 5 min (Figure 6.20). Thus, this exposure dose and time for EGF was used as a receptor stimulant when cells were being treated with aspirin and its analogues.

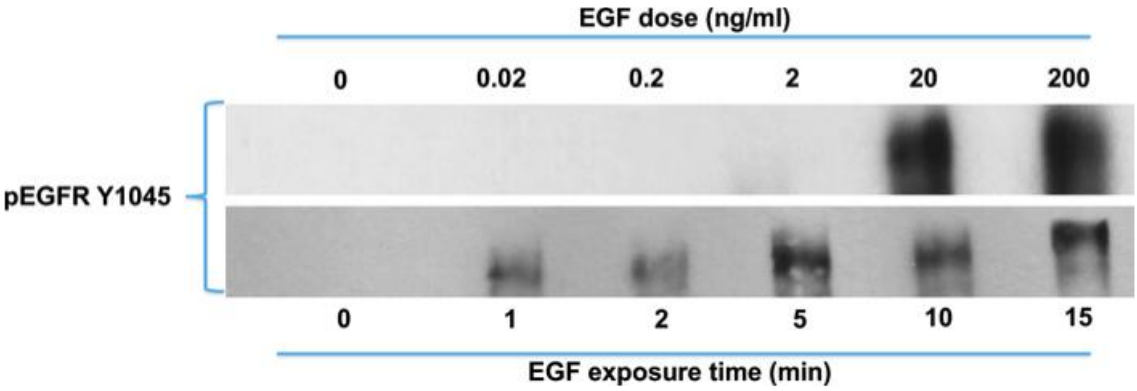

Figure 6.21 EGF dose and exposure time optimization for EGFR stimulation against pY1045 antibody.
SW480 CRC cells were exposed to EGF for 5 min at 0.02 ng/ml, 0.2 ng/ml, 2 ng/ml, 20 ng/ml and 200 ng/ml. Cells were also exposed to EGF at 200 ng/ml for 1 min, 2 min, 5 min, 10 min and 15 min. Cell lysates were separated through SDS-PAGE and then probed with pEGFR Y1045 antibody. Bands were seen at about 180 kDa.

The signal for the phosphorylation of EGF was weak at 1 min and 2 min. However, the signal increased at 5 min and then weakened again after 10 min (Figure 6.21). Lower doses of EGF did not produce any signal, but this appeared at 20 ng/ml and 200 ng/ml. The highest signal for EGF was seen at 200 ng/ml for 5 min. For this reason, the condition adapted for the cell ligand stimulation for extracts to be probed against pY1045 antibody was thus.

Signals to EGF against pY1173 antibody were very weak at 0.02 ng/ml, 0.2 ng/ml and 2 ng/ml with the strongest signal at 200 ng/ml (Figure 6.20). The exposure time course however showed a different pattern from pY1068 and pY1045, with the strongest signal to EGF phosphorylation at 10 min instead of 5 min.

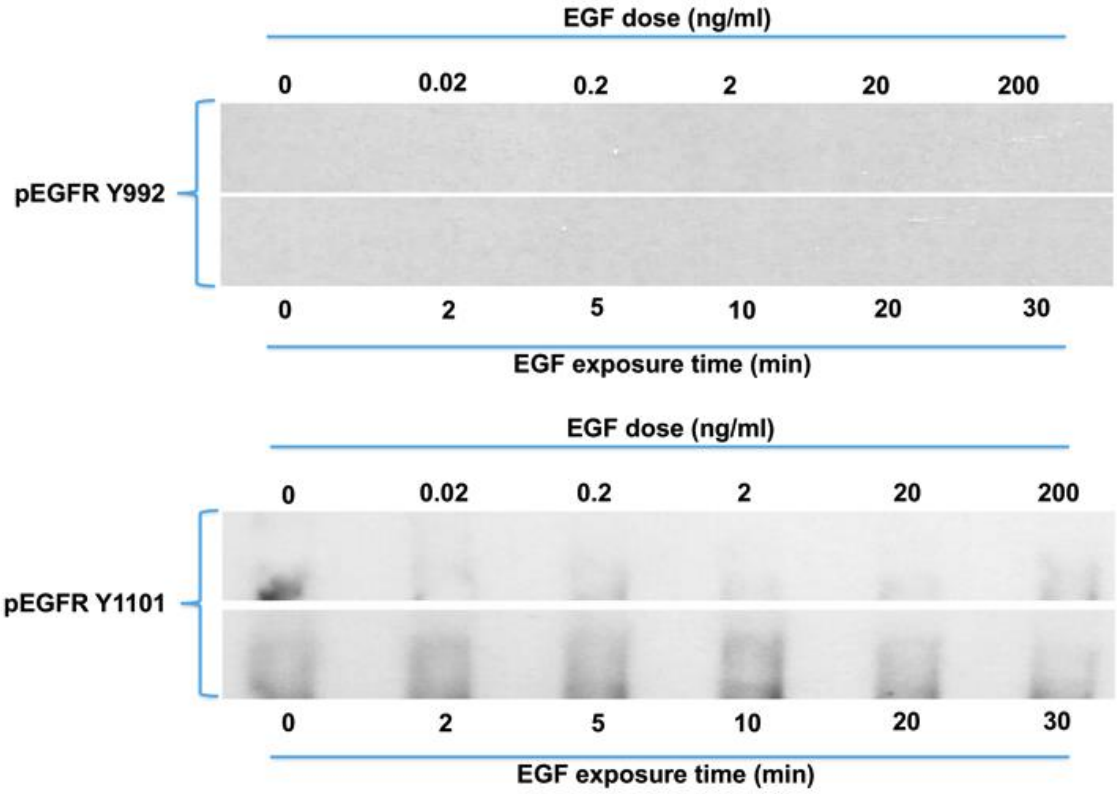

Figure 6.22 EGF dose and exposure time optimization for EGFR stimulation against pY992 and p1101 antibodies.
SW480 CRC cells were exposed to EGF at different concentrations; 0.02 ng/ml, 0.2 ng/ml, 2 ng/ml, 20 ng/ml and 200 ng/ml for 5 min and also exposed at 200 ng/ml for different times; 2 min, 5 min, 10 min, 20 min and 30 min. The cells were then lysed in Laemmli buffer, resolved by SDS-PAGE and then probed with pEGFR Y992 antibody and pEGFR Y1101 antibody. Signals for pY992 and pY1101 were absent over time and at different concentrations.

EGF signals were not observed over time with different doses against pY992 antibody (Figure 6.22). Due to the absence of any EGF signal, indicating that phosphorylation at that Y992 site was not turned on after ligand stimulation or the Abs not working, this site was not studied further with aspirin analogues. Signals for EGF indicating phosphorylation at Y1101 were also not seen at different concentrations and exposure times (Figure 6.22). Due to this, further studies with aspirin analogues in relation to their effect on pY1101 was halted.

SW480 CRC cells were treated with aspirin analogues and lysates probed with three antibodies to tyrosine phosphorylation sites, namely; pEGFR Y1068, pEGFR Y1045 and pEGFR Y1173 to see if these compounds had any effect on EGFR phosphorylation at these sites and ultimately the signalling pathway.

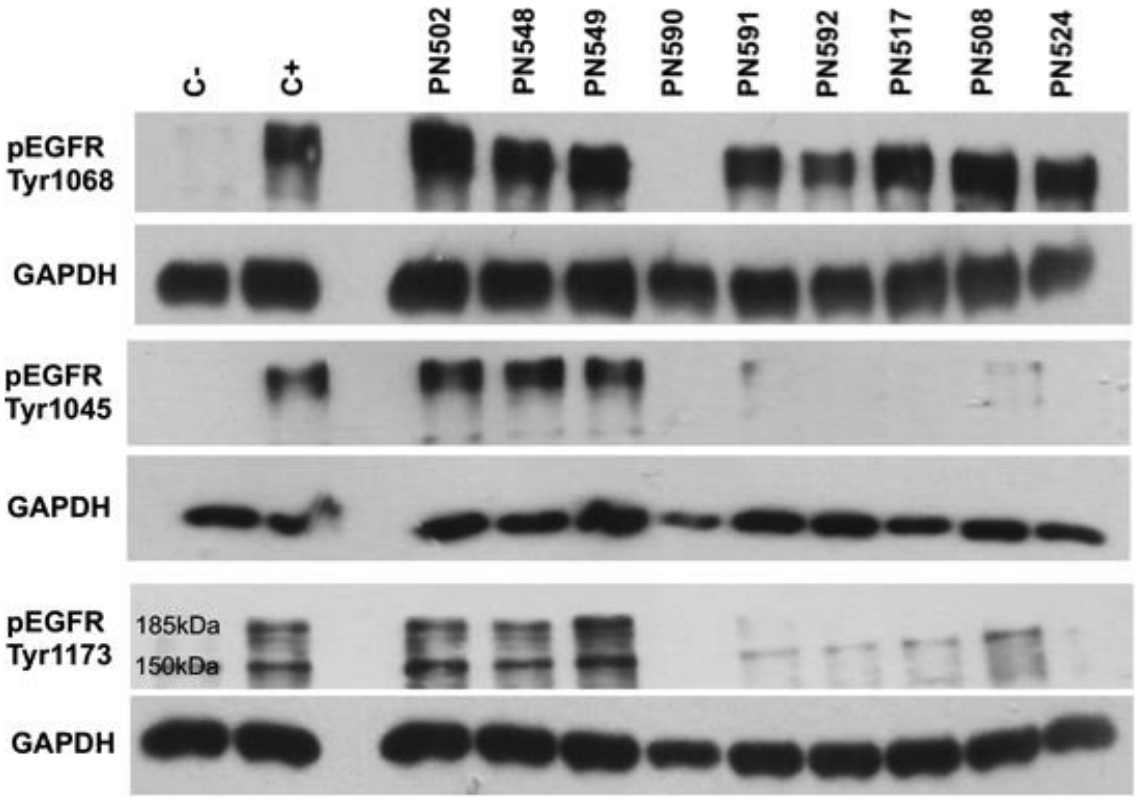

Figure 6.23 Effect of aspirin and its analogues on pEGFR tyrosine kinase phosphorylation sites.
C- represents unstimulated and untreated cell while C+ represents untreated cells stimulated with 200 ng/ml of EGF for 5 min. GAPDH was used as loading control. SW480 CRC cells were treated with 0.5 mM of compounds for 24 h after which ligand was stimulated with EGF (200 ng/ml). Cell lysates were separated through SDS-PAGE and probed with pY1068, pY1045 and pY1173 antibodies. Image is a representation of *n=3*. Bands were seen at about 180 kDa.

With the exception of the thioaspirins, PN590, PN591 and PN592, all the other compounds increased the expression of phosphorylation at Y1068 (Figure 6.23), which is the site responsible for binding to adaptor proteins GRB2 in order to activate the Ras and Mitogen-activated protein kinase (MAPK) pathway (Rojas *et al.*, 1996). However, all compounds with the exception of PN502, PN548 and PN549 decreased expression of phosphorylation at the Y1045 and Y1173 sites (Figure 6.23). It was then decided to carry out a dose response analysis of

these compounds on the individual phosphorylation site affected to see if the effect is dose-dependent or not. Dose responses on pEGFR Y1045 were carried out with PN590, PN591, PN592, PN517, PN508 and PN524.

Dose response blots were initially performed with doses arranged at a descending order. For presentation purposes, the images have been flipped horizontally so that the doses appear at an ascending order.

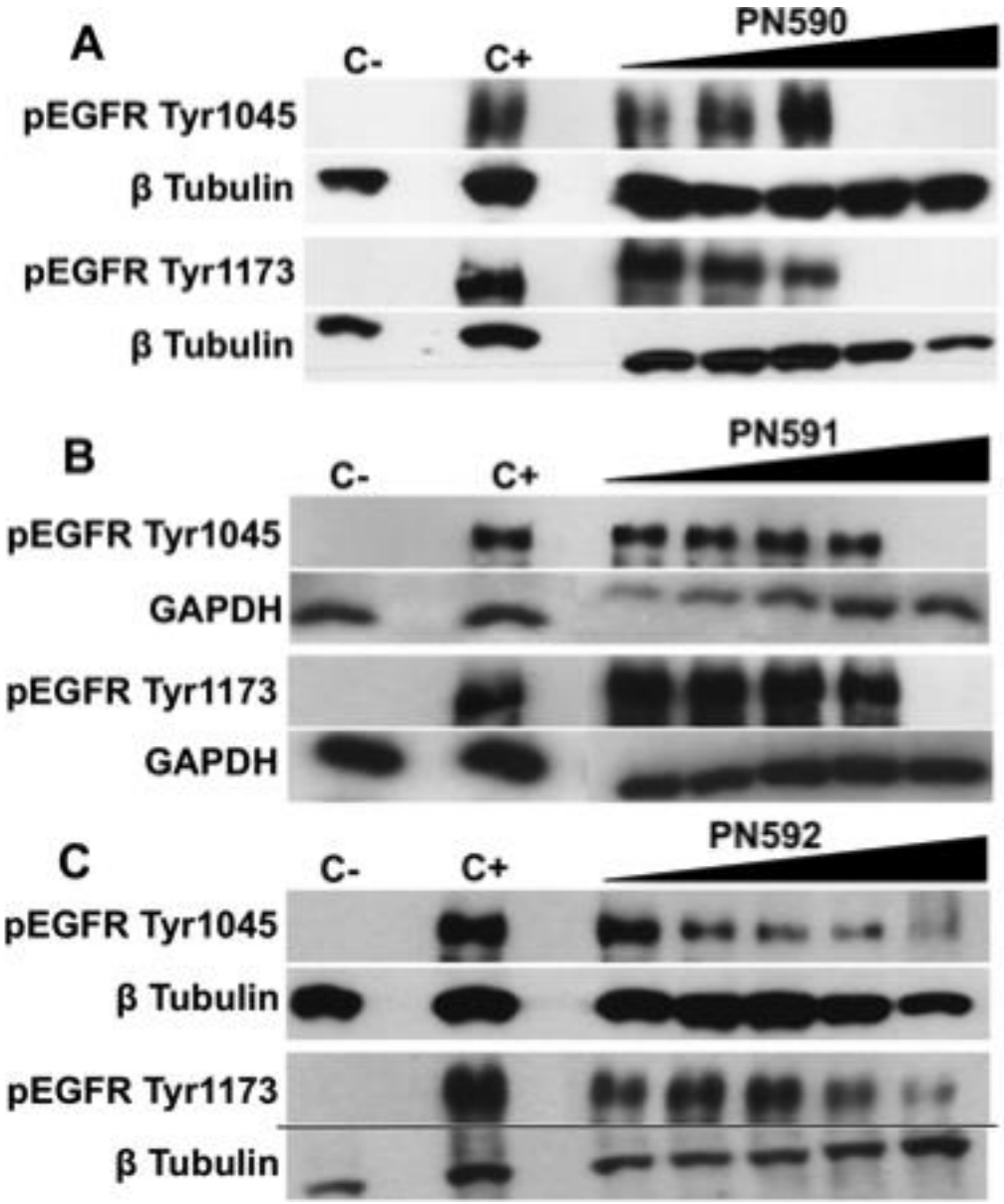

Figure 6.24 Dose response effect of the thioaspirins on the pEGFR Y1045 and Y1173 tyrosine kinase phosphorylation sites.
C- represents unstimulated and untreated cell while C+ represents untreated cells stimulated with 200 ng/ml of EGF for 5 min. β-Tubulin (55 kDa) and GAPDH (35 kDa) were used as loading control. SW480 CRC cells were treated with different doses of PN590 overnight (A) Cells treated with PN591 (B) Cells treated with PN592 (C). The cells were then lysed in Laemmli buffer, resolved by SDS-PAGE and western blotting using antibodies specific to pY1045 and pY1173. Images are a representation of *n=3*. pEGFR Tyr bands were detected around 180 kDa.

The signal that indicates phosphorylation at pY1045 started to get decreased by PN590 at 0.01 mM. But this increased at 0.03 mM and then started to decline at 0.1 mM (Figure 6.24A). Complete disappearance in the signal for phosphorylation at pY1045 and pY1173 by PN590 at 0.3 mM and 0.5 mM concentrations was observed (Figure 6.24A). At pY1173, signal for phosphorylation increased at 0.01 mM, which then started to decrease steadily at 0.03 mM to a complete disappearance of any visible bands at 0.3 mM and 0.5 mM (Figure 6.24A). PN591 appeared to abolish the signal for tyrosine kinase phosphorylation on both sites at 0.5 mM. However, the signal for phosphorylation appreciated at Y1045 from 0.01 mM, which started to decrease at 0.3 mM (Figure 6.24B). At the pY173 site, there was a slight decrease in phosphorylation at 0.01 mM, which then increased at 0.03 mM concentration and then steadily decreased again with an increase in the concentration of the thioaspirin. (Figure 6.24B). This could be due to the inhibition of a negative regulator selectively affected at lower concentrations, with another event taking place at higher concentrations. PN592 also caused a decrease in phosphorylation in a dose dependent manner at Y1045 and Y1173 tyrosine kinase sites (Figure 6.24C). These isomers of thioaspirin, PN591 and PN592 have shown similarities in their effects on SW480 cell line in previous assays, which are different from the effect of the ortho-thioaspirin, PN590. This could be because of the position of the thiol group on the meta- and para- positions of the benzene ring being different from the ortho- position affects their pharmacological action.

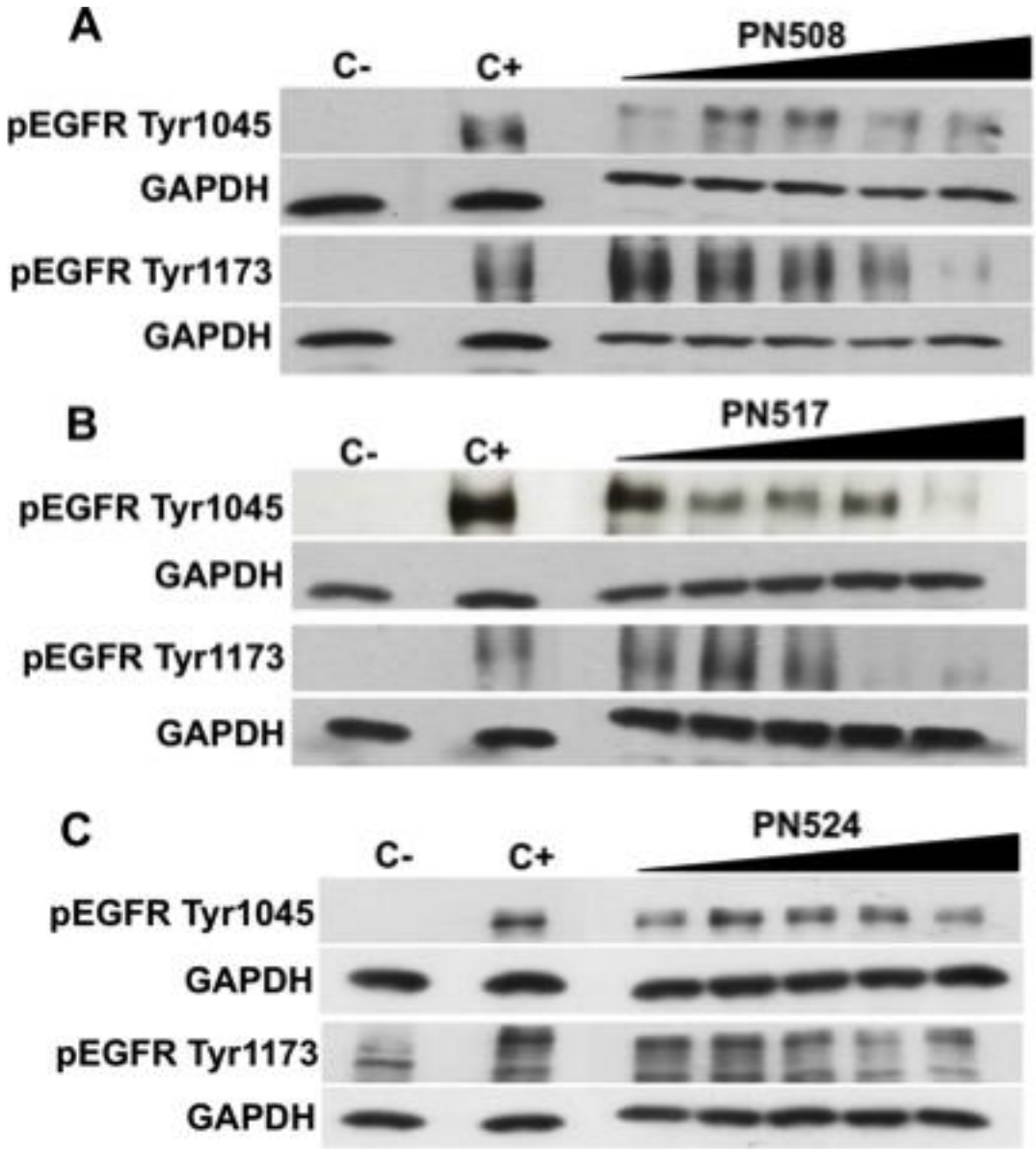

Figure 6.25 Dose response effect of 'diaspirins' on the pEGFR Y1045 and Y1173 tyrosine kinase phosphorylation sites.
C- represents unstimulated and untreated cell while C+ represents untreated cells stimulated with 200 ng/ml of EGF for 5 min. GAPDH (35 kDa) was used as a loading control. SW480 CRC cells were treated with different doses of PN508 overnight (A) Cells treated with PN517 (B) Cells treated with PN524 (C). The cells were then lysed in Laemmli buffer, resolved by SDS-PAGE and western blotting using antibodies specific to pY1045 and pY1173. Images are a representation of *n=3*. pEGFR Tyr bands were detected around 180 kDa.

For the ‘diaspirins’, there was a decrease in the signal for phosphorylation at the Y1045 site in relation to the control stimulated with 200 ng/ml EGF at 0.3 mM and 0.5 mM PN508. There was an increase in phosphorylation at Y1045 when cells were treated with 0.1 mM and 0.03 mM PN508 (Figure 6.25A). In relation to phosphorylation of tyrosine kinase Y1173, PN508 only caused a decrease in signal at 0.5 mM concentration. A decrease in phosphorylation at Y1045 site by PN517 was observed at 0.03 mM and more prominently at 0.5 mM (Figure 6.25B). The reduction in signal for pY1173 was seen at 0.1 mM, which further decreased at 0.3 mM and 0.5 mM (Figure 6.25B). The effect of PN517 on phosphorylation at Y1173 appears to decrease in a dose-dependent fashion. PN524 appeared to have a dose relative inhibitory effect on the signal for pY1045 (Figure 6.25C). However, there was decrease in signal for Y1173 phosphorylation site at 0.3 mM, which seemed to increase at 0.5 mM (Figure 6.25C). Thus, the effect of PN524 on Y1173 tyrosine kinase site appears not to be dose-dependent.

Qualitative EGF internalization assay using immunocytochemistry, showed internalization of EGF to be perturbed after cells were treated with these aspirin analogues for a period of 2 h. It was therefore decided to also treat SW480 cells with these compounds for the same time period in order to find out if there is any effect on pY1045 site, which is responsible for the ubiquitination of the receptor. This experimental condition is to mimic that of the qualitative EGF internalization confocal assay that was based on immunocytochemistry (Figure 6.6 to 6.13).

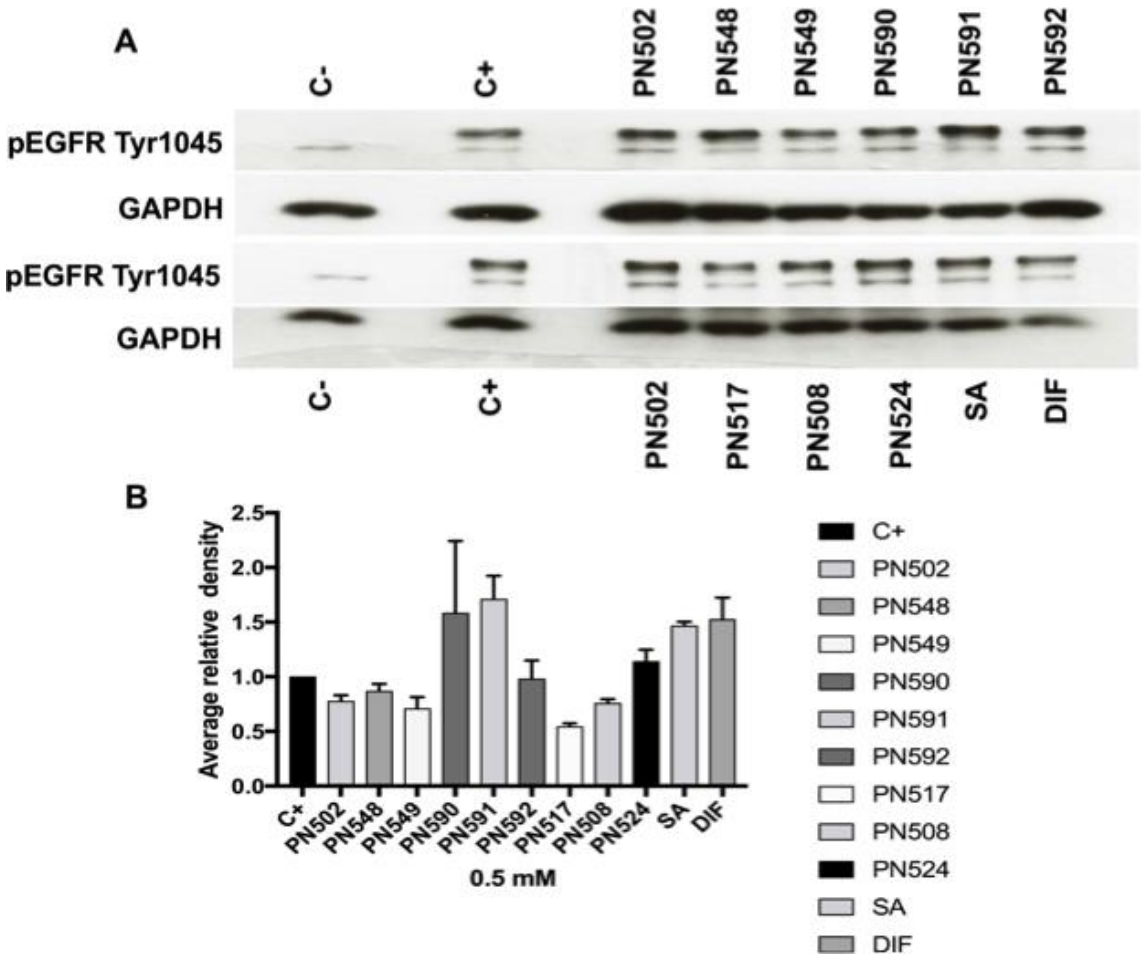

Figure 6.26 Effect of aspirin and its analogues on pEGFR Y1045 site.
C- represents unstimulated and untreated cell while C+ represents untreated cells stimulated with 200 ng/ml of EGF for 5 min. GAPDH was used as loading control. SW480 CRC cells were treated with 0.5 mM of compounds buffered with HEPES (pH8) for 2 h. Cell lysates were then separated through SDS-PAGE and probed with pY1045 antibody (A). Quantitative analysis using Image J of signals to pY1045 (*n=3*) (B). Bands for pY1045 were observed at 185 kDa.

PN517 and PN508, both 'diaspirins', decreased the signal for the pY1045 antibody after treatment of SW480 CRC cells for 2 h (Figure 6.26B) with the salicylate-like compounds, salicylic acid and diflunisal increased the signal for the same phosphorylation site (Figure 6.26B). However, this change in phosphorylation was not significant. The thioaspirins, PN590 and PN591 however significantly increased phosphorylation at Y1045 site after 2 h of

treatment. Surprisingly, after 2 h of treatment with the aspirins, PN502, PN548 and PN549, there was a slight, non-significant decrease in signal for pY1045 in relation to the control stimulated with 200 ng/ml of EGF (Figure 6.26B).

In order to study the possible effects of these aspirin analogues downstream of the EGFR signalling pathway, attempts were made to find out their effects on stat-3 and phosphorylation of stat-3 at Y705.

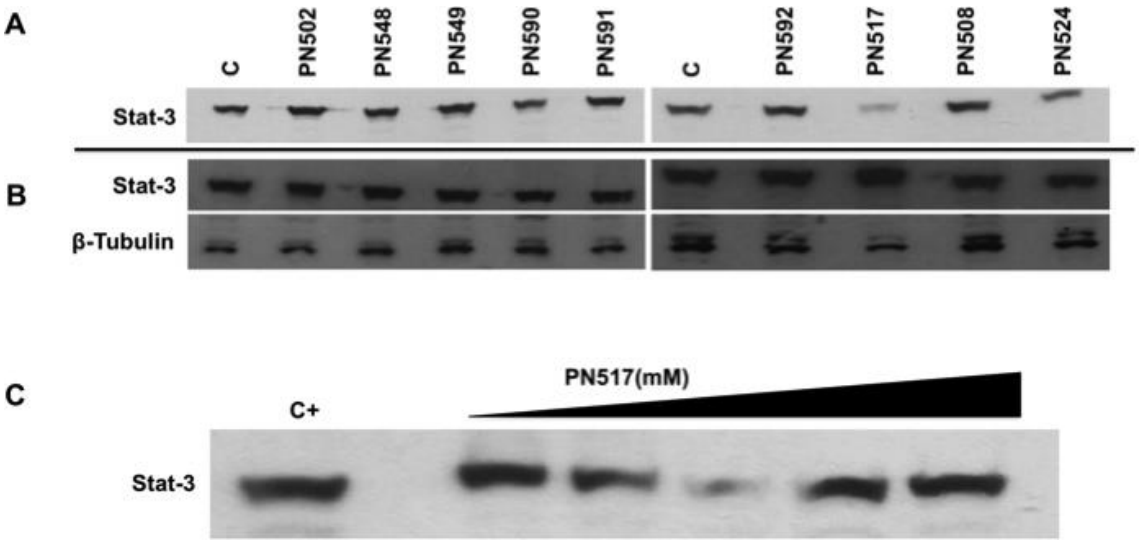

Figure 6.27 Effect of aspirin analogues on stat-3.
C+ represents control/untreated cells. All cells were stimulated with 200 ng/ml of EGF for 5 min. β-Tubulin (55 kDa) was used as loading control. First attempt as 'test-run' without loading control of the treatment of SW480 CRC cells with 0.5 mM of aspirin analogues buffered with HEPES (pH8) overnight. Cell lysates were resolved using SDS-PAGE and probed with stat-3 primary antibody (A). Second attempt of treatment with analogues under the same conditions and probed with antibody specific to stat-3 (B). Cells were treated with increasing doses of PN517 and then lysed with Laemmli buffer, resolved by SDS-PAGE and probed with stat-3 antibody.

On the first attempt, although without a protein loading control, PN517 was found to inhibit the expression of stat-3 (Figure 6.27A). However, after two repeats accompanied by a loading control, it was found out that none of the

compounds had an effect on stat-3 expression; thus, result was not reproducible (Figure 6.27B). In the absence of a loading control in the first attempt, it is likely that the result seen was false and was due to difference in protein volume loaded into SDS-gel wells. To make sure that PN517 definitely did not have any effect on stat-3, a dose-dependent assay was carried out using doses that ranged from 0.01 mM to 0.5 mM (Figure 6.27C). It was observed that PN517 had an effect on stat-3 expression at 0.1 mM (Figure 6.27C). Could this be because PN517 is affecting another target that indirectly affects stat-3? However, this was not investigated further due to time constraint.

If none of the compounds affected the protein stat-3, could they affect the phosphorylation of stat-3? An effect on the phosphorylation of stat-3 indicates an effect on the STAT-signalling pathway as phosphorylation of stat-3 at Y705 allows for stat dimerization and subsequent transcription activation (Schindler and Darnell, 1995). To answer this question SW480 CRC cells were treated with some aspirin analogues and lysates then probed with phospho-stat-3 (Y705) antibody after resolution with SDS-PAGE. Stat-3 was used as a loading control since it appeared to be unaffected by the compounds at 0.5 mM.

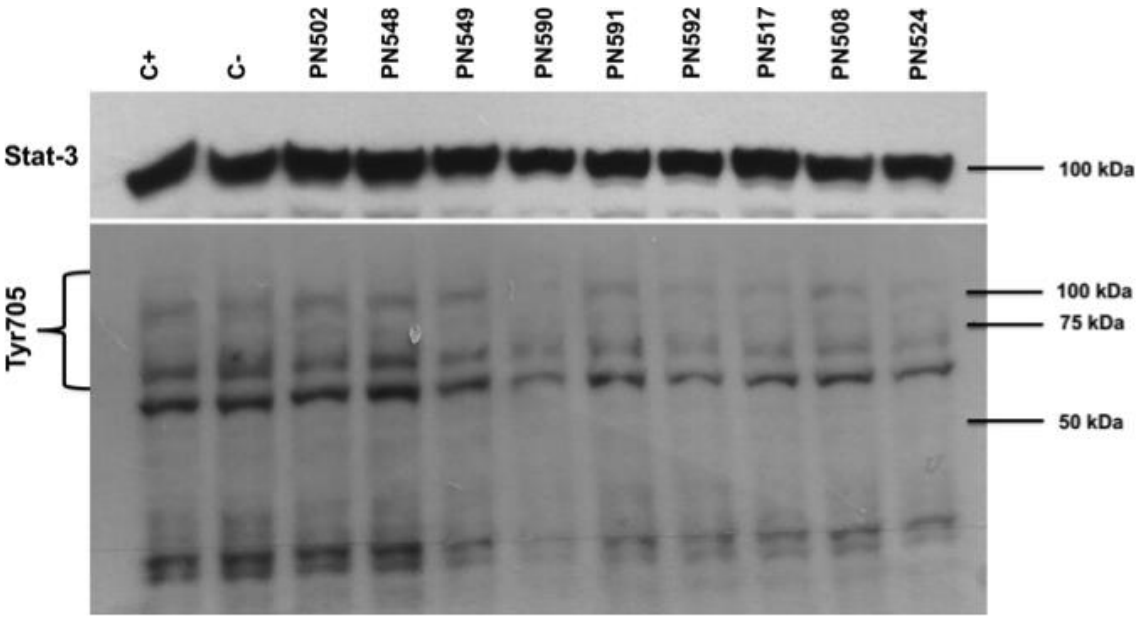

Figure 6.28 Effect of aspirin analogues on stat-3 and Tyr705 phosphorylation. SW480 CRC cells were treated with 0.5 mM of compounds overnight and stimulated with 200 ng/ml of EGF for 5 min. Note the multiple bands around the expected region for Tyr705 band detection.

The bands specific to Y705 was not clear as multiple bands around the region were seen (Figure 6.32). Since the band to stat-3 was observed at 100 kDa, the band to Y705 was expected around that region. This could be an issue of unspecificity of the antibody. In the absence of any clear bands and the period of this study coming to an end, investigation regarding stat-3 and Y705 had to be halted and saved for future studies.

6.5 Discussion

The EGFR signalling pathway is complex (Figure 6.2) and internalization is a significant component of that pathway (Goh *et al.*, 2010, Orth *et al.*, 2006). Herein, it is suggested that aspirin and its analogues can rapidly perturb EGF receptor internalization in SW480 CRC cells (Figures 6.6 to 6.13) and in oesophageal cancer cell lines (Figure 6.14 and 6.15). Thus, causing a delay or halt in EGFR signalling.

Ligand binding can be affected by low pH due to the EGF dissociating itself from the receptor (Roepstorff *et al.*, 2009). Perturbation of internalization due to possible competitive binding between compounds with EGF and change in pH has been addressed by a control binding assay and buffering compounds with HEPES (Figures 6.5 and 6.9) respectively. In another assay, using western blotting, EGFR expression was not significantly different from the control when SW480 CRC cells were treated with aspirin and its analogues buffered with PBS for 24 h (Figure 6.17). When the same experiment was carried out with HEPES being the buffer of choice, diflunisal>PN524>PN517>PN529>salicylic acid decreased EGFR expression (Figure 6.18). PN517, PN524 and diflunisal are all diaspirins, which could explain why they exhibit similar effects to each other and their metabolite, salicylic acid. Salicylic acid, being acidic will cause the dissociation of any ligand present from the receptor (Roepstorff *et al.*, 2009) and may provide a pocket for itself to bind onto the receptor instead. However, over a time period of up to about 18 h (overnight), these compounds at 0.5 mM did not significantly decrease EGFR expression levels (Figure 6.19). HEPES was the buffer of choice later adapted because it is considered as an effective

buffering agent for biological research (Good *et al.*, 1966). EGF used in a concentration greater than 20 ng/ml as a stimulant could lead to the receptor following different pathways (Henriksen *et al.*, 2013), which could either be clathrin dependent or independent (Sigismund *et al.*, 2005) with little being known of the independent pathway (Mayor and Pagano, 2007). It was thus decided to use 20 ng/ml EGF to stimulate the receptor in order to find out if these aspirin analogues disrupt recycling of the EGFR (Sigismund *et al.*, 2008). Aspirin and its analogues perturbed EGF internalization when the receptor was stimulated with 20 ng/ml of EGF (Figure 6.13), which suggests that these aspirin analogues may prevent or delay the EGFR from being recycled back to the cell surface for continuous stimulation of the signalling pathway because stimulating the EGFR with low doses of EGF results in the receptor being recycled back to the cell surface (Sigismund *et al.*, 2008). Perturbation of receptor endocytosis by these aspirin analogues at 20 ng/ml in SW480 CRC cell line (Figure 6.13), OE33 oesophageal cell line (Figure 6.14) and FLO1 oesophageal cell line (Figure 6.15) could lead to the prevention of receptor recycling and thus attenuation of repeated signalling and eventual ubiquitination of the receptor.

Post internalization, the EGFR is translocated to the nucleus where it associates with genes responsible for cell proliferation and thus acting as a transcription factor (Lin *et al.*, 2001). The EGFR also phosphorylates PCNA, while in the nucleus thereby disrupting interaction with MutSα and MutSβ, which are mismatch-recognition proteins. This consequently leads to interruption of

DNA MMR and the proliferation of cells that have damaged DNA, potentially causing genetic instability (Ortega *et al.*, 2015). Time-lapse assay using Confocal Live imaging has further proven that aspirins do perturb internalization of the EGF (Figure 8.22). It has thus been discovered that aspirin and its analogues do prevent the translocation of EGF (and hence EGFR) from the surface of the cell membrane towards the nucleus, which implies that these compounds may have the ability to promote genetic stability in cancer as they will prevent inaccuracy in DNA replication and thus prevent tumour progression. This correlates with observed increase in the expression of hMLH1, hPMS2, hMSH2 and hMSH6 DNA MMR proteins in CRC cell lines (SW480, HCT116, HCT+chr3) after treatment with aspirin (Goel *et al.*, 2003).

Another cause for tumour progression is the sustained activation of Akt, which is dependent on EGFR internalization (Goh *et al.*, 2010). This proposal concurs with Wheeler et al. (2010) and Chan et al. (1999) where it is mentioned that the activation of Akt/mTor pathway results in enhanced cell proliferation by phosphorylating caspase-9, an apoptosis pathway enzyme (Cardone *et al.*, 1998) and BAD, a BCL-2 family member (Datta *et al.*, 1997). Thus, perturbation of receptor internalization will lead to the inactivation of the Akt/mTor pathway, which is favourable in cancer therapy.

In a study carried out in OVCAR-3 ovarian cancer cell line, which overexpresses COX1 enzyme *in vitro*, 1 mM aspirin was found to inhibit EGFR associated Y1068 phosphorylation (Cho *et al.*, 2013) as opposed to what was

observed with 0.5 mM of aspirin and its analogues with the exception of the thioaspirins (Figure 6.23). However, this could be a COX1 dependent effect for aspirins because of COX1 being overexpressed in OVCAR-3 ovarian cell line (Cho *et al.*, 2013) and low levels detected in SW480 (Richter *et al.*, 2001), which is the cell line used in this study.

Furthermore, cyclin D1, an important protein responsible for cell cycle regulation at G_1 to S phase transition (Malumbres and Barbacid, 2009) has been found to be inhibited by PN508 [referred in paper as DiA] and PN517 [referred in paper as F-DiA] (Claudius *et al.*, 2014) and of which is found to interact with nuclear EGFR to cause cell proliferation (Lin *et al.*, 2001).
Diflunisal, a salicylate-like compound with anti-cancer properties (Shirakawa *et al.*, 2016) appeared to totally inhibit EGF internalization (Figure 6.12G, 6.13L), suggesting that it might inhibit signalling of the EGFR pathway. The effect of diflunisal on the EGFR could be an addition to its mechanism of action as potential oral therapy for patients with acute myelogenous leukaemia (Shirakawa *et al.*, 2016).

EGFR is stimulated when bound to EGF, which is then followed by internalization of the receptor and its delivery to early EEA1 endosomes (Zoncu *et al.*, 2009), whereby the receptor is either recycled or delivered to the lysosomes for degradation (Beas *et al.*, 2012, Platta and Stenmark, 2011, Sorkin and von Zastrow, 2009). EEA1 is an effector protein required at the early endosome, which is a compartment responsible for the sorting of ligand-

receptor complexes into late endosomes and lysosomes for degradation or back to the cell surface for recycling (Mu *et al.*, 1995, Shepherd, 1989). This compartmentalization is part of the signalling pathway of the EGFR and takes place after endocytosis of a receptor (Schlessinger, 2000). However, in SW480 cells, it was observed that EGF did not co-localise with EEA1 even after stimulation (Figure 6.6D, 6.10D and 6.13D), which suggests that the receptor may not have been delivered into the endosomes. Previous studies have demonstrated that P53 is involved in the production and regulation of endosomes and exosomes responsible for sorting of receptors either for recycling or degradation (Sun *et al.*, 2016, Yu *et al.*, 2006, Yu *et al.*, 2009) and SW480 cells harbour a mutated *TP53* (Din *et al.*, 2010), which could mean that there is a disruption in the regulation of these endosomes, thus, the absence of co-localization of EGF with EEA1. Nevertheless, PN517, a diaspirin (Figure 6.8F, 6.11F and 6.13H) seems to have restored the regulation of the endosomes for it forced the co-localization of EGF and EEA1. PN590, a thioaspirin (Figure 6.7F and 6.10H) also slightly forced some EGF to co-localize with the EEA1. The possible regulation of endosomes by these aspirin analogues may be due partly to the parent drug and partly to the salicylate moiety because salicylic acid (Figure 6.12F and 6.13J) also forced EGF to co-localise with EEA1. However, further research into this is needed to find out if these aspirin analogues also restore regulation of endosomes rich in Rab5 for early endosomes, Rab4 or Rab11 for endosomes responsible for receptor recycling and Rab7 for late endosomes responsible for the degradation of the EGFR (Flores-Rodriguez *et al.*, 2015, Zerial and McBride, 2001). These late

endosomes, also known as lysosomes are armed with lysosomal proteins such as LAMPs and are as a result of matured EEA1 that acquire Rab7 (Huotari and Helenius, 2011). If lysosomes are the final destination for stimulated EGFR, the receptor is then guaranteed to undergo degradation. This is particularly important because signalling continues even when EGFR has been delivered into the endosomal system (Di Guglielmo *et al.*, 1994).

It is therefore proposed that the signal of the EGFR signalling pathway is attenuated or dulled by these compounds, which led to the question of what happens at the ubiquitination phase of this receptor? The action of these compounds on tyrosine phosphorylation means there might be an effect downstream. The maximal dose and time of exposure for EGF used to stimulate the phosphorylation of specific sites (Y1068, Y1045 and Y1173) was found to be 200 ng/ml for 5 min (Figure 6.20 and 6.21). However, no signal was observed against pY992 and pY1101 antibodies (Figure 6.22). Phosphorylation at Y1101 is Src-dependent and not ligand induced (Biscardi *et al.*, 1999). Thus, phosphorylation is not likely to be activated by EGF stimulation. Another possibility could be that this particular cell line undergoes serine/threonine instead of tyrosine kinase phosphorylation, thus, having a kinase inactive mutant, which does not undergo autophosphorylation on those particular tyrosine residues. This happens if the receptor is missing a portion/portions of the carboxy-terminal tail (Zwang and Yarden, 2006). Frantz and O'Neill, (1995) believed that the effect of salicylates on tyrosine kinases were non-specific. However, contrary to this and in agreement with Kopp and Gosh, (1994), it has

been found that these salicylate compounds have specific effects on various phosphorylation sites. The thioaspirins decreased phosphorylation at Y1068, while the aspirins and 'diaspirins' increased phosphorylation on the same Tyr site (Figure 6.23). In addition, all the compounds with the exception of PN502, PN548 and PN549 decreased phosphorylation at Y1045 and Y1173 (Figure 6.23). With the compounds perturbing EGF internalization, it was quite unexpected for them to also inhibit the phosphorylation of the receptor at the site responsible for ubiquitination. However, the process of EGFR internalization is independent of tyrosine phosphorylation (Wang *et al.*, 2005). In relation to the effect of these compounds on the phosphorylation sites (Y1045 and Y1173) studied (Figure 6.24 and 6.25), dose-dependent effects were observed with some of these compounds, which correlates well with results reported previously (Wang and Xie, 2007). Aspirin and its analogues with the exception of PN590 did not inhibit EGFR phosphorylation at Y1068 (Figure 6.23), but perturbed EGF internalization (Figure 6.6 to 6.13). This is opposed to the notion that EGFR internalization is as a result of tyrosine phosphorylation (Schmidt *et al.*, 2003, Sorkina *et al.*, 2002) but correlates with the early notion that the two processes are independent of each other (Felder *et al.*, 1992, Felder *et al.*, 1990, Honegger *et al.*, 1987). However, these differences in opinion could be due to different cell lines having different requirements for the degree of EGFR phosphorylation and its involvement in EGFR internalization (Jiang *et al.*, 2003).

Chapter 7. General Discussion and Future Studies

7.1 General Discussion

The compounds with single benzene rings, aspirin (PN502) and its isomers, PN548 and PN549 exhibited their effects in a similar manner. Likewise the thioaspirins, PN590, PN591 and PN592 had similar effects different from the 'diaspirins', PN517, PN508 and PN524, which are made up of two benzene rings. Similarities in the effects **(Table 7.1)** exhibited by these compounds on SW480 cells may thus be attributed to their chemical structures **(Table 3.3)**.

In this study, 5-FU decreased the expression of p21 **(Figure 5.2 and 5.3)**, however when used in combination with 3-bromopyruvic acid, an inhibitor of energy metabolism, p21 expression was increased in SW480 cells (Chong *et al.*, 2017). Lung cancer cells, Calu-6 and colon cancer cells, HCT 116 treated with 100 μM of 5-FU for a period of 24 h also down-regulated p21 expression (Esposito *et al.*, 2014). This study has the same dosing and duration of treatment with 5-FU as ours and also agrees with the findings in this study. Along with 5-FU, aspirin and the thioaspirins also decreased the expression of p21 **(Figure 5.3)**. On the other hand, the isomers of aspirin, PN548 and PN549 appear to induce apoptosis in SW480 cells through the BCL2/BAX pathway **(Figure 5.4)** of which was achieved by combining 5-FU and dimethoxycurcumin in SW480 CRC cells (Zhao *et al.*, 2017). The effect of aspirin and the thioaspirins via p21 appear to inhibit the oncogenic activity of the protein (Karimian *et al.*, 2016) and thus hopefully lead to better disease free survival in patients with colorectal cancer (Esposito *et al.*, 2014, Noske *et al.*, 2009, Rau *et al.*, 2003). The apoptotic effect of these compounds is reflected in the ICC

studies using YO-PRO-1® and PI fluorescence dyes as positive stains for apoptosis and necrosis respectively **(Figure 5.6 to 5.11)**. Flow analysis also show apoptosis **(Figure 5.6 to 5.12)** accompanied by a large percentage of late apoptotic/necrotic cells, which could be attributed to harvesting of adherent cells even though this percentage is significantly lower than the percentage of necrotic cells caused by treatment with H_2O_2, which was used as the positive control for necrosis **(Figure 5.13)**. One of the shortcomings of this analysis is the inability to distinguish between late apoptotic and necrotic/dead cells, which is a disadvantage as cells could still be undergoing apoptosis but are then stained with PI and clustered in the UR **(Figure 2.2)** quadrant thereby being forced to be labelled as necrotic or dead cells.

Compounds	Cell proliferation (MTT assay)	% Apoptosis (16 h)	% Apoptosis (40 h)	Apoptosis (ICC)	p21	BCL2	BAX	Synergy at ED_{50}	pY1068	pY1045	pY1173	EGF internalization	EGF co-localization with EEA1
5-FU	↓				↓	↓	↑						
Staurosporine	↓	**41.6**	**21.4**	**+**		**x**	**x**						
PN502 (aspirin)	↓	**0.8**	**11.0**	**+**	↓	**x**	**x**	**CP, OX**	↑	**x**	**x**	**–**	**x**
PN548	↓	**1.5**	**8.7**	**+**	↑	↓	↑	**CP, OX**	↑	**x**	**x**	**–**	**x**
PN549	↓	**1.5**	**12.8**	**+**	↑	↓	↑	**CP, OX**	↑	**x**	**x**	**–**	**x**
PN590	↓	**6.2**	**5.9**	**+**	↓	**x**	**x**	**–**	↓	↓	↓	**––**	**+**
PN591	↓	**0.2**	**1.9**	**+**	↓	**x**	**x**	**–**	↓	↓	↓	**–**	**x**
PN592	↓	**2.5**	**3.6**	**+**	↓	**x**	**x**	**–**	↓	↓	↓	**–**	**x**
PN517	↓							**CP, OX, CB**	↑	↓	↓	**––**	**+++**
PN508	↓							**CP, OX**	↑	↓	↓	**–**	
PN524	↓							**CP, OX**	↑	↓	↓	**–**	**x**
Salicylic acid												**––**	**+**
Diflunisal												**–––**	**x**

Table 7.1 Summary of the effect of aspirin analogues on SW480 CRC cells.

EGFR expression was not significantly different from the control when SW480 cells were treated with aspirin and its analogues buffered with PBS for 24 h **(Figure 6.17)**. When the same experiment was carried out with HEPES being the buffer of choice, diflunisal>PN524>PN517>PN529>salicylic acid decreased EGFR expression. In chapter three, it was found out that PN517 metabolises into salicylate at a faster rate than PN502 **(Figure 3.14)**. Furthermore, PN517, PN524 and diflunisal are all diaspirins, which could explain why they exhibit similar effects to each other and their metabolite, salicylic acid. Salicylic acid, being acidic will cause the dissociation of any ligand present from the receptor (Roepstorff *et al.*, 2009) and may provide a pocket for itself to bind onto the receptor instead. However, over a time period of up to about 18 h (overnight), these compounds at 0.5 mM did not significantly decrease EGFR expression levels during the experimental study.

These compounds perturbed EGF internalization in SW480 cells when the receptor was stimulated with both 100 ng/ml **(Figure 6.6 to 6.12)** and 20 ng/ml of EGF **(Figure 6.13)** and under PBS and HEPES buffering systems. Perturbation of EGF internalization by these compounds was also observed in oesophageal cancer cell lines, OE33 **(Figure 6.14)** and FLO1 **(Figure 6.15)**. This effect will eventually lead to a decrease in proliferation of cancer cells via preventing translocation of the EGFR into the nucleus where it acts as a transcription factor (Lin *et al.*, 2001). The EGFR also phosphorylates PCNA, while in the nucleus thereby disrupting interaction with MutSα and MutSβ, which are mismatch-recognition proteins. This consequently leads to interruption of

DNA MMR and the proliferation of cells that have damaged DNA, potentially causing genetic instability (Ortega *et al.*, 2015). The perturbation of EGF by the aspirins was also observed when a time-lapse assay over a 60 min period using confocal live imaging was adopted **(Screen shots in Figure 8.22 and Movies on DVD)**. It has thus been discovered that aspirin and its analogues do prevent the translocation of EGF from the surface of the cell membrane towards the nucleus, which implies that these compounds may have the ability to promote genetic stability in cancer as they will prevent inaccuracy in DNA replication and thus prevent tumour progression. This correlates with observed increase in the expression of hMLH1, hPMS2, hMSH2 and hMSH6 DNA MMR proteins in CRC cell lines (SW480, HCT116, HCT+chr3) after treatment with aspirin (Goel *et al.*, 2003).

Furthermore, the results show that the aspirin analogues do affect phosphorylation at Tyr1068, in that the thioaspirins, PN590, PN591 and PN592 decrease phosphorylation at Y1068 while the aspirins and ‘diaspirins’ caused an increase in phosphorylation at Y1068 **(Figure 6.23)**, which might suggest that binding of GRB2 to the docking site is regulated, thus could lead to the regulation of EGF-induced Ras/MAPK activation and the signalling pathway altogether. This agrees with published data which shows that in CRC cell lines with high basal EGFR phosphorylation at the Y1068 site correlated with synergistic effects when oxaliplatin and gefitinib were used in combination in that particular cell line and low basal pY1068 was related to antagonistic effects between these compounds (Van Schaeybroeck *et al.*, 2005). It has also been

found that the thioaspirins did not exhibit synergistic effect in SW480 CRC cells at ED_{50} with oxaliplatin **(Table 4.6)**. Thus, an increase in phosphorylation at Y1068 by the aspirins and 'diaspirins' encouraged synergistic effects when combined with oxaliplatin. Nevertheless, further studies will be needed to see the particular effects these compounds have on what particular protein in the EGFR downstream signalling pathway.

The phosphorylated Y1045 is able to bind to Cbl, which eventually leads to endocytosis of the receptor (Levkowitz *et al.*, 1998). These aspirin analogues with the exception of PN502, PN548 and PN549 decreased phosphorylation at this docking site, thus assumed to lead to the perturbation of EGF internalization seen in the qualitative ICC assay. This will eventually affect repetition of signalling **(Figures 6.6 to 6.13)**.

It was observed that EGF did not co-localise with EEA1 even after stimulation in SW480 cells **(Figure 6.6D, 6.10D and 6.13D)**, which suggests that the receptor may have not been delivered into the endosomes. Previous studies have demonstrated that P53 is involved in the production and regulation of endosomes and exosomes responsible for sorting of receptors either for recycling or degradation (Sun *et al.*, 2016, Yu *et al.*, 2006, Yu *et al.*, 2009) and SW480 CRC cells harbour a mutated *TP53* (Din *et al.*, 2010), which could mean that there is a disruption in the regulation of these endosomes, thus, the absence of co-localization of EGF with EEA1. Nevertheless, PN517, a diaspirin **(Figure 6.8F, 6.11F and 6.13H)** seems to have restored the regulation of the endosomes for it forced the co-localization of EGF and EEA1. PN590, a thioaspirin **(Figure 6.7F and 6.10H)** also slightly forced some EGF to co-

localize with the EEA1. The possible regulation of endosomes by these aspirin analogues may be due partly to the parent drug and partly to the salicylate moiety because salicylic acid **(Figure 6.12F and 6.13J)** also forced EGF to co-localise with EEA1. In addition, it has been found out that these aspirin analogues rather quickly breakdown into their precursor salicylate **(Figure 3.13)**.

A previous study has found PN508 (diaspin) and PN517 (fumaryldiaspirin) referred to as DiA and F-DiA respectively to inhibit the stimulation of NFκB in a number of CRC cell lines (Claudius *et al.*, 2014) and in this study it was found out that these aspirin analogues also perturbed internalization of the EGFR and some decreased phosphorylation at Y1045 and Y1173 **(Figure 6.23).** Endogenous EGF as a ligand to the EGFR has been reported to be involved in wound healing process (Schultz *et al.*, 1991, Werner and Grose, 2003) and its inhibition by aspirin via disruption of the hydrophobic surface in mucosal cell membrane (Barrett *et al.*, 2012), thus leading to unhindered spreading of gastric acid and eventually GI toxicity (Lichtenberger *et al.*, 2006, Lichtenberger *et al.*, 2012, Pereira-Leite *et al.*, 2013), which in cancer cell membranes could also cause perturbation of the lipid membrane layer (Alsop *et al.*, 2015) leading to disruption of EGF internalization. This disruption in the lipid bilayer arrangement of EGFR membrane, will surely also disrupt the cascade of signalling pathways. EGFR activates NFκB in a number of cancers (Jorissen *et al.*, 2003, Shostak and Chariot, 2015) such as in A431 cells when stimulated by EGF (Sun and Carpenter, 1998) via phosphorylation of IκBα and degradation thus rendering it incapable of masking NFκB nuclear signals, which ultimately results in nuclear

translocation of NFκB followed by a series of proliferative signals (Beg *et al.*, 1992, Cautain *et al.*, 2015, Habib *et al.*, 2001). This interplay between EGFR and NFκB is as a result of the hyperactivation of NFκB in cells that overexpress EGFR (Lehman et al., 2017), which is found in most CRC cell lines (Spano *et al.*, 2005). EGFR has also been found to activate NFκB in cultured rat aortic smooth muscle cells (Obata *et al.*, 1996), in a number of oestrogen receptor-negative breast cancer cell lines (Biswas *et al.*, 2000) and also results in the promotion of lung carcinogenesis (Saxon *et al.*, 2016). The effect of these aspirin analogues on the EGFR is thus beneficial in cancer therapy. With this in mind, the mechanism of action for these aspirin analogues cannot be concluded until further studies are carried out on the effects to the downstream EGFR signalling pathway. Although PN590 has been found to have cytotoxic and synergy effects with platinum compounds in SW480 cell line, the potential of this compound as an anti cancer compound is let down by its ability to cause nuclear co-localization of β-catenin when dissolved in DMSO **(Figure 5.14B)**, however, this effect is not seen when dissolved in acetone **(Figure 5.14D)**. Thus, dissolution of PN590 in DMSO should be avoided.

Clearly, there are limitations to some of the experimental designs in this study. There is therefore an awareness that further work need to be carried out in order for a conclusion to be drawn. Having said this, more light has been shed on how aspirin and its analogues act in SW480, OE33 and FLO1 cancer cell lines and it is believed that there is hope for these aspirin analogues to be adapted as a more affordable, less toxic therapy for the prevention, treatment and management of cancer.

7.2 Future Studies

Radioligand binding of the EGFR with EGF could act as an assay that will show clearly whether these aspirins act as antagonists by measuring the amount of EGF still bound to the receptor after treatment with aspirin analogues as compared to the amount of bound EGF without treatment with the aspirin analogues.

In this study, it has been shown that aspirin analogues perturb EGF internalization. Could these aspirin analogues then be blocking the clarithrin-dependent pathway in order to mediate degradation of the EGFR by delivering the receptor to the lysosomes? In addition, do PN517, PN590 and salicylic acid promote delivery of EGFR into late endosomes (Rab7 and Lamp2) for degradation or with Rab4 and Rab11, recycling endosome markers, remains open (Flores-Rodriguez *et al.*, 2015, Zerial and McBride, 2001). In other words, do these compounds drive co-localization of EGF with Rab7, Lamp2, Rab4 or Rab11?

These aspirin analogues have been found out to perturb EGF internalization in SW480 cancer cell lines. Could this effect extend to colonocytes from healthy colon tissues?

The phosphorylation of PCNA by EGFR interferes with its interaction with mismatch-recognition proteins MutSα and MutSβ, which leads to the deactivation of DNA mismatch repair (MMR) process (Ortega *et al.*, 2015). Can aspirin and its analogues promote genome stability in cancer by inhibiting the phosphorylation of PCNA when the internalization of EGFR is perturbed?

Do aspirin analogues deregulate NFκB by inhibiting the phosphorylation of IκB alpha at serine 32 and 36 (Habib *et al.*, 2001) in order to prevent its nuclear localization and stop transcription?

Western blot analysis can be used to find out if these compounds interfere with Akt expression and also interfere with phosho-Akt? Data from this analysis could conclude if these compounds have a downstream effect on the EGFR signalling pathway. Another indication of these compounds having a downstream effect on the EGFR signalling pathway is if they have an effect on Stat-3 and phosphor-Stat-3; Stat-5 and phosphor-Stat-5 (Schindler and Darnell, 1995).

For the EGFR phosphorylation experiments using western blot analysis, the receptor was stimulated using 200 ng/ml of EGF. This dose of EGF is now understood to be too high and should be substituted with 20 ng/ml in future experiments.

Is there any link between phosphorylation of EGFR at Y1045, Y1173 and clarithrin? This could be pursued by comparing the levels of phosphorylation of the EGFR at Y1045, Y1173 with levels of clarithrin when treated with these aspirin analogues.

TNF (tumour necrosis factor) regulates proliferation of the intestinal cell line in mice, which is due to downregulation of EGF-dependent EGFR activation (Kaiser and Polk, 1997). Is there a relationship between these aspirin analogues and TNF?

Elevated Akt and STATs signalling are found in cell lines with mutated EGFR (Sordella *et al.*, 2004). An increase in the expression of Akt is also associated

with increase in p21 expression (Karimian *et al.*, 2016). Thus the study of the expression of Akt and STATs in SW480 CRC cell line together with the effect aspirin analogues will have on the expression of Akt and STAT could be beneficial because it shows that this particular cell line may not be responsive to standard therapy. This information could be added to the findings in this study of aspirin (PN502), PN590, PN591 and PN592 decreasing p21 expression **(Figure 5.3)**. Furthermore, cytoplasmic p21 promotes survival by inhibiting apoptosis (Dehennaut *et al.*, 2013). For example, cytoplasmic localization of p21 in testicular cancer cells has been found to safeguard cells from apoptosis caused by cisplatin (Karimian *et al.*, 2016). Immunocytochemistry (ICC) can be used to find out if increases in p21 expression via western blot correlates with p21 expression in the cytoplasmic region of the cells and whether treatment with these compounds cause any changes.

To further study the effects of these aspirin analogues on p21 expression and its effect on apoptosis, the effect of these aspirin analogues on the expression of p53 as a tumour suppressor alongside p21 on SW480 CRC cell line and other cancer cell lines without *TP53* mutations should be investigated. The results could be compared against normal/healthy cell lines. A non-adherent cell line or alternative methods to harvest adherent cells should also be included. For example, the use of RNase A, which enables the removal of cytoplasmic RNA and thus eliminates any false necrotic values due to PI staining (Rieger *et al.*, 2011) could be added to the protocol.

Chapter 8. Appendix

8.1 ^{13}C NMR Spectra for aspirin and its analogues

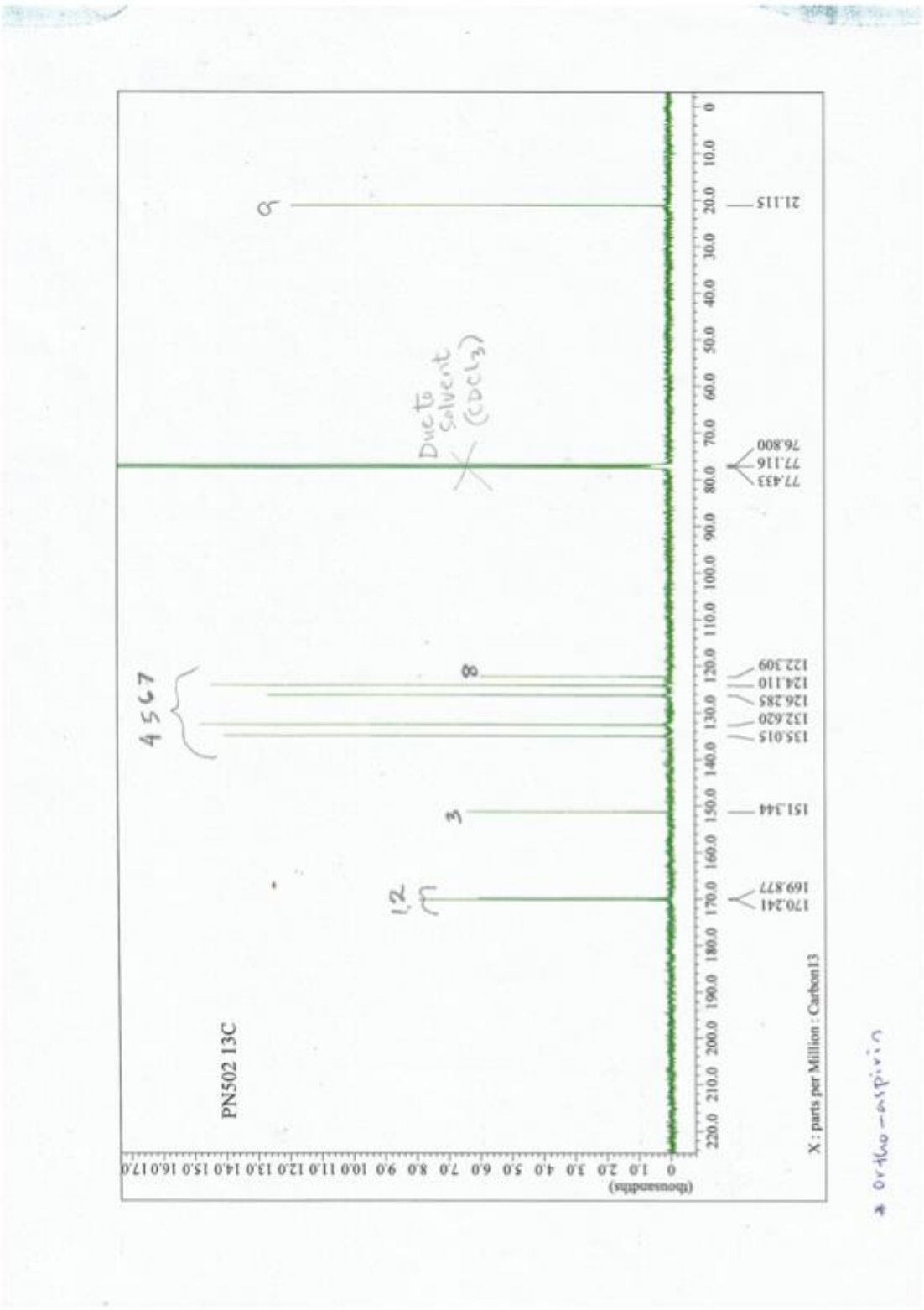

Figure 8.1 ^{13}C NMR spectrum for aspirin (PN502).

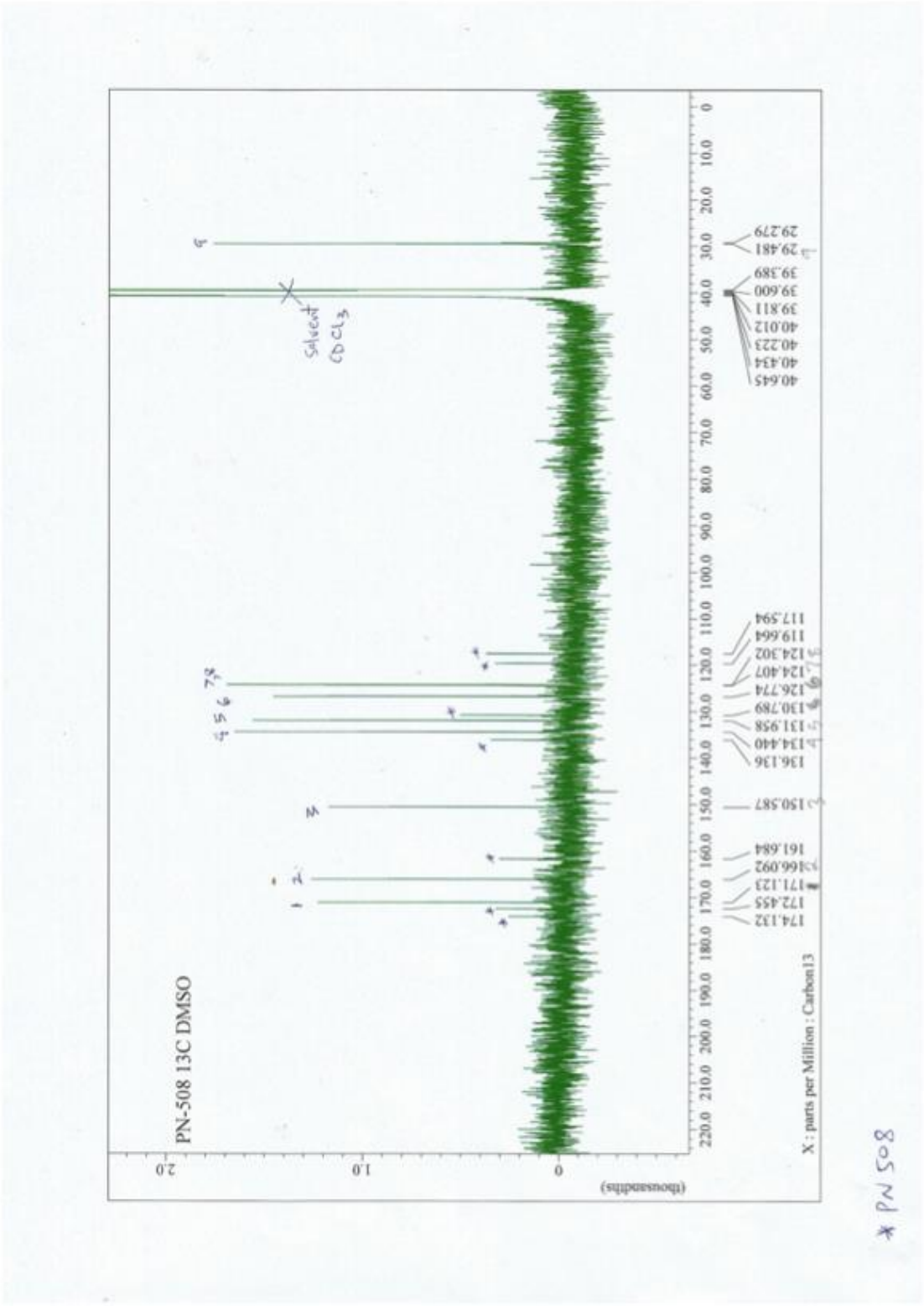

Figure 8.2 ^{13}C NMR spectrum for PN508.

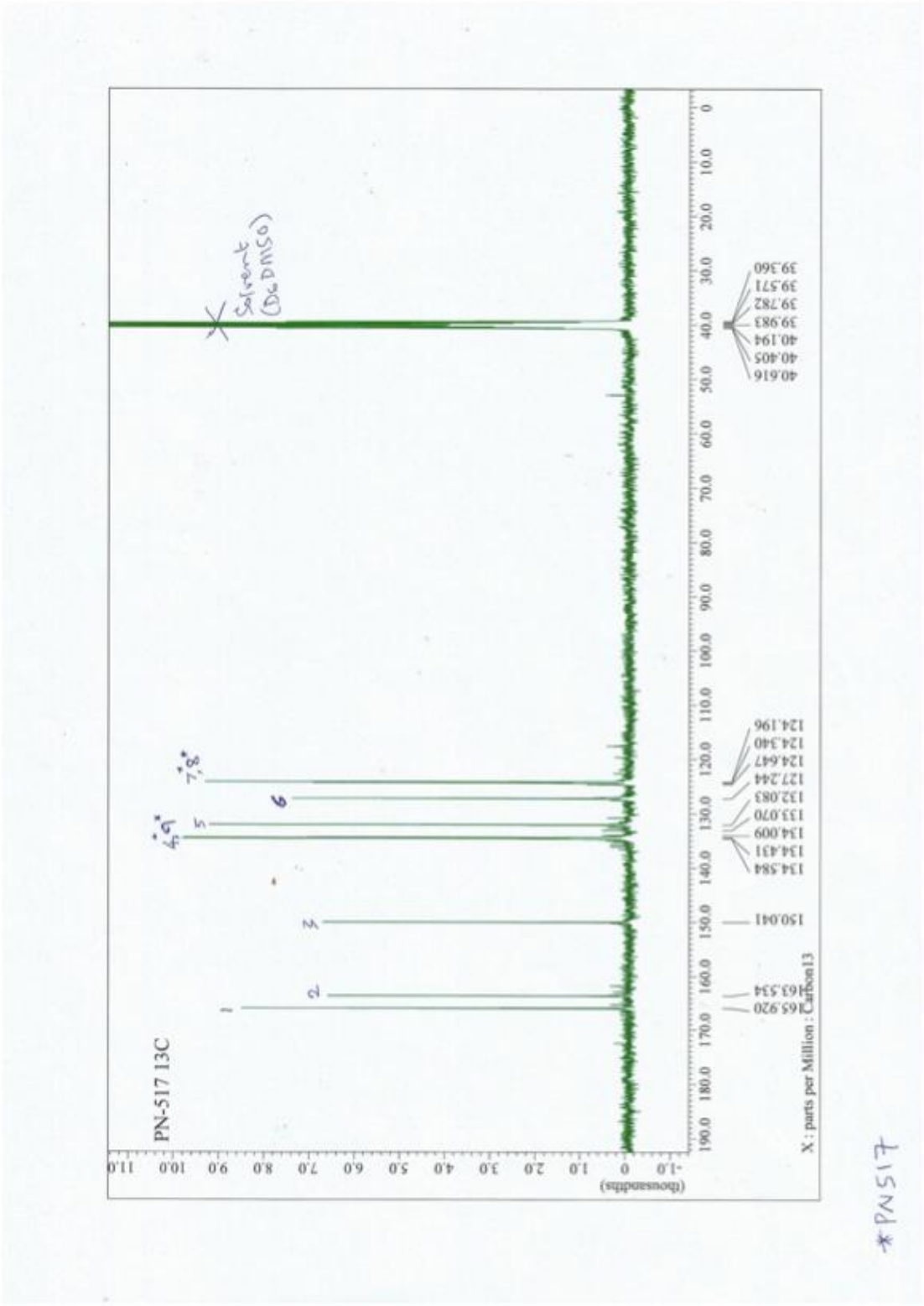

Figure 8.3 ^{13}C NMR spectrum for PN517.

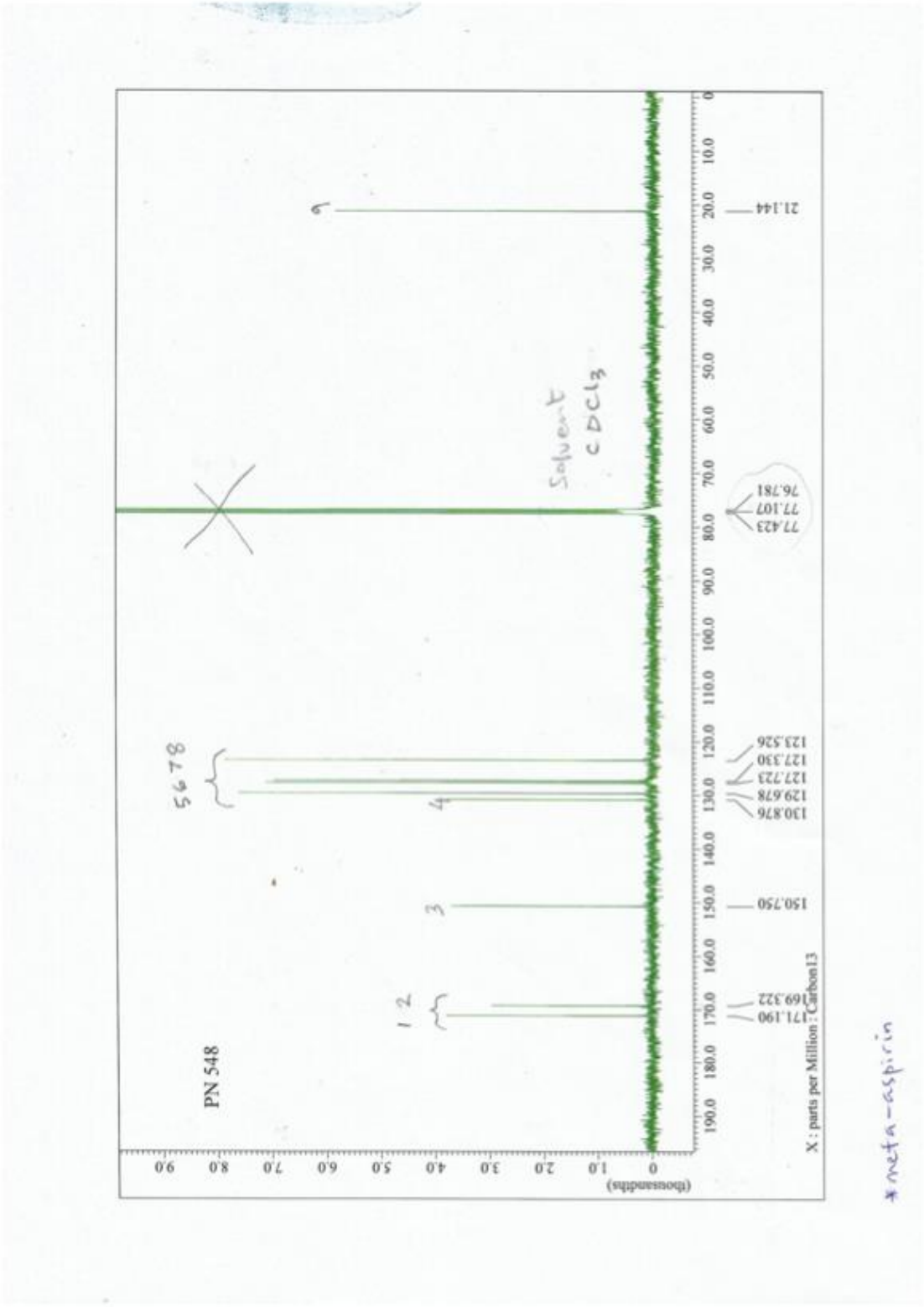

Figure 8.4 ^{13}C NMR spectrum for PN548

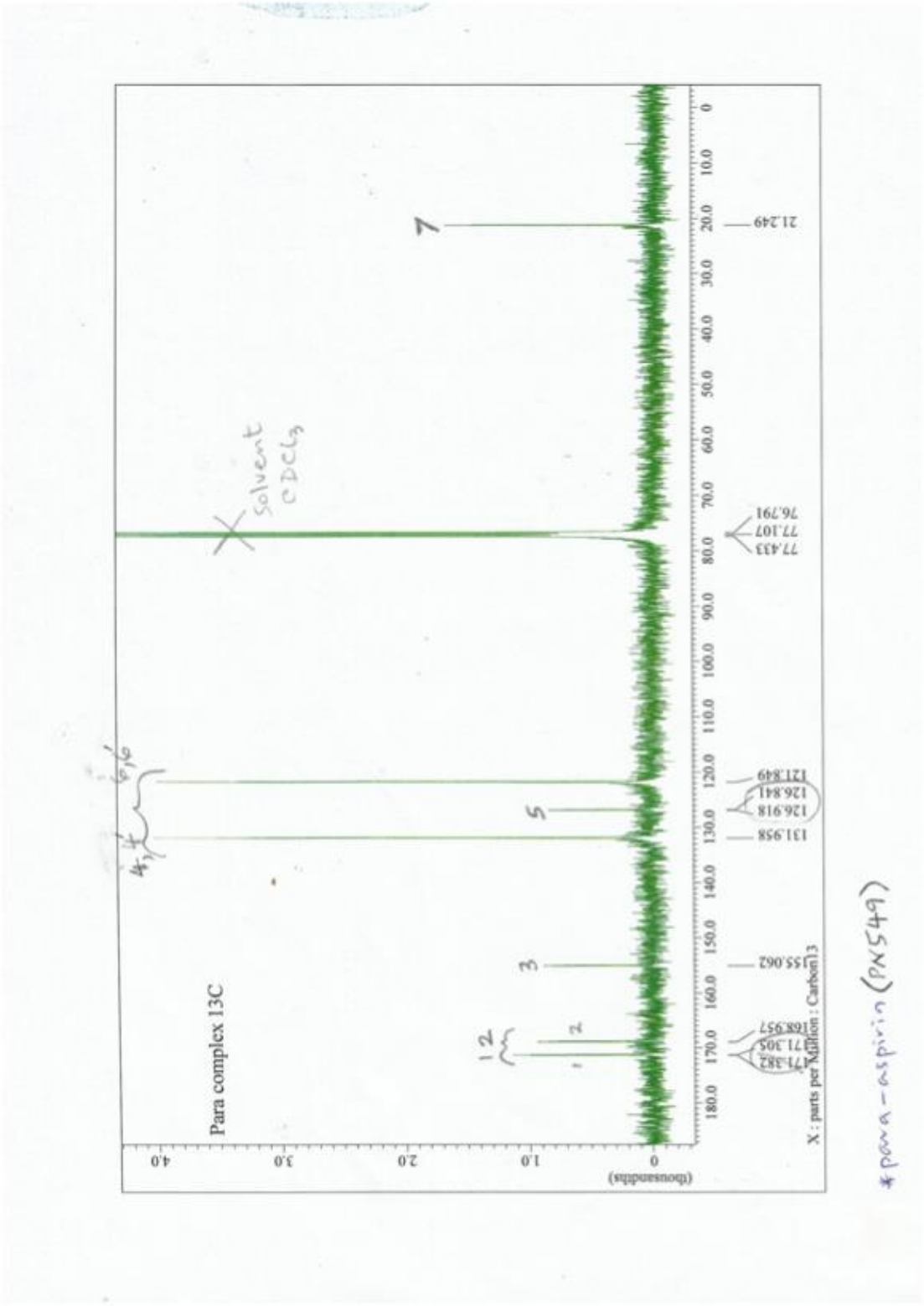

Figure 8.5 ^{13}C NMR spectrum for PN549.

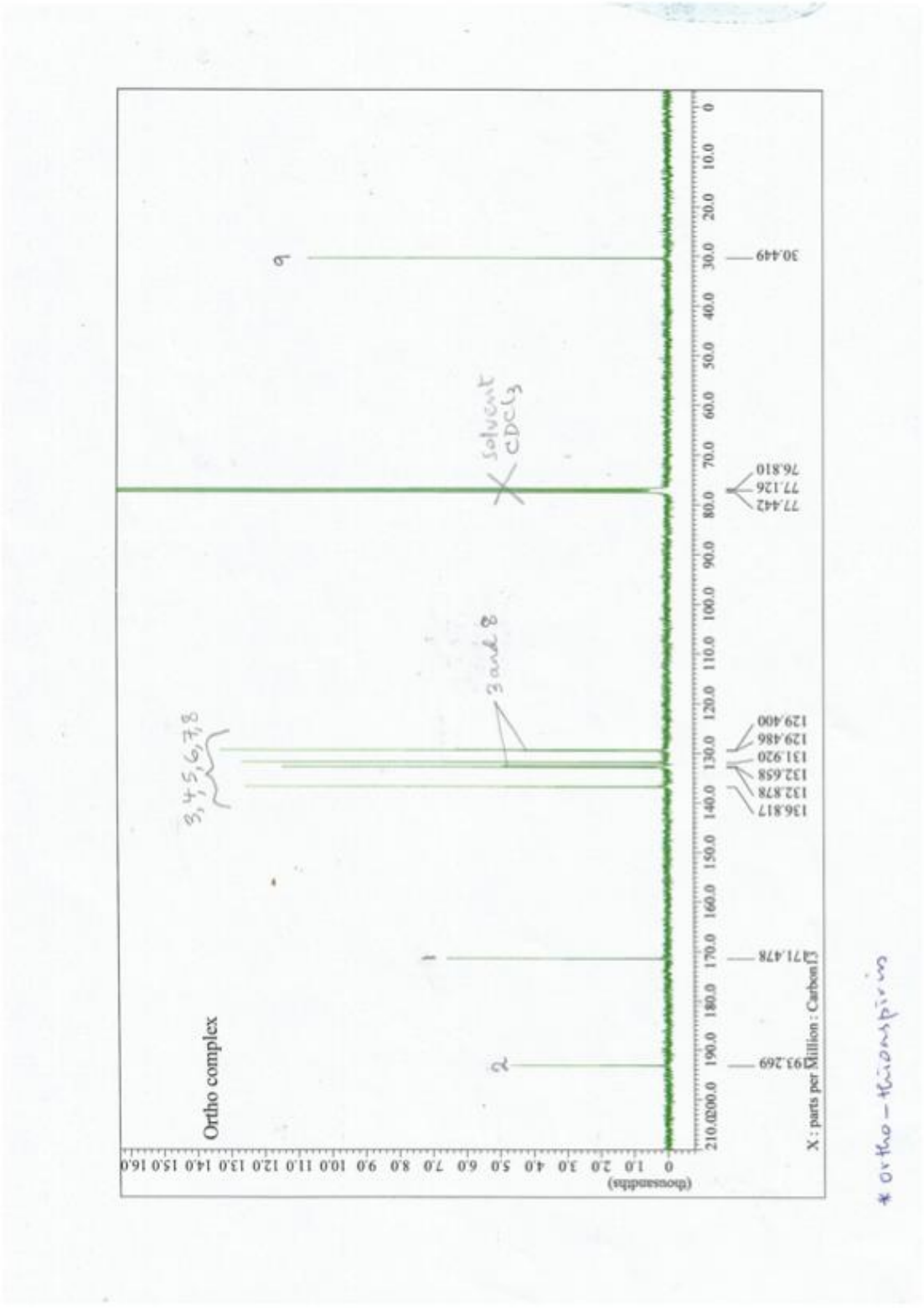

Figure 8.6 ^{13}C NMR spectrum for PN590.

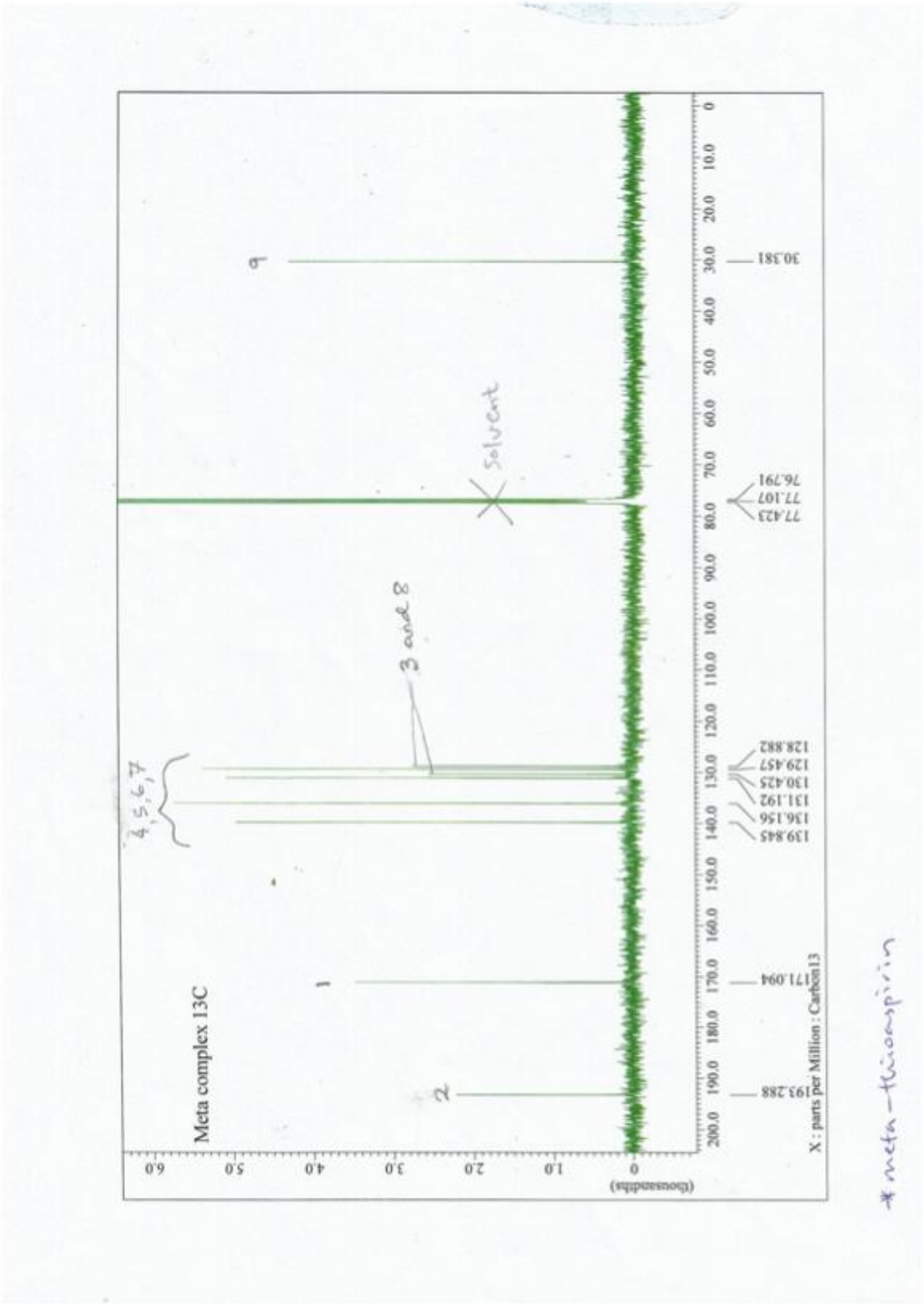

Figure 8.7 ^{13}C NMR spectrum for PN591.

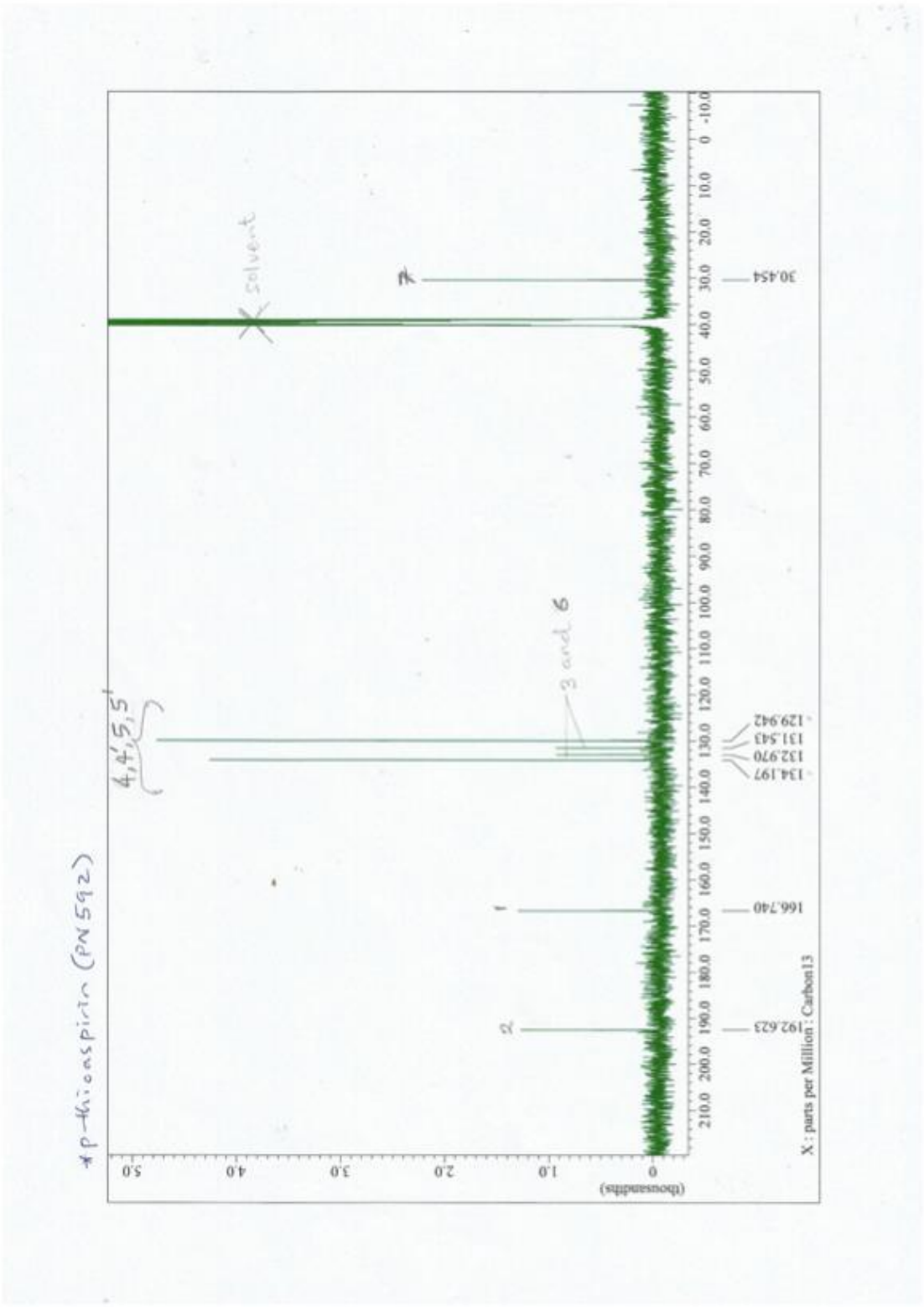

Figure 8.8 ^{13}C NMR spectrum for PN592.

8.2 IR Spectra for aspirin and its analogues

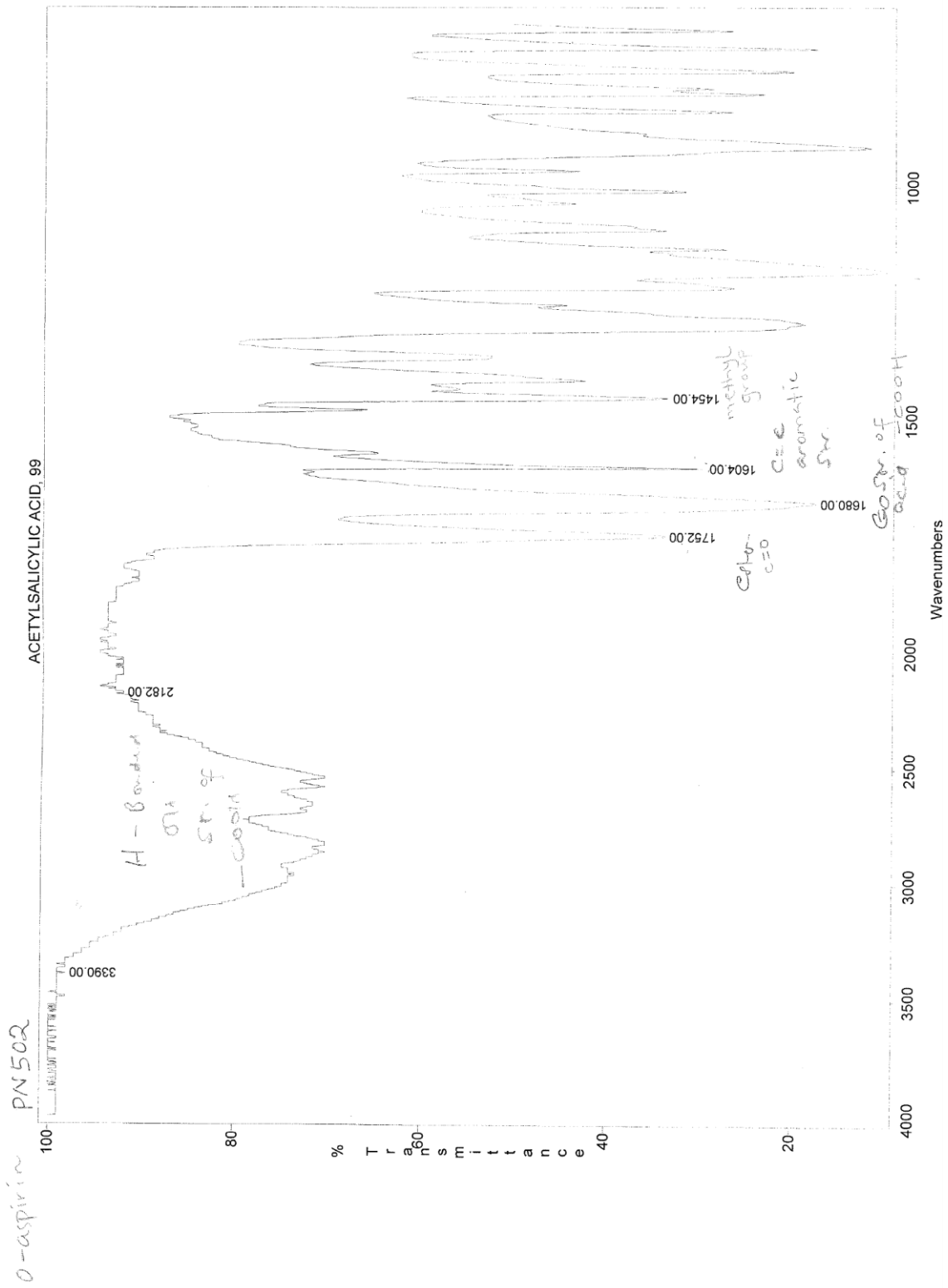

Figure 8.9 IR Spectrum of PN502.

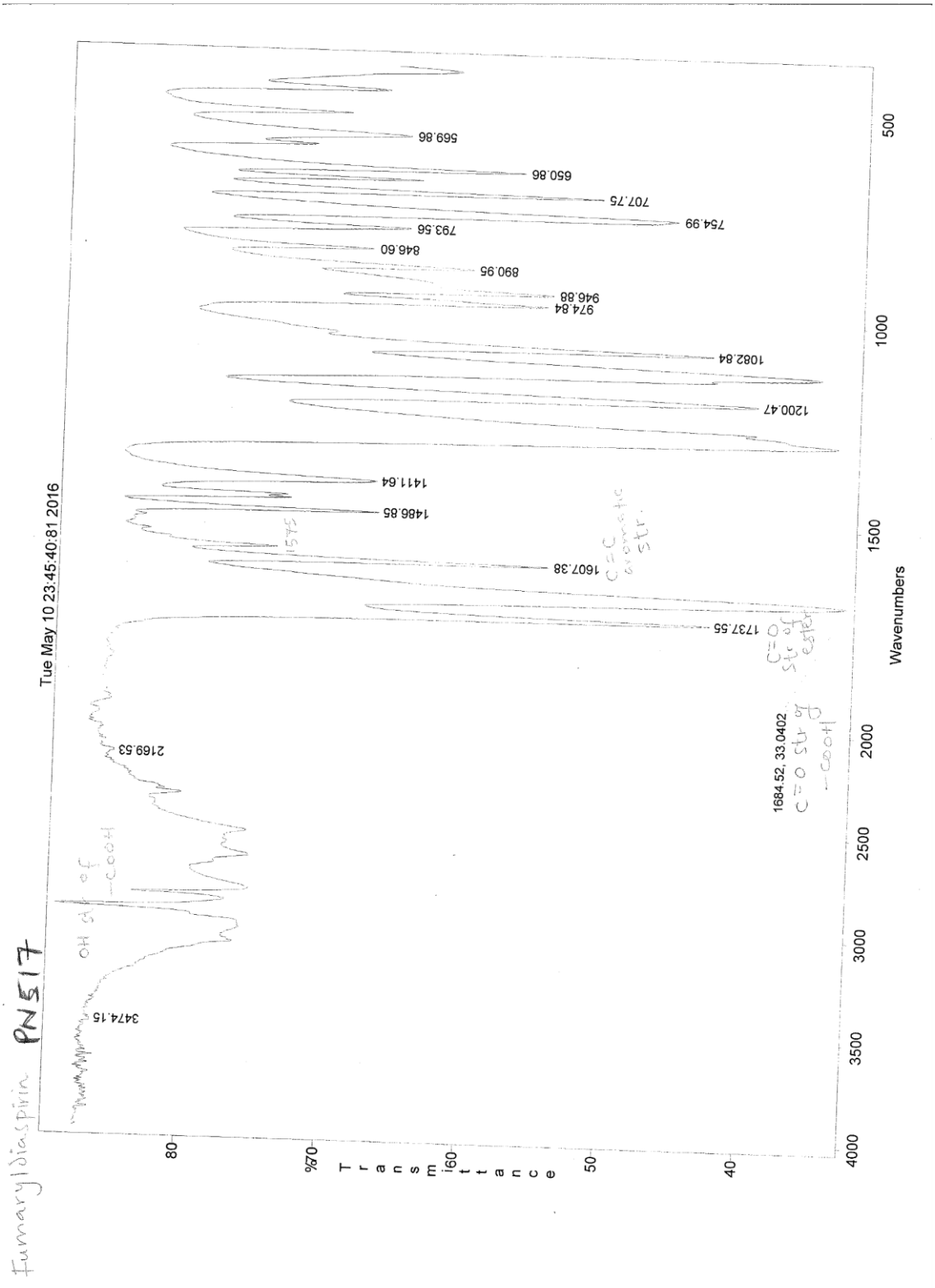

Figure 8.10 IR Spectrum of PN517.

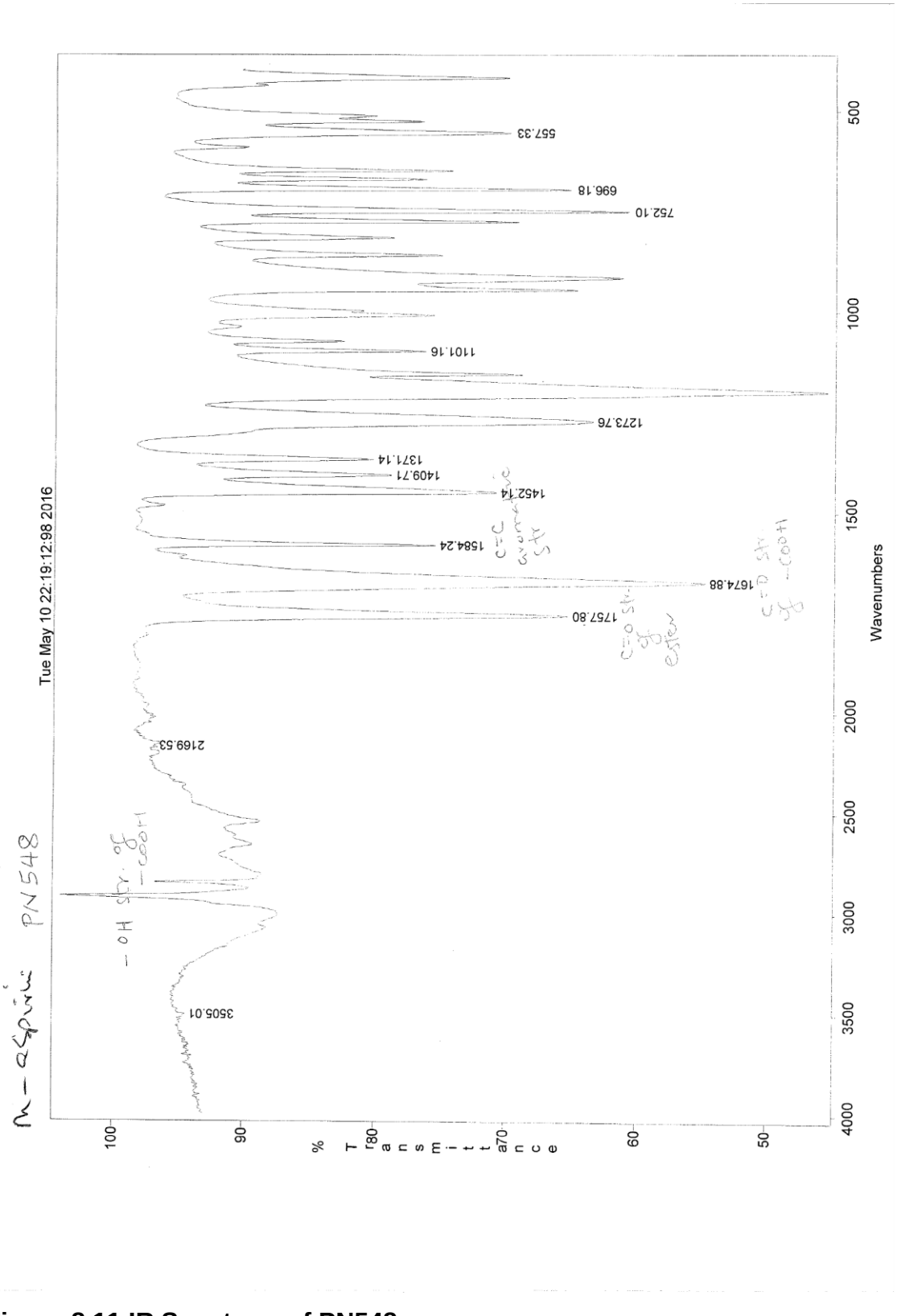

Figure 8.11 IR Spectrum of PN548.

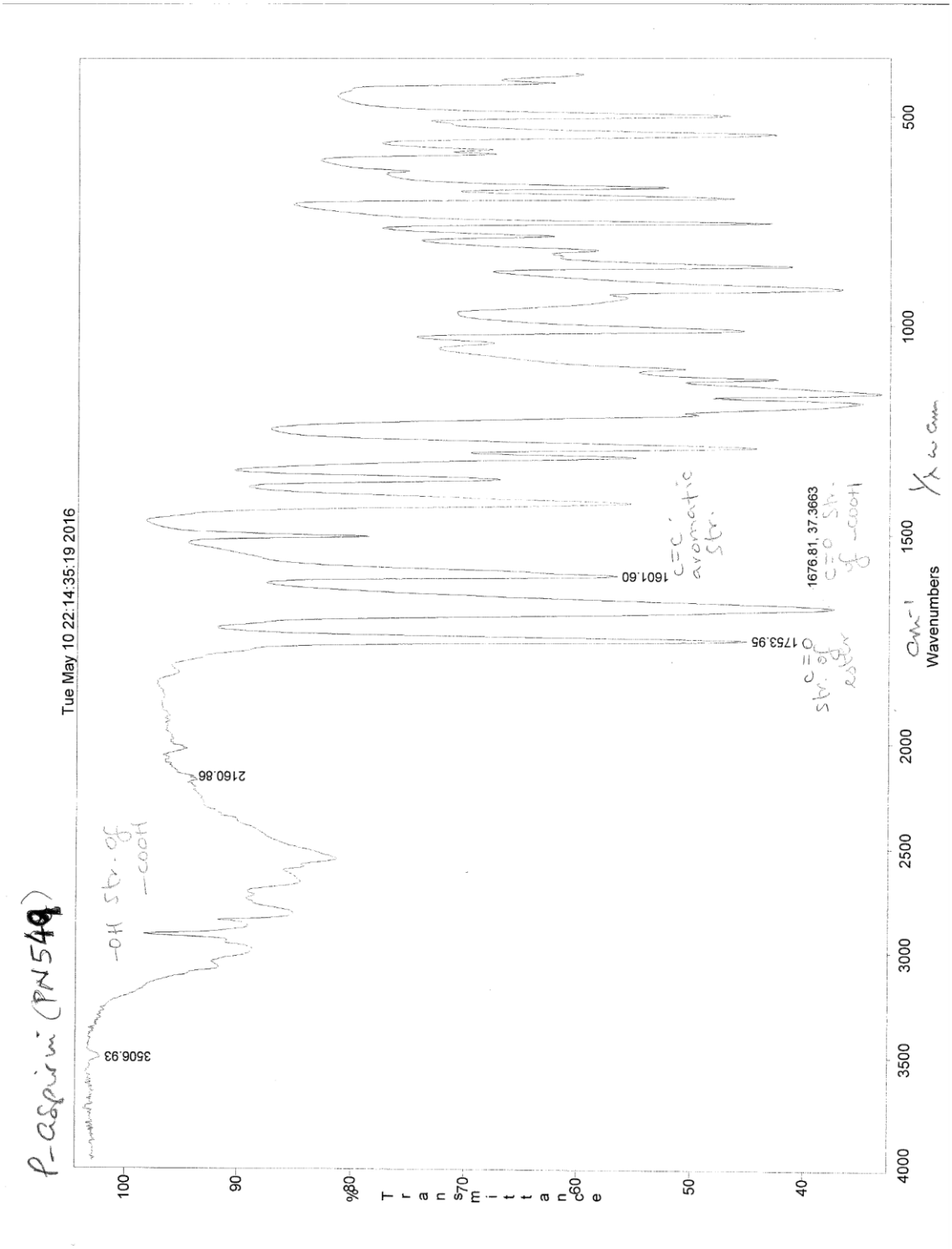

Figure 8.12 IR Spectrum of PN549.

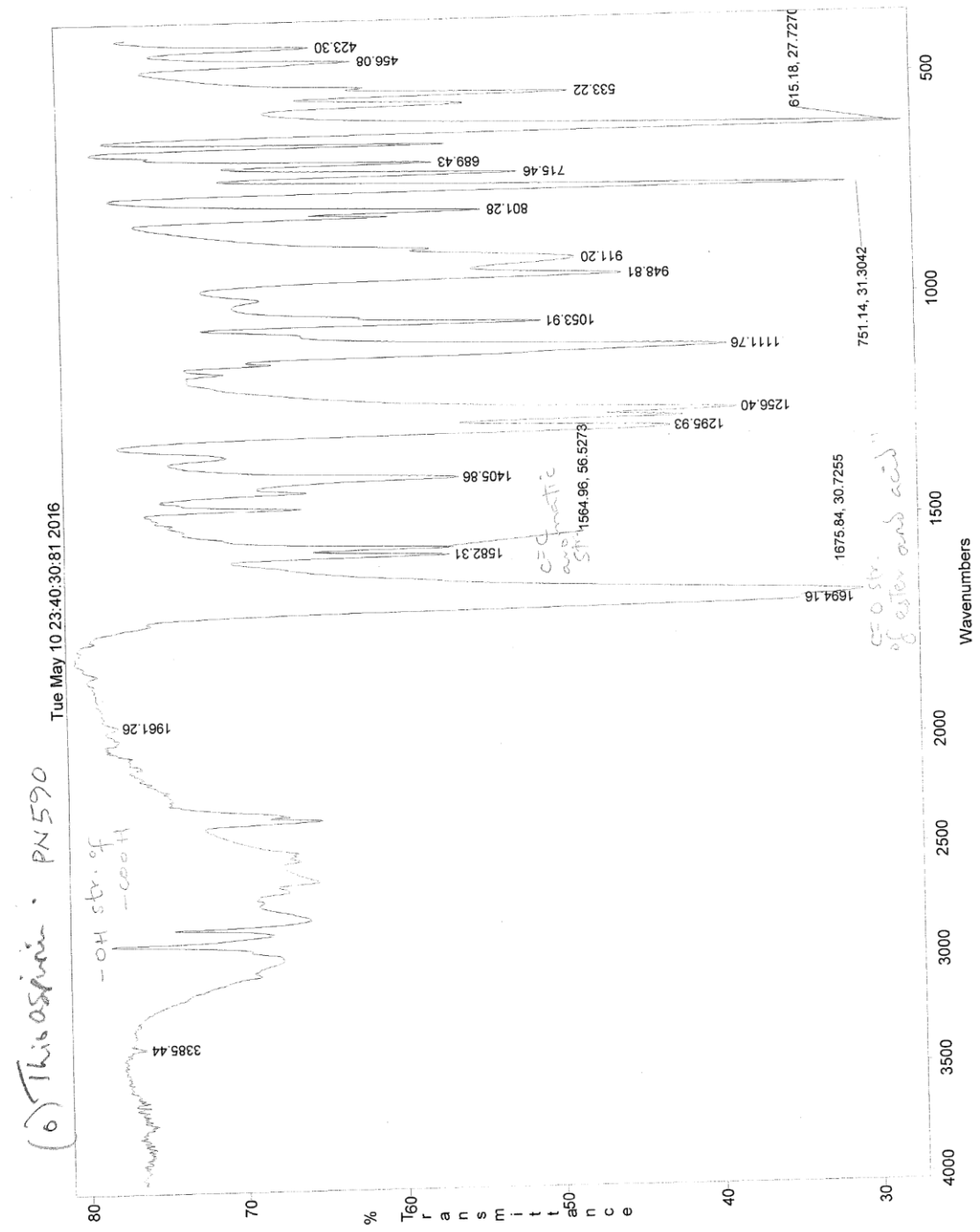

Figure 8.13 IR Spectrum of PN590.

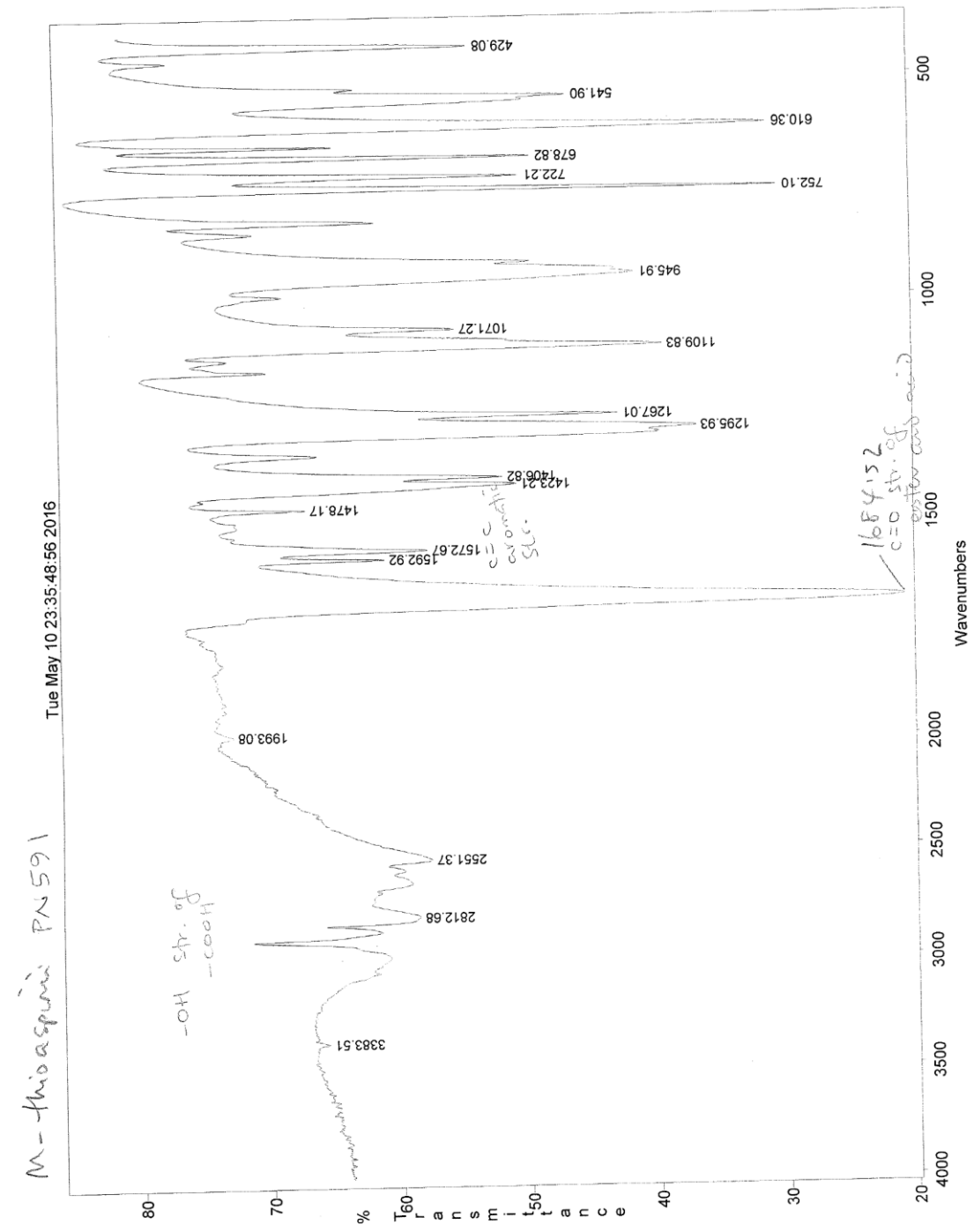

Figure 8.14 IR Spectrum of PN591.

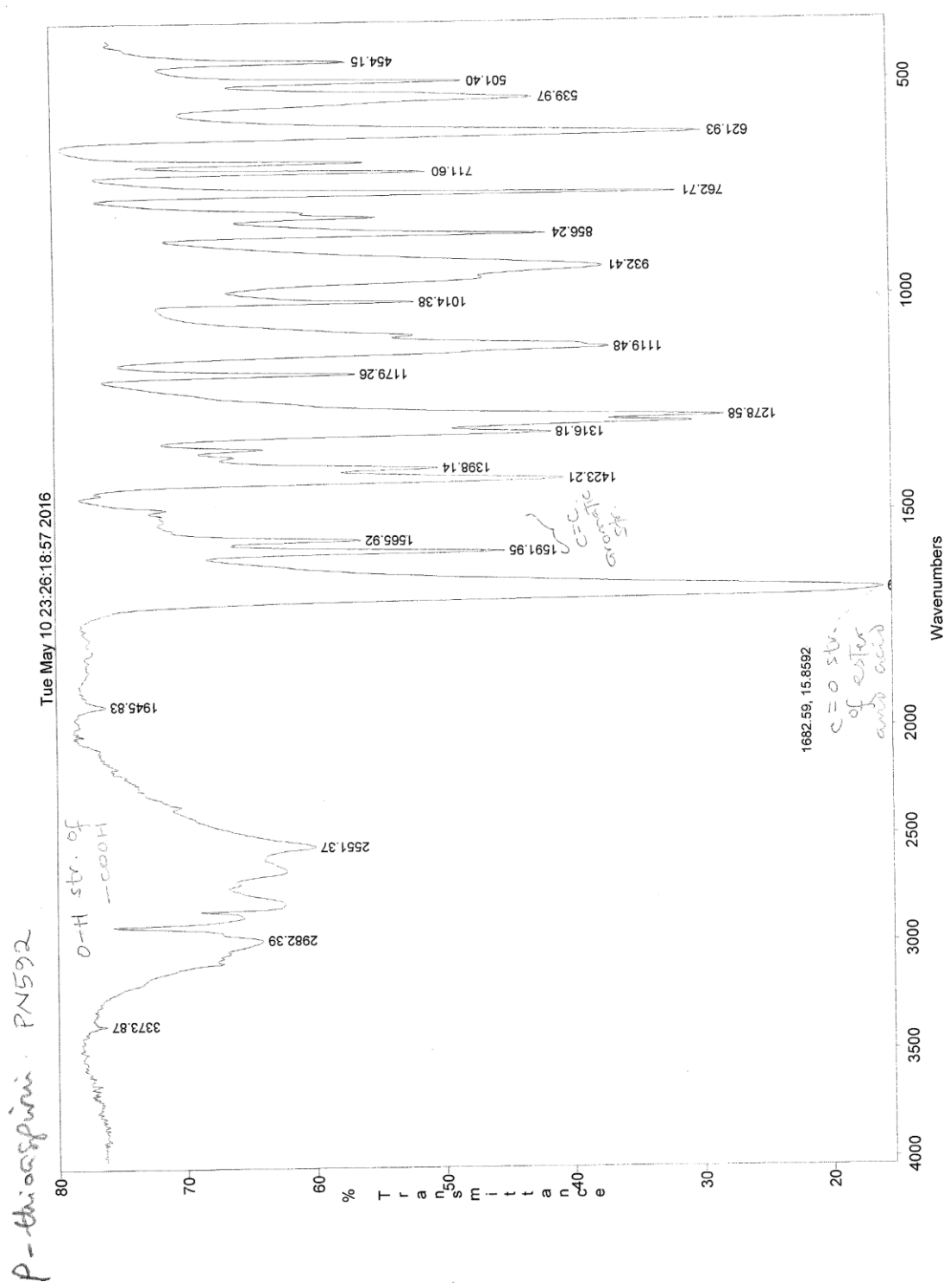

Figure 8.15 IR Spectrum of PN592.

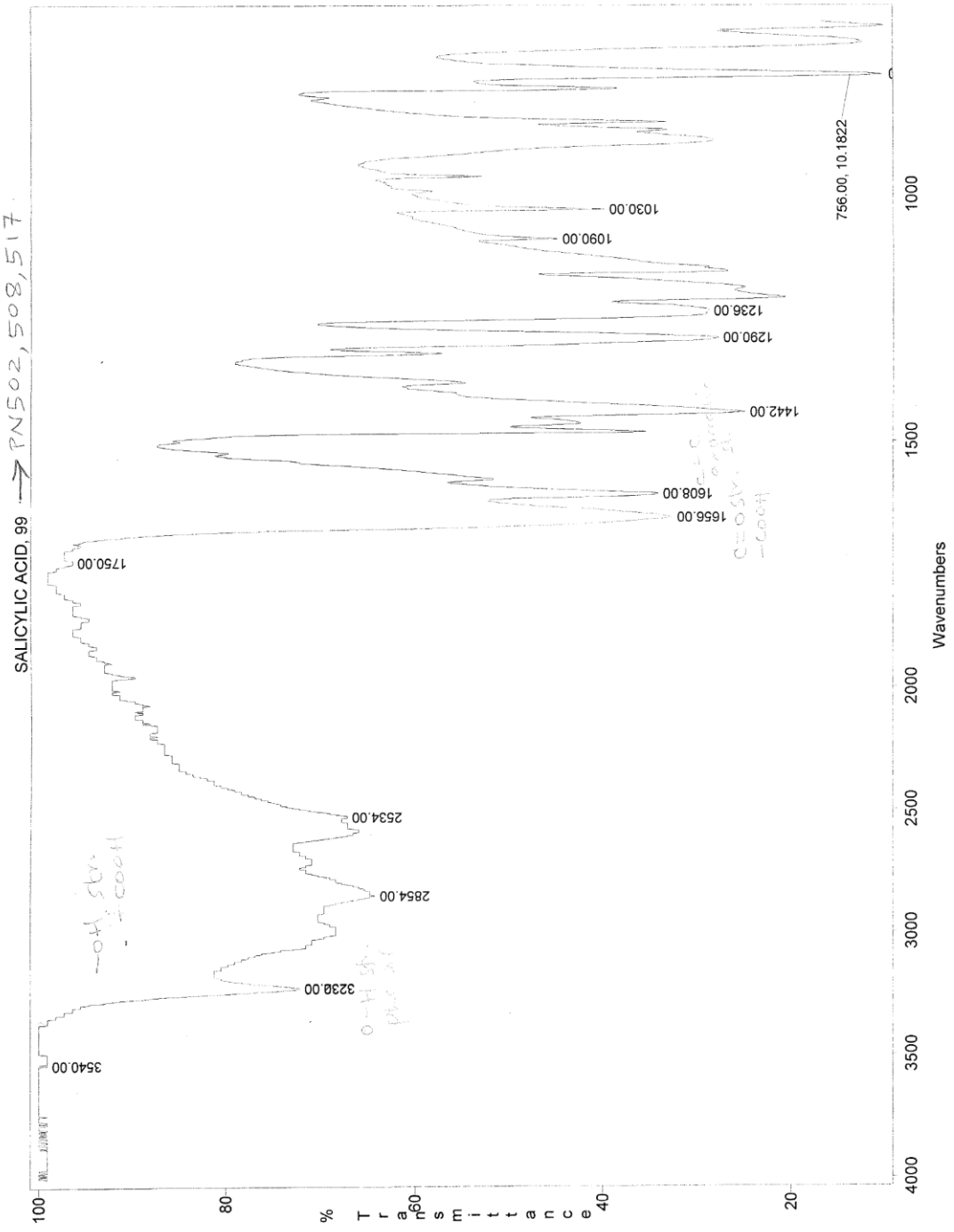

Figure 8.16 IR Spectrum of Salicylic acid.

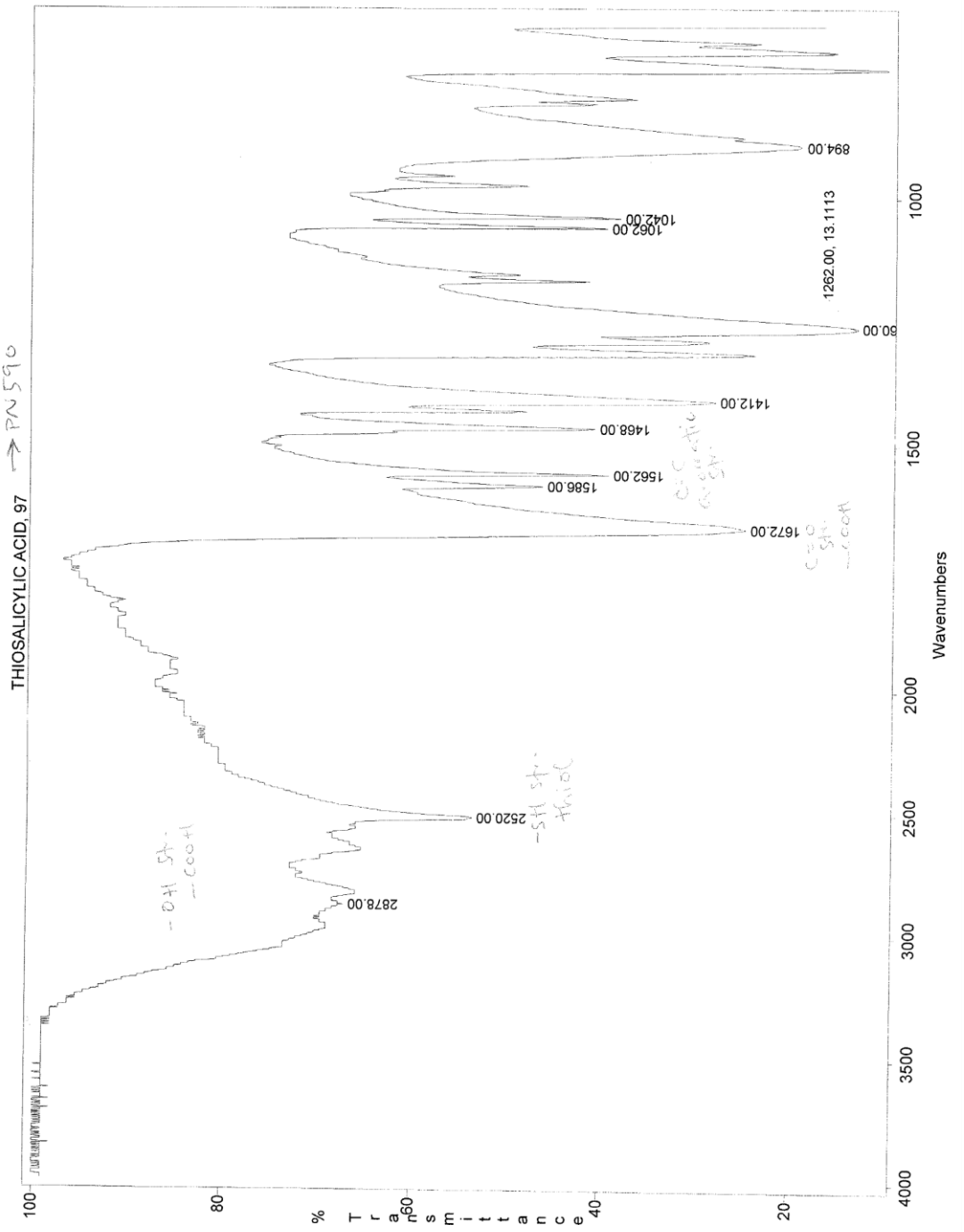

Figure 8.17 IR Spectrum of Thiosalicylic acid.

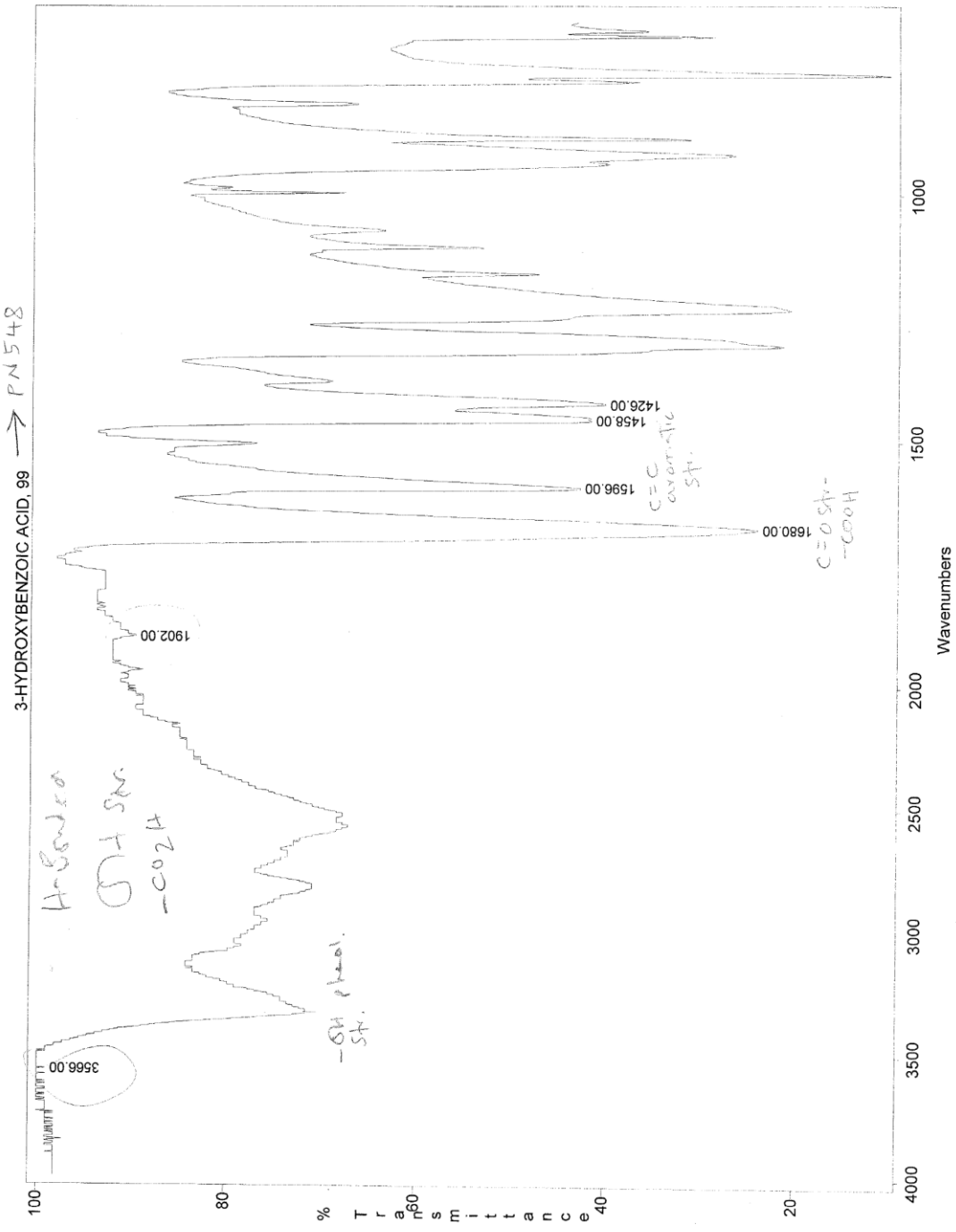

Figure 8.18 IR Spectrum of 3-hydroxybenzoic acid.

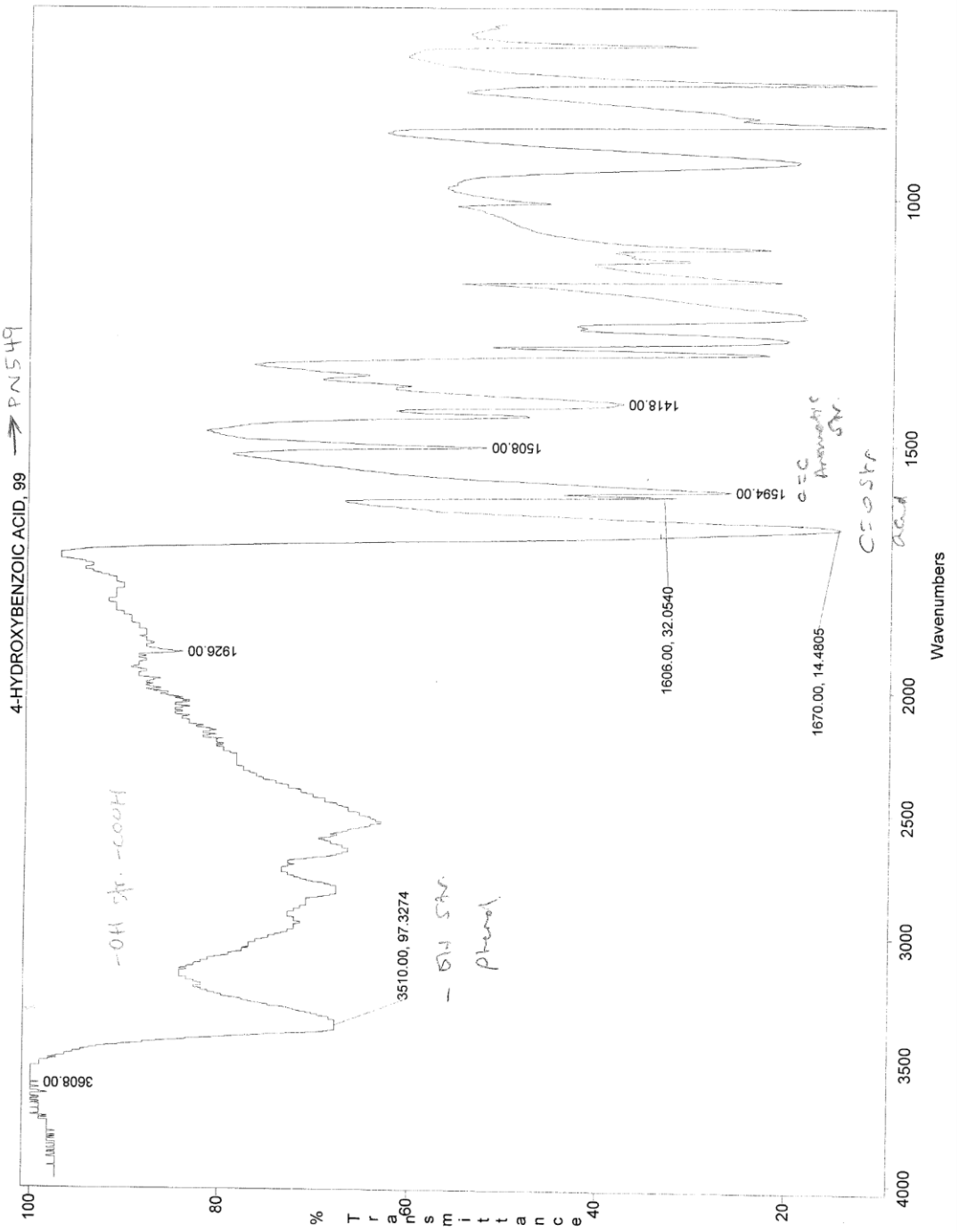

Figure 8.19 IR Spectrum of 4-hydroxybenzoic acid.

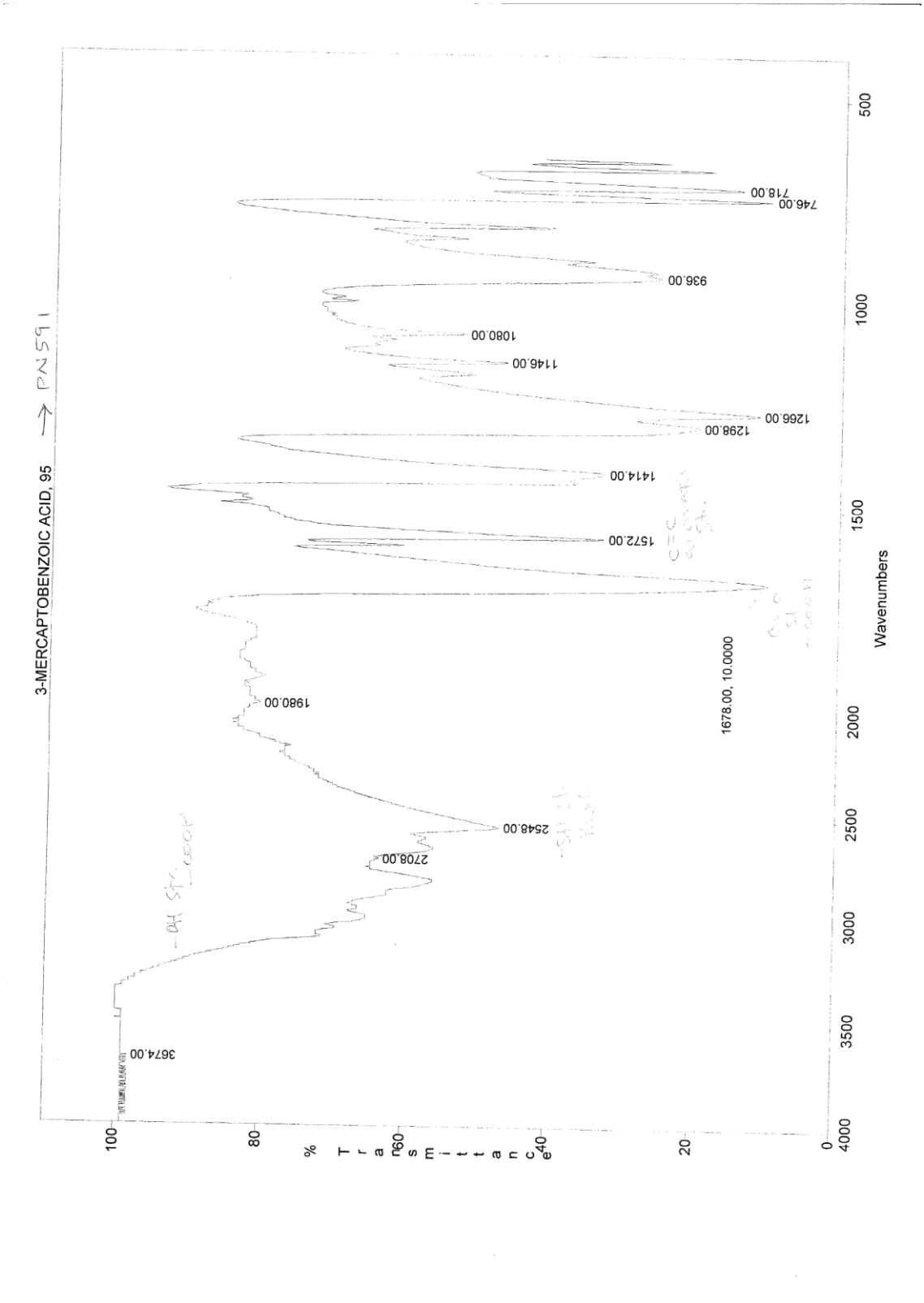

Figure 8.20 IR Spectrum of 3-mercaptobenzoic acid.

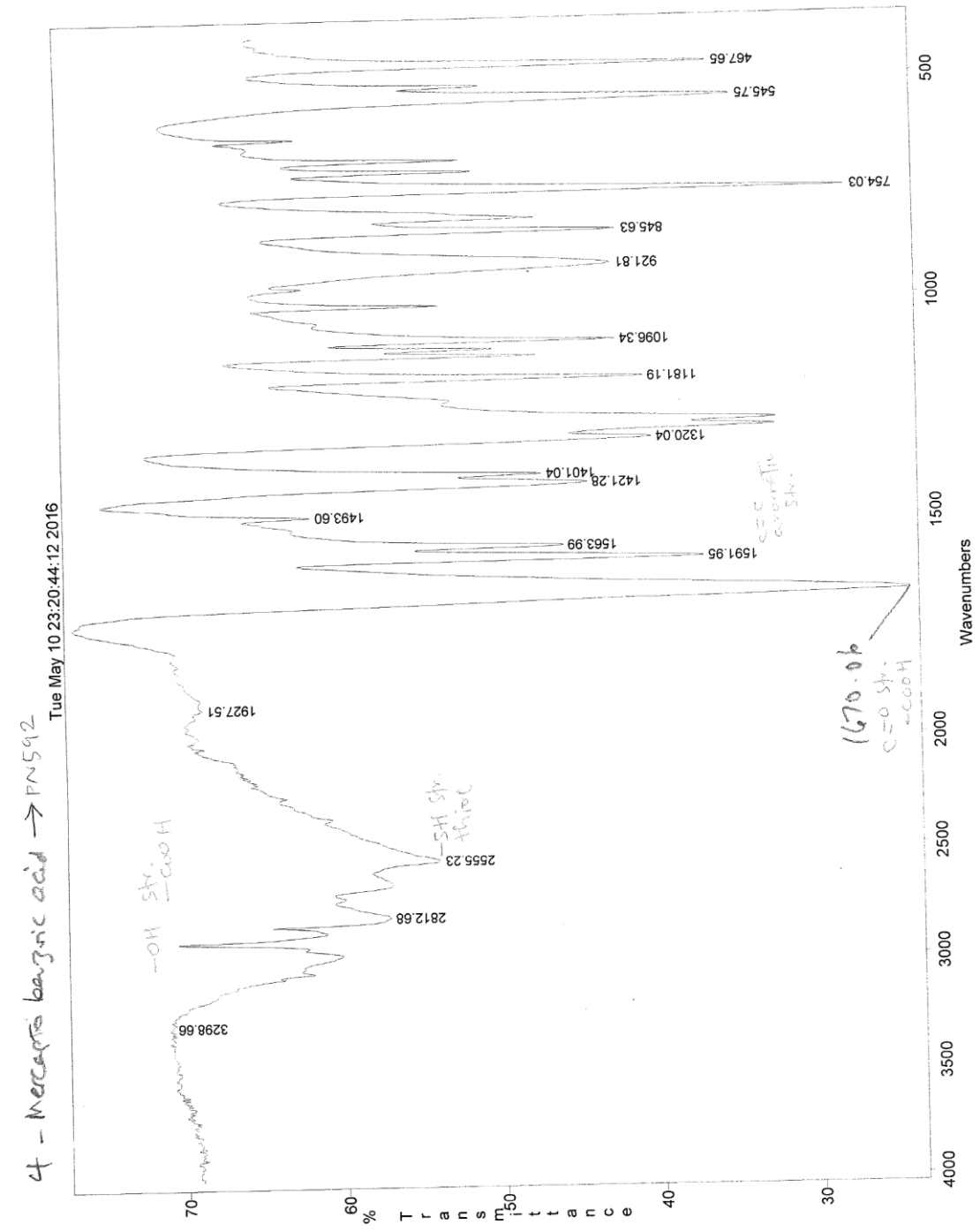

Figure 8.21 IR Spectrum of 4-mercaptobenzoic acid.

8.3 Supplementary: Screen shots and Legend for Live Imaging Movies (on DVD) of EGF in cells incubated with aspirin and aspirin analogue.

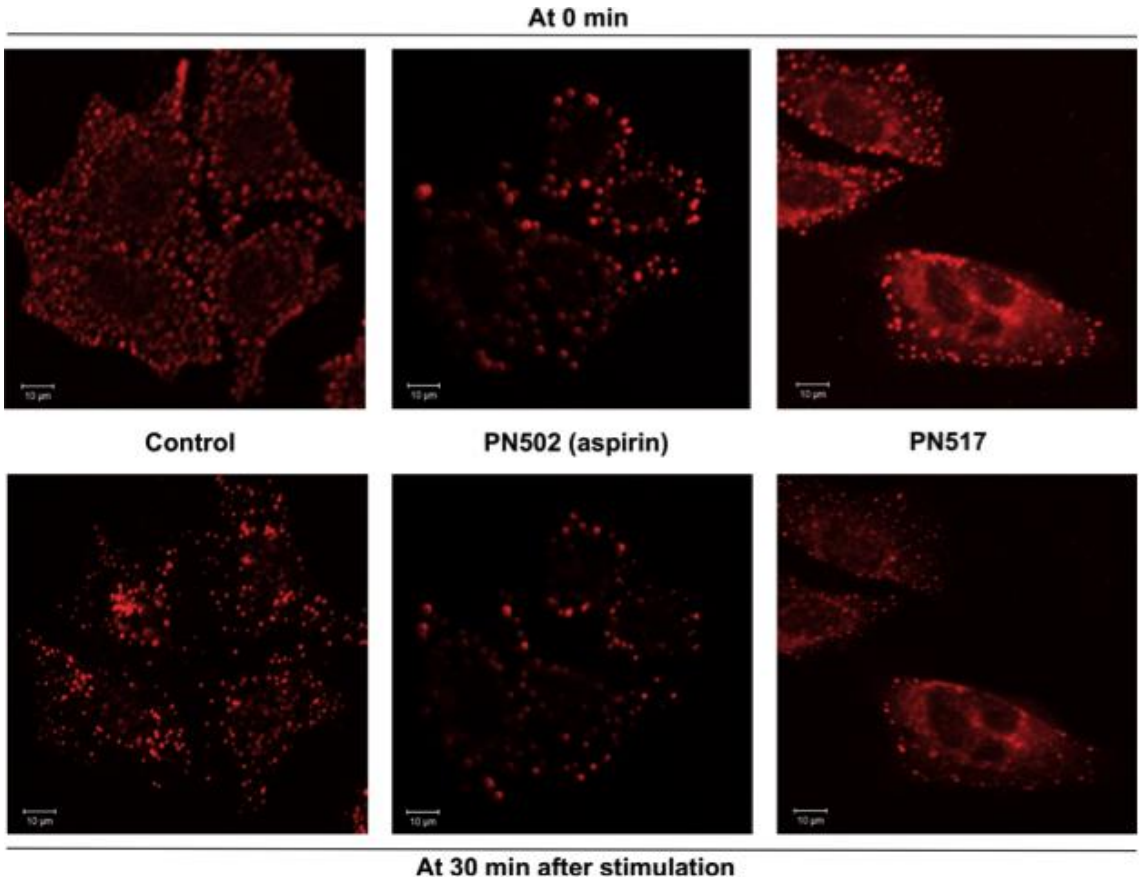

Figure 8.22 Screen shots of Movies showing SW480 CRC cells untreated (control), treated with aspirin and PN517 at 0 min and 30 min after stimulation. EGF was internalized in the untreated cells while internalization was perturbed when cells were treated with 0.5 mM of aspirin and PN517 (Movies are on attached DVD).

Movie 1: Binding and internalisation of EGF control (untreated) in SW480 CRC cell line imaged confocal microscopy uninterruptedly for 60 min. SW40 CRC cells (37°C, 5% CO_2) were exposed to Alexa Fluor® 555 EGF (red). Time series after addition of ligand is 120 cycles at 0.5 min intervals.

Movie 2: Binding and internalisation of EGF after treatment with 0.5 mM aspirin (buffered with HEPES, pH8) for 30 min in SW480 CRC cell line and imaged using confocal microscopy uninterruptedly for 60 min. SW40 CRC cells (37°C, 5% CO_2) were exposed to Alexa Fluor® 555 EGF (red). Time series after addition of ligand is 120 cycles at 0.5 min intervals.
Movie 3: Binding and internalisation of EGF after treatment with 0.5 mM PN517 (buffered with HEPES, pH8) for 30 min in SW480 CRC cell line and imaged using confocal microscopy uninterruptedly for 60 min. SW40 CRC cells (37°C, 5% CO_2) were exposed to Alexa Fluor® 555 EGF (red). Time series after addition of ligand is 120 cycles at 0.5 min intervals.

Reference List

(1992) Modulation of fluorouracil by leucovorin in patients with advanced colorectal cancer: Evidence in terms of response rate. Advanced colorectal cancer meta-analysis project. *J Clin Oncol,* **10**(6)**,** pp. 896-903.

Aaltonen, L.A., Peltomaki, P., Leach, F.S., Sistonen, P., Pylkkanen, L., Mecklin, J.P., Jarvinen, H., Powell, S.M., Jen, J., Hamilton, S.R. and et al. (1993) Clues to the pathogenesis of familial colorectal cancer. *Science,* **260**(5109)**,** pp. 812-816.

Abbas, T. and Dutta, A. (2009) P21 in cancer: Intricate networks and multiple activities. *Nat Rev Cancer,* **9**(6)**,** pp. 400-414.

Adams, J.M. and Cory, S. (1998) The bcl-2 protein family: Arbiters of cell survival. *Science,* **281**(5381)**,** pp. 1322-1326.

Adams, J.M. and Cory, S. (2007) The bcl-2 apoptotic switch in cancer development and therapy. *Oncogene,* **26**(9)**,** pp. 1324-1337.

Ahmed, D., Eide, P.W., Eilertsen, I.A., Danielsen, S.A., Eknaes, M., Hektoen, M., Lind, G.E. and Lothe, R.A. (2013) Epigenetic and genetic features of 24 colon cancer cell lines. *Oncogenesis,* **2**, pp. e71.

Alcindor, T. and Beauger, N. (2011) Oxaliplatin: A review in the era of molecularly targeted therapy. *Curr Oncol,* **18**(1)**,** pp. 18-25.

Algra, A.M. and Rothwell, P.M. (2012) Effects of regular aspirin on long-term cancer incidence and metastasis: A systematic comparison of evidence from observational studies versus randomised trials. *Lancet Oncol,* **13**(5)**,** pp. 518-527.

Ali, R., Baracos, V.E., Sawyer, M.B., Bianchi, L., Roberts, S., Assenat, E., Mollevi, C. and Senesse, P. (2016) Lean body mass as an independent determinant of dose-limiting toxicity and neuropathy in patients with colon cancer treated with folfox regimens. *Cancer Med,* **5**(4)**,** pp. 607-616.

Alroy, I. and Yarden, Y. (1997) The erbb signaling network in embryogenesis and oncogenesis: Signal diversification through combinatorial ligand-receptor interactions. *FEBS Lett,* **410**(1)**,** pp. 83-86.

Alsop, R.J., Toppozini, L., Marquardt, D., Kucerka, N., Harroun, T.A. and Rheinstadter, M.C. (2015) Aspirin inhibits formation of cholesterol rafts in fluid lipid membranes. *Biochim Biophys Acta,* **1848**(3)**,** pp. 805-812.

Alvarado, D., Klein, D.E. and Lemmon, M.A. (2010) Structural basis for negative cooperativity in growth factor binding to an egf receptor. *Cell,* **142**(4)**,** pp. 568-579.

Andre, T., Boni, C., Mounedji-Boudiaf, L., Navarro, M., Tabernero, J., Hickish, T., Topham, C., Zaninelli, M., Clingan, P., Bridgewater, J., Tabah-Fisch, I., de Gramont, A. and Multicenter International Study of Oxaliplatin/5-Fluorouracil/Leucovorin in the Adjuvant Treatment of Colon Cancer, I. (2004) Oxaliplatin, fluorouracil, and leucovorin as adjuvant treatment for colon cancer. *N Engl J Med,* **350**(23)**,** pp. 2343-2351.

Andre, T., Boni, C., Navarro, M., Tabernero, J., Hickish, T., Topham, C., Bonetti, A., Clingan, P., Bridgewater, J., Rivera, F. and de Gramont, A. (2009) Improved overall survival with oxaliplatin, fluorouracil, and leucovorin as adjuvant treatment in stage ii or iii colon cancer in the mosaic trial. *J Clin Oncol,* **27**(19)**,** pp. 3109-3116.

Andreyev, H.J., Norman, A.R., Cunningham, D., Oates, J., Dix, B.R., Iacopetta, B.J., Young, J., Walsh, T., Ward, R., Hawkins, N., Beranek, M., Jandik, P., Benamouzig, R., Jullian, E., Laurent-Puig, P., Olschwang, S., Muller, O., Hoffmann, I., Rabes, H.M., Zietz, C., Troungos, C., Valavanis, C., Yuen, S.T., Ho, J.W., Croke, C.T., O'Donoghue, D.P., Giaretti, W., Rapallo, A., Russo, A., Bazan, V., Tanaka, M., Omura, K., Azuma, T., Ohkusa, T., Fujimori, T., Ono, Y., Pauly, M., Faber, C., Glaesener, R., de Goeij, A.F., Arends, J.W., Andersen, S.N., Lovig, T., Breivik, J., Gaudernack, G., Clausen, O.P., De Angelis, P.D., Meling, G.I., Rognum, T.O., Smith, R., Goh, H.S., Font, A., Rosell, R., Sun, X.F., Zhang, H., Benhattar, J., Losi, L., Lee, J.Q., Wang, S.T., Clarke, P.A., Bell, S., Quirke, P., Bubb, V.J., Piris, J., Cruickshank, N.R., Morton, D., Fox, J.C., Al-Mulla, F., Lees, N., Hall, C.N., Snary, D., Wilkinson, K., Dillon, D., Costa, J., Pricolo, V.E., Finkelstein, S.D., Thebo, J.S., Senagore, A.J., Halter, S.A., Wadler, S., Malik, S., Krtolica, K. and Urosevic, N. (2001) Kirsten ras mutations in patients with colorectal cancer: The 'rascal ii' study. *Br J Cancer,* **85**(5)**,** pp. 692-696.

Artandi, S.E. and DePinho, R.A. (2010) Telomeres and telomerase in cancer. *Carcinogenesis,* **31**(1)**,** pp. 9-18.

Bakhoum, S.F. and Compton, D.A. (2012) Chromosomal instability and cancer: A complex relationship with therapeutic potential. *J Clin Invest,* **122**(4)**,** pp. 1138-1143.

Balkwill, F. and Mantovani, A. (2001) Inflammation and cancer: Back to virchow? *Lancet,* **357**(9255)**,** pp. 539-545.

Barber, T.D., Vogelstein, B., Kinzler, K.W. and Velculescu, V.E. (2004) Somatic mutations of egfr in colorectal cancers and glioblastomas. *N Engl J Med,* **351**(27)**,** pp. 2883.

Barrett, M.A., Zheng, S., Roshankar, G., Alsop, R.J., Belanger, R.K., Huynh, C., Kucerka, N. and Rheinstadter, M.C. (2012) Interaction of aspirin (acetylsalicylic acid) with lipid membranes. *PLoS One,* **7**(4)**,** pp. e34357.

Beas, A.O., Taupin, V., Teodorof, C., Nguyen, L.T., Garcia-Marcos, M. and Farquhar, M.G. (2012) Galphas promotes eea1 endosome maturation and shuts down proliferative signaling through interaction with giv (girdin). *Mol Biol Cell,* **23**(23)**,** pp. 4623-4634.

Beg, A.A., Ruben, S.M., Scheinman, R.I., Haskill, S., Rosen, C.A. and Baldwin, A.S., Jr. (1992) I kappa b interacts with the nuclear localization sequences of the subunits of nf-kappa b: A mechanism for cytoplasmic retention. *Genes Dev,* **6**(10)**,** pp. 1899-1913.

Belly, R.T., Rosenblatt, J.D., Steinmann, M., Toner, J., Sun, J., Shehadi, J., Peacock, J.L., Raubertas, R.F., Jani, N. and Ryan, C.K. (2001) Detection of mutated k12-ras in histologically negative lymph nodes as an indicator of poor prognosis in stage ii colorectal cancer. *Clin Colorectal Cancer,* **1**(2)**,** pp. 110-116.

Benamouzig, R., Uzzan, B., Deyra, J., Martin, A., Girard, B., Little, J., Chaussade, S. and Association pour la Prevention par l'Aspirine du Cancer Colorectal Study, G. (2012) Prevention by daily soluble aspirin of colorectal adenoma recurrence: 4-year results of the apacc randomised trial. *Gut,* **61**(2)**,** pp. 255-261.

Bendell, J.C., Hochster, H., Hart, L.L., Firdaus, I., Mace, J.R., McFarlane, J.J., Kozloff, M., Catenacci, D., Hsu, J.J., Hack, S.P., Shames, D.S., Phan, S.C., Koeppen, H. and Cohn, A.L. (2017) A phase ii randomized trial (go27827) of first-line folfox plus bevacizumab with or without the met inhibitor onartuzumab in patients with metastatic colorectal cancer. *Oncologist,* **22**(3)**,** pp. 264-271.

Benmerah, A. and Lamaze, C. (2007) Clathrin-coated pits: Vive la difference? *Traffic,* **8**(8)**,** pp. 970-982.

Bertrand, R., Solary, E., O'Connor, P., Kohn, K.W. and Pommier, Y. (1994) Induction of a common pathway of apoptosis by staurosporine. *Exp Cell Res,* **211**(2)**,** pp. 314-321.

Berx, G. and van Roy, F. (2009) Involvement of members of the cadherin superfamily in cancer. *Cold Spring Harb Perspect Biol,* **1**(6)**,** pp. a003129.

Bhowmick, N.A. and Moses, H.L. (2005) Tumor-stroma interactions. *Curr Opin Genet Dev,* **15**(1)**,** pp. 97-101.

Bijnsdorp, I.V., Giovannetti, E. and Peters, G.J. (2011) Analysis of drug interactions. *Methods Mol Biol,* **731,** pp. 421-434.

Biscardi, J.S., Maa, M.C., Tice, D.A., Cox, M.E., Leu, T.H. and Parsons, S.J. (1999) C-src-mediated phosphorylation of the epidermal growth factor receptor on tyr845 and tyr1101 is associated with modulation of receptor function. *J Biol Chem,* **274**(12)**,** pp. 8335-8343.

Biswas, D.K., Cruz, A.P., Gansberger, E. and Pardee, A.B. (2000) Epidermal growth factor-induced nuclear factor kappa b activation: A major pathway of cell-cycle progression in estrogen-receptor negative breast cancer cells. *Proc Natl Acad Sci U S A,* **97**(15)**,** pp. 8542-8547.

Blasco, M.A. (2005) Telomeres and human disease: Ageing, cancer and beyond. *Nat Rev Genet,* **6**(8)**,** pp. 611-622.

Bordwell, F.G. and Boutan, P.J. (1956) Conjugative effects in divalent sulphur groupings. *J Am Chem Soc*, **78**, pp. 854-860.

Borthwick, G.M., Johnson, A.S., Partington, M., Burn, J., Wilson, R. and Arthur, H.M. (2006) Therapeutic levels of aspirin and salicylate directly inhibit a model of angiogenesis through a cox-independent mechanism. *FASEB J,* **20**(12)**,** pp. 2009-2016.

Bosetti, C., Rosato, V., Gallus, S., Cuzick, J. and La Vecchia, C. (2012) Aspirin and cancer risk: A quantitative review to 2011. *Ann Oncol,* **23**(6)**,** pp. 1403-1415.

Boveri, T. (2008) Concerning the origin of malignant tumours by theodor boveri. Translated and annotated by henry harris. *J Cell Sci,* **121** Suppl 11-84.

Brown, C.J., Lain, S., Verma, C.S., Fersht, A.R. and Lane, D.P. (2009) Awakening guardian angels: Drugging the p53 pathway. *Nat Rev Cancer,* **9**(12)**,** pp. 862-873.

Bruno, A., Dovizio, M., Tacconelli, S. and Patrignani, P. (2012) Mechanisms of the antitumoural effects of aspirin in the gastrointestinal tract. *Best Pract Res Clin Gastroenterol,* **26**(4)**,** pp. e1-e13.

Burkhart, D.L. and Sage, J. (2008) Cellular mechanisms of tumour suppression by the retinoblastoma gene. *Nat Rev Cancer,* **8**(9)**,** pp. 671-682.

Burn, J., Bishop, D.T., Chapman, P.D., Elliott, F., Bertario, L., Dunlop, M.G., Eccles, D., Ellis, A., Evans, D.G., Fodde, R., Maher, E.R., Moslein, G., Vasen, H.F., Coaker, J., Phillips, R.K., Bulow, S., Mathers, J.C. and International, C.c. (2011a) A randomized placebo-controlled prevention trial of aspirin and/or resistant starch in young people with familial adenomatous polyposis. *Cancer Prev Res (Phila),* **4**(5)**,** pp. 655-665.

Burn, J., Gerdes, A.M., Macrae, F., Mecklin, J.P., Moeslein, G., Olschwang, S., Eccles, D., Evans, D.G., Maher, E.R., Bertario, L., Bisgaard, M.L., Dunlop, M.G., Ho, J.W., Hodgson, S.V., Lindblom, A., Lubinski, J., Morrison, P.J., Murday, V., Ramesar, R., Side, L., Scott, R.J., Thomas, H.J., Vasen, H.F., Barker, G., Crawford, G., Elliott, F., Movahedi, M., Pylvanainen, K., Wijnen, J.T., Fodde, R., Lynch, H.T., Mathers, J.C., Bishop, D.T. and Investigators, C. (2011b) Long-term effect of aspirin on cancer risk in carriers of hereditary colorectal cancer: An analysis from the capp2 randomised controlled trial. *Lancet,* **378**(9809)**,** pp. 2081-2087.

Bustin, S.A. and Murphy, J. (2013) Rna biomarkers in colorectal cancer. *Methods,* **59**(1)**,** pp. 116-125.

Cahill, D.P., Lengauer, C., Yu, J., Riggins, G.J., Willson, J.K., Markowitz, S.D., Kinzler, K.W. and Vogelstein, B. (1998) Mutations of mitotic checkpoint genes in human cancers. *Nature,* **392**(6673)**,** pp. 300-303.

Callahan, M.K., Postow, M.A. and Wolchok, J.D. (2013) Immunomodulatory therapy for melanoma: Ipilimumab and beyond. *Clin Dermatol,* **31**(2)**,** pp. 191-199.

Canel, M., Serrels, A., Frame, M.C. and Brunton, V.G. (2013) E-cadherin-integrin crosstalk in cancer invasion and metastasis. *J Cell Sci,* **126**(Pt 2)**,** pp. 393-401.

Cao, Z., Liu, S., Niu, J., Wei, B. and Xu, J. (2015) Severe hepatoxicity caused by aspirin overdose: A case report. *Front Med,* **9**(3)**,** pp. 388-391.

Cardone, M.H., Roy, N., Stennicke, H.R., Salvesen, G.S., Franke, T.F., Stanbridge, E., Frisch, S. and Reed, J.C. (1998) Regulation of cell death protease caspase-9 by phosphorylation. *Science,* **282**(5392)**,** pp. 1318-1321.

Carmichael, J., DeGraff, W.G., Gazdar, A.F., Minna, J.D. and Mitchell, J.B. (1987) Evaluation of a tetrazolium-based semiautomated colorimetric assay: Assessment of chemosensitivity testing. *Cancer Res,* **47**(4)**,** pp. 936-942.

Carpenter, G. and Cohen, S. (1979) Epidermal growth factor. *Annu Rev Biochem,* **48,** pp. 193-216.

Carpenter, G., Lembach, K.J., Morrison, M.M. and Cohen, S. (1975) Characterization of the binding of 125-i-labeled epidermal growth factor to human fibroblasts. *J Biol Chem,* **250**(11)**,** pp. 4297-4304.

Catlett-Falcone, R., Landowski, T.H., Oshiro, M.M., Turkson, J., Levitzki, A., Savino, R., Ciliberto, G., Moscinski, L., Fernandez-Luna, J.L., Nunez, G., Dalton, W.S. and Jove, R. (1999) Constitutive activation of stat3 signaling confers resistance to apoptosis in human u266 myeloma cells. *Immunity,* **10**(1)**,** pp. 105-115.

Cautain, B., Hill, R., de Pedro, N. and Link, W. (2015) Components and regulation of nuclear transport processes. *FEBS J,* **282**(3)**,** pp. 445-462.

Cavallaro, U. and Christofori, G. (2004) Cell adhesion and signalling by cadherins and ig-cams in cancer. *Nat Rev Cancer,* **4**(2)**,** pp. 118-132.

Chan, A.T., Arber, N., Burn, J., Chia, W.K., Elwood, P., Hull, M.A., Logan, R.F., Rothwell, P.M., Schror, K. and Baron, J.A. (2012) Aspirin in the chemoprevention of colorectal neoplasia: An overview. *Cancer Prev Res (Phila),* **5**(2)**,** pp. 164-178.

Chan, A.T. and Ladabaum, U. (2016) Where do we stand with aspirin for the prevention of colorectal cancer? The uspstf recommendations. *Gastroenterology,* **150**(1)**,** pp. 14-18.

Chan, A.T. and Lippman, S.M. (2011) Aspirin and colorectal cancer prevention in lynch syndrome. *Lancet,* **378**(9809)**,** pp. 2051-2052.

Chan, M., Gravel, M., Bramoulle, A., Bridon, G., Avizonis, D., Shore, G.C. and Roulston, A. (2014) Synergy between the nampt inhibitor gmx1777(8) and pemetrexed in non-small cell lung cancer cells is mediated by parp activation and enhanced nad consumption. *Cancer Res,* **74**(21)**,** pp. 5948-5954.

Chan, T.O., Rittenhouse, S.E. and Tsichlis, P.N. (1999) Akt/pkb and other d3 phosphoinositide-regulated kinases: Kinase activation by phosphoinositide-dependent phosphorylation. *Annu Rev Biochem,* **68**, pp. 965-1014.

Chavrier, P., Parton, R.G., Hauri, H.P., Simons, K. and Zerial, M. (1990) Localization of low molecular weight gtp binding proteins to exocytic and endocytic compartments. *Cell,* **62**(2)**,** pp. 317-329.

Cheng, N., Chytil, A., Shyr, Y., Joly, A. and Moses, H.L. (2008) Transforming growth factor-beta signaling-deficient fibroblasts enhance hepatocyte growth factor signaling in mammary carcinoma cells to promote scattering and invasion. *Mol Cancer Res,* **6**(10)**,** pp. 1521-1533.

Cheung-Ong, K., Giaever, G. and Nislow, C. (2013) DNA-damaging agents in cancer chemotherapy: Serendipity and chemical biology. *Chem Biol,* **20**(5)**,** pp. 648-659.

Cho, M., Kabir, S.M., Dong, Y., Lee, E., Rice, V.M., Khabele, D. and Son, D.S. (2013) Aspirin blocks egf-stimulated cell viability in a cox-1 dependent manner in ovarian cancer cells. *J Cancer,* **4**(8)**,** pp. 671-678.

Chong, D., Ma, L., Liu, F., Zhang, Z., Zhao, S., Huo, Q., Zhang, P., Zheng, H. and Liu, H. (2017) Synergistic antitumor effect of 3-bromopyruvate and 5-fluorouracil against human colorectal cancer through cell cycle arrest and induction of apoptosis. *Anticancer Drugs,* **28**(8)**,** pp. 831-840.

Chou, T.C. (2006) Theoretical basis, experimental design, and computerized simulation of synergism and antagonism in drug combination studies. *Pharmacol Rev,* **58**(3)**,** pp. 621-681.

Chou, T.C. (2010) Drug combination studies and their synergy quantification using the chou-talalay method. *Cancer Res,* **70**(2)**,** pp. 440-446.
Chou, T.C. and Talalay, P. (1984) Quantitative analysis of dose-effect relationships: The combined effects of multiple drugs or enzyme inhibitors. *Adv Enzyme Regul,* **22**, pp**.** 27-55.
Chou, W.Y., Marky, L.A., Zaunczkowski, D. and Breslauer, K.J. (1987) The thermodynamics of drug-DNA interactions: Ethidium bromide and propidium iodide. *J Biomol Struct Dyn,* **5**(2)**,** pp. 345-359.
Chu, H.Y., Zheng, Q.C., Zhao, Y.S. and Zhang, H.X. (2009) Homology modeling and molecular dynamics study on n-acetylneuraminate lyase. *J Mol Model,* **15**(3)**,** pp. 323-328.
Chung, K.Y., Gore, I., Fong, L., Venook, A., Beck, S.B., Dorazio, P., Criscitiello, P.J., Healey, D.I., Huang, B., Gomez-Navarro, J. and Saltz, L.B. (2010) Phase ii study of the anti-cytotoxic t-lymphocyte-associated antigen 4 monoclonal antibody, tremelimumab, in patients with refractory metastatic colorectal cancer. *J Clin Oncol,* **28**(21)**,** pp. 3485-3490.
Ciardiello, F., Caputo, R., Bianco, R., Damiano, V., Fontanini, G., Cuccato, S., De Placido, S., Bianco, A.R. and Tortora, G. (2001) Inhibition of growth factor production and angiogenesis in human cancer cells by zd1839 (iressa), a selective epidermal growth factor receptor tyrosine kinase inhibitor. *Clin Cancer Res,* **7**(5)**,** pp. 1459-1465.
Citri, A. and Yarden, Y. (2006) Egf-erbb signalling: Towards the systems level. *Nat Rev Mol Cell Biol,* **7**(7)**,** pp. 505-516.
Claudius, A.K., Kankipati, C.S., Kilari, R.S., Hassan, S., Guest, K., Russell, S.T., Perry, C.J., Stark, L.A. and Nicholl, I.D. (2014) Identification of aspirin analogues that repress nf-kappab signalling and demonstrate anti-proliferative activity towards colorectal cancer in vitro and in vivo. *Oncol Rep,* **32**(4)**,** pp. 1670-1680.
Cochet, C., Kashles, O., Chambaz, E.M., Borrello, I., King, C.R. and Schlessinger, J. (1988) Demonstration of epidermal growth factor-induced receptor dimerization in living cells using a chemical covalent cross-linking agent. *J Biol Chem,* **263**(7)**,** pp. 3290-3295.
Cohen, S. (1962) Isolation of a mouse submaxillary gland protein accelerating incisor eruption and eyelid opening in the new-born animal. *J Biol Chem,* **237**, pp. 1555-1562.
Collado, M. and Serrano, M. (2010) Senescence in tumours: Evidence from mice and humans. *Nat Rev Cancer,* **10**(1)**,** pp. 51-57.
Colotta, F., Allavena, P., Sica, A., Garlanda, C. and Mantovani, A. (2009) Cancer-related inflammation, the seventh hallmark of cancer: Links to genetic instability. *Carcinogenesis,* **30**(7)**,** pp. 1073-1081.
Colussi, D., Brandi, G., Bazzoli, F. and Ricciardiello, L. (2013) Molecular pathways involved in colorectal cancer: Implications for disease behavior and prevention. *Int J Mol Sci,* **14**(8)**,** pp. 16365-16385.
Connell, W.R., Talbot, I.C., Harpaz, N., Britto, N., Wilkinson, K.H., Kamm, M.A. and Lennard-Jones, J.E. (1994) Clinicopathological characteristics of colorectal carcinoma complicating ulcerative colitis. *Gut,* **35**(10)**,** pp. 1419-1423.

Counter, C.M., Avilion, A.A., LeFeuvre, C.E., Stewart, N.G., Greider, C.W., Harley, C.B. and Bacchetti, S. (1992) Telomere shortening associated with chromosome instability is arrested in immortal cells which express telomerase activity. *EMBO J,* **11**(5)**,** pp. 1921-1929.

Cregan, S.P., Dawson, V.L. and Slack, R.S. (2004) Role of aif in caspase-dependent and caspase-independent cell death. *Oncogene,* **23**(16)**,** pp. 2785-2796.

CRUK (http://www.cancerresearchuk.org/health-professional/cancer-statistics/statistics-by-cancer-type/bowel-cancer#heading-On) [Accessed on 14-07-2017].

Cunningham, D., Humblet, Y., Siena, S., Khayat, D., Bleiberg, H., Santoro, A., Bets, D., Mueser, M., Harstrick, A., Verslype, C., Chau, I. and Van Cutsem, E. (2004) Cetuximab monotherapy and cetuximab plus irinotecan in irinotecan-refractory metastatic colorectal cancer. *N Engl J Med,* **351**(4)**,** pp. 337-345.

Czabotar, P.E., Lessene, G., Strasser, A. and Adams, J.M. (2014) Control of apoptosis by the bcl-2 protein family: Implications for physiology and therapy. *Nat Rev Mol Cell Biol,* **15**(1)**,** pp. 49-63.

Datta, S.R., Dudek, H., Tao, X., Masters, S., Fu, H., Gotoh, Y. and Greenberg, M.E. (1997) Akt phosphorylation of bad couples survival signals to the cell-intrinsic death machinery. *Cell,* **91**(2)**,** pp. 231-241.

Datto, M.B., Hu, P.P., Kowalik, T.F., Yingling, J. and Wang, X.F. (1997) The viral oncoprotein e1a blocks transforming growth factor beta-mediated induction of p21/waf1/cip1 and p15/ink4b. *Mol Cell Biol,* **17**(4)**,** pp. 2030-2037.

Davies, M.A. and Samuels, Y. (2010) Analysis of the genome to personalize therapy for melanoma. *Oncogene,* **29**(41)**,** pp. 5545-5555.

de Gramont, A., Tournigand, C., Louvet, C., Andre, T., Molitor, J.L., Raymond, E., Moreau, S., Vignoud, J., Le Bail, N. and Krulik, M. (1997) [oxaliplatin, folinic acid and 5-fluorouracil (folfox) in pretreated patients with metastatic advanced cancer. The gercod]. *Rev Med Interne,* **18**(10)**,** pp. 769-775.

Deb, J., Dibra, H., Shan, S., Rajan, S., Manneh, J., Kankipati, C.S., Perry, C.J. and Nicholl, I.D. (2011) Activity of aspirin analogues and vanillin in a human colorectal cancer cell line. *Oncol Rep,* **26**(3)**,** pp. 557-565.

DeBerardinis, R.J., Lum, J.J., Hatzivassiliou, G. and Thompson, C.B. (2008) The biology of cancer: Metabolic reprogramming fuels cell growth and proliferation. *Cell Metab,* **7**(1)**,** pp. 11-20.

Decker, S.J. (1990) Epidermal growth factor and transforming growth factor-alpha induce differential processing of the epidermal growth factor receptor. *Biochem Biophys Res Commun,* **166**(2)**,** pp. 615-621.

DeFrancesco, L. (2010) Landmark approval for dendreon's cancer vaccine. *Nat Biotechnol,* **28**(6)**,** pp. 531-532.

Dehennaut, V., Loison, I., Boulay, G., Van Rechem, C. and Leprince, D. (2013) Identification of p21 (cip1/waf1) as a direct target gene of hic1 (hypermethylated in cancer 1). *Biochem Biophys Res Commun,* **430**(1)**,** pp. 49-53.

del Solar, V., Lizardo, D.Y., Li, N., Hurst, J.J., Brais, C.J. and Atilla-Gokcumen, G.E. (2015) Differential regulation of specific sphingolipids in colon cancer cells during staurosporine-induced apoptosis. *Chem Biol,* **22**(12)**,** pp. 1662-1670.

Deng, L., Hu, S., Baydoun, A.R., Chen, J., Chen, X. and Cong, X. (2009) Aspirin induces apoptosis in mesenchymal stem cells requiring wnt/beta-catenin pathway. *Cell Prolif,* **42**(6)**,** pp. 721-730.

Di Fiore, P.P., Pierce, J.H., Kraus, M.H., Segatto, O., King, C.R. and Aaronson, S.A. (1987) Erbb-2 is a potent oncogene when overexpressed in nih/3t3 cells. *Science,* **237**(4811)**,** pp. 178-182.

Di Guglielmo, G.M., Baass, P.C., Ou, W.J., Posner, B.I. and Bergeron, J.J. (1994) Compartmentalization of shc, grb2 and msos, and hyperphosphorylation of raf-1 by egf but not insulin in liver parenchyma. *EMBO J,* **13**(18)**,** pp. 4269-4277.

Din, F.V., Dunlop, M.G. and Stark, L.A. (2004) Evidence for colorectal cancer cell specificity of aspirin effects on nf kappa b signalling and apoptosis. *Br J Cancer,* **91**(2)**,** pp. 381-388.

Din, F.V., Theodoratou, E., Farrington, S.M., Tenesa, A., Barnetson, R.A., Cetnarskyj, R., Stark, L., Porteous, M.E., Campbell, H. and Dunlop, M.G. (2010) Effect of aspirin and nsaids on risk and survival from colorectal cancer. *Gut,* **59**(12)**,** pp. 1670-1679.

Dobo, K.L., Greene, N., Fred, C., Glowienke, S., Harvey, J.S., Hasselgren, C., Jolly, R., Kenyon, M.O., Munzner, J.B., Muster, W., Neft, R., Reddy, M.V., White, A.T. and Weiner, S. (2012) In silico methods combined with expert knowledge rule out mutagenic potential of pharmaceutical impurities: An industry survey. *Regul Toxicol Pharmacol,* **62**(3)**,** pp. 449-455.

Dong, H., Liu, G., Jiang, B., Guo, J., Tao, G., Yiu, W., Zhou, J. and Li, G. (2014) The effects of aspirin plus cisplatin on sgc7901/cddp cells in vitro. *Biomed Rep,* **2**(3)**,** pp. 344-348.

Dong, H., Strome, S.E., Salomao, D.R., Tamura, H., Hirano, F., Flies, D.B., Roche, P.C., Lu, J., Zhu, G., Tamada, K., Lennon, V.A., Celis, E. and Chen, L. (2002) Tumor-associated b7-h1 promotes t-cell apoptosis: A potential mechanism of immune evasion. *Nat Med,* **8**(8)**,** pp. 793-800.

Drew, D.A., Cao, Y. and Chan, A.T. (2016) Aspirin and colorectal cancer: The promise of precision chemoprevention. *Nat Rev Cancer,* **16**(3)**,** pp. 173-186.

Eagle, H. (1971) Buffer combinations for mammalian cell culture. *Science,* **174**(4008)**,** pp. 500-503.

Edinger, A.L. and Thompson, C.B. (2004) Death by design: Apoptosis, necrosis and autophagy. *Curr Opin Cell Biol,* **16**(6)**,** pp. 663-669.

Eiro, N., Gonzalez, L., Gonzalez, L.O., Andicoechea, A., Fernandez-Diaz, M., Altadill, A. and Vizoso, F.J. (2012) Study of the expression of toll-like receptors in different histological types of colorectal polyps and their relationship with colorectal cancer. *J Clin Immunol,* **32**(4)**,** pp. 848-854.

el-Deiry, W.S., Tokino, T., Velculescu, V.E., Levy, D.B., Parsons, R., Trent, J.M., Lin, D., Mercer, W.E., Kinzler, K.W. and Vogelstein, B. (1993) Waf1, a potential mediator of p53 tumor suppression. *Cell,* **75**(4)**,** pp. 817-825.

Elliot Cham, B., Dykman, J.H. and Bochner, F. (1982) Urinary excretion of aspirin. *Br J Clin Pharmacol,* **14**(4)**,** pp. 562-564.

Emlet, D.R., Moscatello, D.K., Ludlow, L.B. and Wong, A.J. (1997) Subsets of epidermal growth factor receptors during activation and endocytosis. *J Biol Chem,* **272**(7)**,** pp. 4079-4086.

Esposito, D., Crescenzi, E., Sagar, V., Loreni, F., Russo, A. and Russo, G. (2014) Human rpl3 plays a crucial role in cell response to nucleolar stress induced by 5-fu and l-ohp. *Oncotarget,* **5**(22)**,** pp. 11737-11751.

Farrell, N., Kiley, D.M., Schmidt, W. and Hacker, M.P. (1990) Chemical-properties and antitumor-activity of complexes of platinum containing substituted sulfoxides [ptcl(r'r''so)(diamine)]no3 - chirality and leaving-group ability of sulfoxide affecting biological-activity. *Inorganic Chemistry,* **29**(3)**,** pp. 397-403.

Felder, S., LaVin, J., Ullrich, A. and Schlessinger, J. (1992) Kinetics of binding, endocytosis, and recycling of egf receptor mutants. *J Cell Biol,* **117**(1)**,** pp. 203-212.

Felder, S., Miller, K., Moehren, G., Ullrich, A., Schlessinger, J. and Hopkins, C.R. (1990) Kinase activity controls the sorting of the epidermal growth factor receptor within the multivesicular body. *Cell,* **61**(4)**,** pp. 623-634.

Ferrara, N. (2009) Vascular endothelial growth factor. *Arterioscler Thromb Vasc Biol,* **29**(6)**,** pp. 789-791.

Fishel, R. and Kolodner, R.D. (1995) Identification of mismatch repair genes and their role in the development of cancer. *Curr Opin Genet Dev,* **5**(3)**,** pp. 382-395.

Flores-Rodriguez, N., Kenwright, D.A., Chung, P.H., Harrison, A.W., Stefani, F., Waigh, T.A., Allan, V.J. and Woodman, P.G. (2015) Escrt-0 marks an appl1-independent transit route for egfr between the cell surface and the eea1-positive early endosome. *J Cell Sci,* **128**(4)**,** pp. 755-767.

Foret, L., Dawson, J.E., Villasenor, R., Collinet, C., Deutsch, A., Brusch, L., Zerial, M., Kalaidzidis, Y. and Julicher, F. (2012) A general theoretical framework to infer endosomal network dynamics from quantitative image analysis. *Curr Biol,* **22**(15)**,** pp. 1381-1390.

Foucquier, J. and Guedj, M. (2015) Analysis of drug combinations: Current methodological landscape. *Pharmacol Res Perspect,* **3**(3)**,** pp. e00149.

Gangadhar, T.C. and Salama, A.K. (2015) Clinical applications of pd-1-based therapy: A focus on pembrolizumab (mk-3475) in the management of melanoma and other tumor types. *Onco Targets Ther,* **8**, pp. 929-937.

Garcia, R. and Jove, R. (1998) Activation of stat transcription factors in oncogenic tyrosine kinase signaling. *J Biomed Sci,* **5**(2)**,** pp. 79-85.

Garcia Rodriguez, L.A., Hernandez-Diaz, S. and de Abajo, F.J. (2001) Association between aspirin and upper gastrointestinal complications: Systematic review of epidemiologic studies. *Br J Clin Pharmacol,* **52**(5)**,** pp. 563-571.

Garcia Rodriguez, L.A., Martin-Perez, M., Hennekens, C.H., Rothwell, P.M. and Lanas, A. (2016) Bleeding risk with long-term low-dose aspirin: A systematic review of observational studies. *PLoS One,* **11**(8)**,** pp. e0160046.

Garcia-Albeniz, X. and Chan, A.T. (2011) Aspirin for the prevention of colorectal cancer. *Best Pract Res Clin Gastroenterol,* **25**(4-5)**,** pp. 461-472.

Garraway, L.A. and Lander, E.S. (2013) Lessons from the cancer genome. *Cell,* **153**(1)**,** pp. 17-37.

Gartel, A.L. (2005) The conflicting roles of the cdk inhibitor p21(cip1/waf1) in apoptosis. *Leuk Res,* **29**(11)**,** pp. 1237-1238.

Gartel, A.L. (2006) Is p21 an oncogene? *Mol Cancer Ther,* **5**(6)**,** pp. 1385-1386.

Gasche, C., Goel, A., Natarajan, L. and Boland, C.R. (2005) Mesalazine improves replication fidelity in cultured colorectal cells. *Cancer Res,* **65**(10)**,** pp. 3993-3997.

Gensini, G.F. and Conti, A.A. (2009) The preventive and therapeutic impact of antiplatelet agents: Past and present. *Minerva Med,* **100**(2)**,** pp. 133-136.

Giancotti, F.G. and Ruoslahti, E. (1999) Integrin signaling. *Science,* **285**(5430)**,** pp. 1028-1032.

GLOBOCAN (http://gco.iarc.fr/today/fact-sheets-cancers?cancer=6&type=0&sex=0) [Accessed on 12-03-2017].

Goel, A., Chang, D.K., Ricciardiello, L., Gasche, C. and Boland, C.R. (2003) A novel mechanism for aspirin-mediated growth inhibition of human colon cancer cells. *Clin Cancer Res,* **9**(1)**,** pp. 383-390.

Goetz, M., Ziebart, A., Foersch, S., Vieth, M., Waldner, M.J., Delaney, P., Galle, P.R., Neurath, M.F. and Kiesslich, R. (2010) In vivo molecular imaging of colorectal cancer with confocal endomicroscopy by targeting epidermal growth factor receptor. *Gastroenterology,* **138**(2)**,** pp. 435-446.

Goggin, P.M., Collins, D.A., Jazrawi, R.P., Jackson, P.A., Corbishley, C.M., Bourke, B.E. and Northfield, T.C. (1993) Prevalence of helicobacter pylori infection and its effect on symptoms and non-steroidal anti-inflammatory drug induced gastrointestinal damage in patients with rheumatoid arthritis. *Gut,* **34**(12)**,** pp. 1677-1680.

Goh, A.M., Xue, Y., Leushacke, M., Li, L., Wong, J.S., Chiam, P.C., Rahmat, S.A., Mann, M.B., Mann, K.M., Barker, N., Lozano, G., Terzian, T. and Lane, D.P. (2015) Mutant p53 accumulates in cycling and proliferating cells in the normal tissues of p53 r172h mutant mice. *Oncotarget,* **6**(20)**,** pp. 17968-17980.

Goh, L.K., Huang, F., Kim, W., Gygi, S. and Sorkin, A. (2010) Multiple mechanisms collectively regulate clathrin-mediated endocytosis of the epidermal growth factor receptor. *J Cell Biol,* **189**(5)**,** pp. 871-883.

Gold, P. and Freedman, S.O. (1965) Demonstration of tumor-specific antigens in human colonic carcinomata by immunological tolerance and absorption techniques. *J Exp Med,* **121**, pp. 439-462.

Goldberg, R.M., Rothenberg, M.L., Van Cutsem, E., Benson, A.B., 3rd, Blanke, C.D., Diasio, R.B., Grothey, A., Lenz, H.J., Meropol, N.J., Ramanathan, R.K., Becerra, C.H., Wickham, R., Armstrong, D. and Viele, C. (2007) The continuum of care: A paradigm for the management of metastatic colorectal cancer. *Oncologist,* **12**(1)**,** pp. 38-50.

Goldstein, I., Marcel, V., Olivier, M., Oren, M., Rotter, V. and Hainaut, P. (2011) Understanding wild-type and mutant p53 activities in human cancer: New landmarks on the way to targeted therapies. *Cancer Gene Ther,* **18**(1)**,** pp. 2-11.

Gong, J., Wang, C., Lee, P.P., Chu, P. and Fakih, M. (2017) Response to pd-1 blockade in microsatellite stable metastatic colorectal cancer harboring a pole mutation. *J Natl Compr Canc Netw,* **15**(2)**,** pp. 142-147.

Good, N.E., Winget, G.D., Winter, W., Connolly, T.N., Izawa, S. and Singh, R.M. (1966) Hydrogen ion buffers for biological research. *Biochemistry,* **5**(2)**,** pp. 467-477.

Grandis, J.R., Drenning, S.D., Zeng, Q., Watkins, S.C., Melhem, M.F., Endo, S., Johnson, D.E., Huang, L., He, Y. and Kim, J.D. (2000) Constitutive activation of stat3 signaling abrogates apoptosis in squamous cell carcinogenesis in vivo. *Proc Natl Acad Sci U S A,* **97**(8)**,** pp. 4227-4232.

Grant, S., Qiao, L. and Dent, P. (2002) Roles of erbb family receptor tyrosine kinases, and downstream signaling pathways, in the control of cell growth and survival. *Front Biosci,* **7**, pp. d376-389.

Green, D.R. and Reed, J.C. (1998) Mitochondria and apoptosis. *Science,* **281**(5381)**,** pp. 1309-1312.

Griffin, M.R., Piper, J.M., Daugherty, J.R., Snowden, M. and Ray, W.A. (1991) Nonsteroidal anti-inflammatory drug use and increased risk for peptic ulcer disease in elderly persons. *Ann Intern Med,* **114**(4)**,** pp. 257-263.

Grivennikov, S.I., Greten, F.R. and Karin, M. (2010) Immunity, inflammation, and cancer. *Cell,* **140**(6)**,** pp. 883-899.

Gross, A., McDonnell, J.M. and Korsmeyer, S.J. (1999) Bcl-2 family members and the mitochondria in apoptosis. *Genes Dev,* **13**(15)**,** pp. 1899-1911.

Grovdal, L.M., Stang, E., Sorkin, A. and Madshus, I.H. (2004) Direct interaction of cbl with ptyr 1045 of the egf receptor (egfr) is required to sort the egfr to lysosomes for degradation. *Exp Cell Res,* **300**(2)**,** pp. 388-395.

Gurpinar, E., Grizzle, W.E. and Piazza, G.A. (2013) Cox-independent mechanisms of cancer chemoprevention by anti-inflammatory drugs. *Front Oncol,* **3**, pp. 181.

Habib, A.A., Chatterjee, S., Park, S.K., Ratan, R.R., Lefebvre, S. and Vartanian, T. (2001) The epidermal growth factor receptor engages receptor interacting protein and nuclear factor-kappa b (nf-kappa b)-inducing kinase to activate nf-kappa b. Identification of a novel receptor-tyrosine kinase signalosome. *J Biol Chem,* **276**(12)**,** pp. 8865-8874.

Hackel, P.O., Zwick, E., Prenzel, N. and Ullrich, A. (1999) Epidermal growth factor receptors: Critical mediators of multiple receptor pathways. *Curr Opin Cell Biol,* **11**(2)**,** pp. 184-189.

Haldar, S., Jena, N. and Croce, C.M. (1995) Inactivation of bcl-2 by phosphorylation. *Proc Natl Acad Sci U S A,* **92**(10)**,** pp. 4507-4511.

Halevy, O., Novitch, B.G., Spicer, D.B., Skapek, S.X., Rhee, J., Hannon, G.J., Beach, D. and Lassar, A.B. (1995) Correlation of terminal cell cycle arrest of skeletal muscle with induction of p21 by myod. *Science,* **267**(5200)**,** pp. 1018-1021.

Hall, M.D., Telma, K.A., Chang, K.E., Lee, T.D., Madigan, J.P., Lloyd, J.R., Goldlust, I.S., Hoeschele, J.D. and Gottesman, M.M. (2014) Say no to dmso: Dimethylsulfoxide inactivates cisplatin, carboplatin, and other platinum complexes. *Cancer Res,* **74**(14)**,** pp. 3913-3922.

Hamdan, J.A., Manasra, K. and Ahmed, M. (1985) Salicylate-induced hepatitis in rheumatic fever. *Am J Dis Child,* **139**(5)**,** pp. 453-455.

Hammarstrom, S. (1999) The carcinoembryonic antigen (cea) family: Structures, suggested functions and expression in normal and malignant tissues. *Semin Cancer Biol,* **9**(2)**,** pp. 67-81.

Hanahan, D. and Folkman, J. (1996) Patterns and emerging mechanisms of the angiogenic switch during tumorigenesis. *Cell,* **86**(3)**,** pp. 353-364.

Hanahan, D. and Weinberg, R.A. (2000) The hallmarks of cancer. *Cell,* **100**(1)**,** pp. 57-70.

Hanahan, D. and Weinberg, R.A. (2011) Hallmarks of cancer: The next generation. *Cell,* **144**(5)**,** pp. 646-674.

Hanson, P.I. and Cashikar, A. (2012) Multivesicular body morphogenesis. *Annu Rev Cell Dev Biol,* **28**, pp. 337-362.

Hardee, M.E., Dewhirst, M.W., Agarwal, N. and Sorg, B.S. (2009) Novel imaging provides new insights into mechanisms of oxygen transport in tumors. *Curr Mol Med,* **9**(4)**,** pp. 435-441.

Harwood, L.M. and Claridge, T.D.W. (1997) *Introduction to organic spectroscopy.* [online] Oxford: Oxford University Press. Available at: <http://wlv.summon.serialssolutions.com/2.0.0/link/0/eLvHCXMwbV07D8IgEL74GDRx8BmfSQdXDaU0wmxsdNe5uVxhrA4mxn8vV-zgY4SBADm447jv-wASuRWbrzvBGUrSHZGOyZAofOCPuFMOMSYUhvQn-T7UmoiELJ3B-FSuZ-RPVIZXfUiVmST1dteEpjJ8LrPzJRDn6NQHIql-c-zUbXYhj1oSvnIhWR9aDCsYQMOWQ-jsa521EaxPXCxeBBbX6H6NgtASRRUIkskmr7fnGGbZ4bw_bvyw-TvlkodJyQn0kOvUy3uFZyumEFkrVOJQFlpYZRWiROk9pvMPiVj6PZnB4Heg-b_OBXQDlSqnA5bQdt5c7apa3gvWoWlL>.

Hatori, A., Shigematsu, A. and Tsuya, A. (1984) The metabolism of aspirin in rats; localization, absorption, distribution and excretion. *Eur J Drug Metab Pharmacokinet,* **9**(3)**,** pp. 205-214.

Hawley, S.A., Fullerton, M.D., Ross, F.A., Schertzer, J.D., Chevtzoff, C., Walker, K.J., Peggie, M.W., Zibrova, D., Green, K.A., Mustard, K.J., Kemp, B.E., Sakamoto, K., Steinberg, G.R. and Hardie, D.G. (2012) The ancient drug salicylate directly activates amp-activated protein kinase. *Science,* **336**(6083)**,** pp. 918-922.

Henriksen, L., Grandal, M.V., Knudsen, S.L., van Deurs, B. and Grovdal, L.M. (2013) Internalization mechanisms of the epidermal growth factor receptor after activation with different ligands. *PLoS One,* **8**(3)**,** pp. e58148.

Herman, J.G., Umar, A., Polyak, K., Graff, J.R., Ahuja, N., Issa, J.P., Markowitz, S., Willson, J.K., Hamilton, S.R., Kinzler, K.W., Kane, M.F., Kolodner, R.D., Vogelstein, B., Kunkel, T.A. and Baylin, S.B. (1998) Incidence and functional consequences of hmlh1 promoter hypermethylation in colorectal carcinoma. *Proc Natl Acad Sci U S A,* **95**(12)**,** pp. 6870-6875.

Hewitt, R.E., McMarlin, A., Kleiner, D., Wersto, R., Martin, P., Tsokos, M., Stamp, G.W. and Stetler-Stevenson, W.G. (2000) Validation of a model of colon cancer progression. *J Pathol,* **192**(4)**,** pp. 446-454.

Hicklin, D.J. and Ellis, L.M. (2005) Role of the vascular endothelial growth factor pathway in tumor growth and angiogenesis. *J Clin Oncol,* **23**(5)**,** pp. 1011-1027.

Higgs, G.A., Salmon, J.A., Henderson, B. and Vane, J.R. (1987) Pharmacokinetics of aspirin and salicylate in relation to inhibition of arachidonate cyclooxygenase and antiinflammatory activity. *Proc Natl Acad Sci U S A,* **84**(5)**,** pp. 1417-1420.

Hollingsworth, M.A. and Swanson, B.J. (2004) Mucins in cancer: Protection and control of the cell surface. *Nat Rev Cancer,* **4**(1)**,** pp. 45-60.

Honegger, A.M., Szapary, D., Schmidt, A., Lyall, R., Van Obberghen, E., Dull, T.J., Ullrich, A. and Schlessinger, J. (1987) A mutant epidermal growth factor receptor with defective protein tyrosine kinase is unable to stimulate proto-oncogene expression and DNA synthesis. *Mol Cell Biol,* **7**(12)**,** pp. 4568-4571.

Huang, E.S., Strate, L.L., Ho, W.W., Lee, S.S. and Chan, A.T. (2010) A prospective study of aspirin use and the risk of gastrointestinal bleeding in men. *PLoS One,* **5**(12)**,** pp. e15721.

Huotari, J. and Helenius, A. (2011) Endosome maturation. *EMBO J,* **30**(17)**,** pp. 3481-3500.

Hynes, N.E. and Lane, H.A. (2005) Erbb receptors and cancer: The complexity of targeted inhibitors. *Nat Rev Cancer,* **5**(5)**,** pp. 341-354.

Idziorek, T., Estaquier, J., De Bels, F. and Ameisen, J.C. (1995) Yopro-1 permits cytofluorometric analysis of programmed cell death (apoptosis) without interfering with cell viability. *J Immunol Methods,* **185**(2)**,** pp. 249-258.

Ikushima, H. and Miyazono, K. (2010) Tgfbeta signalling: A complex web in cancer progression. *Nat Rev Cancer,* **10**(6)**,** pp. 415-424.

Iyer, R.R., Pluciennik, A., Burdett, V. and Modrich, P.L. (2006) DNA mismatch repair: Functions and mechanisms. *Chem Rev,* **106**(2)**,** pp. 302-323.

Jacobson, M.D., Burne, J.F., King, M.P., Miyashita, T., Reed, J.C. and Raff, M.C. (1993) Bcl-2 blocks apoptosis in cells lacking mitochondrial DNA. *Nature,* **361**(6410)**,** pp. 365-369.

Janne, P.A. and Mayer, R.J. (2000) Chemoprevention of colorectal cancer. *N Engl J Med,* **342**(26)**,** pp. 1960-1968.

Jiang, B.H. and Liu, L.Z. (2009) Pi3k/pten signaling in angiogenesis and tumorigenesis. *Adv Cancer Res,* **102**, pp. 19-65.

Jiang, X., Huang, F., Marusyk, A. and Sorkin, A. (2003) Grb2 regulates internalization of egf receptors through clathrin-coated pits. *Mol Biol Cell,* **14**(3)**,** pp. 858-870.

Jiang, X., Overholtzer, M. and Thompson, C.B. (2015) Autophagy in cellular metabolism and cancer. *J Clin Invest,* **125**(1)**,** pp. 47-54.

Johnson, C.C., Hayes, R.B., Schoen, R.E., Gunter, M.J., Huang, W.Y. and Team, P.T. (2010) Non-steroidal anti-inflammatory drug use and colorectal polyps in the prostate, lung, colorectal, and ovarian cancer screening trial. *Am J Gastroenterol,* **105**(12)**,** pp. 2646-2655.

Jorissen, R.N., Walker, F., Pouliot, N., Garrett, T.P., Ward, C.W. and Burgess, A.W. (2003) Epidermal growth factor receptor: Mechanisms of activation and signalling. *Exp Cell Res,* **284**(1)**,** pp. 31-53.

Jurgensmeier, J.M., Xie, Z., Deveraux, Q., Ellerby, L., Bredesen, D. and Reed, J.C. (1998) Bax directly induces release of cytochrome c from isolated mitochondria. *Proc Natl Acad Sci U S A,* **95**(9)**,** pp. 4997-5002.

Kaiser, G.C. and Polk, D.B. (1997) Tumor necrosis factor alpha regulates proliferation in a mouse intestinal cell line. *Gastroenterology,* **112**(4)**,** pp. 1231-1240.

Kane, M.F., Loda, M., Gaida, G.M., Lipman, J., Mishra, R., Goldman, H., Jessup, J.M. and Kolodner, R. (1997) Methylation of the hmlh1 promoter correlates with lack of expression of hmlh1 in sporadic colon tumors and mismatch repair-defective human tumor cell lines. *Cancer Res,* **57**(5)**,** pp. 808-811.

Kang, C.S., Zhang, Z.Y., Jia, Z.F., Wang, G.X., Qiu, M.Z., Zhou, H.X., Yu, S.Z., Chang, J., Jiang, H. and Pu, P.Y. (2006) Suppression of egfr expression by antisense or small interference rna inhibits u251 glioma cell growth in vitro and in vivo. *Cancer Gene Ther,* **13**(5)**,** pp. 530-538.

Kankipati, C. S. (2014) *Investigation into the cytotoxicity of the analogues of salicylic acid to colorectal cancer cells*. Ph.D. Thesis, University of Wolverhampton.

Karim, M.M., Lee, H.S., Kim, Y.S., Bae, H.S. and Lee, S.H. (2006) Analysis of salicylic acid based on the fluorescence enhancement of the as(iii)-salicylic acid system. *Anal Chim Acta,* **576**(1)**,** pp. 136-139.

Karimian, A., Ahmadi, Y. and Yousefi, B. (2016) Multiple functions of p21 in cell cycle, apoptosis and transcriptional regulation after DNA damage. *DNA Repair (Amst),* **42**, pp. 63-71.

Kazerounian, S., Yee, K.O. and Lawler, J. (2008) Thrombospondins in cancer. *Cell Mol Life Sci*, **65**(5), pp. 700-712.

Kennedy, K.M. and Dewhirst, M.W. (2010) Tumor metabolism of lactate: The influence and therapeutic potential for mct and cd147 regulation. *Future Oncol,* **6**(1)**,** pp. 127-148.

Kerrison, S.J.S. and Sadler, P.J. (1985) Pt-195 nmr-studies of platinum(ii) dimethylsulfoxide complexes. *Inorganica Chimica Acta-Articles and Letters,* **104**(3)**,** pp. 197-201.

Khazaie, K., Schirrmacher, V. and Lichtner, R.B. (1993) Egf receptor in neoplasia and metastasis. *Cancer Metastasis Rev,* **12**(3-4)**,** pp. 255-274.

Kieler, M., Scheithauer, W., Zielinski, C.C., Chott, A., Al-Mukhtar, A. and Prager, G.W. (2016) Case report: Impressive response to pembrolizumab in a patient with mismatch-repair deficient metastasized colorectal cancer and bulky disease. *ESMO Open,* **1**(6)**,** pp. e000084.

Kilari, R. S. (2014) *Roles of inositol diphosphates in DNA repair and effects of aspirin analogues on oesophageal cancer*. Ph. D.Thesis, University of Wolverhampton.

Kim, H., Kang, M., Park, Y., Kim, S. and Kang, J. (2013) Stability of an aspirin in the aspirin + curcumin admixture at different storage conditions. *British Journal of Pharmaceutical Research*, **3**(4), pp. 830-838.

Kiyoto, I., Yamamoto, S., Aizu, E. and Kato, R. (1987) Staurosporine, a potent protein kinase c inhibitor, fails to inhibit 12-o-tetradecanoylphorbol-13-acetate-caused ornithine decarboxylase induction in isolated mouse epidermal cells. *Biochem Biophys Res Commun,* **148**(2)**,** pp. 740-746.

Klapper, L.N., Kirschbaum, M.H., Sela, M. and Yarden, Y. (2000) Biochemical and clinical implications of the erbb/her signaling network of growth factor receptors. *Adv Cancer Res,* **77**, pp. 25-79.

Knox, R.J., Friedlos, F., Lydall, D.A. and Roberts, J.J. (1986) Mechanism of cytotoxicity of anticancer platinum drugs: Evidence that cis-diamminedichloroplatinum(ii) and cis-diammine-(1,1-cyclobutanedicarboxylato)platinum(ii) differ only in the kinetics of their interaction with DNA. *Cancer Res,* **46**(4 Pt 2)**,** pp. 1972-1979.

Ko, L.J. and Prives, C. (1996) P53: Puzzle and paradigm. *Genes Dev,* **10**(9)**,** pp. 1054-1072.

Kobayashi, S., Boggon, T.J., Dayaram, T., Janne, P.A., Kocher, O., Meyerson, M., Johnson, B.E., Eck, M.J., Tenen, D.G. and Halmos, B. (2005) Egfr mutation and resistance of non-small-cell lung cancer to gefitinib. *N Engl J Med,* **352**(8)**,** pp. 786-792.

Kodela, R., Chattopadhyay, M., Goswami, S., Gan, Z.Y., Rao, P.P., Nia, K.V., Velazquez-Martinez, C.A. and Kashfi, K. (2013) Positional isomers of aspirin are equally potent in inhibiting colon cancer cell growth: Differences in mode of cyclooxygenase inhibition. *J Pharmacol Exp Ther,* **345**(1)**,** pp. 85-94.

Kohne, C.H. and Lenz, H.J. (2009) Chemotherapy with targeted agents for the treatment of metastatic colorectal cancer. *Oncologist,* **14**(5)**,** pp. 478-488.

Kopp, E. and Ghosh, S. (1994) Inhibition of nf-kappa b by sodium salicylate and aspirin. *Science,* **265**(5174)**,** pp. 956-959.

Krasinskas, A.M. (2011) Egfr signaling in colorectal carcinoma. *Patholog Res Int,* **2011**, pp. 932932.

Kuiper, R.P., Vissers, L.E., Venkatachalam, R., Bodmer, D., Hoenselaar, E., Goossens, M., Haufe, A., Kamping, E., Niessen, R.C., Hogervorst, F.B., Gille, J.J., Redeker, B., Tops, C.M., van Gijn, M.E., van den Ouweland, A.M., Rahner, N., Steinke, V., Kahl, P., Holinski-Feder, E., Morak, M., Kloor, M., Stemmler, S., Betz, B., Hutter, P., Bunyan, D.J., Syngal, S., Culver, J.O., Graham, T., Chan, T.L., Nagtegaal, I.D., van Krieken, J.H., Schackert, H.K., Hoogerbrugge, N., van Kessel, A.G. and Ligtenberg, M.J. (2011) Recurrence and variability of germline epcam deletions in lynch syndrome. *Hum Mutat,* **32**(4)**,** pp. 407-414.

Kune, G.A., Kune, S. and Watson, L.F. (1988) Colorectal cancer risk, chronic illnesses, operations, and medications: Case control results from the melbourne colorectal cancer study. *Cancer Res,* **48**(15)**,** pp. 4399-4404.

Laemmli, U.K. (1970) Cleavage of structural proteins during the assembly of the head of bacteriophage t4. *Nature,* **227**(5259)**,** pp. 680-685.

Laine, L. (2002) The gastrointestinal effects of nonselective nsaids and cox-2-selective inhibitors. *Semin Arthritis Rheum,* **32**(3 Suppl 1)**,** pp. 25-32.

Lane, D.P. (1992) Cancer. P53, guardian of the genome. *Nature,* **358**(6381)**,** pp. 15-16.

Langley, R.E., Burdett, S., Tierney, J.F., Cafferty, F., Parmar, M.K. and Venning, G. (2011) Aspirin and cancer: Has aspirin been overlooked as an adjuvant therapy? *Br J Cancer,* **105**(8)**,** pp. 1107-1113.

Langman, M.J., Weil, J., Wainwright, P., Lawson, D.H., Rawlins, M.D., Logan, R.F., Murphy, M., Vessey, M.P. and Colin-Jones, D.G. (1994) Risks of bleeding peptic ulcer associated with individual non-steroidal anti-inflammatory drugs. *Lancet,* **343**(8905)**,** pp. 1075-1078.

Le Roy, C. and Wrana, J.L. (2005) Clathrin- and non-clathrin-mediated endocytic regulation of cell signalling. *Nat Rev Mol Cell Biol,* **6**(2)**,** pp. 112-126.

Lee, J.W., Soung, Y.H., Kim, S.Y., Park, W.S., Nam, S.W., Lee, J.Y., Yoo, N.J. and Lee, S.H. (2005) Absence of egfr mutation in the kinase domain in common human cancers besides non-small cell lung cancer. *Int J Cancer,* **113**(3)**,** pp. 510-511.

Lee, W., Belkhiri, A., Lockhart, A.C., Merchant, N., Glaeser, H., Harris, E.I., Washington, M.K., Brunt, E.M., Zaika, A., Kim, R.B. and El-Rifai, W. (2008) Overexpression of oatp1b3 confers apoptotic resistance in colon cancer. *Cancer Res,* **68**(24)**,** pp. 10315-10323.

Leibovitz, A., Stinson, J.C., McCombs, W.B., 3rd, McCoy, C.E., Mazur, K.C. and Mabry, N.D. (1976) Classification of human colorectal adenocarcinoma cell lines. *Cancer Res,* **36**(12)**,** pp. 4562-4569.

Leist, M. and Jaattela, M. (2001) Four deaths and a funeral: From caspases to alternative mechanisms. *Nat Rev Mol Cell Biol,* **2**(8)**,** pp. 589-598.

Lemmon, M.A. and Schlessinger, J. (1994) Regulation of signal transduction and signal diversity by receptor oligomerization. *Trends Biochem Sci,* **19**(11)**,** pp. 459-463.

Lemmon, M.A. and Schlessinger, J. (2010) Cell signaling by receptor tyrosine kinases. *Cell,* **141**(7)**,** pp. 1117-1134.

Lengauer, C., Kinzler, K.W. and Vogelstein, B. (1998) Genetic instabilities in human cancers. *Nature,* **396**(6712)**,** pp. 643-649.

Levi, F., Metzger, G., Massari, C. and Milano, G. (2000) Oxaliplatin: Pharmacokinetics and chronopharmacological aspects. *Clin Pharmacokinet,* **38**(1)**,** pp. 1-21.

Levi, F., Misset, J.L., Brienza, S., Adam, R., Metzger, G., Itzakhi, M., Caussanel, J.P., Kunstlinger, F., Lecouturier, S., Descorps-Declere, A. and et al. (1992) A chronopharmacologic phase ii clinical trial with 5-fluorouracil, folinic acid, and oxaliplatin using an ambulatory multichannel programmable pump. High antitumor effectiveness against metastatic colorectal cancer. *Cancer,* **69**(4)**,** pp. 893-900.

Levine, B. and Kroemer, G. (2008) Autophagy in the pathogenesis of disease. *Cell,* **132**(1)**,** pp. 27-42.

Levkowitz, G., Waterman, H., Zamir, E., Kam, Z., Oved, S., Langdon, W.Y., Beguinot, L., Geiger, B. and Yarden, Y. (1998) C-cbl/sli-1 regulates endocytic sorting and ubiquitination of the epidermal growth factor receptor. *Genes Dev,* **12**(23)**,** pp. 3663-3674.

Li, H., Zhu, F., Boardman, L.A., Wang, L., Oi, N., Liu, K., Li, X., Fu, Y., Limburg, P.J., Bode, A.M. and Dong, Z. (2015) Aspirin prevents colorectal cancer by normalizing egfr expression. *EBioMedicine,* **2**(5)**,** pp. 447-455.

Li, L., Geraghty, O.C., Mehta, Z., Rothwell, P.M. and Oxford Vascular, S. (2017) Age-specific risks, severity, time course, and outcome of bleeding on long-term antiplatelet treatment after vascular events: A population-based cohort study. *Lancet*, **390**(10093), pp. 490-499.

Li, M., Wu, X. and Xu, X.C. (2001) Induction of apoptosis in colon cancer cells by cyclooxygenase-2 inhibitor ns398 through a cytochrome c-dependent pathway. *Clin Cancer Res,* **7**(4)**,** pp. 1010-1016.

Li, M.H., Ito, D., Sanada, M., Odani, T., Hatori, M., Iwase, M. and Nagumo, M. (2004) Effect of 5-fluorouracil on g1 phase cell cycle regulation in oral cancer cell lines. *Oral Oncol,* **40**(1)**,** pp. 63-70.

Lichtenberger, L.M., Zhou, Y., Dial, E.J. and Raphael, R.M. (2006) Nsaid injury to the gastrointestinal tract: Evidence that nsaids interact with phospholipids to weaken the hydrophobic surface barrier and induce the formation of unstable pores in membranes. *J Pharm Pharmacol,* **58**(11)**,** pp. 1421-1428.

Lichtenberger, L.M., Zhou, Y., Jayaraman, V., Doyen, J.R., O'Neil, R.G., Dial, E.J., Volk, D.E., Gorenstein, D.G., Boggara, M.B. and Krishnamoorti, R. (2012) Insight into nsaid-induced membrane alterations, pathogenesis and therapeutics: Characterization of interaction of nsaids with phosphatidylcholine. *Biochim Biophys Acta,* **1821**(7)**,** pp. 994-1002.

Lin, S.Y., Makino, K., Xia, W., Matin, A., Wen, Y., Kwong, K.Y., Bourguignon, L. and Hung, M.C. (2001) Nuclear localization of egf receptor and its potential new role as a transcription factor. *Nat Cell Biol,* **3**(9)**,** pp. 802-808.

Liotta, L.A. and Kohn, E.C. (2001) The microenvironment of the tumour-host interface. *Nature,* **411**(6835)**,** pp. 375-379.

Liu, D.S., Duong, C.P., Haupt, S., Montgomery, K.G., House, C.M., Azar, W.J., Pearson, H.B., Fisher, O.M., Read, M., Guerra, G.R., Haupt, Y., Cullinane, C., Wiman, K.G., Abrahmsen, L., Phillips, W.A. and Clemons, N.J. (2017) Inhibiting the system xc-/glutathione axis selectively targets cancers with mutant-p53 accumulation. *Nat Commun,* **8**, pp. 14844.

Liu, W., Zhang, Z., Zhang, Y., Chen, X., Guo, S., Lei, Y., Xu, Y., Ji, C., Bi, Z. and Wang, K. (2015) Hmgb1-mediated autophagy modulates sensitivity of colorectal cancer cells to oxaliplatin via mek/erk signaling pathway. *Cancer Biol Ther,* **16**(4)**,** pp. 511-517.

Loeb, L.A. (1991) Mutator phenotype may be required for multistage carcinogenesis. *Cancer Res,* **51**(12)**,** pp. 3075-3079.

Lowe, S.W., Cepero, E. and Evan, G. (2004) Intrinsic tumour suppression. *Nature,* **432**(7015)**,** pp. 307-315.

Lowe, S.W., Ruley, H.E., Jacks, T. and Housman, D.E. (1993) P53-dependent apoptosis modulates the cytotoxicity of anticancer agents. *Cell,* **74**(6)**,** pp. 957-967.

Luo, H.Y., Wei, W., Shi, Y.X., Chen, X.Q., Li, Y.H., Wang, F., Qiu, M.Z., Li, F.H., Yan, S.L., Zeng, M.S., Huang, P. and Xu, R.H. (2010) Cetuximab enhances the effect of oxaliplatin on hypoxic gastric cancer cell lines. *Oncol Rep,* **23**(6)**,** pp. 1735-1745.
Lynch, D. and Murphy, A. (2016) The emerging role of immunotherapy in colorectal cancer. *Ann Transl Med,* **4**(16)**,** pp. 305.
Maciel, E., Neves, B.M., Santinha, D., Reis, A., Domingues, P., Teresa Cruz, M., Pitt, A.R., Spickett, C.M. and Domingues, M.R. (2014) Detection of phosphatidylserine with a modified polar head group in human keratinocytes exposed to the radical generator aaph. *Arch Biochem Biophys,* **548**, pp. 38-45.
Madshus, I.H. and Stang, E. (2009) Internalization and intracellular sorting of the egf receptor: A model for understanding the mechanisms of receptor trafficking. *J Cell Sci,* **122**(Pt 19)**,** pp. 3433-3439.
Malumbres, M. and Barbacid, M. (2009) Cell cycle, cdks and cancer: A changing paradigm. *Nat Rev Cancer,* **9**(3)**,** pp. 153-166.
Margolis, B. (1992) Proteins with sh2 domains: Transducers in the tyrosine kinase signaling pathway. *Cell Growth Differ,* **3**(1)**,** pp. 73-80.
Masek, V., Anzenbacherova, E., Machova, M., Brabec, V. and Anzenbacher, P. (2009) Interaction of antitumor platinum complexes with human liver microsomal cytochromes p450. *Anticancer Drugs,* **20**(5)**,** pp. 305-311.
Mayor, S. and Pagano, R.E. (2007) Pathways of clathrin-independent endocytosis. *Nat Rev Mol Cell Biol,* **8**(8)**,** pp. 603-612.
Mazel, S., Burtrum, D. and Petrie, H.T. (1996) Regulation of cell division cycle progression by bcl-2 expression: A potential mechanism for inhibition of programmed cell death. *J Exp Med,* **183**(5)**,** pp. 2219-2226.
McDonald, E.R., 3rd and El-Deiry, W.S. (2000) Cell cycle control as a basis for cancer drug development (review). *Int J Oncol,* **16**(5)**,** pp. 871-886.
McGranahan, N., Favero, F., de Bruin, E.C., Birkbak, N.J., Szallasi, Z. and Swanton, C. (2015) Clonal status of actionable driver events and the timing of mutational processes in cancer evolution. *Sci Transl Med,* **7**(283)**,** pp. 283ra54.
McKeague, A.L., Wilson, D.J. and Nelson, J. (2003) Staurosporine-induced apoptosis and hydrogen peroxide-induced necrosis in two human breast cell lines. *Br J Cancer,* **88**(1)**,** pp. 125-131.
McPherson, L.A., Shen, Y. and Ford, J.M. (2014) Poly (adp-ribose) polymerase inhibitor lt-626: Sensitivity correlates with mre11 mutations and synergizes with platinums and irinotecan in colorectal cancer cells. *Cancer Lett,* **343**(2)**,** pp. 217-223.
Melero, I., Gaudernack, G., Gerritsen, W., Huber, C., Parmiani, G., Scholl, S., Thatcher, N., Wagstaff, J., Zielinski, C., Faulkner, I. and Mellstedt, H. (2014) Therapeutic vaccines for cancer: An overview of clinical trials. *Nat Rev Clin Oncol,* **11**(9)**,** pp. 509-524.
Mendelsohn, J. and Baselga, J. (2000) The egf receptor family as targets for cancer therapy. *Oncogene,* **19**(56)**,** pp. 6550-6565.

Mert, H., Tunca, U. and Hizal, G. (2006) Thiophenol derivatives as a reducing agent for *in situ* generation of Cu(I) species via electron transfer reaction in copper-catalyzed living/controlled radical polymerization of styrene. *Journal of Polymer Science*, **44(**20), pp. 5923-5932.
Messa, C., Russo, F., Caruso, M.G. and Di Leo, A. (1998) Egf, tgf-alpha, and egf-r in human colorectal adenocarcinoma. *Acta Oncol,* **37**(3)**,** pp. 285-289.
Mitsudomi, T. and Yatabe, Y. (2010) Epidermal growth factor receptor in relation to tumor development: Egfr gene and cancer. *FEBS J,* **277**(2)**,** pp. 301-308.
Miyoshi, N., Oubrahim, H., Chock, P.B. and Stadtman, E.R. (2006) Age-dependent cell death and the role of atp in hydrogen peroxide-induced apoptosis and necrosis. *Proc Natl Acad Sci U S A,* **103**(6)**,** pp. 1727-1731.
Modrich, P. and Lahue, R. (1996) Mismatch repair in replication fidelity, genetic recombination, and cancer biology. *Annu Rev Biochem,* **65**, pp. 101-133.
Morin, P.J., Kinzler, K.W. and Sparks, A.B. (2016) Beta-catenin mutations: Insights into the apc pathway and the power of genetics. *Cancer Res,* **76**(19)**,** pp. 5587-5589.
Morin, P.J., Sparks, A.B., Korinek, V., Barker, N., Clevers, H., Vogelstein, B. and Kinzler, K.W. (1997) Activation of beta-catenin-tcf signaling in colon cancer by mutations in beta-catenin or apc. *Science,* **275**(5307)**,** pp. 1787-1790.
Morse, M.A., Chaudhry, A., Gabitzsch, E.S., Hobeika, A.C., Osada, T., Clay, T.M., Amalfitano, A., Burnett, B.K., Devi, G.R., Hsu, D.S., Xu, Y., Balcaitis, S., Dua, R., Nguyen, S., Balint, J.P., Jr., Jones, F.R. and Lyerly, H.K. (2013) Novel adenoviral vector induces t-cell responses despite anti-adenoviral neutralizing antibodies in colorectal cancer patients. *Cancer Immunol Immunother,* **62**(8)**,** pp. 1293-1301.
Mosmann, T. (1983) Rapid colorimetric assay for cellular growth and survival: Application to proliferation and cytotoxicity assays. *J Immunol Methods,* **65**(1-2)**,** pp. 55-63.
Mu, F.T., Callaghan, J.M., Steele-Mortimer, O., Stenmark, H., Parton, R.G., Campbell, P.L., McCluskey, J., Yeo, J.P., Tock, E.P. and Toh, B.H. (1995) Eea1, an early endosome-associated protein. Eea1 is a conserved alpha-helical peripheral membrane protein flanked by cysteine "fingers" and contains a calmodulin-binding iq motif. *J Biol Chem,* **270**(22)**,** pp. 13503-13511.
Munemitsu, S., Albert, I., Souza, B., Rubinfeld, B. and Polakis, P. (1995) Regulation of intracellular beta-catenin levels by the adenomatous polyposis coli (apc) tumor-suppressor protein. *Proc Natl Acad Sci U S A,* **92**(7)**,** pp. 3046-3050.
Munn, L.L. (2017) Cancer and inflammation. *Wiley Interdiscip Rev Syst Biol Med,* **9**(2)**,** pp. e1370.
Murphy, R.F. (1991) Maturation models for endosome and lysosome biogenesis. *Trends Cell Biol,* **1**(4)**,** pp. 77-82.

Nan, H., Hutter, C.M., Lin, Y., Jacobs, E.J., Ulrich, C.M., White, E., Baron, J.A., Berndt, S.I., Brenner, H., Butterbach, K., Caan, B.J., Campbell, P.T., Carlson, C.S., Casey, G., Chang-Claude, J., Chanock, S.J., Cotterchio, M., Duggan, D., Figueiredo, J.C., Fuchs, C.S., Giovannucci, E.L., Gong, J., Haile, R.W., Harrison, T.A., Hayes, R.B., Hoffmeister, M., Hopper, J.L., Hudson, T.J., Jenkins, M.A., Jiao, S., Lindor, N.M., Lemire, M., Le Marchand, L., Newcomb, P.A., Ogino, S., Pflugeisen, B.M., Potter, J.D., Qu, C., Rosse, S.A., Rudolph, A., Schoen, R.E., Schumacher, F.R., Seminara, D., Slattery, M.L., Thibodeau, S.N., Thomas, F., Thornquist, M., Warnick, G.S., Zanke, B.W., Gauderman, W.J., Peters, U., Hsu, L., Chan, A.T., Ccfr and Gecco (2015) Association of aspirin and nsaid use with risk of colorectal cancer according to genetic variants. *JAMA,* **313**(11)**,** pp. 1133-1142.

Negrini, S., Gorgoulis, V.G. and Halazonetis, T.D. (2010) Genomic instability--an evolving hallmark of cancer. *Nat Rev Mol Cell Biol,* **11**(3)**,** pp. 220-228.

Nelson, R.L., Davis, F.G., Sutter, E., Sobin, L.H., Kikendall, J.W. and Bowen, P. (1994) Body iron stores and risk of colonic neoplasia. *J Natl Cancer Inst,* **86**(6)**,** pp. 455-460.

Nikoletopoulou, V., Markaki, M., Palikaras, K. and Tavernarakis, N. (2013) Crosstalk between apoptosis, necrosis and autophagy. *Biochim Biophys Acta,* **1833**(12)**,** pp. 3448-3459.

Norbury, C. and Nurse, P. (1992) Animal cell cycles and their control. *Annu Rev Biochem,* **61**, pp. 441-470.

Noske, A., Lipka, S., Budczies, J., Muller, K., Loddenkemper, C., Buhr, H.J. and Kruschewski, M. (2009) Combination of p53 expression and p21 loss has an independent prognostic impact on sporadic colorectal cancer. *Oncol Rep,* **22**(1)**,** pp. 3-9.

Nyati, M.K., Morgan, M.A., Feng, F.Y. and Lawrence, T.S. (2006) Integration of egfr inhibitors with radiochemotherapy. *Nat Rev Cancer,* **6**(11)**,** pp. 876-885.

Obata, H., Biro, S., Arima, N., Kaieda, H., Kihara, T., Eto, H., Miyata, M. and Tanaka, H. (1996) Nf-kappa b is induced in the nuclei of cultured rat aortic smooth muscle cells by stimulation of various growth factors. *Biochem Biophys Res Commun,* **224**(1)**,** pp. 27-32.

Obuch, J.C. and Ahnen, D.J. (2016) Colorectal cancer: Genetics is changing everything. *Gastroenterol Clin North Am,* **45**(3)**,** pp. 459-476.

Odugbemi, T.O., Akinsulire, O.R., Aibinu, I.E. and Fabeku, P.O. (2007) Medicinal plants useful for malaria therapy in okeigbo, ondo state, southwest nigeria. *African Journal of Traditional Complementary and Alternative Medicines,* **4**(2)**,** pp. 191-198.

Ogino, S., Nosho, K., Kirkner, G.J., Kawasaki, T., Meyerhardt, J.A., Loda, M., Giovannucci, E.L. and Fuchs, C.S. (2009) Cpg island methylator phenotype, microsatellite instability, braf mutation and clinical outcome in colon cancer. *Gut,* **58**(1)**,** pp. 90-96.

Oh, B.Y., Lee, R.A., Chung, S.S. and Kim, K.H. (2011) Epidermal growth factor receptor mutations in colorectal cancer patients. *J Korean Soc Coloproctol,* **27**(3)**,** pp. 127-132.

Olayioye, M.A., Neve, R.M., Lane, H.A. and Hynes, N.E. (2000) The erbb signaling network: Receptor heterodimerization in development and cancer. *EMBO J,* **19**(13)**,** pp. 3159-3167.
Ortega, J., Li, J.Y., Lee, S., Tong, D., Gu, L. and Li, G.M. (2015) Phosphorylation of pcna by egfr inhibits mismatch repair and promotes misincorporation during DNA synthesis. *Proc Natl Acad Sci U S A,* **112**(18)**,** pp. 5667-5672.
Orth, J.D., Krueger, E.W., Weller, S.G. and McNiven, M.A. (2006) A novel endocytic mechanism of epidermal growth factor receptor sequestration and internalization. *Cancer Res,* **66**(7)**,** pp. 3603-3610.
Ouyang, N., Williams, J.L. and Rigas, B. (2008) No-donating aspirin inhibits angiogenesis by suppressing vegf expression in ht-29 human colon cancer mouse xenografts. *Carcinogenesis,* **29**(9)**,** pp. 1794-1798.
Pages, F., Galon, J., Dieu-Nosjean, M.C., Tartour, E., Sautes-Fridman, C. and Fridman, W.H. (2010) Immune infiltration in human tumors: A prognostic factor that should not be ignored. *Oncogene,* **29**(8)**,** pp. 1093-1102.
Pan, Z.Q., Reardon, J.T., Li, L., Flores-Rozas, H., Legerski, R., Sancar, A. and Hurwitz, J. (1995) Inhibition of nucleotide excision repair by the cyclin-dependent kinase inhibitor p21. *J Biol Chem,* **270**(37)**,** pp. 22008-22016.
Pao, W., Miller, V.A., Politi, K.A., Riely, G.J., Somwar, R., Zakowski, M.F., Kris, M.G. and Varmus, H. (2005) Acquired resistance of lung adenocarcinomas to gefitinib or erlotinib is associated with a second mutation in the egfr kinase domain. *PLoS Med,* **2**(3)**,** pp. e73.
Papadopoulos, N., Nicolaides, N.C., Wei, Y.F., Ruben, S.M., Carter, K.C., Rosen, C.A., Haseltine, W.A., Fleischmann, R.D., Fraser, C.M., Adams, M.D. and et al. (1994) Mutation of a mutl homolog in hereditary colon cancer. *Science,* **263**(5153)**,** pp. 1625-1629.
Patel, S.G. and Ahnen, D.J. (2014) Prevention of interval colorectal cancers: What every clinician needs to know. *Clin Gastroenterol Hepatol,* **12**(1)**,** pp. 7-15.
Patrignani, P., Sacco, A., Sostres, C., Bruno, A., Dovizio, M., Piazuelo, E., Di Francesco, L., Contursi, A., Zucchelli, M., Schiavone, S., Tacconelli, S., Patrono, C. and Lanas, A. (2017) Low-dose aspirin acetylates cyclooxygenase-1 in human colorectal mucosa: Implications for the chemoprevention of colorectal cancer. *Clin Pharmacol Ther*. **102**, pp. 52-61.
Patrono, C., Baigent, C., Hirsh, J. and Roth, G. (2008) Antiplatelet drugs: American college of chest physicians evidence-based clinical practice guidelines (8th edition). *Chest,* **133**(6 Suppl)**,** pp. 199S-233S.
Patrono, C., Garcia Rodriguez, L.A., Landolfi, R. and Baigent, C. (2005) Low-dose aspirin for the prevention of atherothrombosis. *N Engl J Med,* **353**(22)**,** pp. 2373-2383.
Paulus, H.E., Siegel, M., Mongan, E., Okun, R. and Calabro, J.J. (1971) Variations of serum concentrations and half-life of salicylate in patients with rheumatoid arthritis. *Arthritis Rheum,* **14**(4)**,** pp. 527-532.
Peltomaki, P. (1995) Microsatellite instability and hereditary non-polyposis colon cancer. *J Pathol,* **176**(4)**,** pp. 329-330.

Peltomaki, P. and de la Chapelle, A. (1997) Mutations predisposing to hereditary nonpolyposis colorectal cancer. *Adv Cancer Res,* **71**93-119.
Perazella, M.A. and Markowitz, G.S. (2010) Drug-induced acute interstitial nephritis. *Nat Rev Nephrol,* **6**(8)**,** pp. 461-470.
Perego, P., Giarola, M., Righetti, S.C., Supino, R., Caserini, C., Delia, D., Pierotti, M.A., Miyashita, T., Reed, J.C. and Zunino, F. (1996) Association between cisplatin resistance and mutation of p53 gene and reduced bax expression in ovarian carcinoma cell systems. *Cancer Res,* **56**(3)**,** pp. 556-562.
Pereira, D.A. and Williams, J.A. (2007) Origin and evolution of high throughput screening. *Br J Pharmacol,* **152**(1)**,** pp. 53-61.
Pereira-Leite, C., Nunes, C. and Reis, S. (2013) Interaction of nonsteroidal anti-inflammatory drugs with membranes: In vitro assessment and relevance for their biological actions. *Prog Lipid Res,* **52**(4)**,** pp. 571-584.
Platta, H.W. and Stenmark, H. (2011) Endocytosis and signaling. *Curr Opin Cell Biol,* **23**(4)**,** pp. 393-403.
Podolsky, S.H. and Greene, J.A. (2011) Combination drugs--hype, harm, and hope. *N Engl J Med,* **365**(6)**,** pp. 488-491.
Polyak, K., Xia, Y., Zweier, J.L., Kinzler, K.W. and Vogelstein, B. (1997) A model for p53-induced apoptosis. *Nature,* **389**(6648)**,** pp. 300-305.
Porebska, I., Harlozinska, A. and Bojarowski, T. (2000) Expression of the tyrosine kinase activity growth factor receptors (egfr, erb b2, erb b3) in colorectal adenocarcinomas and adenomas. *Tumour Biol,* **21**(2)**,** pp. 105-115.
Prives, C. and Gottifredi, V. (2008) The p21 and pcna partnership: A new twist for an old plot. *Cell Cycle,* **7**(24)**,** pp. 3840-3846.
Qian, X., Anzovino, A., Kim, S., Suyama, K., Yao, J., Hulit, J., Agiostratidou, G., Chandiramani, N., McDaid, H.M., Nagi, C., Cohen, H.W., Phillips, G.R., Norton, L. and Hazan, R.B. (2014) N-cadherin/fgfr promotes metastasis through epithelial-to-mesenchymal transition and stem/progenitor cell-like properties. *Oncogene,* **33**(26)**,** pp. 3411-3421.
Ramanathan, R.K., Clark, J.W., Kemeny, N.E., Lenz, H.J., Gococo, K.O., Haller, D.G., Mitchell, E.P. and Kardinal, C.G. (2003) Safety and toxicity analysis of oxaliplatin combined with fluorouracil or as a single agent in patients with previously treated advanced colorectal cancer. *J Clin Oncol,* **21**(15)**,** pp. 2904-2911.
Ramjiawan, R.R., Griffioen, A.W. and Duda, D.G. (2017) Anti-angiogenesis for cancer revisited: Is there a role for combinations with immunotherapy? *Angiogenesis,* **20**(2)**,** pp. 185-204.
Rau, B., Sturm, I., Lage, H., Berger, S., Schneider, U., Hauptmann, S., Wust, P., Riess, H., Schlag, P.M., Dorken, B. and Daniel, P.T. (2003) Dynamic expression profile of p21waf1/cip1 and ki-67 predicts survival in rectal carcinoma treated with preoperative radiochemotherapy. *J Clin Oncol,* **21**(18)**,** pp. 3391-3401.
Raymond, E., Faivre, S., Woynarowski, J.M. and Chaney, S.G. (1998) Oxaliplatin: Mechanism of action and antineoplastic activity. *Semin Oncol,* **25**(2 Suppl 5)**,** pp. 4-12.

Resnick, M.B., Routhier, J., Konkin, T., Sabo, E. and Pricolo, V.E. (2004) Epidermal growth factor receptor, c-met, beta-catenin, and p53 expression as prognostic indicators in stage ii colon cancer: A tissue microarray study. *Clin Cancer Res,* **10**(9)**,** pp. 3069-3075.

Ribatti, D. (2009) Endogenous inhibitors of angiogenesis: A historical review. *Leuk Res,* **33**(5)**,** pp. 638-644.

Richter, M., Weiss, M., Weinberger, I., Furstenberger, G. and Marian, B. (2001) Growth inhibition and induction of apoptosis in colorectal tumor cells by cyclooxygenase inhibitors. *Carcinogenesis,* **22**(1)**,** pp. 17-25.

Rieger, A.M., Hall, B.E., Luong le, T., Schang, L.M. and Barreda, D.R. (2010) Conventional apoptosis assays using propidium iodide generate a significant number of false positives that prevent accurate assessment of cell death. *J Immunol Methods,* **358**(1-2)**,** pp. 81-92.

Rieger, A.M., Nelson, K.L., Konowalchuk, J.D. and Barreda, D.R. (2011) Modified annexin v/propidium iodide apoptosis assay for accurate assessment of cell death. *J Vis Exp,* (50)**,** pp. 2597.

Risau, W. and Flamme, I. (1995) Vasculogenesis. *Annu Rev Cell Dev Biol,* **11**, pp. 73-91.

Roderick, P.J., Wilkes, H.C. and Meade, T.W. (1993) The gastrointestinal toxicity of aspirin: An overview of randomised controlled trials. *Br J Clin Pharmacol,* **35**(3)**,** pp. 219-226.

Roepstorff, K., Grandal, M.V., Henriksen, L., Knudsen, S.L., Lerdrup, M., Grovdal, L., Willumsen, B.M. and van Deurs, B. (2009) Differential effects of egfr ligands on endocytic sorting of the receptor. *Traffic,* **10**(8)**,** pp. 1115-1127.

Rojas, M., Yao, S. and Lin, Y.Z. (1996) Controlling epidermal growth factor (egf)-stimulated ras activation in intact cells by a cell-permeable peptide mimicking phosphorylated egf receptor. *J Biol Chem,* **271**(44)**,** pp. 27456-27461.

Roninson, I.B. (2002) Oncogenic functions of tumour suppressor p21(waf1/cip1/sdi1): Association with cell senescence and tumour-promoting activities of stromal fibroblasts. *Cancer Lett,* **179**(1)**,** pp. 1-14.

Rosenberg, S.A., Yang, J.C., Sherry, R.M., Kammula, U.S., Hughes, M.S., Phan, G.Q., Citrin, D.E., Restifo, N.P., Robbins, P.F., Wunderlich, J.R., Morton, K.E., Laurencot, C.M., Steinberg, S.M., White, D.E. and Dudley, M.E. (2011) Durable complete responses in heavily pretreated patients with metastatic melanoma using t-cell transfer immunotherapy. *Clin Cancer Res,* **17**(13)**,** pp. 4550-4557.

Roth, A.D., Tejpar, S., Delorenzi, M., Yan, P., Fiocca, R., Klingbiel, D., Dietrich, D., Biesmans, B., Bodoky, G., Barone, C., Aranda, E., Nordlinger, B., Cisar, L., Labianca, R., Cunningham, D., Van Cutsem, E. and Bosman, F. (2010) Prognostic role of kras and braf in stage ii and iii resected colon cancer: Results of the translational study on the petacc-3, eortc 40993, sakk 60-00 trial. *J Clin Oncol,* **28**(3)**,** pp. 466-474.

Rothwell, P.M., Fowkes, F.G., Belch, J.F., Ogawa, H., Warlow, C.P. and Meade, T.W. (2011) Effect of daily aspirin on long-term risk of death due to cancer: Analysis of individual patient data from randomised trials. *Lancet,* **377**(9759)**,** pp. 31-41.

Rowan, A.J., Lamlum, H., Ilyas, M., Wheeler, J., Straub, J., Papadopoulou, A., Bicknell, D., Bodmer, W.F. and Tomlinson, I.P. (2000) Apc mutations in sporadic colorectal tumors: A mutational "hotspot" and interdependence of the "two hits". *Proc Natl Acad Sci U S A,* **97**(7)**,** pp. 3352-3357.

Rowland, C.E., Belai, N., Knope, K.E. and Cahill, C.L. (2010) Hydrothermal synthesis of disulfide-containing uranyl compounds: In situ ligand synthesis versus direct assembly. *Crystal Growth & Design,* **10**(3)**,** pp. 1390-1398.

Rowland, C.E., Cantos, P.M., Toby, B.H., Frisch, M., Deschamps, J.R. and Cahill, C.L. (2011) Controlling disulfide bond formation and crystal growth from 2-mercaptobenzoic acid. *Crystal Growth & Design,* **11**(4)**,** pp. 1370-1374.

Saltz, L.B., Clarke, S., Diaz-Rubio, E., Scheithauer, W., Figer, A., Wong, R., Koski, S., Lichinitser, M., Yang, T.S., Rivera, F., Couture, F., Sirzen, F. and Cassidy, J. (2008) Bevacizumab in combination with oxaliplatin-based chemotherapy as first-line therapy in metastatic colorectal cancer: A randomized phase iii study. *J Clin Oncol,* **26**(12)**,** pp. 2013-2019.

Samowitz, W.S., Curtin, K., Schaffer, D., Robertson, M., Leppert, M. and Slattery, M.L. (2000) Relationship of ki-ras mutations in colon cancers to tumor location, stage, and survival: A population-based study. *Cancer Epidemiol Biomarkers Prev,* **9**(11)**,** pp. 1193-1197.

Sandler, R.S., Halabi, S., Baron, J.A., Budinger, S., Paskett, E., Keresztes, R., Petrelli, N., Pipas, J.M., Karp, D.D., Loprinzi, C.L., Steinbach, G. and Schilsky, R. (2003) A randomized trial of aspirin to prevent colorectal adenomas in patients with previous colorectal cancer. *N Engl J Med,* **348**(10)**,** pp. 883-890.

Saxon, J.A., Sherrill, T.P., Polosukhin, V.V., Sai, J., Zaynagetdinov, R., McLoed, A.G., Gulleman, P.M., Barham, W., Cheng, D.S., Hunt, R.P., Gleaves, L.A., Richmond, A., Young, L.R., Yull, F.E. and Blackwell, T.S. (2016) Epithelial nf-kappab signaling promotes egfr-driven lung carcinogenesis via macrophage recruitment. *Oncoimmunology,* **5**(6)**,** pp. e1168549.

Schenck, A., Goto-Silva, L., Collinet, C., Rhinn, M., Giner, A., Habermann, B., Brand, M. and Zerial, M. (2008) The endosomal protein appl1 mediates akt substrate specificity and cell survival in vertebrate development. *Cell,* **133**(3)**,** pp. 486-497.

Schetter, A.J., Heegaard, N.H. and Harris, C.C. (2010) Inflammation and cancer: Interweaving microrna, free radical, cytokine and p53 pathways. *Carcinogenesis,* **31**(1)**,** pp. 37-49.

Schindler, C. and Darnell, J.E., Jr. (1995) Transcriptional responses to polypeptide ligands: The jak-stat pathway. *Annu Rev Biochem,* **64**, pp. 621-651.

Schlessinger, J. (2000) Cell signaling by receptor tyrosine kinases. *Cell,* **103**(2)**,** pp. 211-225.

Schmidt, M.H., Furnari, F.B., Cavenee, W.K. and Bogler, O. (2003) Epidermal growth factor receptor signaling intensity determines intracellular protein interactions, ubiquitination, and internalization. *Proc Natl Acad Sci U S A,* **100**(11)**,** pp. 6505-6510.

Schreiber, R.D., Old, L.J. and Smyth, M.J. (2011) Cancer immunoediting: Integrating immunity's roles in cancer suppression and promotion. *Science,* **331**(6024)**,** pp. 1565-1570.

Schror, K. (2011) Pharmacology and cellular/molecular mechanisms of action of aspirin and non-aspirin nsaids in colorectal cancer. *Best Pract Res Clin Gastroenterol,* **25**(4-5)**,** pp. 473-484.

Schultz, G., Rotatori, D.S. and Clark, W. (1991) Egf and tgf-alpha in wound healing and repair. *J Cell Biochem,* **45**(4)**,** pp. 346-352.

Schvartzman, J.M., Sotillo, R. and Benezra, R. (2010) Mitotic chromosomal instability and cancer: Mouse modelling of the human disease. *Nat Rev Cancer,* **10**(2)**,** pp. 102-115.

Schwartzman, R.A. and Cidlowski, J.A. (1993) Apoptosis: The biochemistry and molecular biology of programmed cell death. *Endocr Rev,* **14**(2)**,** pp. 133-151.

Schwenger, P., Bellosta, P., Vietor, I., Basilico, C., Skolnik, E.Y. and Vilcek, J. (1997) Sodium salicylate induces apoptosis via p38 mitogen-activated protein kinase but inhibits tumor necrosis factor-induced c-jun n-terminal kinase/stress-activated protein kinase activation. *Proc Natl Acad Sci U S A,* **94**(7)**,** pp. 2869-2873.

Scott, N., Hatlelid, K.M., MacKenzie, N.E. and Carter, D.E. (1993) Reactions of arsenic(iii) and arsenic(v) species with glutathione. *Chem Res Toxicol,* **6**(1)**,** pp. 102-106.

Seaman, W.E., Ishak, K.G. and Plotz, P.H. (1974) Aspirin-induced hepatotoxicity in patients with systemic lupus erythematosus. *Ann Intern Med,* **80**(1)**,** pp. 1-8.

Sebastian, S., Settleman, J., Reshkin, S.J., Azzariti, A., Bellizzi, A. and Paradiso, A. (2006) The complexity of targeting egfr signalling in cancer: From expression to turnover. *Biochim Biophys Acta,* **1766**(1)**,** pp. 120-139.

Seglen, P.O., Berg, T.O., Blankson, H., Fengsrud, M., Holen, I. and Stromhaug, P.E. (1996) Structural aspects of autophagy. *Adv Exp Med Biol,* **389**, pp. 103-111.

Selvendiran, K., Bratasz, A., Tong, L., Ignarro, L.J. and Kuppusamy, P. (2008) Ncx-4016, a nitro-derivative of aspirin, inhibits egfr and stat3 signaling and modulates bcl-2 proteins in cisplatin-resistant human ovarian cancer cells and xenografts. *Cell Cycle,* **7**(1)**,** pp. 81-88.

Sergent, C., Franco, N., Chapusot, C., Lizard-Nacol, S., Isambert, N., Correia, M. and Chauffert, B. (2002) Human colon cancer cells surviving high doses of cisplatin or oxaliplatin in vitro are not defective in DNA mismatch repair proteins. *Cancer Chemother Pharmacol,* **49**(6)**,** pp. 445-452.

Shepherd, V.L. (1989) Intracellular pathways and mechanisms of sorting in receptor-mediated endocytosis. *Trends Pharmacol Sci,* **10**(11)**,** pp. 458-462.

Shinoura, N., Yoshida, Y., Nishimura, M., Muramatsu, Y., Asai, A., Kirino, T. and Hamada, H. (1999) Expression level of bcl-2 determines anti- or proapoptotic function. *Cancer Res,* **59**(16)**,** pp. 4119-4128.

Shirakata, Y., Kimura, R., Nanba, D., Iwamoto, R., Tokumaru, S., Morimoto, C., Yokota, K., Nakamura, M., Sayama, K., Mekada, E., Higashiyama, S. and Hashimoto, K. (2005) Heparin-binding egf-like growth factor accelerates keratinocyte migration and skin wound healing. *J Cell Sci,* **118**(Pt 11)**,** pp. 2363-2370.

Shirakawa, K., Wang, L., Man, N., Maksimoska, J., Sorum, A.W., Lim, H.W., Lee, I.S., Shimazu, T., Newman, J.C., Schroder, S., Ott, M., Marmorstein, R., Meier, J., Nimer, S. and Verdin, E. (2016) Salicylate, diflunisal and their metabolites inhibit cbp/p300 and exhibit anticancer activity. *Elife,* **5**, pp. e11156.

Shostak, K. and Chariot, A. (2015) Egfr and nf-kappab: Partners in cancer. *Trends Mol Med,* **21**(6)**,** pp. 385-393.

Sigismund, S., Argenzio, E., Tosoni, D., Cavallaro, E., Polo, S. and Di Fiore, P.P. (2008) Clathrin-mediated internalization is essential for sustained egfr signaling but dispensable for degradation. *Dev Cell,* **15**(2)**,** pp. 209-219.

Sigismund, S., Woelk, T., Puri, C., Maspero, E., Tacchetti, C., Transidico, P., Di Fiore, P.P. and Polo, S. (2005) Clathrin-independent endocytosis of ubiquitinated cargos. *Proc Natl Acad Sci U S A,* **102**(8)**,** pp. 2760-2765.

Singh, P.K. and Hollingsworth, M.A. (2006) Cell surface-associated mucins in signal transduction. *Trends Cell Biol,* **16**(9)**,** pp. 467-476.

Smyth, E.M., Grosser, T., Wang, M., Yu, Y. and FitzGerald, G.A. (2009) Prostanoids in health and disease. *J Lipid Res,* **50**, pp. S423-428.

Song, S., Honjo, S., Jin, J., Chang, S.S., Scott, A.W., Chen, Q., Kalhor, N., Correa, A.M., Hofstetter, W.L., Albarracin, C.T., Wu, T.T., Johnson, R.L., Hung, M.C. and Ajani, J.A. (2015) The hippo coactivator yap1 mediates egfr overexpression and confers chemoresistance in esophageal cancer. *Clin Cancer Res,* **21**(11)**,** pp. 2580-2590.

Sordella, R., Bell, D.W., Haber, D.A. and Settleman, J. (2004) Gefitinib-sensitizing egfr mutations in lung cancer activate anti-apoptotic pathways. *Science,* **305**(5687)**,** pp. 1163-1167.

Soria, G. and Gottifredi, V. (2010) Pcna-coupled p21 degradation after DNA damage: The exception that confirms the rule? *DNA Repair (Amst),* **9**(4)**,** pp. 358-364.

Sorkin, A. and Goh, L.K. (2009) Endocytosis and intracellular trafficking of erbbs. *Exp Cell Res,* **315**(4)**,** pp. 683-696.

Sorkin, A. and von Zastrow, M. (2009) Endocytosis and signalling: Intertwining molecular networks. *Nat Rev Mol Cell Biol,* **10**(9)**,** pp. 609-622.

Sorkina, T., Huang, F., Beguinot, L. and Sorkin, A. (2002) Effect of tyrosine kinase inhibitors on clathrin-coated pit recruitment and internalization of epidermal growth factor receptor. *J Biol Chem,* **277**(30)**,** pp. 27433-27441.

Spano, J.P., Fagard, R., Soria, J.C., Rixe, O., Khayat, D. and Milano, G. (2005) Epidermal growth factor receptor signaling in colorectal cancer: Preclinical data and therapeutic perspectives. *Ann Oncol,* **16**(2)**,** pp. 189-194.

Sporn, M.B. (1996) The war on cancer. *Lancet,* **347**(9012)**,** pp. 1377-1381.
Spruce, B.A., Campbell, L.A., McTavish, N., Cooper, M.A., Appleyard, M.V., O'Neill, M., Howie, J., Samson, J., Watt, S., Murray, K., McLean, D., Leslie, N.R., Safrany, S.T., Ferguson, M.J., Peters, J.A., Prescott, A.R., Box, G., Hayes, A., Nutley, B., Raynaud, F., Downes, C.P., Lambert, J.J., Thompson, A.M. and Eccles, S. (2004) Small molecule antagonists of the sigma-1 receptor cause selective release of the death program in tumor and self-reliant cells and inhibit tumor growth in vitro and in vivo. *Cancer Res,* **64**(14)**,** pp. 4875-4886.
Stark, L.A., Din, F.V., Zwacka, R.M. and Dunlop, M.G. (2001) Aspirin-induced activation of the nf-kappab signaling pathway: A novel mechanism for aspirin-mediated apoptosis in colon cancer cells. *FASEB J,* **15**(7)**,** pp. 1273-1275.
Strand, M., Prolla, T.A., Liskay, R.M. and Petes, T.D. (1993) Destabilization of tracts of simple repetitive DNA in yeast by mutations affecting DNA mismatch repair. *Nature,* **365**(6443)**,** pp. 274-276.
Sullivan, S.G., Hussain, R., Glasson, E.J. and Bittles, A.H. (2007) The profile and incidence of cancer in down syndrome. *J Intellect Disabil Res,* **51**(Pt 3)**,** pp. 228-231.
Sun, L. and Carpenter, G. (1998) Epidermal growth factor activation of nf-kappab is mediated through ikappabalpha degradation and intracellular free calcium. *Oncogene,* **16**(16)**,** pp. 2095-2102.
Sun, Y., Zheng, W., Guo, Z., Ju, Q., Zhu, L., Gao, J., Zhou, L., Liu, F., Xu, Y., Zhan, Q., Zhou, Z., Sun, W. and Zhao, X. (2016) A novel tp53 pathway influences the hgs-mediated exosome formation in colorectal cancer. *Sci Rep,* **6**, pp. 28083.
Sutter, A., Amberg, A., Boyer, S., Brigo, A., Contrera, J.F., Custer, L.L., Dobo, K.L., Gervais, V., Glowienke, S., van Gompel, J., Greene, N., Muster, W., Nicolette, J., Reddy, M.V., Thybaud, V., Vock, E., White, A.T. and Muller, L. (2013) Use of in silico systems and expert knowledge for structure-based assessment of potentially mutagenic impurities. *Regul Toxicol Pharmacol,* **67**(1)**,** pp. 39-52.
Tejpar, S., Bertagnolli, M., Bosman, F., Lenz, H.J., Garraway, L., Waldman, F., Warren, R., Bild, A., Collins-Brennan, D., Hahn, H., Harkin, D.P., Kennedy, R., Ilyas, M., Morreau, H., Proutski, V., Swanton, C., Tomlinson, I., Delorenzi, M., Fiocca, R., Van Cutsem, E. and Roth, A. (2010) Prognostic and predictive biomarkers in resected colon cancer: Current status and future perspectives for integrating genomics into biomarker discovery. *Oncologist,* **15**(4)**,** pp. 390-404.
Teramoto, S., Tomita, T., Matsui, H., Ohga, E., Matsuse, T. and Ouchi, Y. (1999) Hydrogen peroxide-induced apoptosis and necrosis in human lung fibroblasts: Protective roles of glutathione. *Jpn J Pharmacol,* **79**(1)**,** pp. 33-40.
Thompson, S.L. and Compton, D.A. (2008) Examining the link between chromosomal instability and aneuploidy in human cells. *J Cell Biol,* **180**(4)**,** pp. 665-672.

Thorat, M.A. and Cuzick, J. (2015) Prophylactic use of aspirin: Systematic review of harms and approaches to mitigation in the general population. *Eur J Epidemiol,* **30**(1)**,** pp. 5-18.

Thorstensen, L., Lind, G.E., Lovig, T., Diep, C.B., Meling, G.I., Rognum, T.O. and Lothe, R.A. (2005) Genetic and epigenetic changes of components affecting the wnt pathway in colorectal carcinomas stratified by microsatellite instability. *Neoplasia,* **7**(2)**,** pp. 99-108.

Tomasetti, C., Li, L. and Vogelstein, B. (2017) Stem cell divisions, somatic mutations, cancer etiology, and cancer prevention. *Science,* **355**(6331)**,** pp. 1330-1334.

Tomasetti, C., Vogelstein, B. and Parmigiani, G. (2013) Half or more of the somatic mutations in cancers of self-renewing tissues originate prior to tumor initiation. *Proc Natl Acad Sci U S A,* **110**(6)**,** pp. 1999-2004.

Tomlinson, I., Ilyas, M., Johnson, V., Davies, A., Clark, G., Talbot, I. and Bodmer, W. (1998) A comparison of the genetic pathways involved in the pathogenesis of three types of colorectal cancer. *J Pathol,* **184**(2)**,** pp. 148-152.

Toscano, F., Parmentier, B., Fajoui, Z.E., Estornes, Y., Chayvialle, J.A., Saurin, J.C. and Abello, J. (2007) P53 dependent and independent sensitivity to oxaliplatin of colon cancer cells. *Biochem Pharmacol,* **74**(3)**,** pp. 392-406.

Touchstone, J.C. (1992) *Practice of Thin Layer Chromatography*. 3rd ed. New York: John Wiley and Sons, Inc., pp. 1-2, 11.

Tran, E., Robbins, P.F., Lu, Y.C., Prickett, T.D., Gartner, J.J., Jia, L., Pasetto, A., Zheng, Z., Ray, S., Groh, E.M., Kriley, I.R. and Rosenberg, S.A. (2016) T-cell transfer therapy targeting mutant kras in cancer. *N Engl J Med,* **375**(23)**,** pp. 2255-2262.

Tutlewska, K., Lubinski, J. and Kurzawski, G. (2013) Germline deletions in the epcam gene as a cause of lynch syndrome - literature review. *Hered Cancer Clin Pract,* **11**(1)**,** pp. 9.

Ushiro, H. and Cohen, S. (1980) Identification of phosphotyrosine as a product of epidermal growth factor-activated protein kinase in a-431 cell membranes. *J Biol Chem,* **255**(18)**,** pp. 8363-8365.

Van Cutsem, E. and Geboes, K. (2007) The multidisciplinary management of gastrointestinal cancer. The integration of cytotoxics and biologicals in the treatment of metastatic colorectal cancer. *Best Pract Res Clin Gastroenterol,* **21**(6)**,** pp. 1089-1108.

van Engeland, M., Ramaekers, F.C., Schutte, B. and Reutelingsperger, C.P. (1996) A novel assay to measure loss of plasma membrane asymmetry during apoptosis of adherent cells in culture. *Cytometry,* **24**(2)**,** pp. 131-139.

van Gurp, M., Festjens, N., van Loo, G., Saelens, X. and Vandenabeele, P. (2003) Mitochondrial intermembrane proteins in cell death. *Biochem Biophys Res Commun,* **304**(3)**,** pp. 487-497.

Van Schaeybroeck, S., Karaiskou-McCaul, A., Kelly, D., Longley, D., Galligan, L., Van Cutsem, E. and Johnston, P. (2005) Epidermal growth factor receptor activity determines response of colorectal cancer cells to gefitinib alone and in combination with chemotherapy. *Clin Cancer Res,* **11**(20)**,** pp. 7480-7489.

Vaughn, C.P., Zobell, S.D., Furtado, L.V., Baker, C.L. and Samowitz, W.S. (2011) Frequency of kras, braf, and nras mutations in colorectal cancer. *Genes Chromosomes Cancer,* **50**(5)**,** pp. 307-312.

Vermes, I., Haanen, C., Steffens-Nakken, H. and Reutelingsperger, C. (1995) A novel assay for apoptosis. Flow cytometric detection of phosphatidylserine expression on early apoptotic cells using fluorescein labelled annexin v. *J Immunol Methods,* **184**(1)**,** pp. 39-51.

Vermeulen, K., Van Bockstaele, D.R. and Berneman, Z.N. (2003) The cell cycle: A review of regulation, deregulation and therapeutic targets in cancer. *Cell Prolif,* **36**(3)**,** pp. 131-149.

Vieira, A.V., Lamaze, C. and Schmid, S.L. (1996) Control of egf receptor signaling by clathrin-mediated endocytosis. *Science,* **274**(5295)**,** pp. 2086-2089.

von Zastrow, M. and Sorkin, A. (2007) Signaling on the endocytic pathway. *Curr Opin Cell Biol,* **19**(4)**,** pp. 436-445.

Vousden, K.H. and Prives, C. (2009) Blinded by the light: The growing complexity of p53. *Cell,* **137**(3)**,** pp. 413-431.

Wang, J. and Xie, X. (2007) Development of a quantitative, cell-based, high-content screening assay for epidermal growth factor receptor modulators. *Acta Pharmacol Sin,* **28**(10)**,** pp. 1698-1704.

Wang, Q., Villeneuve, G. and Wang, Z. (2005) Control of epidermal growth factor receptor endocytosis by receptor dimerization, rather than receptor kinase activation. *EMBO Rep,* **6**(10)**,** pp. 942-948.

Wang, S.C., Nakajima, Y., Yu, Y.L., Xia, W., Chen, C.T., Yang, C.C., McIntush, E.W., Li, L.Y., Hawke, D.H., Kobayashi, R. and Hung, M.C. (2006) Tyrosine phosphorylation controls pcna function through protein stability. *Nat Cell Biol,* **8**(12)**,** pp. 1359-1368.

Warner, T.D., Giuliano, F., Vojnovic, I., Bukasa, A., Mitchell, J.A. and Vane, J.R. (1999) Nonsteroid drug selectivities for cyclo-oxygenase-1 rather than cyclo-oxygenase-2 are associated with human gastrointestinal toxicity: A full in vitro analysis. *Proc Natl Acad Sci U S A,* **96**(13)**,** pp. 7563-7568.

Watson, D.G. (2005) *Pharmaceutical Analysis: A Textbook for Pharmacy Students and Pharmaceutical Chemists*. 2nd ed. London: Elsevier Churchill Livungstone, pp. 315-321.

Weaver, B.A., Silk, A.D., Montagna, C., Verdier-Pinard, P. and Cleveland, D.W. (2007) Aneuploidy acts both oncogenically and as a tumor suppressor. *Cancer Cell,* **11**(1)**,** pp. 25-36.

Weiner, H.L. and Zagzag, D. (2000) Growth factor receptor tyrosine kinases: Cell adhesion kinase family suggests a novel signaling mechanism in cancer. *Cancer Invest,* **18**(6)**,** pp. 544-554.

Weiss, R.B. and Christian, M.C. (1993) New cisplatin analogues in development. A review. *Drugs,* **46**(3)**,** pp. 360-377.

Wells, A. (1999) Egf receptor. *Int J Biochem Cell Biol,* **31**(6)**,** pp. 637-643.

Werner, S. and Grose, R. (2003) Regulation of wound healing by growth factors and cytokines. *Physiol Rev,* **83**(3)**,** pp. 835-870.

Wheeler, D.L., Dunn, E.F. and Harari, P.M. (2010) Understanding resistance to egfr inhibitors-impact on future treatment strategies. *Nat Rev Clin Oncol,* **7**(9)**,** pp. 493-507.

Wherry, E.J. (2011) T cell exhaustion. *Nat Immunol,* **12**(6)**,** pp. 492-499.
Williams, D.H. and Fleming, I. (2008) *Spectroscopic methods in organic chemistry.* [online] 6th ed. London: McGraw-Hill Higher Education. Available at: <http://wlv.summon.serialssolutions.com/2.0.0/link/0/eLvHCXMwbV1LCwIhEB56HAo6tD1oe4DnoFjXTd1ztPQD6rzsmkKXLSjo7-esSfQ4KjIo6Og4830fAIvX0erLJ1CmRMw0NYk0UaIlF5g2pYU0dGM2LsH7Jt8Hr4moCpTOQHwq1jNiEhXhVR9SZTZ-4OiDm0mK5zI7HF3sJRBRGXuOHd-2D8nmw0vC11dI1ocWwgoCaOhqAJ2t11kbwhIl4O9IKnm5nhVxks43cq6IU1xSRPnBIwiz3WG7X1nj-evjJXdTi8fQK7BavbrXqLbTBIhkUpVcSs2RfV6IlJaliJRKTtzGKykLIfg1NP3XOYOuq2DAT4E5tI3dtHpRL_IJn6ppcg>.
Wittig, B., Schmidt, M., Scheithauer, W. and Schmoll, H.J. (2015) Mgn1703, an immunomodulator and toll-like receptor 9 (tlr-9) agonist: From bench to bedside. *Crit Rev Oncol Hematol,* **94**(1)**,** pp. 31-44.
Wlodkowic, D., Telford, W., Skommer, J. and Darzynkiewicz, Z. (2011) Apoptosis and beyond: Cytometry in studies of programmed cell death. *Methods Cell Biol,* **103**, pp. 55-98.
Wolter, K.G., Hsu, Y.T., Smith, C.L., Nechushtan, A., Xi, X.G. and Youle, R.J. (1997) Movement of bax from the cytosol to mitochondria during apoptosis. *J Cell Biol,* **139**(5)**,** pp. 1281-1292.
Woodman, P. (2009) Escrt proteins, endosome organization and mitogenic receptor down-regulation. *Biochem Soc Trans,* **37**(Pt 1)**,** pp. 146-150.
Wyllie, A.H., Kerr, J.F. and Currie, A.R. (1980) Cell death: The significance of apoptosis. *Int Rev Cytol,* **68**, pp. 251-306.
Xiang, B., Snook, A.E., Magee, M.S. and Waldman, S.A. (2013) Colorectal cancer immunotherapy. *Discov Med,* **15**(84)**,** pp. 301-308.
Yan, K.H., Yao, C.J., Chang, H.Y., Lai, G.M., Cheng, A.L. and Chuang, S.E. (2010) The synergistic anticancer effect of troglitazone combined with aspirin causes cell cycle arrest and apoptosis in human lung cancer cells. *Mol Carcinog,* **49**(3)**,** pp. 235-246.
Yang, C., Zhou, Q., Li, M., Tong, X., Sun, J., Qing, Y., Sun, L., Yang, X., Hu, X., Jiang, J., Yan, X., He, L. and Wan, C. (2016) Upregulation of cyp2s1 by oxaliplatin is associated with p53 status in colorectal cancer cell lines. *Sci Rep,* **6**, pp**.** 33078.
Yao, Y.L., Shao, J., Zhang, C., Wu, J.H., Zhang, Q.H., Wang, J.J. and Zhu, W. (2013) Proliferation of colorectal cancer is promoted by two signaling transduction expression patterns: Erbb2/erbb3/akt and met/erbb3/mapk. *PLoS One,* **8**(10)**,** pp. e78086.
Yarden, Y. and Schlessinger, J. (1987) Epidermal growth factor induces rapid, reversible aggregation of the purified epidermal growth factor receptor. *Biochemistry,* **26**(5)**,** pp. 1443-1451.
Yarden, Y. and Ullrich, A. (1988) Growth factor receptor tyrosine kinases. *Annu Rev Biochem,* **57**, pp. 443-478.

Yost, C., Torres, M., Miller, J.R., Huang, E., Kimelman, D. and Moon, R.T. (1996) The axis-inducing activity, stability, and subcellular distribution of beta-catenin is regulated in xenopus embryos by glycogen synthase kinase 3. *Genes Dev,* **10**(12)**,** pp. 1443-1454.

Yu, X., Harris, S.L. and Levine, A.J. (2006) The regulation of exosome secretion: A novel function of the p53 protein. *Cancer Res,* **66**(9)**,** pp. 4795-4801.

Yu, X., Riley, T. and Levine, A.J. (2009) The regulation of the endosomal compartment by p53 the tumor suppressor gene. *FEBS J,* **276**(8)**,** pp. 2201-2212.

Yuan, R. and Lin, Y. (2000) Traditional chinese medicine: An approach to scientific proof and clinical validation. *Pharmacol Ther,* **86**(2)**,** pp. 191-198.

Yuan, Z., Shin, J., Wilson, A., Goel, S., Ling, Y.H., Ahmed, N., Dopeso, H., Jhawer, M., Nasser, S., Montagna, C., Fordyce, K., Augenlicht, L.H., Aaltonen, L.A., Arango, D., Weber, T.K. and Mariadason, J.M. (2009) An a13 repeat within the 3'-untranslated region of epidermal growth factor receptor (egfr) is frequently mutated in microsatellite instability colon cancers and is associated with increased egfr expression. *Cancer Res,* **69**(19)**,** pp. 7811-7818.

Zaugg, R.H., Walder, J.A., Walder, R.Y., Steele, J.M. and Klotz, I.M. (1980) Modification of hemoglobin with analogs of aspirin. *J Biol Chem,* **255**(7)**,** pp. 2816-2821.

Zerial, M. and McBride, H. (2001) Rab proteins as membrane organizers. *Nat Rev Mol Cell Biol,* **2**(2)**,** pp. 107-117.

Zhang, H., Chen, Q.Y., Xiang, M.L., Ma, C.Y., Huang, Q. and Yang, S.Y. (2009) In silico prediction of mitochondrial toxicity by using ga-cg-svm approach. *Toxicol In Vitro,* **23**(1)**,** pp. 134-140.

Zhang, X., Cheng, L., Minn, K., Madan, R., Godwin, A.K., Shridhar, V. and Chien, J. (2014) Targeting of mutant p53-induced foxm1 with thiostrepton induces cytotoxicity and enhances carboplatin sensitivity in cancer cells. *Oncotarget,* **5**(22)**,** pp. 11365-11380.

Zhao, H., Liu, Q., Wang, S., Dai, F., Cheng, X., Cheng, X., Chen, W., Zhang, M. and Chen, D. (2017) In vitro additive antitumor effects of dimethoxycurcumin and 5-fluorouracil in colon cancer cells. *Cancer Med,* **6**(7)**,** pp. 1698-1706.

Zhao, W., Mackenzie, G.G., Murray, O.T., Zhang, Z. and Rigas, B. (2009) Phosphoaspirin (mdc-43), a novel benzyl ester of aspirin, inhibits the growth of human cancer cell lines more potently than aspirin: A redox-dependent effect. *Carcinogenesis,* **30**(3)**,** pp. 512-519.

Zhou, J., Zhou, Y., Yin, B., Hao, W., Zhao, L., Ju, W. and Bai, C. (2010) 5-fluorouracil and oxaliplatin modify the expression profiles of micrornas in human colon cancer cells in vitro. *Oncol Rep,* **23**(1)**,** pp. 121-128.

Zhu, L., Finkelstein, D., Gao, C., Shi, L., Wang, Y., Lopez-Terrada, D., Wang, K., Utley, S., Pounds, S., Neale, G., Ellison, D., Onar-Thomas, A. and Gilbertson, R.J. (2016) Multi-organ mapping of cancer risk. *Cell,* **166**(5)**,** pp. 1132-1146 e1137.

Zimmermann, G.R., Lehar, J. and Keith, C.T. (2007) Multi-target therapeutics: When the whole is greater than the sum of the parts. *Drug Discov Today,* **12**(1-2)**,** pp. 34-42.

Zirbes, T.K., Baldus, S.E., Moenig, S.P., Nolden, S., Kunze, D., Shafizadeh, S.T., Schneider, P.M., Thiele, J., Hoelscher, A.H. and Dienes, H.P. (2000) Prognostic impact of p21/waf1/cip1 in colorectal cancer. *Int J Cancer,* **89**(1)**,** pp. 14-18.

Zoncu, R., Perera, R.M., Balkin, D.M., Pirruccello, M., Toomre, D. and De Camilli, P. (2009) A phosphoinositide switch controls the maturation and signaling properties of appl endosomes. *Cell,* **136**(6)**,** pp. 1110-1121.

Zwang, Y. and Yarden, Y. (2006) P38 map kinase mediates stress-induced internalization of egfr: Implications for cancer chemotherapy. *EMBO J,* **25**(18)**,** pp. 4195-4206.